NASA CR-176,052

NASA-CR-176052
19850022857

Proceedings of the Workshop on Identification and Control of Flexible Space Structures

Volume II

G. Rodriguez
Editor

For Reference

April 1, 1985

NΛSΛ

National Aeronautics and
Space Administration

Jet Propulsion Laboratory
California Institute of Technology
Pasadena, California

NF01777

All Blank Pages

Intentionally Left Blank

To Keep Document Continuity

Proceedings of the Workshop on Identification and Control of Flexible Space Structures

Volume II

G. Rodriguez
Editor

April 1, 1985

NASA

National Aeronautics and
Space Administration

Jet Propulsion Laboratory
California Institute of Technology
Pasadena, California

ABSTRACT

These proceedings report the results of a workshop on identification and control of flexible space structures held in San Diego, CA, July 4-6, 1984. The workshop was co-sponsored by the Jet Propulsion Laboratory and the NASA Langley Research Center, and preceded the 1984 American Control Conference held at the same location. The main objectives of the workshop were to provide a forum to exchange ideas in exploring the most advanced modeling, estimation, identification and control methodologies to flexible space structures. The workshop responded to the rapidly growing interest within NASA in large space systems (space station, platforms, antennas, flight experiments) currently under design. The workshop consisted of surveys, tutorials, contributed papers, and discussion sessions in the following general areas: missions of current interest - space platforms, antennas, and flight experiments; control/structure interactions - modeling, integrated design and optimization, control and stabilization, and shape control; uncertainty management - parameter identification, model error estimation/compensation, and adaptive control; and experimental evaluation - ground laboratory demonstrations and flight experiment designs. Papers and lectures on these topics were presented at a total of fourteen sessions, including three panel discussions.

TABLE OF CONTENTS

VOLUME I

A REDUCING TRANSFORMATION FOR DYNAMICS MODELING OF A CLUSTER OF CONTIGUOUS FLEXIBLE STRUCTURES WITH CONSTRAINTS

R. P. Singh
Honeywell, Inc
Clearwater, FL 33546

P. W. Likins
Lehigh University
Bethlehem, PA 18015

THEME

Large Space Structures (LSS) and other dynamical systems of current interest
are often extremely complex assemblies of rigid and flexible bodies subjected
to kinematical constraints. This paper presents a formulation of the govern-
ing equations of constrained multibody systems via the application of singular
value decomposition (SVD). The resulting equations of motion are shown to be
of minimum dimension.

The motivation for this work was the development of a generic computer program
for simulating space structures and similar electromechanical systems amenable
to mathematical representation as a set of flexible bodies interconnected in a
topological configuration. This representation may include closed loops of
bodies, prescribed motion, or other constraints that may qualify as simple
monholonomic. The equations of motion appropriate for a set of flexible bodies
in an open loop configuration appear in Refs. 1, 2. A computer program
(TREETOPS) developed to simulate the dynamic response of flexible structures
in a topological tree configuration is described in Ref. 3. The SVD technique
of the present paper is being incorporated in an extension of the TREETOPS
program that permits application to constrained systems. This extension
permits direct use of the dynamical equations for the less constrained system
in Refs. 1, 2, with augmentation by kinematical constraint equations and re-
duction of dimension by SVD.

Basically, there are two conceptual approaches to solving the equations of
motion of such systems. (1) One can introduce unknown forces and torques at
the interfaces between constrained bodies (often accomplishing this symbolical-
ly with Lagrange multipliers), and then solve the dynamical equations simul-
taneously with the constraint equations to determine the constraint forces and
torques as well as the kinematical variables, Ref. 4. (2) Alternatively, one
can use the constraint equations to reduce the dimension of the system of
dynamical equations to be solved by partitioning generalized coordinates, Refs.
5, 6. Techniques presented in Refs. 4, 5, 6 may encounter numerical singular-
ities. Also, systems undergoing large motion may present problems of
inconsistency in the constraints such as three dimensional loops during the
system motion becoming two dimensional or one dimensional loops. In what
follows, the SVD method will be shown to avoid mathematical singularities.

CONTENTS

Singular Value Decomposition: Orthogonal decomposition of an mxn matrix L by singular value decomposition is closely related to the eigenvalue-eigenvector decomposition of the symmetric positive semi definite matrices L^TL and LL^T. Let $r \leq m$ be the rank of L. Then there are orthogonal matrices U and V of order mxm and nxn rexpectively such that

$$U^TLV = \begin{bmatrix} \Sigma & 0 \\ 0 & 0 \end{bmatrix} \tag{1}$$
$$= S$$

where $\Sigma = $ diag $(\lambda_1, \lambda_2, \ldots, \lambda_r)$ and $\lambda_1 \geq \lambda_2 \geq \ldots \geq \lambda_r > 0$.

The diagonal elements of the decomposition are called the singular values of the matrix L. The singular values are unique, although U and V are not.

It is easy to verify that

$$V^TL^TLV = \text{diag} (\Sigma^2, 0) \tag{2}$$

Thus $(\lambda_1^2, \ldots, \lambda_r^2)$ must be the nonzero eigenvalues of L^TL arranged in the descending order and the requirement that λ_1 be nonnegative completely determines the λ_1. The eigenvectors of L^TL are the columns of V. If L^TL has a multiple eigenvalue $\lambda^2 > 0$, the corresponding columns of V may be chosen as an orthonormal basis for the space spanned by the eigenvectors corresponding to λ^2.

From eq. (1)

$$L = USV^T \tag{3}$$

Now with proper partitioning of U and V eq. (3) can be expressed as

$$L = \begin{bmatrix} U_1 & \vdots & U_2 \end{bmatrix} \begin{bmatrix} \Sigma & \vdots & 0 \\ 0 & \vdots & 0 \end{bmatrix} \begin{bmatrix} V_1^T \\ V_2^T \end{bmatrix} = U_1 \Sigma V_1^T \tag{4}$$

From the above one obtains

$$U_1 = LV_1 \Sigma^{-1} \tag{5}$$

Thus once V_1 is chosen U_1 is obtained by eq. (5). The matrices U_2 and V_2 may be any matrices with orthonormal columns spanning the null spaces of L^T and L respectively. It is worthwhile to mention that the null space of L is the space of all vectors x such that

$$Lx = 0 \tag{6}$$

With the orthogonal decomposition given by eq. (3), an nxm matrix L^+, called the pseudoinverse of L, is defined by

$$L^+ = V \begin{bmatrix} \Sigma^{-1} & 0 \\ 0 & 0 \end{bmatrix} U^T \tag{7}$$

L^+ is uniquely defined by L; it does not depend on the particular orthogonal decomposition of L.

Application of SVD to Dynamical System with Constraints: Let $q = q_1,\ldots,q_n$ comprise a set of generalized coordinates that fully defines the configuration of dynamical system. The equations of motion of the system can be written as

$$M\ddot{q} = F(\dot{q},q,t) \tag{8a}$$

where the elements of nxn matrix M are functions of q's and the inertia properties of the system; the elements of nxl column vector F are functions of q's, their time derivatives $\dot{q}$'s and applied forces (moments) on the systems. If the generalized coordinates are related by constraint equations then they are not independent and the right hand side of eq. (8a) will also include the non-working forces of constraints. Let the unknown constraint forces be denoted F^C. Now for the general case of constrained dynamical system, eq. (8a) takes the following form

$$M\ddot{q} = F + F^C \tag{8}$$

Suppose however that the constraint equations can be written as

$$A\dot{q} = B \tag{9}$$

where A is of dimension mxn (m<n) and B is an mxl column vector.

Holonomic constraint equations can always be placed in the form of eq. (9) and nonholonomic constraints in the class called Pfaffian or simple have this structure also.

If the rank of matrix A is $r \leq m$ then r of the kinematical variables in q are related by eq. (9) and there are only n-r independent generalized coordinates. In other words the dynamical system possesses n-r degrees of freedom.

The SVD of the mxn matrix A provides

$$A = USV^T \tag{10}$$

The orthogonal matrices U and V (of dimension mxm and nxn respectively) are partitioned as

3

$$U = \begin{bmatrix} U_1 & \vdots & U_2 \end{bmatrix} \tag{11}$$

$$V = \begin{bmatrix} V_1 & \vdots & V_2 \end{bmatrix} \tag{12}$$

where U_1 and V_1 are respectively mxr and nxr matrices; U_2 and V_2 are respectively mx(m-r) and nx(n-r) matrices. Note that r is the rank of A.

Because $AV_2 = 0$, eq. (9) is satisfied by

$$\dot{q} = A^+ B + V_2 \dot{z} \tag{13}$$

for any vector $\dot{z}$, A^+ is the pseudoinverse of A. We shall refer to z as the reduced set of (n-r) coordinates.

Differentiation of eq. (9) with respect to time yields

$$A\ddot{q} = -\dot{A}\dot{q} + \dot{B}$$

or, $A\ddot{q} = B'$ $\qquad\qquad$ (14)

Following eq. (13) express $\ddot{q}$ in terms of $\ddot{z}$ as

$$\ddot{q} = A^+ B' + V_2 \ddot{z} \tag{15}$$

Note from eq. (13) or eq. (15) that V_2 maps the n kinematic variables $\dot{q}$ (or $\ddot{q}$) to n-r variables $\dot{z}$ (or $\ddot{z}$). Thus a consistent set of equations of motion in $\ddot{z}$ is given as

$$V_2^T M V_2 \ddot{z} = V_2^T F + V_2^T F^C - V_2^T M A^+ B' \tag{16}$$

The coefficient of $\ddot{z}$ is a symmetric positive definite matrix with the characteristic of an "inertia matrix" for the reduced set of coordinates z.

With the Lagrange multiplier method, F^C is established via (see Ref. 4)

$$F^C = A^T \alpha \tag{17}$$

where α is the column vector of Lagrange multipliers.

Premultiply eq. (17) by V_2^T to obtain the following

$$V_2^T F^C = V_2^T A^T \alpha \tag{18}$$

$$= (AV_2)^T \alpha$$

$$= 0$$

Thus it is seen that the nonworking constraint forces make no contribution to the equations of motion (eq. (16)) and need not be recorded.

Employing the transformations given by eqs. (13) and (15), the minimum dimension foverning differential equations of motion are given by

$$V_2^T M V_2 \ddot{z} = V_2^T F - V_2^T MA^+ B'$$ (19)

and

$$\dot{q} = A^+ B + V_2 \dot{z}$$ (20)

This method eliminates the forces of constraints which when included serve not only to enlarge the dimension of the dynamical system but also quite often introduce computational problems.

ACKNOWLEDGMENT

REFERENCES

1. Singh, R. P. and Likins, P. W., "Manipulator Interactive Design with Interconnected Flexible Elements", Proceedings of the 1983 Automatic Control Conference, San Francisco, CA., June 1983, pp. 505-512.

2. Singh, R. P., VanderVoort, R. J. and Likins, P. W., "Dynamics of Flexible Bodies in Tree Topology - A Computer Oriented Approach", Proceedings of the 25th SDM and AIAA Dynamics Specialist Conference, Palm Springs, CA., May 1984, Part 2, pp. 327-337.

3. VanderVoort, R. J. and Singh, R. P., "A Pointing Control System Simulation and Generic Model Generator for Multi-Body Flexible Structures" Proceedings of the Ninth DARPA Strategic and Space Symposium, Monterey, CA., October 1983.

4. Bodley, C., Devers, A., Park A. and Frisch, H., "A Digital Computer Program for Dynamic Interaction Simulation of Controls and Structures (DISCOS)", NASA Technical Paper 1219, May 1978.

5. Kane, T. R,. and Wang, C. F., "On the Derivation of Equations of Motion", J. SIAM, Vol. 13, 1965, pp. 487 - 492.

6. Wehage, R. A. and Haug, E. J., "Generalized Coordinate Partitioning for Dimension Reduction in Analysis of Constrained Dynamic Systems", ASME Journal of Mechanical Design, Vol. 104, January 1982, pp. 247-255.

VIBRATION/LIBRATION INTERACTION DYNAMICS DURING THE ORBITER BASED DEPLOYMENT OF FLEXIBLE MEMBERS

V. J. Modi* and A. M. Ibrahim**
The University of British Columbia
Vancouver, B C , Canada V6T 1W5

ABSTRACT

Essential features of a general formulation for studying librational dynamics of a large class of spacecraft during deployment of flexible members are reviewed. The formulation is applicable to a variety of missions ranging from deployment of antennas, booms and solar panels to manufacturing of trusses for space platforms using the Space Shuttle. The governing nonlinear, non-autonomous and coupled equations of motion are extremely difficult to solve even with the help of a computer, not to mention the cost involved. To get some appreciation as to the complex interactions between flexibility, deployment and attitude dynamics as well as to help pursue stability and control analysis, the equations are linearized about their nominal deflected equilibrium configuration. The procedure is applied to the Space Shuttle based deployment of boom and plate-like members. Results suggest substantial influence of the inertia parameter, flexural rigidity of the appendages, orbit eccentricity, deployment velocity, initial conditions, etc. on the system response. The results should prove useful in planning of the Orbiter based experiments aimed at assessing effectiveness of procedures for studying dynamics and control of flexible orbiting members.

C	instantaneous centre of mass of satellite
C_o	centre of mass of satellite before deployment
e	orbit eccentricity
S	centre of mass of the Earth
F_q	generalized force associated with the generalized coordinate q
h	angular momentum per unit mass of satellite
{H}	angular momentum due to deploying and vibrating appendages
H_{mn}	generalized coordinate associated with ϕ_m, ψ_n modes of free-free and fixed-free beams, respectively, to represent plate type appendage oscillations

---

* Professor
**Graduate Research Fellow

$[I]$	satellite inertia diadic
$L^P(t)$, $L^b(t)$	instantaneous length of a deploying plate and beam, respectively
L^P, L^b	fully deployed length
$\{\ell\} \equiv \begin{Bmatrix} \ell \\ m \\ n \end{Bmatrix}$	direction cosines of the unit vector along $\bar{R}_C$ with respect to x,y,z axes, respectively
M_t	total mass of satellite
N_b, N_p	number of beam and plate type appendages, respectively
P_ℓ, Q_ℓ	generalized coordinates associated with ℓth mode of a fixed-free beam vibration
$\bar{R}_C$	position vestor from the Earth centre to the instantaneous centre of mass C.
t	time
T	kinetic energy
U	gravitational potential energy
V	strain energy
x,y,z	body coordinates with origin at C (Figure 3)
X,Y,Z	inertial coordinate system with origin at C_o; Y_o along local vertical Z_o along local horizontal and X_o aligned with orbit normal
α,β,γ	pitch, yaw and roll librational angles (Figure 4)
θ	true anomaly, $\dot{\theta} = \Omega$
μ_e	universal gravitational constant
$\{\omega\}$	satellite angular velocity vector

Subscripts, Superscripts and Miscellaneous Symbols:

$(\cdot)$, $d(\ )/dt$	time rate of change in inertial and reference coordinate systems for vectorial quantity, respectively
$[\ ]$	matrix
$\{\ \}$	vector

II. INTRODUCTION

In the early stages of space exploration when spacecraft tended to be small, mechanically simple, and essentially inflexible, the elastic deformations were relatively insignificant. Numerous investigations involving active and passive stabilization procedures and accounting for internal as well as external forces have been carried out assuming satellites to be rigid [1]. However, in a modern space vehicle carrying light-weight deployable members, which are inherently flexible, this is no longer true. Furthermore, preliminary configurations of the next generation of satellites suggest a trend towards spacecraft with large flexible members. In fact, space engineers are involved in assessing feasibility

of construction of gigantic space stations which cannot be launched in their entirety from the earth, but have to be constructed in space through integration of modular sub-assembies. Assembly of such Space Operations Centres [SOC,2-5] suggests an increasing role of structural flexibility in their dynamical and control considerations.

This being the case, flexibility effects on satellite attitude motion and its control has become a topic of considerable investigation. Over the years, a large body of literature pertaining to the various aspects of satellite system response, stability and control has evolved which has been reviewed quite effectively by Likins, Modi, Williams, Robertson, Lips, Markland and others [6-12].

It should be emphasized that prediction of satellite attitude motion is by no means a simple proposition, even if the system is rigid. Flexible character of the appendages makes the problem enormously complex. It is, therefore, understandable why transient behaviour associated with the critical phase of attitude acquisition and/or deployment related maneuvers has received relatively little attention. On the other hand, although the deployment effects are of a transient nature, they may be felt over a long period of time as a result of relatively small extension rates that are normally associated with large appendages. For example, the Space Shuttle based tethered system extending to 100 km, in which the NASA has shown considerable interest, may take 6-8 hours to deploy and much longer to retrieve.

The complex character of the problem has led to analysis which often involves simplifying assumptions. Lang and Honeycutt [13], as well as Cloutier [14], studied the problem of deployment dynamics representing an appendage by point masses. On the other hand, there are several efforts reported in the literature where authors have treated flexible members as rigid bodies [15-17]. Cherchas and his associates [18,19] as well as Dow et al [20] did analyze systems having flexible membrane or beam type appendages but with a specific configuration. Furthermore, the appendages were considered to be uniform with a fixed deployment velocity. More recently Jankovic [21] investigated dynamics of the CTS solar panels during deployment and correlated measured tip acceleration with the analytical prediction. The librational dynamics of a body deploying two plate type flexible members normal to the orbital plane was studied by Ibrahim and Misra [22]. Effects of deployment velocities and plate properties on the librational response were investigated. A rather general formulation for the class of satellites with flexible deploying beam type appendages has been presented by Lips and Modi [23]. Interaction between the libration dynamics, flexibility and deployment was studied and it was noted that instability may result under certain combinations of system parameters. Recently, Modi and Ibrahim [24] presented a general model for studying librational dynamics of a large class of spacecraft during deployment of arbitrarily oriented beam and/or plate type appendages. The formulation is ideally suited to help assess the effect of complex interactions between flexibility, deployment, attitude dynamics and stability of present as well as the next generation of spacecraft.

Using the linearized form of the general formulation, this paper studies dynamics of the Orbiter based deployment of flexible members during two planned experiments:
(i) Orbiter Mounted Large Platform Assembler Experiment
    Objective here is to establish capability for manufacturing beams, trusses, etc. in space for construction of the SOC. The assembler is fully

9

collapsible and automatically deployed (Figure 1).

(ii) NASA/Lockheed Solar Array Flight Experiment
This experiment involves deployment and retrieval of a solar panel, 101 ft. in length, from the orbiter to generate about 13 kW of additional power. The objective here is to demonstrate in orbit extension/retraction of the lightweight solar array wing developed by Lockheed Missile and Space Company for NASA's Marshall Space Flight Center (Figure 2).

Response of the two systems is obtained over a range of system parameters and external disturbances. Both transient as well as post deployment phases are considered. Results suggest that under critical combination of flexibility, inertia, deployment and orbital parameters, the system can become unstable. The presence of free molecular environmental forces may further accentuate this tendency.

III. OUTLINE OF THE FORMULATION PROCEDURE

Figure 3 shows schematically a satellite with an arbitrarily oriented flexible beam and plate type deployable appendages. The satellite is free to negotiate any specified trajectory around the centre of force. Let the position vector $\bar{R}_c$ and true anomaly θ define the location of the instantaneous centre of mass C of the spacecraft with respect to the inertial coordinate system X, Y, Z having its origin at the centre of the Earth. C_0 represents location of C without any vibrations or asymmetric deployment. An orthogonal orbiting reference frame X_0, Y_0, Z_0 with its origin at C_0 is so oriented that Y_0 and Z_0 are along local vertical and horizontal, respectively, while X_0 is aligned with the orbit normal. The body coordinates x, y, z with origin at C coincide with the orbital coordinates X_0, Y_0, Z_0 in absence of any librations and vibrations.

The orientations of the body axes x, y, z at any instant t relative to the orbital coordinate frame X_0, Y_0, Z_0 can be described by a set of modified Eulerian rotations as follows: γ (roll) about Z_0 giving x', y', z'; β (yaw) about y' resulting in x", y", z" and finally α (pitch) about x" yielding x, y, z (Figure 4).

General formulation of the nonlinear, nonautonomous and coupled equations of motion for this system has been treated in detail earlier in reference 24. Here the attention is focussed on linearization of the equations and modular programming procedure which help isolate the effects of deployment, flexibility, inertia orbital parameters, appendage orientation, deployment rate, etc.

Flexible character of the appendages renders the system hybrid, i.e. the system is described in terms of discrete and distributed coordinates. The resulting governing equations of motion, in general, do not admit to any closed form solution. They are normally transformed into a set of ordinary differential equations using finite element, lumped parameter or assumed mode methods with generalized coordinates depending on time alone. Here, an assumed mode discretization procedure is favoured as the elastic appendage displacements can be represented adequately using a relatively few equations. Displacements of the flexible members are described by linear combinations of space-dependent admissible functions and time-dependent generalized coordinates.

The basic system is so complex that to check the validity of the governing equations and associated program for their integration presents a challenging task. Hence, the formulation can also serve as a comparative validating scheme

in association with other analytical/numerical models when they become available. The dynamical equations would also serve as a basis for assessing the effects of environmental forces and development of control strategies. The kinetic energy of the spacecraft with deploying flexible appendages was shown to be [24]

$$T = T_{orb} + T_{vib} + \{\omega\}^T\{H\} + \frac{1}{2}\{\omega\}^T[I]\{\omega\} \quad , \tag{1}$$

where

T_{orb} = K.E. due to orbital motion

T_{vib} = K.E. component due to pure vibration

$\frac{1}{2}\{\omega\}^T[I]\{\omega\}$ = K.E. due to pure rotation

$\{\omega\}^T\{H\}$ = K.E. due to coupling between vibrational and rotational modes

$\{\omega\}$ = angular velocity vector

$\{H\}$ = angular momentum due to deploying and vibrating appendages

$[I]$ = time dependent inertia matrix.

The gravitational potential energy of the satellite was written as

$$U = -(M_t\mu_e/R_c) - (\mu_e/2R_c^3)tr[I] + (3\mu_e/2R_c^3)\{\ell\}^T[I_n]\{\ell\} \quad . \tag{2}$$

Here the first term represents potential energy due to the satellite treated as a point mass while the rest of the expression is the contribution due to its rotation.

The strain energy stored in the appendages during their vibration had the form

$$V = \{q\}^T[V]\{q\} \quad , \tag{3}$$

where $\{q\}$ represents generalized coordinates associated with the vibration degrees of freedom,

$$\{q\} = \begin{Bmatrix} H_{mni} \\ ---- \\ P_{\ell j} \\ ---- \\ Q_{\ell j} \end{Bmatrix} \quad ,$$

and $[V]$ is a symmetric matrix of vibration modes used to represent flexural deformations of the appendages.

Using the Lagrangian procedure the equations of motion can now be obtained

11

from,

$$\frac{d}{dt}\left(\frac{\partial T}{\partial \dot{q}}\right) - \frac{\partial T}{\partial q} + \frac{\partial(U+V)}{\partial q} = F_q \quad , \tag{4}$$

where:

$$q = R_c, \; \theta, \; \alpha, \; \beta, \; \gamma, \; H_{mni}, \; P_{\ell j}, \; Q_{\ell j};$$

$$m = 1, 2, \cdots, p \; ; \qquad n = 1, 2, \cdots, r \; ;$$

$$i = 1, 2, \cdots, N_p \; ; \qquad \ell = 1, 2, \cdots, s \; ;$$

$$j = 1, 2, \cdots, N_b \; ;$$

hence the satellite dynamics is simulated by a system of q ordinary differential equations of the 2nd order where

$$q = 5 + (p \times r \times N_p) + 2(s \times N_b) \quad .$$

The librational motion of the system and the vibrations of the appendages normally have very little effect on the orbital motion unless the system dimensions become comparable to the position vector R_c. Hence, for most studies, the orbit can be computed using the classical Keplerian relations

$$R_c = h^2 / \mu_e(1 + e \cos \theta) \quad ,$$

$$R_c^2 \theta = h \quad ,$$

where h is the angular momentum per unit mass of the satellite and e the eccentricity of the orbit. The equations of motions in the librational degrees of freedom are

$$\frac{d}{dt}\left(\left\{\frac{\partial \omega}{\partial \dot{q}}\right\}^T \{H\}\right) - \left\{\frac{\partial \omega}{\partial q}\right\}^T \{H\} + \frac{d}{dt}\left(\left\{\frac{\partial H}{\partial \dot{q}}\right\}^T [I] \{\omega\}\right)$$

$$- \left\{\frac{\partial \omega}{\partial q}\right\}^T [I] \{\omega\} + \frac{\partial U}{\partial q} = Q_q \quad , \qquad q = \alpha, \; \beta, \; \gamma \; . \tag{5a}$$

The equations of motions in the vibrational degrees of freedom can now be written as

$$\frac{d}{dt}\left(\frac{\partial T_{vib}}{\partial \dot{q}}\right) - \frac{\partial T_{vib}}{\partial q} + \frac{d}{dt}\left(\left\{\frac{\partial H}{\partial \dot{q}}\right\}^T \{\omega\}\right) - \left\{\frac{\partial H}{\partial q}\right\}^T \{\omega\}$$

$$- \frac{1}{2}\{\omega\}^T \frac{\partial}{\partial q}[I]\{\omega\} + \frac{\partial(U + V)}{\partial q} = Q_q \quad , \qquad q = H_{mni}, \; P_{\ell j}, \; Q_{\ell j} \; . \tag{5b}$$

12

The number of equations representing vibrational motion would depend on the number of modes used,

$$N = \text{number of vibrational equations}$$
$$= (p \times r \times N_p) + 2(s \times N_b) .$$

The governing nonlinear equations were linearized about a nominal equilibrium position to give

$$M\ddot{q} + (\dot{M} + 2G) \dot{q} + (\dot{G} + \dot{C} + K) q + \dot{E} + F = 0 , \qquad (6)$$

where q is a generalized coordinate vector, in general of N dimensions, with elements α, β, γ, H_{mni}, $P_{\ell j}$ and $Q_{\ell j}$. In Equation (6), M, C and K are (NxN) symmetric matrices, while G is skew symmetric of order N. In general, vectors E and F are of N dimensions. It should be emphasized that the nonlinear Equation (5) and its linearized version as given in Equation (6) are rather general. They are valid for any spacecraft with central rigid body carrying arbitrary number and orientation of flexible appendages. Although the derivation used beam and plate type of appendages, the form of the equations remained the same for membrane and tether type of flexible members. Character of the members only affect elements of the coefficient matrices but not their symmetry properties or the general form of the governing equation. The equations are valid for deployment as well as retrieval of appendages.

IV. COMPUTATIONAL CONSIDERATIONS

Refined computational procedure is the key requirement in the numerical solution of such a formidable problem. Hence, a brief statement on the computational considerations would be appropriate. The equations were integrated using an AMDAHL 470-V8 digital computer. Depending upon the stiffness character of the system, two different integration routines were used from computational efficiency considerations. For stiff systems (i.e. those involving widely differing time scales as would be the case for spacecraft with flexible deploying appendages), the routine DGEAR-I.S.M.L. was used which is based on Gear's backward differentiation formulae [25,26]. For rigid spacecraft, the well-known Adam's method with functional iteration was employed. The programs proved to be extremely efficient. In a typical case of a spacecraft deploying one flexible plate-type appendage to 50 m, the three axes librational response of the central rigid body and flexural response of the appendages can be computed in less than 18.271 cpu seconds!

The program is so formulated that it can readily be extended to the nonlinear case. Furthermore, it is written in a modular fashion to help isolate the effects of flexibility, deployment, character and orientation of the appendages, inertia and orbital parameters, number and type of admissible functions, etc. Environmental effects due to solar radiation pressure, aerodynamic forces, Earth's magnetic field interaction, etc. can be incorporated easily through generalized forces. The same is true with internal energy dissipation although in the present analysis the system is considered, purposely, conservative. The total energy of the system is monitored routinely and serves as a check. Furthermore, contributions of its constituents (i.e. T, U, V) to individual degrees of freedom are also computed continuously to provide physical insight into the character of the resulting dynamics and associated energy transfer. Finally, the program can be used to check positive and negative definite character of the Liapounov function, constructed using the stored matrices, thus providing information concerning necessary condition for stability.

V. RESULTS AND DISCUSSION

One can generate an enormous amount of information through a systematic variation of geometric, inertia, orbital, flexibility and deployment parameters together with a variety of initial conditions representing external disturbances. For conciseness only a few of the typical results useful in establishing trends are recorded here.

Calculations were carried out for a plate type appendage deployed from the Orbiter in a circular trajectory. Effects of aerodynamic and solar radiation pressure forces are purposely omitted here to obtain some base information. It is intended to study the environmental effects once there is some appreciation as to the fundamental dynamics. The equations were nondimensionalized using the central rigid body mass (M), radius of gyration corresponding to the maximum moment of inertia (I_{yy} in case of the Orbiter), and angular velocity Ω. Hence, it is not necessary to specify system parameters individually. This is indeed advantageous as the obtained system response remains valid over a range of combinations of variables as long as the dimensionless parameters maintain constant values.

For calculations geometry, inertia, flexibility and deployment rate parameters were taken to be as follows:

Orbiter:

Mass $=$ 79,710 kg

I_{xx} $=$ 8,286,760 kg m^2; $I_{yy} = 8,646,050$ kg m^2; $I_{zz} = 1,091,430$ kg m^2

I_{xy} $=$ 27,116 kg m^2; $I_{xz} = -8,135$ kg m^2; $I_{yz} = 328,108$ kg m^2

Plate

L^P $=$ 50 m, width $=$ 5 m, mass $=$ 260 kg

Flexibility Parameter $= \overline{E}^P = Et^3/12(1-\nu^2)$ Ω^2 I_{yy} $= 0.01$.

Deployment Parameter $= \overline{\dot{L}}^P = \dot{L}_p/\Omega$ $(I_{yy}/M_r)^{1/2}$ $= 0.1$.

Plate Attachment Parameter $P_r =$ (distance of the appendage support point from the Orbiter c.m.)/$(I_{yy}/M_r)^{1/2}$ $= 0$

Here: E $=$ modulus of elasticity of the plate material;
t $=$ plate thickness;
ν $=$ Poisson's ratio.

Beam

The Orbiter has been given an initial angular disturbance in pitch, yaw and roll of

$\alpha(0)$ $=$ $\beta(0)$ $=$ $\gamma(0)$ $=$ 0.001 rad .

Note, the given responses are in absence of any control and damping.

Figure 5 shows librational response of the Orbiter in three different

orientations. As can be expected the Orbiter is stable in the Lagrangian configuration corresponding to the maximum moment of inertia axis aligned with the orbit normal and the minimum moment of inertia axis along the local vertical.

Figure 6 studies the effects of flexibility and deployment for the stable case studied in Figure 5c. The 50 m plate type appendage is considered to be either rigid or flexible and deploying or completely deployed along the local vertical. The Orbiter inertia being extremely large compared to that of the appendage, its librational response in all the cases was found to be essentially the same. However, vibratory response of the flexible appendage shows considerable variation. As expected the deploying appendage experiences high frequency amplitude modulations initially with a progressive increase in period with time. Instability of the generalized coordinate H_{11} associated with the first rigid body free-free and the first fixed-free beam modes is apparent although the response corresponding to the higher modes (H_{22}) is stable.

From the consideration of construction of a space platform using the orbiter it would be useful to assess its stability during deployment in various orientations. Figure 7 addresses this aspect of the problem. The flexible plate is deployed along the maximum moment of inertia axis during three different orientations of the Orbiter. The plate is located in the plane of symmetry of the Orbiter. As both the Orbiter as well as the plate orientations govern the response and stability, the cases considered here represent only a small sample. It is intended to assess how far the Lagrangian stable configuration concept continues to be effective in the presence of flexibility and time dependent inertias. Obviously, a systematic variation in orientations would be necessary to fully understand complex nonlinear interactions. Such studies would help in assessing the extra demand imposed on the Orbiter's control system, fuel used to achieve the control and its effect on the Orbiter's mission life. The results show that the Orbiter continues to be unstable for cases (a) and (b) both in librational and vibrational modes, however, case (c), corresponding to the Lagrangian configuration, remains stable. This would suggest desired orientation for the Orbiter during in-orbit manufacture of structural components for construction of space-platforms.

Figure 8 compares generalized coordinates associated with the first four modes for the three different attitudes of the Orbiter considered in Figure 7. Note, the vibrations continue to be relatively small for the Lagrangian configuration.

Of course, the large amplitude motion data should be treated as qualitative because the general nonlinear, nonautonomous, and coupled equations are linearized here. However, they do suggest trends. Analysis using nonlinear equations is in progress.

VI. CONCLUDING COMMENT

With a relatively general formulation in hand and the program operational, efforts are in progress to develop a comprehensive data bank for spacecraft with flexible appendages. Not only will it prove useful to design engineers involved in planning of future communications satellites but also help in assessing dynamical, stability and control considerations associated with the Orbiter based construction of space-platforms.

ACKNOWLEDGEMENT

REFERENCES

[1] Shrivastava, S.K., Tschann, C., and Modi, V.J., "Librational Dynamics of Earth Orbiting Satellites - A Brief Review," Proceedings of the XIVth Congress of Theoretical and Applied Mechanics, ISTAM Publisher, Kharagpur, India, December 1969, pp. 284-306.

[2] Covington, C., and Piland, R.O., "Space Operations Center - Next Goal for Manned Flight?", Astronautics and Aeronautics, Vol.18, No.9, September 1980 pp.30-37.

[3] Brodsky, R.F., and Morias, B.G., "Space 2020," Astronautics and Aeronautics, Vol.20, No.4, May 1982, pp.30-37.

[4] Burke, B.F., "Radio Telescopes Bigger than the Earth," Astronautics and Aeronautics, Vol.20, No.10, October 1982, pp.44-52.

[5] Joshi, S.M., "Control System Synthesis for a Large Flexible Space Antenna," 33rd Congress of the International Astronautical Federation, Paris, France, September-October 1982, Paper No.82-320.

[6] Likins, P.W., "Dynamics and Control of Flexible Space Vehicles," NASA, TR-32-1329, January 1970.

[7] Likins, P.W., and Bouvier, H.K., "Attitude Control of Nonrigid Spacecraft," Astronautics and Aeronautics, Vol.9, May 1971, pp.64-71.

[8] Modi, V.J., "Attitude Dynamics of Satellites with Flexible Appendages - A Brief Review," Journal of Spacecraft and Rockets, Vol.11, November 1974, pp.743-751.

[9] Williams, C.J.H., "Dynamics Modelling and Formulation Techniques for Non-Rigid Spacecraft," Proceedings of the ESA Symposium on Dynamics and Control of Non-Rigid Spacecraft, ESA SP 117, Frascati, Italy, May 1976, pp.53-70.

[10] Roberson, R.E., "Two Decades of Spacecraft Attitude Control," Journal of Guidance and Control, Vol.2, January-February 1979, pp.3-8.

[11] Lips, K.W., "Dynamics of a Large Class of Satellites with Deploying Flexible Appendages," Ph.D. Dissertation, University of British Columbia, Sept. 1980.

[12] Markland, C.A., "A Review of the Attitude Control of Communications Satellites," 32nd Congress of the International Astronautical Federation, Rome, Italy, 1981, Paper No. IAF-81-344.

[13] Lang, W., and Honeycutt, G.H., "Simulation of Deployment Dynamics of Spinning Spacecraft," NASA, TN-D-4074, 1967.

[14] Cloutier, G.J., "Dynamics of Deployment of Extendible Booms from Spinning Space Vehicles," Journal of Spacecraft and Rockets, Vol.5, No.5, May 1968, pp.547-552.

[15] Bowers, Jr., E.J., and Williams, C.E., "Optimization of RAE Satellite Boom Deployment Timing," Journal of Spacecraft and Rockets, Vol.7, No.9, September 1970, pp.1057-1062.

[16] Hughes, P.C., "Dynamics of a Spin-Stabilized Satellite during Extension of Rigid Booms," CASI Transactions, Vol.5, No.1, 1972, pp.11-19.

[17] Sellapan, R., and Bainum, P.M., "Dynamics of Spin-Stabilized Spacecraft during Deployment of Telescoping Appendages," Journal of Spacecraft and Rockets, Vol.13, No.10, October 1976, pp.605-610.

[18] Cherchas, D.B., "Dynamics of Spin-Stabilized Satellites during Extension of Long Flexible Booms," Journal of Spacecraft and Rockets, Vol.8, No.7, July 1971, pp.802-804.

[19] Cherchas, D.B., and Gossain, D.M., "Dynamics of a Flexible Solar Array during Deployment from a Spinning Spacecraft," CASI Transactions, Vol.7, No.1, 1974, pp.10-18.

[20] Dow, P.C., Scammell, F.H., Murray, F.T., Carlson, N.A., and Buck, I.H., "Dynamic Stability of a Gravity Gradient Stabilized Satellite Having Long Flexible Antennas," Proceedings of the AIAA/JACC Guidance and Control Conference, New York, 1966, pp.285-303.

[21] Jankovic, M.S., "Deployment Dynamics of Flexible Spacecraft," Ph.D. Dissertation, University of Toronto, Institute of Aerospace Studies, 1980.

[22] Ibrahim, A.M., and Misra, A.K., "Attitude Dynamics of a Satellite During Deployment of Large Plate-Type Structures," Journal of Guidance, Control and Dynamics, Vol.5, No.5, September-October 1982, pp.442-447.

[23] Lips, K.W., and Modi, V.J., "General Dynamics of a Large Class of Flexible Satellite Systems," Acta Astronautica, Vol.7, No.2, 1980, pp.1349-1360.

[24] Modi, V.J., and Ibrahim, A.M., "Transient Dynamics during the Space Shuttle Based Manufacture of Structural Components," AIAA 21st Aerospace Sciences Meeting, Reno, Nevada, U.S.A., January 10-13, 1983, Paper No.83-0432; also as "A General Formulation for Librational Dynamics of Spacecraft with Deploying Appendages," Journal of Guidance, Control and Dynamics, AIAA, in press.

[25] Gear, C.W., Numerical Initial Value Problems in Ordinary Differential Equations, Prentice-Hall, Englewood Cliffs, New Jersey, 1971.

[26] Hindmarsh, A.C., "Gear: Ordinary Differential Equation System Solver," Lawrence Livermore Laboratory, Report UCID-30001, Revision 3, December 1974.
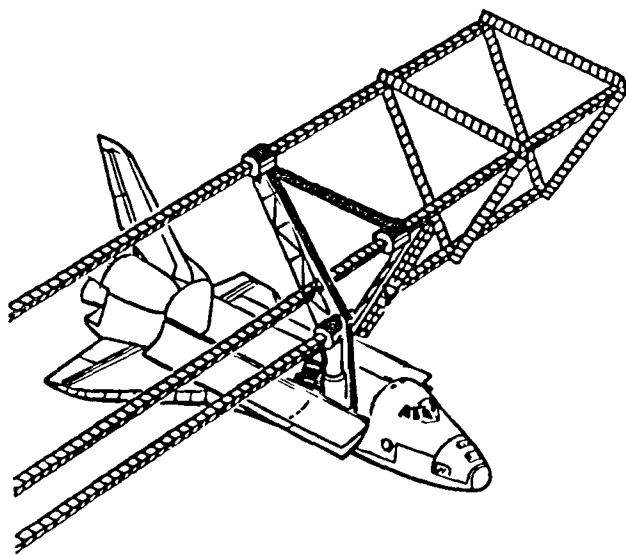
Figure 1   Artists view of the Space
Shuttle based manufacture
of structural components.
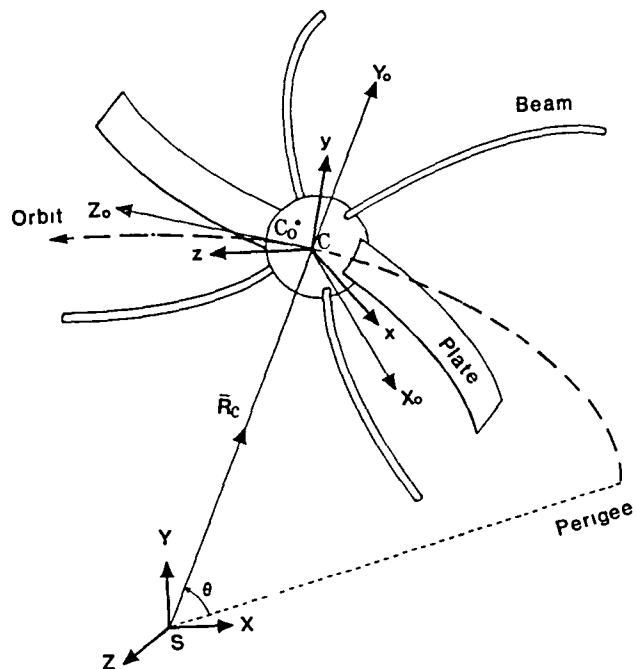
Figure 3   Geometry of orbiting space-
craft with flexible deploying
beam and plate type appendages.
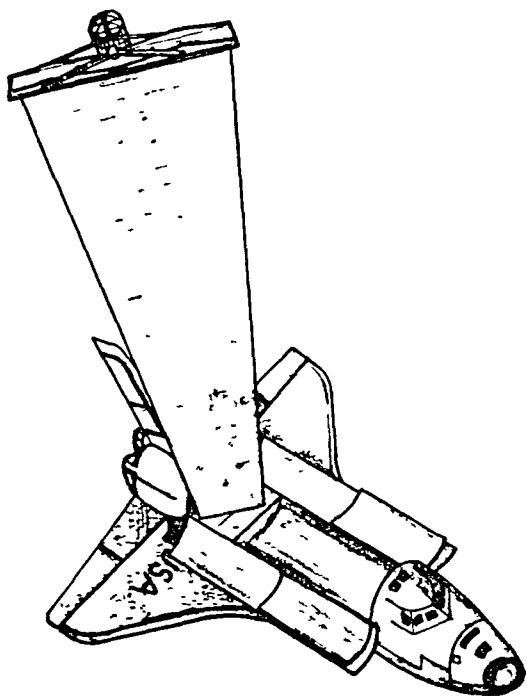
Figure 2   Schematic diagram of the
Orbiter based deployment
of a solar array during
the proposed NASA/Lockheed
experiment.
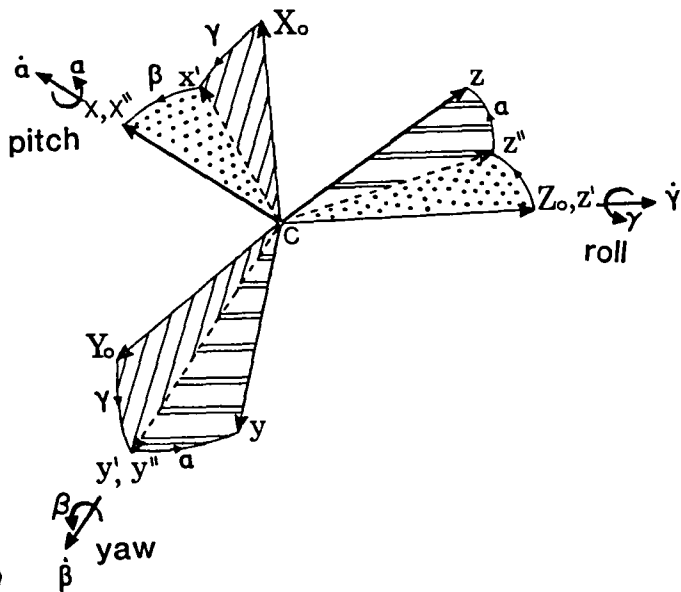
Figure 4   Eulerian rotations showing
roll (γ), yaw (β) and
pitch (α) librations.

18
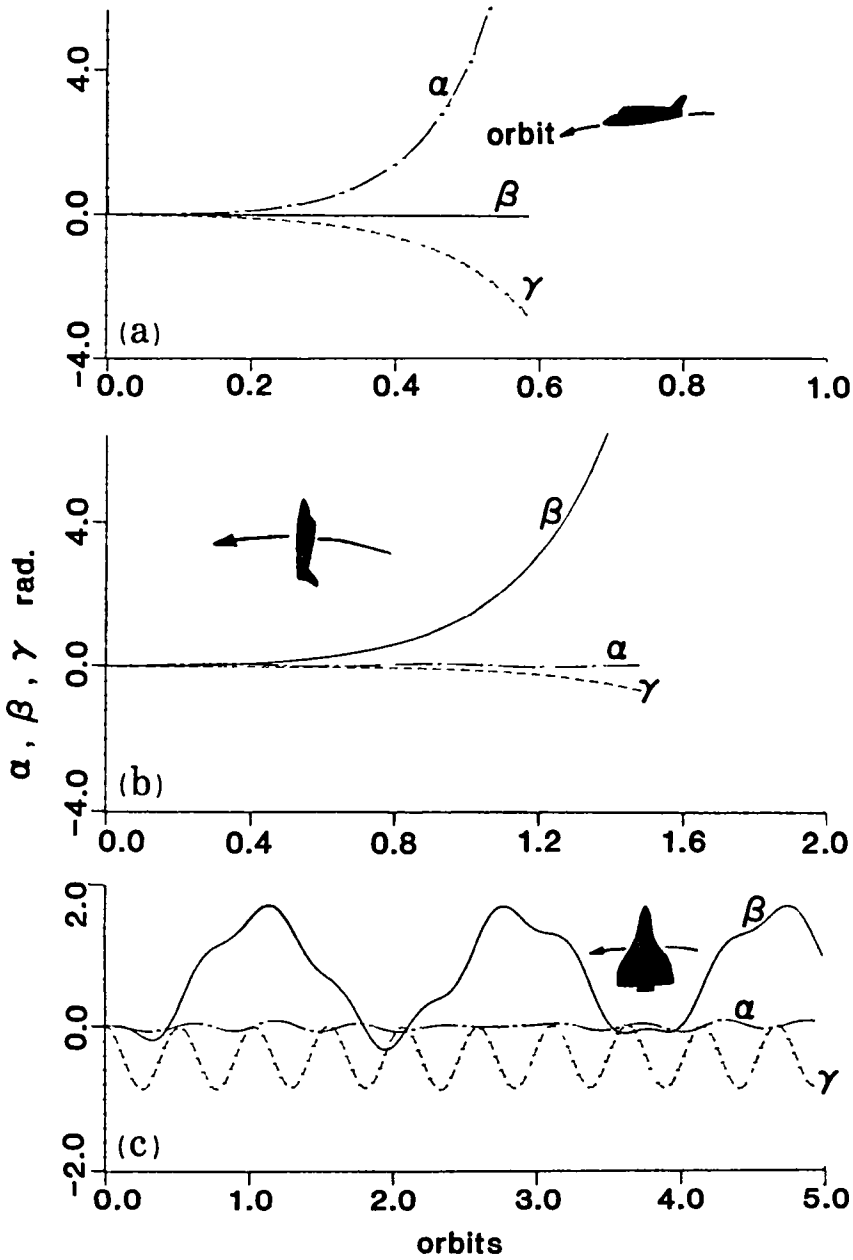
Figure 5 Dynamical response of the Orbiter to a displacement type
disturbance in three different orientations. Note the
Lagrangian configuration (case c) is stable.
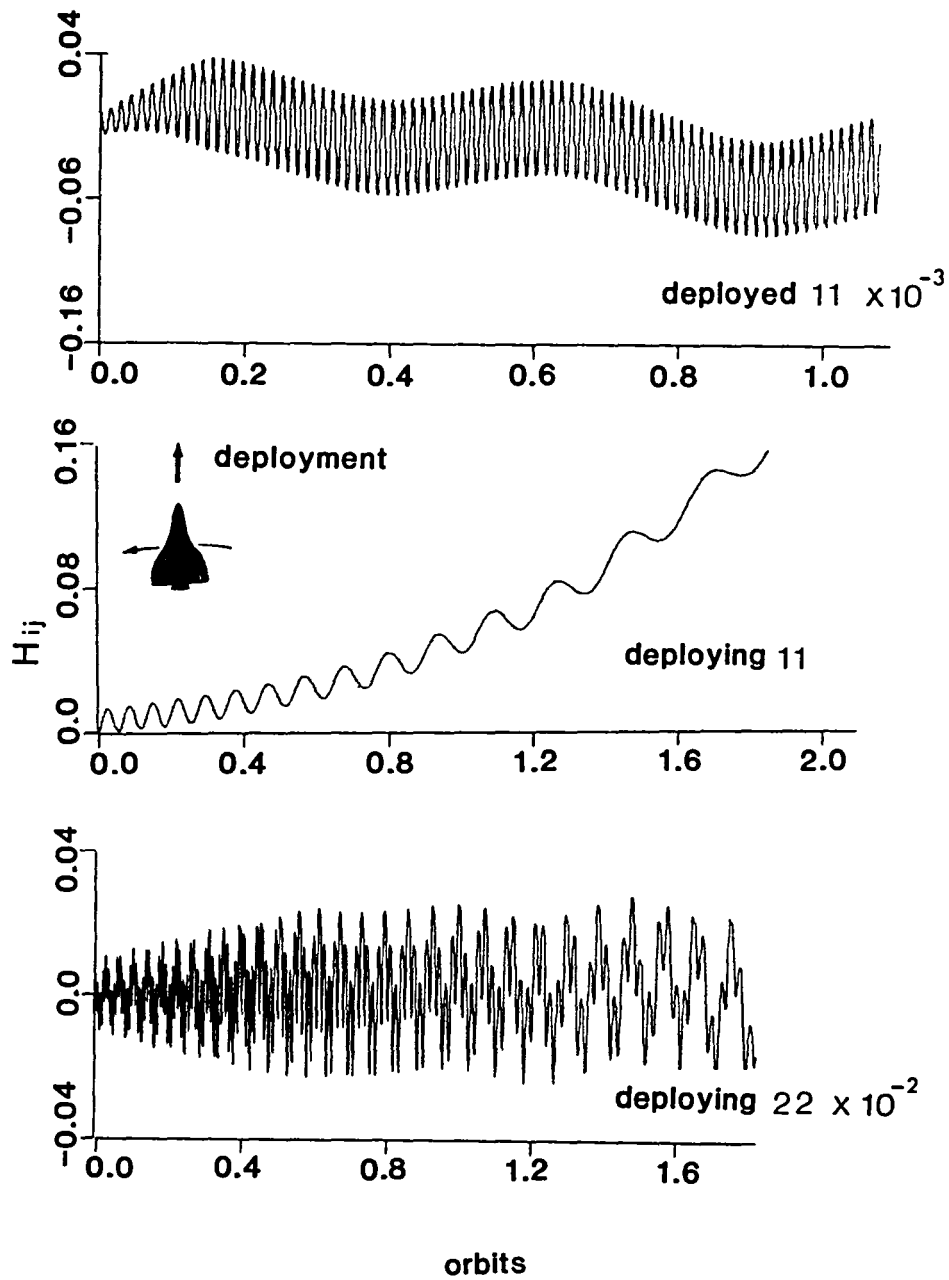
Figure 6 Vibrational characteristics of a flexible plate-type
appendage during and post-deployment phases.
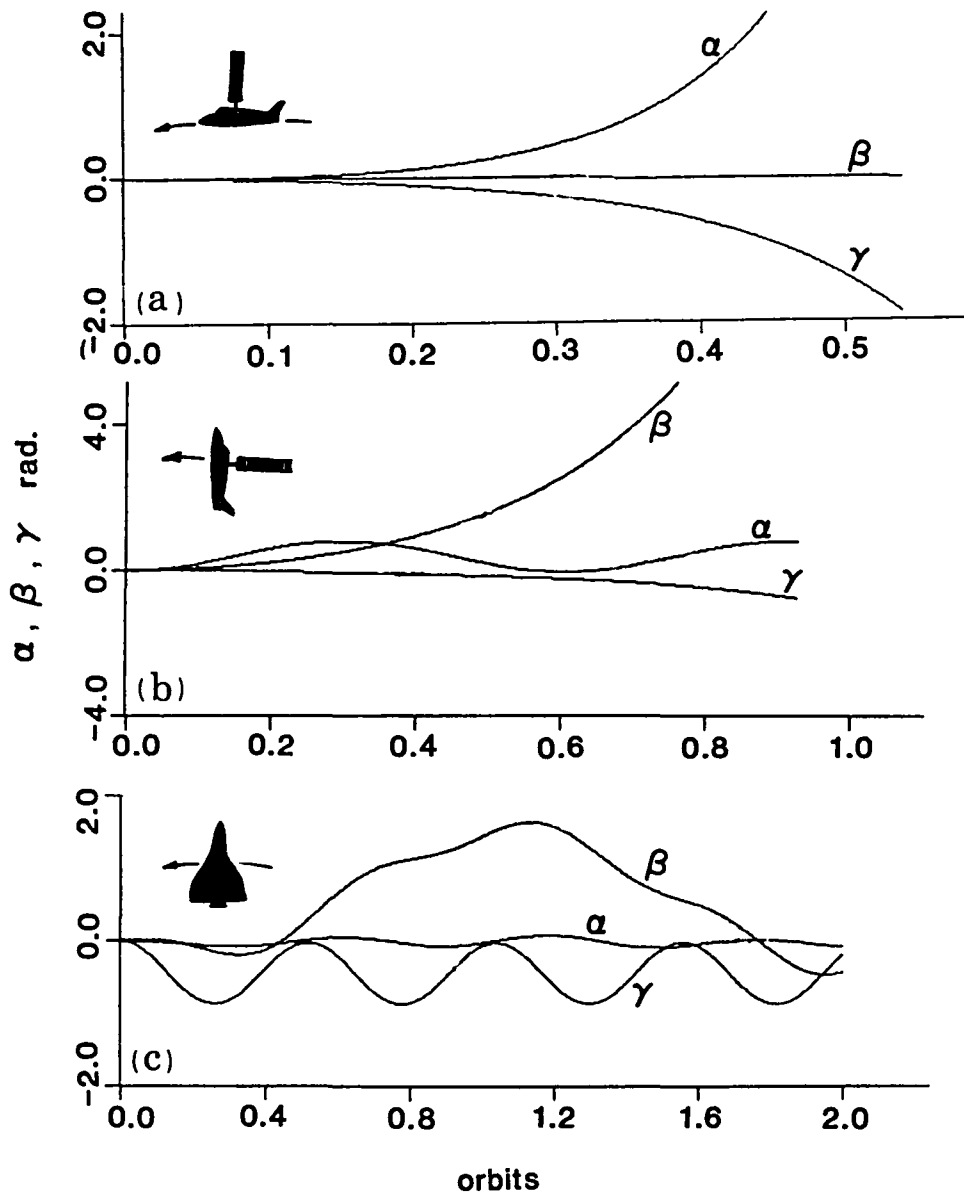
Figure 7   Effect of the Orbiter's initial orientation on the
transient librational response during deployment of
a flexible plate-type appendage along the maximum
moment of inertia axis y.
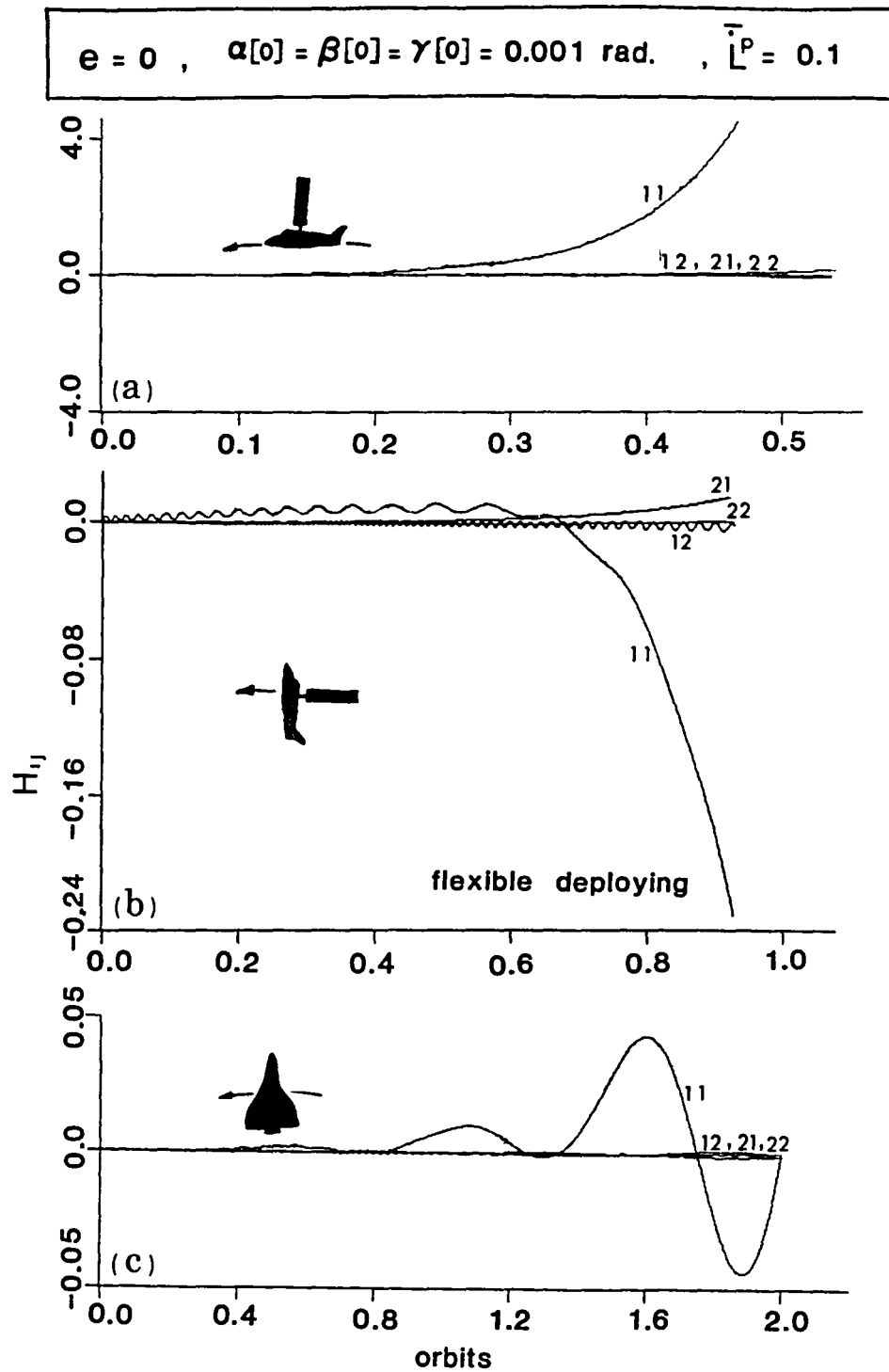
Figure 8 Typical vibrational response of the flexible appendage during the maneuver described in Figure 7.

DESIGN OF MULTIVARIABLE CONTROLLERS USING THE INTEGRATED ANALYSIS CAPABILITY (IAC)

J. A. Bossi*
University of Washington
Seattle, WA 98195

G. A. Price and **S. A. Winkleblack**
Boeing Aerospace Company
Seattle, WA 98124

ABSTRACT

Dynamic analysis and controls design for flexible spacecraft involves high-order dynamic systems with multiple inputs and outputs. Computer tools are essential for such analysis. This paper describes the controls/-structures interaction analysis capability of an inter-disciplinary computer software system, called the Integrated Analysis Capability (IAC), which is being developed by Boeing Aerospace Company for NASA/Goddard SFC. An overview of IAC components and procedures is presented, and an example of a preliminary space station controls design is shown.

I. INTRODUCTION

Since 1979, the Boeing Aerospace Company has been under contract to NASA/Goddard Space Flight Center to develop the Integrated Analysis Capability (IAC), a computer software system for conducting interdisciplinary design analysis and performance evaluation of large space systems. The IAC combines major computer programs used in diverse disciplines (e.g., structural, thermal, and controls analysis) into a single package with a common executive routine and database.

The IAC was developed in three phases. Phase I was a proof of concept code developed during a ten month study which established the IAC development plan. Phase II saw the first operational IAC (level $\emptyset$) delivered to Goddard in 1981. Since that time, the IAC has been used by many individual analysts and on some inter-disciplinary projects within NASA and Boeing. The resulting user group has identified a number of desirable improvements and helped to establish priorities for continued system development. Phase III resulted in the completed version of the IAC (level 1) which will be delivered to Goddard July 15 of this year. The IAC should be available for public use late this summer through the COSMIC Software Distribution Center.

Phase III also produced several pre-programmed modules which permit a complete multivariable linear controller design, from definition of the spacecraft structure (in a NASTRAN [2] format) to final compensator

---

*Consultant, Boeing Aerospace Co.

configuration and simulation. The controller design tools incorporate linear-quadratic synthesis (LQS) theory by use of the ORACLS [3] subroutine package. This paper presents an overview of the IAC components and the procedures for controller design. An example of high-order, multi-input/-multi-output design is presented through an attitude control design for a space station model. A discussion of the tools and procedures used for non-linear multiflexible body control design and simulation is also included.

II. ARCHITECTURE

IAC development has emphasized compatibility with a modern super-minicomputer, and the system is currently resident on the DEC/VAX host machine using the VMS operating system. The system architecture (described in detail in [1]) provides two products:

1) A specific inter-disciplinary analysis capability having a set of interfaced technical modules that deal with coupling of thermal, structures and controls disciplines.

2) A general framework product which serves as an "integrated base" whereby user groups can add desired modules and disciplines.

The IAC architecture is summarized by Figure 1. The three methods of data storage and access are: the IAC user workspace, the host file system, and IAC databases. The user may access this data concurrently with other users directly through the executive, shown at the top of the figure, using one of the many executive Query functions which allow the user to load, view, or manipulate the data in the database. The user also may use the executive to issue Host commands which allows access to data on the host computer. The executive provides the capability to run all the IAC modules. The right side of Figure 1 shows the interaction with the database through support modules, such as the interface modules, graphics packages or user-defined modules. On the left side of Figure 1, the final method of database interaction is shown, namely the technical modules and a list of these modules is shown in Figure 2.

Figure 1 illustrates the framework which allows for data flow between disciplines. More specifically, this flow is defined as a "solution path", a term which refers to a defined sequence of IAC- provided operations. Figure 3 illustrates five standard solution paths which have been defined within the thermal/structures/controls specific capabilities. The stand-alone operation of each technological module is defined as Solution Path I. Paths II and V involve an increasing degree of inter-disciplinary coupling and correspondingly greater complexity.

Solution Path III is the path discussed in this paper. Briefly, Path III accomplishes a Controls/Structures Interaction (CSI) analysis, in either the frequency or time domain, as described in the following sections.

It should be noted that Solution Path V is to be completed at some

24

future time and will provide a fully coupled analysis in the frequency domain, directed at problems such as thermal flutter of long spacecraft members.

Each user-defined solution path is executed by a series of IAC commands. These may include direct interactive commands or references to external host files containing commands. The user may stop along a path to inspect data and review options. This engineer-in-the-loop mode of operation allows flexibility in the development and the use of IAC solution paths.

III. CONTROLS DESIGN FOR FLEXIBLE SPACECRAFT USING IAC

CSI analysis begins with a presumption of small deflections and linear dynamic models with modal damping. For systems of interest, the problem is inherently multivariable, with strong coupling of inputs and outputs to many modes. In its initial form, modules in the IAC have been provided to construct such linear multi-input/multioutput (MIMO) models. Also, driver programs have been developed to permit design of linear proportional controllers, using linear-quadratic synthesis (LQS) techniques, for attitude control and active vibration damping. More recently, modules have been added to provide for linear (and non-linear) simulation capability with closed-loop control.

In this section, the steps involved in linear MIMO controller design will be described and illustrated by use of an example. The example is a Boeing version of an initial operational capability space station.

Finite-Element Structural Model

A NASTRAN [2] case control and bulk data deck to describe the structure of interest must be prepared as a host file (see Figure 1). This host file establishes the order of the desired model for the dynamic system. The IAC is then entered and commands are issued to execute a NASTRAN run in a batch mode. The output from this run is stored in another host file; an interface program (INDA) is then run to format and store the dynamic model data in the database.

As an example of this process, Figure 4 presents a portion of the nodal configuration of a raft-type space station, shown in Figure 5, with solar panels mounted on a boom and gimballed at their centers. Table 1 presents the modal frequencies for a 24-mode model of the structure as generated by NASTRAN. INDA provides this data plus mass properties, node goemetry and the mode shapes to the database.

State Space Model

To construct the actuator and sensor modal distribution matrices, the designer must construct arrays in the database which define the nodal location, orientation, and units for the system inputs (e.g., actuators)

and outputs (e.g., sensors). This can be done manually through the executive Query function. Then an interface program (ABC) is run to form the matrices of a state space model. ABC is a driver program written using ORACLS matrix routines and IAC-provided input/output utilities. The input data for ABC, which must be placed in a host file, can include a value for modal damping of the flexible modes.

Table 2 presents the actuator and sensor data for the example; also included are outputs to be controlled and input disturbances (assumed to occur at the core). The resulting linear model has the standard form

$$\dot{x} = Ax + Bu + Gw, \quad z = Cx + v, \quad y = Hx \quad (1)$$

where x is the state vector, u is the control, w is the disturbance, z is the measurement, v is the measurement noise and y is the controlled output. The A-matrix for this model is generated by ABC in block diagonal form with each 2x2 modal block in companion form, i.e., for the ith-mode

$$A_{11} = \begin{bmatrix} \emptyset & 1 \\ -\omega^2 & -2\zeta\omega \end{bmatrix}$$

where ω is the modal frequency and ζ is its damping ratio. Thus B, G, C, H are modal distribution matrices.

Linear Model Modifications

The model generated by ABC is stored as data structures (i.e., arrays) in the database, and is thus accessible to the designer through the executive Query function. For example, cascade elements such as actuator or sensor dynamic models can be added by extending the arrays; or model order reduction can be accomplished by simple truncation of the arrays or by removing specific rows or columns. These modifications can be accomplished either interactively or by constructing a user-module FORTRAN program which is executed by IAC command.

At Boeing, we have built user-module programs to investigate model order reduction by a technique known as impulse energy analysis [4]. This is a form of modal cost analysis [5] in which unit impulses are applied simultaneously to all inputs and the energy flow to the outputs through each flexible mode is assessed. The modes with largest values are retained in the model. Table 1 includes such an assessment for the example; of the 18 flexible modes, the 6 with largest values were used in the reduced-order model, along with the 6 rigid body modes. The reduced-order C- and H-matrices for this model have been generated by a technique called partial realization [6] which attempts to match the time response of the full-order model in a particular frequency range (here, at low frequency).

LQS Tools

Once a linear model in the form of equation (1), or a reduced order version, has been stored in the database, a state space controller can be designed. One of the controls modules provided with the IAC is a driver program (REGEST) which utilizes the ORACLS subroutine package [3] to apply LQS techniques to the design of a constant-gain state feedback regulator and state estimator. The designer must load into the database, utilizing IAC Query, a set of quadratic weighting matrices for the design, and then construct a host file which tells REGEST the location of the model arrays and design parameters. Various options in the calculations are selected by interactive input during program execution.

The resulting gain matrices are combined with the model to form a dynamic compensator, of the same order as the model, for feedback control. This compensator can be represented by

$$\dot{\hat{x}}' = A'\hat{x}' + B'u + K_e(z - C'\hat{x}'), \quad u = u_c - K_r\hat{x}'$$

$$= (A' - B'K_r - K_eC')\hat{x}' + B'u_c + K_ez$$

$$(3)$$

where the primes refer to the reduced-order model. K_r and K_e are the gain matrices, and u_c is a command input.

For the 12-mode model of the example, Table 3 presents results from REGEST for two selections of weighting of the inputs and outputs described previously. Table 3 lists the eigenvalues for the regulator $A'-B'K_r$, the estimator $A'-K_eC'$, and the compensator $A'-B'K_r-K_eC'$. Note that the regulator design with faster low-frequency poles results in an unstable compensator. This is not uncommon in LQS design and is related to the robustness problems that have been recognized with this design technique.

Stability and Performance

When A', B', C' are not the same as A, B, C, the closed-loop system will not have the eigenvalues predicted by REGEST. Another controls module program (TIMFST) is available to assess the stability of the system that results from combining equation (3) with equation (1). The designer must construct a host file which identifies the appropriate arrays in the database for the system and compensator; the program then provides the eigenvalues of the closed loop system. Initial conditions and system input time functions can also be provided to the program, which then produces a time response by linear simulation.

For the two example designs, Table 4 presents the closed-loop eigenvalues obtained from TIMFST. Note that the unstable compensator produces an unstable system.

IV. MULTI-FLEXIBLE BODY CONTROL DESIGN FOR LINEAR AND NONLINEAR SYSTEMS

As the control design for CSI begins to mature, nonlinearlities must

27

be considered. The IAC contains design modules for nonlinear structural and controls analysis. A significant nonlinearity in structures is exhibited by multiple inter- connected flexible structures. Construction of the space station utilizing the shuttle remote manipulator arm is an example of this type of structure. In this section, the available IAC tools for this task will be described. Example design procedures for interfacing these tools utilizing IAC intermodule data flow will also be discussed.

A block diagram of the design and analysis module interaction with the IAC for this task is shown in Figure 6. The typical control system design consists of three elements: 1) development of the vehicle model for analysis, 2) synthesis and analysis of the control system utilizing linear theory, and 3) performance analysis and verification using nonlinear simulation techniques.

DISCOS (Dynamic Interaction of Controls and Structures) [7] models the dynamics of multi-flexible bodies connected at generalized six degree-of-freedom hinge points. SAMSAN [8] is a collection of state-of-the-art subroutines for classical control system design or high-order systems. SAMSAN was developed primarily for Sampled System Analysis. EASY5 [9] is a control system and plant model development program which contains general purpose time domain simulation and frequency domain analysis tools for nonlinear and linear systems. All of the modules depicted in the figure, with the exception of EASY5 and the combined DISCOS/EASY5 modules developed at Boeing, are contained within the level 1 IAC architecture. The IAC architecture is developed to facilitate inclusion of user selected design and analysis modules that could be used in place of the Boeing modules.

To develop vehicle dynamic models for multi-flexible bodies, the analysis modules NASTRAN, DISCOS, SAMSAN, EASY5 and the interface module INDA are used in a procedure as depicted by the information flow of Figure 6. Thermal deformation data can be included in this development if the design warrants such consideration. The initial step in developing multi-flexible vehicle dynamic models is to create a structural finite element model for each flexible body using NASTRAN. Model definitions in terms of geometry, mass properties, mode shapes and frequencies are entered into the IAC database through INDA. DISCOS can then read this data out of the database and combine it into a coupled flexible body model through its Lagrange multiplier approach. At Boeing, the DISCOS interface to the IAC has been modified so that the user can select the modes to be retained after INDA has loaded the NASTRAN model parameters into the IAC database. The DISCOS model is a complete, general nonlinear dynamic model including all coupling effects and large angle body motions for a multi-flexible body. DISCOS can linearize this model at any userspecified static or dynamic initial condition and load into the database the linear matrices A, B, and C satisfying equation (1) above. Code has been developed in the IAC to store labels for the DISCOS states to assist the user in interpretation of the data.

In order to utilize the DISCOS model in the most efficient manner to address the question of controllability and observability, and to develop reduced-order models for control system design, the DISCOS linearized equations can be restructured into block diagonal model form. A powerful

28

tool for performing this task is a set of subroutines called BLKDRV [10]. These subroutines reside in the SAMSAN library. The most significant advantage of these routines is that they are designed to diagonalize systems with multiple roots while avoiding ill- conditioned results. This is particularly important for the zero frequency (rigid body) roots that are present in the DISCOS linearized model. The SAMSAN routines have been combined together in a user-defined driver program (BLOCKIT), utilizing IACprovided utilities to communicate data to and from the IAC database. This program reads the A, B, C matrices from DISCOS, forms the diagonalized model and returns it to the database for analysis.

The ORACLS routines can be used to synthesize a multivariable controller for this model by an LQS procedure as discussed above. In addition, the linearized vehicle model can be transferred to EASY5 utilizing IAC I/O utilities. The control system designer can combine this plant model with either a linear or nonlinear model of the controller. EASY5 can then be used to perform standard classical frequency domain analysis of the system for either a continuous or discrete system. EASY5 can also be used to run a time domain simulation of the linear vehicle model and either a linearized model of the controller or the complete nonlinear model of the controller. Multivariable controller design parameters developed by a LQS approach using ORACLS can be passed to the EASY5 model through the IAC database to be combined with nonlinear models of sensors and actuators for a more complete analysis of the system.

Final evaluation of system performance and adjustment of control parmeters is performed at Boeing using the DISCOS/EASY5 module. This module combines the nonlinear vehicle dynamic model of DISCOS with the nonlinear model of the controller which is easily defined using the standard components of EASY5 for time domain simulation. The DISCOS vehicle dynamic model and the EASY5 continuous controller states are integrated by the DISCOS numerical integrators to compute the time response. Since DISCOS does not have the capability to compute time responses of digital models, EASY5 complements the DISCOS multiflexible dynamics by providing this capability. Graphics IAC utilities can be used to plot the time history results of the nonlinear controlled multi-flexible body.

REFERENCES

[1]   Vos, R. G. et al, "Development and Use of an Integrated Analysis Capability", Proc. 24th AIAA/ASME/ASCE/AHS Structures, Structural Dynamics and Materials Conference, Paper 83-1017, May 1983.

[2]   "MSC NASTRAN Version 63", Theoretical/User/Programmer/Application Manuals, MacNeal-Schwendler Corporation, 7442 N. Figueroa Street, Los Angeles, CA.

[3]   Armstrong, E. S., "ORACLS - A System for Linear-Quadratic-Gaussian Control Law Design", NASA Technical Paper 1106, April, 1978; also Dekker Publishing, 1980.

[4] Zhao, Rozsa, and Sinha, "On the Selection of the Eigenvalues to be Retained in a Reduced-order Model", Proc. of 19th Allerton Conference on Communication, Control, and Computing, 1981, p. 163.

[5] Skelton and Yousuff, "Component Cost Analysis of Large-Scale Systems", in Advances in Control and Dynamic Systems, Vol. 18, Academic Press, 1982.

[6] Kwong and Chen, "A Quotient Space Analysis of Aggregated Models", IEEE Trans. on A.C., AC-27, No. 1, Feb. 1982.

[7] Bodley, C. S. et al, "A Digital Computer Program for the Dynamic Interaction Simulation of Controls of Structure (DISCOS)", NASA Technical Paper 1219, Volumes I-III, May 1978.

[8] Frisch, H. P., "Modern Numerical Methods for Classical Sampled System Analysis SAMSAN - Version 2", NASA Goddard SFC.

[9] 10208-127-R2, "Mainstream - EKS Capability (IAC) Executive Summary (Level 1)", Boeing Aerospace Co., prepared for Goddard Space Flight Center.

[10] Frisch, H. P., "Reduced Order Feedback Control Equations for Linear Time and Frequency Domain Analysis", NASA Technical Paper 1818, June 1981.

Table 1. Symmetric Space Station, Configuration 1, 24-Mode Model

Eigenvalues of Flexible Modes:[+]

Mode No.	Frequency (rad/sec)	Type	Modal Costs	
7	.527		$.313 \times 10^{-14}$	
8	.531	Solar Array Mast Torsion	$.233 \times 10^{-17}$	
9	.531		$.347 \times 10^{-21}$	
10	.533		$.392 \times 10^{-11}$	
11	.546	Boom Torsion	$.684 \times 10^{-15}$	
12	.599		$.294 \times 10^{-9}$	*
13	.728	Boom Bending	$.623 \times 10^{-11}$	
14	.771		$.312 \times 10^{-11}$	
15	.930		$.461 \times 10^{-9}$	*
16	.967		$.364 \times 10^{-8}$	*
17	1.11		$.125 \times 10^{-17}$	
18	1.12		$.255 \times 10^{-12}$	
19	1.53	Combined Bending	$.243 \times 10^{-12}$	
20	1.57		$.731 \times 10^{-11}$	
21	1.83		$.483 \times 10^{-9}$	*
22	2.75		$.149 \times 10^{-7}$	*
23	2.86		$.398 \times 10^{-13}$	
24	2.87		$.490 \times 10^{-9}$	*

[+] Added Damping Ratio: .0001

31

Table 2. Input and Output Definitions for Space Station Model

3 Actuators:	• Independent torque generation about roll, pitch, yaw, located on the core (at node 100); units: N-m
3 Disturbances:	• Unknown torques about roll, pitch, yaw, located at node 100; units: N-m
9 Sensors:	• Inertial rate about roll, pitch, yaw, located on the core (at node 100); units: rad/sec
	• Angles about roll and pitch, located at node 100; units: rad
	• Relative angles of solar array gimbal about roll and yaw, located at node 105 (relative to node 100); units: rad
	• Relative angles of solar array panel corner about roll and yaw, located at node 310 (relative to node 100); units: rad
3 Control Outputs:	• Inertial angles of solar array gimbal about roll, pitch, yaw, located at node 105; units: rad

Table 3. Eigenvalues of 12-Mode Regulator, Estimator, and Compensator

Case 1: $Q_R = 10^9$		Case 2: $Q_R = 10^{10}$	
Damping Ratio	Frequency (rad/s)	Damping Ratio	Frequency (rad/s)
● Regulator:			
6 Poles at Zero		6 Poles at Zero	
.711	.112	.721	.199
.716	.146	.735	.257
.708	.149	.710	.266
.013	.600	.0396	.605
.0045	.930	.0141	.929
.0039	.967	.0120	.967
.0030	1.83	.0093	1.83
.0072	2.75	.0209	2.75
.0044	2.87	.0121	2.88
● Estimator			
7 Poles at Zero		(Same as Case 1)	
1.0	.00398		
.859	.00691		
.866	.00703		
.0011	.599		
.0209	.929		
.0091	.965		
.0175	1.83		
.302	1.89		
.575	4.19		
● Compensator			
6 Poles at Zero		6 Poles at Zero	
1.0	.0849	1.0	.129
1.0	.101	1.0	.143
.730	.112	.732	.199
1.0	.121	1.0	.257
1.0	.151	1.0	.319
.013	.598	.032	.601
.041	.894	.041	.841
.0068	.961	.011	.961
.012	1.81	.0097	1.82
.127	2.51	-.208	2.88
.820	3.29	1.0	1.46
		1.0	5.89

Table 4. Eigenvalues for 24-Mode System with 12-Mode Compensator

Case 1: $Q_R = 10^9$		Case 2: $Q_R = 10^{10}$	
Damping Ratio	Frequency (rad/s)	Damping Ratio	Frequency (rad/s)
13 Poles at Zero		13 Poles at Zero	
1.0	.00398	1.0	.00398
.859	.00691	.859	.00691
.866	.00703	.866	.00703
.711	.112	.721	.199
.716	.146	.734	.257
.708	.149	.708	.267
.0001	.527	.0001	.527
.0001	.531	.0001	.531
.0001	.531	.0001	.531
.000095	.533	.00038	.534
.0001	.546	.0001	.546
.0011	.599	.0011	.599
.013	.600	.0396	.605
.00011	.728	.00019	.728
.0001	.771	.00011	.771
.0398	.897	.0417	.846
.00022	.930	.00024	.930
.0069	.961	.011	.961
.00026	.967	.00031	.967
.0001	1.11	.0001	1.11
.0001	1.12	.0001	1.12
.0001	1.53	.0001	1.53
.0001	1.57	.0001	1.57
.012	1.81	.0096	1.82
.0001	1.83	.00020	1.83
.126	2.51	.00011	2.75
.000089	2.75	.0001	2.86
.0001	2.86	.000098	2.87
.0001	2.87	-.207	2.88
.817	3.31	1.0	1.56
		1.0	5.85
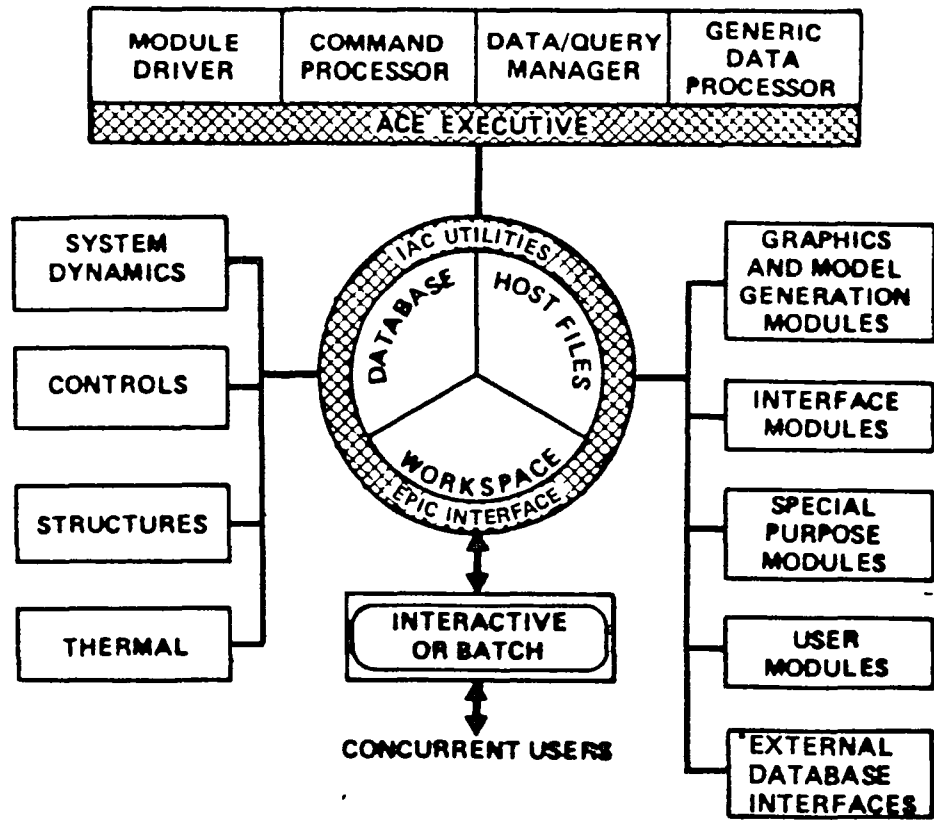
Figure 1.   IAC Architecture

THERMAL

MSC NASTRAN
SINDA
TRASYS

CONTROLS

ORACLS
SAMSAN
MODEL

GRAPHICS

PLOT/MOSAIC
MOVIEBYU
ETC.

SPECIAL PURPOSE

MIMIC
RIM
LINK
ETC.

STRUCTURAL

MSC NASTRAN
COSMIC NASTRAN

SYSTEM DYNAMICS

DISCOS
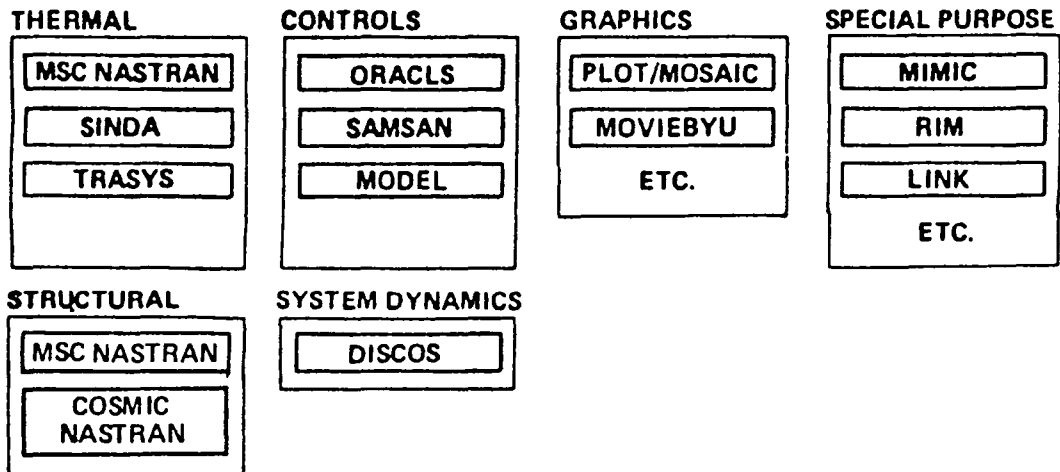
Figure 2.   Discipline Module List

Figure 3. Solution Paths

M = 5.3444 E4 kg

I_x' = 1 42 E6 $kg\text{-}m^2$

I_y' = 1 48 E6 $kg\text{-}m^2$

I_z' = 2.53 E6 $kg\text{-}m^2$
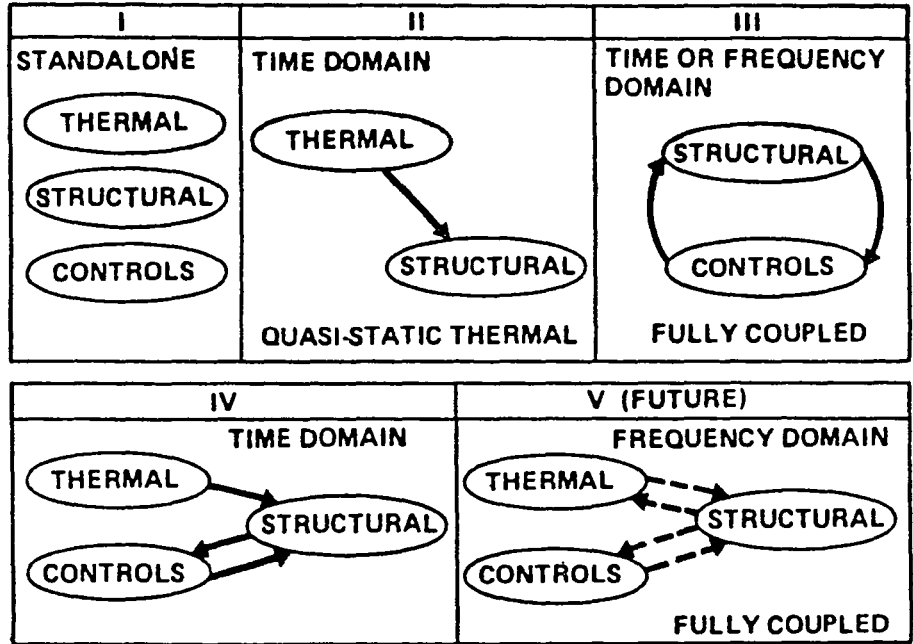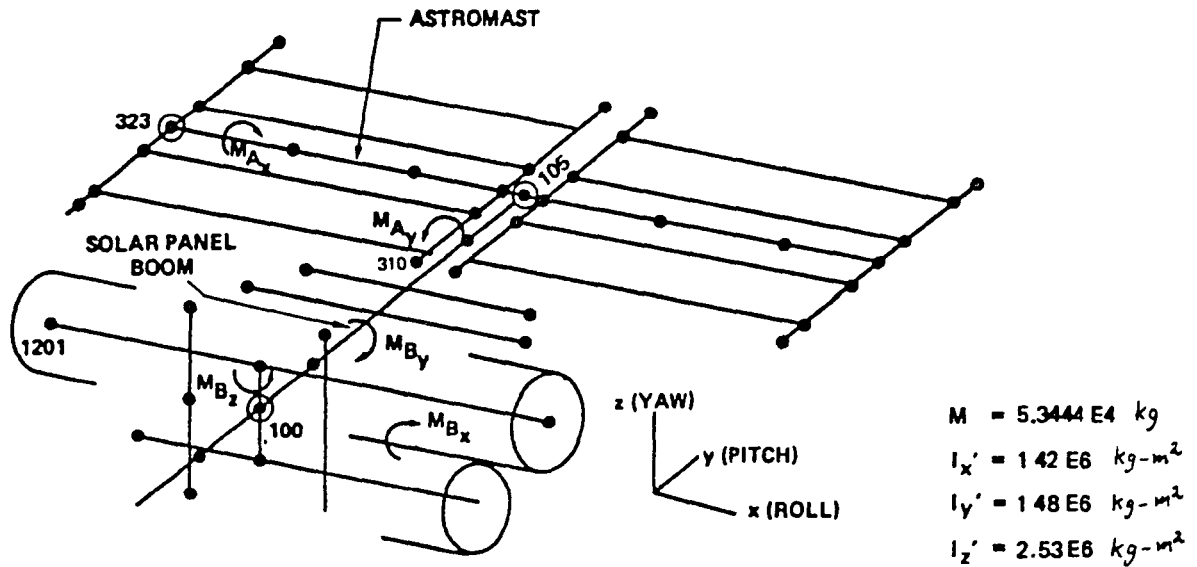
Figure 4. Node Configuration of Space Station Model
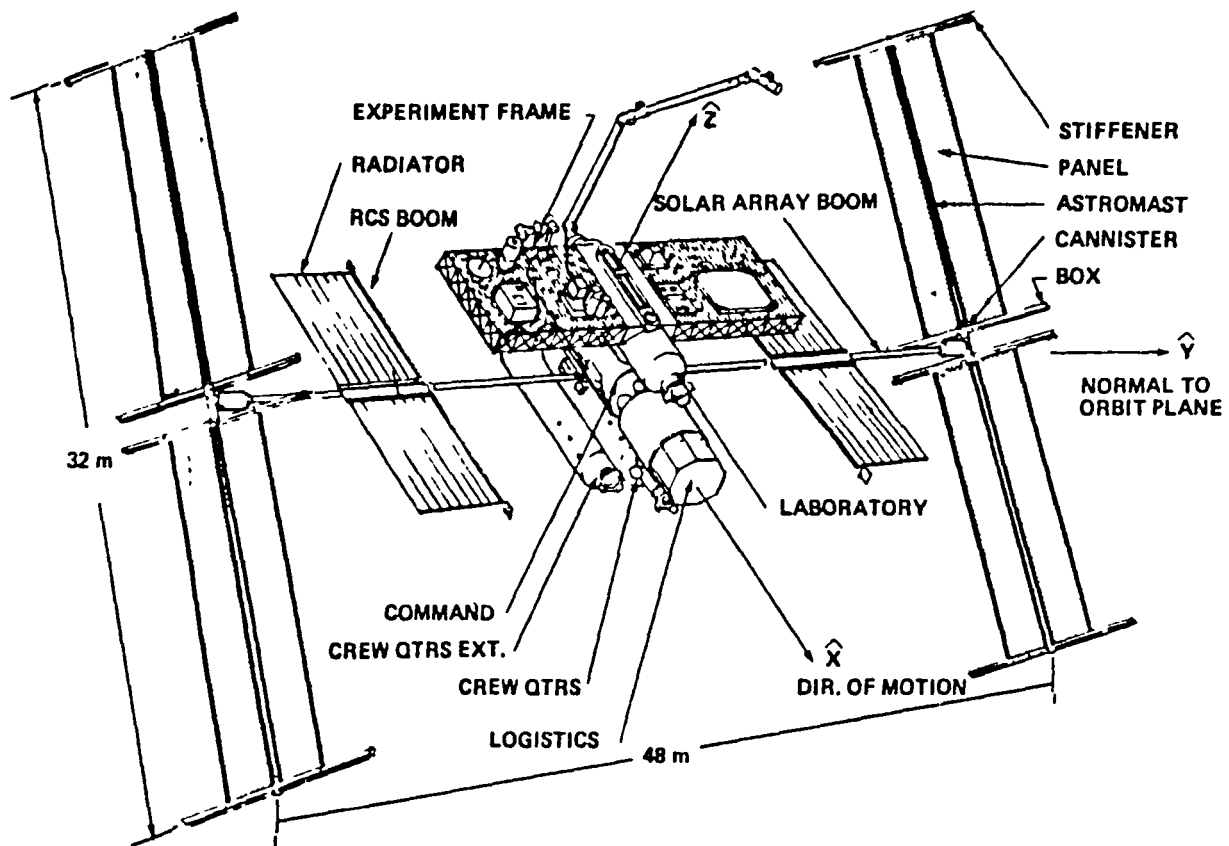
Figure 5. Space Station Configuration
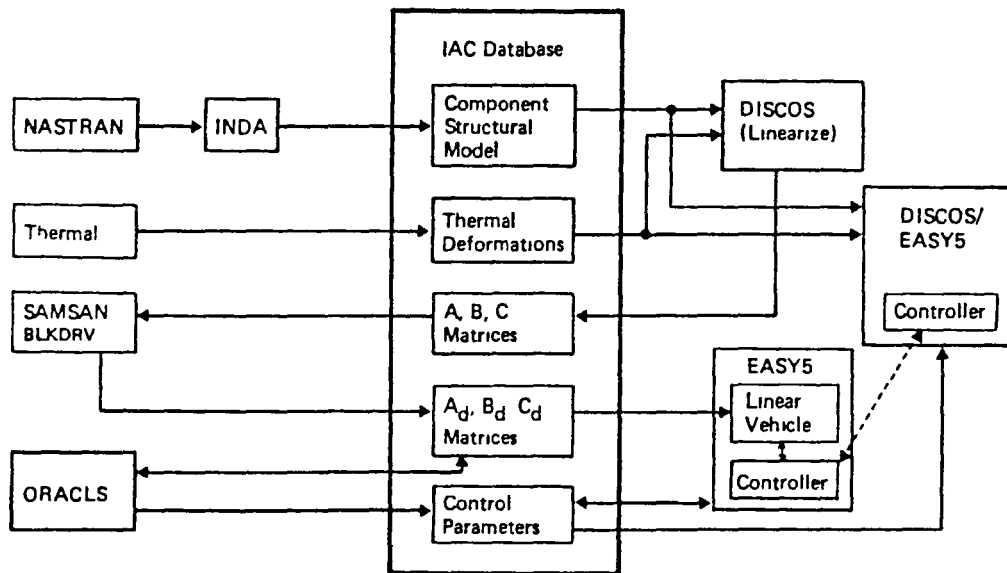
Figure 6. IAC Analysis and Data Flow for Multiflexible
Body Control Design

A STRUCTURAL DYNAMICS APPROACH TO THE SIMULATION OF SPACECRAFT CONTROL/STRUCTURE INTERACTION

J. W. Young*
Structural Dynamics Research Corporation
San Diego, CA 92121

ABSTRACT

A relatively simple approach to the analysis of linear spacecraft control/structure interaction problems is presented. The approach uses a commercially available structural system dynamic analysis package for both controller and plant dynamics, thus obviating the need to transfer data between separate programs. The unilateral coupling between components in the control system block diagram is simulated using sparse matrix stiffness and damping elements available in the structural dynamics code. The approach is illustrated with a series of simple tutorial examples of a rigid spacecraft core with flexible appendages.

I. INTRODUCTION

One of the challenges in the control of large flexible space structures is the dichotomy of analytical disciplines which are critical to the problem: rigid body dynamics, structural dynamics and control. Differences in the formulation and domain of the applicable equations, notation, and jargon lead to problems in communication between analysts. The problem is further exacerbated by the use, typically, of different software programs to analyze the control system and structural dynamics. The purpose of the work reported here is to address this latter difficulty. Specifically, a few "tricks" are played which permit the use of a structural dynamics software program for the analysis of actively controlled structural systems. This alleviates the difficulties associated with the transfer of data between structural and control codes. It also provides a common forum for communication among control and structural analysts.

*Director of Engineering

Following this brief introduction, a structural dynamics approach to the modeling of feedback control systems is presented. Included is a discussion of the fundamental difference between control and structural systems which makes such an approach less than obvious. Next, the method is illustrated in a series of simple tutorial examples of the attitude control of a flexible spacecraft. These examples, incidentally, also clearly illustrate the type and cause of instabilities which can arise in such systems. The paper concludes with a summary.

II. THE APPROACH: THE UNILATERAL STRUCTURAL ELEMENT

The block diagram for a typical feedback control system is shown in Figure 1, which also defines the notation used in this paper. Of course, infinite variations from this basic scheme are possible, but it is sufficiently general for our purposes. Ideally, a system analysis approach would enable the structural dynamicist and control system analyst to model the appropriate boxes in Figure 1 and then assemble the system model using a "building block" [1] technique. A common software package with integrated data base would eliminate many problems associated with different variable definitions, units, data transfer, etc.

The fundamental difficulty in a structural dynamics approach to modeling a control system such as in Figure 1 is that the block diagrams of control engineering show flow of information or signals and not power. It is convenient to think in terms of the power variables, "effort" and "flow," which are often defined in control and system dynamics theory (see, for example, [2]). The product of an effort and flow variable (for example, force times velocity) represents the power exchange between components connected at the degrees of freedom (DOF) where the variables are defined. For a system consisting of interconnected structural components, this power is generally nonzero. In contrast, for a feedback control system, which is dominated by instruments (sensors or transducers) and isolating amplifiers, either the effort or flow variable may be suppressed to nearly zero at many connection points so that essentially no power flows between these components. In the "bond graph" approach to dynamic system analysis [2], the effort and flow variables are treated explicitly, and such a flow of information is represented by an "active bond" involving only one of the power variables. The difference between interacting structural systems (or "multiports") and control systems may also be described in terms of "bilateral" or "unilateral" coupling. Unilateral coupling refers to the flow of one of the two power variables as information without any "back effect" or loading, while bilateral coupling refers to the flow of both power variables, resulting in the transfer of energy. These ideas are summarized in Table 1.

If we temporarily think of the blocks of Figure 1 as structural components, then a structural analyst might create a system structural model using the building block approach or the methods of component mode synthesis. One common way to do this is to represent the structural components by appropriate modal characteristics and couple these components using connectors or "scalar structural elements" (using MSC NASTRAN terminology) such as springs and viscous dampers. By definition such structural elements represent a bilateral coupling between component DOF's. However, depending upon the flexibility of the structural analysis software, it may be quite simple to define a unilateral connection by defining a nonsymmetric matrix structural element. The concept is illustrated in Figure 2 by analogy to a spring connection between two translational DOF's. If we envision the physical spring of Figure 2(a) as grounded at point 2 and excited by a displacement input y_1 at point 1, then it responds with a force f_2 and an equal reaction force f_1. The constitutive equation for this bilateral spring connector is shown in Figure 2(b).

In contrast, a "unilateral" connector may be defined as shown in Figure 2(c), which represents proportional feedback control. A force f_2 proportional to the input signal y_1 is generated by the controller, and no reaction force f_1 is generated. An analogous argument can be made for the case of derivative feedback using a structural element representing viscous damping. An even simpler special case exists in which the control force or torque is applied at the same location and direction as the measurement. This strategy is guaranteed not to drive an otherwise stable system unstable and is often referred to as the ILSM concept (Integrally Located Sensor and Manipulator) or simply as "collocated sensor and actuator." It may be simulated using simple spring and dashpot elements between the sensor/actuator DOF and ground. The stiffness and viscous damping coefficients are defined to be equal to the controller's proportional and derivative gains.

Similar "tricks" can be used to model various compensation filters (for instance, lead, lag, or lag-lead). A structural modeling technique simulating pure integral control has not been determined, but this is not of particular concern because it is also very difficult to physically realize a drift-free, pure integrator. Instead, the usual approach is to use a low pass filter which acts like an integrator for frequencies above the filter bandwidth. This approach can be simulated using structural elements as will be shown by example.

The discussion thus far has focused upon single input, single output systems. However, the modern, state-variable control methods* usually used

*I have differentiated between classical and modern control in terms of the number of inputs and outputs. In fact the more fundamental differences relate to the design objectives and approach and to the domain of the independent variable (that is, frequency versus time). Both control approaches may be applied to any number of inputs and outputs.

for flexible spacecraft controller design involve multi-input, multi-output systems. Ideally, the complete system "state"-- consisting of the displacement and velocity associated with all structural DOF's--is measured and fed back with a gain. This is equivalent to PD control of the component displacement DOF's and is easily simulated in a structural analysis code using unilateral matrix connectors. Thus, the primary additional complication for simulation of state-variable control systems is the probable need for multiple PD controllers. Other complications may arise if, for example, the state equations are based on nonphysical variables (for instance, phase or canonical variables), but in most cases such problems appear to be solvable by defining constraint equations.

III. Examples

In the examples presented here, a commercially available structural system analysis code** based upon the methods of component mode synthesis is used to simulate a variety of control strategies applied to a simple spacecraft model. Many spacecraft can be accurately modeled as a rigid core with flexible appendages. In Example 1, PD and PID control is illustrated for a rigid spacecraft model. Appendage flexibility is added for Example 2, and it is shown that the controls of Example 1 result in an unstable system. Finally, the simplest possible stable control system, in which the sensors and actuators are collocated, is developed in Example 3. This strategy, sometimes referred to as ILSM (Integrally Located Sensors and Manipulators), is also trivially simple to simulate in a structural analysis code, requiring only scalar connectors.

Example 1: PD Control of Rigid Spacecraft

The planar rigid body spacecraft model is shown in Figure 3, which also shows the arbitrarily selected locations of the two sensors and two actuators. First the transfer functions for the plant and controller are derived and the parameter values defined. Next the closed-loop eigenvalues are calculated by hand. Finally, the modeling procedure is described and the resulting modes compared with the previously derived results.

The equation of motion for the planar, rigid spacecraft is simply

$$J\dot{\Theta} = t \tag{1}$$

**SDRC SYSTAN.

where J = Polar moment of inertia about the spacecraft center of gravity (c.g.)

O = Spacecraft rotation about its c.g.

t = Applied torque about c.g.

Referring to Figure 3, the linearized vertical displacement of the appendage tip is

$$y_p = l_s O \qquad (2)$$

The external torque from the two actuators is

$$t = 2fl_A \qquad (3)$$

where f = actuator force.

Combining equations (1) - (3)

$$\frac{J}{2l_S l_A} \ddot{y}_p = f \qquad (4)$$

By taking the Laplace transform of equation (4), the plant transfer function in Figure 1 becomes

$$G_p(s) \triangleq \frac{Y_p(s)}{F(s)} = \frac{2l_s l_A}{Js^2} \qquad (5)$$

By definition of PD control, the controller transfer function of Figure 1 is

$$G_c(s) \triangleq \frac{F_A}{Y_E} = K_p (1 + T_d s) \qquad (6)$$

where K_p = proportional gain

T_d = derivative time

Block diagram algebra yields the following two closed-loop transfer functions

$$\frac{Y_p}{Y_D} = \frac{K_p (1 + T_d s)}{Ms^2 + 2\zeta\omega_n s + K_p} \qquad (7)$$

and

$$\frac{Y_p}{F_D} = \frac{1}{Ms^2 + 2\zeta\omega_n s + K_p} \qquad (8)$$

43

where

$$M \triangleq \frac{J}{2 l_A l_s}$$

$$2\zeta\omega_n = K_p T_d$$

$$\omega_n = \sqrt{\frac{K_p}{M}} \qquad\qquad (9)$$

The controller parameters can be selected to provide any desired value of system natural frequency, ω_n, and damping ratio, ζ. For our numerical simulation assume

$$J = 9000 \text{ lb-s}^2\text{-in}$$

$$l_s = 110 \text{ inches}$$

$$l_A = 60 \text{ inches}$$

If we choose a natural frequency of 1 Hz and 20% damping, equation (9) can be solved for the controller parameters

$$K_p = 26.92 \text{ lb/in}$$

$$T_d = 0.06366 \text{ seconds}$$

Note that we have assumed an ideal measurement system so that sensor dynamics can be ignored. One approach to the simulation of this feedback control system using structural analysis software is to model the total closed loop system using direct matrix input. Thus, the mass, damping, and stiffness terms in the denominator of equations (7) or (8) can be entered directly. However, this approach requires that the analyst perform the block diagram algebra manually and obscures the effects of the individual components of the system; the controller is no longer distinct from the plant. Instead, we can define each of the parts of the block diagram in Figure 1 as distinct entities in the manner described below.

(1) The spacecraft (or "plant" in Figure 1) is modeled as three separate rigid body components representing the core and two appendages. While only one component was required, it was convenient to "swap" the rigid appendages of this example for flexible ones in Example 2.

(2) The two reference inputs are defined as rigid-body components with only one DOF each in the y direction. These DOF's are "grounded" at the system level in order to permit input of the desired position of the appendage tips. In fact, because the entire system has only one independent DOF (Θ_z), these two set-point DOF's cannot be defined independently.

(3) The comparitors and error signals of Figure 1 are created by defining a constraint equation of the form

$$y_E = y_D - y_P \; .$$

(4) Finally, the two PD controllers are defined as sparse, nonsymmetric matrix translational connectors. One point of each connector is connected to the variable created for the error signal, and the second point is connected to the actuator location.

Thus, to provide the unilateral coupling as shown in Figure 2(c), the nonzero elements of the stiffness and viscous damping matrices are defined to be

$$K_p = -26.92 \text{ lb/in}$$
$$C = K_p T_d = -1.714 \text{ lb-s/in}$$

This connector thus generates a force on the spacecraft appendage proportional to the error signal plus its derivative and does not create a back effect or reaction force at the sensor location.

Because the damping term (velocity feedback) results in a nonconservative eigenvalue problem, a complex eigensolution is required, yielding complex conjugate eigenvalues. The code used here lists a modal viscous damping ratio and natural frequency corresponding to each eigenvalue as shown in Figure 4. These values correspond to the hand-calculated ones. The response to a step change in the desired spacecraft attitude is shown in Figure 5. The input was defined as a unit step displacement associated with the two set-point variables. The resulting steady-state appendage tip position is unity, as expected.

Similarly, a ten-pound step disturbance was applied at the right actuator location. This might represent, for example, a bias in the actuator electronics. The appendage response is shown in Figure 6. The predicted steady-state error labeled in the figure agrees with the theoretical value calculated from the equation found in any controls text:

$$e_{ss} = \lim_{s \to o} s \; Y_E(s) \tag{10}$$

For zero set point, using equation (8)

$$Y_E = -Y_P = \left(\frac{-1}{Ms^2 + K_p T_d s + K_p} \right) F_d$$

45

so that

$$\lim_{t \to \infty} y_p = -e_{ss} = \frac{F_d}{K_p} = .186 \tag{11}$$

A value of $F_d = 5$ was used in equation (11) because the ten-pound distur-
bance was applied to the right actuator only and is equivalent to two
five-pound disturbances applied simultaneously to each actuator.

Example 1A: PID Control of Rigid Spacecraft

Integral control action is often used when steady-state error is to be
minimized, and this approach can be applied to the system of Example 1.

The transfer function of the PID controller thus becomes

$$G_c = \frac{F_A}{Y_E} = K_p(1 + T_d s + \frac{1}{T_i s}) \tag{12}$$

where T_i = integral time.

The closed loop system transfer functions then become

$$\frac{Y_p}{Y_d} = \frac{K_p T_d s^2 + K_p s + K_p/T_i}{Ms^3 + K_p T_d s^2 + K_p s + K_p/T_i} \tag{13}$$

$$\frac{Y_p}{F_d} = \frac{s}{Ms^3 + K_p T_d s^2 + K_p s + K_p/T_i} \tag{14}$$

Using equations (10) and (11) it is easy to show that the steady-state error
in response to a step input is exactly zero. Unfortunately, as mentioned in
Section 2, it is difficult to realize pure integral control. We can, however,
approximate PID control using a low pass filter so that the controller
transfer function becomes

$$G_c = K_p(1 + T_d s + \frac{1}{1 + T_i s}) \tag{15}$$

and the closed loop transfer functions become

$$\frac{Y_p}{Y_d} = \frac{K_p T_d s^2 + K_p(1 + T_d/T_i) s + 2K_p/T_i}{Ms^3 + (\frac{M}{T_i} + K_p T_d) s^2 + K_p(1 + \frac{T_d}{T_i}) s + 2K_p/T_i} \tag{16}$$

46

$$\frac{Y_p}{F_d} = \frac{1 + T_i s}{Ms^3 + (\frac{M}{T_i} + K_p T_d) s^2 + K_p (1 + \frac{T_d}{T_i}) s + 2K_p/T_i} \qquad (17)$$

This controller will integrate signals with frequencies much higher than the "break frequency,"

$$\omega_b = \frac{1}{T_i} \text{ (radians/second)} \qquad (18)$$

It can also be shown using equations (10) and (17) that the steady-state error in response to a step disturbance, F_d, is

$$\lim_{t \to \infty} y_p = -e_{ss} = \frac{F_d}{2K_p} \qquad (19)$$

Thus, the first order filter approximation to integral control reduces the steady-state error by half.

We will illustrate the modeling of approximate integral control action by adding a first order filter to Example 1. As shown in Figure 7, the first order filter can be realized using a series spring and damper. Ignoring the second spring element in the figure, it is easy to show that

$$\frac{Y_2}{Y_1} = \frac{1}{1 + T_i s} \qquad (20)$$

where $T_i = \frac{C}{K_1}$.

This transfer function is implemented using sparse, nonsymmetric matrix translational connectors in order to provide the appropriate unilateral coupling. Grid point 1 of spring K_1 is connected to the error signal, and the filtered output is provided at grid point 2. Note that no reaction force is imposed on the error signal because of the sparse stiffness matrix defined in Figure 7 for this connector.

Grid point 1 of spring K_2 is connected to the plant, thus providing the appropriate control force (including gain K_p) without a reaction force on K or C. In addition, a small mass must be included at grid point 2 of C in order that the system mass matrix not be rank deficient. The value of M may be selected so that

$$\omega = \sqrt{K_1/M} > \omega_{max} = \text{maximum frequency of interest}$$

47

The control subsystem of Figure 7 is included with the other entities of Example 1. The parameter values were chosen such that $T_i = 1$ second. The eigensolution is listed in Figure 8. While the natural frequency (see modes 3 and 4) is relatively unchanged compared to Example 1 with PD control, the damping ratio has been decreased from 0.2 to 0.12. This is to be expected because of the destabilizing effects of integral control. Four additional modes have appeared. Two are real eigenvalues associated with the low pass filters for the two I-controllers, and two are artificial, over-damped modes associated with the small mass included to eliminate the rank deficiency of the model. The response to a step change in the desired spacecraft attitude is shown in Figure 9, which may be compared to Figure 5 of Example 1. Finally, the step response to a ten-pound disturbance at the right actuator is shown in Figure 10, which may be compared to Figure 6 from Example 1. The steady-state error has been cut in half as predicted by Equation (19).

Example 2. PD Control of Spacecraft with Flexible Appendages

A more interesting example is obtained by replacing the rigid appendages of Example 1 with flexible ones represented by finite element beam components. The natural frequencies and damping ratios are listed in Table 2. In addition to the rigid-body mode at 1 Hz, we now have the modes associated with the flexible appendages. Note in Table 2 the suspicious negative values of damping for modes 5-9. The significance of negative damping is illustrated by the step response plotted in Figure 11; our spacecraft control system is unstable! A further indication of the problem is the frequency domain response to a white noise disturbance shown in Figure 12. The increase in phase at 22 Hz (modes 5 and 6) and 65 Hz (modes 9 and 10) is also indicative of the instability.

The physical cause for the instability is apparent from Figure 13. The controller was designed for rigid body spacecraft attitude positioning, and the flexibility of the appendages results in spurious feedback signals. Thus, the positive displacement of the right appendage tip in mode 5 (Figure 13) is interpreted by the controller as a rigid body counterclockwise rotation, and a "correction" force is applied which actually pumps more energy into this mode and drives it unstable. The effect is similar with regard to mode 7, also shown in Figure 13, as well as the other modes with negative damping.

The following example illustrates a typical unconditionally stable control for this flexible spacecraft.

48

Example 3. PD Control of Flexible Spacecraft using Collocated Sensors and Actuators.

As discussed in Section 2, the simplest control strategy to simulate using a structural analysis code is PD control where the sensors and actuators are in the same location, sometimes referred to as the ILSM concept. Figure 14 is a display of the flexible spacecraft control system with collocated sensors and actuators. It should be apparent that this control strategy results in a stable system because we have effectively added only springs and dampers to ground. It may at first seem contradictory that we have simulated an active feedback control system using purely passive mechanical elements. However, we have employed the infamous "skyhook" damper which arises in optimum suspension design studies. The problem with regard to the physical realization of this passive design is that "ground" is not available in space!

Table 3 is a listing of the natural frequencies and damping ratios, where it is noted that all damping values are now positive. The well-behaved step and white noise responses are also shown in Figures 15 and 16 for comparison with Examples 1 and 2.

IV. SUMMARY AND CONCLUSIONS

An approach to the analysis of linear spacecraft control/structural interaction has been presented. The method enables the separate dynamic analysis of the controller, the plant, and the closed loop system in a single structural analysis software package. Any structural analysis package with the following capabilities can be used:

(1) System analysis: component mode synthesis, substructuring or the building block approach;

(2) User-definable nonsymmetric structural stiffness and viscous damping elements;

(3) Nonconservative complex eigenvalue solutions;

(4) Time and frequency domain forced response analysis with complex modal systems.

The use of a common structural analysis software package for the analysis of controller, plant, and system dynamics provides a common focus for communication between control and structural analysts and designers and reduces the chance of errors due to transfer of data between separate control and structural analysis codes. In addition, relatively small organizations without extensive control system analysis capabilities and software can begin to model such systems using structural analysis software which they may

already have in-house. Obviously, this approach appeals more to structural analysts because controller and closed-loop dynamics are treated as special cases of structural elements and systems. However, a control-oriented user interface could be developed to minimize this bias. Such an interface would be especially simple to develop for interactive software programs with macro capabilities. The approach has also been applied to control/structural interaction problems associated with non-aerospace systems including the analysis of a Winchester disk drive. No attempt has yet been made, however, to model nonlinear control/structural interaction problems or the controller design synthesis problem.

REFERENCES

[1] Klosterman, A.L., and J.R. Lemon, "Building Block Approach to Structural Dynamics," ASME Publication, 1969 VIBR-30.

[2] Karnopp, D., and R. Rosenberg, System Dynamics: A United Approach, Wiley-Interscience, 1975.

[3] Karnopp, D., and R.R. Allen, "Semiactive Control of Multimode Vibratory Systems Using the ILSM Concept," ASME Paper No. 75-DET-15, 1975.

F_d disturbance input

FIGURE 1 FEEDBACK CONTROL SYSTEM BLOCK DIAGRAM
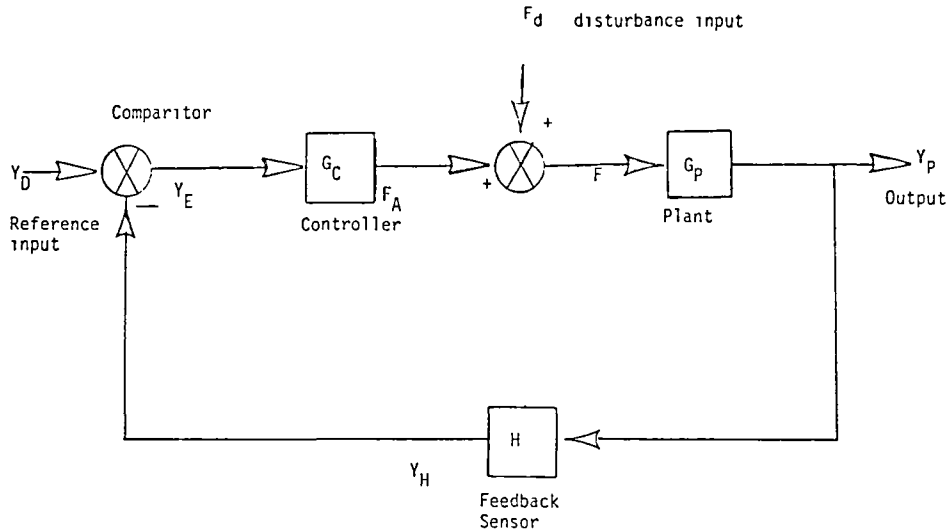
Y_P = OUTPUT OR CONTROLLED VARIABLE

Y_D = REFERENCE INPUT, SET POINT OR DESIRED OUTPUT

Y_H = MEASURED OUTPUT

Y_E = MEASURED ERROR SIGNAL

F_A = ACTUATION SIGNAL FROM CONTROLLER

F_D = DISTURBANCE SIGNAL (NOISE)

F = INPUT SIGNAL TO CONTROLLED OBJECT ("PLANT")

G_C = TRANSFER FUNCTION (LAPLACE DOMAIN) OR IMPULSE RESPONSE FUNCTION (TIME DOMAIN) FOR CONTROLLER

G_P = TRANSFER OR IMPULSE RESPONSE FUNCTION FOR CONTROLLED OBJECT

H = TRANSFER OR IMPULSE RESPONSE FUNCTION FOR FEEDBACK SENSOR

VARIABLES AND FUNCTIONS ARE SCALARS FOR SINGLE INPUT-SINGLE OUTPUT SYSTEMS, BUT ARE VECTORS AND MATRICES FOR MULTI INPUT-MULTI OUTPUT SYSTEMS.

Table 1. The Concepts of Unilateral Versus Bilateral Coupling

Unilateral	Bilateral Coupling
Information or Signal Flow	Power Flow
Control Systems	Structural System
Block Diagrams, Signal Flow Graphs	Bond Graphs
Active Bonds	Passive Bonds
Low Power Flow	High Power Flow
Effort or Flow	Effort and Flow
High Input, Low Output Impedance	Impedance Matching

(A) SCHEMATIC DIAGRAM
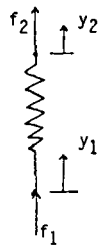
$$\begin{bmatrix} f_1 \\ f_2 \end{bmatrix} = \begin{bmatrix} k & -k \\ -k & k \end{bmatrix} \begin{bmatrix} y_1 \\ y_2 \end{bmatrix}$$

or $f_1 = k(y_1 - y_2) = -f_2$

(B) CONSTITUTIVE EQUATION
FOR PHYSICAL SPRING

$$\begin{bmatrix} f_1 \\ f_2 \end{bmatrix} = \begin{bmatrix} 0 & 0 \\ k & 0 \end{bmatrix} \begin{bmatrix} y_1 \\ y_2 \end{bmatrix}$$

or $f_1 = 0$
$f_2 = ky_1$

(c) CONSTITUTIVE EQUATION FOR A SIMPLE UNIDIRECTIONAL,
UNILATERAL CONNECTOR

FIGURE 2 CONSTITUTIVE EQUATIONS FOR SIMPLE,
UNIDIRECTIONAL TRANSLATIONAL CONNECTORS REPRESENTING
BILATERAL AND UNILATERAL COUPLING

SDRC__I-DEAS 2.0: System Assembly   15-SEP-83 11:12:19
ANALYSIS OF CONTROL SYSTEM ALTERNATIVES FOR A FLEXIBLE SPACECRAFT
RIGID SATELLITE: PROPORTIONAL PLUS DERIVITIVE CONTROL WITH SET POINT

- In-plane rotation only
- $J = 9000$ lb-s^2- inches
- $l_S = 110$ inches
- $l_A = 60$ inches
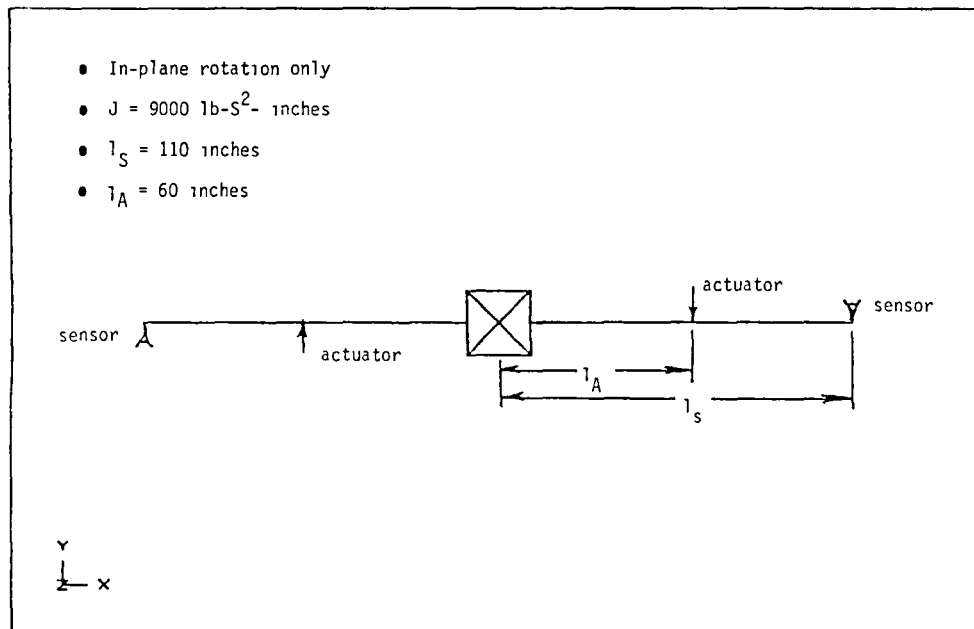
FIGURE 3. SCHEMATIC OF RIGID SPACECRAFT MODEL WITH PD CONTROL.

ANALYSIS OF CONTROL SYSTEM ALTERNATIVES FOR A FLEXIBLE SPACECRAFT
RIGID SATELLITE: PD CONTROL WITH SET POINT
MODE 1 - SPACECRAFT PITCH ABOUT CG
1.99990E-01 (ZETA)   1.00005E+00 (HZ)

```
EIG.    1 ( 2.00E-01, 1.00E+00 HZ) -SPACECRAFT PITCH ABOUT CG
EIG.    2 ( 2.00E-01, 1.00E+00 HZ) -SPACECRAFT PITCH ABOUT CG


            DAMPING   NATURAL
            RATIO   FREQUENCY
```
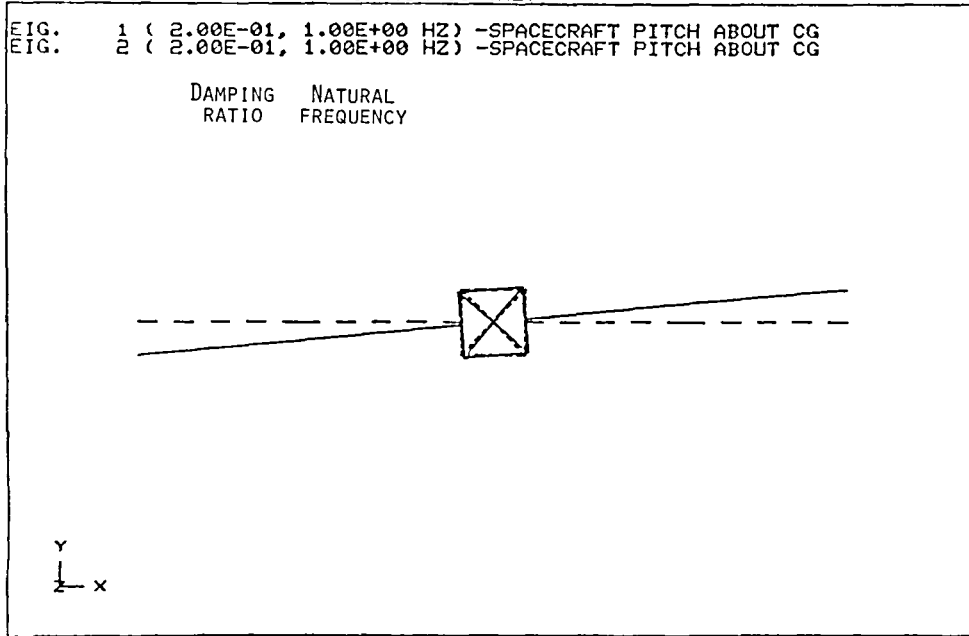
FIGURE 4. EIGENSOLUTION FOR RIGID SPACECRAFT WITH PD CONTROL.

RIGID SATELLITE: PROPORTIONAL PLUS DERIVITIVE CONTROL WITH SET POINT

TIME DOMAIN
RESPONSE OF APPENDAGE TIP TO STEP INPUT

```
1X= 1.59E+00 (ABSCISSA VALUE)
1Y= 1.50E+00 (ORDINATE VALUE)

2X= 2.10E+00
2Y= 7.31E-01

3X= 2.59E+00
3Y= 1.14E+00

4X= 3.08E+00
4Y= 9.24E-01

5X= 6.92E+00
5Y= 9.95E-01

ENTITY=SAT3
UNITS=IN
```

1/ID= 1
APR1:3-2
DISPLACEMENT
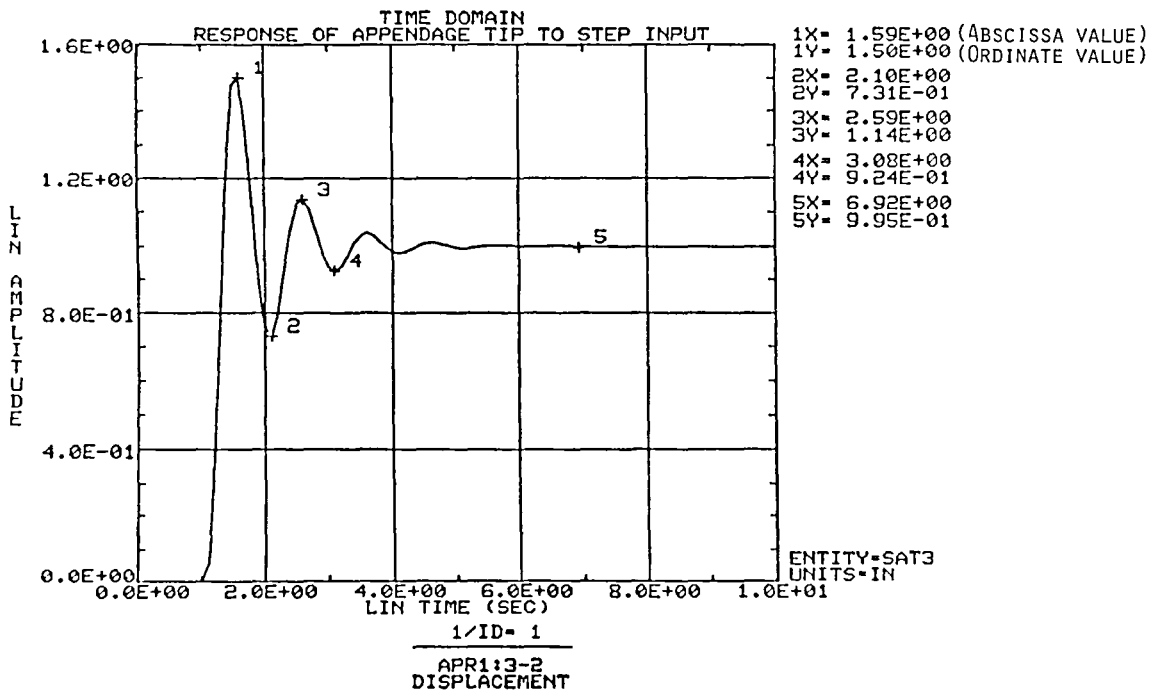
FIGURE 5. STEP INPUT RESPONSE OF THE APPENDAGE TIPS OF PD-CONTROLLED RIGID SPACECRAFT.

53

TIME DOMAIN

RESPONSE TO TEN POUND DISTURBANCE AT RIGHT ACTUATOR

1X= 8.48E+00
1Y= 1.85E-01
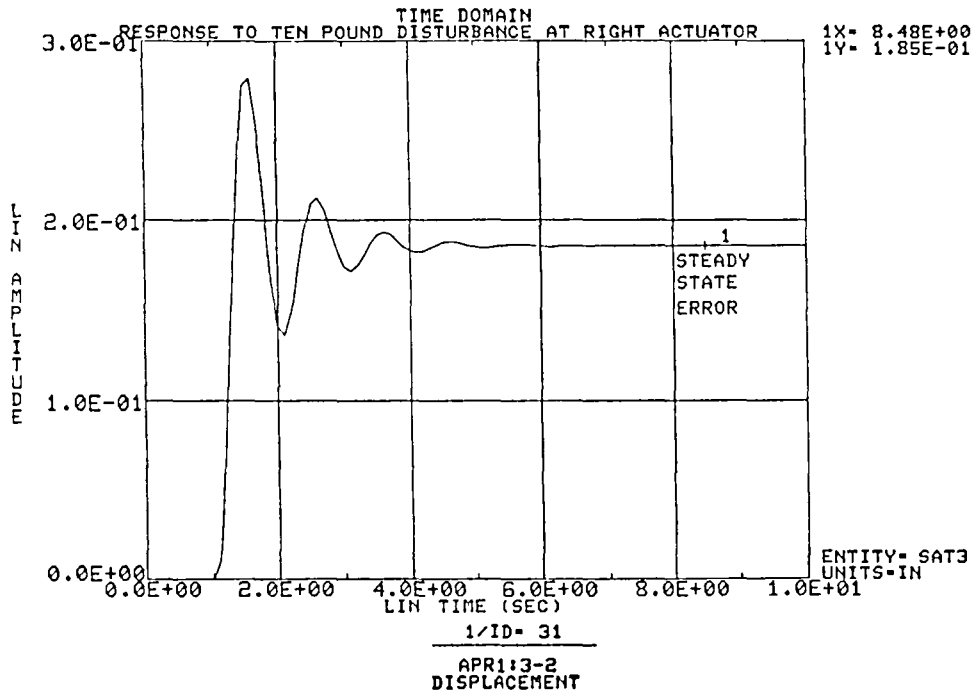
FIGURE 6. APPENDAGE TIP RESPONSE OF PD-CONTROLLED RIGID SPACECRAFT TO 10 POUND STEP DISTURBANCE AT RIGHT ACTUATOR.
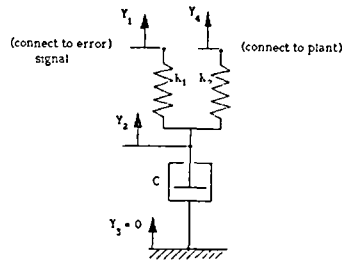
Constitutive equations for structural elements

(1) "Spring," K_1

$$\begin{bmatrix} F_1 \\ F_2 \end{bmatrix} = \begin{bmatrix} 0 & 0 \\ -1 & 1 \end{bmatrix} \begin{bmatrix} Y_1 \\ Y_2 \end{bmatrix}$$

(2) Viscous damper, C

$$\begin{bmatrix} F_2 \\ F_3 \end{bmatrix} = \begin{bmatrix} T_1 & -T_1 \\ -T_1 & T_1 \end{bmatrix} \begin{bmatrix} Y_2 \\ Y_3 \end{bmatrix}$$

(3) "Spring," K_2

$$\begin{bmatrix} F_4 \\ F_2 \end{bmatrix} = \begin{bmatrix} 0 & -k_p \\ 0 & 0 \end{bmatrix} \begin{bmatrix} y_4 \\ y_2 \end{bmatrix}$$

Figure 7 Structural spring and damper components used to model integral control

54

```
#  "P LS S F
EIGENVECTOR NUMBER =    1
EIGENVALUE = (-1 0025E+02    0 0000E+00)
UNDAMPED FREQUENCY (RAD/SEC) = XXXXXXXXXX
UNDAMPED FREQUENCY (HERTZ) = XXXXXXXXXX
VISCOUS DAMPING RATIO = XXXXXXXXXX
MODAL A = ( 3 0565E+03 ,   0 0000E+00)
MODAL B = ( 3 0585E+03 ,   0 0000E+00)

EIGENVECTOR NUMBER =    2
EIGENVALUE  (-2 0276E+00    0 0000E+00)
UNDAMPED FREQUENCY (RAD/SEC) = XXXXXXXXXX
C DAMPED FREQUENCY (HERTZ)   XXXXXXXXXX
VISCOUS DAMPING RATIO   XXXXXXXXXX
MODAL A = (-3 1407E+03    0 0000E+00)
MODAL B = (-6 5b8EE+03 ,   0 0000E+00)

EIGENVECTOR NUMBER =    3
EIGENVALUE = (-7 4308E-01 , -6 1977E+00)
UNDAMPED FREQUENCY (RAD/SEC) =   6 2421E+00
UN AMPED FREQUENCY (HERTZ) =  9 9346E-01
VISCOUS DAMPING RATIO =  1 1904E-01
MODAL A = ( 6 0205E+03 ,   1 2304E+03)
MODAL B = (-3 1445E+03 ,   3 8290E+04)

EIGENVECTOR NUMBER =    4
EIGENVALUE   (-7 4308E-01 ,  6 1977E+00)
UNDAMPED FREQUENCY (RAD/SEC) =   6 2421E+00
UNDAMPED FREQUENCY (HERTZ) =  9 9346E-01
VISCOUS DAMPING RATIO =  1 1904E-01
MODAL A = ( 6 0305E+03 , -1 2304E+03)
MODAL B = (-3 1445E+03 , -3 8290E+04)

EIGENVECTOR NUMBER =    5
EIGENVALUE   (-1 9990E+03    0 0000E+00)
UNDAMPED FREQUENCY (RAD/SEC) = XXXXXXXXXX
C DAMPED FREQUENCY (HERTZ) = XXXXXXXXXX
VISCOUS DAMPING RATIO = XXXXXXXXXX
MODAL A = (-3 0569E+03 ,   0 0000E+00)
MODAL B = (-6 1907E+06 ,   0 0000E+00)

EIGENVECTOR NUMBER =    6
EIGENVALUE = (-1 9990E+03    0 0000E+00)
UNDAMPED FREQUENCY (RAD/SEC) = XXXXXXXXXX
UNDAMPED FREQUENCY (HERTZ) = XXXXXXXXXX
VISCOUS DAMPING RATIO = XXXXXXXXXX
MODAL A = (-3 0569E+03 ,   0 0000E+00)
MODAL B = (-6 1907E+06 ,   0 0000E+00)

OK TO CONTINUE (YES)#
```

Low pass filter (controller) modes

Structural modes

Artificial modes of small mass on I-controller stiffness

FIGURE 8.   EIGENSOLUTION TO EXAMPLE 1A.

Table 2. Listing of natural frequencies and damping ratios for flexible
satellite with P.D. control (only the odd-numbered modes are listed
since the even modes have identical damping ratios and natural
frequencies).

MODE NO.	DAMPING RATIO	NATURAL FREQ (HZ	DESCRIPTION
1	2.01E-01	1.00E+00 Hz	spacecraft pitch about CG
3	2.84E-02	6.53E+00 Hz	first symmetric appendage bending
5	-9.84E-03	2.21E+01 Hz	first antisymmetric appendage bending
7	-9.63E-03	4.04E+01 Hz	second symmetric appendage bending
9	-3.65E-03	6.56E+01 Hz	second antisymmetric appendage bending
11	8.89E-05	1.13E+02 Hz	third symmetric appendage bending
13	9.16E-04	1.34E+-2 Hz	third antisymmetric appendage bending

TIME DOMAIN
RESPONSE OF RIGHT APPENDAGE TIP TO STEP CHANGE IN SET POINT

1X= 1.56E+00
1Y= 1.66E+00
2X= 2.07E+00
2Y= 5.44E-01
3X= 2.57E+00
3Y= 1.31E+00
4X= 3.06E+00
4Y= 7.80E-01
5X= 9.38E+00
5Y= 1.00E+00

ENTITY= SAT7
UNITS=IN

1/ID= 1

APR1:3-2
DISPLACEMENT
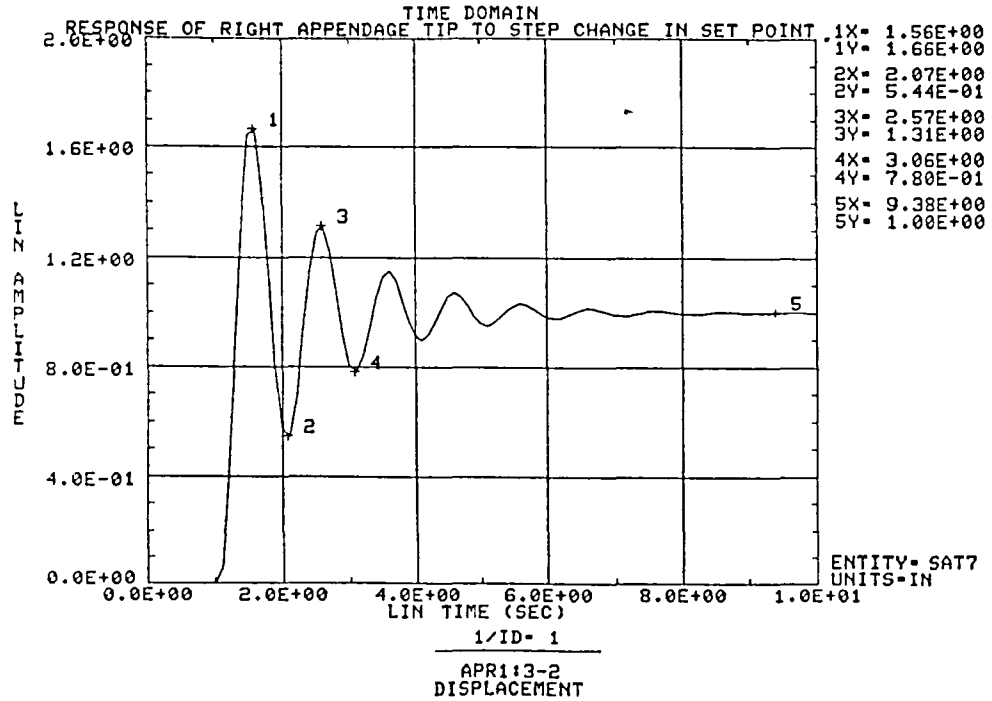
FIGURE 9.   STEP INPUT RESPONSE OF THE APPENDAGE TIPS OF PID-CONTROLLED RIGID SPACECRAFT.

TIME DOMAIN
RESPONSE OF RIGHT APPENDAGE TIP TO 10 LB FORCE DISTURBANCE

1X= 9.38E+00
1Y= 9.27E-02

ENTITY= SAT7
UNITS=IN

1/ID= 31

APR1:3-2
DISPLACEMENT
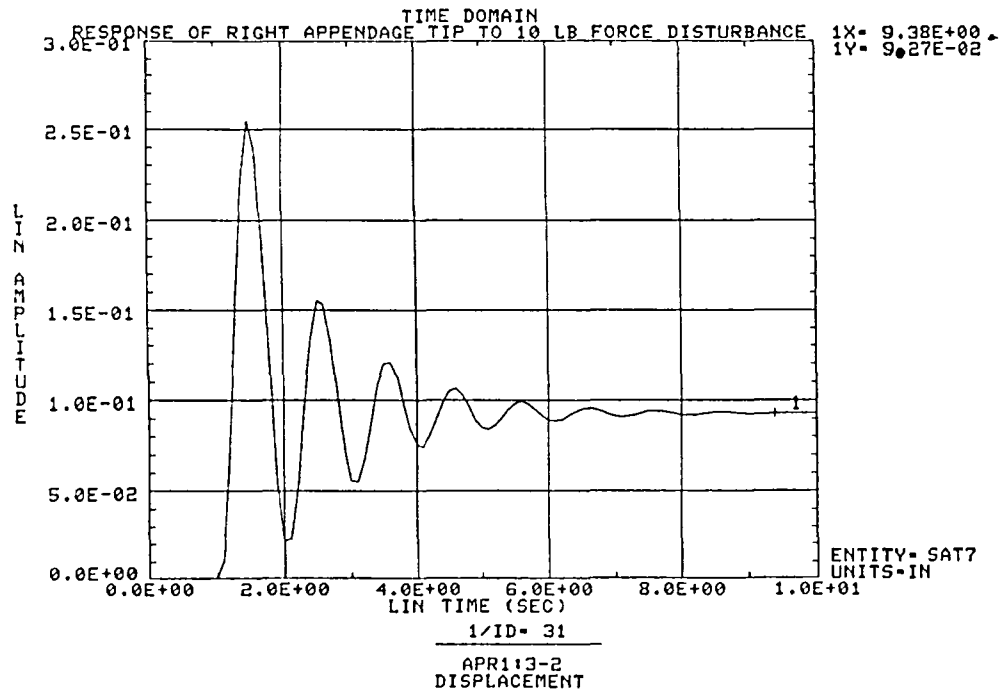
FIGURE 10.   APPENDAGE TIP RESPONSE OF PID-CONTROLLED RIGID SPACECRAFT TO 10 POUND
STEP DISTURBANCE AT THE RIGHT ACTUATOR.

TIME DOMAIN
RESPONSE OF SATELLITE APPENDAGE TIP TO STEP INPUT   1X= 3 55E+00
                                                           1Y= 1 09E+00
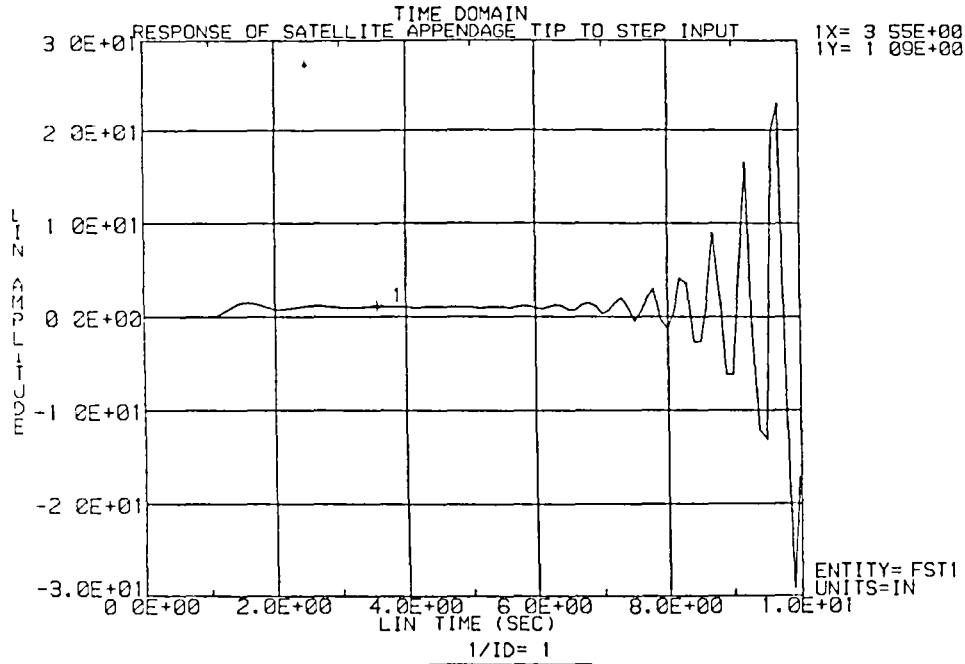
FIGURE 11. STEP INPUT RESPONSE OF APPENDAGE TIP OF PD-CONTROLLED FLEXIBLE SPACECRAFT.

FREQUENCY DOMAIN
RESPONSE OF APPENDAGE TIP TO WHITE NOISE FORCE DISTURBANCE   1X= 9 86E-01
                                                             1Y= 7 66E-03
                                                             2X= 2 23E+01
                                                             2Y= 1 04E-03
                                                             3X= 6 50E+01
                                                             3Y= 4.59E-04
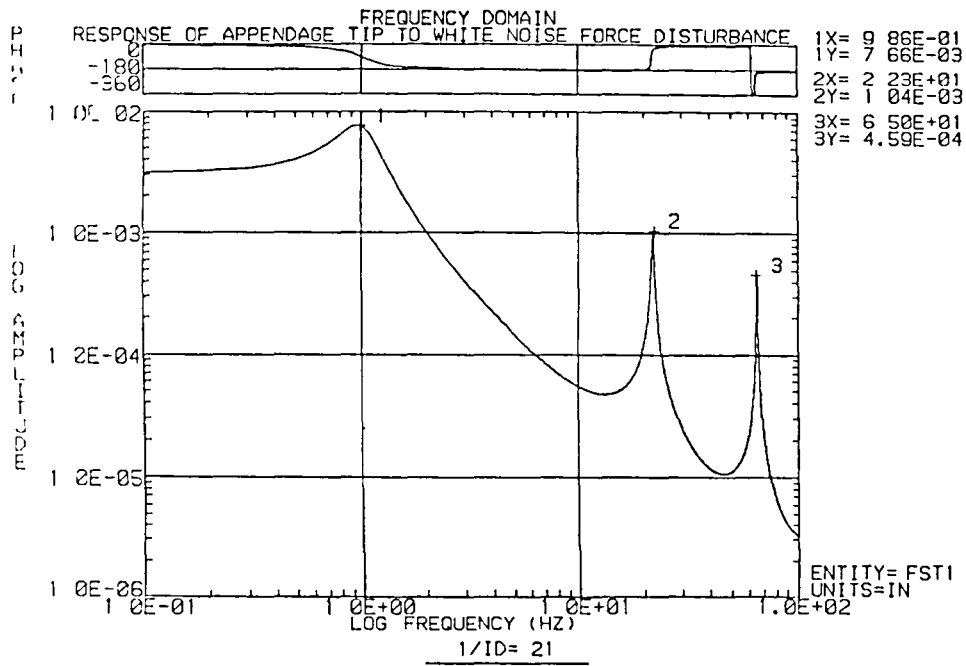
FIGURE 12. FREQUENCY DOMAIN RESPONSE OF APPENDAGE TIP OF FLEXIBLE SPACECRAFT
TO A WHITE NOISE FORCE DISTURBANCE AT THE ACTUATOR LOCATION.
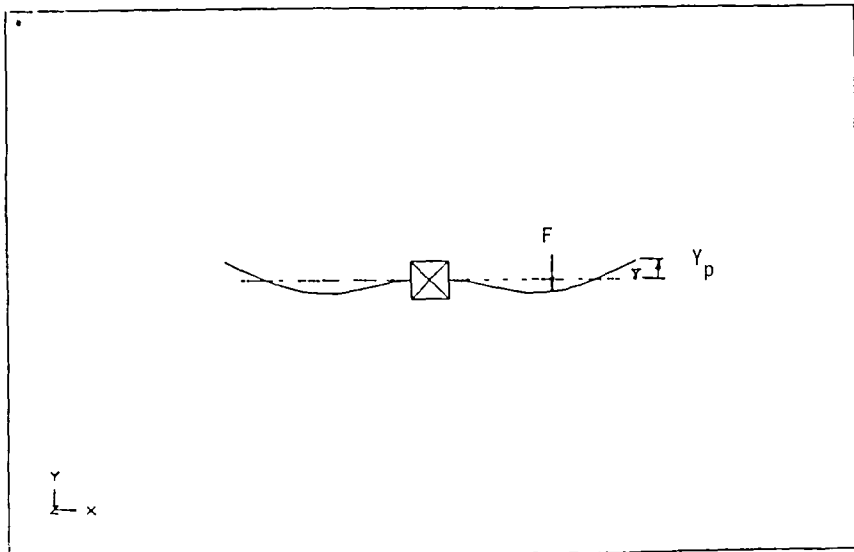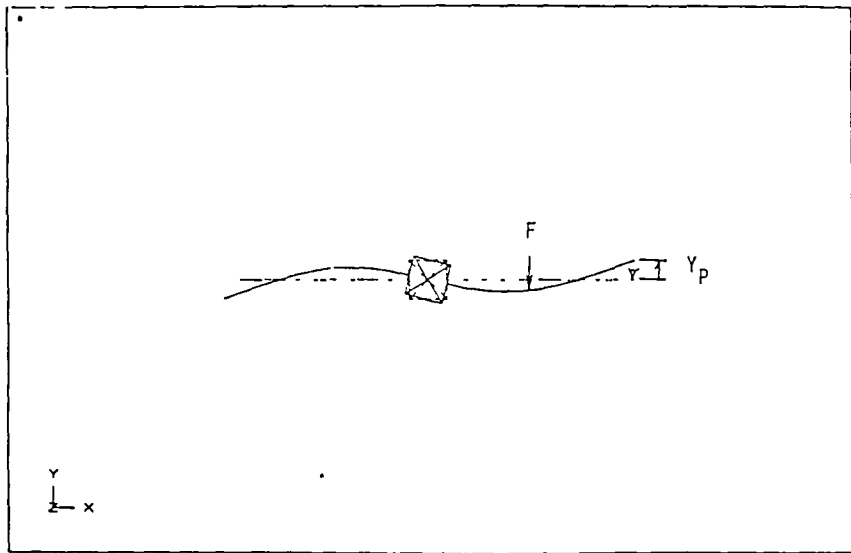
Figure 13   Illustration of destabilizing control
yielding negative damping in modes 5 and 7 of PD-
controlled flexible spacecraft

58
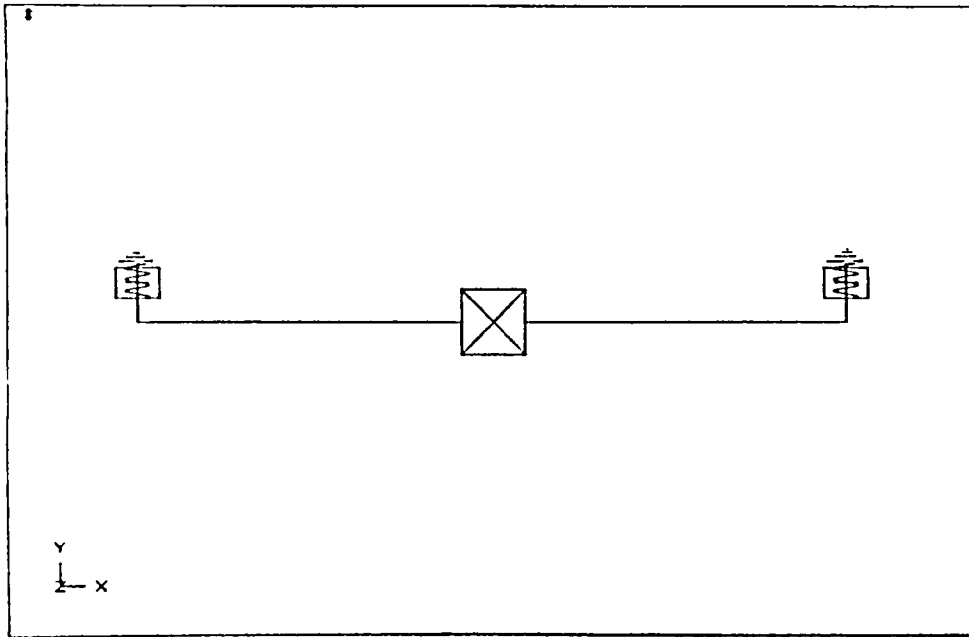
FIGURE 14. SCHEMATIC OF FLEXIBLE SPACECRAFT WITH COLLOCATED SENSOR AND
ACTUATOR AND PD-CONTROL.

Table 3. Listing of damping ratios and natural frequencies for flexible
satellite with collocated sensors and actuators and PD control.

MODE NO.	DAMPING RATIO	NATURAL FREQ. (HZ)	DESCRIPTION
1	1.99E-01	9.99E-01	spacecraft pitch about CG
3	4.52E-02	6.57E+00	first symmetric appendage bending
5	1.13E-02	2.21E+01	first antisymmetric appendage bending
7	7.35E-03	4.04E+01	second symmetric appendage bending
9	3.57E-03	6.56E+01	second antisymmetric appendage bending
11	2.62E-03	1.13E+02	third symmetric appendage bending
13	1.91E-03	1.34E+02	third antisymmetric appendage bending

TIME DOMAIN
RESPONSE OF APPENDAGE TIP TO STEP INPUT

1X= 1.59E+00
1Y= 1.50E+00

2X= 2.11E+00
2Y= 7.28E-01

3X= 2.60E+00
3Y= 1.14E+00

4X= 3.06E+00
4Y= 9.22E-01

5X= 8.83E+00
5Y= 9.95E-01

ENTITY=FST2
UNITS=IN

1/ID= 1

APR2:11-2
DISPLACEMENT
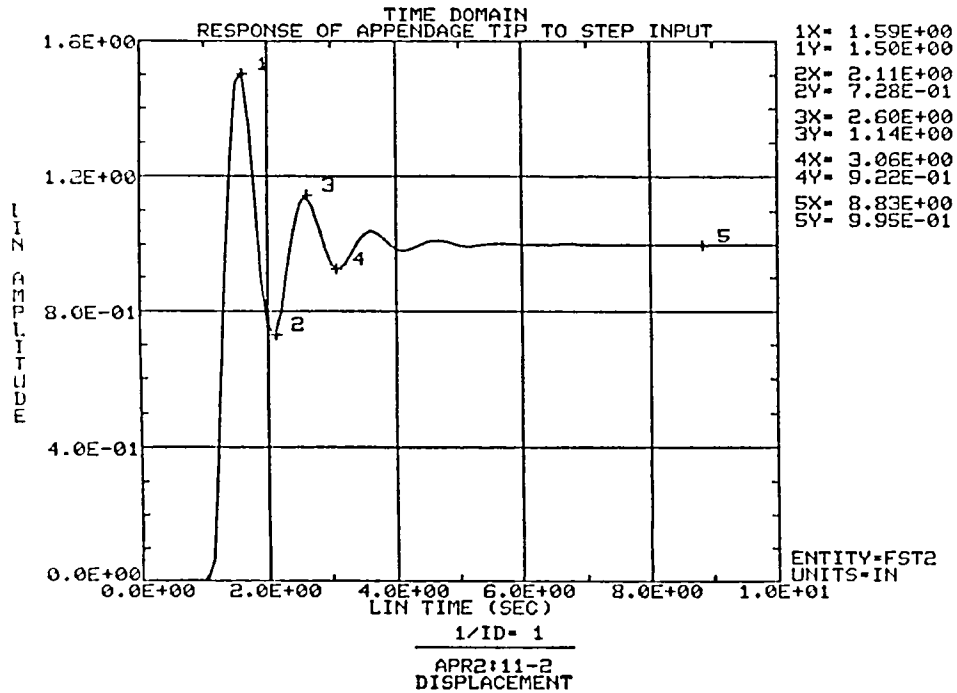
FIGURE 15. STEP INPUT RESPONSE OF THE APPENDAGE TIP OF PD-CONTROLLED
FLEXIBLE SPACECRAFT (COLLOCATED SENSOR AND ACTUATOR).
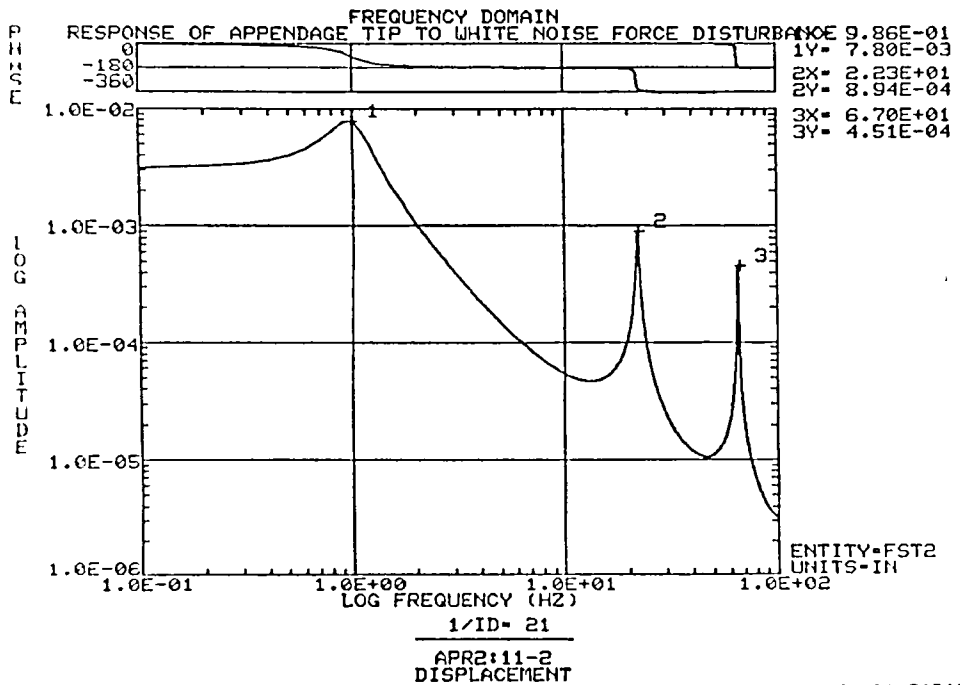
FREQUENCY DOMAIN
RESPONSE OF APPENDAGE TIP TO WHITE NOISE FORCE DISTURBANCE

1Y= 9.86E-01
1Y= 7.80E-03

2X= 2.23E+01
2Y= 8.94E-04

3X= 6.70E+01
3Y= 4.51E-04

ENTITY=FST2
UNITS-IN

1/ID= 21

APR2:11-2
DISPLACEMENT

FIGURE 16. FREQUENTLY DOMAIN RESPONSE OF APPENDAGE TIP OF FLEXIBLE SPACECRAFT
TO A WHITE NOISE FORCE DISTURBANCE (COLLOCATED SENSOR AND ACTUATOR).

60

ATTITUDE CONTROL TRADEOFF STUDY BETWEEN THE USE OF A FLEXIBLE BEAM AND A TETHER CONFIGURATION FOR THE CONNECTION OF TWO BODIES IN ORBIT

S. H. Graff
Jet Propulsion Laboratory
California Institute of Technology
Pasadena, CA 91109

ABSTRACT

Sometimes it is necessary to mount a payload remotely from the main body of a spacecraft or space station. The reasons for this vary from vibration isolation to avoidance of measurement contamination. For example the SP-100 project, which grew out of the increased interest in nuclear power in space for space stations and for deep space explorations, requires separation of the nuclear reactor from the user because of vibration, heat and radiation.

This paper addresses the different attitude control problems for beam and tether configurations. The beam configuration uses a conservative design approach. The vibration, beam flexibility and deployment concerns are analyzed. The tether configuration offers some very attractive design features, but not without several thorny problems. These problems are analyzed in this paper. One configuration will be recommended for the main thrust of the SP-100 design effort based on attitude control considerations.

I. INTRODUCTION

Abundant electrical power is a vital ingredient in our progress in space. This power is needed for large communication and navigation satellites, space stations, and exploration of the solar system.

The SP-100 nuclear space power system is nominally a 100 kW_e power source for applications which require high power and long life. The preliminary set of requirements calls for continuous power delivery for a period of seven years.

SP-100 requires an attitude control development to insure proper utilization of the current and future technology. Total integration of all the system components by JPL requires a design concept for each subsystem which can be used to compare, critique, and assess various designs. The attitude control requirements include high reliability, tolerance of high radiation levels, tolerance of large temperature variations, long system and component lifetimes, the ability to withstand vibrations from rotating and reciprocating machinery, and unique user requirements.

This paper assesses the technology available in the areas of articulation, deployment, dynamics and control of beams and tethers, attitude control constraints, and the hardware commonality. The final conclusions and recommendations provide ideas and rationale for the future efforts.

II. BEAM DYNAMICS AND CONTROL

The SP-100 system may be visualized, as shown in Figure 1, as two bodies B_1 and B_2 connected by a flexible truss B_3, and in orbit around the earth. B_1 is the power generating unit and may or may not be more massive than B_2. Depending on the precise type of power generation system adopted, B_1 may carry rotating or reciprocating machinery as well as working fluids.
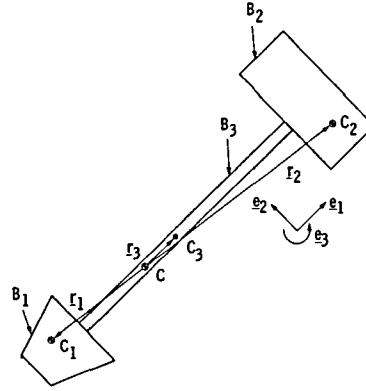
Figure 1:   The SP-100 System

Rigid Body Formulation

General Configuration

As a first step in the modeling of the SP-100, the system will be assumed to comprise two rigid bodies B_1 and B_2 connected by a rigid rod B_3, as shown in Figure 1. The properities m_i and $\underline{I}_i$ represent respectively the mass of body B_i, and the inertia dyadic of body B_i for its center of mass C_i.

The angular momentum of the system may be written as

$$\underline{H} = (\underline{I}_1 + \underline{I}_2 + \underline{I}_3) \cdot \underline{\omega} + \sum m_i \underline{r}_i \times (\underline{\omega} \times \underline{r}_i) \tag{1}$$

where $\underline{\omega}$ is the angular velocity of any of the bodies, and $\underline{r}_i$ is the position vector of C_i with respect to the center of mass C of the whole system. If

$$\underline{I} = \underline{I}_1 + \underline{I}_2 + \underline{I}_3 \tag{2}$$

then

$$\underline{H} = \underline{I} \cdot \underline{\omega} + \sum m_i \underline{r}_i \times (\underline{\omega} \times \underline{r}_i) \tag{3}$$

and

$$\underline{\dot{H}} = \underline{I} \cdot \underline{\dot{\omega}} + \underline{\omega} \times \underline{I} \cdot \underline{\omega} + \sum \{ m_i \underline{r}_i \times (\underline{\dot{\omega}} \times \underline{r}_i) + m_i \underline{r}_i \times [\underline{\omega} \times (\underline{\omega} \times \underline{r}_i)] \} \tag{4}$$

or

$$\dot{\underline{H}} = I \cdot \dot{\underline{\omega}} + \underline{\omega} \times I \cdot \underline{\omega} + \sum m_i \{-\underline{r}_i \times (\underline{r}_i \times \dot{\underline{\omega}}) - \underline{\omega} \times [\underline{r}_i \times (\underline{r}_i \times \underline{\omega})]\} \qquad (5)$$

If matrix formulation is desired, the unit vectors $\underline{e}_1$, $\underline{e}_2$, $\underline{e}_3$, are written as a vector array

$$\{e\} = \begin{bmatrix} \underline{e}_x \\ \underline{e}_y \\ \underline{e}_z \end{bmatrix} \qquad (6)$$

and matrices $\dot{H}$, ω, r_i, and I_i are defined as follows:

$$\underline{H} = \{\underline{e}_x \ \underline{e}_y \ \underline{e}_z\} \begin{bmatrix} H_x \\ H_y \\ H_z \end{bmatrix} = \{\underline{e}\}^T \dot{H} \qquad (7)$$

$$\underline{\omega} = \{\underline{e}_x \ \underline{e}_y \ \underline{e}_z\} \begin{bmatrix} \omega_x \\ \omega_y \\ \omega_z \end{bmatrix} = \{\underline{e}\}^T \omega \qquad (8)$$

$$\underline{r}_i = \{\underline{e}_x \ \underline{e}_y \ \underline{e}_z\} \begin{bmatrix} r_{ix} \\ r_{iy} \\ r_{iz} \end{bmatrix} = \{\underline{e}\}^T r_i \qquad (9)$$

and

$$I_i = \begin{bmatrix} I_{ix} & I_{ixy} & I_{ixz} \\ I_{ixy} & I_{iy} & I_{iyz} \\ I_{ixz} & I_{iyz} & I_{zz} \end{bmatrix} \qquad (10)$$

The matrix equivalent of Equation (5) then becomes

$$\dot{H} = I\dot{\omega} + \tilde{\omega}I\omega + \sum m_i \ (-\tilde{r}_i \tilde{r}_i \omega - \tilde{\omega}\tilde{r}_i \tilde{r}_i \omega) \qquad (11)$$

where the tilde ($\sim$) sign implies the cross operator; for example

$$\tilde{\omega} = \begin{bmatrix} 0 & -\omega_z & \omega_y \\ \omega_z & 0 & -\omega_x \\ -\omega_y & \omega_x & 0 \end{bmatrix}$$

Defining

$$I'_i = I_i - m_i \tilde{r}_i \tilde{r}_i \tag{12}$$

and

$$I' = I'_1 + I'_2 + I'_3 \tag{13}$$

Equation (11) could be written in the more compact and familiar form

$$\underline{H} = I'\omega + \tilde{\omega}I'\omega = M \tag{14}$$

where M is a column vector whose elements are the components of the moment about the system mass center C of the resultant force on the system. Equation (14), supplemented with appropriate kinematical equations and control equations, may be used for the simulation of the motion of the system.

Symmetric Configuration

Real engineering systems of this type usually possess some amount of symmetry. In the specific case of SP-100, it is not unreasonable to assume, for example, that the axis of the rod B_3 passes through all mass centers, and that lines parallel to $\underline{e}_1$, $\underline{e}_2$, and $\underline{e}_3$ are centroidal principal axes for each of the bodies. The equations of motion in this case still have the form of Equation (14); however, the expression for I' is much simpler. For three axis stabilized systems, like the SP-100, it is customary and reasonable to further

assume that $\underline{\omega}$ is small so that the $\tilde{\omega}I'\omega$ term in Equation (14) drops out, leading to the simple decoupled equations

$$\dot{\omega}_x = M_x/I_x$$
$$\dot{\omega}_y = M_y/I_y \qquad (15)$$
$$\dot{\omega}_z = M_z/I_z$$

Flexibility Considerations

Model Description

Once the rigidity assumption of the previous section is discarded, the difficulty becomes one of modeling a system which now includes a flexible beam between two rigid bodies. Several approaches to the analysis of flexible vehicles are treated in references [1] through [4]. When the ultimate aim is to arrive at equations of motion for computer simulation, the dynamical equations must be in a form which facilitates coordinate truncation. This truncation is necessary so that system deformation may be represented by a finite number of "modal" coordinates.

The approach adopted in this study is the hybrid coordinate method of Likins [2]. This method is most useful when portions of an otherwise rigid vehicle undergo deformations that may be reasonably assumed to remain "small." For an efficient use of this method, the SP-100 is modeled, as shown in Figure 2, as a rigid body B_1 with a linearly elastic flexible appendage A. B_1 is taken to be the more massive of the two end masses of the real system, and the other end mass together with the flexible beam constitute the appendage A. Should B_2 be the larger mass, then it would be regarded as rigid and the remainder of the system considered as a flexible appendage.

Appendage Motions Equations

Consider the system in some general configuration depicted in Figure 2. The appendage A undergoes "small" deformations relative to the base B_1, while the motion of B_1 is arbitrary. A is now idealized as a collection of n elastically interconnected discrete rigid sub-bodies, A_s being one such sub-body. Damping is ignored at this point; it will be incorporated
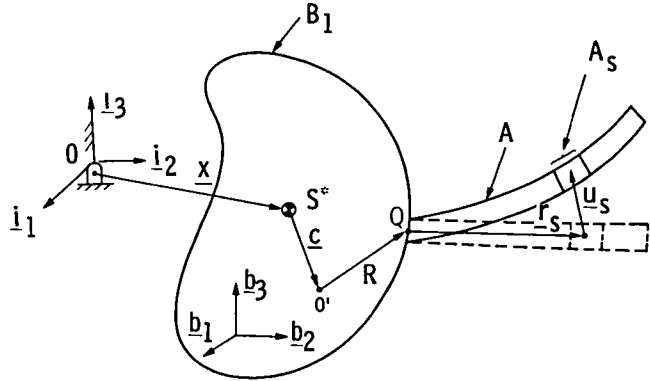
Figure 2: The Flexible Beam Model

in the model at a later stage with the introduction of modal coordinates. The dotted lines in Figure 2 show the position of A before deformation; point 0 is fixed in inertial space, S* is the system mass center, and 0' is the location of S* when the system was undeformed, and is therefore fixed in B_1.

For the sub-body A_s,

$$\underline{F}_s = m_s \underline{\ddot{p}}_s \tag{16}$$

where $\underline{F}_s$ is the resultant force on A_s, m_s is its mass, and $\underline{p}_s$ is the position vector of the center of mass of A_s relative to 0. On the other hand, it is clear from the figure that

$$\underline{p}_s = \underline{X} + \underline{C} + \underline{R} + \underline{r}_s + \underline{u}_s \tag{17}$$

where

$\underline{X}$ is the vector from 0 to S*

$\underline{C}$ is the position vector of 0' relative to S*

$\underline{R}$ is the vector from 0' to a point Q fixed in B_1

$\underline{r}_s$ vector goes from Q to the location of the mass center of

A_s in the undeformed configuration, and

$\underline{u}_s$ is the position vector of the mass center of A_s relative

to its location in the undeformed configuration.

Hence

$$\underline{F}_s = m_s(\underline{\ddot{X}} + \underline{\ddot{C}} + \underline{\ddot{R}} + \underline{\ddot{r}}_s + \underline{\ddot{u}}_s) \tag{18}$$

Column matrices X, C, R, r_s, and u_s are now defined as follows

$$\underline{X} = \{\underline{i}_1 \ \underline{i}_2 \ \underline{i}_3\} \begin{bmatrix} X_1 \\ X_2 \\ X_3 \end{bmatrix} = \{\underline{i}\}^T X \tag{19}$$

$$\underline{C} = \{\underline{b}_1 \ \underline{b}_2 \ \underline{b}_3\} \begin{bmatrix} C_1 \\ C_2 \\ C_3 \end{bmatrix} = \{\underline{b}\}^T C \tag{20}$$

$$\underline{R} = \{\underline{b}_1 \ \underline{b}_2 \ \underline{b}_3\} \begin{bmatrix} R_1 \\ R_2 \\ R_3 \end{bmatrix} = \{\underline{b}\}^T R \tag{21}$$

$$\underline{r}_s = \{\underline{b}_1 \ \underline{b}_2 \ \underline{b}_3\} \begin{bmatrix} r_{s1} \\ r_{s2} \\ r_{s3} \end{bmatrix} = \{\underline{b}\}^T r_s \tag{22}$$

$$\underline{u}_s = \{\underline{b}_1 \ \underline{b}_2 \ \underline{b}_3\} \begin{bmatrix} u_{s1} \\ u_{s2} \\ u_{s3} \end{bmatrix} = \{\underline{b}\}^T u_s \tag{23}$$

It then becomes possible to write Equation 18 in matrix form as

$$F_s = m_s \ [\Lambda\ddot{X} + \ddot{C} + 2\tilde{\omega}\dot{C} + \tilde{\omega}\tilde{\omega}(C+R) - (\tilde{C}+\tilde{R})\dot{\omega} - (\tilde{r}_s + \tilde{u}_s)\dot{\omega} + \tilde{\omega}\tilde{\omega}(r_s + u_s)$$

$$+ 2\tilde{\omega}\dot{u}_s + \ddot{u}_s] \tag{24}$$

where Λ is the transformation matrix between the $\underline{i}$ and $\underline{b}$ bases given by

$$\{\underline{i}\}^T = \{\underline{b}\}^T \Lambda \tag{25}$$

The matrix C represents the motion of the system mass center in B_1, and may be shown to be given by

$$C = - \sum_s \mu_s u_s \tag{27}$$

where $\quad \mu_s = m_s / (\sum m_s)$ $\qquad\qquad\qquad$ (28)

Equation (27) and its time derivatives may be substituted into Equation (24) to give

$$F_s = m_s [\Lambda \ddot{X} + \ddot{u}_s - \sum \mu_k \ddot{u}_k + 2 \tilde{\omega} (u_s - \sum \mu_k u_k) - (\tilde{R} + \tilde{r}_s) \dot{\omega} + \dot{\tilde{\omega}} (u_s - \sum \mu_k u_k)$$
$$+ \tilde{\omega} \tilde{\omega} (R + r_s + u_s - \sum \mu_k u_k)] \tag{29}$$

The equations of rotational motion of A_s are obtained by equating the resultant external torque on A_s to the time rate of change of its inertial angular momentum. Since the rotation of A_s relative to B_1 is due only to "small" structural deformations, this rotation can be represented by the vector

$$\underline{\beta}_s = \beta_{s1} \underline{b}_1 + \beta_{s2} \underline{b}_2 + \beta_{s3} \underline{b}_3 \tag{30}$$

where β_{s1}, β_{s2} β_{s3} are three angles of rotation about the orthogonal axes $\underline{b}_1$, $\underline{b}_2$, $\underline{b}_3$. Hence, the angular velocity matrix ω_s of A_s takes the form

$$\omega_s = \omega + \{ \underline{b} \}^T \dot{\beta}_s \tag{31}$$

Finally, the equations of attitude motion of A_s can be put in the form

$$T_s = I_s (\dot{\omega} + \ddot{\beta}_s) + [I_s \tilde{\omega} + \tilde{\omega} I_s - (\widetilde{I_s \omega})] \dot{\beta}_s + \tilde{\omega} I_s \omega + [I_s \dot{\tilde{\omega}} - (\widetilde{I_s \dot{\omega}}) - \tilde{\omega} (\widetilde{I_s \omega}) + \tilde{\omega} I_s \tilde{\omega}] \beta_s \tag{32}$$

where

T_s is the resultant torque matrix

and I_s is the centroidal inertia matrix of A_s.

For a three-axis stabilized system, Equations (29) and (32) may be linearized in ω. They then reduce respectively to

$$m_s (\ddot{u}_s - \sum \mu_k \ddot{u}_k) = - m_s \Lambda \ddot{X} + (\tilde{R} + \tilde{r}_s) \dot{\omega} + F_s \tag{33}$$

and

$$I_s \ddot{\beta}_s = - I_s \dot{\omega} + T_s \tag{34}$$

Vehicle Motion Equations

Equations (33) and (34) are not sufficient for the complete description of the motions of our system. They will now be supplemented with the dynamical equations of the whole vehicle.

The vehicle translational equation is

$$\underline{F} = m \underline{a}^{s*} \tag{35}$$

where F is the resultant external force on the whole vehicle, m is the total mass, and $\underline{a}^{s*}$ is the acceleration of the system mass center. The matrix form of Equation (35) is

$$F = m\Lambda\ddot{X} \tag{36}$$

and the rotational equations for small ω can be written in the compact form

$$T = I^*\dot{\omega} + \tilde{R}\sum m_s\ddot{u}_s + \sum \tilde{r}_s m_s\ddot{u}_s + \sum I_s\ddot{\beta}_s \tag{37}$$

where I^* is the inertia matrix of the undeformed vehicle for the point $0'$ of Figure 3. A comparison of Equations (15) and (37) indicates that the effects of beam flexibility are contained in the last three terms on the right hand side of Equation (37). Equations (33), (34), (36), and (37) form a set of 6n+6 scalar equations with X, Λ, ω, u_s and β_s (6n+9 in number) as unknowns. And together with a set of kinematical equations relating Λ and ω, and control equations, they are sufficient for the simulation of the motions of the system.
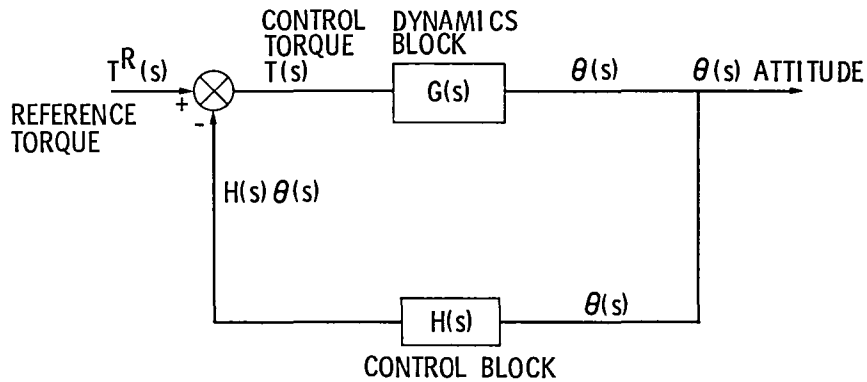
Figure 3: The Control Block Diagram

Modal Truncation

The difficulty with the equations mentioned above is simply their dimension due mainly to the appendage equations whose number is directly proportional to n. The objective in this subsection is to attempt a reduction

70

of the dimension of the equations of motion through some type of coordinate truncation. This naturally involves the introduction of a linear transformation for at least some of the variables, and this transformation must give rise to decoupled equations so as to permit valid truncation. Here, such a transformation is applied to the appendage deformation coordinates only. First, the appendage deformation coordinates are organized into a coordinate matrix q defined as

$$q = [u_1^1 \; u_2^1 \; u_3^1 \; \beta_1^1 \; \beta_2^1 \; \beta_3^1 \; u_1^2 \; u_2^2 \; u_3^2 \; \beta_1^2 \; \beta_2^2 \; \beta_3^2 \; \ldots \; \beta_3^n]^T \tag{38}$$

Because the appendage Equations (33) and (34) are linearized in the deformation coordinates u_s and β_s, these equations can be written in matrix form as

$$M'\ddot{q} + D'\dot{q} + K'q = L' \tag{39}$$

By inspection of Equations (33) and (34), it becomes evident that M' is a constant symmetric matrix. F_s and T_s in Equations (33) and (34) include structural interaction forces and torques between neighboring sub-bodies of A. These interactions may be visualized as linearly elastic and viscous forces and torques that are proportional to the deformation and deformation rates. Hence D' and K' are also constant matrices; all the damping coefficients go into D' and all the stiffnesses go into K'. L' depends on Λ, $\ddot{X}$, and the external applied forces and torques that may appear in F_s and T_s.

Classical modal analysis techniques can be applied to our system by first ignoring damping and considering

$$M'\ddot{q} + K'q = L' \tag{40}$$

This leads to the choice of the normal-mode transformation

$$q = \phi\eta \tag{41}$$

which in turn transforms Equation (39) into

$$\ddot{\eta} + 2\zeta\sigma\eta + \sigma^2\eta = \phi^T L' \tag{42}$$

where η is the column matrix of modal coordinates, σ and ζ are diagonal matrices of natural frequencies and damping ratio, and ϕ is the modal matrix. Equations (42) are now decoupled and may be truncated to a convenient size. If $\bar{\eta}$ is the truncated form of η, the appendage equations now take the form

$$\ddot{\bar{\eta}} + 2\zeta\dot{\bar{\eta}} + \sigma^2\bar{\eta} = \phi^T L' \tag{43}$$

Depending on the number of "modes" retained, this truncated form of the

appendage equations, together with the vehicle equations could constitute a much smaller set of dynamical equations, and therefore much cheaper to integrate on a computer.

Effects of Rotating and/or Reciprocating Machinery

Rigid Formulation

The addition of a rotating element to one of the main bodies of the system introduces a slight change in the equations of attitude motion. For example, let us examine the case of Figure 1 where the connecting rod between B_1 and B_2 is assumed to be rigid, and body B_1 contains a rotor. If this added rotor is axisymmetric, then B_1 is a gyrostat and the system angular momentum is augmented by a term h which represents the angular momentum of the rotor relative to the basebody B_1. Equation (15) then has the matrix form

$$T = I\dot{\omega} + \dot{h} - \tilde{h}\omega \qquad (44)$$

which now includes a "gyroscopic stiffness" term. Hence, the motion of an axisymmetric rotor in B_1 does affect vehicle motion. The importance of this effect depends on the inertia of the rotor, and its spin rate relative to the basebody B_1. If the rotor mass center is offset from the spin axis, the system's dynamics is further complicated by the appearance of new terms involving this offset.

Flexible Body Formulation

In the case of a flexible beam, the presence of a rotor on body B_1 can affect both the appendage equations and the vehicle equations. The appendage equations can only be affected through the column vector C (see Equation (24)) which represents the motion of the system mass center in body B_1. If the rotor is axisymmetric, then the location of the system mass center is not modified by the motion of the rotor, and hence, the appendage equations remain unchanged. This means that the procedure and results of the coordinate matrix truncation are unaffected by the motion of a symmetric rotor in B_1. However, the vehicle equations change slightly because the expression for the angular

72

momentum of the system is modified by the presence of the rotor. The vehicle equation of rotational motion becomes

$$T = I^* \dot{\omega} + \dot{\tilde{h}} - \tilde{h}\omega + \tilde{R} \quad m_s \ddot{u}_s + \sum I_s \ddot{\beta}_s + \sum \tilde{r}_s m_s \ddot{u}_s \qquad (45)$$

The first term on the right hand side of Equation (45) is the rigid body term. It is the only term that would remain if the whole system were one rigid body. The second and third terms are due to the presence of the rotor, and the last three terms are contributions from the system's flexibility.

If the rotor mass center is not located on the spin axis, the rotor's motion will affect the location of the system mass center. That is, the appendage equations will be impacted through the C matrix, and the modal analysis technique used above breaks down because D' and K' are no longer constant matrices.

Control System

Since our system is three-axis stabilized, the elements of the matrix ω are small, and we can let

$$\omega = \dot{\theta} \qquad (46)$$

where
$$\theta = [\theta_1 \ \theta_2 \ \theta_3]^T \qquad (47)$$

and θ_1, θ_2, θ_3 are vehicle rotation angles. If our interest, from controls point of view, is limited to θ, it will be necessary to display clearly the relationship between the control torque T and the rotation angle θ. As a simple example, we consider the case of negligible external force and torque on the appendage. System equations may then be reduced to

$$T = I^* \ddot{\theta} - \delta^T \ddot{\eta} \qquad (48)$$

and
$$\ddot{\eta} + 2\zeta\sigma\dot{\eta} + \alpha^2\bar{\eta} = \delta\ddot{\theta} \qquad (49)$$

The Laplace transform of these equations yields

$$T(s) = s^2 I^* \theta(s) - \delta^T s^2 \bar{\eta}(s) \qquad (50)$$

and
$$s^2\bar{\eta}(s) + 2s\zeta\sigma\bar{\eta}(s) + \bar{\sigma}^2\bar{\eta}(s) = s^2\delta\theta(s) \qquad (51)$$

Equations (50) and (51) can be combined to give

$$\theta(s) = [sI^* - s^4\delta^T D\delta]^{-1} T(s) \qquad (52)$$

where D is a diagonal matrix given by

73

$$D = \begin{bmatrix} \dfrac{1}{s^2+2\zeta_1\sigma_1 s+\sigma_1^2} & & 0 \\ & \dfrac{1}{s^2+2\zeta_2\sigma_2 s+\sigma_2^2} & \\ 0 & & \dfrac{1}{s^2+2\zeta_N\sigma_N s+\sigma_N^2} \end{bmatrix} \tag{53}$$

In the special case when the coordinate truncation is carried down to a single modal coordinate, Equation (52) becomes

$$\Theta(s) = \frac{1}{s^2}\left[I^* - s^2\delta^1 T_\delta 1 \left(\frac{1}{s^2+2\zeta\ \sigma\ s+\sigma^2}\right) \right]^{-1} T(s) \tag{54}$$

A block diagram representation of this control system is shown in Figure 3. If it is further assumed that dynamic response in this single mode representation influences vehicle response about one axis only, and that the inertia matrix I^* is diagonal, then the dynamics block of Figure 3 can be expressed as

$$G(s) = \left[I^*_\alpha s - \frac{s^4(\delta^1_\alpha)^2}{(s^2+2\zeta_1\sigma_1 s+\sigma_1^2)} \right]^{-1} \tag{55}$$

where α is the single axis considered. This expression can eventually be put in the form

$$G(s) = \frac{s^2+2\zeta_1\sigma_1 s+\sigma_1^2}{I^*_\alpha s^2(s^2 E+2\zeta_1\sigma_1 s+\sigma_1^2)} \tag{56}$$

where

$$E = 1 - \frac{(\delta^1_\alpha)^2}{I^*_\alpha} \tag{57}$$

In the case of simple gain control,

$$H(s) = K \text{ (constant)} \tag{58}$$

74

and the characteristic equation becomes

$$s^4(I^*_\alpha E) + s^3(2I^*_\alpha \zeta_1 \sigma_1) + s^2(I^*_\alpha \sigma_1^2 + K) + s(2K\zeta_1\sigma_1) + K\sigma_1^2 = 0$$

An examination of the Routhian array for this system indicates asymptotic stability for positive K.

Findings

The formulation of equations of motion for the SP-100 system could be described as complete. If the connecting structure of the system is assumed to be rigid, the equations of motion are very simple and decoupled. When the flexibility of the structure is taken into account, the system is modeled as a main rigid body with an attached flexible appendage, the other rigid body being assimilated into the appendage. Furthermore, the appendage is modeled as a system of elastically interconnected rigid sub-bodies. The complete dynamical equations of the system are then composed of the appendage equations together with the complete vehicle equations. Truncation of these equations is achieved through modal analysis of the appendage equations. These reduced dynamical equations can then be completed with kinematical and control equations for the purposes of vehicle motion simulation.

When the basebody contains a perfectly axisymmetric rotating or reciprocating sub-body, the effects of the motion of such a rotor are easily accommodated in the analyses presented because they are decoupled from flexibility effects.

A preliminary analysis of the control system using the extreme example of single axis response of an appendage represented by a single modal coordinate, with simple gain control, reveals asymptotic stability in every case.

III. TETHER CONFIGURATION

Extensive work has been done in the dynamics and control of space vehicles. The initial efforts by NASA in the early days of Gemini studied the dynamics and control of short tethers (order of 100 m) to provide gravity

gradient stabilization and spin induced gravity. These activities were accomplished both in orbit and in simulations. Recent efforts have surfaced with emphasis on the uses of long tethers primarily due to the better understanding of the dynamics pioneered by the late Professor Colombo of the Smithsonian Astrophysical Observatory. These efforts have initiated interest in many universities and laboratories to better understand the simulations. The recent emphasis has centered around the new missions that have become better understood since the new dynamical modeling has been discussed in the literature.

Currently, NASA is investigating the concepts of tethers that relate to the Earth resources or Earth oriented activities. The new ideas of gravity gradient induced gravitational forces for manned activities (about 0.1 g), of "free" altitude additions from "spare" masses provided to the shuttle orbits, and of scientific measurements in the upper atmosphere from medium orbits of the orbiters have created much interest in the earth resources and space sciences community.

Two joint U.S.-Italian missions scheduled for 1987 and 1988 will demonstrate the feasibility and benefits of tethered satellite systems deployed from the shuttle orbiter. The tether will be a flexible metallic or synthetic line, 1-2 mm in diameter and 100 Km or more in length, carrying a total payload mass of 500 Kg. Because of the differences in environmental parameters at the outer planets, (such as gravity and aerodrag) the requirements and characteristics of tethers will vary from the above Earth oriented missions. Furthermore, current work on tether dynamics and controls are relatively immature. It is timely to verify the tether concept for applications to future planetary, earth resources, and military missions.

The SP-100 program has two major areas for potential benefit and two areas of smaller potential for future utilization of tether technology. The major aspects of tether technology that apply to SP-100 are 1) radiation attenuation and 2) disturbance isolation. The two ancillary aspects of the tether technology are 1) the ability to provide gravitational fields and 2)

the adjustment capability for attitude control without the use of propellants. These benefits will be discussed further. The concept of tethers and their applications in space have recently identified potential applications to both Earth and interplanetary missions. Notably, tethers can provide unique techniques for scientific measurements. By using a constellation of tethered satellites, simultaneous sampling and multiple measurements of electromagnetic and atmospheric characteristics at stereographic observations, sample retrieval of low altitude atmospheric gases of a planet, such as Jupiter, or a fly-by comet can be easily accomplished across multiple locations. Tethers also provide the option of using less fuel for maneuvers such as spacecraft insertion, orbit adjust, and science probe injection towards planets.

Several representatives of the SP-100 project attended the NASA sponsored Tether Workshop in Williamsburg, Virginia in June 1983 (see reference [6]). Their participation in the Tether Workshop resulted in a better understanding of the current technology and programmatic paths. The emphasis was related to Earth oriented activities and rarely investigated the possibilities of interplanetary activities. A major conclusion from this Tether Workshop was that the modeling of the dynamics and control of orbiting tethers must be investigated thoroughly. The current models vary in assumptions, in structure, and sometimes in conclusions.

The initial assessment of the dynamics and control of tether satellite systems has shown that there are four potential benefits.

(a) Radiation Attenuation: An increase in tether length (r) decreases the amount of shield area to protect a satellite safety zone by a rate of $1/r^2$. A tether on the order of 10 km might render shielding totally unnecessary. See Table 1.

Table 1. Tether Length and Radiation Shield Requirements

Tether Length (M)	Angle for a 500 M diameter Safety Zone	Shield Radius(M)	Shield Area(M^2)
25	84.2	10.0	314.0
50	78.8	5.0	78.5
75	73.3	3.3	34.9
100	68.2	2.5	19.6
250	45.0	1.0	3.1
500	26.6	0.5	0.8

Note: The shield mass is proportional to the shield area.

(b)   Vibration Isolation: A tether system will provide the ability to attenuate vibrations through the use of a tether with very little or no transmission of shear forces. This provides a protection from vibration that must be studied to quantify the effect.

(c)   Gravity Field: The stable tether system will rotate once during each orbit. This slow rotation and long tether length (moment arm) will provide a small amount of artificial gravity through centrifugal force. This could have significant safety implications for the reactor.

(d)   Attitude Adjustment: By placing the center of mass around the attachment point, fine adjustments can be achieved of the attitude of the satellite. This can be accomplished with electromechanical devices instead of costly propellant usage.

IV. COMMONALITY

When the reactor is operational the radiator temperature may be as high as 900° K; when the reactor is shut down, the electronics will need heaters. The electronics temperature range which has been selected is the same as for

78

the Galileo Project, which is from 273° to 328° K with qualification limits at 253° to 348°K.

The potential of propellant line freezing combined with the propellant line deployment problems has led to the decision that each subsatellite, whether deployed by a beam or tether, should have its own set of propellant tanks, propellant lines and thrusters. However, the complete spacecraft will have only one attitude control subsystem.

Since large amounts of electrical power are available, attitude control should emphasize reaction wheels, control moment gyros, magnetic torquers, rather than thrusters as primary devices. Table 2 shows the possible primary effectors and sensors for various mission orbits and trajectories. Magnetic torquers and gravity gradient are viable contenders for the primary system only in low planetary orbits. The exact choice of effectors and sensors depends on mission requirements and further investigation of the SP-100 design.

TABLE 2: Control Implementation

	LOW ORBIT	HIGH ORBIT	HIGHLY ELLIPTICAL ORBIT	INTERPLANETARY
THRUSTERS	X	X	X	X
GRAVITY GRADIENT	X			
MAGNETIC TORQUERS	X			
CONTROL MOMENT GYRO	X	X	X	X
REACTION WHEEL	X	X	X	X
MOMENTUM WHEEL	X	X	X	X
SUN SENSOR	X	X	X	X
STAR SENSOR	X	X	X	X
EARTH SENSOR	X	X	X	X

V. CONCLUSION

The deployable beam configuration uses an off-the-shelf item with a 20:1 expansion ratio. Thus a 25 meter beam uses slightly more than one meter of shuttle cargo bay length. The dynamics are well understood, although the power and attitude control cable deployment with the beam is a concern. This is a good conservative approach for today.

Tethers offer a low radiation user environment and vibration isolation. There are many advantages for applications of tethers which are harder to achieve with the beam configuration: radiation isolation, artificial gravity, and vibration isolation are three. While tether materials and fabrication need further study, this is a good approach for future space power applications. Tethers are not included in the baseline system at the present time; however, the study effort should continue to insure that the benefits could be incorporated if they fulfill their potential.

The following area are being developed futher:

In the beam dynamics area, the dynamics model will be put into a computer simulation. Further, modeling and subsequent incorporation into the simulation program are required to quantify:

1. the effects of fluid motion in the basebody on the dynamic behavior of the system;

2. the effects of rotating or reciprocating machinery in the base body, particularly when the rotating body is non-axisymmetric. This may lead to a strong coupling between the motion of the rotor and appendage deformations.

The controls work presented in this paper is very preliminary in the sense that the final results were restricted to a single mode representation and a single axis control. A generalization to several modes and three axes

control is needed. Furthermore, a decision on the exact location of sensors and effectors in the light of the existing constraints still has to be made; and this will have an impact on the final form of the control equations.

Tether dynamics and controls will be investigated further with an emphasis on application to the next generation SP-100.

VI. ACKNOWLEDGMENTS

The authors thank Dr. F. Eke, Dr. R. A. Laskin and P. A. Swan for their technical advice on dynamics, modal truncation and tethers.

VII. REFERENCES

[1]   Likins, P. W., "Dynamics and Control of Flexible Space Vehicles," JPL Technical Report 32-1329, 15 January 1970.

[2]   Likins, P. W., and Fleischer, G. E., "Results of Flexible Spacecraft Attitude Control Studies Utilizing Hybrid Coordinates," AIAA Journal of Spacecraft, Vol. 8, No. 3, 1971.

[3]   Williams, C.J.H., "Dynamics Modeling and Formulation Techniques for Non-Rigid Spacecraft," Proceedings of a Symposium on Dynamics and Control of Non-Rigid Spacecraft, Frascati, Italy, 24-26 May 1976.

[4]   Kane, T. R., Likins, P. W., and Levinson, D. A., Spacecraft Dynamics, McGraw Hill Book Company, 1983.

[5]   "Applications of Tethers in Space Workshop, Executive Summary", 15-17 June 1983.

SOME ASYMPTOTIC PROBLEMS IN THE OPTIMAL CONTROL OF DISTRIBUTED SYSTEMS

J. L. Lions
College de France
Chaire d'Analyse Mathématique des Systémes et de leur Contrôle
Paris, France
and
INRIA (Institut National de Recherche en Informatique et en Automatique)
B.P. 105, 78153 Le Chesnay Cedex, France

ABSTRACT

We consider the optimal control of structures which consist of composite materials or of perforated materials. Asymptotic formula, derived from the so-called homogenization theory, are presented which allow to "replace" very complicated problems by much simpler ones.

I. INTRODUCTION

Large space structures lead to very many new questions in the Optimal Control of Distributed Systems.

In this paper, we wish to concentrate on *some asymptotic problems*, where, it *could* happen that new methods currently available or in the process of development, could be of some practical interest.

More specifically, let us consider a *state equation given by*

$$A_\varepsilon(y_\varepsilon(v)) = \mathcal{B}v \tag{1.1}$$

where A_ε is a partial differential operator which depends on a "small" parameter ε ; we write (1.1.) in a formal fashion, i.e. without making precise the hypotheses on A_ε , neither the boundary conditions (nor the initial conditions if A_ε is an evolution operator). In (1.1) v denotes the control variable ; v can be a boundary control, or a pointwise control. We assume that (1.1) *admits a unique solution,* denoted by $y_\varepsilon(v)$[1]. Let the *cost function* be given, again formally, by

$$J_\varepsilon(v) = \phi(y_\varepsilon(v)) + \psi(v). \tag{1.2}$$

If $\mathcal{U}_{ad}$ denotes the set of admissible controls, we want to find

$$\inf J_\varepsilon(v), \quad v \in \mathcal{U}_{ad}. \tag{1.3}$$

Let u_ε be the (or a) solution of (1.3). *The problem we are interested in consists in finding the behaviour of* $\inf J_\varepsilon(v)$ *as* $\varepsilon \to 0$, *and also the behaviour of* u_ε. ∎

The general motivation for looking at problems of this sort is clear : we want to find an approximated problem, say a first order approximated problem, the

---

[1] For various applications, in particular in the field of Biochemistry, there is a great interest in studying the control of systems where this hypothesis *is not true* (these are the so-called *multi-state systems*). We refer to E.J.DOEDEL, M.C.DUBAN, G. JOLY & J.P.KERNEVEZ [1] , J.P.KERNEVEZ & J.L.LIONS [2] , J.L.LIONS [3] .

solution of which is simpler (and, hopefully, *much* simpler !) than the solution of the problem in its original formulation.

In what follows we are going to present some new examples of such situations.

We are going to consider the control of structures which consist of *composite materials* (sections 2 and 3 below) or of *perforated materials* (sections 4 and 5).

The general result will be of the following type : we shall find, in a constructive way, an operator $\mathcal{A}$ such that the state equation

$$\mathcal{A}y(v) = \mathcal{B}v \qquad (1.4)$$

"replaces" (in a much simpler way) equation (1.1) ; we shall also find a cost function

$$\mathcal{J}(v), \text{ function of } v \text{ and of } y(v) \text{ the solution of } (1.4) \qquad (1.5)$$

derived from $J_\varepsilon(v)$ (in a fashion which may not be entirely trivial ; cf. section 5), such that, as $\varepsilon \to 0$, one has

$$\inf J_\varepsilon(v) \, , \, v \in \mathcal{U}_{ad} \to \inf \mathcal{J}(v), \, v \in \mathcal{U}_{ad}. \qquad (1.6)$$

As we shall see the operator $\mathcal{A}$ (and the cost function $\mathcal{J}$) have to be computed (in the situations considered here) in a non trivial way ([1]).

The plan is as follows :

2. Composite materials. Stationary situations.
3. Composite materials. Problems of evolution.
4. Perforated materials (I).
5. Perforated materials (II).

The techniques used here are based on some general principles in the Asymptotic Calculus of Variations (cf. J.L. LIONS [4]) and on the asymptotic expansions for composite materials and perforated materials which are given for *periodic* structures in A. BENSOUSSAN, J.L. LIONS and G. PAPANICOLAOU [5] E. SANCHEZ-PALENCIA [6] (and the bibliography therein) and in J.L. LIONS [7].

In this paper, we explain, in a formal way, how the various formulas can be constructively computed. The complete proofs are not given here ; they will be presented in J.L. LIONS [8] Many open questions still remain ; some are indicated in this paper. In the framework of perforated materials, it is extremely interesting to study situations where one has *two* parameters : in the notations of Section 4, Fig. 2, it would correspond to an obstacle $\mathcal{O}_\mu$ depending on a *second* small parameter μ ([2]) ; one obtains then homogenized coefficients $q_{ij}(\mu)$ which are functions of μ, and one next looks for an asymptotic expansion of $q_{ij}(\mu)$. This is not presented here, because for the *control* of such structures many open questions remain ([3]).

Of course this paper is *not* a survey of "all" asymptotic methods which can be used in optimal control ! This would be an hopeless task, since, in principle at least, "all" asymptotic methods used in the *analysis* of physical problems can be adapted (of course with some new difficulties). Let us only mention here the possibility of using

---

([1]) Remark 5.2., section 5 below, gives an example where we conjecture that $\mathcal{U}_{ad}$ has to be replaced by another (non trivial) set $\hat{\mathcal{U}}_{ad}$.

([2]) This is in order to simplify structures called "carcasses" in G.P. PANACENKO [9].

([3]) For the *analysis* of such problems, without control, a book by N.C. BAHBALOV and G.P. PANACENKO [10] (not available to the A. at the time of writing) is to appear.

techniques of singular perturbations and of stiff problems.(Cf. J.L. LIONS [7]).
Asymptotic expansions for some of the Riccati's systems corresponding to problems
studied here are given in J.L. LIONS [11].

2. COMPOSITE MATERIALS. STATIONARY SITUATION.

Composite materials considered here are supposed to have *a periodic struc-
ture* ; they are, for instance, reinforced materials with fibers arranged in a per-
iodic way (in the so-called matrix). We suppose that the size of the period (which
is supposed to be the same along all directions, but this is just a matter of conv-
enience) is *small* compared with the size of the whole object we want to control.
This period will be denoted by ε.

In mathematical terms, an example (actually, a very simple example) can be
formulated as follows.

Let Ω be a bounded open set of $\mathbb{R}^3$, with smooth boundary Γ.

Let $Y =]0,1[^3$ and let us consider functions $a_{ij}(\xi)$ which are Y-periodic,
i.e. which have period 1 in all variables ξ_1, ξ_2, ξ_3. We suppose that these
functions are smooth (this is by no means compulsory !) and we assume that ([1])

$$a_{ij}(\xi)\lambda_i\lambda_j \geq \alpha \,\lambda_i\lambda_i \quad , \quad \alpha > 0, \; \forall \, \lambda_i \in \mathbb{R} \, , \; \forall \, \xi \in Y. \tag{2.1}$$

Let a_o be another Y-periodic function, such that

$$a_o(\xi) \geq \alpha_o > 0. \tag{2.2}$$

For every $\varepsilon > 0$ we define the *elliptic operator*

$$A_\varepsilon = - \frac{\partial}{\partial x_i} \left(a_{ij}(\tfrac{x}{\varepsilon}) \frac{\partial}{\partial x_j} \right) + a_o(\tfrac{x}{\varepsilon}) \, . \tag{2.3}$$

This operator models physical situations where one has a periodic composite
material ; for instance $a_{ij}(\xi)$ can be "large" on the fiber and "small" on the
matrix. ∎

For any given $\varepsilon > 0$, the *state of the system* will be given by $y_\varepsilon = y_\varepsilon(v)$,
the solution of

$$A_\varepsilon y_\varepsilon(v) = f \quad \text{in} \quad \Omega \, , \tag{2.4}$$

where f is given in $L^2(\Omega)$, subject to the Neumann boundary condition

$$\frac{\partial y_\varepsilon(v)}{\partial \nu_{A_\varepsilon}} = v \quad \text{on} \quad \Gamma. \quad ([2]) \tag{2.5}$$

([1]) We use the summation convention of repeated indices.

([2]) $\dfrac{\partial}{\partial \nu_{A_\varepsilon}} = a_{ij}(\tfrac{x}{\varepsilon}) \, \nu_i \, \dfrac{\partial}{\partial x_j}$, $\nu = \{\nu_i\} = $ normal to Γ directed towards the exterior

of Ω.

To fix ideas, let us assume that the *cost function* is given by

$$J_\epsilon(v) = \int_\Gamma (y_\epsilon(v) - z_d)^2 \, d\Gamma + N \int_\Gamma v^2 \, d\Gamma \qquad (2.6)$$

where z_d is given in $L^2(\Gamma)$ and where N is given >0.

The problem is then to find

$$\left| \begin{array}{l} \inf J_\epsilon(v) \ , \\[6pt] v \in U_{ad} \end{array} \right. \qquad (2.7)$$

where

$$U_{ad} = \text{closed convex subset of } L^2(\Gamma). \qquad \blacksquare \qquad (2.8)$$

The difficulty of the problem lies in the computational aspects of (2.7), i.e in the computational difficulties of $y_\epsilon(v)$ when ϵ is small compared to the size of Ω . Indeed any approximation, should it be by difference or finite element methods, will have to take into account the complicated composite structure of the material and will lead to very large linear algebraic systems.

This is a well known difficulty met in all composite structures.

A method to turn this difficulty, at least in part, is to seek for an *asymptotic expansion* of $y_\epsilon(v)$ and of $J_\epsilon(v)$, as explained in the Introduction. $\blacksquare$

Let us explain the result one can obtain along these lines, making things more precise step by step.

As we shall see below, there exists a so-called *homogeneous operator* $\mathcal{A}$, which is a second order elliptic operator with constant coefficients :

$$\left| \begin{array}{l} \mathcal{A} = -q_{ij} \dfrac{\partial^2}{\partial x_i \partial x_j} + q_o \\[12pt] q_{ij} \ , \ q_o = \text{constants to be computed below,} \end{array} \right. \qquad (2.9)$$

such that, for fixed v , one has, as $\epsilon \to 0$,

$$\left| \begin{array}{l} y_\epsilon(v) \to y(v) \quad \text{in } L^2(\Omega) \ , \\[10pt] \dfrac{\partial y_\epsilon(v)}{\partial x_i} \to \dfrac{\partial y(v)}{\partial x_i} \text{ in } L^2(\Omega) \quad \text{weakly} \end{array} \right. \qquad (2.10)$$

where

$$\left| \begin{array}{l} \mathcal{A} \, y(v) = f \quad \text{in } \Omega, \\[10pt] \dfrac{\partial y(v)}{\partial \nu} = v \quad \text{on } \Gamma. \end{array} \right. \qquad (2.11)$$

There one considers the cost function

$$\mathcal{J}(v) = \int_\Gamma (y(v) - z_d)^2 \, d\Gamma + N \int_\Gamma v^2 \, d\Gamma \qquad (2.12)$$

and the new problem

86

$$\inf_{v \in \mathcal{U}_{ad}} \mathcal{J}(v) \qquad\qquad (2.13)$$

One can show that, as $\varepsilon \to 0$, *problem* (2.7) *converges towards problem* (2.13). ∎

Remark 2.1

More precisely, if u_ε (resp. u) is the optimal control for (2.7) (resp. (2.13)) , then $u_\varepsilon \to u$ in $L^2(\Gamma)$, and

$$J_\varepsilon(u_\varepsilon) \to \mathcal{J}(u) . \qquad\qquad ∎$$

Remark 2.2

The coefficients q_{ij} are the so-called *effective coefficients* of the composite material. They are independent of Ω . ∎

Remark 2.3

Assuming that we can compute the q_{ij}'s , the problem has been reduced to a much simpler one. ∎

Remark 2.4

The question of *error estimates* is, in general, open. ∎

Computation of the q_{ij}'s.

We recall here the formula which are given in A. BENSOUSSAN, J.L. LIONS and G. PAPANICOLAOU [5] (consult also the Bibliography of this book, and references given to I. BABUSKA, J. KELLER, E. SANCHEZ PALENCIA, L. TARTAR, and to E. DE GIORGI and his school ; cf. also F. MURAT and L. TARTAR [13]).

To obtain q_0 is trivial. One only takes the *average* of a_0 :

$$q_0 = \int_Y a_0(\xi)d\xi \qquad\qquad (2.14)$$

But the q_{ij}'s are *not at all* the averages of $a_{ij}(\xi)$.

We can suppose that v is fixed in (2.4)(2.5) and we can write y_ε instead of $y_\varepsilon(v)$. We look for y_ε in the form (ansatz)

$$y_\varepsilon = y_0(x,\xi) + \varepsilon y_1(x,\xi) + \varepsilon^2 y_2(x,\xi) + \ldots \qquad\qquad (2.15)$$

where

$$\begin{vmatrix} y_j = y_j(x,\xi) \text{ is defined in } \Omega \times Y, \\[2mm] y_j \text{ is Y-periodic in } \xi , \end{vmatrix} \qquad\qquad (2.16)$$

and where in (2.15) ξ is to be replaced by $\frac{x}{\varepsilon}$.

The ansatz (2.15) takes care of the "double structure" connected with composite materials : the global structure of Ω , and the periodic structure connected with fibers.

Remark 2.5

The ansatz (2.15) is of course reminiscent of the *multi-scale expansions*, with fast and slow variables, which have proven to be so useful in stiff problems of evolution. ∎

The next step is to make a formal computation, by using (formally) the expansion (2.15) into (2.4).

We introduce

$$A_\varepsilon = \varepsilon^{-2} A_o + \varepsilon^{-1} A_1 + A_2 \tag{2.17}$$

where

$$A_o = - \frac{\partial}{\partial \xi_i} a_{ij}(\xi) \frac{\partial}{\partial \xi_j} \; , \tag{2.18}$$

$$A_1 = - \frac{\partial}{\partial \xi_i}(a_{ij}(\xi) \frac{\partial}{\partial x_j}) - \frac{\partial}{\partial x_i}(a_{ij}(\xi) \frac{\partial}{\partial \xi_j}) \; , \tag{2.19}$$

$$A_2 = - \frac{\partial}{\partial x_i}(a_{ij}(\xi) \frac{\partial}{\partial x_j}) + a_o(\xi) \; ; \tag{2.20}$$

we obtain

$$\left|\begin{array}{l} A_o \, y_o = 0 \; , \\[2mm] A_o y_1 + A_1 y_o = 0 \; , \\[2mm] A_o y_2 + A_1 y_1 + A_2 y_o = f \; , \; \ldots \end{array}\right. \tag{2.21}$$

We recall that y_o, y_1, y_2, ... should be Y-periodic in ξ .

Therefore $(2.21)_1$ implies that y_o *does not depend on* ξ :

$$y_o(x,\xi) = y_o(x) \quad . \tag{2.22}$$

Using (2.22), $(2.21)_2$ reduces to

$$A_o y_1 = \frac{\partial a_{ij}(\xi)}{\partial \xi_i} \frac{\partial y_o(x)}{\partial x_j} \tag{2.23}$$

so that y_1 can be compiled by separation of variables. .

If we introduce

$$\left|\begin{array}{l} A_o \chi^j = - \dfrac{\partial a_{ij}(\xi)}{\partial \xi_i} \quad \text{in } Y \; , \\[4mm] \chi^j \text{ periodic,} \qquad \displaystyle\int_Y \chi^j \, d\xi = 0 \end{array}\right. \tag{2.24}$$

then

$$y_1 = -\chi^j(\xi) \frac{\partial y_o(x)}{\partial x_j} + \tilde{y}_1(x) \quad .$$

(2.25)

It remains to solve $(2.22)_3$ in Y , i.e.

$$\left| \begin{array}{l} A_o y_2 = f - A_1 y_1 - A_2 y_o \quad , \\ \\ y_2 \quad \text{periodic in } Y . \end{array} \right.$$

(2.26)

Problem (2.26) admits a solution iff

$$\int_Y (f - A_1 y_1 - A_2 y_o) \, d\xi = 0$$

i.e.

$$\int_Y (A_1 y_1 + A_2 y_o) \, d\xi = f(x) \quad \forall \, x \quad .$$

(2.27)

This gives

$$\mathcal{A} y_o = f \quad \text{in } \Omega$$

(2.28)

where q_o *is given by (2.14) and where*

$$q_{ij} = \int_Y [a_{ij}(\xi) - a_{ik}(\xi) \frac{\partial \chi^j}{\partial \xi_k}(\xi)] \, d\xi \quad .$$

(2.29)

Remark 2.6

We already said that the q_{ij}'s are *not* the averages of the a_{ij}'s ; formula (2.29) makes this remark precise ; the term

$$-\int_Y a_{ik} \frac{\partial \chi^j}{\partial \xi_k} \, d\xi$$

in (2.29) may be thought of as a *corrector* to the average of a_{ij}. ∎

Remark 2.7

Of course the previous derivation is *formal*. For justification of this computation (there are several methods to make this justification), we refer to the book of A. BENSOUSSAN, G. PAPANICOLAOU and the A. (loc. cit.), and to the bibliography therein. ∎

Remark 2.8

Special care should be taken in order to obtain that

$$\frac{\partial y}{\partial \nu_A} = v$$

but this can be done.

The final result is

the optimal control problem (2.7), *for the composite structure, can be "replaced" by the analogous problem, for the homogeneous structure : the new state equation is given by* (2.11), *the cost function by* (2.12), *and the homogeneous operator is given by* (2.9) *with* q_{ij} *given by* (2.29).

Remark 2.9

There are programs which compute the a_{ij}'s. Cf. D. BEGIS, S. DINARI, G. DUVAUT, A. HASSIM, F. PISTRE [14]. ∎

3. COMPOSITE MATERIALS. PROBLEM OF EVOLUTION

Let us consider, with the same notations than in Section 1, the *hyperbolic state equation*

$$\frac{\partial^2 y_\varepsilon(v)}{\partial t^2} + A_\varepsilon y_\varepsilon(v) = f \quad \text{in} \quad \Omega \times]0,T[= Q \qquad (3.1)$$

where f is given in $L^2(Q)$, $T > 0$ given, where $y_\varepsilon(v)$ is subject to the *initial* and *boundary conditions* :

$$\left|\begin{array}{l} y_\varepsilon(v) = \dfrac{\partial}{\partial t} y_\varepsilon(v) = 0 \quad \text{for} \quad t = 0 \ , \\[4mm] \dfrac{\partial y_\varepsilon(v)}{\partial \nu_{A_\varepsilon}} = v \quad \text{on} \quad \Sigma = \Gamma \times]0,T[\quad , \end{array}\right. \qquad (3.2)$$

where v is given in $L^2(\Sigma)$.

For every v , problem (3.1)(3.2) admits a unique (weak) solution, denoted by $y_\varepsilon(v) = y_\varepsilon(x,t;v)$.

The cost function is given (to fix ideas) by

$$J_\varepsilon(v) = \int_\Omega (y_\varepsilon(x,T;v) - z_d(x))^2 \, dx + N \int_\Sigma v^2 \, d\Sigma \ , \qquad (3.3)$$

and we are looking for

$$\left|\begin{array}{l} \inf J_\varepsilon(v) \ , \\[2mm] v \in \mathcal{U}_{ad} \end{array}\right. \qquad (3.4)$$

where

$$\mathcal{U}_{ad} = \text{closed convex subset of } L^2(\Sigma). \qquad \blacksquare \qquad (3.5)$$

The difficulties are, at least formally, of the same nature than in Section 2. The very complicated structure of A_ε makes it difficult any computation of the state $y_\varepsilon(v)$ for v given – and a fortiori any algorithm connected with (3.4).

An answer (at least a partial answer) is provided by the following result, the proof of which is technically a little bit complicated :

$$\text{as } \varepsilon \to 0, \quad \inf_{v \in \mathcal{U}_{ad}} J_\varepsilon(v) \to \inf_{v \in \mathcal{U}_{ad}} \mathcal{J}(v) , \tag{3.6}$$

where

$$\mathcal{J}(v) = \int_\Omega (y(x,T;v) - z_d)^2 dx + N \int_\Sigma v^2 d\Sigma \tag{3.7}$$

where the state $y(v)$ *is now given by the homogenized problem*

$$\left| \begin{array}{l} \dfrac{\partial^2 y(v)}{\partial t^2} + \mathcal{Q} y(v) = f \quad \text{in} \quad Q , \\[2ex] y(v) = \dfrac{\partial}{\partial t} y(v) = 0 \quad \text{at} \quad t = 0 , \\[2ex] \dfrac{\partial y(v)}{\partial \nu} = v \quad \text{on} \quad \Sigma ; \end{array} \right. \tag{3.8}$$

in (3.8), $\mathcal{Q}$ is the homogenized operator constructed in Section 2.

Remark 3.1

The proof of (3.6) uses the techniques of Section 2, the Laplace transform in time and some functional analysis. Details will be given in J.L LIONS [8] ∎

Remark 3.2

In the one-dimensional case, formula (2.29)[1] gives

$$q = \frac{1}{\int_Y a^{-1}(\xi) d\xi} \qquad \qquad \blacksquare$$

Remark 3.3

We do not have error estimates. ∎

Remark 3.4

The homogenization process *changes the speed of propagation.* This may affect results connected with *controllability.* Many more efforts will be necessary in order to clarify this point. ∎

Remark 3.5

What we have said extends to *other boundary conditions* and to other models : systems of elliptic equations, higher order equations, etc.. ∎

_____

[1] Which is valid in any space dimension.

Summary

In Sections 2 and 3 we have presented examples of the general situation given in the Introduction (Section 1) where the limit operator $\mathcal{A}$ (with the notations of (1.4)) is not obvious.

In the following sections we are going to present other examples where again $\mathcal{A}$ is not obvious to find and *where also* $\mathcal{J}$ may not be obvious to find (section 5).

4. PERFORATED MATERIALS (I).

We consider the domain Ω_ε which consists (cf. Fig. 1) of the half space $x_n > 0$, minus the set of "holes" of size ε and arranged in a periodical manner.

More precisely, in the ξ-space (cf. Fig. 2) we consider

$$\mathcal{Y} = Y \setminus \mathcal{O} . \qquad (4.1)$$

Then each hole equals $\varepsilon\mathcal{O}$ and they are arranged in a periodical manner, with period ε in all directions.

If $S = \partial\mathcal{O}$, we denote by $S\varepsilon$ the *union* of the boundaries of the holes in Ω_ε (cf. Fig. 1). Therefore

$$\partial\Omega_\varepsilon = S_\varepsilon \cup \Gamma , \qquad (4.2)$$

where

$$\Gamma = \{x | \ x_n\}= 0 .$$

We set

$$x' = \{x_1, \ \dots \ , x_{n-1}\} ,$$
$$\xi' = \{\xi_1, \ \dots \ , \xi_{n-1}\} .$$

In the applications, n will equal 2 or 3.

Figure 1

Remark 4.1

Of course, in possible applications, Ω_ε will be a *bounded* domain. The method we are going to present applies to such situations. ∎

Figure 2

Setting of the problem.

We assume that the *state* is given by :
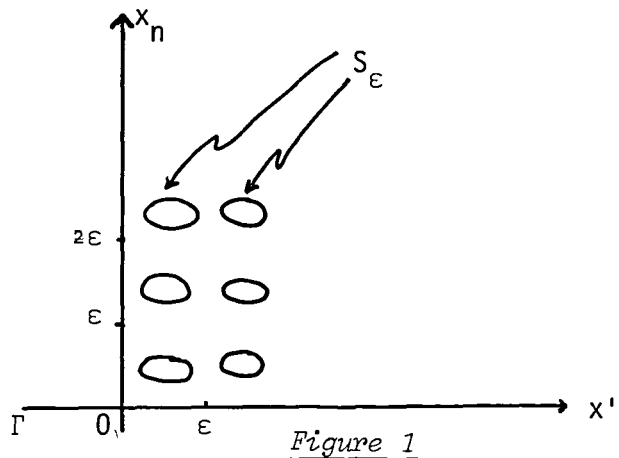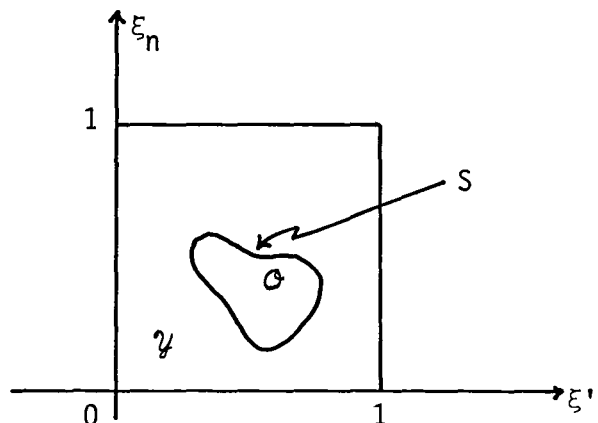
$$\left| \begin{array}{l} - \Delta y_\varepsilon(v) + y_\varepsilon(v) = f \quad \text{in} \quad \Omega_\varepsilon \ , \\[2mm] \dfrac{\partial y_\varepsilon(v)}{\partial \nu} = v \quad \text{on} \quad \Gamma \\[2mm] \dfrac{\partial y_\varepsilon(v)}{\partial \nu} = 0 \quad \text{on} \quad S_\varepsilon \end{array} \right. \qquad (4.3)$$

(where $\dfrac{\partial}{\partial \nu}$ stands for the normal derivative, directed towards the exterior of Ω_ε).
The cost function is given[1] by

$$J_\varepsilon(v) = \int_\Gamma (y_\varepsilon(v) - z_d)^2 \, d\Gamma + N \int_\Gamma v^2 \, d\Gamma \qquad (4.4)$$

and we are looking for

$$\inf J_\varepsilon(v) \ , \quad v \in \mathcal{U}_{ad} \ , \qquad (4.5)$$

where

$$\mathcal{U}_{ad} = \text{closed convex subset of } L^2(\Gamma). \qquad \blacksquare \qquad (4.6)$$

One can prove a result which is along the same lines of previous sections, but with different technical details : *there exists an homogeneous operator $\mathcal{A}$ [2], elliptic with constant coefficients, such that, as $\varepsilon \to 0$, problem* (4.5) *tends to the following one* :

the state equation is given by

$$\mathcal{A}y(v) = f \quad \text{in} \quad \Omega \qquad (4.7)$$

$$\frac{\partial y(v)}{\partial \nu} = \frac{1}{|\mathcal{Y}|} v \quad \text{on} \quad \Gamma, \qquad |\mathcal{Y}| = \text{volume of } \mathcal{Y} \ ;$$

the cost function is given by

$$\mathcal{J}(v) = \int_\Gamma (y(v) - z_d)^2 \, d\Gamma + N \int_\Gamma v^2 \, d\Gamma \qquad (4.9)$$

and one looks for

$$\inf \mathcal{J}(v) \ , \quad v \in \mathcal{U}_{ad} \ . \qquad (4.10)$$

Remark 4.2

Provided one knows how to compute $\mathcal{A}$, the practical interest of a result of this type is to replace the very complicated problem (4.3)(4.4)[3] by a rather standard linear-quadratic problem. $\qquad \blacksquare$

---

[1] We take examples somewhat similar to the ones in Sections 2 and 3, but the the method presented is general.

[2] To be given explicitely below.

[3] It is clear that any discretization of Ω_ε is complicated.

<u>How to obtain $\mathcal{Q}$.</u>

We consider (4.3) with *fixed* v. Therefore, we write y_ϵ instead of $y_\epsilon(v)$. We define

$$\left|\begin{array}{l} a_\epsilon(\varphi,\psi) = \int_{\Omega_\epsilon} \left(\dfrac{\partial \varphi}{\partial x_i}\dfrac{\partial \psi}{\partial x_i} + \varphi\psi\right)dx \ , \\[4mm] a_\epsilon(\varphi) = a_\epsilon(\varphi,\varphi) \quad , \\[4mm] L_\epsilon(\varphi) = \int_{\Omega_\epsilon} f\ \varphi\ dx + \int_\Gamma v\ \varphi\ d\Gamma \ . \end{array}\right. \tag{4.11}$$

Then y_ϵ is the solution of

$$\left|\begin{array}{l} \inf \ [\tfrac{1}{2} a_\epsilon(\varphi) - L_\epsilon(\varphi)] \ , \\[3mm] \varphi \in H^1(\Omega_\epsilon) \ , \end{array}\right. \tag{4.12}$$

where

$$H^1(\Omega_\epsilon) = \{\varphi \mid \varphi, \dfrac{\partial \varphi}{\partial x_1}, \dots, \dfrac{\partial \varphi}{\partial x_n} \in L^2(\Omega_\epsilon)\} \quad .$$

Let us introduce the Y-periodic function $m(\xi)$ defined by

$$m(\xi) = 1 \quad \text{in } \mathcal{Y} \ , \quad = 0 \text{ in } \mathcal{O} \ ; \quad \text{then, if } m^\epsilon(x) < m(\dfrac{x}{\epsilon}) \ , \text{ we have}$$

$$\left|\begin{array}{l} a_\epsilon(\varphi) = \int_\Omega m^\epsilon(x)[\,|\nabla\varphi|^2 + \varphi^2]\,dx \ , \\[4mm] L_\epsilon(\varphi) = \int_\Omega m^\epsilon f\ \varphi\ dx + \int_\Gamma v\ \varphi\ d\Gamma. \end{array}\right. \tag{4.13}$$

In order to solve (4.7) we now use ideas coming from the Asymptotic Calculus of Variations as given in J.L. LIONS [4] [7] .

We take in (4.12) φ given by[1]

$$\varphi = \varphi_o(x,\xi) + \epsilon\varphi_1(x,\xi) + \dots \tag{4.14}$$

where

$$\left|\begin{array}{l} \varphi_j(x,\xi) \ \text{ is defined in } \ \Omega \times \mathcal{Y} \ , \\[3mm] \varphi_j(x,\xi) \ \text{ is Y-periodic in } \xi \end{array}\right. \tag{4.15}$$

and where in (4.14) we replace ξ by $\dfrac{x}{\epsilon}$.

If we use (4.14) in (4.13), we obtain

$$a_\epsilon(\varphi) = \int_\Omega m^\epsilon(x)\ [(\nabla_x \varphi_o + \nabla_\xi \varphi_1)^2 + \varphi_o^2]\,dx + \dots \tag{4.16}$$

under the assumption that

$$\nabla_\xi \varphi_o = 0 \,[2] \ , \tag{4.17}$$

---

[1] Compare to the ansatz (2.15)

[2] A necessary condition for $a^\epsilon(\varphi)$ to remain bounded as $\epsilon \to 0$.

94

and

$$L_\varepsilon(\varphi) = \int_\Omega m^{\frac{\varepsilon}{2}} f \,\varphi_o \, dx + \int_\Gamma v \,\varphi_o \, d\Gamma + \ldots \tag{4.18}$$

where in (4.16) and (4.18) the ... stand for terms in ε, ε^2 , ...
We observe next that, as $\varepsilon \to 0$

$$\int k(x,\tfrac{x}{\varepsilon}) dx \longrightarrow \iint_{\Omega \times Y} k(x,\xi) dx d\xi \tag{4.19}$$

if $k(x,\xi)$ is reasonably regular and is Y-periodic in ξ, and that

$$\int_\Gamma \ell(x',\tfrac{x'}{\varepsilon}) dx' \longrightarrow \iint_{\Gamma \times Y'} \ell(x',\xi') dx' d\xi' \quad , \tag{4.20}$$

$Y' =]0,1[^{n-1}$, $\ell(x',\xi')$ being Y'-periodic in ξ'.

Therefore, the first term of the expansion (4.16) converges, as $\varepsilon \to 0$, towards

$$\hat{a}(\varphi_o,\varphi_1) = \iint_{\Omega \times Y} m(\xi) \, [(\nabla_x \varphi_o + \nabla_\xi \varphi_1)^2 + \varphi_o^2] dx d\xi \tag{4.21}$$

and the first term in the expansion (4.18) converges towards

$$\hat{L}(\varphi_o) = \iint_{\Omega \times Y} m(\xi) f \varphi_o dx d\xi + \iint_{\Gamma \times Y'} v \varphi_o dx' d\xi'. \tag{4.22}$$

Since $m(\xi) = 1$ in $\mathcal{Y}$ and $= 0$ in $\mathcal{O}$, and since according to (4.17) φ_o does not depend on ξ , (4.21)(4.22) give :

$$\left|
\begin{aligned}
\hat{a}(\varphi_o,\varphi_1) &= \iint_{\Omega \times \mathcal{Y}} [\,(\nabla_x \varphi_o + \nabla_\xi \varphi_1)^2 + \varphi_o^2] dx d\xi, \\
\hat{L}(\varphi_o) &= |\mathcal{Y}| \int_\Omega f \varphi_o dx + \int_\Gamma v \,\varphi_o dx' \quad ,
\end{aligned}
\right. \tag{4.23}$$

where $\qquad |\mathcal{Y}| = \int_Y m(\xi) d\xi.$

Then one can prove (using techniques of D. CIORANESCU and J. SAINT JEAN PAULIN [15]) that problem (4.12) gives in the limit :

$$\left|
\begin{aligned}
&\inf \, [\hat{a}(\varphi_o,\varphi_1) - \hat{L}(\varphi_o)] \quad , \\
&\varphi_o \in H^1(\Omega) \quad , \\
&\varphi_1 \quad \text{such that} \quad \nabla_\xi \varphi_1 \in L^2(\Omega \times \mathcal{Y})^n.
\end{aligned}
\right. \tag{4.24}$$

If in (4.24) one minimizes firstly in φ_1 , and if y_o, y_1 denotes a solution of this problem, one has

$$\iint_{\Omega \times \mathcal{Y}} (\nabla_x y_o + \nabla_\xi y_1) \nabla_\xi \varphi_1 dx d\xi = 0 \quad \forall\, \varphi_1 \; ; \tag{4.25}$$

this variational equation can be rewritten

$$\iint_{\Omega \times \mathcal{Y}} \nabla_\xi y_1 \, \nabla_\xi \varphi_1 \, dx d\xi = - \int_\Omega \frac{\partial y_o}{\partial x_j}(x) dx \int_S \nu_j(\xi) \, \varphi_1 \, dS \qquad (4.26)$$

where $\nu = \{\nu_j\}$ denotes the normal to S directed towards the exterior of $\mathcal{Y}$. In (4.21) x plays the role of a *parameter* and one can separate variables. If we define χ^j by (¹)

$$\left|\begin{array}{l} - \Delta_\xi \chi^j = 0 \quad \text{in} \ \mathcal{Y} \ , \\[2mm] \chi^j \text{ is periodic in } \xi \ , \\[2mm] \dfrac{\partial \chi^j}{\partial \nu} = \nu_j \quad \text{on} \ S \end{array}\right. \qquad (4.27)$$

then

$$y_1 = - \chi^j(\xi) \, \frac{\partial y_o}{\partial x_j}(x) \ . \qquad (4.28)$$

Minimizing (4.24) in φ_o gives

$$\iint_{\Omega \times \mathcal{Y}} (\nabla_x y_o + \nabla_\xi y_1) \, \nabla_x \varphi_o \, dx d\xi + \iint_{\Omega \times \mathcal{Y}} y_o \varphi_o \, dx d\xi =$$

$$= |\mathcal{Y}| \int_\Omega f \varphi_o \, dx + \int_\Gamma v \varphi_o d\Gamma$$

i.e.

$$\int_\Omega q_{ij} \frac{\partial y_o}{\partial x_j} \frac{\partial \varphi_o}{\partial x_i} \, dx + \int_\Omega y_o \varphi_o dx = \int_\Omega f \, \varphi_o dx + \frac{1}{|\mathcal{Y}|} \int_\Gamma v \, \varphi_o d\Gamma \quad (4.29)$$

where

$$q_{ij} = \frac{1}{|\mathcal{Y}|} \int_\mathcal{Y} (\delta_i^j - \frac{\partial \chi^j}{\partial \xi_i}) d\xi. \qquad (4.30)$$

We have obtained explicitely the operator $\mathcal{Q}$ *of* (4.7) :

$$\mathcal{Q} = - q_{ij} \frac{\partial^2}{\partial x_i \partial x_j} \ , \quad q_{ij} \ \textit{given by} \ (4.30).$$

Boundary condition (4.8) follows from (4.29). ∎

(¹) Compare to (2.24) ; χ^j is defined up to an additive constant ; remember that $\int_S \nu_j dS = 0.$

96

One obtains similar results for *evolution problems*.   ▊

Summary.

In the example we have just given, the "limit" state equation is obtained through a non trivial operator $\mathcal{A}$ - with the functional $\mathcal{J}$ (in the notations of the Introduction) obtained in an obvious manner.

We now give an example of a situation where $\mathcal{J}$ is not entirely obvious.

5. PERFORATED MATERIALS (II).

We consider the same geometrical situation than in Section 4, but we assume now that the *state* $y_\epsilon(v)$ is given by

$$- \epsilon^2 \, \Delta y_\epsilon(v) + y_\epsilon(v) = 0 \quad \text{in} \quad \Omega_\epsilon \, , \tag{5.1}$$

subject to

$$\epsilon \frac{\partial y_\epsilon}{\partial \nu}(v) = v \quad \text{on} \quad \Gamma \tag{5.2}$$

and to

$$y_\epsilon(v) = 0 \quad \text{on} \quad S_\epsilon. \tag{5.3}$$

The main difference of the present situation and the one of Section 4 lies in the fact that we have now the Dirichlet's boundary condition on S_ϵ instead of the Neumann boundary condition.

Let the *cost function* be given, as in Section 4, by

$$J_\epsilon(v) = \int_\Gamma [y_\epsilon(v) - z_d]^2 \, d\Gamma + N \int_\Gamma v^2 d\Gamma, \tag{5.4}$$

and we consider the problem

$$\inf J_\epsilon(v) \, , \quad v \in \mathcal{U}_{ad} \, , \tag{5.5}$$

$$\mathcal{U}_{ad} = \text{closed convex subset of } L^2(\Gamma). \tag{5.6}$$

Again, we want to find a "simple" limit problem.   ▊

The present question is solved, at the time of writing, only for the case

$$\mathcal{U}_{ad} = L^2(\Gamma). \tag{5.7}$$

We have to use here a more complicated ansatz. This is because *boundary layers* appear in the present situation. We consider

$$v = v_o(x', \xi') + \epsilon v_1(x', \xi') + \dots \tag{5.8}$$

where

$v_j(x',\xi')$ is defined in $\Gamma \times Y'$

v_j is Y' periodic in ξ' ; (5.9)

If in (5.1)(5.2)(5.3) we choose v by (5.8), we obtain an expansion

$$y_\varepsilon(v) = y_o(v_o) + \varepsilon y_1(v_o,v_1) + \dots \qquad (5.10)$$

where formula to compute y_o , y_1 , $\dots$ are given below ; $y_o(v_o)$ is a function of x and $\xi = x/\varepsilon$, defined as explained below, *periodic with respect to* ξ'.

Then

$$J_\varepsilon(v_o+\varepsilon v_1+ \dots) = \int_\Gamma (y_o(v_o)-z_d)^2 d\Gamma + N \int_\Gamma v_o^2 d\Gamma + \dots \qquad . \quad (5.11)$$

Using (4.20), we see that it is reasonable[1] to replace the first term in the expansion (5.11) by

$$\iint_{\Gamma\times Y'} (y_o(v_o)-z_d)^2 dx'd\xi' + N \iint_{\Gamma\times Y'} v_o^2 dx'd\xi' \quad . \qquad \blacksquare \quad (5.12)$$

We now show how to compute $y_o(v_o)$[2]. We introduce (cf. Fig. 3) the set $\mathcal{G}$ which consists of $Y'\times]0,+\infty[$, minus $\mathcal{O} \cup \mathcal{O}_1 \cup \mathcal{O}_2 \cup \dots$

where $\mathcal{O}_1$ (resp. $\mathcal{O}_2$, $\dots$) is obtained by translating $\mathcal{O}$ in the ξ_n direction by +1 (resp.+2, ..).

We then define $y_o(v_o)$ as the solution of

$$-\Delta_\xi y_o+y_o = 0 \text{ in } \mathcal{G}$$

$$y_o = 0 \text{ on } \partial\mathcal{O}\cup\partial\mathcal{O}_1 \cup \partial\mathcal{O}_2 \cup \ .. \quad (5.13)$$

$$-\frac{\partial y_o}{\partial\xi_n} = v_o \text{ on } Y'.$$

In (5.13) v_o is a function of x' and ξ', x' playing the role of a parameter.
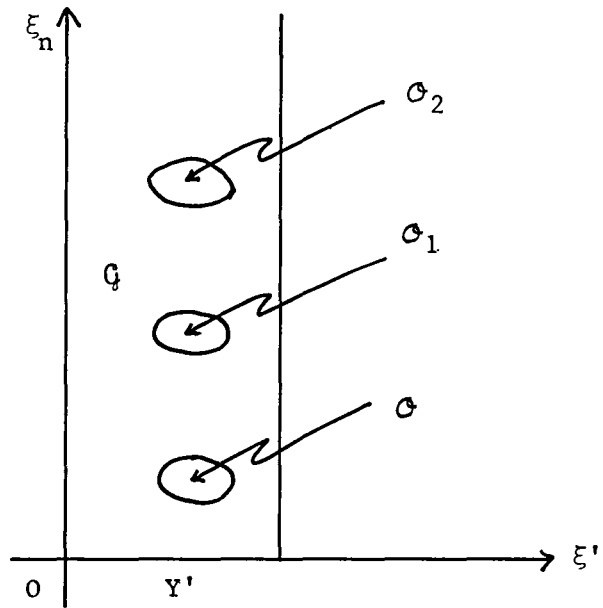
Figure 3.

In the notations of the Introduction, *the operator* $\mathcal{Q}$ *is now given by* (5.13) *and the cost function* $\mathcal{J}$ *is now given by* (5.12).

---

[1] This can be rigorously justified.

[2] Technical details, which are a little bit heavy, will be given in J.L. LIONS $\lceil 8 \rceil$.

Remark 5.1

One can give, in the present situation, a complete expansion of the optimal control u_ε. Cf. J.L. LIONS [8] . ∎

Remark 5.2

If $\hat{u}_{ad} \subset L^2(\Gamma)$, we *conjecture* that the infimum in the limit problem has to be taken on

$$\hat{u}_{ad} = \{v \mid v = v(x',\xi') \in L^2(\Gamma \times Y'), \int_{Y'} v(x',\xi')d\xi' \in u_{ad}\}. \blacksquare (5.14)$$

REFERENCES

[1] Doedel, E.J., Duban, M.C., Joly, G. and Kernevez, J.P., "Optimal Control of Systems with multiple steady-states". Proc. VIth International Conference on Analysis and Optimization of Systems, Nice, France June 19-22, 1984, ed. by A.Bensoussan and J.L. Lions, Lecture Notes in Control and Information Science, Springer-Verlag, pub., to appear.

[2] Kernevez, J.P. and Lions, J.L. To appear.

[3] Lions, J.L. "Contrôle des systèmes distribués singuliers", Gauthier Villars, Paris, 1983. [English translation is underway, to appear, trad. T.I.S., Tonbridge, U.K., publ. Gauthier Villars, Paris].

[4] Lions, J.L. "Asymptotic Calculus of Variations", in "Singular Perturbations and Asymptotics", Acad. Press, pp. 277-196.

[5] Bensoussan, A., Lions, J.L., Papanicolaou, G. "Asymptotic Analysis for periodic Structures". Studies in Mathematics and its Applications, vol. 5 (1978), North-Holland (Amsterdam).

[6] Sanchez Palencia, E. "Non Homogeneous Media and Vibration Theory". Lecture Notes in Physics, 127 (1980), Springer-Verlag.

[7] Lions, J.L. "Some Methods in the Variational Analysis of Systems and their Control". Science Press, Beijing (PRC) (1981). English trans. Gordon & Breach.

[8] Lions, J.L. Lectures in the Collège de France, 1984-1985 and book in preparation.

[9] Panacenko, G.P., "Homogenization principles ... for "carcasses" structures". Doklady Akad. Nauk, t. 263 (1982), N° 1, pp. 35-40.

[10] Bahbalov, N.C. and Panacenko, G.P. Book to appear.

[11] Lions, J.L. "Perturbations singulières dans les problèmes aux limites et en Contrôle optimal". Lecture Notes in Mathematics, Springer Verlag 323 (1973).

[12] Lions, J.L. "Remarques sur les problèmes d'homogénéisation dans des milieux à structure périodique et sur quelques problèmes raides". Cours CEA-EDF-INRIA, July 1983, to appear in Eyrolles, Collection "Direction des Etudes et Recherches EDF".

[13] Murat, F. and Tartar, L. "Calcul des variations et homogénéisation". Cours CEA-EDF-INRIA, July 1983, to appear in Eyrolles, Collection "Direction des Etudes et Recherches EDF".

[14] Régis, D., Dinari, S., Duvaut, G., Hassim, A., Pistre, F. "MODULEF et les matériaux composites". Proc. Sixth International Conference on "Computing Methods in Engineering and Applied Sciences", Versailles, Dec. 1983, R. Glowinski and JL. Lions, ed., to appear in North-Holland INRIA Conferences series.

[15] Cioranescu, D. and Saint Jean Paulin, J. "Homogenization in open sets with holes". J.M.A.A. 71 (1979), pp. 590-607.

-§-

FINITE CONTROL IN UNDERDAMPED DISTRIBUTED PARAMETER SYSTEMS*

D. J. Inman
University at Buffalo
State University of New York
Buffalo, NY 14260

1. INTRODUCTION

In the development of the theory of control for large flexible space structures, two important questions have been raised about the effect of using finite dimensional controls on inherently distributed parameter structures. The first question raised [1] has come to be known as control spillover [2]. Spillover can roughly be defined as the effect of energy added to unmodeled modes of a structure by the action of control laws derived from information about the modeled modes only. More recently, the question of whether or not a control law based on finite dimensional approximations of the distributed system will converge to a control law which is optimal for the full distributed parameter model has been raised. Gibson [3] has shown that the answer to this question is yes if enough damping is modeled. The result presented here, shows that both of these problems i.e. spillover and convergence, are manageable when the distributed parameter system under consideration is underdamped [4-5].

Specifically, a class of distributed parameter systems is defined using Hilbert space methods based on a partial differential equation model of a structure. In this space a simple, easy to check definition of underdamping is constructed based on the well known single degree of freedom concept of critical damping. It is then shown that if a given distributed parameter system satisfies this definition, each mode of the modal expansion of the solution is in fact an underdamped function of time. It is noted that a distributed parameter system which is underdamped is also uniformly exponentially stable. By appealing to the work of Gibson [3], a finite dimensional model of the system will yield satisfactory control laws. Furthermore, it is shown that the assumption of the underdamping also allows straightforward computation of rough bounds on the magnitude of the unmodeled or residual modes for a modal truncation scheme. Hence, underdamped systems are precisely that class of distributed parameter systems which are not likely to have spillover problems and which will yield convergence of finite dimensional control laws to control laws which are optimal for the full distributed parameter model of the system.

2. PROBLEM DEFINITION

We wish to consider systems governed by the following:

$$u_{tt}(x,t) + L_1[u_t(x,t)] + L_2[u(x,t)] = f(x,t) \text{ in } \Omega \qquad (2.1)$$

101

$$B[u(x,t)] = 0 \qquad\qquad \text{on } \partial\Omega \qquad (2.2)$$

where

a $(\cdot)_t$ indicates partial differentiation of $(\cdot)$ with respect to t;

b Ω is bounded, open region in R^n, n=1,2, or 3 with boundary $\partial\Omega$;

c L_1, L_2 are linear spatial differential operators of order n_1, n_2, respectively, and are symmetric on the domain $D(L) = \{u(\cdot, t) \in L^2(\Omega)$ such that all partial derivatives with respect to x of order up to and including k are in $L^2(\Omega)$ where $k=\max(2n_1, n_2)$ and $B[u(x,t)]=0$ for $x \in \partial\Omega$, for all $t \geq 0.\}$;

d L_2 is further assumed to be self adjoint, M-accretive and to have a compact inverse;

e   B is a linear operator (and may be a differential operator of order up to $\max(n_1, n_2)-1$) which reflects boundary conditions;

f $f(x,t)$ represents applied excitations and/or control forces.

With additional assumptions equations (2.1) and (2.2) can adequately describe vibration problems related to damped beams, plates, shells, etc. In particular, we will be interested in the case where $f(x,t)$ represents the action of discrete actuators as control forces.

Here $L^2(\Omega)$ denotes the Hilbert space of all square integrable functions in the Lebesgue sense defined by inner product and norm

$$\langle u, v \rangle = \int_\Omega uv dx \qquad\qquad (2.3)$$

$$||u|| = \langle u, u \rangle^{1/2} \qquad\qquad (2.4)$$

3. PREVIOUS WORK

When the function $f(x,t)$ is taken to be a control force of the form

$$f(x,t) = \sum_{i=1}^{P} k_i \delta(x-x_i) u(x,t) + \sum_{i=1}^{P} c_i \delta(x-x_i) u_t(x,t), \qquad (3.1)$$

equation (2.1) represents a reasonable formulation of the control problem usually stated for the control of flexible structures by using position and velocity feedback at P points on the structure. Here δ indicates the Dirac delta function. The control problem is to choose the constants c_i and k_i so that the response of (2.1) has certain specified properties.

The common approach to solving the problem, as first indicated by Berkman and Karnopp [1], is to truncate (2.1) into a finite dimensional problem. The general philosophy here being that for the free structure,

the system can always be truncated at a large enough value of N (say the number of modes kept in a modal expansion of the solution) so that the response can be modeled as accurately as desired. With control applied to the structure, the truncated model is then split into two parts. The first part consists of a certain number of modes which define the controlled system. This is the model of the structure used in solving for the values of the control gains; c_i and k_i. The remaining portion of the truncated model, referred to as residual modes, are not considered in the control problem. However, since the action of the control also adds energy to the residual modes and hence the total response, the response may be effected in an undesirable way. This has been discussed by a number of authors (see [6] for instance). This action is referred to as control spillover into the residual modes.

Another approach to examining the effects of using a finite dimensional control law on a distributed parameter (flexible) system is to examine the convergence of the truncated control system and structure to a control law that is valid (optimal) for the full distributed system. Gibson [3] has examined this problem and found that if enough damping is modeled in the system that one can expect the finite dimensional control law to be valid for the full distributed system and that the free response of the system will have a uniform decay rate.

Both of these previously addressed problems, i.e. convergence and spillover, address the important question of the validity of a finite dimensional model of a distributed parameter system subject to finite dimensional control. In the following it will be shown that underdamped distributed parameter systems, as defined in the next section, are exactly that class of systems which are well behaved with respect to convergence and spillover.

4. UNDERDAMPED SYSTEMS

It is well known that for a single degree of freedom discrete mass system, consisting of a mass, viscous damper and linear spring, the response, $x(t)$, will be underdamped if and only if the discrimanent of the associated characteristic equation is negative. This concept can be defined and used for distributed parameter systems (2.1) as well. This has been done for the special case of proportional damping [4] and generalized using heuristic arguments in [5]. In what follows the extension is made rigorous.

Before proceeding with a formal definition and proof, an overview of the result is in order. First, since L_2 is assumed to have a compact inverse and is self adjoint, it has associated with a complete set of eigenfunctions $\{\emptyset_n(x)\}_{n=1}^{\infty}$ [7]. These functions are used to expand the solution of (2.1) in a uniformly convergent infinite series, i.e.,

$$u(x,t) = \sum_{n=1}^{\infty} a_n(t)\emptyset_n(x) \tag{4.1}$$

The system defined by (2.1) is then defined to be underdamped if each of

103

the temporal functions, $a_n(t)$ are underdamped. That is, if each $a_n(t)$ has the form

$$a_n(t) = e^{-\zeta_n \omega_n t} \sin(\omega_n t \theta_n) . \qquad (4.2)$$

It is first shown that if the operator

$$4L_2 - L_1^2 \qquad (4.3)$$

is coercive then each $a_n(t)$ will have the form of (4.2). Then it is shown that (4.2) yields the convergence of (4.1) to a solution of (2.1).

With a further assumption on the smallest eigenvalue of L_1 or L_2, i.e. that the smallest eigenvalue of at least one of the operators is greater than unity, it can be shown that the coercive condition on (4.3) yields Gibson's convergence criteria and allows a bound to be calculated for the residual modes of Balas [6] in the decoupled case.

Definition 4.1   The system (2.1) is said to be <u>underdamped</u> if each temporal coefficient in the series solution (4.1) is an underdamped function of time.

Theorem 4.1   With the assumptions stated for (2.1) and the additional assumption that L_1 is positive definite on $D(L)$, the system described by (2.1) is underdamped if the operator

$$4L_2 - L_1^2$$

is coercive. That is if there exists a real number ρ such that

$$4\langle u, L_2 u \rangle - \langle u, L_1^2 u \rangle \geq \rho ||u||^2 \qquad (4.4)$$

for all u in $D(L)$.

Proof: Under the stated assumptions, L_2 has a complete set of normalized eigenfunctions denoted $\{\emptyset_n(x)\}_{n=1}^{\infty}$. As a possible solution for (2.1), examine the terms $a_n(t)\emptyset_n(x)$. Substitution of this term into (2.1) yields

$$\ddot{a}_n(t)/_n(x) + \dot{a}_n(t)L_1\emptyset_n(x) + a_n(t)L_2\emptyset_n(x) = 0 \qquad (4.5)$$

Premultiplying (4.5) by $\emptyset_n(x)$ and integrating over $D(L)$ yields that the characteristic roots associated with the initial value problem for $a_n(t)$ are determined by the discriminant (details can be found in [5]) given by

$$d(\emptyset_n) = \langle \emptyset_n, L_1\emptyset_n \rangle^2 - 4\langle \emptyset_n, L_2\emptyset_n \rangle \qquad (4.6)$$

By applying the Cauchy inequality to the term $\langle \emptyset_n, L_1\emptyset_n \rangle^2$ and comparing (4.6) and (4.4) we see that $d(\emptyset_n) < 0$ for any choice of $\emptyset_n$. Hence, each of the functions $a_n(t)$ must have the form given in (4.2) and are underdamped functions of time.

Next consider the function $u(x,t)$ given by

104

$$u(x,t) = \sum_{n=1}^{\infty} a_n(t)\emptyset_n(x) \tag{4.7}$$

and note that each term satisfies (2.1). Hence (4.7) will be a solution of (2.1) if (4.7) converges. In fact, since

$$\sum_{n=1}^{\infty} |a_n(t)|^2 < \infty \quad \text{for all } t > 0 \tag{4.8}$$

the Riesz-Fischer Theorem [8] yields the convergence of (4.7). In fact, by examining $|\dot{a}_n|$ and $|a_n|$

$$u_t = \sum_{n=1}^{\infty} \dot{a}_n(t)\emptyset_n(x) \tag{4.9}$$

and

$$u_{tt} = \sum_{n=1}^{\infty} \ddot{a}_n(t)\emptyset_n(x) \tag{4.10}$$

also converge. In addition, since the operator L_2 has a compact inverse, $L_2u(x,t)$ can also be expanded (see page 261 of [7]) as

$$L_2u(x,t) = \sum_{n=1}^{\infty} \mu_n a_n(t)\emptyset_n(x) \tag{4.11}$$

$$= \sum_{n=1}^{\infty} \mu_n \langle u, \emptyset_n \rangle \emptyset_n(x) \tag{4.12}$$

which converges uniformly and where μ_k are the eigenvalues of L_2.

Next consider the term $L_1 u_t(x,t)$ and note that

$$||L_1 u_t - \sum_{n=1}^{k} \dot{a}_n(t)L_1\emptyset_n(x)|| = ||L_1(u_t - \sum_{n=1}^{j} \dot{a}_n\emptyset_n)|| \tag{4.13}$$

and

$$||L_1(u_t - \sum_{n=1}^{k} \dot{a}_n\emptyset_n)|| = (y, L_1^2 y)^{1/2} \tag{4.14}$$

where $y = u_t - \sum_{n=1}^{k} a_n\emptyset_n$ since L_1 is symmetric. However, since $4L_2 - L_1^2$ is coercive.

$$0 < \langle y, L_1^2 u \rangle \leq 4 \langle y, L_2 y \rangle \tag{4.15}$$

and

$$\langle y, L_1^2 y \rangle^{1/2} \leq 2 \langle y, L_2 y \rangle^{1/2} = 2 \langle L_2^{1/2} y, L_2^{1/2} y \rangle^{1/2} \tag{4.16}$$

where $L_2^{1/2}$ is the maximally accretive square root of L_2 (see [7] page 283) which also has eigenfunctions $\emptyset_n(x)$. Thus,

$$\left\| L_1 u_t - \sum_{n=1}^{k} \dot{a}_n L_1 \emptyset_n \right\| \leq 2 \left\| L_2^{1/2} u_t - \sum_{n=1}^{k} \dot{a}_n L_2 \emptyset_n \right\| . \tag{4.17}$$

But, $L_2^{1/2}$ also has compact inverse so this last term converges uniformly, i.e.

$$L_2^{1/2} u_t \rightarrow \sum_{n=1}^{\infty} \dot{a}_n \mu_n^{1/2} \emptyset_n(x) \tag{4.18}$$

and hence

$$L_1 u_t = \sum_{n=1}^{\infty} \dot{a}_n L_1 \emptyset_n(x) \tag{4.19}$$

Thus (4.7) is the solution of (2.1) with each temporal coefficient underdamped.

5. GIBSON'S CONVERGENCE CRITERIA

Gibson has shown [3] that for the linear modal regulation problem associated with (2.1), a control scheme based on finite dimensional modeling of (2.1) will approach a control law which is optimal for the full system as the dimension of the model increases, if sufficient damping is modeled to provide a uniform decay rate for the free system. In this case the actual system is guaranteed to perform satisfactorily. Specifically, Gibson showed that if, in addition to the assumptions made for equation (2.1), L_1 is positive definite and the operators L_1 and L_2 are such that there exists a real number $\gamma \geq 0$ such that

$$\| L_1 u \| \leq \gamma^2 \| L_2 u \| \tag{5.1}$$

for all $u \in D(L)$, then the free system has a uniform decay rate. In addition as the number of modeled modes increases the modal control approaches the optimal control of the full system.

Gibson's assumptions are the same as the assumptions made for (2.1) with the addition of condition (5.1). The next theorem, however, shows that (5.1) follows from assuming that the structure to be controlled is underdamped.

106

<u>Theorem 5.1</u>   If either $||L_1u||>1$ or $||L_2u||>1$ and if $4L_2-L_1^2$ is coercive then there exists a real number, γ, such that unequality (5.1) holds.

Proof.   Since $4L_2-L_1^2$ is coercive, there exists a real number $\rho>0$ such that

$$4\langle u,L_2u\rangle - \langle L_1u,L_1u\rangle > \rho||u||^2 \qquad u\in D(L) \tag{5.2}$$

Next consider the Cauchy inequality applied to $\langle u,L_2u\rangle$. This yields

$$\langle u,L_2u\rangle \le ||u||\,||L_2u|| . \tag{5.3}$$

Combining (5.2) and (5.3) yields

$$||u||\,||L_2u|| \ge \langle u,L_2u\rangle \ge \frac{||L_1u||^2 + \rho||u||}{4} \ge \frac{1}{4}||L_1u||^2 .$$

Since $||u||$ is less than some constant for all u (or we can consider all u such that $||u||=1$) the above is of the form

$$\gamma^2||L_2u|| \ge ||L_1u||^2 \tag{5.4}$$

Now either $||L_1u||\ge1$ and $||L_1u||^2>||L_1u||$ so that

$$\gamma^2||L_2u|| > ||L_1u|| \text{ for all } u\in D(L) \tag{5.5}$$

or $||L_2u|| > 1$ so that $\gamma^4||L_2u||^2\ge\gamma^2||L_2u||>||L_1u||^2$, and

$$\gamma^2||L_2u|| \ge ||L_1u|| \text{ for all } u\in D(L) . \tag{5.6}$$

Thus in a slightly restricted sense, the underdamping condition is that which is required to insure the convergence and stability problems delineated in [3].

6. SPILLOVER BOUNDS

To a lesser extent, the underdamping condition allows bounds to be calculated for the spillover terms defined in [6]. Specifically, if the operators L_1 and L_2 are further restricted to commute, i.e. $L_1L_2=L_2L_1$ on $D(L)$, then the assumption of underdamping allows a simple bound on the spillover terms to be calculated.

Let $u_r(t)$ denote an uncontrolled or residual mode. Here $r>N$ where N is the number of modes kept in the truncated version of (2.1). In this case the underdamping assumption allows the truncated version of (2.1) to be decoupled and solved analytically (details can be found in [10]). Each residual mode has a temporal coefficient of the form

107

$$a_r(t) = e^{-\beta_r t} \left[\frac{\dot{a}_r(o) + \beta_r a_r(o)}{\omega_r} \sin\omega_r t + u_r(o)\cos\omega_r t \right] \tag{6.1}$$

$$+ \sum_{j=1}^{4n} \int_0^t q_j \bar{f}_j(\tau) e^{-\beta_r(t-\tau)} \sin\omega_r(t-\tau)d\tau$$

where

$\beta_r = \lambda_r^{(1)}/2$, the rth/eigenvalue of L_1

$\omega_r = \sqrt{\lambda_r^{(2)}}$, the rth/eigenvalue of L_2

$a_r(o) = \langle u(x,o), \emptyset_r(x) \rangle$ = initial condition

$\dot{a}_r(o) = \langle u_t(x,o), \emptyset_r(x) \rangle$ = initial condition

q_j = gain constants of the controller

$\bar{f}_j(\tau) = e^{-\sigma_j t}$ or $e^{-\sigma_j t} \sin(\bar{\omega}_j t - \theta_j)$
    where $\sigma_j, \bar{\omega}_j$ and θ_j are positive real numbers prescribed by the controller-observer system

n = number of modeled modes.

A simple bound on $a_r(t)$ can be calculated from (6.1) by merely allowing the sine terms to be replaced by 1. This yields, as a first estimate

$$[a_r(t)]_{max} = H_r e^{-\beta_r t} + \sum_{j=1}^{4n} q_j \int e^{-(\sigma_j-1)\tau - \beta_r t} d\tau \tag{6.2}$$

where

$$H_r = \left[\frac{[\dot{a}_r(o) + \beta_r a_r(o)]^2}{\omega_r^2} + a_r^2(o) \right]^{1/2} .$$

While these bounds are not tight enough to insure performance specifications, they do indicate that no instability will occur due to control spillover.

SUMMARY

It has been shown that the nature of the coefficient operators corresponding to the stiffness and damping of a distributed system determine if a given system is underdamped. Underdamped structures are then shown to be that class of structures which are suitable for control by point actuators in the sense that they are not likely to cause difficulty when truncated models are used in control design.

108

The result encourages further research in the area of computing more precise bounds on the truncated and residual modes of underdamped structures.

REFERENCES

[1] Berkman, and Karnopp, D., "Complete Response of Distributed Systems Controlled by a Finite Number of Linear Feedback Loops", ASME Journal of Engineering for Industry, Vol. 91, pp. 1063-1068, 1969.

[2] Balas, M.J., "Feedback Control of Flexible Systems", IEE Transactions on Automatic Control, Vol. AC-23, #4, pp. 673-679, 1978.

[3] Gibson, J.S., "An Analysis of Optimal Modal Regulation: Convergence and Stability", SIAM Journal of Control and Optimization, Vol. 19, pp. 686-706, 1981.

[4] Inman, D.J. and Andry, A.N., Jr., "The Nature of the Temporal Solutions of Damped Distributed Systems with Classical Normal Modes", ASME Journal of Applied Mechanics, Vol. 49, pp. 867-870, 1982.

[5] Inman, D.J., "Oscillatory Damped Distributed Parameter Systems", Mechanics Research Communications", Vol. 9, No. 2, pp. 101-108, 1982.

[6] Balas, M.J., "Modal Control of Certain Flexible Dynamic Systems", SIAM Journal of Control and Optimization, Vol. 16, pp. 450-462, 1978.

[7] Kato, T., Perturbation Theory for Linear Operators, Springer Verlag, New York, 1966, p. 169.

[8] Stakgold, Ivar, Boundary Value Problems of Mathematical Physics, Vol. I, Macmillan Co., 1967, p. 122.

[9] Ng, C.K. and Inman, D.J., "Active Control of Decoupled Underdamped Systems", Proceedings of the AIAA 25th SDM Conference Part II, May 1984, pp. 192-200.

Errata

2nd page d under 2.2 should read "... self adjoint, coercive ..." instead of M-accretive
3rd page 3rd line under part 4 should read: "... discriminant ..."
4th page equation (4.2), aregument of the sine function should read: $(\omega_n t + \theta_n)$

NEW DIRECTIONS IN ASYMPTOTICALLY STABLE FINITE-DIMENSIONAL ADAPTIVE CONTROL OF LINEAR DISTRIBUTED PARAMETER SYSTEMS

M. J. Balas
Rensselaer Polytechnic Institute
Troy, NY 12181

ABSTRACT

Distributed Parameter Systems (DPS), such as systems described by partial differential equations, require infinite-dimensional state space descriptions to correctly model their dynamical behavior. However, any adaptive control algorithm must be finite-dimensional in order to be implemented via on-line digital computers. Finite-dimensional adaptive control of linear DPS requires stability analysis of nonlinear, time-varying, infinite-dimensional systems.

The structure of nonadaptive finite-dimensional control of linear DPS is summarized as it relates to the existence of limiting systems for adaptive control. Two candidate schemes for finite-dimensional adaptive control of DPS are described and critical issues in infinite-dimensional stability analysis are discussed, in particular, the invariance Principle, Center Manifold Theory, and Relationships Between Input-Output and Internal Stability.

1.0 INTRODUCTION

By <u>distributed parameter systems</u> (DPS) we mean those dynamical systems whose description requires an infinite-dimensional state space, for example, systems described by partial differential equations. Many engineering applications such as chemical processes, large flexible spacecraft, and plasma fusion reactors are DPS.

The linear DPS of interest will be modeled by the following <u>state space form</u>:

$$\begin{cases} \dfrac{\partial v(t)}{\partial t} = A\, v(t) + Bf(t); \quad v(o) = v_o \\[2em] y(t) = C\, v(t) \end{cases} \tag{1.1}$$

where the <u>state</u> $v(t)$ is in an infinite-dimensional Hilbert space H with inner product $(\cdot,\cdot)$ and corresponding norm $||\cdot||$. The bounded operators B and C have finite ranks M and P, respectively, and $f(t)$, $y(t)$ represent the inputs for M linear actuators and the outputs from P linear sensors, respectively. Thus,

$$Bf(t) = \sum_{i=1}^{M} b_i \, f_1(t) \tag{1.2}$$

and

$$y(t) = [y_1(t), \ldots, y_P(t)]^T \text{ with}$$

$$y_j(t) = (c_j, v(t)) : 1 \leq j \leq P \tag{1.3}$$

where b_1 and c_j belong to H. In finite-dimensional theory, A would be a matrix, but here the operator A is a closed, linear, unbounded differential operator with domain $D(A)$ dense in H. Furthermore (1.1)-(1.3) represents some <u>well-posed</u> physical system, which in mathematical terms is the weak formulation of (2.1):

$$\begin{cases} v(t) = U(t) \, v_o + \int_0^t U(t-\tau) \, Bf(\tau) d\tau \\ \\ y(t) = Cv(t) : t \geq 0 \end{cases} \tag{1.4}$$

where v_o is <u>any</u> initial state in H and $U(t)$ is the C_o-semigroup of bounded operators generated on H by A. This latter means:

$$U(t+\tau) = U(t) \, U(\tau) : t \geq 0, \tau \geq 0 \tag{1.5a}$$

$$U(o) = I \tag{1.5b}$$

$$\lim_{t \to 0^+} [U(t)-I] \, v = 0 ; v \text{ in } H \tag{1.5c}$$

$$Av = \lim_{t \to 0^+} [\frac{U(t)-I}{t}]v ; v \text{ in } D(A) \tag{1.5d}$$

Note that the semigroup $U(t)$ evolves the initial condition v_o forward in time. When v_o is in $D(A)$ and $f(t)$ has continuous first derivative, $v(t)$ also is differentiable, lies in $D(A)$ for a $t \geq 0$, and satisfies (2.1). However, any v_o in H and any square-integrable $f(t)$ will satisfy the weak formulation (2.4) and yield states $v(t)$ in H for all $t \geq 0$. Consequently, (2.4) is much easier to work with in infinite-dimensions and is more likely to represent the actual physical system being modeled by (1.1). This form, (1.1) or (1.4), models most practical <u>interior control problems</u> for linear DPS where the actuator and sensor influence functions are given by b_1 and c_j, respectively.

For example, control of the damped wave equation on a region $\Omega \subseteq R^n$ by a single actuator and sensor is described by (for $\varepsilon > 0$):

$$\begin{cases} \dfrac{\partial^2 u(x,t)}{\partial t^2} + \varepsilon \dfrac{\partial u(x,t)}{\partial t} - A_o u(x,t) = b(x)\, f(t) \\[12pt] y(t) = \displaystyle\int_\Omega c(x)\, u(x,t)\, dx \end{cases} \tag{1.6}$$

where $u(x,t)$ is the displacement from equilibrium of Ω and the influence functions b and c can be taken as approximations of Dirac delta functions at the location of the actuator and sensor. The operator A_o is the Laplacian given by

$$A_o u(x,t) = \sum_{\ell=1}^{n} \frac{\partial^2 u(x,t)}{\partial x_\ell^2} \tag{1.7}$$

on $D(A_o) \equiv \{u(x,t)\ \varepsilon H_o \,|\, u(x,t)$ is smooth and $u(x,t) = 0$ on the boundary of $\Omega\}$. The domain $D(A_o)$ is dense in $H_o \equiv L^2(\Omega)$ with the usual inner product $(\cdot,\cdot)_o$. This can be put into the form (1.1) by choosing the state $v(t) = [u(x,t),$ $\dfrac{\partial u(x,t)}{\partial t}]^T$ in $H \equiv D(A_o^{\frac{1}{2}}) \times H_o$ with the energy inner product:

$$(v,\omega) = (A_o^{\frac{1}{2}} v_1,\ A_o^{\frac{1}{2}} \omega_1)_o + (v_2,\ \omega_2)_o \tag{1.8}$$

The operator A in (1.1) becomes

$$A = \begin{bmatrix} 0 & I \\ -A_o & -\varepsilon I \end{bmatrix} \tag{1.9}$$

and the rest follows.

Linear boundary control problems for DPS have a form somewhat different from (1.1); however, they can often be recast as equivalent interior control problems of the form (1.1) [1].

The Hille-Yosida Theorem provides conditions under which an operator A generates a C_o-semigroup $U(t)$ satisfying:

$$||U(t)|| \le K e^{-\sigma t},\ t \ge 0 \tag{1.10}$$

where $K \ge 1$ and σ real. The necessary and sufficient conditions are given for the resolvent operator $R(\lambda,A) \equiv (\lambda I - A)^{-1}$:

$$||R(\lambda,A)^n|| \le \frac{K}{(\lambda+\sigma)^n}\ ;\ n = 1,\ 2,\ \ldots \tag{1.11}$$

for all real $\lambda > -\sigma$ in the resolvent set of A, $\rho(A) = \{\lambda$ complex $|R(\lambda,A)$ is a bounded operator on $H\}$. The spectrum of A, $\sigma(A) = \rho(A)^c$ is much more complicated in infinite-dimensions, but, in finite-dimensions, it consists only of the

(finite number of) eigenvalues of A. We say that A is exponentially stable when σ > 0 in (1.10). i.e. the semi-group U(t) generated by A decays exponentially at the rate σ. There are many other types of stability in infinite-dimensions, but no others provide the safety of a stability margin σ; therefore, this seems like the kind of stability of most practical interest for engineering applications where there is always some uncertainty in the model of the DPS.

No matter what the purpose of feedback control for a DPS, the controller must be finite-dimensional in order to be implemented by on-line digital computers with limited memory and meory access. Of course, in many applications the controller is required to automatically adapt to a system with poorly known parameters; this adaptation should take place in a stable way in order to be effective. The majority of results for stable adaptive control are for finite-dimensional systems and require the controller dimension to be the same as that of the plant. For DPS, this is impossible to achieve and, hence model reduction and reduced-order adaptive control are involved; see e.g. [2]-[3]. This is also the case for very large-scale finite-dimensional systems which are to be controlled by very low-order controllers. Much of what we will say here applies to the large-scale system problems, but our focus will be on critical issues for infinite-dimensional systems.

In Section 2.0, we review our results on the mathematical structure of stable nonadaptive finite-dimensional control of DPS. This will indicate what it is possible to accomplish in the limiting case and guide us toward reasonable expectations for adaptive control.

In Section 3.0, we present two finite-dimensional adaptive control schemes for DPS. These by no means exhaust the possibilities but will give us some points of reference. In Section 4.0, we consider possible ways to prove stability of adaptive control for DPS. Even for linear, time-invariant DPS, the closed-loop analysis for finite-dimensional adaptive control requires stability theory for nonlinear, time-varying, infinite-dimensional systems. We concentrate in this section on time-domain rather than input-output methods. Finally, in Section 5.0 we summarize critical issues for adaptive DPS control generated by Sec. 3.0 and 4.0.

We do not wish to give the impression that this is the definitive work on stable adaptive control of infinite-dimensional systems. This is a new area of research and, although several applications of adaptive control for DPS have been successful in computer simulation, the corresponding stability analysis has not been done. We hope to indicate here where the difficulties of such analysis arise and to suggest some potential directions for solution.

2.0 THE MATHEMATICAL STRUCTURE OF STABLE NONADAPTIVE DPS CONTROL

This section summarizes results on nonadaptive DPS control presented in [1] and [4]-[6].

Finite-dimensional, continuous-time controllers will have the form:

$$\begin{cases} f(t) = L_{11} \, y(t) + L_{12} \, z(t) & \text{(2.1a)} \\ \dot{z}(t) = L_{12} \, y(t) + L_{22} \, z(t) = Fz(t) + EF(t) \cdot z(o) = z_o & \text{(2.1b)} \end{cases}$$

with

$$\begin{cases} L_{21} = K + EL_{11} \\ L_{22} = F + EL_{12} \end{cases} \qquad \text{(2.1c)}$$

where $z(t)$ belongs to R^α for some non-negative integer α. We call the special case $\alpha = 0$: <u>static feedback</u>; otherwise, when $\alpha > 0$, we have <u>dynamic feedback</u>. Although the actual digital computer implementation of such controllers requires a discrete-time formulation of (2.1), we will consider the continuous-time formulation for simplicity; however, see [5] for the corresponding discrete-time results.

We say that (A,B) in (1.1) has a pair of <u>stabilizing subspaces</u> (H_N, H_R) if the following hold:

$$H = H_N \oplus H_R \qquad \text{(2.2a)}$$

$$\dim H_N = N < \infty \; \& \; H_R \text{ closed} \qquad \text{(2.2b)}$$

and $A_o \equiv A + BG$ generates an exponentially stable C_o-semigroup $U_o(t)$, i.e.

$$||U_o(t)|| \le K_o e^{-\sigma_o t}; \; t \ge 0 \qquad \text{(2.2c)}$$

with $K_o \ge 1$ and $\sigma_o > 0$, where

$$G = GP_N \; (\text{ or } GP_R = 0) \qquad \text{(2.2d)}$$

with (P_N, P_R) the projections defined by (2.2a). Thus, stabilizing subspaces guarantee that the <u>projection feedback law</u>:

$$f(t) = GP_N \, v(t) \qquad \text{(2.3)}$$

can produce an exponentially stable closed-loop system (1.1) and (2.3). Usually, we assume that σ_o is specified; hence, (1.1) may have stabilizing subspaces for some values σ_o but not for others (clearly, if it has them for some $\sigma_o > 0$ then it will have them for all smaller values $0 < \sigma \le \sigma_o$). Of course, it should be noted that (2.3) is an <u>ideal</u> control law which cannot in general be generated from the sensor outputs (1.3). Our main result will show that, at best, <u>every finite-dimensional controller (2.1) asymptotically reproduces (2.3) for a special pair of stabilizing subspaces.</u>

Consider the linear operator $Q:D(A) \to R^\alpha$ which satisfies the <u>nonsymmetric Riccati equation</u>:

$$0 = W \equiv L_{21}C + L_{22}Q - O(A + BL_{11}C) - QBL_{12}Q \qquad (2.4)$$

Clearly, (2.4) is nonlinear in Q and O is obviously bounded (also, finite-rank). The following is the main structural result:

Theorem 1: Assume v_o is in D(A). Given any controller of the form (2.1) satisfying the following:

(a) a solution Q for (2.4) exists and

(b) $\tilde{F} \equiv L_{22} - QBL_{12}$ is stable in the finite-dimensional sense, then the closed-loop (1.1) and (2.1) is exponentially stable if and only if $(\tilde{H}_N, \tilde{H}_R)$ are stabilizing subspaces for (A, B) in (1.1), where $\tilde{H}_N \equiv N(\tilde{Q})^{\perp}$ and $\tilde{H}_R \equiv N(\tilde{Q})$ and $\tilde{Q} \equiv \begin{bmatrix} C \\ Q \end{bmatrix}$. The dim $\tilde{H}_N = N \leq P + \alpha < \infty$. Furthermore, the control law (2.1a) converges asymptotically in time to the projection control law (2.3) i.e., $\lim_{t \to \infty} [f(t) \quad G\tilde{P}_N v(t)] = 0$, where $(\tilde{P}_N, \tilde{P}_R)$ are the (orthogonal) projections defined by $(\tilde{H}_N, \tilde{H}_R)$.

This result says that, as long as (2.4) has a solution which produces a stable $\tilde{F}$, the finite-dimensional controller will asymptotically reproduce a certain projection feedback law (2.3); thus, exponential closed-loop stability is only attainable by finite-dimensional control when it is attainable by orthogonal projection feedback on the finite-dimensional subspace $\tilde{H}_N$. This is a time-domain characterization of the α-dimensional stabilizing controllers for (1.1).

The proof is given in [1]. The special case

$$E = Q B \qquad (2.5)$$

in (2.1b) leads to a linear version of (2.4):

$$0 = KC + FQ - QA \qquad (2.6)$$

with $\tilde{F} = F$. Such a controller contains a reduced-order observer for the DPS; however, in general (2.5) is not satisfied, e.g. for controllers based on reduced-order models of (1.1), and the more general result of Theo. 1 is needed.

In the above analysis the subspaces $(\tilde{H}_N, \tilde{H}_R)$ are determined by the controller (2.1) and are not very accessible. A more practical approach is to specify a pair of subspaces (H_N, H_R) and perform a model reduction of the DPS (1.1). The closed-loop stability analysis of the corresponding finite-dimensional controller is performed afterward. Since there are many ways to perform model reduction, there are many possibilities for the finite-dimensional controller; however, not all of them will be stable. We define a pair of model reducing subspaces (H_N, H_R) for (1.1) by the following:

$$H = H_N \oplus H_R : \qquad (2.7a)$$

$$\dim H_N = N < \infty \ , \quad H_R \text{ closed} \tag{2.7b}$$

$$H_N \subseteq D(A) \ , \tag{2.7c}$$

the reduced-order model (A_N, B_N, C_N) is stabilizable and detectable in the finite-dimensional sense, (2.7d) the C_o-semigroup $U_R(t)$ generated by A_R is exponentially stable, i.e.

$$||U_R(t)|| \le K_R e^{-\sigma_R t} \ ; \quad t > 0 \tag{2.7e}$$

with $K_R \ge 1$ and $\sigma_R > 0$.

where $A_N \equiv P_N A P_N$, $B_N \equiv P_N B$, $C_N \equiv C P_R$, and $A_R \equiv P_R A P_R$ with (P_N, P_R) the projections defined by (2.7a). The <u>model reduction</u> of (1.1) produced by (H_N, H_R) yields the <u>reduced-order model</u> (ROM): (A_N, B_N, C_N), and from this ROM the following <u>ROM based finite-dimensional controller</u> is obtained:

$$
\begin{cases}
f(t) = G_N \hat{v}_N(t) \\[2mm]
\dfrac{\partial \hat{v}_N(t)}{\partial t} = A_N \hat{v}_N(t) + B_N f(t) + K_N(y(t) - \hat{y}_N(t)) \\[2mm]
\hat{y}_N(t) = C_N \hat{v}_N(t); \quad \hat{v}_N(o) = 0
\end{cases}
\tag{2.8}
$$

This is a special case of (2.1) with

$$L_{11} = 0, \quad L_{12} = G_N, \quad L_{21} = K_N, \quad \text{and} \quad L_{22} = A_N - K_N C_N + B_N G_N \tag{2.9}$$

The gains G_N and K_N can be chosen so that

$$A_N - K_N C_N \quad \text{and} \quad A_N + B_N G_N \quad \text{are stable} \tag{2.10}$$

However, in general (2.8) does not asymptotically reconstruct the projection $v_N(t) \equiv P_N v(t)$. Let $e_N(t) \equiv \hat{v}_N(t) - v_N(t)$ and from (1.1) and (2.8) obtain (when $v_o \in D(A)$):

$$
\begin{cases}
\dfrac{\partial v(t)}{\partial t} = (A + B G_N P_N) v(t) + B G_N e_N(t); \quad v(o) = v_o \tag{2.11a} \\[2mm]
\dfrac{\partial e_N(t)}{\partial t} = \Delta_{NR} v(t) + (A_N - K_N C_N) e_N(t); \quad e_N(o) = -P_N v_o \tag{2.11b}
\end{cases}
$$

where $\Delta_{NR} \equiv K_N C_R - A_{NR}$, $C_R \equiv C P_R$, and $A_{NR} \equiv P_N A P_R$. The following result gives conditions under which the closed-loop is stable with the controller (2.8):

<u>Theorem 2</u>: If (H_N, H_R) are model reducing subspaces for (1.1) and both $||\Delta_{NR}||$ and $||A_{NR}||$ are sufficiently small, then the above are stabilizing subspaces for (1.1) also and the closed-loop (1.1) and (2.8) will be exponentially stable when

117

the gains G_N and K_N are chosen to satisfy (2.10).

This result was proved in [6] and uses semigroup perturbation theory to give bounds on the smallness required for $||\Delta_{NR}||$ and $||A_{NR}||$.

To compare this with Theo. 1, let $\tilde{e}_N(t) \equiv e_N(t) + Q_N v(t) = \hat{v}_N(t) - (P_N - Q_N) v(t)$ (2.12)

where $Q_N : D(A) \rightarrow H_N$ is a linear operator solution of the following:

$$0 = W_N = \Delta_{NR} - F_N Q_N (A + BG_N P_N) - Q_N BG_N Q_N \qquad (2.13)$$

where $F_N = A_N - K_N C_N$. From (2.11) - (2.13), the closed-loop becomes:

$$\begin{cases} \dfrac{\partial v(t)}{\partial t} = \tilde{A}_o v(t) + BG_N \, \tilde{e}_N(t) & (2.14a) \\[2mm] \dfrac{\partial \tilde{e}_N(t)}{\partial t} = \tilde{F}_N \, e_N(t) & (2.14b) \end{cases}$$

where $A_o \equiv A + BG_N (P_N - Q_N)$ and $\tilde{F}_N \equiv F_N + Q_N BG_N$. Consequently, we can obtain:

<u>Theorem 3</u>: Assume (H_N, H_R) are model reducing subspaces for (1.1). If Q_N solves (2.13) then $Q = P_N - Q_N$ solves (2.4). Furthermore, if $\tilde{F}_N = F_N + Q_N BG_N$ is stable, then $\tilde{F} = \tilde{F}_N$ is stable and the closed-loop (1.1) and (2.8) is exponentially stable if and only if $\hat{H}_N = N(P_N - Q_N)^{\perp}$ and $\hat{H}_R = N(P_N - Q_N)$ are stabilizing subspaces for (A,B) in (1.1), where (P_N, P_R) are the model reducing projections. The proof is given in [1]. Therefore, the relationship of the model reduction approach to the structural results is through the triangularizing transformation Q_N in (2.12) and the model reducing projection P_N. Their difference forms Q in (2.4) and this generates the stabilizing subspaces $(\hat{H}_N, \hat{H}_R)$ produced by the ROM-based controller (2.8). Only in the <u>very special case</u> where $\Delta_{NR} = 0$ does $0 = P_N$ (i.e. $Q_N = 0$) and $(\hat{H}_N, \hat{H}_R)$ become

$$\begin{cases} \hat{H}_N = N(P_N)^{\perp} = R(P_R)^{\perp} = H_R^{\perp} \\[2mm] \hat{H}_R = N(P_N) = R(P_R) = H_R \end{cases}$$

This yields $\hat{H}_N = H_N$ and $\hat{H}_R = H_R$ when (H_N, H_R) are orthogonal.

Although the above only characterizes the stabilizing <u>nonadaptive</u> controllers for DPS, it tells us what is possible in the limiting case. In other words, <u>there must exist some finite-dimensional nonadaptive controller which stabilizes the DPS and this becomes the limit of the corresponding adaptive controller.</u> If the limiting case is a linear controller (highly likely), then the above results tell us what the structure of this limit must be. These limits are, in fact, the "equilibrium points" for the stability analysis.

3.0 SOME ADAPTIVE CONTROL SCHEMES FOR DPS

There are infinitely many ways to generate adaptive controllers for DPS; a few of them might actually be stable. The most obvious procedure is to generate a reduced-order model (ROM) of the DPS and use any of the myriad finite-dimensional adaptive control schemes as though the ROM were the true DPS. Of course, even though the scheme may be stable with the ROM, it need not be stable with the actual DPS due to unmodeled residual dynamics.

When (H_N, H_R) are a pair of model reducing subspaces as in (2.7) with corresponding projections (P_N, P_R), they produce a decomposition of the DPS (1.1):

$$\frac{\partial v_N}{\partial t} = A_N v_N + A_{NR} v_R + B_N f \tag{3.1a}$$

$$\frac{\partial v_R}{\partial t} = A_{RN} v_N + A_R v_R + B_R f \tag{3.1b}$$

$$y = C_N v_N + C_R v_R \tag{3.1c}$$

where $v_N = P_N v$, $v_R = P_R v$, $A_N = P_N A P_N$, $B_N = P_N B$, $C_N = C P_N$, $A_{NR} = P_N A P_R$, etc. The corresponding ROM is obtained by ignoring all residual terms (setting $v_R = 0$):

$$\frac{\partial v_N}{\partial t} = A_N v_N + B_N f \tag{3.2a}$$

$$y_N = C_N v_N \tag{3.2b}$$

Whenever an operator $T: H_N \rightarrow H_R$ exists satisfying:

$$T A_N - A_R T + A_{RN} - T A_{NR} T = 0 \tag{3.3}$$

it is possible to block-triangularize (3.1) with $\begin{bmatrix} I & 0 \\ T & I \end{bmatrix}$ so that $A_{RN} = 0$; see [3]. Consequently, we will assume:

$$A_{RN} = 0 \tag{3.4}$$

Suppose we want to control (1.1) to adaptively follow a reference model:

$$\frac{\partial v_m}{\partial t} = A_m v_m + B_m \tilde{f} \tag{3.5}$$

where A_m has desired properties, e.g. stability. If dim v_m = dim v, i.e. the reference model is infinite-dimensional, then we try the following adaptive control law:

$$f(t) = Q(t) \tilde{f}(t) + Q(t) F(t) v(t) \tag{3.6}$$

Let $e(t) \equiv v_m(t) - v(t)$ and, from (1.1),(3.5), and (3.6), we obtain:

$$\frac{\partial e}{\partial t} = A_m e + (A_m - A - BQF)v + (B_m - BQ)\tilde{f} \tag{3.7}$$

Suppose there exist constant <u>exact model matching gains</u> Q_e and F_e such that

$$BQ_e = B_m \tag{3.8a}$$

$$A + B_m F_e = A_m \tag{3.8b}$$

Let $\Phi(t) \equiv [F_e - F(t) \vdots Q^{-1}(t) - Q_e^{-1}] = [\Phi_1(t) \vdots \Phi_2(t)]$ and obtain:

$$\frac{\partial e}{\partial t} = A_m e + B_m \Phi z \tag{3.9}$$

where $z \equiv \begin{bmatrix} v \\ f \end{bmatrix}$. Now, we try a Lyapunov function of the form:

$$V(t) = 1/2[(e, Pe) + tr \, \Phi^* \, \Gamma^{-1} \Phi] \tag{3.10}$$

where Φ^* is the adjoint operator for Φ, $\Gamma \equiv diag \, [\Gamma_1 \Gamma_2]$, and P is a bounded symmetric positive definite operator satisfying:

$$(A_m v, \, Pv) + (Pv, \, A_m v) = -||v||^2 \tag{3.11}$$

for all v in $D(A_m)$. Formally calculating the derivative of V, we obtain:

$$\dot{V}(t) = -\frac{||v(t)||^2}{2} \leq 0 \tag{3.12}$$

when $tr \, \Phi^* \, \Gamma^{-1} \Phi = -(e, \, PB_m \Phi z)$ \hfill (3.13)

From (3.13) we can obtain the appropriate <u>adaptation laws</u> for Lyapunov stability. Further, use of <u>La Salle's Invariance Principle</u> [7] guarantees global asymptotic stability for the case of <u>finite-dimensional plants</u> [8]. However, the extension of this principle to <u>infinite-dimensional plants</u>, e.g. [9], Theo. 4.2, p. 168, does not yield very useful results. This is true because a continuous Lyapunov function generally yields bounded positive orbits but this does not give the necessary precompactness (a bounded set is precompact in a finite-dimensional space but not in an infinite-dimensional one).

Even if the above stability analysis were successful, the <u>adaptive control laws (3.6) and (3.13) could not be implemented.</u> They require instantaneous knowledge of the infinite-dimensional plant and model states, and this is not available either from sensor outputs or on-line computation. This adaptive control algorithm is infinite-dimensional. Therefore, we must modify the adaptive controller so that we shall obtain a <u>finite-dimensional adaptive control algorithm.</u>

<u>Assume</u>:

(a) dim v_m = dim v_N = N < ∞ and A_m stable.

(b) $C_N = I_N$, i.e. there are N linearly independent sensor outputs.

120

(c) the <u>modified exact model matching conditions</u> are satisfied:

$$A_N + B_m F_e = A_m \qquad (3.14a)$$

$$(B_N + C_R B_R)\, Q_e = B_m \qquad (3.14b)$$

The <u>desired-performance</u> will be that $\tilde{e}(t) \equiv v_m(t) - y(t) \to 0$ as $t \to \infty$, since $y(t)$ is the best estimate we have of $v_N(t)$, this is the most we can expect from the reduced-order formulation. Note that

$$\tilde{e}(t) = e(t) - C_R v_R(t) \qquad (3.15)$$

because $y(t) = v_N(t) + C_R v_R(t)$.

The <u>adaptive control law</u> is given by

$$f(t) = Q(t)\ \tilde{f}(t) + Q(t)\ F(t)\ y(t) \qquad (3.16)$$

where the <u>adaptation laws</u> are

$$\dot{F}(t) q_1 = \Gamma_1\ B_m^{\ *}\ P_m \tilde{e}(t)(y(t),\ q_1) \qquad (3.17a)$$

$$\dot{Q}^{-1}(t) q_2 = -\Gamma_2\ B_m^{\ *}\ P_m \tilde{e}(t)(f(t),\ q_2) \qquad (3.17b)$$

for all q_1 in H and q_2 in R^M. The positive definite operator P_m satisfies:

$$A_m^{\ *}\ P_m + P_m\ A_m = -\ I \qquad (3.18)$$

because A_m is stable with rank N. Note that this adaptive controller requires only available measured information $y(t)$ and is a finite-dimensional algorithm.

The <u>stability analysis</u> proceeds as before. We try a Lyapunov function of the form:

$$V(t) = 1/2[(\tilde{e}(t),\ P\tilde{e}(t)) + tr\ \Phi^*(t)\ \Gamma^{-1}\Phi(t)] \qquad (3.19)$$

From (3.1), we obtain

$$\frac{\partial e}{\partial t} = A_m \tilde{e} + B_m\ \Phi\ z_N + W_R\ v_R \qquad (3.20)$$

where $W_R \equiv (A_m - B_N QF - B\Phi_2 QF - B_m\Phi_1)\ C_R - C_R(A_R + B_R QFC_R) + A_{NR}$ and $z_N = \begin{bmatrix} y \\ f \end{bmatrix}$.

Formal calculation of the derivative yields:

$$\dot{V}(t) = -\ 1/2||\tilde{e}||^2 + (\tilde{e},\ P_m W_R v_R) \leq -\ 1/2R(t)||\tilde{e}(t)|| \qquad (3.21)$$

where $R(t) \equiv ||\tilde{e}(t)|| - ||P_m||\ ||W_R(t)||\ ||v_R(t)||$. Also, from (3.1b) and (3.16), we have

$$\frac{\partial v_R}{\partial t} = A_R v_R - B_R OF\tilde{e} + B_R QFv_m + B_R Q\tilde{f} \tag{3.22}$$

The following stability result holds:

<u>Theorem 4</u>: If the parameter errors $\Phi(t)$ and the adaptive gains $Q(t)$, $F(t)$ remain bounded and $B_R = 0$, then $\tilde{e}(t)$ is <u>ultimately bounded</u>, i.e. there is a neighborhood S of the origin such that $\lim_{t \to \infty} e(t) \epsilon S$.

The proof of this result follows from the facts: $||W_R(t)||$ is bounded and A_R is exponentially stable (see 2.7e). It uses an argument similar to [10] Theo. 16 with Lyapunov functions for infinite-dimensional systems which can be carried out rigorously; see [9] Chapt. IV.

We should note that Theo. 4 requires too strong a set of hypotheses to be very useful. Moreover, for all of that we still only get that $\tilde{e}(t)$ is ultimately bounded. This shows that even the simplest finite-dimensional adaptive control laws for DPS require a much more complicated stability analysis.

A somewhat different approach to finite-dimensional adaptive control of DPS is given in the following:

<u>Assume</u> there exist v^*, f^* such that:

$$v^* = S_{11} v_m + S_{12} \tilde{f} \tag{3.23a}$$

$$f^* = S_{21} v_m + S_{22} \tilde{f} \tag{3.23b}$$

where v_m and f come from (3.5) and

$$\frac{\partial v^*}{\partial t} = A v^* + Bf^* \tag{3.24a}$$

$$y^* \equiv C v^* = y_m \equiv C_m v_m \tag{3.24b}$$

Furthermore, we <u>assume</u> dim $v_m = N < \infty$. For <u>step inputs</u>, i.e. $\tilde{f}(t)$ constant, it follows that

$$S_{11} A_m = A S_{11} + B S_{21} \tag{3.25a}$$

$$S_{11} B_m = A S_{12} + B S_{22} \tag{3.25b}$$

Also, from (3.24b), we have

$$C S_{11} = C_m \tag{3.26a}$$

$$C S_{12} = 0 \tag{3.26b}$$

In more compact form, (3.25) and (3.26) become:

122

$$\begin{bmatrix} A & B \\ C & 0 \end{bmatrix} \begin{bmatrix} S_{11} & S_{12} \\ S_{21} & S_{22} \end{bmatrix} = \begin{bmatrix} S_{11}A_m & S_{11}B_m \\ C_m & 0 \end{bmatrix} \qquad (3.27)$$

When the operator equation (3.27) is solvable for S_{ij}, there exist trajectories of the DPS (1.1) which are generated by a finite-dimensional model (3.5). These trajectories will be the "equilibria" for the stability analysis of the adaptive control algorithm; we do not need to know these trajectories explicitly - only that they exist. See also [11] where a "tuned system" is required to exist for the input-output stability analysis.

Let $e(t) \equiv v(t) - v^*(t)$ and we obtain

$$\begin{cases} \dfrac{\partial e}{\partial t} = (A + B\,G\,C)e \\ e(o) = e_o \end{cases} \qquad (3.28)$$

when we apply the following <u>nonadaptive control law</u>:

$$f(t) = f^*(t) + G(y(t) - y_m(t)) = S_{21}v_m(t) + S_{22}\tilde{f}(t)$$

$$+ G(y(t) - y_m(t)) \qquad (3.29)$$

This control law requires knowledge of the <u>output error</u>, $y - y_m$, the finite-dimensional model state v_m, and the step input command $\tilde{f}(t)$. If the DPS (A,B, C) can be <u>output feedback stabilized</u>, i.e. There exists a gain operator G such that A + BCG generates an exponentially stable C_o-semigroup, then $\lim\limits_{t \to \infty} e(t) = 0$.

The control law (3.29) requires knowledge of the gains S_{21}, S_{22} and G which exist but may not be available in an explicit form. This leads us to an <u>adaptive</u> version of (3.29):

$$f(t) = S_{21}(t)\,v_m(t) + S_{22}(t)\,\tilde{f}(t) + G(t)(y(t) - y_m(t)) \qquad (3.30)$$

From (3.30) and (1.1), we obtain

$$\begin{cases} \dfrac{\partial e(t)}{\partial t} = (A + BG(t)C)\,e(t) + BL(t)\,z(t) \\ e(o) = e_o \end{cases}$$

where $L(t) \equiv [L_1(t) \vdots L_2(t)]$, $L_1(t) \equiv S_{21}(t) - S_{21}$, $L_2(t) \equiv S_{22}(t) - S_{22}$, and

$$z(t) \equiv \begin{bmatrix} v_m(t) \\ f(t) \end{bmatrix}$$

As before, we can try a Lyapunov function of the form:

$$V(t) \equiv 1/2[(e, Pe) + \text{tr } \Delta G^* \Gamma_1 \Delta G + \text{tr } L^* \Gamma_2 L] \tag{3.32}$$

where

$$(A_c v, Pv) + (Pv, A_c v) = -||v||^2 \tag{3.33}$$

for all v in $D(A)$ and $A_c \equiv A + BGC$ exponentially stable. This will lead to the appropriate <u>adaptation laws</u> so that $e(t)$ is stable, but we must find some other way to show $\overline{\lim_{t \to \infty} e(t)} = 0$.

The above approach for generating finite-dimensional adaptive control laws for DPS is presently under consideration in [25]. It seems possible to arrive at reasonable conditions on the DPS (1.1) which will permit stable finite-dimensional adaptive control. Note that the results of Sec. 2.0 are useful for assessment of the output feedback stabilizability of (A,B,C).

The two adaptive algorithms for DPS developed in this section illustrate the difficulties present for stability analysis of adaptive DPS. In the next section, we present some methods for DPS stability analysis.

4.0 ADAPTIVE DPS STABILITY ANALYSIS

We have already mentioned the popular use of La Salle's Invariance Principle for stability analysis of finite-dimensional systems. Its extension to infinite-dimensions is not nearly as valuable a tool due to the fact that bounded sets are not precompact in infinite-dimensional spaces. However, in [12]-[14], the idea of imbedding the original dynamical system in an "extended system" is used. The original system on a Banach space H is embedded in a larger space H_e where the identification map $i: H \to H_e$ is a <u>compact operator</u>, i.e. it maps bounded sets into precompact ones. This usually involves Sobolev norms and associated spaces. Then solutions of the original system have limit sets in H_e where the generalized invariance principle holds. Also, see [9] Chapt. IV.

Another approach that seems especially amenable to finite-dimensional adaptive control of DPS is the center manifold theory; see [15]. Consider DPS of the form:

$$\begin{cases} \dfrac{\partial v}{\partial t} = Av + N(v) \\ v(o) = v_o \end{cases} \tag{4.1}$$

where A generates a C_o-semigroup $U(t)$ on a Banach space H and $N: H \to H$ is smooth, i.e. has a uniformly continuous second derivative with $N(0) = 0$ and $N'(0) = 0$. We consider <u>weak solutions</u> of (4.1), i.e. continuous solutions $v(t)$ in H of the <u>integral equation</u>:

$$v(t) = U(t) v_o + \int_0^t U(t-\tau)N(v(\tau))d\tau \tag{4.2}$$

124

for any v_o in H. The <u>following assumptions</u> are made:

(a) $H = H_N \oplus H_R$ where dim $H_N = N < \infty$ and H_R is closed,

(b) H_N is A-invariant, i.e. $A(H_N) \subseteq H_N$, and $A_N \equiv P_N A P_N$ is stable, where (P_N, P_R) are the projections associated with (H_N, H_R).

(c) $A_R \equiv P_R A P_R$ generates the C_o-semigroup $U_R(t)$ on H_R with

$$||U_R(t)|| \leq K_R e^{-\sigma_R t}, \quad t \geq 0 \tag{4.3}$$

where $K_R \geq 1$ and $\sigma_R > 0$.

Let $x \epsilon H_N$ and $y \epsilon H_R$ and define $f(x,y) \equiv P_N N(x+y)$, $g(x,y) \equiv P_R N(x+y)$. Thus, (4.1) may be written:

$$\begin{cases} \dfrac{\partial x}{\partial t} = A_N x + f(x,y) & (4.4a) \\[2mm] \dfrac{\partial y}{\partial t} = A_R y + g(x,y) & (4.4b) \end{cases}$$

A <u>center manifold</u> is an invariant manifold for (4.4) which is tangent to H_N at the origin.

<u>Theorem 5</u>: There exists a center manifold for (4.4), i.e. $y = h(x)$ for $||x|| < \delta$ and h has a continuous second derivative. The equation on the <u>center manifold</u> is

$$\frac{\partial \omega}{\partial t} = A\omega + f(\omega, h(\omega)) \tag{4.5}$$

<u>Theorem 6</u>: If the zero solution of (4.5) is stable, asymptotically stable, or unstable, then the zero solution of (4.4) is stable, asymptotically stable, or unstable respectively.

The proofs of Theos. 5 and 6 are given in [15]. They allow us to conclude stability of a nonlinear DPS by determining the stability of the (finite-dimensional) nonlinear system (4.5) which is obtained via the center manifold and projection onto the finite-dimensional subspace H_N. This seems quite closely related to the results of Sec. 2.0 for linear DPS, i.e. we.would expect that our <u>finite-dimensional</u> adaptive controllers would stabilize the DPS (1.1) if a center manifold associated with some finite-dimensional subspace H_N would yield a stable finite-dimensional system (4.5) on H_N. This should follow from Theo. 6, although it must be extended to time-varying nonlinearities for application to adaptive control. One difficulty with the center manifold theory is the need for H_N to be invariant under the linear operator A. Thus implies <u>modal subspaces</u> H_N and H_R must be used as the theory now stands; perhaps, it can be modified so

_that "almost-invariant" subspaces, e.g. Galerkin subspaces, are acceptable.

Finally, the use of input-output stability methods is presently having a great deal of success in finite-dimensional, nonadaptive control, e.g. [16]-[17]. Also, the general approach has begun to be used for adaptive control in [11] and [18]. An _input-output mapping_ of the form:

$$q(t) = (Tu)(t) \tag{4.6}$$

is said to be $\underline{L^2\text{-stable}}$ if $u \epsilon L^2(0,\infty, H)$ implies $q \epsilon L^2$ and

$$||q||_2 \leq M||u||_2 \tag{4.7}$$

where $||q||_2 \equiv (\int_0^\infty ||q(t)||^2 dt)^{1/2}$. Other types of input-output stability involve the L^p spaces for integers $p = 1$ or $p \geq 3$. For finite-dimensional systems, L^2-stability implies internal stability for any minimal state-space realization of (4.6), i.e. the states are exponentially stable [19]; however, for infinite-dimensional systems, this is not necessarily the case. Yet for DPS (1.1), it is the stability of the full state $v(t)$ which we want to guarantee. Consequently, there is a need for some relationships between input-output and internal stability of DPS to be developed.

One such result is the following:

Theorem 7: Consider the DPS

$$\begin{cases} \dfrac{\partial v}{\partial t}(t) = A\, v(t) + h(t,v(t)) \\ v(o) = v_o \end{cases} \tag{4.8}$$

where A generates an exponentially stable C_o-semigroup $U(t)$, i.e.

$$||U(t)|| \leq Ke^{-\sigma t}, \; t \geq 0 \tag{4.9}$$

with $K \geq 1$ and $\sigma > 0$ and $h:R^+ x H \to H$ is continuous. If the input-output mapping (4.6) is L^2-stable where

$$\begin{cases} q(t) = h(t,\omega(t)) \\ \omega(t) = u(t) + \int_0^t U(t-\tau)q(\tau)d\tau \end{cases} \tag{4.10}$$

then (4.8) is globally asymptotically stable, i.e. $\lim_{t \to \infty} v(t) = 0$ for any v_o in H.

The proof of this is given in the Appendix; see also [20] and [21] for similar relationships.

A particular application of Theo. 7 would be to apply some nonlinear adaptive

control law:

$$f(t) = \gamma(t, y(t)) \tag{4.11}$$

to a DPS of the form (1.1). We may think of (1.1) and (4.11) as an _infinite-dimensional error model_. Let $h(t,v(t)) \equiv B(t,Cv(t))$ in Theo. 7 and consider (4.6) defined by

$$\begin{cases} q(t) = \gamma(t,\omega(t)) & \text{(4.12a)} \\[2mm] \omega(t) = Cv(t) = u(t) + C \int_0^t U(t-\tau)Bq(\tau)d\tau & \text{(4.12b)} \\[2mm] u(t) = C \ U(t) \ v_o & \text{(4.12c)} \end{cases}$$

If the linear DPS (4.1)) is exponentially stable and the input-output map defined by (4.12) is L^2-stable, then

$$\lim_{t \to \infty} y = \lim_{t \to \infty} \omega(t) = 0 \tag{4.13}$$

for any v_o in H. In general, this does _not_ say:

$$\lim_{t \to \infty} v(t) = 0 \tag{4.14}$$

It only says $v(t)$ is attracted to the null space of the output operator C. Even though the linear system (A,C) is observable in the DPS sense [23], this does not guarantee (4.14) for the nonlinear system (1.11) and (4.11).

Note that (4.12) has the block-diagram form of Figure 1.
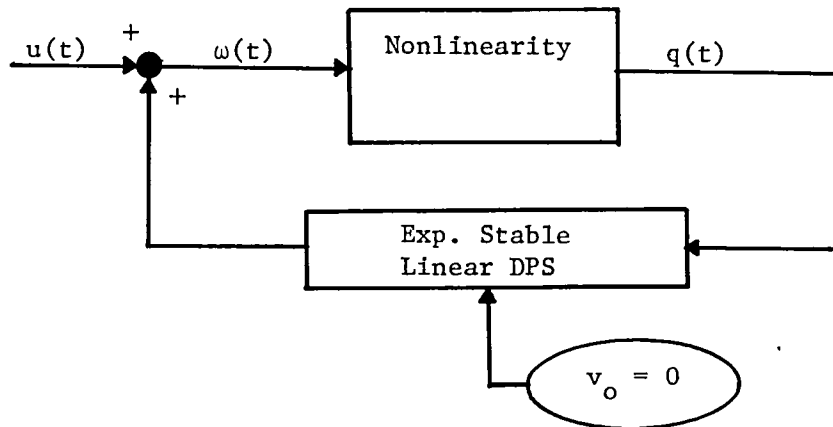
5.0 CRITICAL ISSUES IN INFINITE-DIMENSIONAL STABILITY ANALYSIS

As we have pointed out here, there are substantial differences in nonlinear stability analysis for finite and infinite dimensional systems. Some of the critical issues already presented are

(1) the DPS (1.1) is linear time-invariant, and infinite-dimensional but the adaptive controller must be a finite-dimensional algorithm,

(2) the stability analysis must be done for a nonlinear, time-varying infinite-dimensional system,

(3) limiting solutions should exist, i.e. non-adaptive finite-dimensional controllers of the DPS to which the adaptive laws can converge,

(4) the La Salle Invariance Principle, which is so useful in finite-dimensional stability analysis, does not immediately extend to infinite-dimensions due to the fact that a bounded set is not necessarily precompact,

(5) the Center Manifold Theory seems to extend nonlinear stability results from finite to infinite dimensions in a natural way but it implies that the critical part of this analysis will occur on a finite-dimensional subspace (similar to the linear stability situation),

(6) the use of input-output stability results is much more limited for DPS unless relationships can be found for internal stability (it is the internal state of a DPS which must be stabilized by adaptive control).

Useful references for further consideration of these stability issues for DPS are [9], [15], and [21]. Also, see the survey [24]. Further results on question (6) for the nonadaptive case appear in [26]-[28].

APPENDIX: PROOF OF THEO. 7

Consider v_o in H and

$$v(t) = U(t) \, v_o + \int_0^t U(t-\tau)h(\tau,v(\tau))d\tau$$

Thus $v(t) = \omega(t)$ for $u(t) \equiv U(t) \, v_o$. Clearly this particular u is in L^2 because

$$||u||_2^2 = \int_0^\infty ||u(t)||^2 \, dt \leq K^2 \int_0^\infty e^{-2\sigma t} dt = \frac{K^2}{2\sigma}.$$ Also $\lim_{t\to\infty} u(t) = 0$ due to (4.9).

Since T in (4.6) is L^2-stable, we have q in L^2; hence, ω is in L^2 from (4.10).

Let $z(t) \equiv \int_0^{t/2} U(t-\tau)q(\tau)d\tau$ and we assert that $\lim_{t\to\infty} z(t) = 0$: Consider $z(t) =$

$$\int_0^{t/2} U(t-\tau)q(\tau)d\tau + \int_{t/2}^t U(t-\tau)q(\tau)d\tau = \int_{t/2}^t U(\tau)q(t-\tau)d\tau + \int_{t/2}^t U(t-\tau)q(\tau)d\tau$$

$$\therefore \; ||z(t)|| \leq K[\int_{t/2}^t e^{-\sigma t} ||q(t-\tau)||d\tau + \int_{t/2}^t e_\tau^{-\sigma(t-\tau)} ||q(\tau)||d\tau]$$

$$\leq K[(\int_{t/2}^t e^{-2\sigma\tau}d\tau)^{1/2} (\int_{t/2}^t ||q(t-\tau)||^2 d\tau)^{1/2}$$

$$+ (\int_{t/2}^t e^{-2\sigma(t-\tau)}d\tau)^{1/2} (\int_{t/2}^t ||q(\tau)||^2 d\tau)^{1/2}]$$

$$\leq K \, [(\frac{e^{-\sigma t}-e^{-2\sigma t}}{2\sigma})^{1/2} \, (\int_{0}^{\infty} ||q(\tau)||^2 d\tau)^{1/2}$$

$$+ (\frac{1-e^{-\sigma t}}{2})^{1/2} \, (\int_{t/2}^{\infty} ||q(\tau)||^2 d\tau)^{1/2}]$$

This follows from the Cauchy-Schwarz Inequality and the fact that q is in L^2. Now

$$\lim_{t \to \infty} ||z(t)|| \leq K[0 \cdot ||q||_2 + \frac{1}{2\sigma} \, .$$

$$\lim_{t \to \infty} (\int_{t/2}^{\infty} ||q(\tau)||^2 d\tau)^{1/2}]$$

From [22], when q is in L^2, we have

$$\lim_{t \to \infty} \int_{t}^{\infty} ||q(\tau)||^2 d\tau = 0. \quad \text{Therefore,}$$

$\lim_{t \to \infty} z(t) = 0$. But, because $v = \omega = u + z$, we have the desired result. $\#$

REFERENCES

[1] M. Balas, "Feedback Control of Linear Distributed Parameter Systems: What Can Be Accomplished With A Finite-Dimensional Controller?", Proc. IFAC Plenary Lecture, Symp. on Large Scale Systems, Warsaw, Poland, 1983.

[2] M. Balas and C.R. Johnson, Jr., "Adaptive Control of Distributed Parameter Systems: The Ultimate Reduced-Order Problem", Proc. of 18th IEEE Control and Decision Conf., Ft. Lauderdale, Fl., 1979.

[3] M. Balas and C.R. Johnson, Jr., "Adaptive Identification and Control of Large-Scale or Distributed Parameter Systems Using Reduced-Order Models, 2nd Yale Conf. on Appl. of Adaptive Control, Yale University, New Haven, CT., 1982.

[4] M. Balas, "The Structure of Discrete and Continuous-Time Control of Linear Distributed Parameter Systems", Conf. on Info. Scie. and Systems, The Johns Hopkins University, Baltimore, MD, 1983.

[5] M. Balas, "The Structure of Discrete-Time Finite-Dimensional Control of Distributed Parameter Systems", J. Math Analy. & Appl. (to appear).

[6] M. Balas, "The Mathematical Structure of the Feedback Control Problem for Linear Distributed Parameter Systems With Finite-Dimensional Controllers", Proc. of the Conf. on Control Theory for Distributed Parameter Systems, Vorau, Austria, 1982.

[7] J. La Salle, "Some Extensions of Liapunov's Second Method", IRE Trans. Circuit Theory, CT-7, 520-527, 1960.

[8] K.S. Narendra & P. Kudva, "Stable Adaptive Schemes for System Identification and Control, Part I", IEEE Trans. Systems, Man and Cybernetics, SMC-4, 542-551, 1974.

[9] J. Walker, Dynamical Systems and Evolution Equations: Theory and Applications, Plenum Press, NY, 1980.

[10] J. La Salle and S. Lefschetz, Stability by Liapunov's Direct Method, Academic Press, NY, 1961.

[11] C.R. Johnson, Jr. and R. Kosut, "Robustness of Reduced-Order Adaptive Model Following", Proc. of 3rd Yale Workshop on Applications of Adaptive Systems Theory, Yale University, New Haven, CT. 1983.

[12] J. Hale and E. Infante, "Extended Dynamical System and Stability Theory", Proc. of Nat. Acad. of Sci., Vol. 58, 504-509, 1967.

[13] J. Hale, "Dynamical Systems and Stability", J. Math. Analy. & Appl., Vol. 26, 39-59, 1969.

[14] M. Slemrod, "An Invariance Principle for Dynamical Systems in Hilbert Space With Applications to Asymptotic Stability of Equilibrium', Doctoral Dissertation, Appl. Math. Division, Brown University, Providence, RI, 1969.

[15] J. Carr, Applications of Center Manifold Theory, Springer-Verlag, New York, 1981.

[16] C. Desoer, R-W Liu, J. Murray, and R. Saeks, "Feedback System Design: The Fractional Representation Approach to Analysis and Synthesis", IEEE Trans. Autom. Contr., AC-25, 399-412, 1980.

[17] M. Vidyasagar, H. Schneider, and B. Francis, "Algebraic and Topological Aspects of Feedback Stabilization", IEEE Trans. Autom. Contr., AC-27, 880-894, 1982.

[18] R. Kosut and B. Friedlander, "Robust Adaptive Control: Conditions for Global Stability", IEEE Trans. Autom. Contr. (to appear).

[19] B.D.O. Anderson, "External and Internal Stability of Linear Systems - A New Connection", IEEE Trans. Autom. Contr., AC-17, 107-111, 1972.

[20] C. Desoer and M. Vidyasagar, Feedback Systems: Input-Output Properties, Academic Press, NY, 1975.

[21] J. Willems, "A Survey of Stability of Distributed Parameter Systems", in Control of Distributed Parameter Systems, Joint Automatic Contr. Conf., Boulder, Colorado, M. Athans (ed.) Am. Soc. of Mech. Engr., NY, 1969.

[22] H. Royden, <u>Real Analysis</u>, Macmillan, NY, 1963.

[23] A. Balakrishnan, <u>Applied Functional Analysis</u>, Springer, NY, 1976.

[24] J. Casti, "Recent Developments and Future Perspectives in Nonlinear System Theory", SIAM Review, Vol. 24, 301-331, 1982.

[25] M. Balas, H. Kaufman, & J. Wen, "Stable Direct Adaptive Control of Linear Infinite-Dimensional Systems Using A Command Generator Tracker Approach", This Proceedings.

[26] C. Nett, C. Jacobson, and M. Balas, "Fractional Representation Theory: Robustness Results With Applications To Finite-Dimensional Control of a Class of Linear Distributed Systems", Proc. of IEEE Control and Decision Conf., San Antonio, TX, 1983.

[27] C. Jacobson, "Some Aspects of the Structure and Stability of a Class of Linear Distributed Systems", Rensselaer Polytechnic Institute Robotics and Automation Laboratory, Troy, New York, RAL Report, May 1984.

[28] C. Nett, "The Fractional Representation Approach to Rubust Linear Feedback Design: A Self-Contained Approach", Rensselaer Polytechnic Institute Robotics and Automation Laboratory, Troy, New York, RAL Report, May 1984.

A FACTORIZATION APPROACH TO THE LINEAR REGULATOR QUADRATIC COST PROBLEM

M. H. Milman
Jet Propulsion Laboratory
California Institute of Technology
Pasadena, CA 91109

ABSTRACT

A factorization approach to the linear regulator quadratic cost problem is developed. This approach makes some new connections between optimal control, factorization, Riccati equations and certain Wiener-Hopf operator equations. Applications of the theory to systems describable by evolution equations in Hilbert space and differential delay equations in Euclidean space are presented.

1.   **Notation and problem statement.** For any Banach space Y, $|y|$ will denote the norm of an element $y \epsilon Y$; $B(Y,Z)$ will denote the space of bounded linear maps from Y into Z and we will write $B(Y)$ for $B(Y,Y)$. Let $[0,t_f]$ denote a bounded interval in R and let Σ denote the class of Borel subsets of $[0, t_f]$. Let U and X denote real separable Hilbert spaces with resolutions of the identity $E_U: \Sigma \to B(U)$ and $E_X: \Sigma \to B(X)$. We shall assume that both E_U and E_X are absolutely continuous, i.e. the measures $|E_U(\omega)u|^2$ and $|E_X(\omega)x|^2$ are absolutely continuous with respect to Lebesgue measure λ for each $u \epsilon U$ and $x \epsilon X$.

Our objective is to develop the optimal control law for the following regulator problem:

$$\min_{u,x} J(u,x) = |u|^2 + |x|^2 \tag{1.1}$$

subject to the constraint

$$x = f + Tu \tag{1.2}$$

where f, $x \epsilon X$, $u \epsilon U$ and $T \epsilon B(U,X)$ is causal ($E_X(0,t) \, TE_U(0,t) = E_X(0,t)T$ for all t). We shall also use the notations $P^t = E(0,t)$ and $P_t = I-P^t$. Typically U and X represent L_2 – spaces over Hilbert spaces (finite or infinite dimensional), T is an integral operator, and E_U and E_X are the resolutions induced by multiplication by the characteristic function, i.e. for $\omega \epsilon \Sigma$

$$[E_U(\omega)u](t) = \begin{cases} u(t) & t \epsilon \omega \\ 0 & t \notin \omega. \end{cases} \tag{1.3}$$

We will henceforth refer to the resolution of the identity above as the truncation resolution.

Although at this level of generality, we cannot meaningfully develop a feedback solution to the optimization problem (1.1) – (1.2), the causality of T together with another hypothesis that will be introduced shortly permits the synthesis of a control law that is intermediate between open and closed loop. Heuristically this can be described as a feedback on the space of possible trajectories of the system. In the examples it will be seen that this "mid-way" formulation of the control law leads to new derivations of the feedback gains for some systems described by evolution operators in Hilbert space and delay equations in R^N. These derivations illuminate some connections between optimal control, factorization of operators and Riccati equations. It is anticipated that these connections can be exploited to produce approximation schemes for the optimal control laws associated with large space structure applications.

2. **Main results.** In this section we consider the control problem (1.1) – (1.2) under the additional hypothesis on T:

H1: There exists a constant α and a probability measure μ such that μ is absolutely continuous with respect to Lebesgue measure and

$$|TE(\omega)| \leq \alpha \sqrt{\mu(\omega)} \qquad \text{for all } \omega \epsilon \Sigma \tag{2.1}$$

Whenever a map K satisfies (2.1) we write $K<\mu$.

Example 2.1. Suppose U and X are L_2 – spaces over the Hilbert spaces H_1 and H_2 and the resolutions E_U and E_X are the truncation resolutions (cf (1.3)). Then it can be shown that any map K of the form

$$K u: t \to \int_0^1 K(t,s)u(s)ds$$

with $K(t,s)\epsilon B(H_1,H_2)$ and $|K(\cdot,\cdot)|\epsilon L_2((0,1) \times (0,1))$ satisfies H1.

More generally, any Hilbert-Schmidt map satisfies the hypothesis above [11].

Assuming a map $K\epsilon B(U,X)$ satisfies H1, the adjoint $K^*\epsilon B(X,U)$ induces a mapping $F(K^*)$ from the space of μ–square integrable functions with values in X, $L_2((0,1), X;\mu)$, into U in the following way:

Let $x\epsilon L_2((0,1)), X;\mu)$ be simple, say $x(t) = \Sigma x(\omega_i)(t)x_i$. Define $F(K^*)x$ by

$$F(K^*)x = \sum E_U(\omega_i)K^*x_i.$$

Then for the simple function x,

$$|F(K^*)x|^2 = \sum|E_U(\omega_i)K^*x_i|^2 \leq \sum|x_i|^2\mu(\omega_i) = \int |x|^2 d\mu.$$

Thus $F(K^*)$ extends by continuity to $B (L_2((0,1), X;\mu), U)$. Note also that if we introduce the truncation resolution $\widetilde{E}$ on $L_2((0,1),X;\mu)$, then $F(K^*)$ has the property that $E_U(\omega)F(K^*) = F(K^*) \widetilde{E}(\omega)$ for all $\omega\epsilon\Sigma$. This mapping together with its commutativity property with respect to E_U and $\widetilde{E}$ plays an important role in what follows. For now we note the following result from [10].

Proposition 2.2. In the setting of Example 2.1 suppose further that
$\underset{t,s}{\text{esssup}} |K(t,s)| < \infty$. Then $K,K^*<\lambda$ (Lebesgue measure) and

$$F(K)x:t \to \int_0^1 K (t,s,)x(t)(s)ds.$$

Returning to the control problem (1.1) –(1.2), standard arguments give the optimal solution as

$$\hat{u} = -(I + T^*T)^{-1}T^*f. \tag{2.2}$$

Now suppose for each $t\epsilon[0,1]$ a new problem is defined by introducing a new forcing term f_t and imposing the additional constraint that $u\epsilon P_t U$. Then the optimal control for this problem has the form

$$\hat{u}_t = -(I + P_t T^*TP_t)^{-1}P_t T^*f_t. \tag{2.3}$$

Since $P_o = I$, the solutions u and u_o coincide when $f_o = f$. More generally it can be shown that the selection

$$f_t = P_t [TP^*u + f] \tag{2.4}$$

results in $\hat{u}_t = \hat{u}$ for all t. Thus given any partition of $[0,1]$, $0 = t_o, < t_1, < ... < t_n = 1$, it follows that

$$\hat{u} = -\Sigma E_U(\omega_i) [I + P_{t_i} T^*TP_{t_i}]^{-1}P_{t_i} T^*f_{t_i}, \quad \omega_i = [t_i, t_{i+1}). \tag{2.5}$$

As defined by (2.4), f_t has the interpretation of being the response of the system after "time" t to a control input that terminates at t. Heuristically, f_t is the information derived from the knowledge of the system state at time t. In this context the solution (2.5) is no longer open loop since it can be updated with more current information.

Our "intermediate" feedback solution results from taking the limit in (2.5). Before doing so it is necessary to introduce the following theorems from [11].

Theorem 2.3. Let μ be a probability measure absolutely continuous with respect to Lebesgue measure and suppose $K\epsilon B(U)$ with $K<\mu$ and $I+K$ positive definite and invertible. Then there exists a unique causal $V\epsilon B(U)$ with $V, V^* <\mu$ such that

$$I + K = (I+V^*) (I+V).$$

Theorem 2.4. If $V\epsilon B(U)$ is causal (or anticausal) and $V<\mu$, then V is quasinilpotent.

Another useful result which can be deduced using the two theorems above is the following.

Theorem 2.5. Suppose $K\epsilon B(X)$ with $K<\mu$ and $I+K$ positive definite and invertible. Let $B\epsilon B(U,X)$ have the property that $E_X(\omega)B = BE_U(\omega)$ for all $\omega\epsilon\Sigma$. Then there exists a unique causal $Z\epsilon B(X)$ with $Z,Z^*<\mu$ such that

$$K = Z + Z^* + Z^*BB^*Z.$$

From the hypotheses on T it follows from Theorem 2.3 that $(I + T^*T)$ has the factorization

$$I + T^*T = (I + V^*)(I + V).\qquad(2.6)$$

Since V is causal and $V < \mu$, from Theorem 2.4 and the resolvent expression,

$$V + W + WV = 0,$$

it is evident that $T\,(I + V)^{-1} < \mu$. Hence, $F((I + V^*)^{-1} T^*) \epsilon B(L_2\,((0,1),\ X;\mu),\ U)$. Noting that the X-valued function

$$f(t) = P_t\,[TP^t u + f]\qquad(2.7)$$

is continuous (from the strong continuity of P^t), we obtain

$$F((I + V^*)^{-1} T^*)\ f(\cdot)\ \epsilon U.$$

Here we have used the fact μ has finite measure so that $C([0,1],X) \hookrightarrow L_2((0,1),\ X;\mu)$.

With this background the expression for the limiting control law in (2.5) can now be given.

Theorem 2.6. Let V and $f(\cdot)$ be defined as in (2.6) and (2.7) respectively. Then the optimal control law for (2.1) – (2.2) has the representation

$$\hat{u} = -F\,((I + V^*)^{-1} T^*)f\,(\cdot).$$

In the examples of the next section we shall see that the transition from the solution above to the closed loop solutions is accomplished in a somewhat straightforward fashion once the proper identification of various operators is made.

3.   Examples. Our first example concerns systems governed by differential equations in Hilbert space (cf [1], [4], [7], [8]). Let H_1 and H_2 denote real separable Hilbert spaces and let $U = L_2((0,1),\ H_1)$ and $X = L_2\,((0,1),\ H_2)$. The dynamics of the system are defined as

$$x(t) = S(t)\,x_0 + \int_0^1 S(t-\sigma)Bu(\sigma)d\sigma,\qquad(3.1)$$

where $x_0 \epsilon H_2$, $x(\cdot)\epsilon X$, $u\,(\cdot)\epsilon U$, $B\epsilon B(H_1,\ H_2)$ and $S(t)$ is a strongly continuous semigroup on H_2. The cost functional is defined

$$J(u,x) = \int_0^t |x(t)|^2 + |u(t)|^2\ dt.\qquad(3.2)$$

In this setting $f = S(\cdot)x_0$, T is the integral operator defined in (3.1), and E_U and E_X are the truncation resolutions. It is straightforward to verify that T is causal and that $T < \lambda$. Thus the representation of Theorem 2.6 holds.

We now proceed to develop the usual form of the solution. First let us introduce the map $s : X \to L_2((0,1), X)$ by

$$[sx](t) : \sigma \to \begin{cases} 0 & \sigma < t \\ S(\sigma - t)x(t) & \sigma \geq t. \end{cases}$$

Using the truncation resolution $\tilde{E}$ on $L_2((0,1), X)$ it is evident that $\tilde{E}s = sE_X$. From Theorem 2.6 we have

$$\hat{u} = -F((I+V^*)^{-1}T^*) f(\cdot).$$

But,

$$f(t) : \sigma \to \begin{cases} 0 & \sigma < t \\ S(\sigma)x_0 + \displaystyle\int_0^t S(\sigma - s)Bu(s)ds & \sigma \geq t \end{cases}$$

$$= \begin{cases} 0 & \sigma < t \\ S(\sigma - t) \left[S(t)x_0 + \displaystyle\int_0^t S(t-s)Bu(s)ds \right. & \sigma \geq t \end{cases}$$

$$= \begin{cases} 0 & \sigma < t \\ S(\sigma - t)x(t) & \sigma \geq t. \end{cases}$$

Thus

$$\hat{u} = -F((I+V^*)^{-1}T^*)s\,\hat{x}(\cdot) \tag{3.3}$$

Now let $\omega \epsilon \Sigma$. It follows from the properties of $F(\cdot)$ and s that

$$E_U(\omega)F((I+V^*)^{-1}T^*)s = F((I+V^*)^{-1}T^*)E(\omega)s = F((I+V^*)^{-1}T^*)s\,E_X(\omega). \tag{3.4}$$

And since U and X are L_2 - spaces, a result from [10] together with the commutativity above implies the existence of a strongly measurable essentially bounded $B(H_2, H_1)$ - valued function $K(t)$ such that

$$[F((I+V^*)^{-1}T^*)s\,x(\cdot)](t) = K(t)x(t) \qquad \text{a. e.} \tag{3.5}$$

for every $x(\cdot) \epsilon X$. This result with (3.3) gives the feedback form

$$\hat{u}(t) = -K(t)\hat{x}(t). \tag{3.6}$$

We will now show that $K(t) = B^*P(t)$ where $P(t)$ is the unique solution to the Riccati equation

138

$$P(t)x = \int_t^1 S^*(\sigma-t) \{I - P^*(\sigma)BB^*P(\sigma)\} S(\sigma-t)x \, d\sigma, \quad x\epsilon \, H_2 \tag{3.7}$$

Probably the quickest way of demonstrating this (and existence and uniqueness of solutions to (3.7)) makes use of the generalized factorization of Theorem 2.5.

Let S denote the mapping in B(X),

$$Sx:t \to \int_o^t S(t-\sigma)x(\sigma)d\sigma.$$

An application of Theorem 2.5 yields the factorization

$$S^*S = Z + Z^* + Z^*BB^*Z, \qquad Z,Z^* < \lambda. \tag{3.8}$$

Since $T^*T = BS^*SB$, from uniqueness it is evident that $V = B^*ZB$. Thus it follows

$$B^*Z = (I + B^*Z^*B)^{-1}(B^*S^*S - B^*Z^*)$$

$$= [(I+V^*)^{-1}T^*S]_+ ,$$

where the notation $[\cdot]_+$ is used to denote the causal part of an operator. From here it is not difficult to argue (see [10]) that

$$B^*Z = F((I+V^*)^{-1}T^*)s \, S.$$

Thus B^*Z is an integral operator with kernel $K(t)S(t-\sigma)$. A similar argument yields

$$Z = F((I+Z^*BB^*)^{-1}S^*)s \, S. \tag{3.9}$$

Hence, Z has kernel of the form $P(t)S(t-\sigma)$ (cf (3.5)). And standard arguments (see for example Zaanen [12]) show that $B^*P(t) S(t-\sigma) = K(t) S (t-\sigma)$ for a.e. t,σ. And since $S(t) \to I$ strongly as $t \to 0$, we have $K(t) = B^*P(t)$ a.e. It remains to verify (3.7). Using the notation $Z = PS$ (where $[Px](t) = P(t)x(t)$), (3.8) implies

$$PS = S^* [I-P^*BB^*P]S - S^*P^*$$

In terms of the kernels of these maps it follows that for a.e. t,σ with $t \geq \sigma$,

$$P(t)S(t-\sigma) = \int_t^1 S^*(s-t) \{I - P^*(s)BB^*P(s)\}S (s-\sigma) \, ds.$$

Again using the fact that S(t)→I strongly as t→0, it is evident that the equation above implies (3.7). Uniqueness follows because the argument here is essentially reversible, i.e. two distinct solutions of (3.7) will result in distinct factorizations of (3.8); which is impossible by Theorem 2.5.

We also note that embedded in the argument above is the result that the Volterra factor V is an integral operator with kernel V(t,σ) = K(t)S(t−σ).

Our next example concerns the hereditary system ([2], [5], [9])

$$\dot{x}(t) = L(t, x_t) + B\,u\,(t) \qquad t \geq 0 \quad (3.10)$$

$$x(t) = \phi(t) \qquad\qquad -r \leq t \leq 0,$$

(3.10)

where for each t, $u(t) \in R^M$, $x(t) \in R^N$, $B \in B(R^M, R^N)$, $\phi\,(\cdot) \in C\,([-r,0],\,R^N)$

and

$$L(t, x_t) = \int_{-r}^{o} d_\Theta \eta\,(t,\Theta)\,x\,(t+\Theta)$$

The standard hypotheses are imposed on $\eta\,(\cdot,\cdot)$ so that (3.10) has a unique absolutely continuous solution given by the following variation of constants formula (see [6]):

$$x(t) = Y(t,0)\,\phi\,(0) + \int_{-r}^{0} d_\beta\,\{\int_{o}^{t} Y(t,\alpha)\,\eta\,(\alpha,\beta-\alpha)\,d\alpha\}\,\phi\,(\beta) \qquad (3.11)$$

$$+ \int_{o}^{t} (Y(t,\sigma)\,Bu\,(\sigma)d\sigma$$

The only property of $Y\,(\cdot,\cdot)$ we call attention to here is that it is bounded on bounded subsets of the plane. The cost functional we attach to (3.10) is once again

$$J(u,x) = \int_{o}^{1} |x\,(t)|^2 + |u(t)|^2\,dt. \qquad (3.12)$$

We will basically use the same setup as in the previous example: That is, we take $U = L_2\,((0,1), R^M)$, $X = L_2\,((0,1),\,R^N)$, and E_U and E_X as the truncation resolutions. For the forcing term we take $f(\cdot) \in X$,

$$f(t) = Y(t,0)\,\phi(0) + \int_{-r}^{o} d_\beta\,\{\int_{o}^{t} Y\,(t,\alpha)\,\eta(\alpha,\beta-\alpha)\,d\alpha\}\,\phi(\beta).$$

And T is the operator

$$Tu:t \to \begin{cases} 0 & t < 0 \\[2mm] \displaystyle\int_0^t Y(t,\sigma)\, Bu(\sigma)\,d\sigma. & t \geqq 0. \end{cases}$$

Since $Y(\cdot,\cdot)$ is bounded, once again we have $T < \lambda$. Thus Theorem 2.6 applies, i.e.

$$\hat{u} = -F\,((I+V^*)^{-1}T^*)\,z(\cdot).$$

In this case, for $s \geqq t$

$$z(t):s \to Y(s,0)\,\phi(0) + \int_{-r}^{0} d_\beta \left\{ \int_0^s Y(s,\alpha)\,\eta(\alpha,\beta-\alpha)\,d\alpha \right\} \phi(\beta)$$

$$+ \int_0^t Y(s,\alpha)\,Bu(\alpha)\,d\alpha.$$

But this is recognized as the solution to

$$\dot{x}(s) = L(s,x_s) \qquad\qquad s \geqq t$$

$$x(s) = \hat{x}(s) \qquad\qquad t-r \leqq s \leqq t.$$

Hence, the variation of constants formula implies

$$z(t):s \to Y(s,t)\,\hat{x}(t) + \int_{t-r}^{t} d_\beta \left\{ \int_t^s Y(s,\alpha)\,\eta(\alpha,\beta-\alpha)\,d\alpha \right\} \hat{x}(\beta). \tag{3.13}$$

Now since T has bounded kernel, T^*T necessarily has bounded kernel. It can then be shown that V also is an integral operator with bounded kernel. Thus since V is quasinilpotent, consideration of the Neumann series for $(I+V^*)^{-1}$ leads to the conclusion that $(I+V^*)^{-1}T^*$ is an integral operator with bounded kernel, say $K(t,s)$. Proposition 2.2 and (3.13) then imply

$$\hat{u}(t) = -\int_t^1 K(t,s)\left\{ Y(s,t)\hat{x}(t) + \int_{t-r}^{t} d_\beta \left\{ \int_t^s Y(s,\alpha)\,\eta(\alpha,\beta-\alpha)\,d\alpha \right\} \hat{x}(\beta) \right\} ds$$

$$= -\int_t^1 K(t,s)\left\{ Y(s,t)\hat{x}(t) + \int_t^s Y(s,\alpha)\int_{t-r}^{t} d_\beta\,\eta(\alpha,\beta-\alpha)\,\hat{x}(\beta)\,d\alpha \right\} ds.$$

141

Defining the kernel $P(t,\alpha)$,

$$P(t,\alpha) = \int_{\alpha}^{1} K(t,s)Y(s,\alpha)\, ds, \tag{3.14}$$

it follows that the optimal control has the feedback representation

$$\hat{u}(t) = -P(t,t)\, x(t) - \int_{t}^{\min(t-r,1)} P(t,\alpha) \left\{ \int_{t-r}^{t} d_{\beta}\, \eta\,(\alpha,\beta-\alpha)\, \hat{x}(\beta) \right\} d\alpha.$$

If we introduce the operator $S \in B(X)$,

$$Sx : t \to \int_{-r}^{t} Y(t,\sigma)\, x(\sigma)\, d\sigma,$$

it can be shown that the operator P with kernel $P(t,\alpha)$ satisfies the Wiener-Hopf equation

$$P = \{T^*S\}_- - \{PBT^*S\}_-$$

$$= \{[I-PB]\, T^*S\}_-.$$

This equation is equivalent to

$$P(t,s) = H(t,s) - \int_{t}^{1} P(t,\sigma)BH\,(\sigma,s)\, d\sigma, \tag{3.15}$$

where

$$H(t,s) = \int_{\max(t,s)}^{1} B'Y'\,(\sigma,t)\, Y\,(\sigma,s)\, d\sigma.$$

The equation above was derived earlier by Manitius [9] using a different approach. This equation can also be viewed as a parametrized family of Fredholm equations (in the parameter t). We note however that its solution is given in (3.14), and in our approach (3.15) is a consequence of the connection between factorization and Wiener-Hopf equations.

4.   Concluding remarks. The basic problem formulation could have been made slightly more general by allowing X to be a Banach space and replacing the norm term, $|\cdot|_X^2$, in the cost with a non-negative definite bilinear functional on X×X. A slightly different interpretation of B_X becomes necessary as well as some minor technical modifications in many of the arguments. We also note that the B-operators in each of the examples could have been generalized considerably to accommodate problem formulations which encompass a variety of control delays.

Although we have not focused on any of the numerical aspects of the examples we have considered, the approach here may have some applications in this area. For example, in practical applications the control space U is most often of the form $U = L_2$ $((0, 1), R^M)$. And since the factorization involves the operator $T^*T \epsilon B(U)$, the equation which defines the factor V is an integral equation of the form

$$K(t,s) = V(t,s) + \int_s^1 V'(\sigma,t) V(\sigma,s)\, d\sigma, \qquad s \leq t$$

where $V(t,s)$, $K(t,s) \epsilon R^{M \times M}$. (Here $K(t,s)$ is the kernel defining T^*T.) Thus, regardless of the dimensionality of the state space, the basic nonlinear aspect of the control problem can be reduced to the integral equation (with finite dimensional kernels) above. A similar situation develops in the infinite-time problem. In this case, the analogous factorization problem is the classical Wiener-Hopf factorization (see [3]).

In developing practical approximation schemes for control laws, properties of the factorization together with the generalizations discussed above can be used to obtain convergence estimates for the approximate control laws and gains. We very briefly outline how such an approach can work in the setting of the example involving the hereditary system.

Here we let X denote the Banach space $C([0,1], R^N)$ and let $< \cdot , \cdot >_n$ denote a sequence of bilinear functionals corresponding to quadratures. The family of projections P_X^t on X are defined

$$P_X^t y : s \rightarrow \begin{cases} y(s) & s \leq t \\ \\ y(t) & s \geq t . \end{cases}$$

Replacing the cost on the state in (3.12) by the functional $< \cdot , \cdot >_n$ leads to a control problem with solution kernel $P_n(t,\alpha)$. It can be shown that the kernel $P_n(t,\alpha)$ is "semi-separable", i.e. is of the form $p_n(t)q_n(\alpha) \chi[t,1](\alpha)$. It can also be shown that p_n and q_n can be generated by solutions of finite-dimensional differential equations (given the fundamental matrix $Y(t,s)$). Furthermore, by using continuous dependence properties of the associated factorization problems, L_2 convergence estimates can be established for the approximating kernels on both the square and the diagonal.

REFERENCES

1. A. V. Balakrishnan, "Applied Functional Analysis", Springer-Verlag, N.Y., 1976.

2. H. T. Banks and J. A. Burns, Hereditary control problems: Numerical methods based on averaging approximations, SIAM J. Control Optimization, 16, (1978), pp. 169-208.

3. J. H. Davis, Wiener-Hopf methods for open-loop unstable distributed systems, SIAM J. Control Optimization, 17, (1979), pp. 713-728.

4. J. S. Gibson, The Riccati integral equations for optimal control problems on Hilbert space, SIAM J. Control Optimization, 17, (1979), pp. 537-565.

5. J. S. Gibson, Linear-quadratic optimal control of hereditary differential systems: Infinite dimensional Riccati equations and numerical approximations, SIAM J. Control Optimization, 21, (1983), pp. 95-139.

6. J. Hale, "Theory of Functional Differential Equations," Springer-Verlag, N. Y., 1977.

7. J. L. Lions, "Optimal Control of Systems Governed by Partial Differential Equations," Springer-Verlag, Dunod, 1969.

8. D. L. Lukes and D. L. Russell, The quadratic criterion for distributed systems, SIAM J. Control Optimization, 7, (1969), pp. 101-121.

9. A. Manitius, Optimal control of linear time-lag processes with quadratic performance indexes in Proc. of Fourth IFAC Congress, Warsaw, Poland, (1969), pp. 16-28.

10. M. Milman, Special factorization and Riccati integral equations, J. Math. Anal. Appl., 100, (1984), pp. 155-187

11. M. Milman and A. Schumitzky, On a class of operators on Hilbert space with applications to factorization and systems theory, J. Math. Anal Appl., 99, (1984), pp. 494-512

12. A. C. Zaanen, "Linear Analysis", Interscience Publishers, Inc., N.Y. 1953.

APPROXIMATION TECHNIQUES FOR PARAMETER ESTIMATION AND FEEDBACK CONTROL FOR DISTRIBUTED MODELS OF LARGE FLEXIBLE STRUCTURES

H. T. Banks
Brown University
Providence, RI 02912

I. G. Rosen
Charles Stark Draper Laboratory
Cambridge, MA 02139

ABSTRACT

We discuss approximation ideas that can be used in parameter estimation and feedback control for Euler-Bernoulli models of elastic systems. Focusing on parameter estimation problems, we outline how one can obtain convergence results for cubic spline-based schemes for hybrid models involving an elastic cantilevered beam with tip mass and base acceleration. Sample numerical findings are also presented.

I. INTRODUCTION

In this lecture we discuss some approximation techniques that may be used in algorithms for parameter estimation and/or feedback control in distributed models such as those arising in models typical of large flexible space structures. The focus of our recent efforts has been the development and analysis of computational algorithms, e.g., convergence analysis, numerical implementation (software development) and testing. While the ideas involved are also applicable to the computation of feedback controls, we restrict our discussions here to some of our efforts on techniques in the context of parameter estimation or "inverse" problems: given observations of a system, determine parameters in models which best describe structural/material properties manifested by the system in response to perturbations (loading, etc.).

The importance of such problems is twofold: (i) parameter estimation can be viewed as a primary tool in on-orbit model development and analysis where one seeks to understand elastic/viscoelastic material properties such as damping, stiffness, etc. and to detect changes in these due to aging, prolonged stress, etc.; (ii) parameter estimation is a precursor to and integral part of development of sophisticated feedback control laws (via feedback operators satisfying infinite dimensional Riccati equations involving functional parameters of the system).

Many of the structures of interest to aerospace engineers entail systems composed of composite materials in rather complex geometric/structural configurations. The need for methods to investigate such variable structure distributed models has, in our opinion, been clearly established in a number of

recent efforts including [1], [2], [3], [4]. A number of investigations of parameter estimation in models for elastic beams have involved approximation results (the Trotter-Kato theorem) from linear semigroup theory. In particular, problems for simple beams have been treated in this manner in [5], [6], [7], [8]. In [9] the Trotter-Kato ideas are employed to establish results for hybrid models similar to those introduced later in this presentation and which are important in the study of shuttle-deployed payloads. However, in some instances it is advantageous to use an alternate approach involving a variational (weak) formulation of the system equations along with estimates in the spirit of those found in numerous papers on finite element techniques in structural problems. In [10] such a treatment was given for damped cantilevered Euler-Bernoulli beams. In this presentation we outline this approach in the context of models for beams with tip masses and base acceleration. Full details of our results in this direction will be given in a more lengthy manuscript currently in preparation.

Fundamental to our discussions is a conceptual framework in which one has a dynamical model with "states" $u(t,x)$, $0 < t < T$, $x \in \Omega$, and "parameters" $q(t,x)$, $q \in Q$, where Q is an admissible class of parameter functions. The state system is an initial-boundary value problem involving a hybrid model (parameter dependent and coupled partial differential equations/ordinary differential equations). One is given observations (data) $\bar{u}_{ij}$ for $u(t_i,x_i)$ and seeks to solve the optimization problem of finding parameters $\bar{q}$ in the feasible parameter set Q which give a best (in the least squares sense) fit of the model to the data.

We formulate this problem in an abstract setting with Hilbert state space V and parameter space Q. For computational purposes we then approximate V and Q by finite dimensional spaces V^N and Q^M respectively. We illustrate these ideas with a specific model and particular classes of approximations in our subsequent discussions here.

II. THE IDENTIFICATION PROBLEM

We consider a flexible beam of length ℓ, spatially varying stiffness EI and linear mass density ρ which is clamped at one end and free at the other with an attached tip mass of magnitude m (see Figure 2.1).

Figure 2.1

146
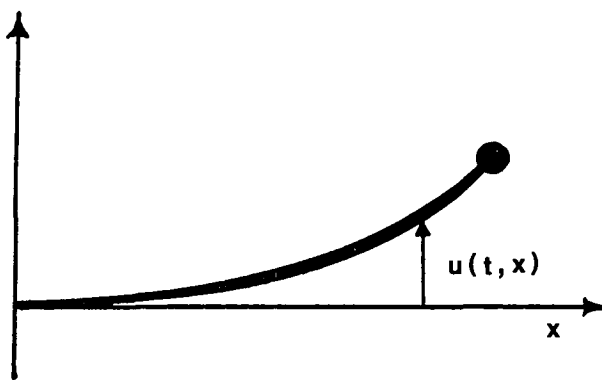
Using the Euler–Bernoulli theory to describe the transverse vibrations of the beam we obtain the partial differential equation (see [11], [12])

$$\rho(x)D_t^2 u(t,x) + D_x^2 EI(x)D_x^2 u(t,x) = D_x \sigma(t,x)D_x u(t,x) + f(t,x),$$

$$x \in (0,\ell), \ t \in (0,T), \qquad (2.1)$$

for the transverse displacement u where σ denotes the internal tension, f is the net externally applied transverse or lateral load, and $D_t = \partial/\partial t$, $D_x = \partial/\partial x$. Use of principles of elementary Newtonian mechanics (i.e., force and moment balance equations) yields the boundary conditions at the free end. From translational equilibrium we obtain

$$mD_t^2 u(t,\ell) - D_x EI(\ell)D_x^2 u(t,\ell) = -\sigma(t,\ell)D_x u(t,\ell) + g(t), \quad t \in (0,T), \quad (2.2)$$

where g is the net external force on the tip mass. In a similar manner, requiring rotational equilibrium, we have

$$D_x^2 u(t,\ell) = 0, \qquad t \in (0,T). \qquad (2.3)$$

The geometric boundary conditions (zero displacement and zero slope) at the clamped end are given by

$$u(t,0) = 0, \qquad t \in (0,T), \qquad (2.4)$$

and

$$D_x u(t,0) = 0, \qquad t \in (0,T), \qquad (2.5)$$

respectively. The initial conditions are in the form of initial displacement

$$u(0,x) = \phi(x), \qquad x \in [0,\ell], \qquad (2.6)$$

and initial velocity

$$D_t u(0,x) = \psi(x), \qquad x \in [0,\ell]. \qquad (2.7)$$

In order to characterize solutions to the hybrid system (2.1) – (2.7) of ordinary and partial differential equations, boundary and initial conditions, we formally represent it as an abstract second-order system. Consider

147

$$M_0 D_t^2 \hat{u}(t) + A_0 \hat{u}(t) = B_0(t)\hat{u}(t) + \hat{F}(t), \quad t \in (0,T), \tag{2.8}$$

$$\gamma_0 \hat{u}(t) = 0 \qquad\qquad \gamma_1 \hat{u}(t) = 0 \qquad\qquad \gamma_2 \hat{u}(t) = 0$$
$$\text{at } x = 0, \qquad\qquad \text{at } x = 0, \qquad\qquad \text{at } x = \ell, \tag{2.9}$$

$$\hat{u}(0) = \hat{\phi}, \qquad D_t \hat{u}(0) = \hat{\psi}, \tag{2.10}$$

where $\hat{u}(t) = (u(t,\ell), u(t,\cdot))$, and the operators M_0, A_0, $B_0(t)$ and γ_i, $i = 0,1,2$ are defined by (for $\hat{v} = (v(\ell),v) \in R \times H^0(0,\ell)$)

$$M_0 \hat{v} = (mv(\ell), \rho v),$$

$$A_0 \hat{v} = (-D_x EI(\ell) D_x^2 v(\ell), D_x^2 EID_x^2 v)$$

$$B_0(t)\hat{v} = (-\sigma(t,\ell)D_x v(\ell), D_x \sigma D_x v)$$

and

$$\gamma_i \hat{v} = D_x^i v, \qquad\qquad i = 0,1,2,$$

$$\hat{F}(t) = (g(t),f(t,\cdot)), \quad \hat{\phi} = (\phi(\ell),\phi), \quad \text{and} \quad \hat{\psi} = (\psi(\ell),\psi).$$

Define the Hilbert space H by

$$H = R \times H^0(0,\ell)$$

with innerproduct

$$\langle(\eta,\phi),(\xi,\psi)\rangle_H = \eta\xi + \langle\phi,\psi\rangle_0$$

where $\{H^1, \langle\cdot,\cdot\rangle_i\}$ denote the usual Sobolev spaces together with the usual

Sobolev inner products. Let V be the Hilbert space defined by

$$V = \{(\eta,\phi) \in H : \phi \in H^2(0,\ell), \; \phi(0) = D\phi(0) = 0, \; \eta = \phi(\ell)\}$$

together with the innerproduct

$$\langle \hat{\phi}, \hat{\psi} \rangle_V = \langle D^2\phi, \; D^2\psi \rangle_0,$$

where $\hat{\phi} = (\phi(\ell),\phi)$, $\hat{\psi} = (\psi(\ell),\psi) \in V$. It is easily shown that V is dense in H and choosing H as our pivot space we have the continuous embeddings $V \subset H \subset V^*$ where V^* is the space of continuous linear functionals on V.

Of particular interest to us here will be the notion of a weak solution to (2.8) – (2.10). Interpreting the derivatives in the definitions of the operators A_0, $B_0(t)$ and γ_i in the distributional sense, we rewrite (2.8) – (2.10) in variational form as

$$\langle M_0 \, D_t^2\hat{u}(t),\hat{\theta} \rangle_H + a(\hat{u}(t),\hat{\theta}) = b(t)(\hat{u}(t),\hat{\theta}) + \langle \hat{F}(t),\hat{\theta} \rangle_H, \qquad (2.11)$$

$$\hat{\theta} \in V, \; t \in (0,T)$$

$$\hat{u}(0) = \hat{\phi}, \qquad D_t\hat{u}(0) = \hat{\psi} \qquad (2.12)$$

where the sesquilinear forms a and $b(t)$ on $V \times V$ are defined by

$$a(\hat{\phi},\hat{\psi}) = \langle EID_x^2\phi, D_x^2\psi \rangle_0$$

and

$$b(t)(\hat{\phi},\hat{\psi}) = -\langle \sigma D_x\phi, D_x\psi \rangle_0$$

respectively, and the H innerproduct is interpreted as the duality pairing between V^* and V (see [13], [14]) wherever appropriate. Under the assumption that $EI, \rho \in L_\infty(0,\ell)$, $\sigma \in L_2([0,T],H^1(0,\ell))$, $f \in L_2([0,T], H^0(0,\ell))$ and $g \in L_2(0,T)$, it is not difficult to show (see [15]) that the system (2.11), (2.12) admits a unique solution $\hat{u}$ with values in V and which satisfies $u \in C([0,T],V)$, $D_t u \in C([0,T],H)$ and $D_t^2 u \in L_2([0,T],V^*)$. The existence of strong solutions can be demonstrated by rewriting (2.8) – (2.10) as an equivalent first-order system and using linear semigroup theory [16], [17] and evolution operators. The details involve standard ideas for evolution systems such as those found in [17] and under additional regularity assumptions (e.g., $EI \in H^2(0,\ell)$, $\sigma \in C^1([0,T], H^1(0,\ell))$,

$\hat{\phi} \in V \cap \{(v(\ell),v)|v \in H^4(0,\ell), D^2v(\ell) = 0\}$, $\hat{\psi} \in V$), one can argue existence of strong solutions (i.e., $\hat{u} \in C([0,T],V)$, $D_t\hat{u} \in C([0,T],H)$, $D_t^2\hat{u} \in L_2([0,T],H)$ with $\hat{u}$ satisfying (2.8), (2.9) almost everywhere on $[0,T]$) with sufficient smoothness to carry out the convergence arguments underlying the results presented in the next section.

In formulating the identification problem, for ease of exposition we assume that we wish to identify the parameters m, EI, ρ and σ only. We do note, however, that our general approach is in fact applicable to a wider class of problems involving the estimation of the forcing terms and initial conditions (see [18], [19]). Let Q be a compact subset of $\mathcal{Q} = R \times L_\infty(0,\ell) \times L_\infty(0,\ell) \times L_2([0,T],H^0(0,\ell))$. We assume that we have been provided with displacement observations $\{\overline{u}(t_i,x_j) : i=1,\cdots,\mu, j=1,\cdots,\nu\}$ at times $t_i \in [0,T]$ and positions $x_j \in [0,\ell]$ and formulate the identification problem as a least squares fit to data:

(ID): Find $q = (m,EI,\rho,\sigma) \in Q$ which minimizes

$$J(q;\hat{u}) = \sum_{i=1}^{\mu} \sum_{j=1}^{\nu} |u(t_i,x_j) - \overline{u}(t_i,x_j)|^2,$$

subject to $\hat{u}(t) = (u(t,\ell),u(t,\cdot))$ being the solution to (2.11), (2.12) corresponding to $q \in Q$.

III. THE APPROXIMATION SCHEME

Our approximation scheme is based upon the use of a standard (finite element) Galerkin approach to construct a sequence of finite dimensional approximating identification problems. For each $N = 1,2,\cdots$, let $V^N \subset V$ be a finite dimensional subspace of H. Let P^N denote the orthogonal projection of H onto V^N with respect to the H innerproduct. The Galerkin equations for the system (2.11), (2.12) are

$$\langle M_0 D_t^2 \hat{u}^N(t),\theta^N \rangle_H + a(\hat{u}^N(t),\theta^N) = b(t)(\hat{u}^N(t),\theta^N) + \langle \hat{F}(t),\theta^N \rangle_H, \qquad (3.1)$$

$$\theta^N \in V^N, \ t \in (0,T),$$

$$\hat{u}^N(0) = P^N\hat{\phi}, \qquad D_t\hat{u}^N(0) = P^N\hat{\psi}, \qquad (3.2)$$

where $\hat{u}^N(t) = (u^N(t,\ell), u^N(t,\cdot)) \in V^N$. The approximating identification problems then take the form

150

(IDN): Find $q^N = \left(m^N, EI^N, \rho^N, \sigma^N\right) \in Q$ which minimizes $J(q;\hat{u}^N)$ subject to $\hat{u}^N$ being the solution to (3.1), (3.2) corresponding to $q \in Q$.

Of particular interest to us here is a scheme involving the use of cubic spline functions. Let $\{B_j^N\}_{j=1}^{N+1}$ denote the (modified) cubic B-splines on the interval $[0,\ell]$ corresponding to the uniform partition $\{0, \frac{\ell}{N}, \frac{2\ell}{N}, \cdots, \ell\}$ which satisfy $B_j^N(0) = DB_j^N(0) = 0$, $j = 1,2,\cdots,N+1$. Let $V^N = \text{span}\{(B_j^N(\ell), B_j^N)\}_{j=1}^{N+1}$. Then $V^N \subset V$ and (3.1), (3.2) take the form

$$M^N \ddot{w}^N(t) + A^N w^N(t) = B^N(t)w^N(t) + F^N(t), \quad t \in (0,T) \tag{3.3}$$

$$w^N(0) = [W^N]^{-1} w_0^N, \qquad \dot{w}^N(0) = [W^N]^{-1} w_1^N \tag{3.4}$$

where

$$\hat{u}^N(t) = \sum_{j=1}^{N+1} w_j^N(t)\left(B_j^N(\ell), B_j^N\right),$$

$$[M^N]_{ij} = mB_i^N(\ell)B_j^N(\ell) + \int_0^\ell \rho B_i^N\, B_j^N,$$

$$[A^N]_{ij} = \int_0^\ell EID^2B_i^N\, D^2B_j^N,$$

$$[B^N(t)]_{ij} = \int_0^\ell \sigma(t,\cdot)DB_i^N\, DB_j^N,$$

$$[F^N(t)]_i = g(t)B_i^N(\ell) + \int_0^\ell f(t,\cdot)B_i^N,$$

$$[w_0^N]_i = \phi(\ell)B_i^N(\ell) + \int_0^\ell \phi B_i^N,$$

$$[w_1^N]_i = \psi(\ell)B_i^N(\ell) + \int_0^\ell \psi B_i^N,$$

and

$$[W^N]_{ij} = B_i^N(\ell)B_j^N(\ell) + \int_0^\ell B_i^N\, B_j^N, \quad i,j = 1,2,\cdots,N+1.$$

Our convergence results for the cubic spline approximation schemes are summarized in the following two theorems.

Theorem 1. Suppose $\{q^N\} \subset Q$ with $q^N \to q$ as $N \to \infty$. Suppose further that $\hat{u}(q)$, the solution to (2.11), (2.12) corresponding to $q \in Q$ is a strong solution. Then if $\hat{u}^N(q^N)$ is the solution to (3.1), (3.2) corresponding to q^N we have

$$|\hat{u}^N(q^N) - \hat{u}(q)|_V \to 0 \quad \underline{\text{and}} \quad |D_t\hat{u}^N(q^N) - D_t\hat{u}(q)|_H \to 0,$$

as $N \to \infty$ for each $t \in [0,T]$.

Theorem 2. Let $\overline{q}^N$ be a solution to problem (IDN). Then the sequence $\{\overline{q}^N\}$ admits a convergent subsequence $\{\overline{q}^{N_k}\}$ with $\overline{q}^{N_k} \to \overline{q}$ as $k \to \infty$. Moreover, $\overline{q}$ is a solution to problem (ID).

Theorem 1 can be established using approximation properties of cubic splines (see [20]) and variational arguments which are similar in spirit to those found in [21] for second-order hyperbolic systems and in [10] for damped cantilevered beams without tip mass. Continuous dependence of J and $\hat{u}^N$ and compactness of Q allow us to conclude that problem (IDN) admits a solution. The existence of a convergent subsequence also follows from the compactness of Q. Finally an application of Theorem 1 yields

$$J(\overline{q},\hat{u}(\overline{q})) = \lim_{k \to \infty} J(\overline{q}^{N_k}, \hat{u}^{N_k}(\overline{q}^{N_k})) \leqslant \lim_{k \to \infty} J(q, \hat{u}^{N_k}(q)) = J(q,\hat{u}(q))$$

for all $q \in Q$ and Theorem 2 is thus proven.

Although the state equation in problem (IDN) is finite dimensional, the admissible parameter space Q is a function space and hence the minimization of J is over an infinite dimensional space. We briefly indicate a means of overcoming this difficulty which involves the introduction of a second level of approximation into our scheme. A detailed discussion of these ideas along with several numerical examples for problems with parabolic, hyperbolic, and simple Euler-Bernoulli equations can be found in [22], [23], and [7] respectively.

For each $M = 1,2,\cdots$, define the set $Q^M \subset Q$ by $Q^M = I^M(Q)$ where I^M is a mapping which satisfies

Q1. $I^M : Q \to Q$ is continuous

Q2. $I^M(q) \to q$ as $M \to \infty$ uniformly in q for all $q \in Q$.

The approximating identification problems now take the form

<u>(IDNM)</u>: Find $q_M^N = (m_M^N, EI_M^N, \rho_M^N, \sigma_M^N) \in Q^M$ which minimizes $J(q; \hat{u}^N)$ subject to $\hat{u}^N$ being the solution to (3.1), (3.2) corresponding to q.

Typically, the spaces Q^M and the mappings I^M are realized using finite dimensional spaces of interpolating linear or cubic spline functions. In this case under sufficient regularity assumptions on Q, it can be shown that conditions Q1 and Q2 above are satisfied.

Using conditions Q1, Q2, and the compactness of Q, one can readily establish a convergence result analogous to that given in Theorem 2. Specifically, if $\{\overline{q}_M^N\}$ is any sequence of solutions to the problems (IDNM), there exists a convergent subsequence $\{\overline{q}_{M_j}^{N_k}\}$ with $\overline{q}_{M_j}^{N_k} \to \overline{q}$ as $N_k \to \infty$, $M_j \to \infty$, where $\overline{q}$ is a solution to (ID).

IV. A NUMERICAL EXAMPLE

We present a representative example to illustrate some of the numerical results we have obtained using the methods outlined above. Further details and other numerical findings will be presented elsewhere.

We consider the problem of estimating the spatially invariant stiffness EI and linear mass density ρ of a cantilevered beam of length $\ell = 1$ with an attached tip mass at the free end of unknown magnitude m which is also to be identified. We also assume that the entire system is subjected to a time varying base acceleration $a_0(t)$. The internal tension σ is then given by (see [9], [12])

$$\sigma(t,x) = - a_0(t)\big(\rho(\ell-x) + m\big).$$

The system was assumed to be initially at rest $(\phi = \psi = 0)$ and then acted upon by the distributed transverse load

$$f(t,x) = e^x \sin 2\pi t$$

and point load at the tip

$$g(t) = 2e^{-t}.$$

The base acceleration a_0 was taken to be

$$a_0(t) \doteq \begin{cases} 1 & 0 < t < 1.5 \\ 0 & t > 1.5 \end{cases}.$$

"Observations" (i.e., displacement values to be used as data in the inverse algorithm) at positions $x_j = .75$, .875, 1.0 at times $t_i = .5$, $1.0, \cdots, 5.0$ were generated using the "true" values of the parameters $m = 1.5$, $EI = 1.0$, and $\rho = 3.0$, the first two natural modes of the unforced, unaccelerated system and a standard Galerkin scheme. The approximating optimization problems were solved using a Levenberg-Marquardt iterative steepest descent method. "Start up" values for the parameters to be estimated were chosen as $m_0 = 1.7$, $EI_0 = .7$ and $\rho_0 = 2.7$. The initial value problem (3.3), (3.4) was solved at each iteration using a variable step size Adams predictor corrector method. The system did not appear to be stiff. Our results are summarized in Table 4.1 below.

N	$\overline{EI}^N$	$\overline{\rho}^N$	$\overline{m}^N$	$\overline{J}^N$	CPU (min/sec)
2	1.0016	3.0997	1.4793	$.17 \times 10^{-4}$	0/18.01
3	1.0012	3.0636	1.4873	$.18 \times 10^{-4}$	0/35.93
4	1.0009	3.0414	1.4921	$.19 \times 10^{-4}$	1/26.19
5	1.0006	3.0306	1.4944	$.19 \times 10^{-4}$	4/15.87
6	1.0012	3.0319	1.4944	$.35 \times 10^{-4}$	5/21.34

REFERENCES

[1] Sun, C. T., Kim, B. J., and Bagdanoff, J. L., "On the Derivation of Equivalent Simple Models for Beam and Plate-like Structures in Dynamic Analysis," Proc. AIAA Specialists Conference, Atlanta, GA, April 6-8, 1981, pp. 523-532.

[2] Chen, C. C. and Sun, C. T., "Transient Analysis of Large Frame Structures by Simple Models," Proc. of Symposium on Engineering Science and Mechanics, (National Cheng Kung University, December 28-31, 1981), pp. 753-775; also to appear in J. Astronaut. Sci.

[3] Noor, A. K. and Anderson, C. M., "Analysis of Beam-like Lattice Trusses," Comp. Meth. Appl. Mech. Engr., 20, 1979, pp. 53-70.

[4] Juang, J. N. and Sun, C. T., "System Identification of Large Flexible Structures by Using Simple Continuum Models," J. Astronaut. Sci., 31, 1983, pp. 77-98.

[5] Banks, H. T. and Crowley, J. M., "Parameter Estimation for Distributed Systems Arising in Elasticity," Proc. Symposium on Engineering Sciences and Mechanics, (National Cheng Kung University, December 28-31, 1981) pp. 158-177; LCDS Technical Report 81-24, Brown University, November 1981.

[6] Banks, H. T. and Crowley, J. M., "Parameter Estimation in Timoshenko Beam Models," LCDS No. 82-14, Brown University, June 1982; J. Astronaut. Sci., 31, 1983, pp. 381-397.

[7] Banks, H. T. and Crowley, J. M., "Parameter Identification in Continuum Models," LCDS Report M-83-1, Brown Univeristy, March 1983; Proc. 1983 American Control Conference, San Francisco, June, 1983.

[8] Kunisch, K. and Graif, E., "Parameter Estimation for the Euler-Bernoulli Beam," Inst. für Math. Bericht 83-26, Techn. Universität Graz, December 1983.

[9] Rosen, I. G., "A Numerical Scheme for the Identification of Hybrid Systems Describing the Vibration of Flexible Beams with Tip Bodies," Report CSDL-P-1893, Draper Laboratory, 1984.

[10] Banks, H. T. and Crowley, J. M., "Estimation of Material Parameters in Elastic Systems," LCDS Technical Report No. 84-20, Brown University, June 1984.

[11] Clough, R. W. and Penzien, J., Dynamics of Structures, McGraw Hill, New York, 1975.

[12] Storch, J. and Gates, S., "Transverse Vibration and Buckling of a Cantilevered Beam with Tip Body Under Axial Acceleration," J. Sound and Vibration, to appear, 1985.

155

[13] Aubin, J. P., <u>Approximation of Elliptic Boundary Value Problems</u>, Wiley-Interscience, New York, 1972.

[14] Oden, J. T. and Reddy, J. N., <u>Mathematical Theory of Finite Elements</u>, Wiley-Interscience, New York, 1976.

[15] Lions, J. L., <u>Optimal Control of Systems Governed by Partial Differential Equations</u>, Springer, New York, 1971.

[16] Yosida, K., <u>Functional Analysis</u>, Springer, New York, 1966.

[17] Pazy, A., <u>Semigroups of Linear Operators and Applications to Partial Differential Equations</u> Springer-Verlag, New York, 1983.

[18] Banks, H. T., Crowley, J. M., and Kunisch, K., "Cubic Spline Approximation Techniques for Parameter Estimation in Distributed Systems," LCDS Technical Report 81-25, Brown University, November 1981, IEEE. Trans. Auto. Control, AC-28, 1983, pp. 773-786.

[19] Banks, H. T., Daniel (Lamm), P., and Kareiva, P., "Estimation Techniques for Transport Equations," LCDS Technical Report 83-23, Brown University, July 1983, to appear in Proc. International Conference on Mathematics in Biology and Medicine (Bari, Italy, July 1983), Springer Lecture Notes in Biomath.

[20] Schultz, M. H., <u>Spline Analysis</u>, Prentice-Hall, Englewood Cliffs, NJ, 1973.

[21] Dupont, T., "L_2-Estimates for Galerkin Methods for Second-Order Hyperbolic Equations," SIAM J. Numer. Anal., 10, 1973, pp. 880-889.

[22] Banks, H. T. and Daniel (Lamm), P., "Estimation of Variable Coefficients in Parabolic Distributed Systems," LCDS Report No. 82-22, Brown University, September 1982, to appear IEEE Trans. Auto. Control.

[23] Banks, H. T. and Murphy, K. A., "Estimation of Coefficients and Boundary Parameters in Hyperbolic Systems," LCDS Technical Report No. 84-5, Brown University, February 1984.

SPACE STATION PARAMETRIC MODELS

M. Hamidi and S. J. Wang
Jet Propulsion Laboratory
California Institute of Technology
Pasadena, CA 91109

ABSTRACT

One of the most complex large space structural systems is a space station. An initial operation center station consisting of four sun-pointing solar array panels, four radiator panels, a main supporting structure, and several pressurized modules, referred to here as the four-panel planar configuration, is modeled mathematically in detail. Two models are developed: a distributed parameter model and a finite-element one. The former is derived using the Lagrangian approach with partial differential equations and subsequently discretized to a finite dimensional model. The latter is generated with a standard finite-element technique. The distributed parameter model is intended for performance evaluation, whereas the finite-element model, due to its simplicity and shorter turn-around time, is ideal for first order analysis.

The results of this work confirm the findings of an earlier study of a two-panel station configuration - that the solar panels dominate the flexible dynamics and that the payload control bandwidth is well within the dynamic range of the station. Consequently, significant interactions between the payloads and the station are expected.

157

I. INTRODUCTION

The space station is a complex large space deployable system. Many of its structural components are large in size and low in mass density. In contrast to the more traditional spacecraft, the characteristics of these large space systems are determined not only by the rigid body dynamics but also by the flexible body motion. Two approaches are generally used for developing mathematical models of large flexible structures: the distributed parameter method and the finite-element method. In this paper, the two methods are used to develop two different dynamic models for a four-panel station configuration.

The four-panel planar configuration as shown in Figure 1 consists of four solar panels with split resource modules, each resource module is associated with two 100 ft by 50 ft solar panels and two 70 ft by 20 ft radiators. The main structure of the station measures 280 feet in length and supports the two resource modules, several pressurized modules, a 30-foot service truss, and payloads. The pressurized modules are sized 22 ft by 14 ft diameter as determined by the space shuttle payload bay size. The station has a ground weight of 223,000 lbs, and the moments of inertia I_{xx} = 1.4910^7, I_{yy} = 3.37×10^6, and I_{zz} = 1.63×10^7 slug-ft^2. The center of mass is nearly at the center of the structure, or X = −1.235 ft, Y = Z = 0.

The solar panels are hinged to rotate about the roll (X) and pitch (Y) axes for solar inertial pointing, the radiators are also hinged for articulation, and the core or the bus of the station is pointed to the nadir direction.

Due to their large size and flexibility, the solar panels are the dominant factor for the flexible body dynamics.
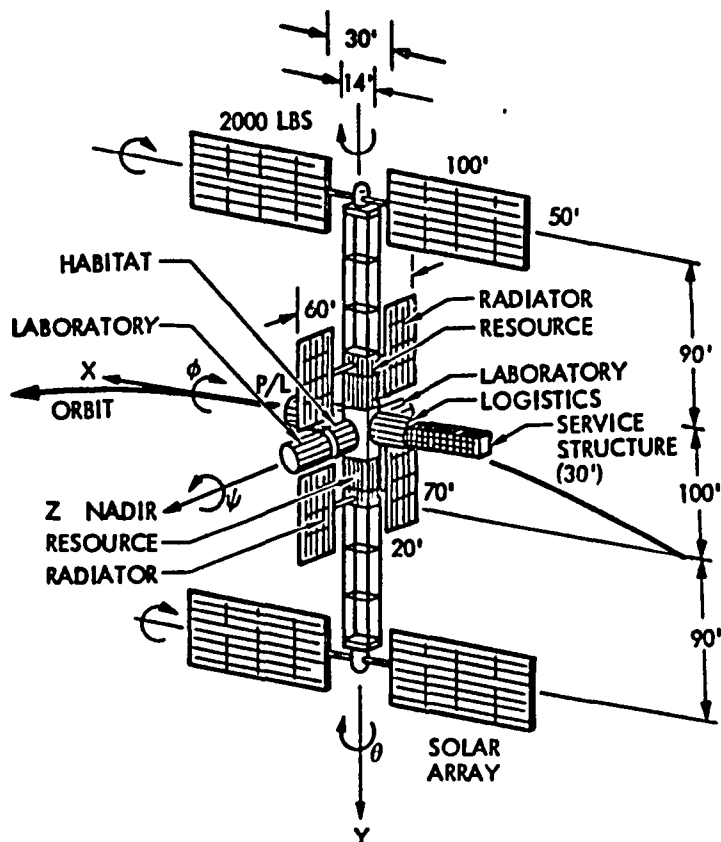
Figure 1. Four-panel planar configuration

Two dynamic models for this configuration have been developed, the distributed parameter model and the finite-element model. The distributed parameter model is developed for the purpose of in-depth analysis and performance evaluation. Dynamics in the full three dimensional space including the elastic body motions, interbody coupling, and orbital effects are derived, discretized, and truncated to a finite dimensional model. The derivation of this model constitutes the major effort of this paper.

While the high order distributed parameter model is for performance evaluation and analysis of higher order effects, the lower order finite-element model is developed for first order analysis with simplicity and fast turn-around time. The details of this model development are discussed

in Ref. 1. The results are included here for the sake of completeness.

II. DISTRIBUTED PARAMETER MODEL

The following assumptions were made for the modeling:

- The main structure and the various modules are rigid and rigidly attached,

- The radiators and the solar panels are hinge attached to the main structure and can be approximated by homogeneous plates, clamped on one side, free on the other three.

The assumption regarding the rigidity of the main structure is a first approximation to simplify the modeling procedure. It is justified by the fact that the main structure is at least one order of magnitude stiffer than the solar panels and their supporting trusses. The homogeneous plate approximation to the radiators and solar panels is merely made for the purpose of obtaining their modal shapes and frequencies. Any other approximation leading to the same quantities, e.g., a finite element model, can be used equally well in the space station modeling procedure.

The dynamics of the space station are obtained using the Lagrangian formalism. First, the potential and kinetic energies of the system are computed as quadratic forms of some adequately defined state space vector and its time derivative. The dynamics are subsequently derived by performing the classical differentiations.

ENERGY COMPUTATIONS

Let XYZ be an inertial frame of reference. The motion of the space station will be determined by the displacement of a body frame xyz attached at the point o, the center of the main structure, with respect to XYZ. The

160

axes ox, oy, oz are depicted on Figure 2: oz is parallel to the trusses supporting the radiators - nadir pointing in the normal mode of operation, oy lies along the main structure and ox forms a right-hand coordinate frame with oy and oz.
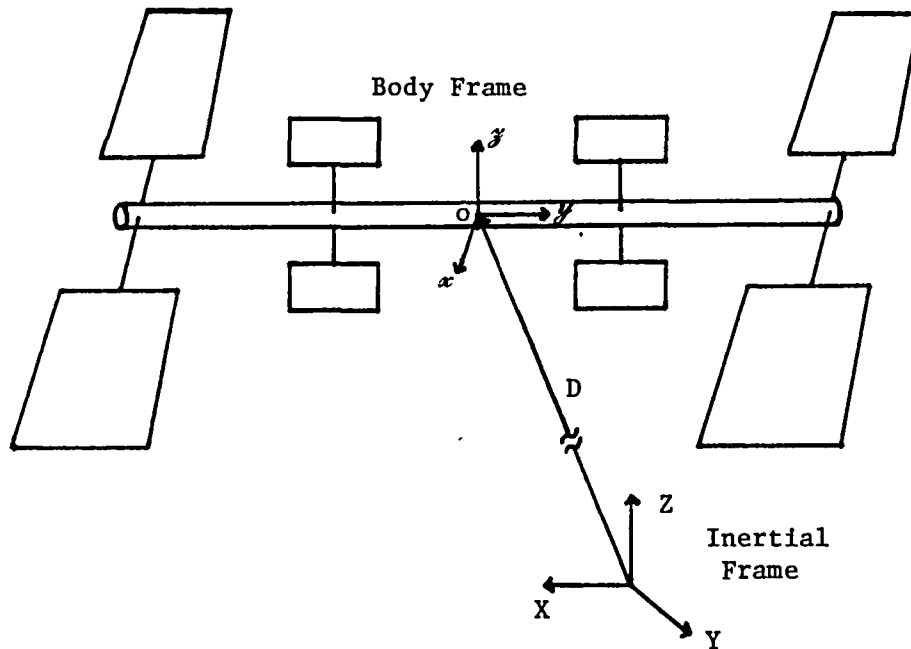
Figure 2. Reference frames

The main structure and the modules form a rigid body. The kinetic energy associated with their motion is given by:

$$T_{RB} = \frac{1}{2} M_{RB} \dot{D}.\dot{D} + \frac{1}{2} \dot{\Omega}^T I_{RB}\dot{\Omega}$$

where M_{RB} and I_{RB} are the mass and moment of inertia of the rigid body in the xyz frame, respectively, D is the vector from the origin of the inertial frame XYZ to the origin of the body frame xyz, and Ω the rotation angle of the frame xyz with respect to the inertial frame. The dots designate differentiation with respect to time.

161

POTENTIAL AND KINETIC ENERGY OF THE RADIATORS

In order to avoid the sun, the radiators are hinged and can rotate about the y and z directions. They are attached to the main structure by short trusses which we consider to be rigid. We will study the deformation of each radiator in a frame $x_R y_R z_R$ parallel to the frame xyz, and placed at the point o_R, the center of the radiator at rest (Fig. 3). In the first
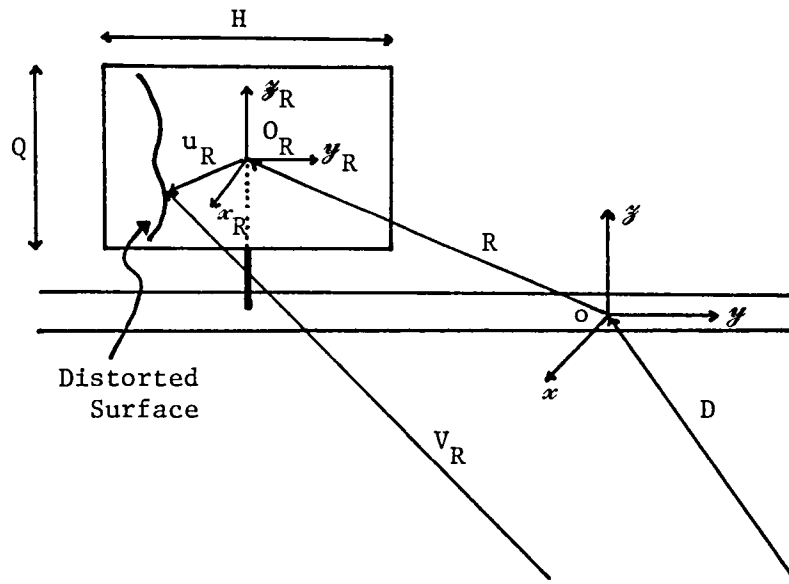
Figure 3. Radiator deformation

order of approximation the radiator plate is supposed to have out-of-plane deformations only. Thus the vector u_R from o_R to a running point of the radiator can be decomposed as:

$$u_R = r + u_r$$

where $r = (o \ y \ z)^T$ is the vector position of the point at rest and $u_r = (u \ o \ o)^T$ is the distortion of the plate at the given point. In the sequel the notation u will be used to designate both the vector u_r and the deformation u. It will be clear by the context which one is meant.

Potential energy

The potential energy stored in the distortion of each radiator is given by[2]:

$$K_R = \frac{1}{2} F_R \int_{-H/2}^{H/2} \int_{-Q/2}^{Q/2} [(\partial^2 u/\partial^2 y)^2 + (\partial^2 u/\partial^2 z)^2 + 2\nu_R(\partial^2 u/\partial y^2)(\partial^2 u/\partial z^2)$$
$$+ 2(1-\nu_R)(\partial^2 u/\partial y \partial z)^2] dz dy$$

where ν_R is the radiator's Poisson ratio and F_R its flexural rigidity. Note that:

$$F_R = E_R A_R^3 / 12(1-\nu_R^2)$$

with A_R designating the radiator's thickness and E_R its Young modulus.

Kinetic energy

The kinetic energy associated with the radiator's motion is given by:

$$T_R = \frac{1}{2} \int_{radiator} \rho_R (dV_R/dt).(dV_R/dt) ds$$

where ρ_R is the mass density of the radiator and V_R the vector position of a running point of the radiator in the inertial frame.

Figure 3 schematizes a decomposition of the vector V_R:

$$V_R = D + R + u_R = D + R + r + u.$$

D, r and u are already defined; R is the vector oo_R.

Let $\beta = (o \ \beta_y \ \beta_z)^T$ be the rotation of the radiator with respect to the main structure. To evaluate dV_R/dt, it should be noted that the frame $x_R y_R z_R$ undergoes a rotation of $\beta + \Omega$ and the frame xyz a rotation of Ω. Thus:

$$dV_R/dt = \dot{D} + \dot{u} + \dot{\Omega}x(R + r + u) + \dot{\beta}x(r + u)$$

which leads to

$$(dV_R/dt).(dV_R/dt) = [\dot{D} + \dot{u} + \dot{\Omega}x(R + r + u) + \dot{\beta}x(r + u)].[\dot{D} + \dot{u}$$

$$+ \dot{\Omega}x(R + r + u) + \dot{\beta}x(r + u)]$$

$$= \dot{D}.\dot{D} + \dot{u}.\dot{u} + [\dot{\Omega}x(R + r + u)].[\dot{\Omega}x(R + r + u)]$$

$$+ [\dot{\beta}x(r + u)].[\dot{\beta}x(r + u)] + 2\dot{D}.\dot{u} + 2\dot{D}.\dot{\Omega}x(R + r + u)$$

$$+ 2\dot{D}.\dot{\beta}x(r + u) + 2\dot{u}.\dot{\Omega}x(R + r + u) + 2\dot{u}.\dot{\beta}x(r + u)$$

$$+ 2[\dot{\Omega}x(R + r + u)].[\dot{\beta}x(r + u)]$$

Note that

$$[\dot{\Omega}x(R + r + u)].[\dot{\Omega}x(R + r + u)] = \dot{\Omega}.\dot{\Omega}[(R + r + u).(R + r + u)]$$

$$- [\dot{\Omega}.(R + r + u)][\dot{\Omega}.(R + r + u)]$$

$$= \dot{\Omega}^T[(R + r + u)^T(R + r + u)E - (R + r + u)(R + r + u)^T]\dot{\Omega}$$

where E is the identity matrix of order 3. Similarly,

$$[\dot{\beta}x(r + u)].[\dot{\beta}x(r + u)] = \dot{\beta}^T[(r + u)^T(r + u)E - (r + u)(r + u)^T]\dot{\beta}$$

Also:

$$\dot{D}.[\dot{\Omega}x(R + r + u)] = \dot{\Omega}^T[(R + r + u)x\dot{D}]$$

$$\dot{D}.[\dot{\beta}x(r + u)] = \dot{\beta}^T[(r + u)x\dot{D}]$$

$$\dot{u}.[\dot{\Omega}x(R + r + u)] = \dot{\Omega}^T[(R + r)x\dot{u}]$$

$$\dot{u}.[\dot{\beta}x(r + u)] = \dot{\beta}^T(r \ x \ \dot{u})$$

since $u \ x \ \dot{u} = 0$, u and $\dot{u}$ being colinear.

Finally:

$$[\dot{\Omega}x(R + r + u)].[\dot{\beta}x(r + u)] = (\dot{\Omega}.\dot{\beta})[(R + r + u).(r + u)]$$

$$- [\dot{\beta}.(R + r + u)][\dot{\Omega}.(r + u)]$$

$$= \dot{\Omega}^T[(r + u)^T(R + r + u)E - (r + u)(R + r + u)^T]\dot{\beta}$$

$$= \dot{\beta}^T[(R + r + u)^T(r + u)E - (R + r + u)(r + u)^T]\dot{\Omega}$$

Substituting these expressions in the expression for T_R leads to:

$$T_R = \frac{1}{2} \int_R \rho_R (dV_R/dt) \cdot (dV_R/dt) ds$$

$$= \frac{1}{2} \left\{ M_R \dot{D}^T \dot{D} + \int_R \rho_R \dot{u}^2 ds + \dot{\Omega}^T [(R^T R E - RR^T) M_R + \int_R \rho_R (r^T r E - rr^T) ds \right.$$

$$+ \int_R \rho_R (u^T u E - uu^T) ds + \int_R \rho_R (2R^T r E - Rr^T - rR^T) ds$$

$$+ \int_R \rho_R (2R^T u E - Ru^T - uR^T) ds - \int_R \rho_R (2r^T u - ru^T - ur^T) ds] \dot{\Omega}$$

$$+ \dot{\beta}^T [\int_R \rho_R (r^T r E - rr^T) ds + \int_R \rho_R (u^T u E - uu^T) ds + \int_R \rho_R (2r^T u E - ru^T - ur^T) ds] \dot{\beta}$$

$$+ 2 \dot{D}^T \int_R \rho_R \dot{u} ds + 2 \dot{\Omega}^T [M_R R x \dot{D} + (\int_R \rho_R r ds) x \dot{D} + (\int_R \rho_R u ds) x \dot{D}]$$

$$+ 2 \dot{\beta}^T [(\int_R \rho_R r ds) x \dot{D} + (\int_R \rho_R u ds) x \dot{D}] + 2 \dot{\Omega}^T [Rx \int_R \rho_R \dot{u} ds$$

$$+ \int_R \rho_R r x \dot{u} ds] + 2 \dot{\beta}^T \int_R \rho_R (r x \dot{u}) ds + 2 \dot{\Omega}^T [(\int_R \rho_R r ds)^T RE - (\int_R \rho_\rho r ds) R^T$$

$$+ (\int_R \rho_R u ds)^T RE - (\int_R \rho_R u ds) R^T + \int_R \rho_R (r^T r E - rr^T) ds + \int_R \rho_R (u^T u E - uu^T) ds$$

$$+ \int_R \rho_R (2r^T u E - ru^T - u^T r) ds] \dot{\beta} \right\}$$

where $M_R = \int_R \rho_R ds$ is the mass of the radiator.

The expression for T_R can be simplified by noting that since u is infinitesimal, all the expressions containing u can be neglected in first approximation. Moreover, assuming that the center of mass of the radiator is at its geometrical center, $\int_R \rho_R r ds = 0$.

The expression for the kinetic energy is therefore reduced to

$$T_R = \frac{1}{2} [M_R \dot{D}^T \dot{D} + \int_R \rho_R \dot{u}^2 ds + \dot{\Omega}^T (I_{OR} + I_R) \dot{\Omega} + \dot{\beta}^T I_R \dot{\beta} + 2 \dot{D}^T \int_R \rho_R \dot{u} ds$$

$$+ 2 M_R \dot{\Omega}^T \tilde{R} \dot{D} + 2 \dot{\Omega}^T \left(\tilde{R} \int_R \rho_R \dot{u} ds + \int_R \rho_R r x \dot{u} ds \right) + 2 \dot{\beta}^T \int_R \rho_R r x \dot{u} ds + 2 \dot{\Omega}^T I_R \dot{\beta}]$$

where:

$$I_{OR} = M_R (R^T R E - RR^T)$$

$$I_R = \int_R \rho_R (r^T r E - rr^T) ds$$

and $\tilde{R}$ is a matrix such that $\tilde{R}\dot{D} = R \times \dot{D}$.

POTENTIAL AND KINETIC ENERGY OF THE BOOMS SUPPORTING THE SOLAR PANELS

The motion of each boom is tracked in a frame $x_b y_b z_b$ placed at the hinge attaching the boom to the main structure, and parallel to the frame xyz initially when the hinge angles are zero. Thus x_b is along the length
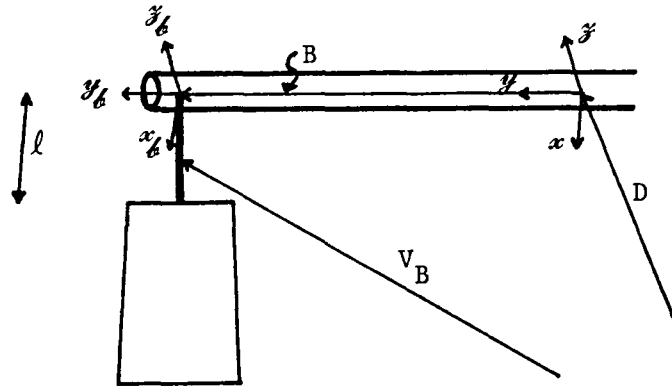
Figure 4. Boom's Reference

of the boom at rest. The hinge allows rotations about the axes x_b and y_b but not z_b. Thus the rotation of the frame $x_b y_b z_b$ with respect to the inertial frame is: $\alpha + \Omega$ where $\alpha = (\alpha_x \ \alpha_y \ 0)^T$ is the rotation with respect to the frame xyz and Ω is the rigid body rotation of the space station, i.e. the rotation of xyz with respect to the inertial frame. The boom is supposed to have deflections $Y_B(x,t)$ and $Z_B(x,t)$ along the axes y_b and z_b and torsion $\theta_B(x,t)$ about the axis x_b.

Potential energy:

The potential energy stored in the boom is given by:

$$K_B = \frac{1}{2} \int_0^\ell \left[GJ(\partial\theta_B/\partial x)^2 + EI_y(\partial^2 Y_B/dx^2)^2 + EI_z(\partial^2 Z_B/\partial x^2)^2 \right]dx$$

Note: ℓ is the length of the boom.

Kinetic energy:

The kinetic energy associated with the motion of the boom is given by:

$$T_B = \frac{1}{2} \int_0^{\ell} [\rho_B \, (dV_B/dt).(dV_B/dt) + J \, \dot{\theta}^2{}_B] dx$$

where V_B is the vector position of a running point of the boom in the inertial frame. Designating by B the vector from the origin of the xyz frame to the origin of $x_b y_b z_b$, we can write:

$$V_B = D + B + \begin{pmatrix} x \\ Y_B \\ Z_B \end{pmatrix}$$

Thus

$$dV_B/dt = \dot{D} + \begin{pmatrix} 0 \\ \dot{Y}_B \\ \dot{Z}_B \end{pmatrix} + \dot{\Omega} x B + (\dot{\Omega} + \dot{\alpha}) x \begin{pmatrix} x \\ Y_B \\ Z_B \end{pmatrix}$$

and

$$(dV_B/dt).(dV_B/dt) = \dot{D}.\dot{D} + \dot{Y}_B{}^2 + \dot{Z}_B{}^2 + \dot{\Omega}^T(B^TBE - BB^T)\dot{\Omega} +$$

$$(\dot{\Omega} + \dot{\alpha})^T \left[(x^2 + Y^2{}_B + Z^2{}_B)E - \begin{pmatrix} x \\ Y_B \\ Z_B \end{pmatrix} (x \; Y_B \; Z_B') \right] (\dot{\Omega} + \dot{\alpha})$$

$$+ 2\dot{D}.\begin{pmatrix} 0 \\ \dot{Y}_B \\ \dot{Z}_B \end{pmatrix} + 2\dot{D}.\dot{\Omega} x B + 2\dot{D}.(\dot{\Omega} + \dot{\alpha}) x \begin{pmatrix} x \\ Y_B \\ z_B \end{pmatrix} +$$

$$+ 2\begin{pmatrix} 0 \\ \dot{Y}_B \\ \dot{Z}_B \end{pmatrix} . \left[\dot{\Omega} x B + (\dot{\Omega} + \dot{\alpha}) x \begin{pmatrix} x \\ Y_B \\ Z_B \end{pmatrix} \right] + 2(\dot{\Omega} x B) . \left[(\dot{\Omega} + \dot{\alpha}) x \begin{pmatrix} x \\ Y_B \\ Z_B \end{pmatrix} \right]$$

In first approximation, Y_B and Z_B can be neglected in comparison to x. Remark that:

$$(\dot{\Omega} x B) . \left[(\dot{\Omega} + \dot{\alpha}) x \begin{pmatrix} x \\ o \\ o \end{pmatrix} \right] = \left[\dot{\Omega}.(\dot{\Omega} + \dot{\alpha}) \right] \left[B.\begin{pmatrix} x \\ o \\ o \end{pmatrix} \right] - \left[B.(\dot{\Omega} + \dot{\alpha}) \right] \left[\dot{\Omega}.\begin{pmatrix} x \\ o \\ o \end{pmatrix} \right]$$

$$= - \left[B.(\dot{\Omega} + \dot{\alpha}) \right] \left[\dot{\Omega}.\begin{pmatrix} x \\ o \\ o \end{pmatrix} \right] = -\dot{\Omega}^T \begin{pmatrix} x \\ o \\ o \end{pmatrix} B^T (\dot{\Omega} + \dot{\alpha})$$

since B having the form $(o\ B_y\ o)^T$ leads to $B.\begin{pmatrix}x\\o\\o\end{pmatrix} = 0.$

T_B is expressed as:

$$T_B = \frac{1}{2}\int_0^\ell \rho_B\Big\{J\dot\theta^2_B + \dot{D}.\dot{D} + \dot{Y}^2_B + \dot{Z}^2_B + \dot\Omega^T(B^TBE - BB^T)\dot\Omega$$

$$+ (\dot\Omega + \dot\alpha)^T\left[x^2E - \begin{pmatrix}x\\o\\o\end{pmatrix}(x\ o\ o)\right](\dot\Omega + \dot\alpha) + 2\dot{D}^T\begin{pmatrix}o\\\dot{Y}_B\\\dot{Z}_B\end{pmatrix} + 2\dot\Omega^T Bx\dot{D}$$

$$+ 2(\dot\Omega + \dot\alpha)^T\begin{pmatrix}x\\o\\o\end{pmatrix}x\dot{D} + 2\dot\Omega^T Bx\begin{pmatrix}o\\\dot{Y}_B\\\dot{Z}_B\end{pmatrix} + 2(\dot\Omega + \dot\alpha)^T\begin{pmatrix}x\\o\\o\end{pmatrix}x\begin{pmatrix}o\\\dot{Y}_B\\\dot{Z}_B\end{pmatrix}$$

$$- 2\dot\Omega^T\begin{pmatrix}x\\o\\o\end{pmatrix}B^T(\dot\Omega + \dot\alpha)\Big\}\,dx$$

$$= \frac{1}{2}\Big\{\int_0^\ell \rho_B(J\dot\theta^2_B + \dot{Y}^2_B + \dot{Z}^2_B)dx + M_B\dot{D}.\dot{D} + M_B\dot\Omega^T(B^TBE - BB^T)\dot\Omega$$

$$+ (\dot\Omega + \dot\alpha)^T I_s(\dot\Omega + \dot\alpha) + 2\dot{D}^T\int_0^\ell \rho_B\begin{pmatrix}o\\\dot{Y}_B\\\dot{Z}_B\end{pmatrix}dx + 2\dot\Omega^T B\,M_B\dot{D} + \int_0^\ell \rho_B\begin{pmatrix}o\\\dot{Y}_B\\\dot{Z}_B\end{pmatrix}dx$$

$$+ 2(\dot\Omega + \dot\alpha)^T\left[\left(\int_0^\ell \rho_B\begin{pmatrix}\tilde{x}\\o\\o\end{pmatrix}dx\right)\dot{D} + \int_0^\ell \rho_B\begin{pmatrix}\tilde{x}\\o\\o\end{pmatrix}\begin{pmatrix}o\\\dot{Y}_B\\\dot{Z}_B\end{pmatrix}dx\right] - 2\dot\Omega^T\int_0^\ell \rho_B\begin{pmatrix}x\\o\\o\end{pmatrix}dx\,B^T(\dot\Omega + \dot\alpha)\Big\}$$

where:

M_B is the mass of the boom,

$$I_s \triangleq \int_0^\ell \rho_B\left[x^2E - \begin{pmatrix}x\\o\\o\end{pmatrix}(x\ o\ o)\right]dx = \frac{1}{3}M_B\ell^2\begin{pmatrix}0&0&0\\0&1&0\\0&0&1\end{pmatrix}$$

if the boom is homogeneous.

POTENTIAL AND KINETIC ENERGY OF SOLAR PANELS
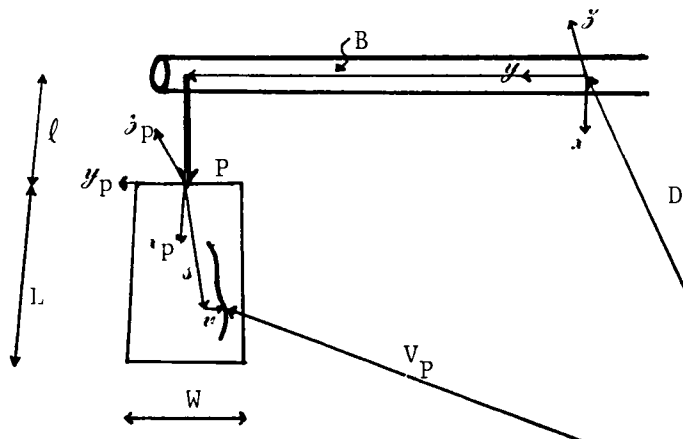
Figure 5. Solar Panel Distortions

Let us choose the reference frame $x_p y_p z_p$ parallel to $x_b y_b z_b$ when hinge angles are zero and placed at the tip of the boom. For the same considerations as in the case of the radiators, the solar panels are supposed to have out of plane distortions only.

Potential energy:

The potential energy stored in a solar panel is given by:

$$K_p = \frac{1}{2} F_p \int_0^L \int_{-W/2}^{W/2} \left[(\partial^2 v/\partial x^2)^2 + (\partial^2 v/\partial y^2)^2 + 2\nu_p (\partial^2 v/\partial x^2)(\partial^2 v/\partial y^2) \right.$$

$$\left. + 2(1-\nu_p)(\partial^2 v/\partial x \partial y)^2 \right] dy dx$$

where L and W are the length and width of the solar panel, respectively, and the other terms are defined as for the radiators.

Kinetic energy:

The kinetic energy due to the solar panel's distortion is given by:

$$T_p = \int_{panel} \rho_p (dV_p/dt).(dV_p/dt) \; ds$$

where panel V_p is the vector position of a running point of the panel in

169

the inertial reference frame. As can be seen in Figure 5:

$$V_p = D + B + P + v_p$$

D and B have been previously defined. $P = \begin{pmatrix} \ell & Y_B(\ell) & Z_B(\ell) \end{pmatrix}^T$ is the vector

position of the tip of the boom, i.e. the origin of the frame $x_p y_p z_p$, in

the frame $x_b y_b z_b$. v_p is the vector from the origin of the frame $x_p y_p z_p$ to

the point on the solar panel. Note that as in the case of the radiator v_p

can be decomposed in two components:

$$v_p = s + v$$

where $s = (x\ y\ o)^T$ represents the position of the point at rest and

$v = (o\ o\ v)^T$ its deformation. Also as for the radiator's case we will use

the same symbol for the vector v, and its non-zero component; the context

will indicate which one is meant. Hence $V_p = D + B + P + s + v$.

To compute the time derivative of V_p, let us observe that the frame

$x_p y_p z_p$ is rotated not only by Ω and α but also by the rotation Ω_p produced

at the tip of the boom, due to its deformations, namely:

$$\Omega_p \triangleq \begin{pmatrix} \theta_B \big|_{x=\ell} \\ -\partial Z_B / \partial x \big|_{x=\ell} \\ \partial Y_B / \partial x \big|_{x=\ell} \end{pmatrix}$$

Thus:

$$dV_p/dt = \dot{D} + \dot{P} + \dot{v} + \dot{\Omega}x(B + P + s + v) + \dot{\alpha}x(P + s + v)$$
$$+ \dot{\Omega}_p x(s + v)$$

To evaluate T_p, we have to compute the following terms:

$$\left[\dot{\Omega}x(B + P + s + v) \right] \cdot \left[\dot{\Omega}x(B + P + s + v) \right] =$$

$$\dot{\Omega}^T \left[(B + P + s + v)^T(B + P + s + v)E - (B + P + s + v)(B + P + s + v)^T \right] \dot{\Omega}$$

$$= \dot{\Omega}^T \left[(B^T B + P^T P + s^T s + v^T v + 2B^T P + 2B^T s + 2B^T v + 2P^T s + 2P^T v + 2s^T v)E \right.$$

$$\left. - (BB^T + PP^T + ss^T + vv^T + BP^T + PB^T + Bs^T + sB^T + Bv^T + vB^T \right.$$

170

$$+ Ps^T + sP^T + Pv^T + vP^T + sv^T + vs^T)\Big]\dot{\Omega}$$

In first approximation, we will neglect infinitesimal terms, i.e. all the terms with v will be neglected, and P will be reduced to $(\ell\ o\ o)^T$, which leads to B.P = 0 since B = $(0\ B\ 0)^T$. Thus:

$$\Big[\dot{\Omega}x(B + P + s + v)\Big].\Big[\dot{\Omega}x(B + P + s + v)\Big] = \dot{\Omega}^T\Big[(B^2 + \ell^2 + s^Ts + 2B^Ts$$
$$+ 2P^Ts)E - (BB^T + PP^T + ss^T + BP^T + PB^T + Bs^T + sB^T + Ps^T + sP^T)\Big]\dot{\Omega}$$

$$\Big[\dot{\alpha}x(P + s + v)\Big].\Big[\dot{\alpha}x(P + s + v)\Big] = \dot{\alpha}^T\Big[(P + s + v)^T(P + s + v)E -$$
$$(P + s + v)(P + s + v)^T\Big]\dot{\alpha} \simeq \dot{\alpha}^T\Big[(\ell^2 + s^Ts + 2P^Ts)E - (PP^T + ss^T$$
$$+ Ps^T + sP^T)\Big]\dot{\alpha}$$

$$\Big[\dot{\Omega}_px(s + v)\Big].\Big[\dot{\Omega}_px(s + v)\Big] \simeq \dot{\Omega}^T_p(s^TsE - ss^T)\dot{\Omega}_p$$

$$\Big[\dot{\Omega}x(B + P + s + v)\Big].\Big[\dot{\alpha}x(P + s + v)\Big] = (\dot{\Omega}.\dot{\alpha})\Big[(B + P + s + v).(P + s + v)\Big]$$
$$-\Big[(B + P + s + v).\dot{\alpha}\Big]\Big[\dot{\Omega}.(P + s + v)\Big] = \dot{\Omega}^T\Big[(P + s + v)^T(B + P + s + v)E$$
$$- (P + s + v)(B + P + s + v)^T\Big]\dot{\alpha} \simeq \dot{\Omega}^T\Big[(\ell^2 + s^Ts + 2P^Ts + s^TB)E$$
$$- (PP^T + ss^T + PB^T + Ps^T + sP^T + sB^T)\Big]\dot{\alpha}$$

$$\Big[\dot{\Omega}x(B + P + s + v)\Big].\Big[\dot{\Omega}_px(s + v)\Big] = (\dot{\Omega}.\dot{\Omega}_p)\Big[(B + P + s + v).(s + v)\Big]$$
$$- \Big[(B + P + s + v).\dot{\Omega}_p\Big]\Big[\dot{\Omega}.(s + v)\Big] \simeq \dot{\Omega}^T\Big[(s^Ts + B^Ts + P^Ts)E$$
$$- (ss^T + sB^T + sP^T)\Big]\dot{\Omega}_p$$

$$\Big[\dot{\alpha}x(P + s + v)\Big].\Big[\dot{\Omega}_px(s + v)\Big] = (\dot{\alpha}.\dot{\Omega}_p)\Big[(P + s + v).(s + v)\Big]$$
$$- \Big[(P + s + v).\dot{\Omega}_p\Big]\Big[(s + v).\dot{\alpha}\Big] \simeq \dot{\alpha}^T\Big[(s^Ts + P^Ts)E - (ss^T + sP^T)\Big]\dot{\Omega}_p$$

Thus T_p can be written as:

$$T_p = \frac{1}{2}\int_{panel}\rho_p(dV_p/dt).(dV_p/dt)ds$$

$$= \frac{1}{2}\left\{M_p\dot{D}.\dot{D} + M_p\dot{P}.\dot{P} + \int_{panel}\rho_p\dot{v}.\dot{v}\ ds + \dot{\Omega}^T\left\{M_p\Big[(B^2 + \ell^2)E - (BB^T + PP^T)\Big]\right.\right.$$

$$\left.\left. + I_p + 2(B^T + P^T)CE - C(B^T + P^T) - (B + P)C^T - M_p(BP^T + PB^T)\right\}\dot{\Omega}\right.$$

$$+ \dot{a}^T \Big[M_p(\ell^2 E - PP^T) + I_p + 2P^T CE - (PC^T + CP^T) \Big] \dot{a} + \dot{\Omega}_p{}^T I_p \dot{\Omega}_p + 2M_p \dot{D} \cdot \dot{P}$$

$$+ 2\dot{D} \int_{panel} \rho_p \dot{v} ds + 2M_p \dot{\Omega}^T \widetilde{(B + P)} \dot{D} + 2\dot{\Omega}^T \widetilde{CD} + 2M_p \dot{a}^T \widetilde{P} \dot{D} + 2\dot{a}^T \widetilde{CD} + 2\dot{\Omega}_p{}^T \widetilde{CD}$$

$$+ 2M_p \dot{\Omega}^T \widetilde{(B + P)} \dot{P} + 2\dot{P} \int_{panel} \rho_p \dot{v} ds + 2\dot{\Omega}^T \widetilde{CP} + 2\dot{a}^T (M_p \widetilde{P} + \widetilde{C}) \dot{P} + 2\dot{\Omega}_p{}^T \widetilde{CP}$$

$$+ 2\dot{\Omega}^T \widetilde{(B + P)} \int_{panel} \rho_p \dot{v} ds + 2\dot{\Omega}^T \int_{panel} \rho_p \widetilde{s} \dot{v} ds + 2\dot{a}^T \widetilde{P} \int_{panel} \rho_p \dot{v} ds + 2\dot{a}^T \int_{panel} \rho_p \widetilde{s} \dot{v} ds$$

$$+ 2\dot{\Omega}_p{}^T \int_{panel} \rho_p \widetilde{s} \dot{v} ds + 2\dot{\Omega}^T \Big[M_p(\ell^2 E - PP^T) + I_p + 2P^T CE - PC^T - CP^T - M_p PB^T \Big]$$

$$+ C^T BE - CB^T \Big] \dot{a} + 2\dot{\Omega}^T \Big[I_p + B^T CE - CB^T + P^T CE - CP^T \Big] \dot{\Omega}_p + 2\dot{a}^T \Big[I_p + P^T CE$$

$$- CP^T \Big] \dot{\Omega}_p \Big\}$$

where M_p is the mass of the solar panel,

$$I_p \triangleq \int_{panel} \rho_p (s^T s E - ss^T) ds \quad \text{its inertia with respect to } x_p y_p z_p, \text{ and}$$

$$C \triangleq \int_{panel} \rho_p s ds$$

Defining:

$$I_{OP} = M_p(\ell^2 E - PP^T) + 2P^T CE - PC^T - CP^T$$

$$I_{OB} = M_p(B^2 E - BB^T) + 2B^T CE - BC^T - CB^T$$

the expression for T_p can be rearranged as:

$$T_p = \frac{1}{2} \Big\{ M_p \Big[\dot{D}^T \dot{D} + \dot{Y}_B{}^2(\ell) + \dot{Z}_B{}^2(\ell) \Big] + \int_{panel} \rho_p \dot{v} \cdot \dot{v} ds + \dot{\Omega}^T \Big[I_p + I_{OP} + I_{OB}$$

$$- M_p(BP^T + PB^T) \Big] \dot{\Omega} + \dot{a}^T (I_p + I_{OP}) \dot{a} + \dot{\Omega}_p{}^T I_p \dot{\Omega}_p + 2M_p \dot{D} \cdot \dot{P} + 2\dot{D}^T \int_{panel} \rho_p \dot{v} ds$$

$$+ 2\dot{\Omega}^T \Big\{ \Big[M_p \widetilde{(B + P)} + \widetilde{C} \Big] \dot{D} + \Big[M_p \widetilde{(B + P)} + \widetilde{C} \Big] \dot{P} + \widetilde{(B + P)} \int_{panel} \rho_p \dot{v} ds +$$

172

$$+ \int_{\text{panel}} \rho_p \tilde{s} \dot{v} ds + (I_p + I_{OP} - M_p PB^T + C^T BE - CB^T)\ddot{\alpha} + (I_p + B^T CE - CB^T)$$

$$+ P^T CE - CP^T)\dot{\Omega}_p\} + 2\dot{\alpha}^T\left[(M_p\tilde{P} + \tilde{C})\dot{D} + (M_p\tilde{P} + \tilde{C})\dot{P} + \tilde{P}\int_{\text{panel}} \rho_p \dot{v} ds\right.$$

$$+ \int_{\text{panel}} \rho_p \tilde{s}\dot{v} ds + (I_p + P^T CE - CP^T)\dot{\Omega}_p\bigg] + 2\dot{\Omega}_p^T(\tilde{C}\dot{D} + \tilde{C}\dot{P} + \int_{\text{panel}} \rho_p \tilde{s}\dot{v} ds)$$

$$+ 2\dot{P}^T\int_{\text{panel}} \rho_p \dot{v} ds\bigg\}$$

EQUATIONS OF MOTION

The Lagrangian formalism is used to derive the equations of motion. It is therefore desirable to define a state space vector W_c such that the kinetic energy of the system can be written as $\frac{1}{2} W_c^T M_c W_c$ and its potential energy as $\frac{1}{2} W_c K_c W_c$ for some operator M_c and K_c.

Kinetic energy

The kinetic energy of the system is evidently the sum of the kinetic energy of its different parts. It is given by:

$$T = T_{RB} + \sum_{i=1}^{4} (T_{Ri} + T_{Bi} + T_{Pi})$$

where the index i refers to the four different radiators, booms and panels attached to the main structure

$$T = \frac{1}{2}\left\{\left[M_{RB} + \sum_{i=1}^{4}(M_{Ri} + M_{Bi} + M_{Pi})\right]\dot{D}^T\dot{D} + \dot{\Omega}^T\left\{I_{RB} + \sum_{i=1}^{4}\left[I_{ORi} + I_{Ri}\right.\right.\right.$$

$$+ M_{Bi}(B_i^T B_i E - B_i B_i^T) + I_{si} - 2\left(\int_0^{\ell_i} \rho_{Bi}\binom{x}{0}dx\right)B_i^T + I_{Pi} + I_{OPi} + I_{OBi}$$

$$- M_{Pi}(B_i P_i^T + P_i B_i^T)\bigg]\bigg\}\dot{\Omega} + \sum_{i=1}^{4}\left\{\int_{Ri}\rho_{Ri}\dot{u}_i^2 ds + \dot{\beta}_i^T I_{Ri}\dot{\beta}_i + \int_0^{\ell_i}\rho_{Bi}(J_i\dot{\theta}_{Bi})^2\right.$$

173

$$+ \dot{Y}_{B1}^2 + \dot{Z}_{B1}^2)dx + M_{P1}\dot{P}_i \cdot \dot{P}_i + \dot{\Omega}_{P1}^T I_{P1}\dot{\Omega}_{P1} + \dot{\alpha}_i^T(I_{si} + I_{P1} + I_{OPi})\dot{\alpha}_i$$

$$+ \int_{P1} \rho_{P1}\dot{v}_i \cdot \dot{v}_i ds\Big\} + 2\dot{D}^T \sum_{i=1}^{4}\Big\{-\Big[M_{R1}\tilde{R}_i + M_{B1}\tilde{B}_i + \int_0^{\ell_i} \rho_{Bi}\begin{pmatrix}\dot{\tilde{x}}\\o\\o\end{pmatrix}dx$$

$$+ M_{P1}\widetilde{(B_1 + P_1)} + \tilde{C}_i\Big]\dot{\Omega} + \int_{Ri}\rho_{Ri}\dot{u}_i ds + \int_0^{\ell_1}\rho_{Bi}\begin{pmatrix}o\\\dot{Y}_{Bi}\\\dot{Z}_{Bi}\end{pmatrix}dx + M_{P1}\dot{P}_i - \tilde{C}_i\dot{\Omega}_{Pi}$$

$$-\Big[\int_0^{\ell_i}\rho_{B1}\begin{pmatrix}\tilde{x}\\o\\o\end{pmatrix}dx + M_{Pi}\tilde{P}_i + \tilde{C}_i\Big]\dot{\alpha}_i + \int_{Pi}\rho_{P1}\dot{v}_i ds\Big\} + 2\dot{\Omega}^T\sum_{i=1}^4\Big\{\tilde{R}_i\int_{Ri}\rho_{R1}\dot{u}_i ds$$

$$+ \int_{R1}\rho_{R1}\tilde{r}\dot{u}_i ds + I_{Ri}\dot{\beta}_1 + \tilde{B}_i\int_0^{\ell_i}\rho_{Bi}\begin{pmatrix}o\\\dot{Y}_{Bi}\\\dot{Z}_{Bi}\end{pmatrix}dx + \int_0^{\ell_i}\rho_{Bi}\begin{pmatrix}\tilde{x}\\o\\o\end{pmatrix}\begin{pmatrix}o\\\dot{Y}_{Bi}\\\dot{Z}_{Bi}\end{pmatrix}dx$$

$$+ \Big[M_{P1}\widetilde{(B_i + P_1)} + \tilde{C}_i\Big]\dot{P}_i + (I_{P1} + B_i^T C_i E - C_i B_i^T + P_i^T C_i E - C_1 P_i^T)\dot{\Omega}_{P1}$$

$$+ \Big[I_{P1} + I_{OPi} - M_{Pi}P_i B_1^T + C_i^T B_i E - C_i B_i^T + I_{si} - \int_0^{\ell_i}\rho_{Bi}\begin{pmatrix}x\\o\\o\end{pmatrix}dx\, B_1^T\Big]\dot{\alpha}_i$$

$$+ \widetilde{(B_1 + P_i)} \int\rho_{P1}\dot{v}_i ds + \int\rho_{Pi}\tilde{s}\dot{v}_1 ds + \sum_{i=1}^4\Big\{2\dot{\beta}_i^T \int_{Ri}\rho_{Ri}\tilde{r}\dot{u}ds$$

$$- 2\Big[\int_0^{\ell_1}\rho_{Bi}\begin{pmatrix}\tilde{x}\\o\\o\end{pmatrix}\begin{pmatrix}o\\\dot{Y}_{Bi}\\\dot{Z}_{Bi}\end{pmatrix}^T dx\Big]\dot{\alpha}_i + 2\dot{P}_1^T\Big[-\tilde{C}_i\dot{\Omega}_{P1} + \int_{P_1}\rho_{Pi}\dot{v}_1 ds - (M_{Pi}\tilde{P}_i + \tilde{C}_i)\dot{\alpha}_i\Big]$$

$$+ 2\dot{\Omega}_{Pi}^T\Big[(I_{Pi} + P_1^T C_i E - P_i C_i^T)\dot{\alpha}_i + \int_{P1}\rho_{Pi}\tilde{s}\dot{v}ds\Big] + 2\dot{\alpha}_i^T(\tilde{P}_i\int_{P1}\rho_{P1}\dot{v}_1 ds + \int_{Pi}\rho_{Pi}\tilde{s}\dot{v}_1 ds)\Big\}\Big\}$$

Using the state vector W_c:

$$W_c \triangleq (D \quad \Omega \quad u_1 \quad \beta_1 \quad \theta_{B1} \quad Y_{B1} \quad Z_{B1} \quad \Omega_{P1} \quad \alpha_1 \quad v_1 \quad u_2 \quad \beta_2$$

$$\theta_{B2} \quad Y_{B2} \quad Z_{B2} \quad \Omega_{P2} \quad \alpha_2 \quad v_2 \quad u_3 \quad \beta_3 \quad \theta_{B3} \quad Y_{B3} \quad Z_{B3} \quad \Omega_{P3}$$

$$\alpha_3 \quad v_3 \quad u_4 \quad \beta_4 \quad \theta_{B4} \quad Y_{B4} \quad Z_{B4} \quad \Omega_{P4} \quad \alpha_4 \quad v_4)^T$$

the kinetic energy T can be expressed as

$$T = \frac{1}{2} \, \dot{W}_c^{\,T} M_c \dot{W}_c$$

where M_c is a matrix of operators.

Potential energy:

The total potential energy of the system is given by:

$$K = \sum_{i=1}^{4} (K_{Ri} + K_{Bi} + K_{Pi})$$

$$= \frac{1}{2} \sum_{i=1}^{4} \left\{ F_{Ri} \int_{-H_{i/2}}^{H_{i/2}} \int_{-Qi/2}^{Qi/2} \left[(\partial^2 u_i/\partial y^2)^2 + (\partial^2 u_i/\partial z^2)^2 + 2\nu_{Ri}(\partial^2 u_i/\partial y^2) \right. \right.$$

$$\left. (\partial^2 u_i/\partial z^2) + 2(1-\nu_{Ri})(\partial^2 u_i/\partial y \partial z)^2 \right] dz\,dy + \int_{o}^{\ell_i} \left[G_i J_i (\partial \theta_{Bi}/\partial x)^2 \right.$$

$$\left. + E_i I_{yi}(\partial^2 Y_{Bi}/\partial x^2)^2 + E_i I_{zi}(\partial^2 Z_{Bi}/\partial x^2)^2 \right] dx + F_{Pi} \int_{o}^{L_i} \int_{-W_{i/2}}^{W_{i/2}} \left[(\partial^2 v_i/\partial x^2)^2 \right.$$

$$\left. + (\partial^2 v_i/\partial y^2)^2 + 2\nu_{Pi}(\partial^2 v_i/\partial x^2)(\partial^2 v_i/\partial y^2) + 2(1 - \nu_{Pi})(\partial^2 v_i/\partial x \partial y)^2 \right] dx\,dy \right\}$$

We are going to show that with suitable boundary conditions on u_i, θ_{Bi}, Y_{Bi}, Z_{Bi} and v_i, and a suitable matrix operator K_c, the potential energy can also be put in the form

$$K = \frac{1}{2} \, W_c^{\,T} K_c W_c \quad .$$

Consider the first set of integrals in the sum, giving the potential energy of the radiators. Successive integration by parts will yield:

$$\int_{-Q/2}^{Q/2}\int_{-H/2}^{H/2}(\partial^2 u/\partial y^2)^2 dy\ dz = \int_{-Q/2}^{Q/2}[(\partial u/\partial y)(\partial^2 u/\partial y^2) - u(\partial^3 u/\partial y^3)]\Big|_{-H/2}^{H/2} dz$$

$$+ \int_R u(\partial^4 u/\partial y^4) ds$$

$$\int_{-H/2}^{H/2}\int_{-Q/2}^{Q/2}(\partial^2 u/\partial z^2)^2 dz\ dy = \int_{-H/2}^{H/2}[(\partial u/\partial z)(\partial^2 u/\partial z^2) - u(\partial^3 u/\partial z^3)]\Big|_{-Q/2}^{Q/2} dy$$

$$+ \int_R u(\partial^4 u/\partial z^4) ds$$

$$\int_{-Q/2}^{Q/2}\int_{-H/2}^{H/2}(\partial^2 u/\partial y^2) \cdot (\partial^2 u/\partial z^2) dy\ dz = \int_{-Q/2}^{Q/2}[(\partial u/\partial y)(\partial^2 u/\partial z^2)$$

$$-u(\partial^3/\partial y\partial z^2)]\Big|_{y=-H/2}^{y=H/2} dz + \int_R u(\partial^4 u/\partial x^2\,\partial z^2) ds$$

$$also = \int_{-H/2}^{H/2}[(\partial u/\partial z)(\partial^2 u/\partial y^2) - u(\partial^3 u/\partial z\,\partial y^2)]\Big|_{z=-Q/2}^{z=Q/2} dy$$

$$+ \int_R u(\partial^4 u/\partial x^2\partial z^2) ds$$

$$\int_{-H/2}^{H/2}\int_{-Q/2}^{Q/2}(\partial^2 u/\partial y\ \partial z)^2 dz\ dy = \int_{-H/2}^{H/2}\Big\{[(\partial u/\partial y)(\partial^2 u/\partial y\ \partial z)]\Big|_{z=-Q/2}^{z=Q/2}$$

$$- \int_{Q/2}^{Q/2}(\partial u/\partial y)(\partial^3 u/\partial y\ \partial z^2) dz\Big\}\ dy$$

$$= \Big\{\Big[u(\partial^2 u/\partial y\ \partial z)\Big]_{z=-Q/2}^{z=Q/2}\Big\}_{y=-H/2}^{y=H/2} - \int_{-H/2}^{H/2}[(\partial^3/\partial y^2\partial z)u]\Big|_{z=-Q/2}^{z=Q/2} dy$$

$$- \int_{-Q/2}^{Q/2}[u(\partial^3 u/\partial y\ \partial z^2)]\Big|_{y=-H/2}^{y=H/2} dz + \int_R u(\partial^4 u/\partial y^2\ \partial z^2) ds$$

Hence with the following boundary conditions which correspond to the radiator being clamped at z = -Q/2 and free on other boundaries, namely:

$$u(y, -Q/2) = (\partial u/\partial z)\Big|_{z=-Q/2} = 0\quad ;$$

$$(\partial^2 u/\partial z^2) + \nu_R(\partial^2 u/\partial y^2) = (\partial^3 u/\partial z^3) + (2 - \nu_R)(\partial^3 u/\partial z\ \partial y^2) = 0$$

for $z = Q/2$;

$$(\partial^2 u/\partial y^2) + \nu_R(\partial^2 u/\partial z^2) = (\partial^3 u/\partial y^3) + (2 - \nu_R)(\partial^3 u/\partial y\ \partial z^2) = 0$$

for $x = \pm\ H/2$;

and

$$u(\partial^2 u/\partial y\ \partial z)\bigg|_{\substack{y\ =\ \pm\ H/2 \\ z\ =\ Q/2}} = 0 \quad .$$

The expression for K_R, the potential energy of the radiator, reduces to:

$$K_R = \frac{1}{2}\ F_R \int_R u\ \nabla^4 u\ ds$$

where $\nabla^4 \overset{\Delta}{=} (\nabla^2)^2 = [(\partial^2/\partial y^2) + (\partial^2/z^2)]^2$

Similarly, for the solar panels, with the boundary conditions:

$$v(o,y) = (\partial v/\partial x)\big|_{x=0} = 0 \quad ;$$

$$(\partial^2 v/\partial x^2) + \nu_p(\partial^2 v/\partial y^2) = (\partial^3 v/\partial x^3) + (2 - \nu_p)(\partial^3 v/\partial x\ \partial y^2) = 0$$

for $x = L$;

$$(\partial^2 v/\partial y^2) + \nu_p(\partial^2 v/\partial x^2) = (\partial^3 v/\partial y^3) + (2 - \nu_p)(\partial^3 v/\partial y\ \partial x^2) = 0$$

for $y = \pm\ W/2$;

and $v(\partial^2 v/\partial x\ \partial y)\bigg|_{\substack{x\ =\ L \\ y\ =\ \pm\ W/2}} = 0$

which correspond to a plate clamped at $x = 0$, free at the other edges, the

expression for the potential energy stored in the solar panel reduces to:

$$K_{PL} = \frac{1}{2}\ F_p \int_P v\ \nabla^4 v\ ds$$

As for the boom:

$$\int_0^{\ell} (\partial\theta_B/\partial x)^2 dx = [\theta_B(\partial\theta_B/\partial x)]_0^{\ell} - \int_0^{\ell} \theta_B(\partial^2\theta_B/\partial x^2) dx$$

$$\int_0^{\ell} (\partial^2 Y_B/\partial x^2)^2 dx = [(\partial Y_B/\partial x)(\partial^2 Y_B/\partial x^2) - Y_B(\partial^3 Y_B/\partial x^3)]_0^{\ell}$$

$$+ \int_0^{\ell} Y_B(\partial^4 Y_B/\partial x^4) dx$$

$$\int_0^{\ell} (\partial^2 Z_B/\partial x^2)^2 dx = [(\partial Z_B/\partial x)(\partial^2 Z_B/\partial x^2) - Z_B(\partial^3 Z_b/\partial x^3)]_0^{\ell}$$

$$+ \int_0^{\ell} Z_B(\partial^4 Z_B/\partial x^4) dx$$

Thus, with the boundary conditions

$$\theta_B(0,t) = Y_B(0,t) = Z_B(0,t) = (\partial Y_B/\partial x)\Big|_{x=0} = (\partial Z_B/\partial x)\Big|_{x=0} = 0, \text{ clamped at } 0;$$

$$(\partial\theta_B/\partial x)\Big|_{x=\ell} = (\partial^2 Y_B/\partial x^2)\Big|_{x=\ell} = (\partial^2 Z_B/\partial x^2)\Big|_{x=\ell}$$

$$= (\partial^3 Y_B/\partial x^3)\Big|_{x=\ell} = (\partial^3 Z_B/\partial x^3)\Big|_{x=\ell} = 0 \text{ , free at } \ell \text{ ;}$$

the potential energy for the boom is given by:

$$K_B = \frac{1}{2} \int_0^{\ell} \{EI_Y(Y_B (\partial^4 Y_B/\partial x^4) + EI_Z Z_B(\partial^4 Z_B/\partial x^4) - GJ\theta_B(\partial^2\theta_B/\partial x^2)\} dx$$

With these considerations, the total potential energy can be expressed as:

$$K = \frac{1}{2} W_C^T K_C W_C$$

with the obvious definition for K_C.

We have thus obtained a simple expression for the Lagrangian $\mathscr{L}$ of the system.

$$\mathscr{L} = T - V = \frac{1}{2}\dot{W}_C^T M_C \dot{W}_C - \frac{1}{2} W_C^T K_C W_C$$

The equations of motion are obtained by employing the fact that for any virtual displacement compatible with the system's constraints, and for any times t_1 and t_2 one must have

$$\delta \left(\int_{t_1}^{t_2} \mathscr{L} dt \right) = 0$$

(in other words, the integral of $\mathscr{L}$ between two arbitrary times t_1 and t_2 is stationary), which yields:

$$M_C \ddot{W}_C + K_C W_C = 0$$

III. DISCRETIZATION AND IMPLEMENTATION

Discretization

The equations of motion with the matrix operators M_C and K_C are not easy to use. The following procedure describes an approach to obtain a finite-dimensional approximation of M_C and K_C.

Let a^2_n and ϕ_n be the eigenvalues and eigenfunctions of the operator ∇^4 with the boundary conditions described for u; and let ψ_n be the eigenfunctions of ∇^4 corresponding to the boundary conditions described for v. These eigenvalues and eigenfunctions are described in reference 3.

Note furthermore that the eigenvalue problem

$$-(d^2 f/dx^2) = \lambda f , \qquad f(0) = 0 , \quad f'(\ell) = 0$$

has the eigenfunctions

$$\eta_n = \sin (2n-1)\pi x/2\ell$$

corresponding to the eigenvalues

$$c_n = [(2n-1)\pi/2\ell]^2$$

and that the problem

$$d^4 f/dx^4 = \lambda f , \qquad f(0) = f'(0) = 0 , \quad f''(\ell) = f'''(\ell) = 0$$

has the eigenfunctions

$$\zeta_n = \cosh d_n x - \cos d_n x - \sigma_n(\sinh d_n x - \sin d_n x)$$

where $\sigma_n = (\sinh d_n \ell - \sin d_n \ell)/(\cosh d_n \ell + \cos d_n \ell)$

and d_n is such that

$$\cos d_n \ell \cosh d_n \ell + 1 = 0$$

The corresponding eigenvalues are $\lambda = d_n^4$. Moreover:

$$\int_0^\ell \eta_m(x) \; \eta_n(x) \; dx = \ell/2 \delta_{mn}$$

and

$$\int_0^\ell \zeta_m(x) \; \zeta_n(x) \; dx = \ell \delta_{mn}$$

We will express u, v, θ_B, Y_B, Z_B in the basis of these eigenfunctions:

$$u(r, \; t) = \sum_{n=1}^\infty u_n(t) \; \phi_n(r)$$

$$v(s, \; t) = \sum_{n=1}^\infty v_n(t) \; \psi_n(s)$$

$$\theta_B(x, \; t) = \sum_{n=1}^\infty \theta_{Bn}(t) \; \eta_n(x)$$

$$Y_B(x, \; t) = \sum_{n=1}^\infty y_{Bn}(t) \; \zeta_n(x)$$

$$Z_B(x, \; t) = \sum_{n=1}^\infty z_{Bn}(t) \; \zeta_n(x)$$

where

$$u_n(t) = \int_R u(r, \; t) \; \phi_n(r) ds$$

$$v_n(t) = \int_P v(s, \; t) \; \psi_n(s) ds$$

$$\theta_{Bn}(t) = \int_B \theta_B(x, t)\eta_n(x)dx$$

$$y_{Bn}(t) = \int_B Y_B(x, t)\,\zeta_n(x)dx$$

$$z_{Bn}(t) = \int_B Z_B(x, t)\,\zeta_n(x)dx$$

The approximations to the variables u, v, θ_B, Y_B, Z_B are obtained by truncating the infinite series to finite summations. Using these approximations for the radiator:

$$\int_R \rho_R \, \dot{u}\, ds = \int_R \rho_R \sum_{n=1}^{N_u} \dot{u}_n(t)\phi_n(r)ds = \sum_{n=1}^{N_u} \dot{u}_n(t)f_n = \mathscr{F}^T \dot{\mathscr{U}}$$

where

$$\mathscr{U} = (u_1, u_2 \ldots u_{Nu})^T, \quad \mathscr{F} = (f_1, f_2 \ldots f_{Nu})^T \text{ and } f_n = \int_R \rho_R \phi_n(r)ds$$

$$\int_R \rho_R \, y\dot{u}\, ds = \int_R \rho_R y \sum_{n=1}^{N_u} \dot{u}_n(t)\phi_n(r)ds = \sum_{n=1}^{N_u} \dot{u}_n(t)g_{yn} = \mathscr{G}_y^T \dot{\mathscr{U}}$$

where $\mathscr{G}_y = (g_{y1} \quad g_{y2} \cdots g_{yNu})^T$ and $g_{yn} = \int_R \rho_R y\,\phi_n(r)ds$

$$\int_R \rho_R z \, \dot{u}\, ds = \mathscr{G}_z^T \dot{\mathscr{U}}$$

where

$$\mathscr{G}_z = (g_{z1}, g_{z2} \cdots g_{zNu})^T \quad \text{and} \quad g_{zn} = \int_R \rho_R z \, \phi_n(r)ds$$

$$\int_R \rho_R \, \dot{u}^2 ds = \int_R \rho_R \left(\sum_{n=1}^{N_u} \dot{u}_n(t)\,\phi_n(r)\right)\left(\sum_{n=1}^{N_u} \dot{u}_n(t)\,\phi_n(r)\right) ds = \dot{\mathscr{U}}^T F \dot{\mathscr{U}}$$

181

where F is the matrix with elements $F_{mn} = \int_R \rho_R \, \phi_m(r) \, \phi_n(r) ds$

Similarly, for the panels,

$$\int_P \rho_p \, \dot{v} \, ds = \mathscr{P}^T \dot{\mathscr{V}} \qquad\qquad \int_P \rho_p \dot{v}^2 \, ds = \dot{\mathscr{V}}^T \mathscr{O} \dot{\mathscr{V}}$$

$$\int_P \rho_p \, x \, \dot{v} \, ds = \mathscr{Q}_x^T \dot{\mathscr{V}} \qquad\qquad \int_P \rho_p \, y \, \dot{v} \, ds = \mathscr{Q}_y^T \dot{\mathscr{V}}$$

with:

$$\dot{\mathscr{V}} = (v_1 \quad v_2 \ \cdots \ v_{Nv})^T,$$

$$\mathscr{P} = (p_1 \quad p_2 \ \cdots \ p_{Nv})^T, \qquad\qquad p_n = \int_P \rho_p \, \psi_n(s) ds$$

$$\mathscr{Q}_x = (q_{x1} \quad q_{x2} \ \cdots \ q_{xNv})^T, \qquad\qquad q_{xn} = \int_P \rho_p \, x \, \psi_n(s) ds$$

$$\mathscr{Q}_y = (q_{y1} \quad q_{y2} \ \cdots \ q_{yNv})^T, \qquad\qquad q_{yn} = \int_P \rho_p \, y \, \psi_n(s) ds$$

$$\mathscr{O} = [\mathscr{O}_{mn}] = \left[\int_P \rho_p \, \psi_m(s) \, \psi_n(s) ds \right]$$

For the boom:

$$\int_0^\ell \rho_B \dot{\theta}_B^2(x, \ t) dx = \int_0^\ell \rho_B \left(\sum_{m=1}^{N_\theta} \dot{\theta}_m(t) \eta_m(x) \right) \left(\sum_{n=1}^{N_\theta} \dot{\theta}_n(t) \eta_n(x) \right) \ dx = \dot{\mathscr{T}}^T N \dot{\mathscr{T}}$$

assuming that the boom is uniform

$$= (\rho_B \, \ell/2) \dot{\mathscr{T}}^T E_{N_\theta} \dot{\mathscr{T}} = (M_B/2) \dot{\mathscr{T}}^T E_{N_\theta} \dot{\mathscr{T}}$$

where:

$$N = [N_{mn}] = \int_0^\ell \rho_B \eta_m(x) \eta_n(x) dx, \quad m, n = 1, \ldots N_\theta$$

E_{N_θ} is the identity matrix of order N_θ and

182

$$\mathcal{T} = (\theta_1 \quad \theta_2 \quad \ldots \quad \theta_{N_\theta})^T$$

$$\int_o^\ell \rho_B \dot{Y}_B^2(x, t)dx = \int_o^\ell \rho_B \left(\sum_{m=1}^{N_y} \dot{y}_{Bm}(t)\, \zeta_m(x)\right)\left(\sum_{n=1}^{N_y} \dot{y}_{Bm}(t)\, \zeta_n(x)\right) dx = \dot{\mathcal{Y}}^T_U \dot{\mathcal{Y}}$$

$$= \rho_B \ell\, \dot{\mathcal{Y}}^T E_{N_y} \dot{\mathcal{Y}} = M_B \dot{\mathcal{Y}} E_{N_y} \dot{\mathcal{Y}} \text{ if the boom is uniform.}$$

Where $U = [U_{mn}] = \int_o^\ell \rho_B \zeta_m(x)\zeta_n(x)dx \qquad m, n = 1, \ldots N_y$

E_{N_y} is the identity matrix of order N_y and

$$\mathcal{Y} = (y_{B1} \quad y_{B2} \quad \ldots \quad y_{BN_y})^T$$

$$\int_o^\ell \rho_B \dot{Y}_B(x, t)dx = \sum_{n=1}^{N_y} \dot{y}_{Bn}(t) \int_o^\ell \rho_B \zeta_n(x)dx = \mathcal{S}_y^T \dot{\mathcal{Y}}$$

where

$$\mathcal{S}_y = (s_1 \quad s_2 \quad \ldots \quad s_{N_y})^T \,, \quad s_n = \int_o^\ell \rho_B \zeta_n(x)dx$$

$$\int_o^\ell \rho_B\, x\, \dot{Y}_B(x, t)dx = \sum_{n=1}^{N_y} \dot{y}_{Bn} \int_o^\ell \rho_B x\, \zeta_n(x)dx = \Gamma_y^T \mathcal{Y}$$

where

$$\Gamma_y = (\gamma_1 \quad \gamma_2 \quad \ldots \quad \gamma_{N_y})^T \,, \quad \gamma_n = \int_o^\ell \rho_B x\, \zeta_n(x)dx$$

Similarly:

$$\int_o^\ell \rho_B \dot{Z}_B^2(x, t)dx = \dot{\mathcal{Z}}^T V \dot{\mathcal{Z}} = M_B \dot{\mathcal{Z}}^T E_{Nz} \dot{\mathcal{Z}} \text{ if the boom is uniform}$$

$$\int_o^\ell \rho_B \dot{Z}_B(x, t)dx = \mathcal{S}_z^T \dot{\mathcal{Z}}$$

$$\int_o^\ell \rho_B x \dot{Z}_B(x, t)dx = \Gamma_z^T \dot{\mathcal{Z}}$$

where $V = V_{mn} = \int_o^\ell \rho_B \zeta_m(x)\zeta_n(x)dx \qquad m, n = 1, \ldots, N_z$

E_{N_z} is the identity matrix of order N_z,

$$\mathscr{Z} = (z_{B1} \quad z_{B2} \quad \cdots \quad z_{BN_z})^T$$

$$\mathscr{S}_z = (s_1 \quad s_2 \quad \cdots \quad s_{N_z})^T \text{ and } \Gamma_z = (\gamma_1 \quad \gamma_2 \quad \cdots \quad \gamma_{N_z})^T$$

Also:

$$\int_R u \, \nabla^4 u \, ds = \int_R \left(\sum_{m=1}^{N_u} u_m(t) \, \phi_m(r) \right) \left(\sum_{n=1}^{N_u} u_n(t) \quad a^2_{\ n} \, \phi_n(r) \right) \, dr$$

$$= \sum_{m,n=1}^{N_u} u_n \, u_m \int_R a_n^2 \, \phi_n(r) \, \phi_m(r) dr$$

$$= \sum_{m,n=1}^{N_u} \left[u_n \, u_m \, (a_n^2 + a_m^2)/2 \right] \quad \int_R \phi_n(r) \quad \phi_m(r) dr$$

$$= \mathscr{U}^T \mathscr{K}_U \mathscr{U}$$

where $\mathscr{K}_U$ is the self-adjoint, positive definite matrix whose elements are:

$$(\mathscr{K}_U)_{mn} = \left[(a_n^2 + a_m^2)/2 \right] \int_R \phi_n(r) \quad \phi_m(r) dr$$

Note that if $\phi_n(r)$, $n=1, \ldots, N_u$ are orthonormal:

$$\mathscr{K}_U = \text{diag } [a_1^2 \quad a_2^2 \quad \cdots \quad a^2_{\ N_u}]$$

Analogously:

$$\int_p v \, \nabla^4 \, vds = \mathscr{V} \mathscr{K}_v \mathscr{V}$$

where $\mathscr{K}_v$ is the $N_v \times N_v$ self-adjoint positive definite matrix whose elements are:

$$(\mathscr{K}_v)_{m,n} = \left[(a_m^2 + a_n^2)/2 \right] \int_p \psi_n(r) \quad \psi_m(r) \, dr$$

If $\psi_n(r)$, $n=1, \ldots, N_v$ are orthonormal:

$$\mathscr{K}_v = \text{diag } [a_1^2 \quad a_2^2 \quad \cdots \quad a_{N_v}^2]$$

$$\int_0^\ell \theta_B(-\partial^2 \theta/\partial x^2)dx = \int_0^\ell \left(\sum_{m=1}^{N_\theta} \theta_{Bm}(t)\eta_m(x)\right)\left(\sum_{n=1}^{N_\theta} \theta_{Bn}(t)[(2n-1)^2\pi^2/4\ell^2]\eta_n(x)\right)dx$$

$$= \sum_{m,n=1}^{N_\theta} \theta_{Bm}(t)\ \theta_{Bn}(t)[(2n-1)^2\pi^2/4\ell^2] \int_0^\ell \eta_m(x)\eta_n(x)dx$$

$$= \sum_{m,n=1}^{N_\theta} \theta_{Bm}(t)\ \theta_{Bn}(t)[(2n-1)^2\pi^2/4\ell^2](\ell/2)\delta_{nm}$$

$$= \sum_{n=1}^{N_\theta} [(2n-1)^2\pi^2/8\ell]\ \theta_{Bn}^2(t) = \mathscr{T}^T\mathscr{K}_\theta\mathscr{T}$$

where

$$\mathscr{K}_\theta = \text{diag } [\pi^2/8\ell \quad 9\pi^2/8\ell \ .\ .\ .\ (2N_\theta -1)^2\pi^2/8\ell]$$

$$\int_0^\ell Y_B(\partial^4 Y_B/\partial x^4)dx = \int_0^\ell \left(\sum_{m=1}^{N_y} y_{Bm}(t)\ \zeta_m(x)\right)\left(\sum_{n=1}^{N_y} y_{Bn}(t)d_n^4\zeta_n(x)\right)dx$$

$$= \sum_{m,n=1}^{N_y} y_{Bm}(t)y_{Bn}(t)d_n^4 \int_0^\ell \zeta_m(x)\ \zeta_n(x)dx$$

$$= \sum_{m,n=1}^{N_y} y_{Bm}(t)y_{Bn}(t)d_n^4\ell\delta_{mn} = \ell\sum_{n=1}^{N_y} d_n^4 y_{Bn}^2(t) = \mathscr{Y}^T\mathscr{K}_y\mathscr{Y}$$

where

$$\mathscr{K}_y = \text{diag } [d_1^4\ell \quad d_2^4\ell \ .\ .\ .\ d_{N_y}^4\ell]$$

and similarly:

$$\int_0^\ell Z_B(\partial^4 Z_B/\partial x^4)dx = \mathscr{Z}^T\mathscr{K}_Z\mathscr{Z}$$

where

$$\mathscr{K}_Z = \text{diag } [d_1^4\ell \quad d_2^4\ell \ .\ .\ .\ d_{N_z}^4 \ell]$$

185

Implementation

Before proceeding to substitute the various discretized variables in the expressions for the kinetic and potential energies, consider the discretization of P and Ω_p.

$$\dot{P} = \begin{pmatrix} 0 \\ \dot{Y}_B(\ell) \\ \dot{Z}_B(\ell) \end{pmatrix} = \begin{pmatrix} 0 \\ \sum_{n=1}^{Ny} \dot{y}_{Bn}(t)\zeta_n(\ell) \\ \sum_{n=1}^{Nz} \dot{z}_{Bn}(t)\zeta_n(\ell) \end{pmatrix} \triangleq \begin{pmatrix} 0 \\ \dot{\mathscr{Y}}^T\zeta_y(\ell) \\ \dot{\mathscr{Z}}^T\zeta_z(\ell) \end{pmatrix}$$

where

$$\zeta_y(\ell) \triangleq (\zeta_1(\ell) \quad \zeta_2(\ell) \quad \ldots \quad \zeta_{N_y}(\ell))^T \text{ and}$$

$$\zeta_z(\ell) \triangleq (\zeta_1(\ell) \quad \zeta_2(\ell) \quad \ldots \quad \zeta_{N_z}(\ell))^T$$

Thus:

$$\dot{P}\cdot\dot{P} = \dot{\mathscr{Y}}^T\zeta_y(\ell)\zeta_y^T(\ell)\dot{\mathscr{Y}} + \dot{\mathscr{Z}}\zeta_z(\ell)\zeta_z^T(\ell)\dot{\mathscr{Z}}$$

$$\dot{\Omega}_p = d/dt \begin{pmatrix} \theta_B(\ell,t) \\ \partial Z_B/\partial x|_{x=\ell} \\ \partial Y_B/\partial x|_{x=\ell} \end{pmatrix} = \begin{pmatrix} \sum_{n=1}^{N\theta} \dot{\theta}_{Bn}(t)\eta_n(\ell) \\ \sum_{n=1}^{Nz} \dot{z}_{Bn}(t)d\zeta_n(x)/dx|_{x=\ell} \\ \sum_{n=1}^{Ny} \dot{y}_{Bn}(t)d\zeta_n(x)/dx|_{x=\ell} \end{pmatrix} \triangleq \begin{pmatrix} \dot{\mathscr{T}}^T\eta(\ell) \\ \dot{\mathscr{Z}}^Td\zeta_z(\ell)/dx \\ \dot{\mathscr{Y}}^Td\zeta_y(\ell)/dx \end{pmatrix}$$

186

where

$$\eta(\ell) = (\eta_1(\ell) \quad \eta_2(\ell) \quad \ldots \ldots \quad \eta_{N_\theta}(\ell))^T$$

Kinetic energy:

Let us now proceed with the substitutions. We will obtain:

$$T = \frac{1}{2}\Bigg\{ M\dot{D}^T\dot{D} + \dot{\Omega}^T I\dot{\Omega} + \sum_{i=1}^{4}\Big\{ \dot{\mathcal{U}}_i{}^T F_i \dot{\mathcal{U}}_i + \dot{\beta}_i{}^T I_{R_i}\dot{\beta}_i + J_i\dot{\mathcal{T}}_i{}^T N_i\dot{\mathcal{T}}_i + \dot{\mathcal{Y}}_i{}^T U_i \dot{\mathcal{Y}}_i$$

$$+ \dot{\mathcal{F}}_1 V_1 \dot{\mathcal{F}}_1 + M_{Pi}(\dot{\mathcal{Y}}_i{}^T \zeta_{yi}(\ell)\zeta_{yi}{}^T(\ell)\dot{\mathcal{Y}}_i + \dot{\mathcal{F}}_i{}^T\zeta_{Zi}(\ell)\zeta_{Zi}{}^T(\ell)\dot{\mathcal{F}}_i)$$

$$+ \dot{\mathcal{F}}_i{}^T\eta_i(\ell)(I_{P_1})_{11}\eta_i{}^T(\ell)\dot{\mathcal{F}}_i + 2\dot{\mathcal{F}}_i{}^T\eta_i(\ell)(I_{Pi})_{12}[d\zeta_{Zi}(\ell)/dx]^T\dot{\mathcal{F}}_i$$

$$+ 2\dot{\mathcal{F}}_i{}^T\eta_i(\ell)(I_{Pi})_{13}[d\zeta_{Yi}(\ell)/dx]^T\dot{\mathcal{Y}}_i + \dot{\mathcal{F}}_i{}^T[d\zeta_{Zi}(\ell)/dx](I_{Pi})_{22}$$

$$[d\zeta_{Zi}(\ell)/dx]^T\dot{\mathcal{F}}_i + 2\dot{\mathcal{F}}_i{}^T[d\zeta_{Zi}(\ell)/dx](I_{Pi})_{23}[d\zeta_{Yi}(\ell)/dx]^T\dot{\mathcal{Y}}_i$$

$$+ \dot{\mathcal{Y}}_i{}^T[d\zeta_{Yi}(\ell)/dx](I_{P_1})_{33}[d\zeta_{Yi}(\ell)/dx]^T\dot{\mathcal{Y}}_i + \dot{a}_i{}^T(I_{si} + I_{Pi} + I_{Opi})\dot{a}_i$$

$$+ \dot{\mathcal{V}}_i{}^T\mathcal{O}_i\dot{\mathcal{V}}_i \Big\} + 2\dot{D}^T\sum_{i=1}^{4}\Big\{-[M_{R_1}\widetilde{R}_i + M_{Bi}\widetilde{B}_i + \int_0^{\ell_i}\rho_{Bi}\begin{pmatrix}\widetilde{x}\\0\\0\end{pmatrix}dx + M_{Pi}(\widetilde{B_i + P_i}) + \widetilde{C}_i]\dot{\Omega}$$

$$+ \begin{pmatrix}\mathcal{F}_1{}^T\dot{\mathcal{U}}_1\\0\\0\end{pmatrix} + \begin{pmatrix}0\\\mathcal{P}_{yi}{}^T\dot{\mathcal{Y}}_i\\\mathcal{P}_{zi}{}^T\dot{\mathcal{F}}_i\end{pmatrix} + M_{Pi}\begin{pmatrix}0\\\zeta_{yi}{}^T(\ell)\dot{\mathcal{Y}}_i\\\zeta_{zi}{}^T(\ell)\dot{\mathcal{F}}_i\end{pmatrix} - \widetilde{C}_i\begin{pmatrix}\eta_i{}^T(\ell)\dot{\mathcal{F}}_i\\[d\zeta_{zi}(\ell)/dx]^T\dot{\mathcal{F}}_1\\[d\zeta_{yi}(\ell)/dx]^T\dot{\mathcal{Y}}_i\end{pmatrix}$$

$$- \Big[\int_0^{\ell_i}\rho_{Bi}\begin{pmatrix}\widetilde{x}\\0\\c\end{pmatrix}dx + M_{Pi}\widetilde{P}_i + \widetilde{C}_i\Big]\dot{a}_i + \begin{pmatrix}0\\0\\\mathcal{P}_i{}^T\dot{\mathcal{V}}_i\end{pmatrix}\Big\} + 2\dot{\Omega}^T\sum_{i=1}^{4}\Big\{\widetilde{R}_i\begin{pmatrix}\mathcal{F}_1{}^T\dot{\mathcal{U}}_1\\0\\0\end{pmatrix} + \begin{pmatrix}0\\\mathcal{G}_{zi}{}^T\dot{\mathcal{U}}_1\\-\mathcal{G}_{yi}{}^T\dot{\mathcal{U}}_1\end{pmatrix}$$

$$+ I_{R_1}\dot{\beta}_i + \tilde{B}_1\begin{pmatrix} 0 \\ \mathscr{S}_{y_1}{}^T\dot{y}_1 \\ \mathscr{S}_{z_1}{}^T\dot{\mathcal{P}}_1 \end{pmatrix} + \begin{pmatrix} 0 \\ -\Gamma_{z_i}{}^T\dot{\mathcal{P}}_1 \\ \Gamma_{y_1}{}^T\dot{y}_1 \end{pmatrix} + [M_{P_i}\widetilde{(B_i + P_1)} + \tilde{C}_i]\begin{pmatrix} 0 \\ \varsigma_{y_i}{}^T(\ell)\dot{y}_i \\ \varsigma_{z_i}{}^T(\ell)\dot{\mathcal{P}}_i \end{pmatrix}$$

$$+ (I_{P_1} + B_1{}^T C_1 E - C_i B_1{}^T + P_i{}^T C_i E - C_1 P_1{}^T)\begin{pmatrix} \eta_i{}^T(\ell)\dot{\mathcal{J}}_1 \\ [d\varsigma_{z_i}(\ell)/dx]^T\dot{\mathcal{P}}_1 \\ [d\varsigma_{y_i}(\ell)/dx]^T\dot{y}_1 \end{pmatrix} + [I_{P_i}$$

$$+ I_{OP_i} - M_{P_1}P_1 B_1{}^T + C_i{}^T B_1 E - C_i B_1{}^T + I_{s_i} - \left(\int_0^{\ell_i}\rho_{B_i}\begin{pmatrix} x \\ o \\ o \end{pmatrix}dx\right)B_i{}^T]\dot{a}_i$$

$$+ \widetilde{(B_1 + P_1)}\begin{pmatrix} 0 \\ 0 \\ \mathscr{P}_i{}^T\dot{\mathscr{V}}_1 \end{pmatrix} + \begin{pmatrix} \mathscr{D}_{y_i}{}^T\dot{\mathscr{V}}_1 \\ -\mathscr{D}_{x_1}{}^T\dot{\mathscr{V}}_1 \\ 0 \end{pmatrix}\} + \sum_{i=1}^{4}\{2\dot{\beta}_i{}^T\begin{pmatrix} 0 \\ \mathscr{G}_{z_i}{}^T\dot{\mathscr{W}}_1 \\ \mathscr{G}_{y_i}{}^T\dot{\mathscr{W}}_1 \end{pmatrix}$$

$$+ 2(0 \quad \dot{\mathcal{J}}_1{}^T\Gamma_{z_i} - \dot{y}_1{}^T\Gamma_{y_i})\dot{a}_i + 2(0 \quad \dot{y}_1{}^T\varsigma_{y_i}(\ell) \quad \dot{\mathcal{P}}_1{}^T\varsigma_{z_i}(\ell))\begin{bmatrix} -\tilde{C}_i \begin{pmatrix} \eta_i{}^T(1)\dot{\mathcal{J}}_i \\ [d\varsigma_{z_i}(\ell)/dx]^T\dot{\mathcal{P}}_i \\ [d\varsigma_{y_i}(\ell)/dx]^T\dot{y}_i \end{pmatrix}$$

$$+ \begin{pmatrix} 0 \\ 0 \\ \mathscr{P}_1{}^T\mathscr{V}_1 \end{pmatrix} - (M_{P_i}\widetilde{P}_i + \tilde{C}_1)\dot{a}_i] + 2(\dot{\mathcal{J}}_i{}^T\eta_i(\ell) \quad \dot{\mathcal{P}}_i{}^T d\varsigma_{z_i}(\ell)/dx \quad \dot{y}_i{}^T d\varsigma_{y_1}(\ell)/dx)$$

$$\begin{bmatrix} (I_{P_1} + P_1{}^T C_1 E - P_i C_1{}^T)\dot{a}_i + \begin{pmatrix} \mathscr{D}_{y_i}{}^T\dot{\mathscr{V}}_1 \\ -\mathscr{D}_{x_i}{}^T\dot{\mathscr{V}}_1 \\ 0 \end{pmatrix}] + 2\dot{a}_i{}^T[\widetilde{P}_i\begin{pmatrix} 0 \\ 0 \\ \mathscr{P}_i{}^T\mathscr{V}_i \end{pmatrix} + \begin{pmatrix} \mathscr{D}_{y_i}{}^T\dot{\mathscr{V}}_1 \\ -\mathscr{D}_{x_i}{}^T\dot{\mathscr{V}}_1 \\ 0 \end{pmatrix}] \end{bmatrix}$$

where:

$$M \underset{=}{\Delta} M_{RB} + \sum_{i=1}^{4}(M_{R_1} + M_{B_1} + M_{P_i}) \quad \text{and}$$

$$I \underset{=}{\Delta} I_{RB} + \sum_{i=1}^{4}[I_{OR_i} + I_{R_i} + M_{B_i}(B_i{}^T B_i E - B_i B_i{}^T) + I_{s_i} - \left(\int_0^{\ell_i}\rho_{B_i}\begin{pmatrix} x \\ o \\ o \end{pmatrix}dx\right)B_1{}^T$$

$$- B_i\left(\int_0^{\ell_i}\rho_{B_i}\begin{pmatrix} x \\ o \\ o \end{pmatrix}dx\right)^T + I_{P_1} + I_{OP_1} + I_{OB_1} - M_{P_1}(B_1 P_1{}^T + P_i B_1{}^T)]$$

Using the state vector W_D:

$$W_D \triangleq (D \quad \Omega \quad \alpha_1 \quad \alpha_2 \quad \alpha_3 \quad \alpha_4 \quad \beta_1 \quad \beta_2 \quad \beta_3 \quad \beta_4 \quad \mathcal{U}_1 \quad \mathcal{U}_2$$

$$\mathcal{U}_3 \quad \mathcal{U}_4 \quad \mathcal{T}_1 \quad \mathcal{Y}_1 \quad \widetilde{\mathcal{T}}_1 \quad \mathcal{V}_1 \quad \mathcal{T}_2 \quad \mathcal{Y}_2 \quad \widetilde{\mathcal{T}}_2 \quad \mathcal{V}_2 \quad \mathcal{T}_3 \quad \mathcal{Y}_3$$

$$\widetilde{\mathcal{T}}_3 \quad \mathcal{V}_3 \quad \mathcal{T}_4 \quad \mathcal{Y}_4 \quad \widetilde{\mathcal{T}}_4 \quad \mathcal{V}_4)^T$$

the kinetic energy can be put in the form:

$$T = \frac{1}{2}\dot{W}_D{}^T M_D \dot{W}_D$$

The matrix M_D is easily obtained from the discretization procedure.

Potential energy:

The expression for the discretized system's potential energy is much simpler to write:

$$K = \frac{1}{2}\sum_{i=1}^{4}(F_R\mathcal{U}_i\mathcal{K}_{u_i}\mathcal{U}_i + G_iJ_i\mathcal{T}_i^T\mathcal{K}_{\theta i}\mathcal{T}_i + E_iI_{y_i}\mathcal{Y}_i^T\mathcal{K}_{y_i}\mathcal{Y}_i$$

$$+ E_iI_{z_i}\widetilde{\mathcal{T}}_i^T\mathcal{K}_{z_i}\widetilde{\mathcal{T}}_i + F_{p_i}\mathcal{V}_i^T\mathcal{K}_{v_i}\mathcal{V}_i)$$

This can easily be put in the form:

$$K = \frac{1}{2}W_D{}^T K_D W_D$$

with the matrix K_D properly defined.

IV. FINITE-ELEMENT MODEL

Referring to Fig. 6, the main structure is modeled as two flexible beams which are rigidly attached to the core body. The solar panels are treated as flexible beams attached to the ends of the main structure. Two payloads, assumed rigid for simplicity, are hinge connected to the core body. To keep the model to a tractable size, the beams are assumed torsionally stiff, and hence, only bending angles and the associated deflections are modeled.

Let Z_1, ..., Z_7 be the out-of-plane linear deformations at the various

189

locations of the beams; $\theta_1,\ldots,\theta_7$ be the corresponding bending angles in the pitch or Y-axis direction; Φ_2, Φ_4, and Φ_6 be the bending angles in the roll or X-axis direction; and γ_{8x}, γ_{8y}, γ_{9x}, γ_{9y} be the payload inertial attitude angles and γ'_{8x}, γ'_{8y}, γ'_{9x} and γ'_{9y} be the corresponding hinge angles. Since the beams are assumed torsionally stiff, the following constraints apply:

$$\theta_2 = \theta_6 = \theta_4$$
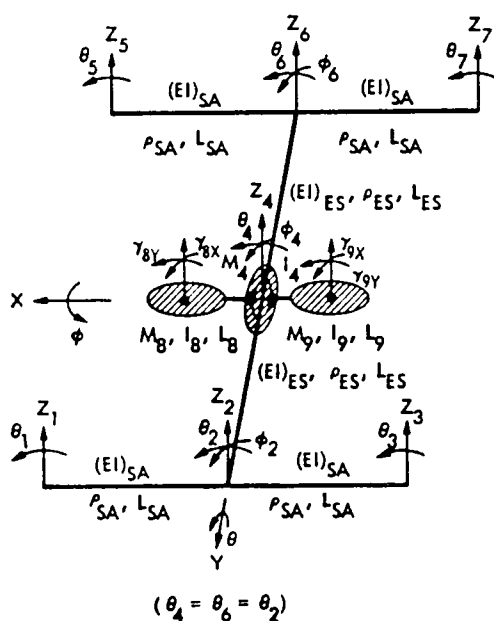
Figure 6. 19-DOF finite-element model for the four-panel planar configurations

Employing finite-element techniques [4,1], the mass and stiffness matrices for the following equation of motion are obtained:

$$M\ddot{Z} + KZ = F$$

where the force vector F and the system displacement vector Z are

$$P = \begin{bmatrix} F_s \\ -\,-\,- \\ F_p \end{bmatrix} \quad \text{and} \quad Z = \begin{bmatrix} Z_s \\ -\,-\,- \\ Z_p \end{bmatrix}$$

with

$$F_S = (F_1,\ T_{1\Theta},\ F_3,\ T_{3\Theta},\ F_2,\ T_{2\phi},\ F_4,\ T_{4\Theta},\ T_{4\phi},\ F_6,\ T_{6\phi},\ F_5,\ T_{5\Theta},\ F_7,\ T_{7\Theta})^T$$

$$F_p = (T_{8x},\ T_{9x},\ T_{8y},\ T_{9y})^T$$

$$Z_S = (Z_1,\ \Theta_1,\ Z_3,\ \Theta_3,\ Z_2,\ \phi_2,\ Z_4,\ \Theta_4,\ \phi_4,\ Z_6,\ \phi_6,\ Z_5,\ \Theta_5,\ Z_7,\ \Theta_7)^T$$

$$Z_p = (\gamma'_{8x},\ \gamma'_{9x},\ \gamma'_{8y},\ \gamma'_{9y})^T$$

where the subscripts S and P refer to the station and payloads, respectively.

The mass and stiffness matrices are partitioned accordingly. Let M_C and M_D be the consistent, and discrete mass matrices, respectively. The system's matrix is

$$M = M_C + M_D$$

with

$$M_C = \begin{bmatrix} M_{SC} & \vdots & 0_{15 \times 4} \\ -\,-\,-\,-\,- & \vdots & -\,-\,-\,- \\ 0_{4 \times 15} & \vdots & 0_{4 \times 4} \end{bmatrix}$$

and

$$M_D = \begin{bmatrix} M_{SD} + M'_{SD} & \vdots & M_{PSD}^T \\ -\,-\,-\,-\,-\,-\,- & \vdots & -\,-\,-\,- \\ M_{PSD} & \vdots & M_{PD} \end{bmatrix}$$

where

$$
\mathbf{M_{SC}} =
\begin{bmatrix}
156a & 22L_sa & 0 & 0 & 54a & 0 & 0 & 13L_sa & 0 & 0 & 0 & 0 & 0 & 0 & 0 \\
22L_sa & 4L_s^2a & 0 & 0 & 13L_sa & 0 & 0 & 3L_s^2a & 0 & 0 & 0 & 0 & 0 & 0 & 0 \\
0 & 0 & 156a & 22L_sa & 54a & 0 & 0 & 13L_sa & 0 & 0 & 0 & 0 & 0 & 0 & 0 \\
0 & 0 & 22L_sa & 4L_s^2a & 13L_sa & 0 & 0 & 3L_s^2a & 0 & 0 & 0 & 0 & 0 & 0 & 0 \\
54a & 13L_sa & 54a & 13L_sa & 312a+156b & 22L_eb & 54b & 0 & 13L_eb & 0 & 0 & 0 & 0 & 0 & 0 \\
0 & 0 & 0 & 0 & 22L_eb & 4L_e^2b & 13L_eb & 0 & 3L_e^2b & 0 & 0 & 0 & 0 & 0 & 0 \\
0 & 0 & 0 & 0 & 54b & 13L_eb & 312b & 0 & 0 & 54b & 13L_eb & 0 & 0 & 0 & 0 \\
13L_sa & 3L_s^2a & 13L_sa & 3L_s^2a & 0 & 0 & 0 & 16L_s^2a & 0 & 0 & 0 & 13L_sa & 3L_s^2a & 13L_sa & 3L_s^2a \\
0 & 0 & 0 & 0 & 13L_eb & 3L_e^2b & 0 & 0 & 8L_e^2b & 13L_eb & 3L_e^2b & 0 & 0 & 0 & 0 \\
0 & 0 & 0 & 0 & 0 & 0 & 54b & 0 & 13L_eb & 156b+312a & 22L_eb & 54a & 13L_sa & 54a & 13L_sa \\
0 & 0 & 0 & 0 & 0 & 0 & 13L_eb & 0 & 3L_e^2b & 22L_eb & 4L_e^2b & 0 & 0 & 0 & 0 \\
0 & 0 & 0 & 0 & 0 & 0 & 0 & 13L_sa & 0 & 54a & 0 & 156a & 22L_sa & 0 & 0 \\
0 & 0 & 0 & 0 & 0 & 0 & 0 & 3L_s^2a & 0 & 13L_sa & 0 & 22L_sa & 4L_s^2a & 0 & 0 \\
0 & 0 & 0 & 0 & 0 & 0 & 0 & 13L_sa & 0 & 54a & 0 & 0 & 0 & 156a & 22L_sa \\
0 & 0 & 0 & 0 & 0 & 0 & 0 & -3L_s^2a & 0 & -13L_sa & 0 & 0 & 0 & -22L_sa & 4L_s^2a
\end{bmatrix}
$$

with $\quad a = \dfrac{\rho_s L_s}{420} \quad$ and $\quad b = \dfrac{\rho_e L_e}{420}$.

and

$$\mathbf{M_{SD}} = \text{diag}\,(0,0,0,0,0,0,M_4,I_{4yy},I_{4xx},0,0,0,0,0,0)$$

$$
\mathbf{M'_{SD}} =
\begin{bmatrix}
0_{6\times6} & \vline & & 0_{6\times3} & & \vline & 0_{6\times6} \\
\hline
& \vline & m_8+m_9 & m_9L_9-m_8L_8 & 0 & \vline & \\
0_{3\times6} & \vline & m_9L_9-m_8L_8 & m_8L_8^2+m_9L_9^2+I_{8YS}+I_{9YS} & 0 & \vline & 0_{3\times6} \\
& \vline & 0 & 0 & I_{8YS}+I_{9YS} & \vline & \\
\hline
0_{6\times6} & \vline & & 0_{6\times3} & & \vline & 0_{6\times6}
\end{bmatrix}
$$

192

$$
M_{PD} = \begin{bmatrix}
I_{8XS} & 0 & 0 & 0 \\
0 & I_{9XS} & 0 & 0 \\
0 & 0 & I_{8YS} + m_8 L_{8b}^2 & 0 \\
0 & 0 & 0 & I_{9YS} + m_9 L_{9b}^2
\end{bmatrix}
$$

$$
M_{PSD} = \begin{bmatrix}
& 0 & 0 & I_{8XS} & \\
& 0 & 0 & I_{9XS} & \\
0_{4\times6} & -m_8 L_{8b} & I_{8YS} + m_8 L_{8a} L_{8b} + m_8 L_{8b}^2 & 0 & 0_{4\times6} \\
& m_9 L_{9b} & I_{9YS} + m_9 L_{9a} L_{9b} + m_9 L_{9b}^2 & 0 &
\end{bmatrix}
$$

The system's stiffness matrix is given by

$$
K = \begin{bmatrix}
K_s & 0_{15\times4} \\
0_{4\times15} & 0_{4\times4}
\end{bmatrix}
$$

with

$$
K_S =
\begin{bmatrix}
6\alpha & 3l_s\alpha & 0 & 0 & -6\alpha & 0 & 0 & 3l_s\alpha & 0 & 0 & 0 & 0 & 0 & \cdot & \cdot \\
3l_s\alpha & 2l_s^2\alpha & 0 & 0 & 3l_s\alpha & 0 & 0 & l_s^2\alpha & 0 & 0 & 0 & 0 & 0 & 0 & 0 \\
0 & 0 & 6\alpha & 3l_s\alpha & 6\alpha & 0 & 0 & 3l_s\alpha & 0 & 0 & 0 & 0 & 0 & 0 & 0 \\
0 & 0 & 3l_s\alpha & 2l_s^2\alpha & 3l_s\alpha & 0 & 0 & l_s^2\alpha & 0 & 0 & 0 & 0 & 0 & 0 & 0 \\
6\alpha & 3l_s\alpha & 6\alpha & 3l_s\alpha & 12\alpha+6\beta & 3l_e\beta & 6\beta & 0 & 3l_e\beta & 0 & 0 & 0 & 0 & 0 & 0 \\
0 & 0 & 0 & 0 & 3l_e\beta & 2l_e^2\beta & 3l_e\beta & 0 & l_e^2\beta & 0 & 0 & 0 & 0 & 0 & 0 \\
0 & 0 & 0 & 0 & 6\beta & 3l_e\beta & 12\beta & 0 & 0 & -6\beta & 3l_e\beta & 0 & 0 & 0 & 0 \\
3l_s\alpha & l_s^2\alpha & 3l_s\alpha & l_s^2\alpha & 0 & 0 & 0 & 8l_s^2\alpha & 0 & 0 & 0 & 3l_s\alpha & l_s^2\alpha & 3l_s\alpha & l_s^2\alpha \\
0 & 0 & 0 & 0 & 3l_e\beta & l_e^2\beta & 0 & 0 & 4l_e^2\beta & 3l_e\beta & l_e^2\beta & 0 & 0 & 0 & 0 \\
0 & 0 & 0 & 0 & 0 & 0 & -6\beta & 0 & 3l_e\beta & 12\alpha+6\beta & 3l_e\beta & -6\alpha & 3l_s\alpha & 6\alpha & 3l_s\alpha \\
0 & 0 & 0 & 0 & 0 & 0 & 3l_e\beta & 0 & l_e^2\beta & 3l_e\beta & 2l_e^2\beta & 0 & 0 & 0 & 0 \\
0 & 0 & 0 & 0 & 0 & 0 & 0 & 3l_s\alpha & 0 & -6\alpha & 0 & 6\alpha & 3l_s\alpha & 0 & 0 \\
0 & 0 & 0 & 0 & 0 & 0 & 0 & l_s^2\alpha & 0 & 3l_s\alpha & 0 & 3l_s\alpha & 2l_s^2\alpha & 0 & 0 \\
0 & 0 & 0 & 0 & 0 & 0 & 0 & 3l_s\alpha & 0 & 6\alpha & 0 & 0 & 0 & 6\alpha & 3l_s\alpha \\
0 & 0 & 0 & 0 & 0 & 0 & 0 & l_s^2\alpha & 0 & 3l_s\alpha & 0 & 0 & 0 & 3l_s\alpha & 2l_s^2\alpha
\end{bmatrix}
$$

where $\alpha = \dfrac{2(EI)_s}{L_s^3}$ and $\beta = \dfrac{2(EI)_e}{L_e^3}$.

V. MODAL PROPERTIES FOR THE FINITE-ELEMENT MODEL

Let $\eta(t)$, Λ, and Φ be the modal amplitude vector, eigenvalue matrix, and eigenvector matrix, respectively. Let $Z(t) = \Phi\eta(t)$. Substitute this into the equation of motion and premultiply it by Φ^T. Since $\Phi^T M \Phi = I$ and $\Phi^T K \Phi = \Lambda$, one obtains the following dynamical equation in modal form,

$$\ddot{\eta} + \Lambda\eta = \Phi^T F$$

where $\Lambda = \text{diag}(\omega_1^2, \ldots, \omega_{19}^2)$. Adding damping terms,

$$\ddot{\eta} + \text{diag}(2\zeta_1\omega_1, \ldots, 2\zeta_{19}\omega_{19})\dot{\eta} + \text{diag}(\omega_1^2, \ldots, \omega_{19}^2)\eta = \Phi^T F$$

The corresponding damped dynamical equation in physical coordinates can be obtained through the inverse transformation. Let D be the damping factor matrix, one has

$$D = \Phi^{-T} \text{diag}(2\zeta_1\omega_1, \ldots, 2\zeta_{19}\omega_{19})\Phi^{-1}$$

and the equation of motion becomes,

$$M\ddot{Z} + D\dot{Z} + KZ = F$$

To obtain the modal properties, i.e. to determine the eigenvalues and eigenvectors, for the open loop system, one can either free the hinges for the payloads, or clamp them. For the latter case, the result is a 15-coordinate system with 12 flexible modes and 3 rigid body modes. For the former case, however, a 19-coordinate system results since the payloads are considered rigid bodies and the hinges are freed, it ends up with 4 additional rigid or zero frequency modes. Since this does not yield additional information, only the clamped-hinge case is considered in this paper.

The modal frequencies and mode shapes for the four-panel planar configuration with clamped-hinge case are shown in Fig. 7. These modes are divided into three groups. The first bending group consists of 6 modes with frequencies ranging from 0.115 Hz to 0.302 Hz. These modes are formed with the first symmetric or antisymmetric bending of the three major structures, i.e., the two solar panel pairs and the main structure. The second bending group is caused by the second symmetric or the antisymmetric bending of the three major structures. The frequencies for this group are

much higher than those of the first group and range from 1.67 Hz to 2.34 Hz. The third group consists of three rigid body modes with zero frequencies.

The structural and mass parameters used for generating these modes are shown in Fig. 6. The flexural rigidity $(EI)_s = 9.48 \times 10^6$ lb-ft^2 has been used for the solar panels and a value of an order of magnitude higher has been used for the main structure.

VI. SUMMARY AND CONCLUSIONS

The development of two parametric models for a four-panel planar initial space station is described. The derivations of the distributed parameter model are presented in detail with the hope that the same method and procedures can be employed for stations with different configurations or for changes within the same configuration class. The 19-DOF finite-element model is also described here but with much less detail as its more complete treatment is discussed in Ref 1.

With the availability of the 19-DOF and a lower-DOF[1] space station models, the frequency characteristics of the various dynamical systems in the space station environment are identified as shown in Fig. 8.

For a nominal orbital altitude of 400 km, the orbital period is 92.61 minutes or a rate of 1.8×10^{-4} Hz. For altitudes close to 400 km, the rate will be inside the shaded narrow region in Fig. 8. The solar panel libration frequency for quasi-solar-inertial pointing [5] will be twice the orbital rate as shown in Fig. 8. A low bandwidth attitude control system for the space station will have a bandwidth in the range of 0.001 Hz to 0.005 Hz. The two-panel low DOF model and the four-panel finite-element

MODE 4
$\omega_4 = 0.11526$ Hz

MODE 5
$\omega_5 = 0.16961$ Hz

MODE 6
$\omega_6 = 0.17794$ Hz

MODE 7
$\omega_7 = 0.21767$ Hz

MODE 8
$\omega_8 = 0.28061$ Hz

MODE 9
$\omega_9 = 0.30205$ Hz

(a) First bending group

MODE 10
$\omega_{10} = 1.6663$ Hz

MODE 11
$\omega_{11} = 1.6714$ Hz

MODE 12
$\omega_{12} = 1.7533$ Hz

MODE 13
$\omega_{13} = 1.7638$ Hz

MODE 14
$\omega_{14} = 2.3364$ Hz

MODE 15
$\omega_{15} = 2.3389$ Hz

(b) Second bending group

MODE 1
$\omega_1 = 0$

MODE 2
$\omega_2 = 0$

MODE 3
$\omega_3 = 0$
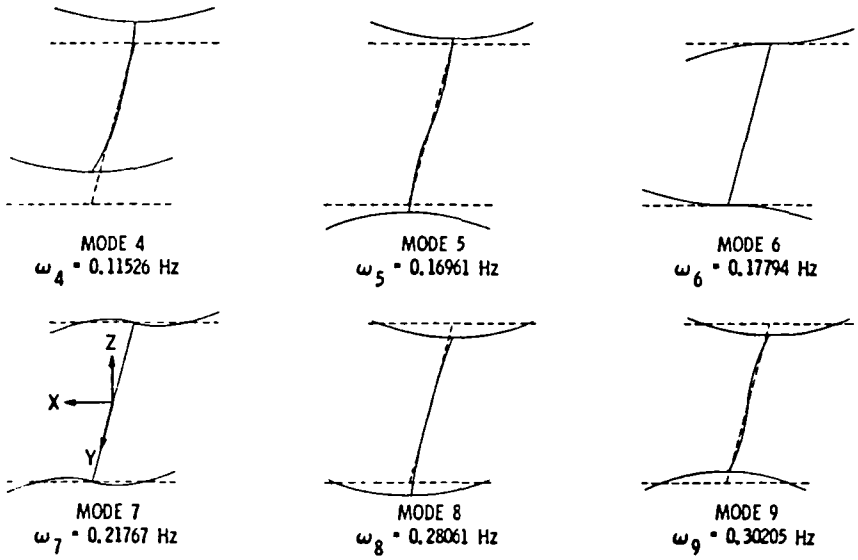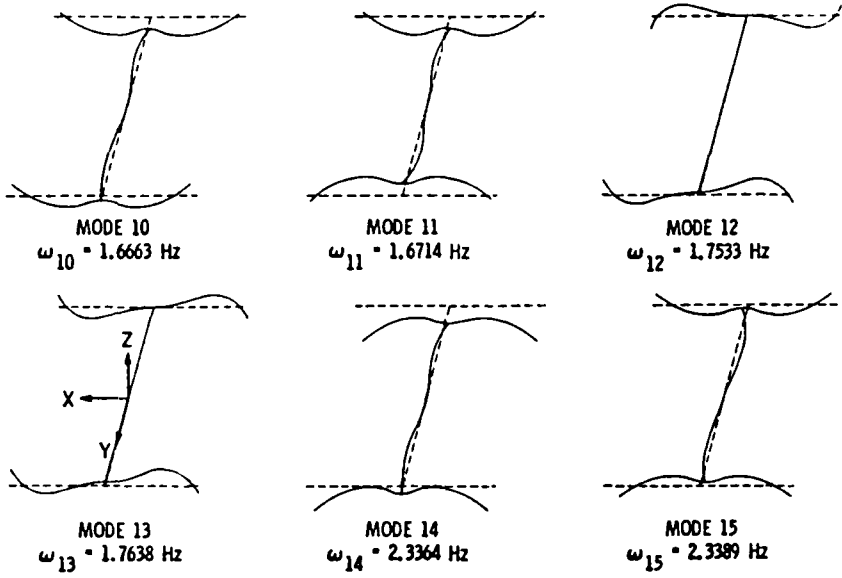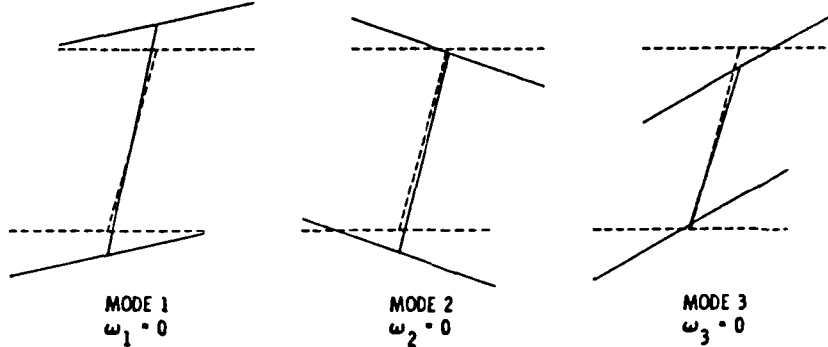
(c) Rigid body modes

Figure 7.   Four-Panel space station modal properties

197
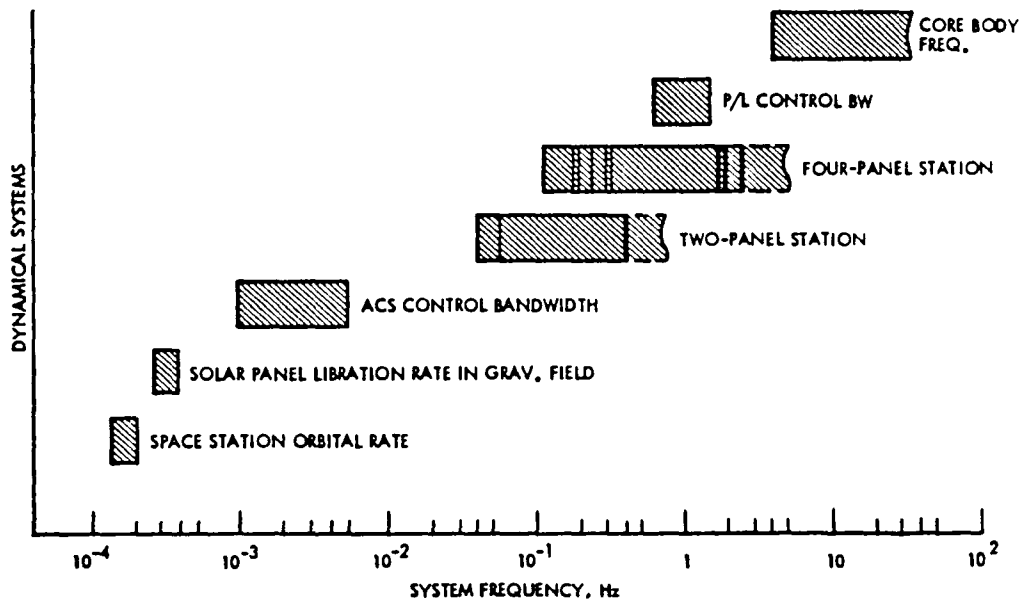
Figure 8. Frequency characteristics of space station dynamical systems

model are shown in Fig. 8 with their modeled frequencies identified by vertical lines. The dashed regions extending the modeled modes represent the modal spectra that are not included in the models. The payload attitude control systems for a range of applications will have bandwidths in a range centered at 1 Hz. The core body including the pressurized modules should have structural frequencies above 9 Hz. The figure indicates that the spectral separations of the orbital rate, the attitude controllers, and the low frequency modes of the station structure are reasonable. However, the same cannot be said about the structural modes and the payload controls. For instance, the payload bandwidth falls between the modes of the first and the second bending groups. This result strongly suggests that decoupling control of the payload is required.

REFERENCES

1. Wang, S.J., C.H.C. Ih, Y.H. Lin, and E. Mettler, "Space Station Dynamic Modeling, Disturbance Accommodation, and Adaptive Control," paper presented at the 1984 Workshop on Identification and Control of Flexible Space Structures, June 4-6, San Diego, California.

2. Timoshenko and Gere, _Theory of Elastic Stability_, McGraw-Hill, Second Edition, 1961, pp. 335-340.

3. Leissa, A.W., _Vibration of Plates_, NASA Report SP 160, NASA, Washington, D.C., 1969, p. 41.

4. Clough, R.W. and J. Penzien, _Dynamics of Structures_, McGraw-Hill, New York, N.Y., 1975.

5. Juang, J.N. and S.J. Wang, "An Investigation of Quasi-Inertial Attitude Control for a Solar Power Satellite," _Space Solar Power Review_, Vol. 3, pp. 337-352, 1982.

APPROXIMATION OF OPTIMAL INFINITE DIMENSIONAL COMPENSATORS FOR FLEXIBLE STRUCTURES

J. S. Gibson, D. L. Mingori, A. Adamian, and **F. Jabbari**
University of California
Los Angeles, CA 90024

1.   Introduction

The infinite dimensional LQG problem for a distributed system results in an optimal compensator which is infinite dimensional. Although such a compensator cannot be built, it can serve as a guide for designing a good finite dimensional compensator. Since the ideal infinite dimensional compensator produces optimal system performance, a finite dimensional compensator which approximates the ideal compensator should produce near-optimal performance.

In this paper, we discuss the infinite dimensional compensator for a large class of flexible structures, modeled as distributed systems, and outline an approximation scheme for designing finite dimensional compensators to approximate the infinite dimensional compensator. The approximation scheme is applied to develop a compensator for a space antenna model based on wrap-rib antennas being built currently. While the present model has been simplified, it retains the salient features of rigid body modes and several distributed components of different characteristics.

The control and estimator gains are represented by functional gains, which provide graphical representations of the control and estimator laws. These functional gains also indicate the convergence of the finite dimensional compensators and show which modes the optimal compensator ignores.

Of course, the practical value of this compensator design method depends on whether the infinite dimensional compensator can be approximated by a finite dimensional compensator of sufficiently low order. For the antenna problem here, a related paper [6] develops a reduced order compensator based on the large order approximation in this paper to the infinite dimensional compensator.

2. Abstract Control System

The space antenna model used here falls into the large class of flexible structures represented by the abstract control system

$$(2.1) \quad M_o x + D_o \dot{x} + A_o x = B_o u + \nu_1,$$

$$(2.2) \quad y = C_o x + \nu_o$$

where the generalized displacement $x(t)$ is in a real Hilbert space H, the control $u(t) \epsilon \; R^m$, the measurement $y(t) \epsilon \; R^p$. The disturbance ν_1 and the noise ν_o are zero-mean Gaussian white noise processes, as in the standard finite dimensional LQG problem. The mass operator M_o is bounded, selfadjoint and coercive on H, B_o is bounded from R^m to H and C_o is bounded from H to R^p. The unbounded stiffness operator A_o is selfadjoint and bounded below, with compact resolvent, and the damping operator D_o is symmetric, nonnegative and A_o-bounded. (See [5] for the terminology).

As usual, by _natural_ _modes_ we mean the eigenvectors x_j of the problem

$$(2.3) \quad \omega_j^2 \; M_o \; x_j = A_o x_j, \quad j = 1,2,\cdots,$$

where the ω_j's are the natural frequencies of the structure. In the antenna problem, as in most structure control problems, the only nonpositive eigenvalues of A_o are zero eigenvalues corresponding to rigid body modes. When these rigid body modes are controllable, they are contained in the positive eigenspace of $B_o B_o^*$, so that the operator

$$(2.4) \quad \tilde{A}_o = A_o + B_o B_o^* \geq m > 0,$$

for some positive m; i.e., $\tilde{A}$ is coercive.

Next, we define the strain-energy space $V = D(\tilde{A}_o^{\frac{1}{2}})$ with inner product

$$(2.5) \quad <v_1, v_2>_V = <\tilde{A}_o^{\frac{1}{2}} v_1, \; \tilde{A}_o^{\frac{1}{2}} v_2>_H.$$

This is a natural space for the generalized displacement because usually, as in our example, $\|x\|_V^2$ is just twice the sum of the elastic strain energy and the squares of the rigid body displacements.

To write (2.1) in first order form, we define the energy space $E = V \times H_M$ where H_M is H with the equivalent kinetic-energy inner product

$$(2.6) \quad \langle h_1, h_2 \rangle_M = \langle M h_1, h_2 \rangle_H.$$

Thus $\|\dot{x}\|_M^2$ is twice the kinetic energy in the structure. Now we can write (2.1) as

$$(2.7) \quad \dot{z} = Az + Bu + \hat{v}_1,$$

$$(2.8) \quad y = Cz + v_0,$$

where

$$(2.9) \quad z = \begin{pmatrix} x \\ \dot{x} \end{pmatrix} \quad, \quad \hat{v}_1 = \begin{pmatrix} 0 \\ v_1 \end{pmatrix} \quad, \quad B = \begin{bmatrix} 0 \\ B_0 \end{bmatrix}$$

and

$$(2.10) \quad A = \begin{bmatrix} 0 & I \\ -M_0^{-1} A_0 & -M_0^{-1} D_0 \end{bmatrix} \quad, \quad D(A_0) \times D(A_0) \subset D(A).$$

As in [3, Sec. 2], D(A) is chosen uniquely so that A generates a C_0-semigroup $T(\cdot)$ on E.

3. Infinite Dimensional LQG Problem

As in the finite dimensional case, a separation principle [1,2] allows us to design the optimal compensator by solving the deterministic optimal regulator problem and the stochastic state-estimation problem separately. The infinite dimensional optimal control problem is to choose u to minimize

$$(3.1) \qquad J = \int_0^\infty (<Qz, z>_E + <Ru, u>_{R^m}) dt,$$

where z is the solution to (2.7), $Q = Q*$ is a nonnegative bounded linear operator on E, and $R = R*>0$.

To simplify certain technicalities about existence of solutions to the LQG problem, we will assume that $D_0 + B_0 B_0^*$ is coercive, which means that the flexible components of the structure have coercive damping, and that Q is coercive, which guarantees that the optimal closed-loop system is uniformly exponentially stable.

For this deterministic problem, the optimal control has the feedback form

$$(3.2) \qquad u = - Kz,$$

where

$$(3.3) \qquad K = -R^{-1}B^*\Pi$$

and Π is the unique nonnegative selfadjoint element of $L(E)$ which satisfies the infinite dimensional Riccati equation

$$(3.4) \qquad A^*\Pi + \Pi A - \Pi BR^{-1}B^* \Pi + Q = 0$$

See [1,2,3].

The minimum-variance estimator, or infinite dimensional Kalman filter, is [1,2]

$$(3.5) \qquad \dot{\hat{z}} = A\hat{z} + Bu + G(y-C\hat{z}),$$

where

204

$$(3.6) \qquad G = \Pi C^* \hat{R}^{-1}$$

and $\hat{\Pi}$ satisfies the Riccati equation

$$(3.7) \qquad A\hat{\Pi} + \hat{\Pi}A^* - \hat{\Pi}C^*\hat{R}^{-1} C\hat{\Pi} + \hat{Q} = 0.$$

The pxp matrix $\hat{R}$ and the bounded nonnegative operator $\hat{Q} = \hat{Q}^*$ are the covariance operators for v_0 and v_1, respectively. We assume that any undamped modes are observable, so that the closed-loop estimator is uniformly exponentially stable.

The optimal compensator consists of the infinite dimensional estimator (3.5) and the control law

$$(3.8) \qquad u = - K\hat{z},$$

where K is given by (3.3). With (3.8), (3.5) becomes

$$(3.9) \qquad \dot{\hat{z}} = A_c\hat{z} + Gy,$$

where

$$(3.10) \qquad A_c = A - BK - GC$$

Note that the optimal compensator has the irrational transfer function

$$(3.11) \qquad K[sI - A_c]^{-1}G.$$

205

4. Functional Gains

When there is a single actuator ($m=1$), the operator $\mathcal{B}_0$ is actually an element of H and $\mathcal{B}\varepsilon E$. Hence

$$(4.1) \qquad Kz = R^{-1}B^{*}\Pi z = <\Pi BR^{-1}, z>_E,$$

or

$$(4.2) \qquad Kz = <f, x>_V + <g, x>_M$$

where

$$(4.3) \qquad \binom{f}{g} = \Pi BR^{-1}$$

with $f\varepsilon V$ and $g\varepsilon H_M = H$. We call f and g __functional__ __control__ __gains__.

Similarly, for a single sensor, the measurement y is a scalar and $C^{*}\varepsilon E$. Then

$$(4.4) \qquad G = \hat{\Pi}C^{*}\hat{R}^{-1} = \binom{\hat{f}}{\hat{g}}$$

where $\hat{f}\varepsilon V$ and $\hat{g}\varepsilon H$ are __functional__ __estimator__ __gains__.

For the multi-input-multi-output case, there is a pair of functional gains for each actuator and for each sensor.

5. Approximation

To obtain a sequence of approximating finite dimensional LQG problems, we use a Ritz-Galerkin approximation scheme for (2.1). We assume a sequence of linearly independent basis vectors e_i, which are complete in V. The nth approximate solution to (2.1) is

$$(5.1) \qquad x_n(t) = \sum_{i=1}^{n} a_i^n(t) e_i,$$

which is in V_n = span $(e_1, \ldots, e_n)$. We will need both V_n and H_{Mn}, which are the same set but have the V and H_M inner products, respectively.

Initially, let us consider the case $\nu_1 = 0$ in (2.1). Then the coefficients $a_i^n(t)$ satisfy

$$(5.2) \qquad M_{on} \ddot{a}^n + D_{on} \dot{a}^n + A_{on} a^n = B_{on} u,$$

where $a^n(t)$ is the n-vector containing $a_i^n(t)$, $i = 1, \ldots, n$. The mass, damping and stiffness matrices are given respectively by

$$(5.3) \qquad M_{on,ij} = <e_i, e_j>_M = <M_o e_i, e_j>_H,$$

$$(5.4) \qquad D_{on,ij} = <D_o e_i, e_j>_H,$$

$$(5.5) \qquad A_{on,ij} = <A_o e_i, e_j>_H.$$

In general, (5.3) and (5.4) are valid only if the basis vectors are in $D(A_o)$. Otherwise, we use

$$(5.5') \qquad A_{on,ij} = <e_i, e_j>_V - <B_o^* e_i, B_o^* e_j>_H$$

(recall (2.4) and (2.5)) and a similar expression for D_{on} (in our model, D_o is essentially a scalar times A_o.) Also,

$$(5.6) \qquad B_{on,ij} = <e_i, B_{oj}>, \quad i = 1, \ldots, n \quad j = 1, \ldots, m.$$

The convergence of such approximations and the corresponding finite dimensional optimal control problems is discussed in [3] for $e_1 \epsilon D(A_0)$, which includes the cases where the basis vectors are either natural modes of the structure or component modes. Here, we only outline the formulation of the sequence of n-order LQG problems. The most efficient way to do this is to note that, with (5.1), (5.2) is equivalent to the following differential equation on H_{Mn} = span $(e_1, \ldots, e_n)$:

$$(5.7) \qquad M_{on} \ddot{x}_n + D_{on} \dot{x}_n + A_{on} x_n = B_{on} u \; ,$$

where M_{on}, D_{on}, A_{on} and B_{on} are the operators on H_{Mn} determined by the matrices in (5.3) - (5.5) and the identification (5.1). Of course, we can write (5.7) as

$$(5.8) \qquad \dot{z}_n = A_n z_x + B_n u$$

with $z_n = \binom{x_n}{\dot{x}_n}$.

For (5.7) and (5.8), the optimal regulator problem leads to the finite dimensional Riccati equation

$$(5.9) \qquad A_n^* \Pi_n + \Pi_n A_n - \Pi_n B_n R^{-1} B_n^* \Pi_n + Q_n = 0,$$

where the operator Q_n is defined as follows. Let $E_n = V_n \times H_{Mn}$ and denote by P_n the projection of E onto E_n. Then

$$Q_n = P_n Q_n P_n \big|_{E_n}.$$

With this Q_n and our preceding hypotheses about damping and the completeness of the e_1's in V, the Π_n of (5.9) is guaranteed to converge strongly to the solution Π of the infinite dimensional Riccati equation (3.4).

The functional control gains in (4.3) are approximated by

$$(5.10) \qquad \binom{f_n}{g_n} = \Pi_n B_n R^{-1}.$$

The strong convergence of Π_n and B_n implies that f_n converges in V to f and g_n converges in H to g.

The functional control gains f_n and g_n are associated with the nth order control law

$$(5.11) \quad u = - K_n z_n = - <f_n, z_n>_V - <g_n, \dot{z}_n>_M,$$

with

$$(5.12) \quad K_n = R^{-1} B_n^* \Pi_n.$$

To approximate the infinite dimensional compensator, we construct a finite dimensional state estimation

$$(5.13) \quad \dot{\hat{z}}_n = A_n \hat{z}_n + B_n u + G_n(y - C_n \hat{z}_n),$$

where

$$(5.14) \quad G_n = \hat{\Pi}_n C_n^* \hat{R}^{-1}$$

and $\hat{\Pi}_n$ satisfies the Riccati equation

$$(5.15) \quad A_n \hat{\Pi}_n + \hat{\Pi}_n A_n^* - \hat{\Pi}_n C_n^* R^{-1} C_n \hat{\Pi}_n + \hat{Q}_n = 0.$$

The operator $\hat{Q}_n$ is given by

$$(5.16) \quad \hat{Q}_n = P_n \hat{Q} P_n$$

for $\hat{Q}$ the covariance of the process noise ν_1 in (2.7). As before, R is the covariance of the measurement noise ν_0.

We now have the components of the nth approximation to the infinite dimensional compensator. The nth finite dimensional compensator consists of (5.13) and the control law

$$(5.17) \quad u = - K \hat{z}_n.$$

This compensator has the rational transfer function

(5.18) $K_n[sI - A_{cn}]^{-1} G_n$

where

(5.19) $A_{cn} = A_n - B_n K_n - G_n C_n$.

For each $s \epsilon \rho(A_c)$, this transfer function approaches the value of the transfer function in (3.11) as n increases.

6. Application to Space Antenna

We have applied the compensator design procedure of the preceding sections to the control of a large space antenna model, which is based on the Lockheed wrap-rib antenna. Our model is shown in Figure 1. Since this is our first application to a truly complex structure, we have simplified the model by taking the antenna to be flat and using eight instead of the actual 48 ribs. Otherwise, the parameters of the model are based on the physical parameters of the 48 rib antenna as nearly as possible.

As shown in Figure 1, our antenna consists of a rigid hub, eight ribs and a mesh reflecting surface. The ribs are modeled as cantilevered beams, and the mesh is modeled as a membrane. The center of the hub is fixed, but the hub can rotate out of plane. Hence, there are two out-of-plane rigid body modes. For more discussion of this model, see [4].

The actuators apply torques to the hub, and the sensors measure the rigid-body rotation of the hub and the displacement of the tip of each rib. We have designed a compensator to control the linear out-of-plane motion of the antenna.

The symmetry of the antenna reduces the complexity of the design process because, for small displacements, the motion of the antenna can be separated into two sets of orthogonal modes controlled independently by one actuator. Each set of modes consists of those modes that are either symmetric or asymmetric about one of the torque axes. Modes symmetric or asymmetric about both axes are uncontrollable. Although the compensator can control only the controllable modes, these are the only modes that are excited by rotating the antenna.

Viscoelastic damping is modeled in both ribs and mesh. If the stiffness operator A_0 is separated into rib and mesh components as

$$(6.1) \qquad A_0 = A_0^r + A_0^m \, ,$$

then the damping operator is

$$(6.2) \qquad \mathcal{D}_0 = .001 \; A_0^r + .003 \; A_0^m \, .$$

This structural damping couples the natural modes - but not controllable and uncontrollable modes.

For the performance index (3.1), we take $Q = I$ and $R = .1I$. For the disturbance $\hat{v}_1$ and measurement noise, we take

$$\hat{Q} = \begin{bmatrix} 0 & 0 \\ 0 & I \end{bmatrix} \quad \text{and} \quad \hat{R} = .01I.$$

The generalized displacement vector x for this system has components representing each of the two out-of-plane rigid body angles, the out-of-plane elastic deformation of each rib and of each mesh. The basic space H is then

$$(6.3) \qquad H = R^2 \times \underbrace{L_2(0,\ell) \times L_2(\Omega)}_{\substack{\text{for each rib and} \\ \text{mesh}}} \times \ldots \times L_2(0,\ell) \times L_2(\Omega),$$

where ℓ is the length of the ribs and Ω is area of each mesh sector. The strain-energy space V is like H with $L_2(0,\ell) \times L_2(\Omega)$ replaced by $H^2(0,\ell) \times H^1(\Omega)$.

The functional gains have the form

$$(6.4) \qquad f = (\alpha_1, \alpha_2, \underbrace{\phi_f^r, \phi_f^m, \ldots, \phi_f^r, \phi_f^m}_{\substack{\text{functions for} \\ \text{each rib and} \\ \text{mesh}}})$$

Figures 2-5 show our approximations to the functions ϕ_f^r, ϕ_g^r, ϕ_f^m and ϕ_g^m for the control gains. Because of symmetry, these functions are the same for each sector. The functions ϕ_f^m and ϕ_g^m are plotted along the center line of a mesh sector.

We used a finite element approximation of the structure to determine the natural modes of the individual components and of the entire antenna. After some numerical work, we decided that it was most convenient and efficient to use the antenna modes for the basis vectors in the compensator approximation described in Section 5. The converged functional gains in Figures 2-5 are for 21 controllable modes. With this number of modes, we also achieved convergence of the estimator functional gains.

212

References

1. A. V. Balakrishnan, <u>Applied Functional Analysis</u>, Springer-Verlag, 1981.

2. R. F. Curtain and A. J. Pritchard, <u>Infinite Dimensional Linear Systems Theory</u>, Springer-Verlag, 1978.

3. J. S. Gibson, "An Analysis of Optimal Modal Regulation: Convergence and Stability," <u>SIAM J. Contro. Opt.</u>, Vol. 19, No. 5, September, 1981.

4. H. R. Textron Report #956541-2, December 1983.

5. T. Kato, <u>Perturbation Theory for Linear Operators</u>, Springer-Verlag, 1976.

6. D. L. Mingori, J. S. Gibson, P. Blelloch, and A. Adamian, "Control of a Flexible Space Antenna: A Finite Dimensional Perspective Based on Distributed Parameter Theory," presented at the "Workshop on Identification and Control of Flexible Structures", San Diego, CA, June 4-6, 1984.

SENSORS

TORQUERS
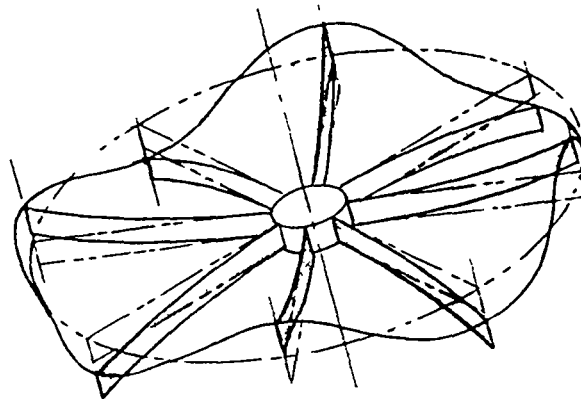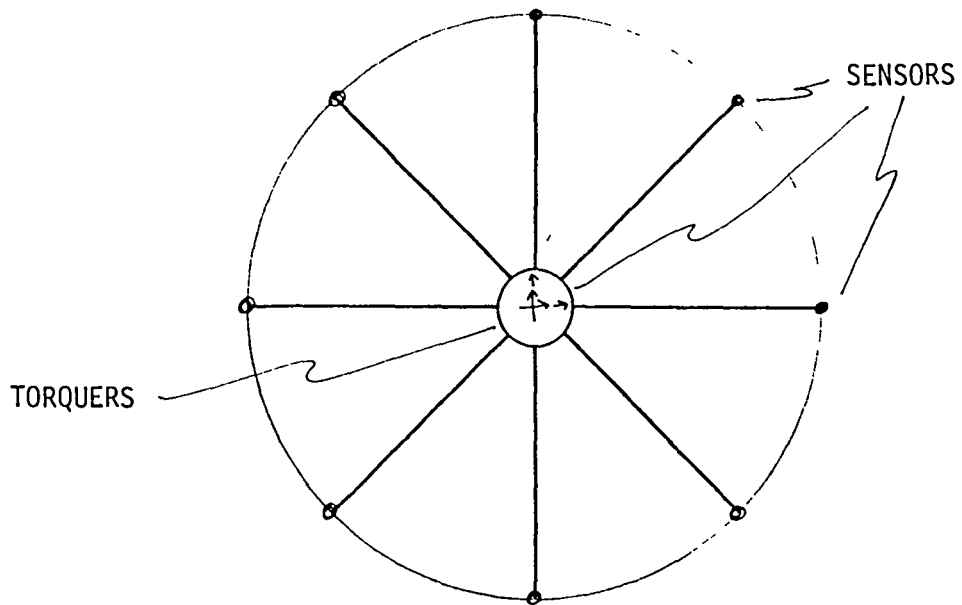
MODEL DATA (based on 48 rib Lockheed wrap rib antenna):

Hub Radius: 46 in.   Hub Weight: 1000 lbs.

Hub Inertias: $I_{xx} = I_{yy} = 342$ lb-in-sec^2
              $I_{zz} = 684$ lb-in-sec^2

Rib Length: 86 ft.   Rib Weight: 115 lb. per rib

Rib stiffness: EI = 4.05×10^7 lb-in^2

Mesh Weight: 6.94 lb per sector

Figure 1

214
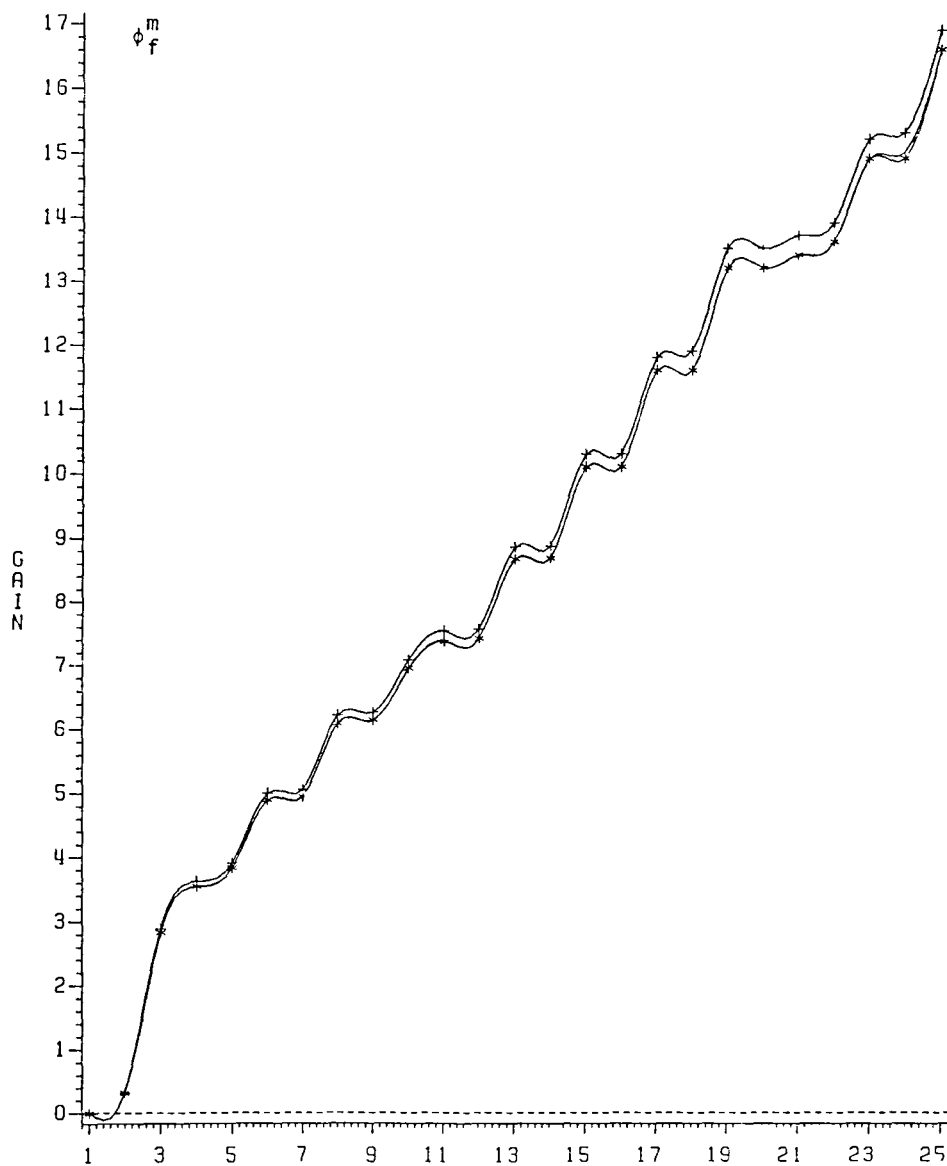
GAIN OF THE BEAM

Figure 2

GAIN OF THE BEAM

Figure 3

GAIN OF THE MESH

Figure 4

GAIN OF THE MESH

Figure 5

CONTROL OF A FLEXIBLE SPACE ANTENNA:
A FINITE DIMENSIONAL PERSPECTIVE BASED ON
DISTRIBUTED PARAMETER THEORY

D. L. Mingori, J. S. Gibson, P. Blelloch, and **A. Adamian**
University of California
Los Angeles, CA 90024

ABSTRACT

LQG based compensators are developed using a design approach
which blends finite dimensional and infinite dimensional control
theory. A feature of the approach is that model reduction, control
law design and estimator design are accomplished in an integrated
manner producing a reduced order model that is appropriate for the
particular control problem. The method is used to develop a
compensator for a flexible space antenna. The antenna compensator
is further simplified using balanced realizations.

I. INTRODUCTION

In Ref. [1] the notion of functional gains has been developed
in an infinite dimensional context and applied to a flexible space
antenna. In this paper, similar ideas are developed, but in a
finite dimensional context. Although some of the rigor of the
mathematical development is lost, a description of the approach in
finite dimensional terms may make it more accessible to engineers
who are not familiar with functional analysis. A finite dimensional
formulation also recognizes that control system designers are
frequently provided with a plant model which is based on a finite
element analysis and is, therefore, finite dimensional. The ap-
proach presented here preserves the feature of Ref. [1], that
the reduced order design model, the control law and the estimator
are produced simultaneously as the steps of the procedure are
worked out. The design model is thus an appropriate one for the
control problem that has been posed.

II. PLANT DESCRIPTION AND CONTROL OBJECTIVES

The approach assumes that a large order description of the
plant is available in state variable form:

(1) $\qquad \dot{x} = Ax + Bu + w \quad ; \quad E[ww^T] = \hat{Q}$

The measurement equation is in the form:

(2) $\qquad z = Mx + v \quad ; \quad E[vv^T] = \hat{R}$

and the output equation is given as:

(3) $\qquad y = Cx$

(The output is in general distinct from the measurements and represents those variables we wish to control. In special cases, the output can be the same as the measurements.)

The matrices in Eqs. (1-3) have the following dimensions:

$x, w = (nx1) \quad ; \quad A, \hat{Q} = (nxn) \quad ; \quad z, v = (qx1)$

$B = (nxp) \quad ; \quad u = (px1) \quad ; \quad M = (qxn) \quad ;$

$\hat{R} = (qxq) \quad ; \quad y = (rx1) \quad , \quad c = (rxn)$

A quadratic performance index for the control problem is introduced as

(4) $\quad J = \int_0^\infty [y^T y + u^T Ru]dt = \int_0^\infty [x^T c^T Cx + u^T Ru]dt$

where R is positive definite, the pair (A,B) is controllable, and the pair (A,C) is observable.

III. GAINS FOR THE CONTROL PROBLEM

Introduce a set of linearly independent basis vectors e_i for approximating the state vector x.

(5) $\quad e_i = \begin{bmatrix} e_{i1} \\ e_{i2} \\ \vdots \\ e_{in} \end{bmatrix} \qquad i = 1,2,\ldots,r1 < n$

(6) $\quad e^T = \begin{bmatrix} e_1 & \vdots & e_2 & \vdots \cdots \vdots & e_{r1} \end{bmatrix} \quad ; \quad e^T = (n \times r1)$

Then x may be approximated as

(7) $\quad x \doteq x_{r1} = e^T a$

The (r1x1) vector a is a vector of state variables which will become the reduced state vector. Substitute (7) into (1), (4) to obtain (after some manipulation)

(8) $\quad \dot{a} = A_{r1} a + B_{r1} u$

(9) $\quad J = \int_0^\infty [a^T Q_{r1} a + u^T Ru] dt$

where

(10) $\quad A_{r1} \triangleq [ee^T]^{-1} e A e^T \quad ; \quad B_{r1} \triangleq [ee^T]^{-1} eB$

(11) $\quad Q_{r1} \triangleq e C^T C e^T$

(w has been omitted in Eq. (8) since it is not needed for the regulator problem.) Eqs. (8) and (9) represent a reduced order state equation and performance index, respectively. Using standard methods, a feedback gain matrix K_{r1} can be obtained for this reduced order problem. The reduced feedback law becomes

(12) $\quad u = - K_{r1} a$

Using Eq. (7) we can express a as a function of x.

(13) $\quad a = [ee^T]^{-1} ex$

Substitute (13) into (12) to obtain

(14) $\quad u = - K_n(r1)x$

221

where

$$(15) \quad K_n(rl) \triangleq K_{rl}[ee^T]^{-1}e$$

$K_n(rl)$ represents an approximation of the pxn feedback gain matrix based on a reduced problem of order rl. The exact feedback gain matrix for the full order problem of Eqs. (1) and (4) would be $K_n(n)$.

Often it is unnecessary to solve the full order problem to obtain $K_n(n)$. Instead one can solve a sequence of lower order problems proceeding as follows:

1) Select a number of linearly independent vectors as in Eq. (6)

2) Formulate and solve a reduced order problem as defined by Eqs. (8-12)

3) Calculate $K_n(rl)$ according to Eq. (15)

4) Enlarge the number of basis vectors included in e^T and repeat steps 2) and 3)

5) When $K_n(rl)$ ceases to change as additional basis vectors are added to e^T, terminate the procedure.

The "convergence" of $K_n(rl)$ as rl is increased may be measured in terms of any appropriate matrix norm. When the norm of the difference between successive approximations of $K_n(rl)$ becomes small, it is an indication that $K_n(rl)$ is a good approximation of $K_n(n)$. It is further an indication that the reduced order model for the current rl (Eqs. 8-11) is a suitable model for the control problem that has been posed. In fact, if rl is approaching n and $K_n(rl)$ is still changing as new basis vectors are added, one may conclude that the full order model is inadequate for the control problem at hand. In this case, either a larger model must be obtained, the level of performance must be reduced, or the physical system must be changed, e.g., by introducing additional passive damping, moving actuators, stiffening members, etc.

IV.   GAINS FOR THE ESTIMATION PROBLEM

As in the control problem, a set of linearly independent basis functions is used to approximate the n dimensional state vector x.

To emphasize that these basis vectors need not be the same as those used in the control problem, they will be denoted by f_i, $i = 1$, 2, $\cdots$, $r2 < n$. In general $r2$ will be different from $r1$. Thus,

$$(16) \quad f_i = \begin{bmatrix} f_{i1} \\ f_{i2} \\ \vdots \\ f_{in} \end{bmatrix} \qquad i = 1, \cdots, r2 < n \quad ; \quad r2 \geq r1$$

$$(17) \quad f^T = [f_1 \vdots f_2 \vdots \cdots \vdots f_{r2}] \quad ; \quad f^T = (n \times r2)$$

Then the approximation of x based on f^T is

$$(18) \quad x \doteq x_{r2} = f^T b$$

Substituting (18) into (1) and (2) yields (after some manipulation) a reduced order state equation and measurement equation in terms of b.

$$(19) \quad \dot{b} = A_{r2} b + B_{r2} u + w_{r2}$$

$$(20) \quad z = M_{r2} b + v$$

where

$$(21) \quad A_{r2} \triangleq [ff^T]^{-1} f A f^T \quad ; \quad B_{r2} \triangleq [ff^T]^{-1} f B$$

$$(22) \quad M_{r2} \triangleq M f^T \quad ; \quad w_{r2} \triangleq [ff^T]^{-1} f w$$

Also,

$$(23) \quad E[w_{r2} w_{r2}^T] = [ff^T]^{-1} f \hat{Q} f^T [ff^T]^{-1} = \hat{Q}_{r2}$$

$$(24) \quad E[vv^T] = \hat{R}$$

An optimal estimator based on (19) - (24) will have the form

$$(25) \quad \dot{\hat{b}} = A_{r2} \hat{b} + B_{r2} u + G_{r2}(z - M_{r2} \hat{b})$$

where G_{r2} is determined as the solution of

$$G_{r2} = P_{r2}M_{r2}^T \hat{R}^{-1}$$

(26)

$$A_{r2}P_{r2} + P_{r2}A_{r2}^T - P_{r2} M_{r2}^T \hat{R}^{-1}M_{r2}P_{r2} + \hat{Q}_{r2} = 0$$

An equation for estimating X_{r2} can be developed from Eqs. (18) and (25):

(27)
$$\dot{\hat{x}}_{r2} = f^T A_{r2}[ff^T]^{-1}f \hat{x}_{r2} + f^T B_{r2}u$$
$$+ f^T G_{r2}[z-M_{r2}[ff^T]^{-1}f \hat{x}_{r2}]$$

Eq. (27) may be compared with the full order estimator which has form:

(28) $\dot{\hat{x}} = A \hat{x} + Bu + G_n[z-M\hat{x}]$

A key thing to note in this comparison is the form of the estimator gain. As more basis vectors are added to f^T (i.e., r2 is increased), we will expect to see $f^T G_{r2}$ approach G_n. Thus $f^T G_{r2}$ represents an approximation of G_n which can be used as a guide for determining when the r2 basis vectors in f^T are adequate for constructing a reduced order estimator. The procedure is analogous to that used in the control problem, and may be summarized as follows:

1) Select a number of linearly independent vectors as in Eq. (17)

2) Formulate and solve a reduced order problem as defined by Eqs. (19) - (26).

3) Calculate $G_n(r2)$ using

(29) $G_n(r2) = f^T G_{r2}$

4) Enlarge the number of basis vectors included in f^T and repeat steps 2) and 3).

5) When $G_n(r2)$ ceases to change as additional vectors are added to f^T, terminate the procedure.

Using any appropriate matrix norm, one may examine the norm of the difference between successive approximations of G_n. When

this norm becomes small, it is an indication that $G_n(r2)$ is a good approximation of G_n and that the reduced order model used to generate $G_n(r2)$ is an appropriate one for constructing a reduced order estimator. The observation made at the end of Section III also applies here if $G_n(r2)$ continues to change as r2 approaches n. Note that if the estimator design procedure reveals that some of the basis vectors in e^T which were important for the control problem are not needed in f^T, the corresponding states will not be estimated and the control law cannot be implemented. In this case, sensors should be moved or added until good estimates can be obtained for all of the states which must be fed back.

V. CONSTRUCTION OF THE COMPENSATOR

After completing the procedures described in Sections III and IV, one should emerge with sets of basis functions suitable for the control and estimation problems, and good approximations of the full order control and estimation gains. To be conservative, control and estimation gains can be recomputed, using the union of the basis functions from the control and estimation problems. The compensator then consists of the following equations:

$$(30) \quad u = -K_n(r1)\hat{x}_{r2}$$

$$(31) \quad \hat{x}_{r2} = f^T \hat{b}$$

$$(32) \quad \dot{\hat{b}} = A_{r2} \hat{b} + B_{r2} u + G_{r2}(z - M_{r2}\hat{b})$$

In transfer matrix form, these equations become:

$$(33) \quad u = - K_n(r1)f^T[sI - A_c]^{-1} G_{r2} z$$

where

$$(34) \quad A_c \triangleq A_{r2} - B_{r2} K_n(r1)f^T - G_{r2} M_{r2}$$

Because of the "convergence" issues that were addressed in constructing the compensator described by Eqs. (33) and (34), this compensator should be an excellent approximation of the full order compensator even though it is based on reduced order calculations.

VI. SIMPLIFICATION OF THE COMPENSATOR: AN EXAMPLE

Although developed here entirely in finite dimensional terms, the procedure described above is identical to that used in Ref. 1, where an infinite dimensional perspective is employed. Thus the spacecraft example worked out in that reference serves equally well to illustrate the procedure developed here. It is assumed that the reader has access to Ref. 1. The gain matrices $K_n(r1)$ and $G_n(r2)$ of the present paper are analogous to the functional gains of Ref. 1.

The spacecraft example of Ref. 1 involves 3 sensors and one actuator. Thus the transfer matrix of the compensator correspond-ing to Eq. (33) is a 1x3 matrix in which each element is a transfer function. The frequency response of the (1,1) element of this matrix is displayed in Fig. 1. This transfer function is based on a model of 42nd order and thus it has 42 poles and 41 zeros. Although the procedure used to generate the compensator produces a suitable reduced order model for the control and estimation problem at hand, there is no guarantee that it is the lowest order model that would work. It is frequently possible to simplify the compensator further without significant loss of performance.

To illustrate this assertion, the order of the compensator of Fig. 1 has been reduced using the technique of balanced state space representations (Ref. 2,3). These methods were applied directly to the compensator and not to the physical model (though application to the physical model may be useful when selecting the basis functions for e^T and f^T). In essence, the method involves transformation to a ("balanced") representation where the states can be ordered in terms of the importance of their contributions to the transfer matrix. Then the least important states may be truncated until significant features of the transfer matrix begin to be lost.

Figures 2 through 4 show the frequency response of the (1,1) element of the transfer matrix as its order is reduced from 42 to 34 to 20 and finally to 16. It seems clear that a reduction from 42nd order to 34th order can be accomplished without any loss of performance. Some features begin to disappear upon further reduction, but the basic character of the frequency response is preserved. Further work is necessary to ascertain how important the loss of various features would be.

VII. CONCLUSIONS

The methods presented in this paper are based on results from infinite dimensional control theory, but they can be described and used in a finite dimensional context. This blend leads to an approach which employs powerful ideas on convergence, and is

also quite practical for systems of realistic complexity.

Appropriate reduced order models are generated simultaneously with the developemt of the compensator. The required models change as a function of changes in the performance demanded, sensor and actuator location, inherent damping, disturbances, etc. Thus they are driven by the control and estimation problems at hand.

The compensator which emerge are very close to the "ideal" compensators which would be obtained with a very large order model. However, some simplification is frequently possible. The method of balanced realizations has been found effective for this purpose.

REFERENCES

[1] Gibson, J. S., Mingori, D. L., Adamian, A. and Jabbari, F., "Approximation of Optimal Infinite Dimensional Compensators for Flexible Structures," presented at the "Workshop on Identification and Control of Flexible Structures", San Diego, CA, June 4-6, 1984.

[2] Moore, B. C., "Principal Component Analysis in Linear Systems: Controllability, Observability and Model Reduction," IEEE Trans. on Auto Control, Vol. AC-26, No. 1, Feb. 1981, pp. 17-32

[3] Pernebo, L., and Silverman, L. M., "Model Reduction via Balanced State Space Representations," IEEE Trans. on Auto Control, Vol. AC-27, No. 2, Apr. 1982.

BODE DIAGRAM
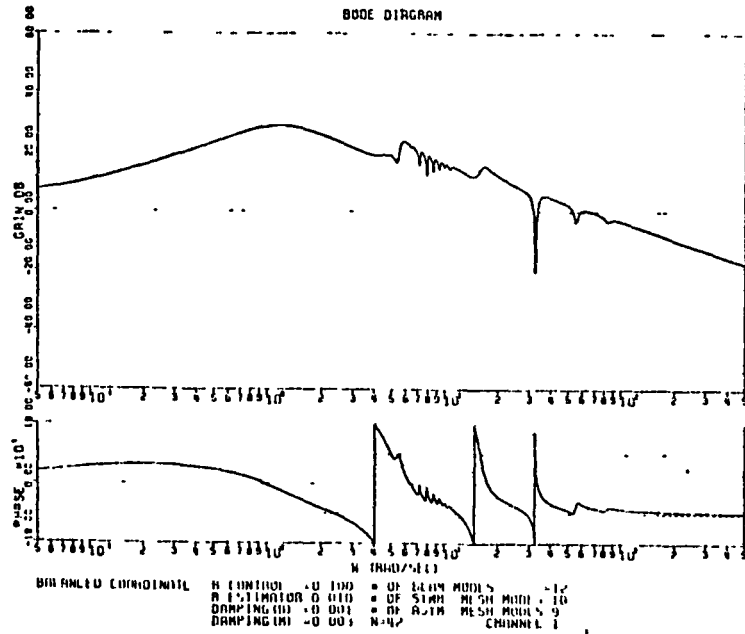
Fig. 1 Frequency Response of a 42nd order
Compensator for a Space Antenna.

BODE DIAGRAM
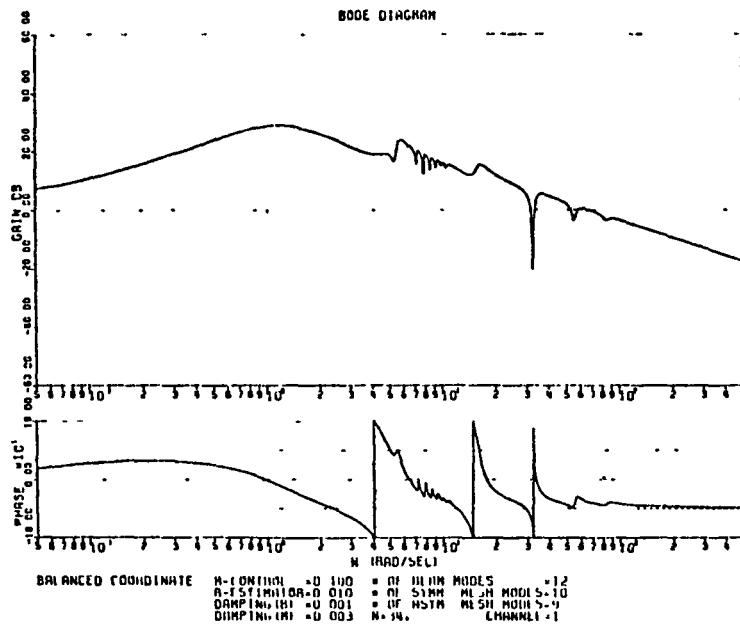
Fig. 2 Frequency Response of a 34th order
Approximation of the Compensator of Fig. 1.

BODE DIAGRAM

BALANCED COORDINATE
K CONTROL =0 100	# OF BEAM MODES	12
R ESTIMATOR=0 010	# OF STMM MESH MODE = 10
DAMPING(B) =0 001	# OF ASTM MESH MODES=9
DAMPING(M) =0 003	N=22	CHANNEL=1
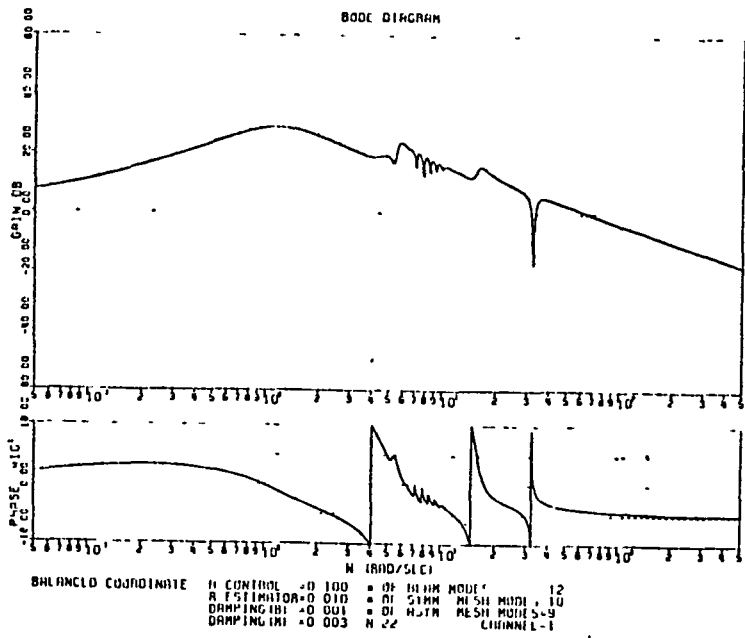
Fig. 3 Frequency Response of a 22nd order
Approximation of the Compensator of Fig. 1.

BODE DIAGRAM

BALANCED COORDINATE
R-CONTROL =0.100	# OF BEAM MODES	=12
R-ESTIMATOR=0 010	# OF STMM MESH MODES=10
DAMPING(B) =0 001	# OF ASTM MESH MODES=9
DAMPING(M) =0 003	N=16	CHANNEL=1
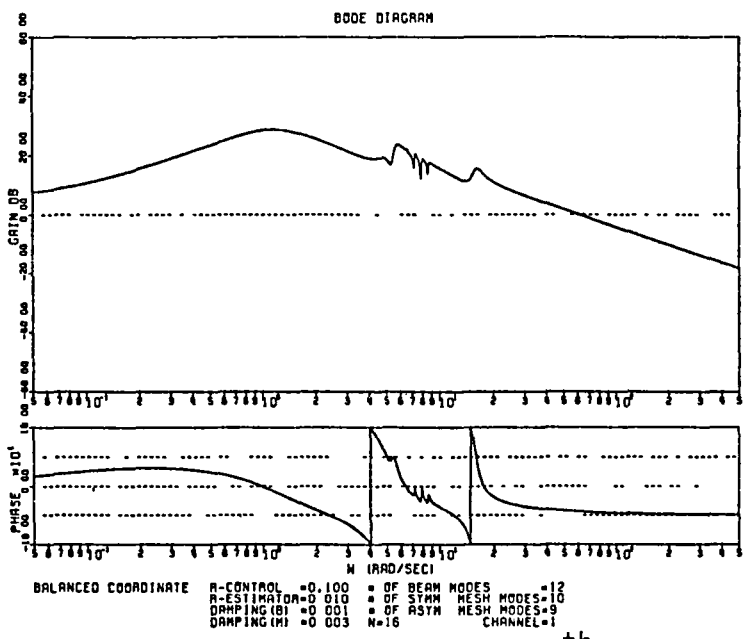
Fig. 4 Frequency Response of a 16th order
Approximation of the Compensator of Fig. 1

229

AN INTEGRATED CONTROL AND MINIMUM MASS STRUCTURAL OPTIMIZATION ALGORITHM FOR LARGE SPACE STRUCTURES

A. Messac*
The Charles Stark Draper Laboratory
Cambridge, MA 02139

J. Turner and K. Soosaar
Cambridge Research
Belmont, MA 02178

Abstract

This paper proposes a new approach for solving dual structural-control optimization problems for high-order flexible space structures, where reduced-order structural models are employed and minimum mass designs are sought. For a given initial structural design, a quadratic control cost is minimized subject to a constant-mass constraint. The sensitivity of the optimal control cost with respect to the structural design variables is then determined and used to obtain successive structural redesigns, using a constrained gradient optimization algorithm. This process is repeated until the constrained control cost sensitivity becomes negligible. The minimum mass design is obtained by solving a sequence of neighboring optimal constant mass designs, where the sequence of optimal performance indices has a minimum at the optimal minimum mass design. A numerical example is presented which demonstrates that this new approach effectively addresses the problem of dual optimization for potentially very high-order structures.

---

*Doctoral Candidate in the Department of Aeronautical and Astronautical Engineering, M.I.T., Draper Fellow

I. Introduction

One important variable, which determines the cost of transporting a payload to orbit, is its total mass. Consequently, at the structural design stage, a strong effort is made to optimize the structure for the mission at hand. Minimum mass and maximum structural eigenvalues constitute the two most frequently used structural optimization criteria (Refs. 1-7). The resulting structure is generally highly flexible and often requires active control (Refs. 8-12). As a result, subsequent to the structural design, the control engineer attempts to determine the optimal control strategy necessary to accomplish the mission.

Traditionally, the problem of optimal structural design and that of optimal control design are solved with little or no interaction. As a result, the "global design" is not optimal. In an effort to overcome this situation, we present in this paper a new method for simultaneously optimizing the structural and control design. There are two key features of the proposed method. First, a reduced-order model for the equations of motion is used which dramatically lowers the computational cost. Second, a minimum mass design is obtained by solving a sequence of neighboring optimal constant mass designs, and selecting the design which yields the minimum performance index as a function of total system mass. A numerical solution for the problem of optimal spacecraft slewing maneuvers of a structurally-optimal minimum mass design for a spacecraft is presented.

232

This dual optimization problem has previously been considered by Hale (Refs. 13, 14) for problems involving simple structures and by Messac and Turner (Refs. 14, 15) for problems of high structural dimension.

In the interests of computational efficiency, the problem is formulated in modal- rather than physical-space. As a result, the order of the TPBVP is dictated, no longer by the complexity of the structure (i.e., order of the mass and stiffness matrices), but rather by the number of structural modes which participate in the dynamic excitation of the spacecraft. The total number of such modes rarely exceeds a dozen in most practical applications.

Specifically, we seek the optimal structural design that enables the slewing maneuver and vibration suppression of the spacecraft to be performed optimally, while first keeping the total mass constant and secondly allowing the total mass to vary in an effort to obtain a minimum mass design.

II.   Generic Problem Statement
A.   Performance Index Definition

We seek the structural design that minimizes the following performance index

$$J = \frac{1}{2} x_f^T S(d)x_f + \frac{1}{2} \int_o^{t_f} \left[x^T Q(d)x + u^T Ru \right] dt \tag{1}$$

subject to the following linear time-invariant plant dynamics equation

$$\dot{x}(t) = A(d)x(t) + B(d)u(t) \tag{2}$$

233

where the total mass m_T and initial state x_0 are given. In the above equation d is the design variable vector, t_f and x_f are the final time and final state respectively, $x(t)$ the state vector, $u(t)$ the control force vector, S and Q are real positive semi-definite matrices, R is a real positive definite matrix, and S, Q, and R are defined in Appendix B.

Equation (2) is obtained by first deriving second-order ordinary differential equations of motion of the form

$$M(d)\ddot{w}(t) + K(d)w(t) = E(d)u(t) \tag{3}$$

where $M(d)$ and $K(d)$ represent the $(N \times N)$ symmetric mass and stiffness matrices, $w(t)$ is a generalized coordinate vector for the elastic and rigid-body motions, $E(d)$ is an $(N \times N_c)$ control influence matrix which determines the point of application of the generalized control forces. Equation (3) is transformed to modal coordinates by carrying out an eigenvalue analysis and normalizing the modes ϕ such that $\phi^T M \phi = I$ and $\phi^T K \phi = \Lambda$. By retaining only those modes - numbering $N_m < N$ - which significantly participate in the dynamic response of the structure, a reduced-order state space model of the form of Eq. (2) is obtained by defining

$$A(d) = \begin{bmatrix} 0 & \Lambda(d) \\ I & 0 \end{bmatrix} \tag{4}$$

$$B(d) = \begin{bmatrix} \phi^T E(d) \\ 0 \end{bmatrix} \tag{5}$$

$$x^T = \{ \dot{\eta}^T , \eta^T \} \tag{6}$$

where A and B are of order $(2N_m \times 2N_m)$ and $(2N_m \times N_c)$ respectively, η is a vector of modal coordinates, and I is an identity matrix.

B. Dependence of x_o on the Design Variable

As shown in Ref. (16) the initial condition vector x_o is an explicit function of the design vector d, as follows:

$$x_o = \Pi(d) \left\{ \begin{array}{c} \dot{w}_o \\ w_o \end{array} \right\} \tag{8}$$

where

$$\Pi(d) = \text{Block Diag.} \left[\phi^T(d)M(d), \ \phi^T(d)M(d) \right] \tag{9}$$

The initial condition dependence on the design vector d is important for both the constant and minimum mass design optimization processes.

Furthermore, as shown in Ref. (16) the partial derivative of x_o with respect to the design vector d is given by

$$\frac{\partial x_o}{\partial d} = \frac{\partial \Pi(d)}{\partial d} \, \Xi x_o \tag{10}$$

where

$$\Xi(d) = \text{Block Diag.} \left[\phi, \ \phi \right] \tag{11}$$

235

III. Optimization Problem Solution

A. Optimal Control Design

As shown in Refs. (9, 15, 16) the optimal control solution for Eqs. (1) and (2) is given by

$$X(t) = e^{Dt}X(o) \quad ; \quad X = \left[x^T \lambda^T\right]^T \tag{12}$$

$$u(t) = -R^{-1}B^T\lambda(t) \quad ; \quad \lambda \text{ is the costate vector} \tag{13}$$

where

$$D(d) = \begin{bmatrix} A(d) & -B(d)R^{-1}B^T(d) \\ -Q(d) & -A^T(d) \end{bmatrix} \tag{14}$$

$$e^{Dt} = \begin{bmatrix} \Psi_{11}(t) & \Psi_{12}(t) \\ \Psi_{21}(t) & \Psi_{22}(t) \end{bmatrix} \tag{15}$$

As shown in Ref. (16) the solution for the initial costate $\lambda(o)$ is given by

$$\lambda(0) = Hx_o \tag{16}$$

where

$$H = -H_A^{-1}H_B \tag{17}$$

236

and

$$H_A = -S\Psi_{21}(t_f) + \Psi_{22}(t_f) \qquad (18)$$

$$H_B = -S\Psi_{11}(t_f) + \Psi_{12}(t_f) \qquad (19)$$

Moreover, from Ref. 11, it follows that the control cost of Eq. (1) can be written as

$$J(d) = \frac{1}{2} x_o^T(d)H(d)x_o(d) \qquad (20)$$

The solution for J(d) above corresponds to solving a time-varying Riccati equation, as a result the gains for the control are time-varying. For many problems, however, we are interested in constant feedback gains for the control. For optimization problems where constant gains are required, Eq. (20) becomes

$$J(d) = \frac{1}{2} x_o^T(d) \ P_{ss}(d) \ x_o(d) \qquad (21)$$

where P_{ss} is the solution to the algebraic Riccati equation

$$0 = A^T P_{ss} + P_{ss} A - P_{ss} BR^{-1}B^T P_{ss} + Q \qquad (22)$$

The key feature of Eqs. (20) and (21) is that time has disappeared from the problem formulation. As a result, the optimization problem becomes an algebraic minimization problem for the design vector d.

B.   **Iterative Structural Redesigns—Constant Mass Case**

So far, we have determined the optimal control cost associated with a given set of design variables d, as defined by Eq. (20). We now present the numerical scheme which is used to minimize the control cost by iteratively refining d.

To this end, we first express the constant mass requirement as $p^T d = m_T$, where d is the design variable vector, m_T the given total mass, and p a vector of structural parameters. More specifically, in terms of changes in the design variables Δd, the constant mass constraint follows as

$$p^T \Delta d = 0 \tag{23}$$

In order to establish a constrained optimization algorithm which takes into account Eq. ( ), we first determine the normalized gradient vector $\alpha = -\dfrac{\partial J}{\partial d} \Big/ \left\lVert \dfrac{\partial J}{\partial d} \right\rVert$ (Appendix A) where $\lVert * \rVert$ denotes the Euclidian norm (see Figure 1). We subsequently make use of the Orthogonal-Projection-Theorem (Ref. 17) which states that the projection of the vector α onto the surface of constant mass represents the direction of greatest decrease in J which also satisfies Eq. (23). As a result, the desired change in the design variable vector, to within a multipicative constant c, becomes

$$\Delta d = c \left\{ \alpha - \frac{\alpha^T p}{p^T p} p \right\} \tag{24}$$

The performance index partial derivatives for Eq. (20) are listed in Appendix A. The corresponding performance index partial derivatives for the constant gain case of Eq. (21) are listed in Appendix C.

238

From a geometrical point of view, the above equation clearly states that when $\alpha^T p = \left|\left|\alpha\right|\right| \cdot \left|\left|p\right|\right|$, the gradient vector α is orthogonal to the constant-mass-constraint plane and $\Delta d = 0$; thus no further improvement can be made and a minimum has been reached (see Figure 1). On the other hand, when $\alpha^T p = 0$, the gradient vector lies in the constant mass plane and Eq. (24) requires $\Delta d = c\alpha$; thus great improvement can be made.

In order to monitor progress towards the optimum dual design, the following convergence parameter is defined

$$\beta = \frac{\left|\alpha^T p\right|}{\left|\left|\alpha\right|\right| \cdot \left|\left|p\right|\right|} \tag{25}$$

which is equal to 0 for the worst possible design, and 1 for the optimal design where $\left|*\right|$ denotes absolute value.

The constant c in Eq. (23) can be chosen in the beginning of the optimization process such that a given small fraction of the total design-mass is displaced. Examination of Eq. (23) reveals the desirable property that the norm of Δd decreases monotonically as the optimal design is being approached. Once c is chosen, the following step sizes are then automatically determined. The dually optimal design is reached when the parameter β satisfies the inequality $\left|1-\beta\right| < \epsilon_1$, where ϵ_1 is user specified.

C.   Iterative Structural Redesigns--Minimum Mass Case

To find the minimum mass design we employ a coarse grid search as a function of total system mass. As depicted in the hypothetical example of the following figure, the sequence of performance indices as a function of the total system mass (i.e., m_i, $i = 0, \ldots, 5$) has a minimum

239

near m_2. As a result, the search procedure requires that the direction yielding

$$\partial J/\partial m \quad < \quad 0$$

must be determined. Once the search direction is known, the next issue is to determine what values for d should be used.
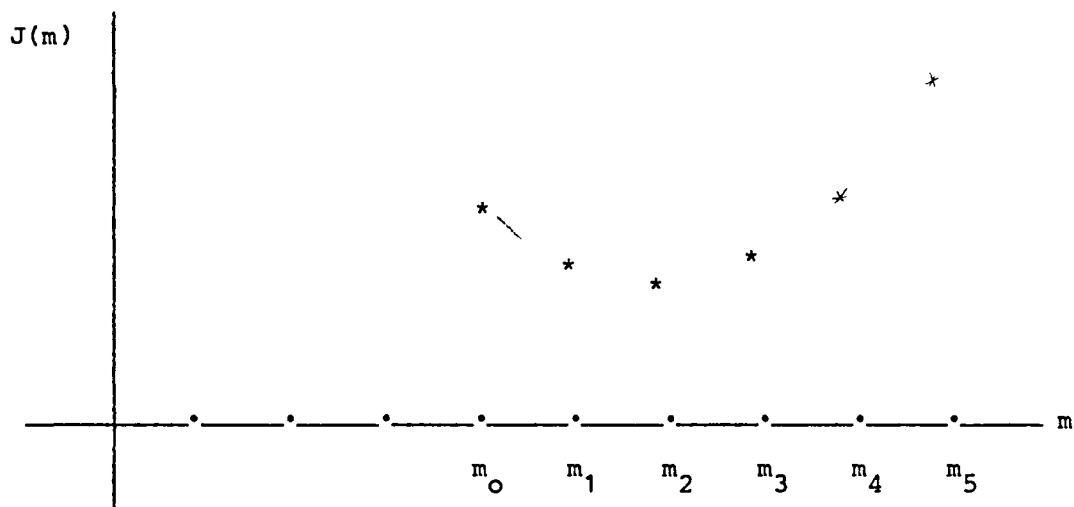
One simple technique readily suggests itself. First, we can make the "optimistic assumption" that all design variables scale according to the following equation:

$$p^T d_{k+1} \quad = \quad m_{K+1} \tag{26}$$

where

$$d_{k+1} \quad = \quad (1 + \alpha_{k+1}) \, dk \qquad\qquad m_{k+1} \quad = \quad m_k + \Delta m_{k+1}$$

which leads to

$$\alpha_{k+1} \quad = \quad \Delta m_{k+1}/m_k \tag{27}$$

240

Second, using this technique we then compute a sequence of performance index costs, as follows:

$$J(d_{k+1}) = \frac{1}{2} x_o^T(d_{k+1}) \; H(d_{k+1}) \; x_o(d_{k+1}) \qquad (k = 0, 1, \ldots) \qquad (28)$$

Once a minimum has been passed, we assume that in the vicinity of the minimum mass design, the performance index can be modeled as a quadratic polynomial in the total mass, as follows:

$$J(d,m) \approx am^2 + bm + c \qquad (29)$$

The a, b, c coefficients above are then recovered by evaluating J(d, m) at three adjacent points where the minimum is contained, leading to a simple linear system which defines the solution.

The optimal minimum mass solution is then found by differentiating the expression for J(d, m) above with respect to m, yielding

$$0 = 2am^* + b \quad ---> \quad m^* = -b/2a \qquad (30)$$

Subject to the m^* found above, an estimate of d is obtained and the constant mass algorithm of Section III.B is used to refine the design vector d.

A local search is then conducted in order to verify that the minimum mass solution has indeed been obtained.

More elaborate algorithms for obtaining extrapolated estimates of d_{k+1} based on back values of d_k, d_{k-1}, ..., naturaly suggest themselves; however, the efficacy of these approaches are not considered in this paper.

241

IV.   Illustrative Example

A.   Structural Model

The example problem analyzed in this paper consists of a linear structure which has the following characteristics (see Figure 2):

- 20 extensional finite elements of equal length

- 21 nodal displacements which coincide with the lumped masses

- uniform mass density $\rho = 100$ kg/m^3

- uniform Young's modulus $E = 800$ N/m^2

- equal initial cross-sectional areas which constitute the design parameters (see Fig. 2)

- length $\ell = 3$m

- a control force applied to the left-most structural node (see Figure 2).

This structure has been selected because it offers two desirable features. First, in order to verify the ability of the proposed approach to optimize higher-order structures through reduced-order modelling, it was deemed necessary to analyze a structure which is composed of more than 15 elements (clearly this objective has been met.) Second, the structure is simple enough so as to allow physical interpretation of the results.

B.   Optimal vs. Non-Optimal Dynamic Response

In the control problem considered here, it is desired to perform a rest-to-rest maneuver where the rigid body modal displacement takes on the initial value of 30.0 and the final value of 0.0 in 2 seconds (Figure 3). As shown in Figure 3, the optimal control performance is greatly improved through successive iterative structural redesigns, where the "optimal" control design of the initial structure is contrasted to that of the final - optimal - structure. There are two salient features of the dynamic

response. First, the peak values of these time-varying quantities are significantly higher in the case of the non-optimal structural design. In particular, the optimal design requires a peak control force 3.4 times lower, and the resulting elastic deflection is 3.07 and 4.96 times lower for the first and second mode, respectively. Second, the optimal dynamic responses are typically smoother in the case of the optimal structural design.

C.   Control Cost Decrease

As previously stated, each step of the redesign process is responsible for a decremental change in the control cost J at each redesign stage. Figure 4 clearly depicts the expected monotonic decrease in J: 83% from the initial to final structural design in 45 iterations. Clearly, this represents a dramatic decrease in the optimal cost. At a value of the convergence parameter β of 0.95, the optimal design was considered reached, in order to prevent the last design variable from vanishing. It is anticipated that further gains in system performance can be achieved by: i) allowing the total mass to be a design variable; ii) allowing the elements of the control weighting matrices S, Q, and R to be design variables (Appendix B); and iii) allowing the sensor and actuator locations to be design variables. However, these extensions are not considered here.

D.   Inclusion of a Tip Mass

In an effort to determine a minimum-mass design, we add a tip mass of 15.0 kg to the right of the previously mentioned structure (Figure 8), with the understanding that it does not constitute a design variable, and is not to be changed during the optimization process. As can be established intuitively, without the tip mass the resulting minimum-mass would be simply zero--a trivial case. We then follow the previously outlined

243

optimization process to determine both the associated constant-mass and minimum-mass designs (Figures 8, 9). The optimal constant-mass design offered a decrease in the control cost of 82%; the subsequent optimal minimum-mass design resulted in an additional 3% decrease in control cost together with a 71% decrease in design mass. Finally, we make the interesting observation that the inclusion of the tip mass drastically changed the nature of the optimal structure (Figures 2 and 8).

E.   Consequences of Mode Shape Derivatives

Often, in structural analyses involving the variations of eigenvalues and eigenvectors, the structural designer only accounts for the changes in the eigenvalues. While in many cases such action is acceptable, in many others the omission of the eigenvector sensitivities leads to erroneous results. Unfortunately, the problem dealt with in this paper belongs to the latter class of problems. To see this we refer to Figure 5, where we observe that the first eigenvalues which participate in the dynamic response increase (see Figure 6). Furthermore, we make the important observation that the eigenvector nodal-displacements which are close to the point of application of the force decrease, while the others increase. (We recall that the force vector is applied to the left, see Figure 2.) Physically, the smaller nodal displacement at the force-application-point leads to reduced structural excitation (Ref. 18).

We finally note that the effect of the mode shape sensitivity is contained in the control-influence-coefficient matrix B (see Eq. (5)), and thus conclude that the eigenvalue derivative, alone, will not capture the ingredients neccesary for convergence toward the global optimum.

The basic algorithm is formulated in Figure 7.

V   Conclusion

In this paper we present an approach for solving a dual structural-control problem which involves high-order structures through a reduced-order model. The validity of the theory developed is demonstrated by using a structural model of 20 finite-elements. The significant findings of this paper are: i) the use of reduced-order models has a tremendous impact on the computer time required in the optimization process and may be necessary in the optimization of high-order structures; ii) the implementation of a constant mass optimization leads to a dramatic decrease in the control cost; iii) the use of mode shape derivatives are required for convergence towards the global optimum; and iv) the use of the eigenvalue and eigenvector extrapolation formulas of Appendix A makes the reduced-order model formulation a practical numerical technique (indeed, the exact eigen solution was computed only three times during the constant-mass optimization process).
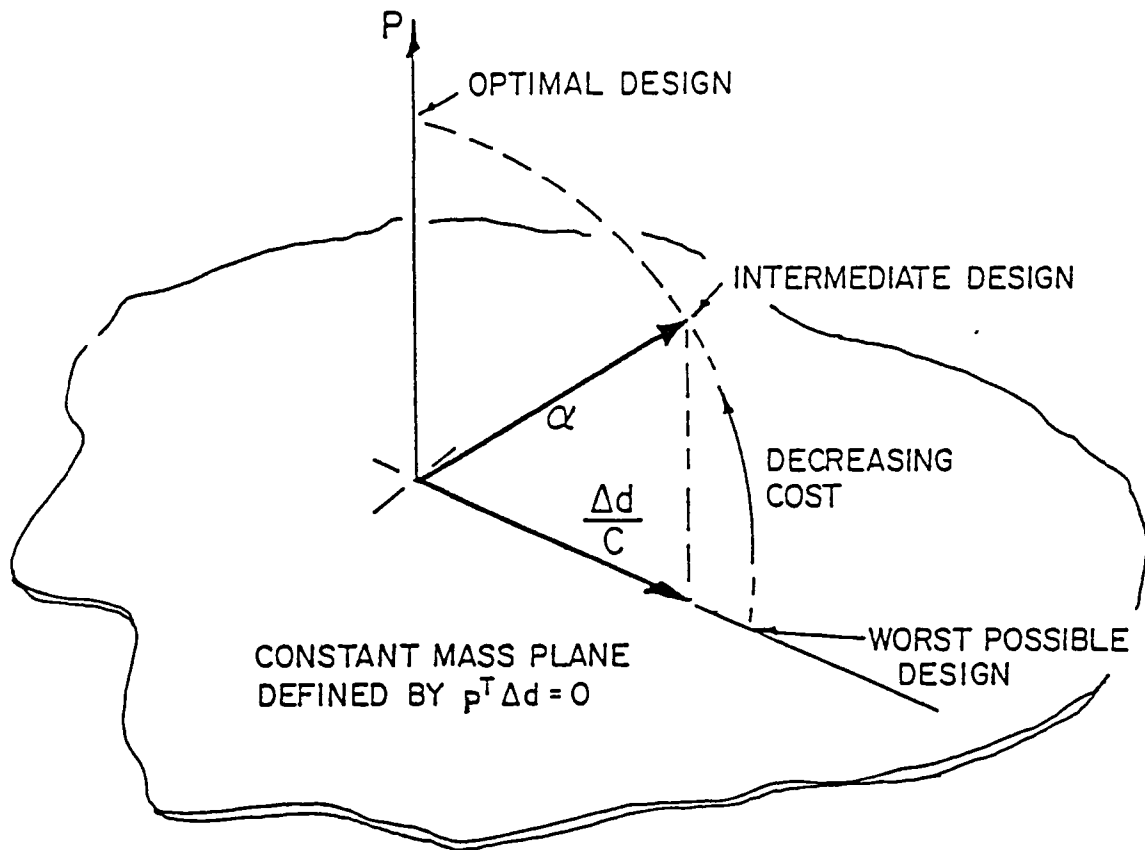
α = NEGATIVE OF NORMALIZED COST GRADIENT VECTOR

$$\Delta d = C \left(\alpha - \frac{\alpha^T P}{P^T P} P \right)$$

Figure 1. Gradient vector with respect to the constant-mass plane.
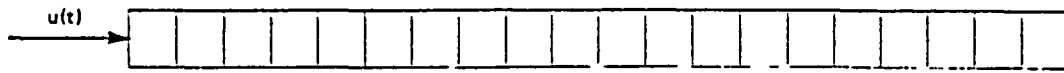
INITIAL DESIGN
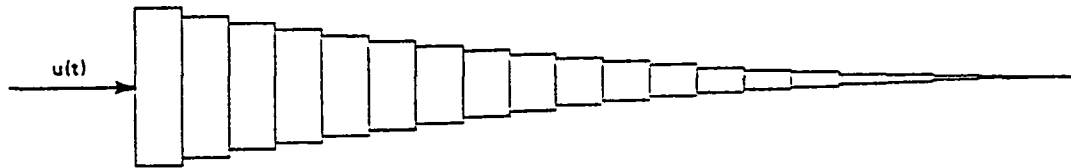
FINAL DESIGN

- BOTH DESIGNS HAVE EQUAL TOTAL MASS
- u(t) = CONTROL FORCE

Figure 2. Initial vs. final structural design.
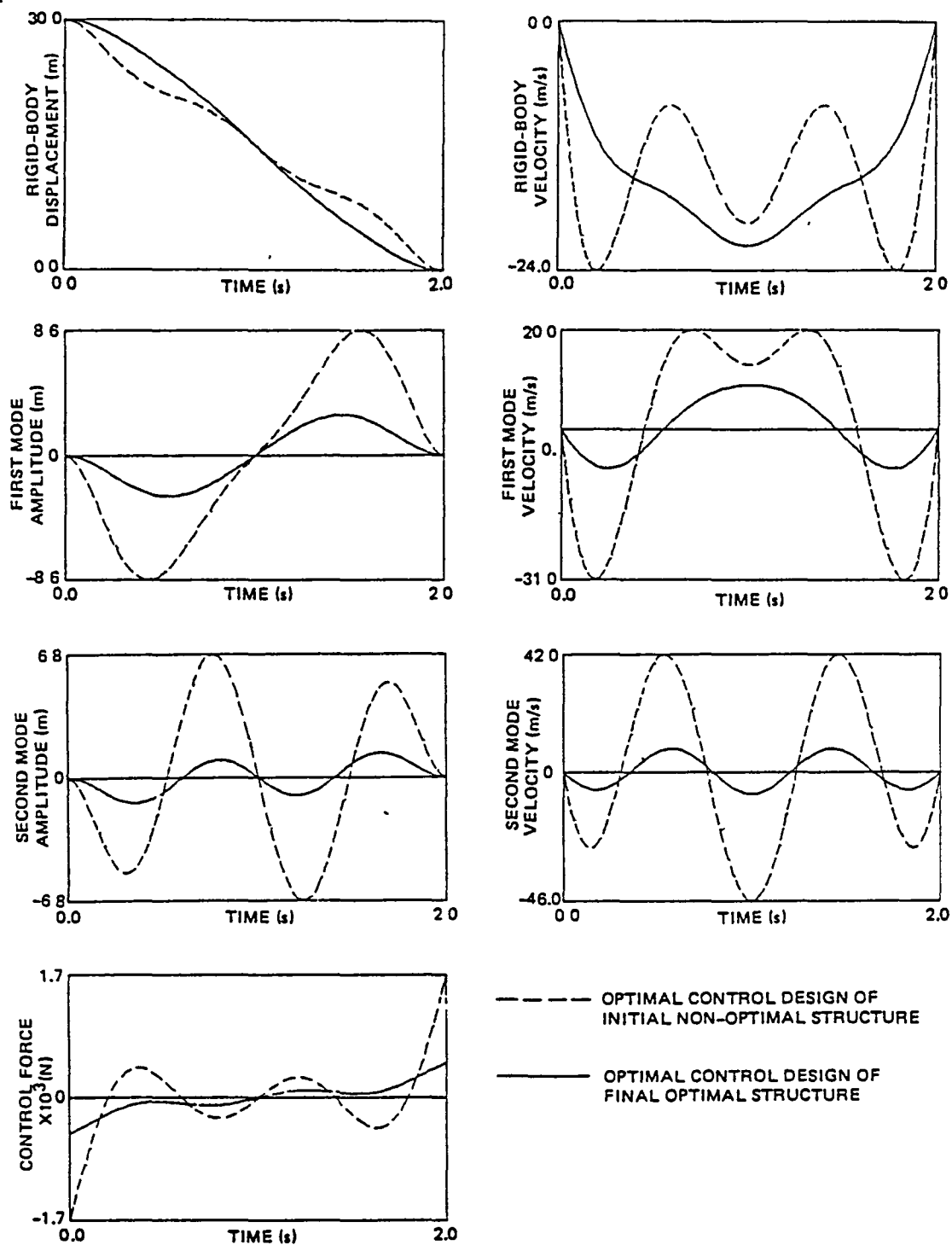
Figure 3. Optimal control design of initial vs. final-optimal-
structural design.
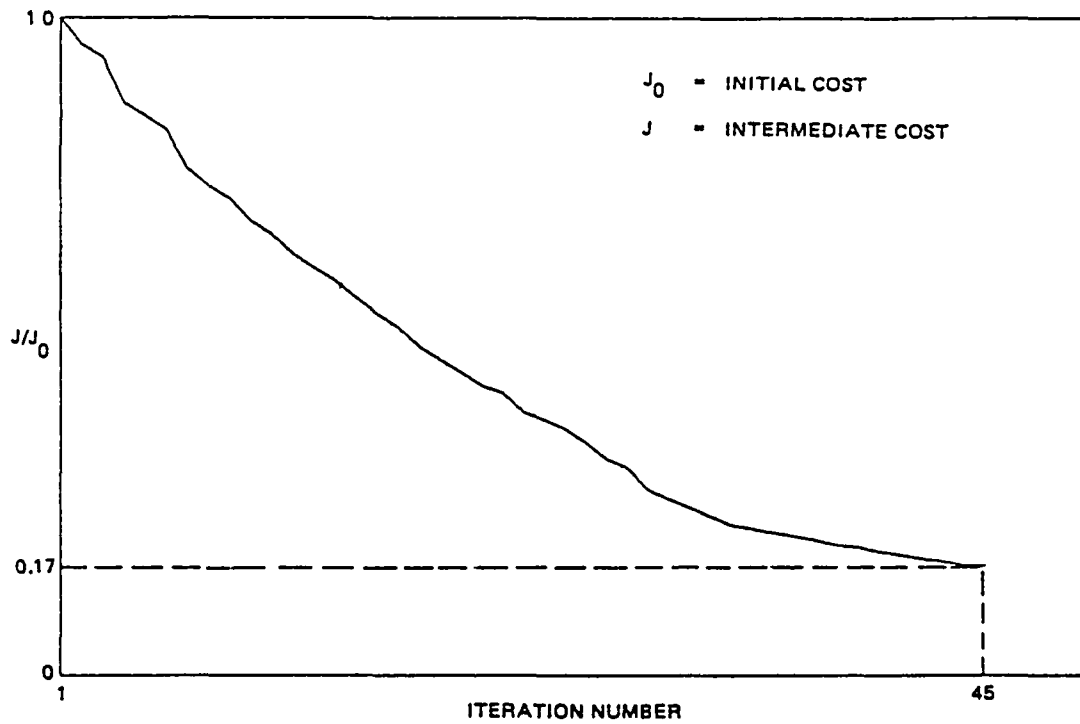
Figure 4. Monotonic decrease of optimal control cost during the "dual" optimization process.

$\lambda_0 = 88$

$\lambda_f = 166$

FIRST MODE

$\lambda_0 = 34.8$

$\lambda_f = 47.9$

SECOND MODE

$\lambda_0 = 77.5$

$\lambda_f = 93.5$

THIRD MODE

$\lambda_0 = 135\,0$

$\lambda_f = 152.0$
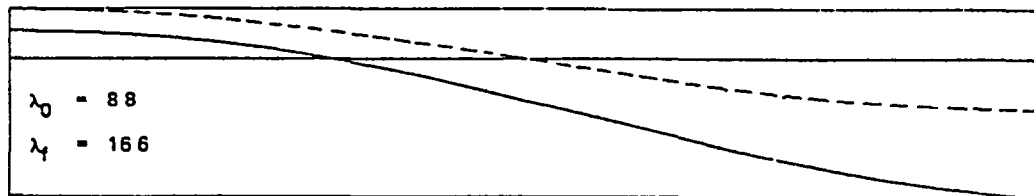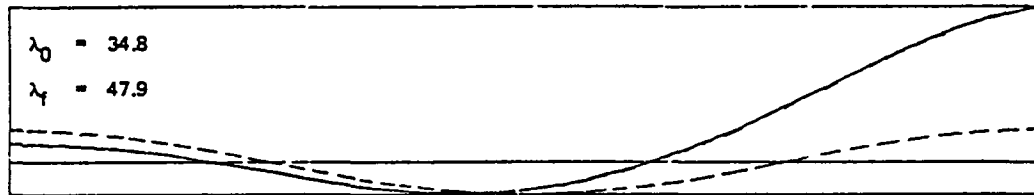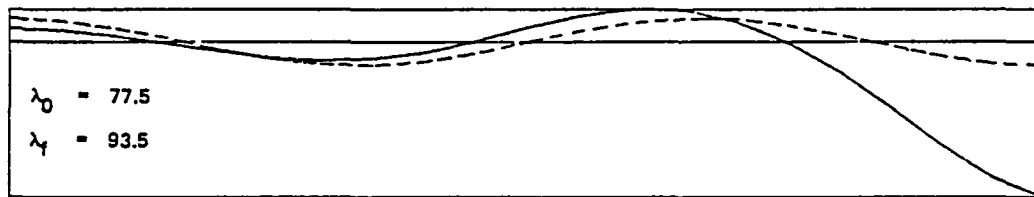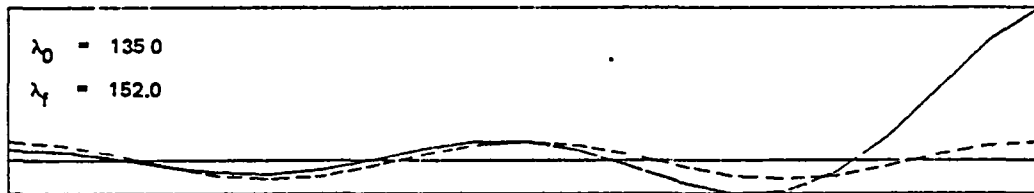
FOURTH MODE

- - - - INITIAL STRUCTURAL MODE SHAPE

——— FINAL OPTIMAL MODE SHAPE

λ_0 = INITIAL EIGENVALUES $(rad/s)^2$

λ_f = FINAL EIGENVALUES $(rad/s)^2$

The modes are normalized such that $\phi^T M \phi = 1$.

Figure 5.   Initial vs. final eigenstructure.

Structural Spectrum ($\frac{rad}{s}$)^2		
Mode #	Initial	Optimal
1	0.0	0 0
2	8.8	16 6
3	34.8	47 9
4	77.5	93.5
5	135.0	152 0
6	208.0	223.0
7	293.0	306.0
8	388.0	398.0
9	491.0	498.0
10	600 0	603.0
11	711.0	711 0
12	822.0	818.0
13	931.0	923.0
14	1034.0	1023.0
15	1129.0	1115.0
16	1214.0	1198.0
17	1286.0	1269.0
18	1345.0	1328.0
19	1387.0	1374 0
20	1413.0	1405.0
21	1422 0	1422 0

Structural Designs		
Design Par. #	Initial	Optimal
1	0.1451	0.405
2	0 1451	0.363
3	0.1451	0.326
4	0.1451	0 291
5	0.1451	0.258
6	0.1451	0.227
7	0.1451	0.198
8	0.1451	0.171
9	0.1451	0.146
10	0.1451	0.122
11	0.1451	0.101
12	0.1451	0.082
13	0.1451	0.065
14	0.1451	0.050
15	0.1451	0.037
16	0.1451	0 026
17	0 1451	0 017
18	0.1451	0.010
19	0.1451	0.005
20	0 1451	0 002

Figure 6. Structural spectrum and structural design parameters for the initial and final-optimal design.
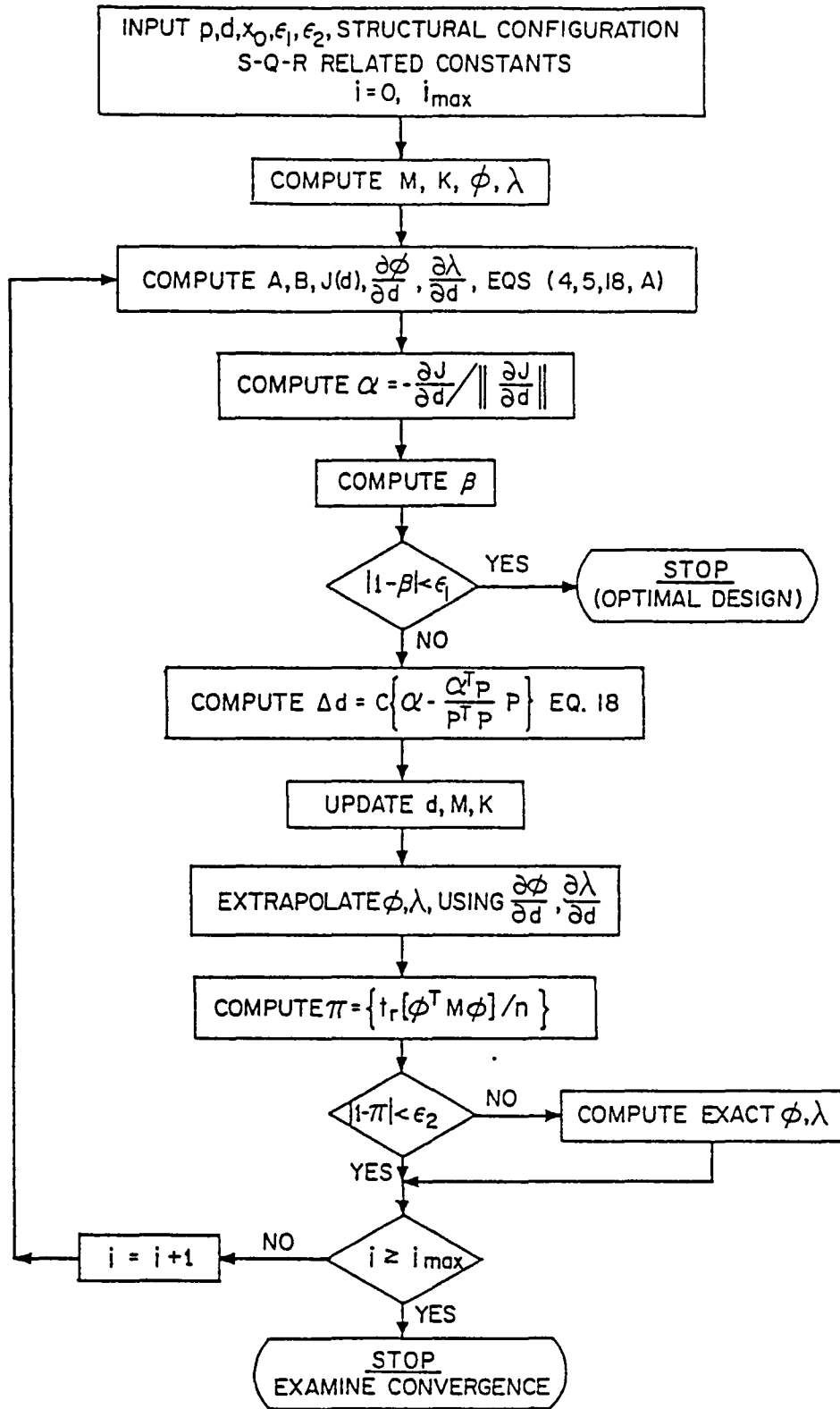
Figure 7. Differential correction algorithm.

252

Initial Design

Optimal Constant-Mass Design

Optimal Minimum-Mass Design

■   Non-Structural Mass

u(t)   Control Force
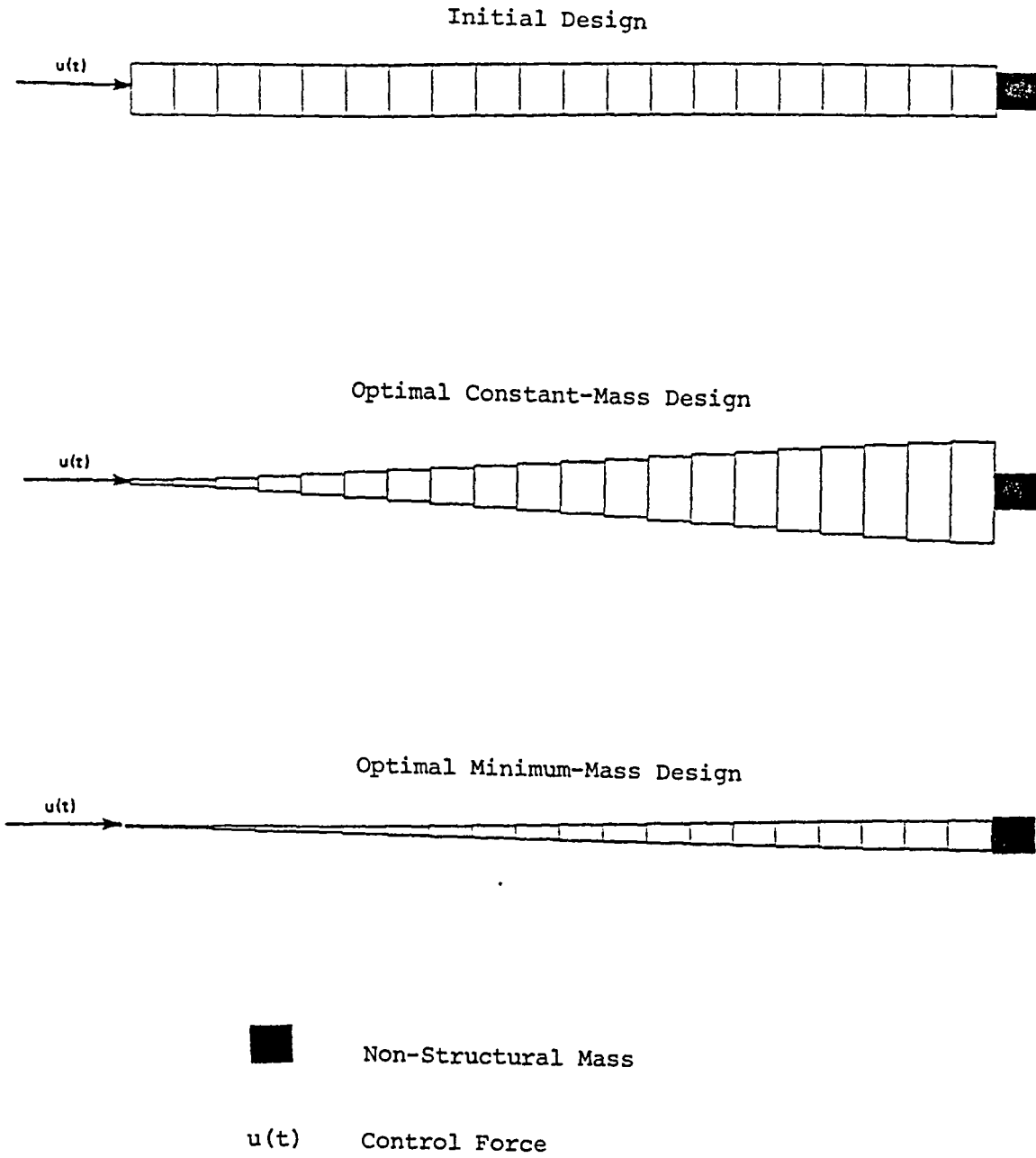
Figure 8.   Structural Designs (Tip Mass Added)

Design Parameter No.	Initial Design	Constant-Mass Optimal Design	Minimum-Mass Optimal Design
1	0.1451	0 0016	0.0042
2	0.1451	0 0147	0 0053
3	0.1451	0.0290	0.0085
4	0.1451	0 0435	0.0128
5	0.1451	0.0582	0.0171
6	0.1451	0.0730	0 0214
7	0.1451	0 0881	0 0258
8	0.1451	0.1033	0.0303·
9	0 1451	0 1187	0 0348
10	0.1451	0 1342	0 0394
11	0.1451	0.1500	0 0440
12	0.1451	0 1659	0 0486
13	0 1451	0.1820	0.0534
14	0 1451	0 1983	0.0581
15	0.1451	0 2148	0 0630
16	0 1451	0.2314	0 0678
17	0.1451	0 2483	0.0728
18	0.1451	0 2653	0 0778
19	0.1451	0 2825	0 0798
20	0.1451	0.2988	0.0859

Figure 9.   Structural Design Parameters (Tip Mass Added)

254

REFERENCES

1. Pierson, B.L., "A Survey of Optimal Structural Design Under Dynamic Constraints," International Journal For Numerical Methods in Engineering, Vol. 4, pp. 491-499, 1972.

2. Sheu, C.Y., and W. Prager, "Recent Developments in Optimal Structural Design," Applied Mechanics, Rev. 21, pp. 985-992, 1968.

3. Turner, M.J., "Design of Minimum-Mass Structures With Specified Natural Frequencies," AIAA Journal, 5, pp. 406-412, 1967.

4. McIntosh, S.C., and F.E. Eastep, "Design of Minimum-Mass Structure With Specified Stiffness Properties," Vol. 6, No. 5, AIAA Journal, pp. 962-964, 1968.

5. Bellagamba, L., and T.Y. Yang, "Minimum-Mass Truss Structure With Constraints on Fundamental Natural Frequency," Vol. 19, No. 11, AIAA Journal, pp. 1452-1458, (AIAA 81-4295).

6. Carmichael, D.G., "Structural Modelling and Optimization," Ellis Horwood, Ltd., Halsted Press: a division of John Wiley & Sons, 1981.

7. Morris, A.J., Editor, "Foundations of Structural Optimization: A Unified Approach," John Wiley & Sons, Ltd., 1982.

8. Turner, J.D., and H.M. Chun, "Optimal Feedback Control of a Flexible Spacecraft During a Large Angle Rotational Maneuver," presented as Paper No. 82-1589 at the AIAA Guidance and Control Conference, San Diego, CA, August 9-12, 1982.

9. Turner, J.D., and H.M. Chun, "Optimal Distributed Control of a Flexible Spacecraft Using Control Rate Penalties in the Controller Design," presented as Paper No. 82-1438 at the AIAA Guidance and Control Conference, San Diego, CA, August 9-12, 1982.

10. Kirk, D.E., Optimal Control Theory, "An Introduction," Printice-Hall, Inc., 1970.

11. Kwakernaak, H., and R. Sivan, "Linear Optimal Control Systems," John Wiley & Sons, Inc., 1972.

12. Meirovitch, L., and H. Oz, "Modal-Space Control of Distributed Gyroscopic Systems," Journal of Guidance and Control, Vol. 3, No. 2, pp. 140-150, 1980.

13. Hale, A.L., R.J. Lisowski, and W.E. Dahl, "Optimizing Both the Structure and the Control of Maneuvering Flexible Spacecraft," presented as Paper No. 83-377 at the AAS/AIAA Astrodynamics Specialist Conference, Lake Placid, NY, August 22-25, 1983.

14. Hale, A.L., and R.J. Lisowski, "Optimal Simultaneous Structural and Control Design of Maneuvering Flexible Spacecraft," presented at the Fourth VPI & SU/AIAA Symposium on Dynamics and Control of Large Space Structures, Blacksburg, VA, June 6-8, 1983.

15. Messac, A., and J.D. Turner, "Dual Structural-Control Optimization of Large Space Structures: Progress Report," presented at the NASA Symposium on Recent Experiences in Multidisciplinary Analysis and Optimization, Langley Research Center, Hampton, VA, April 24-26, 1984.

16. Messac, A., and J.D. Turner, "Dual Structural-Control Optimization of Large Space Structures," presented at the AIAA Dynamics Specialist Conference, Palm Springs, CA, May 17-18, 1984.

APPENDIX A

PERFORMANCE INDEX GRADIENT

The partial derivatives of J(d) in Eq. (16) with respect to the i-th design variable follows as

$$\partial J/\partial d_i = (1/2)x_0^T(\partial H/\partial d_i) x_0$$

$$+ (\partial x_0/\partial d_i)^T H x_0 \tag{A-1}$$

where

$$\partial H/\partial d_i = H_A^{-1}(\partial H_A/\partial d_i)H_A^{-1}H_B - H_A^{-1}(\partial H_B/\partial d_i) \tag{A-2}$$

$$\partial H_A/\partial d_i = -(\partial S/\partial d_i)\Psi_{21} - S(\partial \Psi_{21}/\partial d_i) + \partial \Psi_{22}/\partial d_i \tag{A-3}$$

$$\partial H_B/\partial d_i = -(\partial S/\partial d_i)\Psi_{11} - S(\partial \Psi_{11}/\partial d_i) + \partial \Psi_{12}/\partial d_i \tag{A-4}$$

and $\partial x_0/\partial d_i$ is given by Eq. ( ).

The partial derivatives for the state transition matrix of Eq. (15) with respect to the i-th design variable can be expressed as (Ref-18)

$$\partial \Psi/\partial d_i = e^\Gamma \int_0^1 e^{-\Gamma\sigma}[\partial\Gamma/\partial d_i]e^{\Gamma\sigma}d\sigma \tag{A-5}$$

$$
= \begin{bmatrix} \partial \Psi_{11}/\partial d_{\iota} & \partial \Psi_{12}/\partial d_i \\ \\ \partial \Psi_{21}/\partial d_{\iota} & \partial \Psi_{22}/\partial d_{\iota} \end{bmatrix} \begin{matrix} \} \ 2 \ N_m \\ \\ \} \ 2 \ N_m \end{matrix}
$$

$$
\underline{\hspace{1cm} 2 \ N_m \hspace{1cm}} \quad \underline{\hspace{1cm} 2 \ N_m \hspace{1cm}}
$$

where

$$
\partial \Gamma / \partial d_{\iota} = \begin{bmatrix} \partial (A t_f)/\partial d_i & -\partial (B R^{-1} B^T t_f)/\partial d_i \\ \\ -\partial (Q t_f)/\partial d_i & -\partial (A^T t_f)/\partial d_{\iota} \end{bmatrix} \tag{A-6}
$$

and

$$
\Gamma = D t_f
$$

$$
\partial A / \partial d_i = \begin{bmatrix} 0 & \cdot & -\partial \Lambda / \partial d_{\iota} \\ \\ 0 & & 0 \end{bmatrix} \tag{A-7}
$$

$$
\partial B / \partial d_i = \begin{bmatrix} \partial (\phi^T E)/\partial d_i \\ \\ 0 \end{bmatrix} \tag{A-8}
$$

It is understood that the chain rule is to be applied to produce the appropriate expressions in Eqs. (A-6) and (A-8).

The structural eigenvalue and eigenvector partials required in Eqs. (A-6-8), follow as (Ref. 15)

$$\partial \lambda_j / \partial d_i = \underline{\phi}_j^T \left[\partial K / \partial d_i - \lambda_j (\partial M / \partial d_i) \right] \underline{\phi}_j \qquad \text{(A-9)}$$

$$\partial \underline{\phi}_j / \partial d_1 = \sum_{\substack{k=1 \\ k \neq j}}^{n} a_k \underline{\phi}_k + a_j \underline{\phi}_j \qquad \text{(A-10)}$$

$$a_r = \begin{cases} \underline{\phi}_r^T \left[\partial K / \partial d_i - \lambda_k (\partial M / \partial d_1) \right] \underline{\phi}_k / (\lambda_k - \lambda_r) & , \ r \neq k \\[2em] \phi_r^T \left[\partial M / \partial d_i \right] \phi_r / 2 & , \ r = k \end{cases} \qquad \text{(A-11)}$$

Since the calculation of the structural eigen solution and associated partials is costly, we use the following analytic continuation formulas for extrapolating these important qualities.

$$\lambda_j (d+\Delta d) \approx \lambda_j (d) + \sum_{j=1}^{n} (\partial \lambda_j / \partial d_i) \Delta d_j \qquad \text{(A-12)}$$

$$\underline{\phi}_j (d+\Delta d) \approx \underline{\phi}_j (d) + \sum_{j=1}^{n} (\partial \underline{\phi}_j / \partial d_1) \Delta d_j \qquad \text{(A-13)}$$

where Δd is the current differential correction vector for the design variables. The partial derivatives of $\underline{\lambda}_j$ and $\underline{\phi}_j$ are then produced by substituting the results of Eqs. (A-12) and (A-13) into Eqs. (A-9 through A-11). In order to monitor the validity of the first-order extrapolation formulas above we test the following inequality:

$$\left| \text{TRACE} (\phi^T M \phi)/N_m - 1 \right| = \begin{cases} < \epsilon_2 & \text{use Eqs. (A-12) and (A-13)} \\[1.5em] \geq \epsilon_2 & \text{compute the exact solution} \\ & \text{for } \phi \text{ and } \lambda \end{cases}$$

where ϵ_2 is user specified.

259

STATE TRANSITION MATRIX SENSITIVITY CALUCLATION

To efficiently compute the state-transition-matrix partial derivatives of Eq. (A-5), we first express the matrix $\Gamma = Dt_f$ in terms of the following right and left eigenvector description:

$$\Gamma R = R\gamma, \quad \Gamma^T L = L\gamma, \quad L^T R = I$$

$$\text{(A-14)}$$

$$\Gamma = R\gamma L^T, \quad \gamma = \text{Diag.} \left[\gamma_1, \ldots, \gamma_{N_m} \right]$$

where R and L denote the normalized right and left eigenvector matrices, respectively, leading to

$$e^{\Gamma\sigma} = R \, e^{\gamma\sigma} L^T \tag{A-15}$$

$$e^{-\Gamma\sigma} = R e^{-\gamma\sigma} L^T$$

Introducing the expressions above into Eq. (A-5) we find

$$\partial\Psi/\partial d_i = R e^{\Gamma} \dot{H}_i L^T \tag{A-17}$$

where

$$H_i = \int_0^1 e^{-\gamma\sigma} G_i \, e^{\gamma\sigma} d\sigma \tag{A-18}$$

$$G_i = L^T (\partial\Gamma/\partial d_i) R \tag{A-19}$$

The pq-th term of Eq. (A-18) can further be written as

$$\left[H_i\right]_{pq} = \int_0^1 \left[G_i\right]_{pq} e^{(\gamma_q - \gamma_p)\sigma} \, d\sigma \qquad \text{(A-20)}$$

or, upon carrying out the integral above analytically we find

$$\left[H_i\right]_{pq} = \begin{cases} \left[G_i\right]_{pq} (e^{(\gamma_q - \gamma_p)} - 1)/(\gamma_q - \gamma_p) & , \quad q \neq p \\ \left[G_i\right]_{pq} & , \quad q = p \end{cases} \qquad \text{(A-21)}$$

The important feature of the calculation above is that one set of right and left eigenvectors produces the sensitivity partials for all the design variables.

261

APPENDIX B

CONTROL PENALTY MATRICES S, Q, AND R

The matrices S, Q, and R define the weights imposed on the final state, the intermediate states, and the control, respectively (see Eq. (1)).

Motivated by the desire to minimize the sum of the square of the physical nodal displacements and velocities, we write

$$w^T w \approx (\phi \eta)^T (\phi \eta)$$

$$\approx \eta^T [\phi^T \phi] \eta \qquad (B-1)$$

where modal trunction has already taken place, $\dot{w}$ is defined by Eq. (3), and

$$\dot{w}^T \dot{w} \approx \dot{\eta}^T [\phi^T \phi] \dot{\eta} \qquad (B-2)$$

We further let

$$\theta = \lfloor \phi^T \phi \rfloor$$

and recall that

$$x^T = \{\dot{\eta}^T , \eta^T\}$$ (B-3)

As a result, the form of the matrix Q which has resulted in desirable dynamic responses is given by

$$Q = \begin{bmatrix} \Theta_1 & 0 \\ 0 & \Theta_2 \end{bmatrix}$$ (B-4)

where

$$[\Theta_1]_{ij} = \begin{cases} 5[\Theta]_{ij} & \text{for any } i \text{ or } j = 1 \text{ (rigid-body velocity)} \\ \\ 0.1[\Theta]_{ij} & \text{for any } i \text{ or } j > 1 \text{ (flexible-body velocity)} \end{cases}$$

$$[\Theta_2]_{ij} = \begin{cases} [\Theta]_{ij} & \text{for any } i \text{ or } j = 1 \text{ (rigid-body displacement)} \\ \\ 0.01[\Theta]_{ij} & \text{for any } i \text{ or } j \text{ greater than 2 (flexible-body displacement)} \end{cases}$$

and $[*]_{ij}$ denotes the ij-th element of "*". The matrix S was chosen to be equal to 10^9 times the matrix Q. Finally, the control penalty matrix has one entry equal to 0.5.

263

APPENDIX C

STEADY-STATE CONTROL GAIN OPTIMIZATION PARTIALS

The partial derivative of $J(d)$ in Eq. (21) with respect to the
i-th design variable follows as

$$\partial J/\partial d_i = (1/2) X_o^T (\partial P_{ss}/\partial d_i) X_o$$

$$+ (\partial X_o/\partial d_i)^T P_{ss} X_o \qquad (C-1)$$

where $\partial X_o \partial d_i$ is given by Eq. (10), and the solution for $\partial P_{ss}/\partial d_i$
is defined by the following algebraic Lyapunov equation:

$$\bar{A}^T (\partial P_{ss}/\partial d_i) + (\partial P_{ss}/\partial d_i)\bar{A} = -(\partial A/\partial d_i)^T P_{ss} - P_{ss}(\partial A/\partial d_i)$$

$$+ P_{ss}\left[(\partial B/\partial d_i)R^{-1}B^T + BR^{-1}(\partial B/\partial d_i)^T\right] P_{ss}$$

$$- \partial Q/\partial d_i \qquad (C-2)$$

where $\partial A/\partial d_i$ is defined by Eq. (A-7), $\partial B/\partial d_i$ is defined by Eq. (A-8),
and

$$\partial Q/\partial d_i = \text{Block Diag.} \left[\partial \Theta_1/\partial d_i, \partial \Theta_2/\partial d_i\right]$$

where Θ_2 and Θ_2 are defined by Eq. (B-4).

The solution for Eq. (C-2) is efficiently obtained by first expressing the $\bar{A}$ matrix in terms of the following right and left eigenvector description:

$$\bar{A}R = R\gamma \quad , \quad \bar{A}^T L = L\gamma \quad , \quad L^T R = I$$

$$\bar{A} = R\gamma L^T \quad , \quad \gamma = \text{Diag.} \left[\gamma_1, \ldots, \gamma_{2N_m} \right]$$

where R and L denote the normalized right and left eigenvector matrices, respectively.

Introducing the expressions above for $\bar{A}$ into Eq. (C-2), we obtain

$$(L\gamma R^T)(\partial P_{ss}/\partial d_i) + (\partial P_{ss}/\partial d_i)(R\gamma L^T) = \Xi \tag{C-3}$$

where Ξ denotes the right-hand side of Eq. (C-2).

Pre-multiplying Eq. (C-3) by R^T and post-multiplying the resulting equation by R, leads to

$$\gamma T + T\gamma = R^T \Xi R \tag{C-4}$$

where $T = R^T(\partial P_{ss}/\partial d_i)R$. Since γ is diagonal, the solution for T follows as

$$[T]_{ij} = [R^T \Xi R]_{ij}/(\gamma_i + \gamma_j) \tag{C-5}$$

where we assume that $\gamma_i + \gamma_j \neq 0$ and $[*]_{ij}$ denotes the ij-th element of the bracketed matrix.

The solution for $\partial P_{ss}/\partial d_i$ follows as

$$\partial P_{ss}/\partial d_i = LTL^T \qquad (C\text{-}6)$$

The important feature of the calculation above is that one set of right and left eigenvectors produces the sensitivity partials for all the design variables.

It is important to observe when comparing the complexity of the partial derivatives in Eq. (A-2) and (C-2), that the dimension of the state transition matrix partial $\partial\Psi/\partial d_i$ is $4N_m \times 4N_m$, whereas the dimension of steady-state Riccati matrix partial is $2N_m \times 2N_m$. Thus the cost associated with solving the steady state version is considerably less.

CHARACTERISTIC ELASTIC SYSTEMS OF TIME-LIMITED OPTIMAL MANEUVERS

A. L. Hale* and R. J. Lisouski**
University of Illinois at Urbana—Champaign
Urbana, IL 61801

ABSTRACT

This paper extends earlier work by the authors on optimizing an elastic system and its active control Maneuvers from an initial state to a final state in a finite time interval are considered. An active generalized control force that accomplishes the desired maneuver of a prespecified system is optimal if it minimizes a given quadratic cost function By also varying a set of design parameters, the elastic system can be determined so as to further minimize the cost function. Here, the elastic system that minimizes the actual control cost is compared with the system that minimizes the ratio of actual cost to the cost of optimally maneuvering a rigid system of the same inertial properties. It is shown that an elastic system corresponding to an extremum of the ratio is actually a characteristic of the time-limited maneuver. Because both the spatial domain and the time interval are fixed, a characteristic elastic system is tuned to the specified temporal boundary conditions. The implication for rest-to-rest, spinup, and spin reversal maneuvers of spacecraft is that the optimal control for a characteristic elastic spacecraft is identical to the optimal control for the same spacecraft as if it were rigid.

1. INTRODUCTION

The concern is with flexible structures whose elastic deformations can interact significantly with an active control system. As in [1-5], the optimal integrated design of a structure and its active control is explicitly addressed

A specific objective for the integrated optimization must first be identified. To this end, maneuvers are considered mainly because maneuvering loads are a significant source of large magnitude disturbances, at least for spacecraft. Example sources of loads are thruster firings for station keeping maneuvers, and abrupt reaction wheel and/or thruster excitation for rapid large angle rotational maneuvers These control actions necessarily affect the entire structure because they require changing the motion of the body as if it were rigid. They also define a well-posed structure/control optimization problem. The objective is to balance structural inertia (e. g, mass) with required control energy The two components of this objective are contradictory for many flexible structures and they can be thought of as separate entries of a vector valued cost (objective) function to be minimized. Then, minimizing a scalar function that is a linear combination of the vector's entries leads to a Pareto-optimal solution [2] At one extreme of the Pareto-optimization the objective is quite narrow: what structure/control minimizes total control energy? The solution to this

problem is of especial significance and it is the problem addressed herein.

The outline of the paper is as follows Section 2 presents a brief statement of the integrated optimization problem addressed. It is a parametric optimal control problem [6] for the simultaneous design of a structure and its active control Similar problems have been considered in a number of papers by the authors [1-4] and in the thesis [5] A slightly different approach than that of [1-5] has also been presented recently in [7]. As in [1-5], maneuvers from an initial state to a final state in a specified finite time interval are considered here The main new contribution of this paper is that solutions that minimize actual control cost are now compared with solutions that minimize the ratio of actual control cost to the cost of optimally controlling a rigid body of the same inertial properties. When minimizing the later ratio of costs, a characteristic value problem arises. Hence, its solutions are referred to as characteristic elastic systems for the time-limited optimal maneuver in question. Section 3 solves both integrated problems associated with a rest-to-rest translational maneuver of an idealized elastic system that has only two natural modes of vibration, one being a rigid body mode and the other an elastic mode. The system has one free structural parameter and by its choice the natural frequency of the elastic mode can be assigned. The example is simple enough that the essential ingredients of the solution can be obtained analytically Thus, the minima of both criteria can be compared without introducing significant numerical errors. On the other hand, Sec. 4 presents numerical solutions for a rest-to-rest single axis rotational maneuver of a symmetric four boom structure The results are contained also in [3] and [5] but interpreted here in the context of characteristic elastic systems

2. OPTIMAL INTEGRATED STRUCTURE/CONTROL DESIGN - PROBLEM STATEMENTS

2 1 *Minimizing Actual Control Cost*

We consider the specified terminal value maneuver of a flexible structure in the specified finite time interval $0 \le t \le t_f$ In this subsection, a control vector $E(t) \in R^{N_c}$ and a vector of structural parameters $\xi \in R^{N_d}$ are desired that minimize the cost function

$$J(E,\xi) = \int_0^{t_f} \frac{1}{2}(E^T R E) dt ,$$ (1)

subject to the following differential equation constraints, specified initial values, specified final values, and inequality constraints, respectively,

$$M(\xi)\ddot{U}(t) + K(\xi)U(t) = GE(t) ,$$ (2a)

$$U(0) = U_0 , \quad \dot{U}(0) = V_0 ,$$ (2b,c)

$$U(t_f) = U_f , \quad \dot{U}(t_f) = V_f ,$$ (2d,e)

$$\xi_i \ge 0 , \quad i=1,2, \quad ,N_d$$ (2f)

In (1), R is an $N_c \times N_c$ positive definite symmetric weighting matrix, and in (2a-e) $U(t) \in R^N$ is the generalized displacement vector, and $M(\xi)$ and $K(\xi)$ are the $N \times N$ symmetric mass matrix and stiffness matrix, respectively For simplicity, other explicit constraints are not considered. The constraints (2f), where ξ_i is the ith entry of ξ, are intended to represent non-negativity constraints on physical parameters such as structural member widths, lengths, and/or cross sectional areas. The specified terminal values (2b-e) define the desired maneuver, and (2a) is assumed to be obtained by discretizing the equations of motion of an actual distributed structure by the finite element method.

The necessary conditions are derived by the calculus of variations and their derivation is discussed in [4]. The differential equation constraints (2a) are invoked by introducing a vector U^* of adjoint displacements (Lagrange multipliers) and appending the constraints to (1). After doing so, the variations of E, U, U^* are arbitrary so that their coefficients all vanish, leading to the $2N+N_c$ necessary conditions for an optimal control

$$E(t) = R^{-1}G^T U^*(t)$$ (3a)

$$M(\xi)\ddot{U}(t) + K(\xi)U(t) = GE(t)$$ (3b)

$$M(\underline{\xi})\underline{\Pi}^{*}(t) + K(\underline{\xi})\underline{\Pi}^{*}(t) = \underline{0} \tag{3c}$$

When a parameter is on the boundary of the admissible parameters, the variation of that particular parameter must itself vanish. However, in the neighborhood of extrema not on the boundary the coefficient of the variation of each ξ_i vanishes, leading to the N_d necessary conditions

$$L_i = \int_0^{t_f} \underline{\Pi}^{*T} \left[\frac{\partial M}{\partial \xi_i} \underline{\Pi} + \frac{\partial K}{\partial \xi_i} \underline{\Pi} \right] dt = 0, \quad i=1,2, \quad ,N_d \tag{3d}$$

The necessary conditions (3) are a hybrid system of nonlinear equations which must be solved numerically [2,3,5] For specified parameters ξ, (3a-c) are linear. In conjunction with (2b-e), they represent a two-point boundary value problem for an optimal control. Once the optimal control problem is solved, the N_d entries L_i of the gradient of J with respect to ξ can be evaluated. The gradient is then used in a projected gradient iterative algorithm for determining an admissible minimizing value of ξ. Because the numerical solution for even relatively simple structures can be computationally expensive, it is natural to consider representing the flexible structure by a truncated number n ($n \leq N$) of its lowest modes of free vibration [3-5,7] The parameter optimization is then based on a reduced-order model of dimension n. For details regarding the numerical procedure we use and reduced-order models, the reader should consult [3-5]

2.2 Minimizing the Ratio of Actual Control Cost to Rigid Body Control Cost

Next, for comparison, we consider a control vector $\underline{F}(t) \in R^{N_c}$ for the actual elastic system, a control vector $\underline{F}_R(t) \in R^{N_c}$ for a rigid body of the same inertial properties, and a vector of structural parameters $\underline{\xi} \in R^{N_d}$ Values of the parameters are desired that minimize a function which is the the ratio of cost functions for the actual system and for the rigid body, namely,

$$\lambda = \frac{J(\underline{F},\underline{\xi})}{J_R(\underline{F}_R,\underline{\xi})} = \frac{\int_0^{t_f} \frac{1}{2}(\underline{F}^T R\underline{F}) dt}{\int_0^{t_f} \frac{1}{2}(\underline{F}_R^T R\underline{F}_R) dt} \tag{4}$$

The minimization of λ is subject to the constraints (2a-e) for the actual structure, the inequality constraints (2f), as well as the following differential equation constraints, and specified initial and final values for the rigid body,

$$m_R(\underline{\xi})\underline{u}_R(t) = g_R \underline{F}_R(t), \tag{5a}$$

$$u_R(0) = u_{R0}, \quad u_R(0) = u_{R0} \tag{5b,c}$$

$$u_R(t_f) = u_{Rf}, \quad u_R(t_f) = u_{Rf} \tag{5d,e}$$

In (5a-e), $u_R(t) \in R^{n_R}$ is the generalized displacement vector for the rigid body, and $m_R(\underline{\xi})$ is the $n_R \times n_R$ symmetric mass matrix. The specified terminal values (5b-e) define the desired rigid body maneuver. Moreover, (5a) is obtained from (2a) by transforming to a set of reduced coordinates that span the space of rigid body modes. For simplicity, we make the assumption that by varying the parameters no additional rigid body degrees of freedom are introduced. Then, the transformation itself is performed by constraining $\underline{\Pi}$ to be a linear combination of n_R constant vectors φ_{Ri} that span the space of rigid body modes, i e., by writing

$$\underline{\Pi}(t) = \sum_{i=1}^{n_R} \varphi_{Ri} u_R = \Phi_R u_R \tag{6}$$

By definition, the vectors φ_{Ri} have the property $K\varphi_{Ri}=\underline{0}$, which holds for all admissible values of $\underline{\xi}$ even though K depends on $\underline{\xi}$ and φ_{Ri} does not. Hence, upon substituting (6) into (2a) and premultiplying by Φ_R^T one obtains (5a) where

$$m_R(\underline{\xi}) = \Phi_R^T M(\underline{\xi})\Phi_R, \quad g_R = \Phi_R^T G \tag{7a,b}$$

Finally, the ratio (4) is meaningful only if the maneuver of the actual flexible structure is intimately related

269

to the maneuver of its corresponding rigid model. Our practical interest is in maneuvers of the flexible structure for which the terminal conditions (2b-e) specify rigid body motions only, so that elastic deflections and velocities are zero at the terminal times. Then, the terminal conditions (5b-e) for the rigid body are a projection of (2b-c), where $u_{R0} = (\Phi_R^T M \Phi_R)^{-1} \Phi_R^T M U_0$ and a similar expression holds for each of (5c,d,e). Of course, for a rigid body the elastic deflections are zero for all time, and the orthogonal complement of (5b-e) for the elastic modes is, therefore, trivially satisfied.

Again the necessary conditions are derived by the calculus of variations. The differential equation constraints (2a) and (5a) are invoked by introducing $\underline{\lambda}^*$ and u_R^* and appending the constraints to the numerator and denominator of (4), respectively. Taking the variation leads to conditions (3a-c) for the optimal control of the actual structure, to the $2n_R + N_c$ necessary conditions for the optimal control of the corresponding rigid body, namely,

$$\underline{\lambda}_R(t) = R^{-1} g_R^T u_R^*(t) \tag{8a}$$

$$m_R(\xi) \ddot{u}_R = g_R \underline{\lambda}_R \tag{8b}$$

$$m_R(\xi) \ddot{u}_R^* = \underline{0} \tag{8c}$$

and, finally, to the N_d necessary conditions (for extrema not on the boundary of admissible parameters) for the parameters ξ_i,

$$L_{\lambda i} = \int_0^{t_f} \underline{\lambda}^T \left[\frac{\partial M}{\partial \xi_i} \underline{\lambda} + \frac{\partial K}{\partial \xi_i} \underline{\lambda} \right] dt - \lambda \int_0^{t_f} u_R^T \frac{\partial m_R}{\partial \xi_i} u_R dt = 0 , \quad i = 1, 2, \cdots, N_d \tag{9}$$

Note that although M varies with ξ so that the terminal values (5b-e) also vary, no additional terms appear in the necessary conditions (8a-c) and (9). This is because a complete set of rigid body modes is used, i. e., the space spanned by the columns of Φ_R is invariant.

The function λ is a classic form, namely, the ratio of two positive functions of ξ. It is, therefore, no surprise that the conditions (9) have the classic form of a characteristic value problem. Clearly, the best we can do is to have the cost for the flexible structure to be equal to the cost for the same structure as if it were rigid. The characteristic values of λ are, therefore, all unity. Corresponding to each value of $\lambda^{(r)} = 1$ is a characteristic vector of structural parameters $\xi^{(r)}$ ($r = 1, 2, \cdots$). The parameter vectors correspond to local minima of (4), and their actual values for most elastic systems must be found numerically. Note that the same numerical procedure that is used to minimize J can also be used to minimize λ once one notices that the coefficient of λ in (9) vanishes if the equations of motion (2a) are normalized by the total inertia.

3. SIMPLE TWO DEGREE OF FREEDOM EXAMPLE

The concepts advanced in Sec. 2 are not particularly complex. Nevertheless, the reader may question our claim that minima of λ are indeed unity and a characteristic of the particular maneuver. We demonstrate the behavior in this section by considering a rest-to-rest translational maneuver of two equal masses of mass m connected by a uniform elastic bar. The bar is idealized as a single finite element in axial extension. It has the mass per unit of volume γ, the length l, the modulus of elasticity E, and the cross-sectional area A. The uniform area A is free to be designed. The maneuver is to be accomplished with only a single control force acting at one of the end masses. Hence, the cross-sectional area A cannot become zero without losing the ability to translate the second mass.

The equations of motion for this system have the form of (2a) with $N = 2$, $N_c = 1$, $N_d = 1$, $\underline{U} = \{U_1, U_2\}^T$, $\xi_1 = A$, and

$$M(A) = \begin{bmatrix} 1 + \frac{\gamma L}{3m} A & \frac{\gamma L}{6m} A \\ \frac{\gamma L}{6m} A & 1 + \frac{\gamma L}{3m} A \end{bmatrix} , \quad K(A) = \frac{EA}{mL} \begin{bmatrix} 1 & -1 \\ -1 & 1 \end{bmatrix} , \quad G = \begin{Bmatrix} \frac{1}{m} \\ 0 \end{Bmatrix} \tag{10a,b,c}$$

Due to symmetry, the eigenvectors (not normalized) are always

270

$$\varphi_R = \begin{Bmatrix} 1 \\ 1 \end{Bmatrix} \quad , \quad \varphi_E = \begin{Bmatrix} 1 \\ -1 \end{Bmatrix} \tag{11a,b}$$

where φ_R is the rigid body mode, and φ_E is the elastic mode The equations of motion can be decoupled by transforming to modal coordinates The decoupled equations again have the form (2a) with $\underline{U}=\{u_R,\ u_E\}^T$ and

$$M(A) = \begin{bmatrix} 2+\dfrac{\gamma L}{m}A & 0 \\ 0 & 2+\dfrac{\gamma L}{3m}A \end{bmatrix} \quad , \quad K(A) = \begin{bmatrix} 0 & 0 \\ 0 & \dfrac{4EA}{mL} \end{bmatrix} \quad , \quad G = \begin{Bmatrix} \dfrac{1}{m} \\ \dfrac{1}{m} \end{Bmatrix} \tag{12a,b,c}$$

A control force F, a scalar in this problem, is desired that translates the system between the following terminal conditions (in modal coordinates)

$$\underline{U}_0 = \underline{0} \ , \quad \underline{V}_0 = \underline{0} \ , \quad \underline{U}_f = \begin{Bmatrix} 1 \\ 0 \end{Bmatrix} \ , \quad \underline{V}_f = \underline{0} \tag{13a-d}$$

and that minimizes (1) with $R=1$ Because the equations of motion are decoupled, the optimal control, the modal displacements, and the modal velocities can be obtained easily In terms of four constants $C_1,\quad ,C_4$ depending on the final conditions (13c,d), one obtains

$$F = \frac{1}{m}\Big[C_1 + C_2 t + C_3\cos\omega t + C_4\sin\omega t\Big] \tag{14}$$

$$u_R = \frac{1}{(2+\dfrac{\gamma L}{m}A)m^2}\left[C_1\frac{t^2}{2} + C_2\frac{t^3}{6} + \frac{C_3}{\omega^2}\Big(1-\cos\omega t\Big) + \frac{C_4}{\omega^2}\Big(\omega t - \sin\omega t\Big)\right] \tag{15a}$$

$$u_E = \frac{1}{(2+\dfrac{\gamma L}{3m}A)m^2}\left[\frac{C_1}{\omega^2}\Big(1-\cos\omega t\Big) + \frac{C_2}{\omega^3}\Big(\omega t - \sin\omega t\Big)\right.$$

$$\left. + \frac{C_3}{2\omega}t\sin\omega t + \frac{C_4}{2\omega^2}\Big(\sin\omega t - \omega t\cos\omega t\Big)\right] \tag{15b}$$

$$u_R = \frac{1}{(2+\dfrac{\gamma L}{m}A)m^2}\left[C_1 t + C_2\frac{t^2}{2} + \frac{C_3}{\omega}\sin\omega t + \frac{C_4}{\omega}\Big(1 - \cos\omega t\Big)\right] \tag{15c}$$

$$u_E = \frac{1}{(2+\dfrac{\gamma L}{3m}A)m^2}\left[\frac{C_1}{\omega}\sin\omega t + \frac{C_2}{\omega^2}(1 - \cos\omega t) + \frac{C_3}{2\omega}\Big(\omega t\cos\omega t + \sin\omega t\Big) + \frac{C_4}{2}t\sin\omega t\right] \tag{15d}$$

where the natural frequency of the elastic mode is

$$\omega = \left(\frac{12EA}{6mL + \gamma L^2 A}\right)^{\frac{1}{2}} \tag{16}$$

Of course, the four specified initial conditions (13a,b) are already reflected in (15a-d) and, as already mentioned, the four specified final conditions (13c,d) yield four equations for the constants C_1, C_2, C_3, and C_4 It is easiest to compute the constants numerically. However, the control cost J can be evaluated analytically in terms of the constants. The resulting expression is evaluated numerically once the constants are known. One can also easily determine the optimal control and optimal control cost for the rigid body of mass $(2m+\gamma LA)$, respectively,

$$F_R = \frac{6}{t_f^2}(2m+\gamma LA)\left[1 - \frac{2t}{t_f}\right] \tag{17a}$$

$$J_R = 6\left[\frac{1}{t_f^3}\right](2m + \gamma LA)^2 \qquad (17b)$$

The ratio (4) is, therefore, readily computed for comparison to J

The actual control cost J is plotted verses frequency $(\frac{\omega}{2\pi})$ in Fig 1 for the specific values $t_f = 1$, $m = 1$, $\gamma = 1$, $L = 1$, and $E = 10000$ The area A is also shown, although the frequency is not a linear function of A. The chosen values of E, m, L, and γ allow a great deal of freedom in assigning ω by varying A Note the many local minima in Fig 1 and the trend toward increasing cost with structural frequency The frequencies and areas of the minima are shown in Table 1, along with the corresponding values of the cost. For comparison, the ratio λ is plotted in Fig 2, and the frequencies and areas of the minima are also shown in Table 1 Note that the minima of the ratio are all equal to 1. Moreover, the minima of the ratio occur at nearly the same frequencies (areas) as the minima of the actual control cost The value of the actual optimal control cost is very slightly higher for a value of A that corresponds to a minimum of λ rather than a minimum of J However, the price in choosing a value that corresponds to a minimum of λ is worth paying, particularly because of the meaning of the minima of λ.

To see the meaning of the minima of λ, we shall now substantiate our claim that minima of λ occur at frequencies that are exactly tuned to the optimal control for the rigid body. To this end, the rigid body control force (17d) can be written as $F_R = a(1 - \frac{2t}{t_f})$. Let us apply this force to the actual flexible structure. The equation of motion for the elastic mode has the form

$$\ddot{u}_E + \omega^2 u_E = b\left[1 - \frac{2t}{t_f}\right] \qquad (18)$$

where b is the appropriate participation of the force in the modal equation. Note that ω and b both depend on A, the design parameter. Using the initial conditions $u_E(0) = \dot{u}_E(0) = 0$, the solution of (18) is

$$u_E(t) = \frac{2b}{\omega^3 t_f}\sin\omega t - \frac{b}{\omega^2}\cos\omega t + \frac{b}{\omega^2}\left[1 - \frac{2t}{t_f}\right] \qquad (19)$$

Our desire is that the modal displacement and velocity are quiescent at the final time, i. e., $u_E(t_f) = \dot{u}_E(t_f) = 0$ These final conditions are generally not met because the force F_R is generally not a control force for the elastic body However, the possibility exists that by chosing ω (equivalently A) the final conditions can be met. Two equations for ω result by invoking the final conditions, namely,

$$\frac{2}{\omega^3 t_f}\sin\omega t_f - \frac{1}{\omega^2}\cos\omega t_f - \frac{1}{\omega^2} = 0 \qquad (20a)$$

$$\frac{2}{\omega^2 t_f}\cos\omega t_f + \frac{1}{\omega}\sin\omega t_f - \frac{2}{\omega^2 t_f} = 0 \qquad (20b)$$

Equations (20a,b) are transcendental equations in terms of ω, and values of ω that satisfy both equations simultaneously can be found numerically. This yields an infinite number of *characteristic* natural frequencies, although only N of them are applicable to the discretized systems considered here The first 25 frequencies $(\frac{\omega}{2\pi})$ are listed in Table 2 Comparing the frequencies of the minima of λ with those in Table 2 reveals that the minima of λ occur at precisely the *characteristic* frequencies. The implication is that the optimal control for an elastic system with all natural frequencies at values of ω satisfying (20a,b) is the same as the optimal rigid body control. Here, the rigid body control performs a rest-to-rest maneuver. The rigid body control for other maneuvers, such as spinup and spin reversal maneuvers, yields different characteristic natural frequencies Therefore, a characteristic elastic system depends on the specific maneuver

Of course, a structure composed of two masses connected by a uniform elastic bar is not representative of an actual complex structure, and in particular a large space structure Moreover, the concept of a characteristic elastic system for the maneuver is degenerate when only one elastic mode is present The real allure of the concept is in placing natural frequencies of all elastic modes (or at least a number of the

lowest modes) of a complex structure at values satisfying (20a,b) In complex systems with many elastic modes, the placement of natural frequencies at the characteristic values may not always be possible, and having values in order of Table 2 is also not necessary

4 SINGLE AXIS ROTATIONAL MANEUVER OF A SYMMETRIC FOUR BOOM STRUCTURE

We now consider a single axis rest-to-rest rotational maneuver of an idealized four boom flexible structure (Fig 3) This structure is more representative and it poses several of the problems just discussed. The booms are identical and only antisymmetric bending deflections are allowed. A control torque $f_1(t)$ acts on the rigid hub Although shown in Fig 3, the boom torques f_2 are not used here Each boom is modeled by four finite elements of equal length, constant thickness, and variable width (Fig 4). Thus, the structural design parameters are ξ_1, ξ_2, ξ_3, and ξ_4, where ξ_1 is the root width and ξ_4 is the tip width. Equations of motion are given in [2,3,5] The full dimension of the discrete equations is $N=9$ The same rest-to-rest maneuver and parameters as in [3,5] are used here. Specifically, the structure is slewed from rest and $\vartheta=0$ to rest and $\vartheta=1$ in one unit of time using only the hub torque The booms' elastic deformations are quiescent initially and specified to be quiescent at the final time To keep the computation cost low, the parameter optimization is based on a reduced-order model that contains only the first four ($n=4$) natural modes of free vibration [3-5] The modes are updated at each change of the parameters ξ. Of course, when the optimal control for the reduced-order model is applied to the full-order model the residual modes are also excited. Because the residual modes are not considered in calculating the control, their final displacements and velocities are not necessarily quiescent.

First, we consider minimizing the actual control cost J for the maneuver The optimal parameters (in the sense of minimizing J) are presented in Table 3. For comparison, a non-optimal set of constant parameters, each of which is the average value of the optimal parameters, is also included. The natural frequencies corresponding to the eigenvalues used in the reduced-order model are listed along with the natural frequencies corresponding to the residual modes. The table also includes the final values for the residual mode displacements and velocities for both cases. The residual mode responses result from taking the optimal control for the reduced-order model and applying it to the full-order model. Time histories obtained from the full-order simulations are shown in Fig. 5 and Fig 6 for the optimal and non-optimal cases, respectively. Figure 7 presents the magnitude spectrum of the control for the two cases. The optimal parameter case is shown in solid lines and the non-optimal parameter case in dashed lines. Many attractive properties are observed as a consequence of chosing optimal parameters. For example, the optimal control for the optimal structure is both lower in magnitude and has less excitation at high frequencies than the optimal control for the structure with non-optimal parameters. The tip deflections and velocities are also much lower for the optimal structure Because the parameters are determined so as to minimize J, however, the structure is not tuned exactly to the maneuver This is seen by observing the full-order simulation results in Table 4, where an optimal control for the corresponding rigid optimal and rigid non-optimal structure is applied to the full-order model of the structure While the modal excitation at the final time for the optimal structure is much less than that for the non-optimal structure, it's level is significant.

Next, we shall consider a characteristic structure corresponding to the same rest-to-rest maneuver By chosing the $N_d=4$ parameters ξ_i, only four elastic modes can be assigned. The rigid body mode is always a characteristic of the maneuver Hence, $n=5$ natural frequencies can be chosen to satisfy the conditions (20a,b). However, it is not possible in this example to assign the first five frequencies in order of Table 2. This is due to the coarse structural discretization in which only four finite elements are used. Instead, we assign the rigid body mode with $\omega=0$ (a trivial assignment), and the first elastic mode with $\omega=1.4303$ The remaining freedom in chosing the parameters allows assigning $\omega=3.4709$, $\omega=7.4865$, and $\omega=17.4942$. The parameters are presented in Table 5 along with all associated natural frequencies For the four parameter case considered here, values of the parameters to assign characteristic frequencies can be determined by trial and error, although many simple numerical algorithms to accomplish the same goal can be concocted.

Because the first five natural frequencies are characteristic frequencies for the maneuver, the optimal control for the rigid body does a remarkably good job maneuvering the actual flexible structure. Table 5 presents the final values of modal displacement and velocity for all elastic modes when the rigid body optimal control torque is applied. Note that the level of excitation at $t=t_f=1$ is small for all modes It is

273

slightly higher for modes 6-9 because the frequencies of these modes were not explicitly assigned. Figure 8 presents the time histories for the maneuver of the tuned structure, the characteristic structure. The optimal control is computed based on all nine modes. For comparison, Fig 9 presents time histories for the full-order simulation when the optimal control for the rigid body is applied to the actual flexible structure. There is no noticeable difference between the two figures. The magnitude spectrum of the optimal control based on all nine modes is plotted as a solid line in Fig 10. Also, on Fig 10 is the magnitude spectrum for the rigid body control (a dashed line). The first noticeable difference between the two occurs at frequencies above 20 Hz where the natural frequencies were not assigned.

An additional interpretation of the characteristic frequencies of Table 2 is now noted. The values of Table 2 are precisely the frequencies of the notches in the magnitude spectrum of the optimal rigid body control (see Fig 10). In effect, the characteristic structure is a filter that does not pass the rigid body control input.

Finally, it is interesting to observe the difference between the natural frequencies obtained by minimizing J and those obtained by minimizing λ (the minima of λ are shown in Table 2). The difference is small in the four parameter case, and decreases as we increase the number of parameters (Table 6). Moreover, as the number of parameters is increased, it is possible to obtain frequencies near more of the lowest values in Table 2. This is seen in Table 6, where eight and sixteen parameter results are displayed.

5. CONCLUDING REMARKS

The concept of a characteristic elastic system for a time-limited optimal maneuver has been discussed. The concept may or may not be useful in practice. Nevertheless, it is fundamentally important because it allows a physical understanding of the interaction between a flexible structure and its optimal time-limited control. The concept is also particularly satisfying because of its simplicity. In particular, an infinite number of characteristic elastic systems exist, and one need not choose the one with the lowest mass even though it is probably the one of most practical interest. Moreover, it has been graphically illustrated that the ratio of actual optimal control cost to optimal rigid body control cost, while unity at specific points for a flexible structure, approaches unity everywhere as the structure is stiffened. Thus, the concept is consistent with the fact that the flexibility effects are relatively unimportant when maneuvering stiff structures.

ACKNOWLEDGMENT

REFERENCES

[1] Hale, A. L. and Lisowski, R J., "Optimal Simultaneous Structural and Control Design of Maneuvering Flexible Spacecraft," *Proceedings of the Fourth VPI&SU AIAA Symposium on Dynamics and Control of Large Structures*, Blacksburg, Virginia, June 6-8, 1983

[2] Hale, A L., Lisowski, R J., and Dahl, W E., "Optimizing Both the Structure and the Control of Maneuvering Flexible Spacecraft," *Proceedings of the AAS AIAA Astrodynamics Conference*, Lake Placid, New York, August 22-24, 1983.

[3] Lisowski, R J and Hale, A. L, "Optimal Design for Single Axis Rotational Maneuvers of a Flexible Structure," *Proceedings of the AIAA Dynamics Specialists Conference*, Palm Springs, California, May 12-14, 1984.

[4] Hale, A. L and Lisowski, R J, "Reduced-Order Modeling Applied to Optimal Design of Maneuvering Flexible Structures," *Proceedings of the 1984 American Control Conference*, San Diego, California, June 6-8, 1984.

[5] Lisowski, R J., "Optimizing Parameters and Controls For Maneuvering Flexible Structures," Ph. D Thesis, University of Illinois at Urbana-Champaign, May 1984.

[6] Leitmann, G , *The Calculus of Variations and Optimal Control*, Plenum Press, New York, 1981

[7] Messac, A and Turner, J D , "Dual Structural-Control Optimization of Large Space Structures," Presented at the *AIAA Dynamics Specialists Conference*, Palm Springs, California, May 12-14, 1984.

Table 1				
Comparison of Control Cost Minima for the Simple Example				
Minima of the Cost Ratio		Minima of the Actual Cost		
AREA	FREQ(HZ)	AREA	FREQ(HZ)	COST
0 00404	1 4303	0.00403	1 4293	24 097
0 01196	2 4590	0 01193	2 4542	24 287
0 02387	3 4709	0 02369	3 4575	24 574
0 03983	4.4774	0.03933	4 4489	24 959
0.05990	5 4815	0 05876	5 4297	25 445
0 08416	6 4844	0 08190	6 3979	26 034

Table 2	
Characteristic Natural Frequencies	
for Rest-to-Rest Maneuver	
MODE NUMBER	NATURAL FREQUENCY(HZ)
0	0 0000
1	1 4303
2	2 4590
3	3 4709
4	4.4774
5	5 4815
6	6 4844
7	7 4965
8	8 4881
9	9 4893
10	10 4903
11	11 4912
12	12 4919
13	13 4925
14	14 4930
15	15 4935
16	16 4939
17	17 4942
18	18 4945
19	19.4948
20	20 4951
21	21.4953
22	22 4955
23	23 4957
24	24 4959
25	25 4960

Table 3 Parameters, Frequencies, and Residual Response of Four Boom Structure $(N_d=1,\ n=1)$						
DESIGN PARAMETERS	OPTIMAL 07533, 04065, 01837, 00723			NON-OPTIMAL 03539		
MODELED NATURAL FREQUENCIES (HZ)	0, 1 396, 3 434, 7 508			0, 778, 3 972, 11 097		
RESIDUAL MODE	NATURAL FREQ(HZ)	FINAL DISPL	FINAL VELOC	NATURAL FREQ(HZ)	FINAL DISPL	FINAL VELOC
5	17 354	9×10^{-5}	-2×10^{-2}	21 864	5×10^{-4}	3×10^{-2}
6	23 558	6×10^{-6}	5×10^{-3}	40 650	-3×10^{-5}	-1×10^{-2}
7	40 627	-4×10^{-6}	$-.2 \times 10^{-3}$	65 279	1×10^{-5}	$-.6 \times 10^{-3}$
8	72 831	$-.7 \times 10^{-6}$	-2×10^{-4}	103 480	-2×10^{-6}	2×10^{-4}
9	141 034	-2×10^{-6}	2×10^{-4}	169 779	-4×10^{-7}	4×10^{-4}

Table 4 Residual Response of Four Boom Structure with Rigid Body Optimal Control $(N_d=4,\ n=1)$						
DESIGN PARAMETERS	OPTIMAL 07533, 04065, 01837, 00723			NON-OPTIMAL 03539		
RESIDUAL MODE	NATURAL FREQ(HZ)	FINAL DISPL	FINAL VELOC	NATURAL FREQ(HZ)	FINAL DISPL	FINAL VELOC
2	1 396	-6×10^{-3}	2×10^{-1}	0 778	5×10^{-1}	3×10^{1}
3	3 434	7×10^{-4}	-7×10^{-2}	3 972	6×10^{-3}	$.1 \times 10^{-1}$
4	7 508	-8×10^{-5}	-1×10^{-2}	11 097	4×10^{-4}	2×10^{-2}
5	17 354	$.8 \times 10^{-5}$	-2×10^{-2}	21 864	$.5 \times 10^{-5}$	5×10^{-3}
6	23 558	6×10^{-6}	5×10^{-3}	40 650	9×10^{-6}	$.2 \times 10^{-3}$
7	40 627	$-.4 \times 10^{-6}$	-2×10^{-3}	65 279	$.3 \times 10^{-6}$	9×10^{-4}
8	72 831	-6×10^{-6}	-2×10^{-3}	103 480	7×10^{-7}	4×10^{-4}
9	141 034	-2×10^{-6}	2×10^{-4}	169 770	6×10^{-6}	5×10^{-5}

Table 5
Parameters, Frequencies, and Residual Response
For Structure with Five Characteristic Frequencies
($N_d=4$, $n=1$)

DESIGN PARAMETERS		07132, 04079, 01906, 00779	
RESIDUAL MODE	NATURAL FREQ(HZ)	FINAL DISPL	FINAL VELOC
2	1 4303	-3×10^{-7}	-1×10^{-5}
3	3 4709	-9×10^{-9}	2×10^{-6}
4	7.4865	-3×10^{-9}	4×10^{-6}
5	17 4942	2×10^{-7}	-6×10^{-4}
6	24 3927	1×10^{-5}	$-.5 \times 10^{-3}$
7	42 0657	-2×10^{-5}	1×10^{-3}
8	72 1615	$-.8 \times 10^{-6}$	$.1 \times 10^{-3}$
9	136 5019	-4×10^{-7}	7×10^{-4}

Table 6
Parameters and Lowest Eight Natural Frequencies of Four Boom Structure
($n=4$)

$N_d=8$		$N_d=16$	
OPTIMAL PARAMETERS	NATURAL FREQUENCIES(HZ)	OPTIMAL PARAMETERS	NATURAL FREQUENCIES(HZ)
01623	0.	.08733	0
.04658	1 395	.06572	1.410
.03657	2.444	.05220	2 453
.02744	4.504	.04260	4 453
.01831	8.887	.03500	7.010
.01070	15.177	02879	10 931
.00638	22 871	.02371	16 148
00200	28 220	.01952	23.118
		.01620	
		.01357	
		.01118	
		.00877	
		00616	
		.00364	
		.00200	
		00085	

Figure 1
Actual Control Cost vs. Frequency - Simple Example
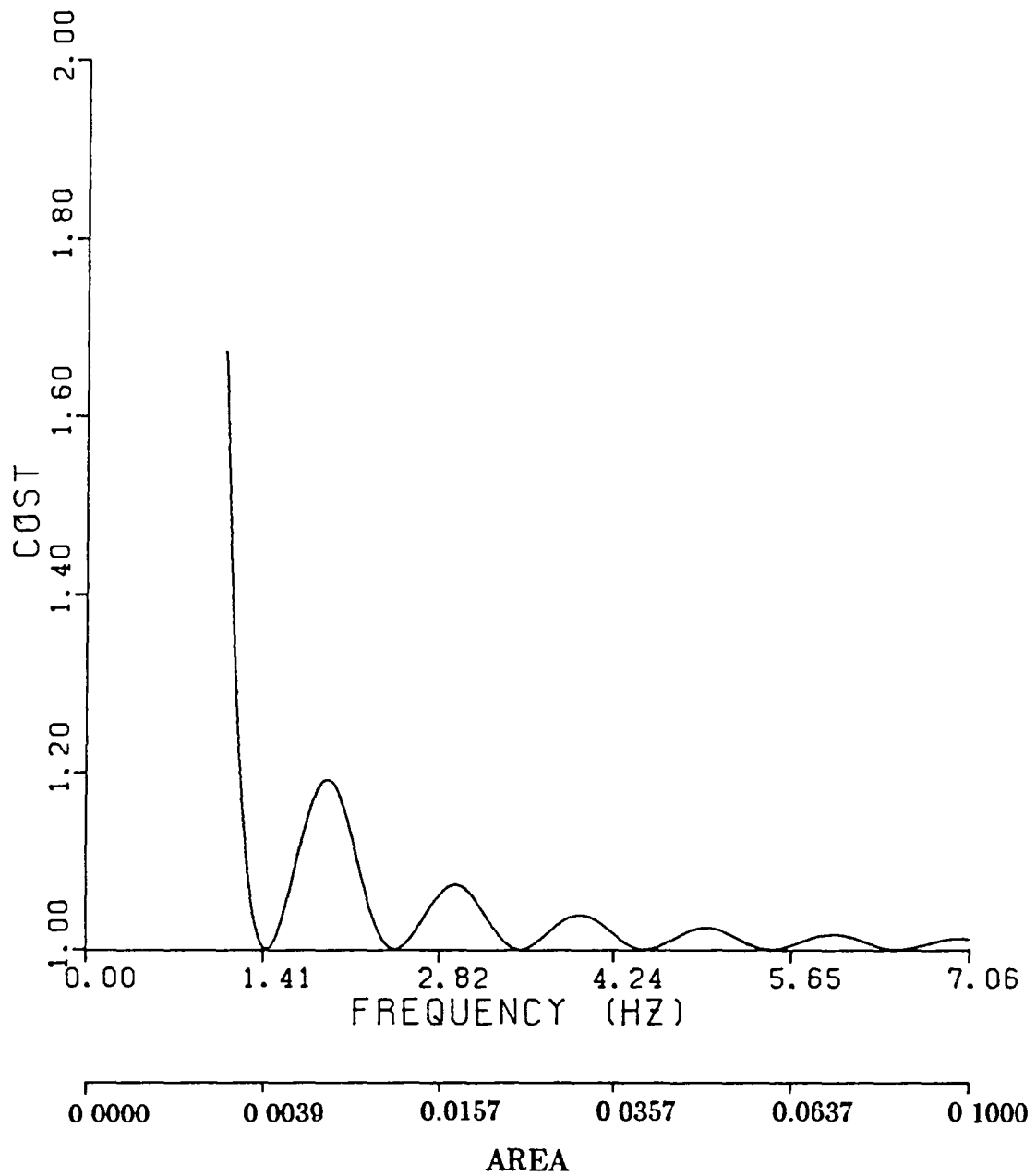
Figure 2
Ratio of Control Costs vs. Frequency - Simple Example
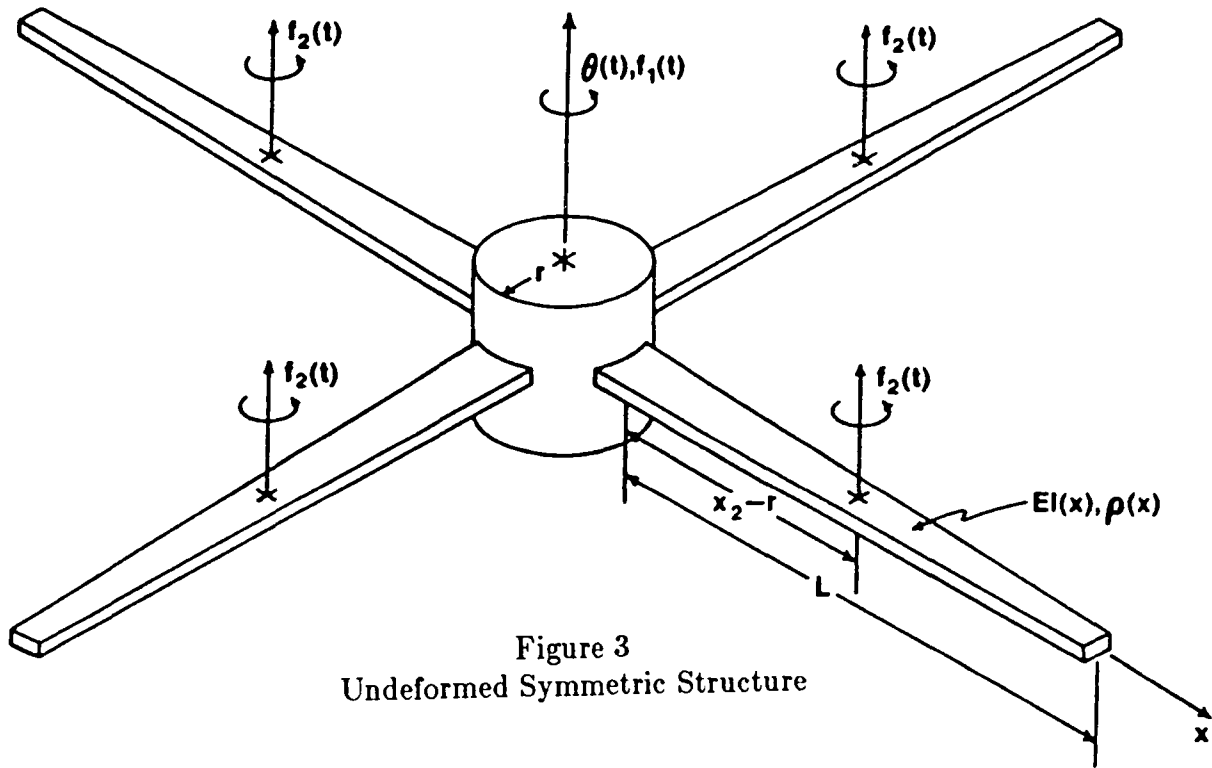
Figure 3
Undeformed Symmetric Structure

EI(x), ρ(x)
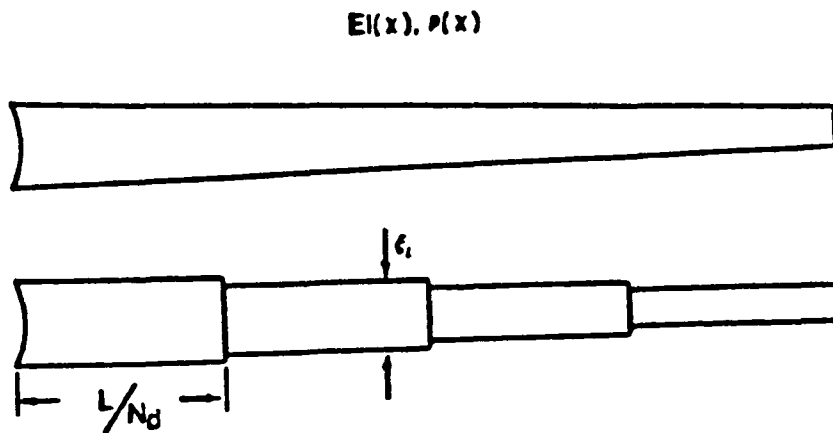
Figure 4
Finite Element Model of Flexible Boom

280
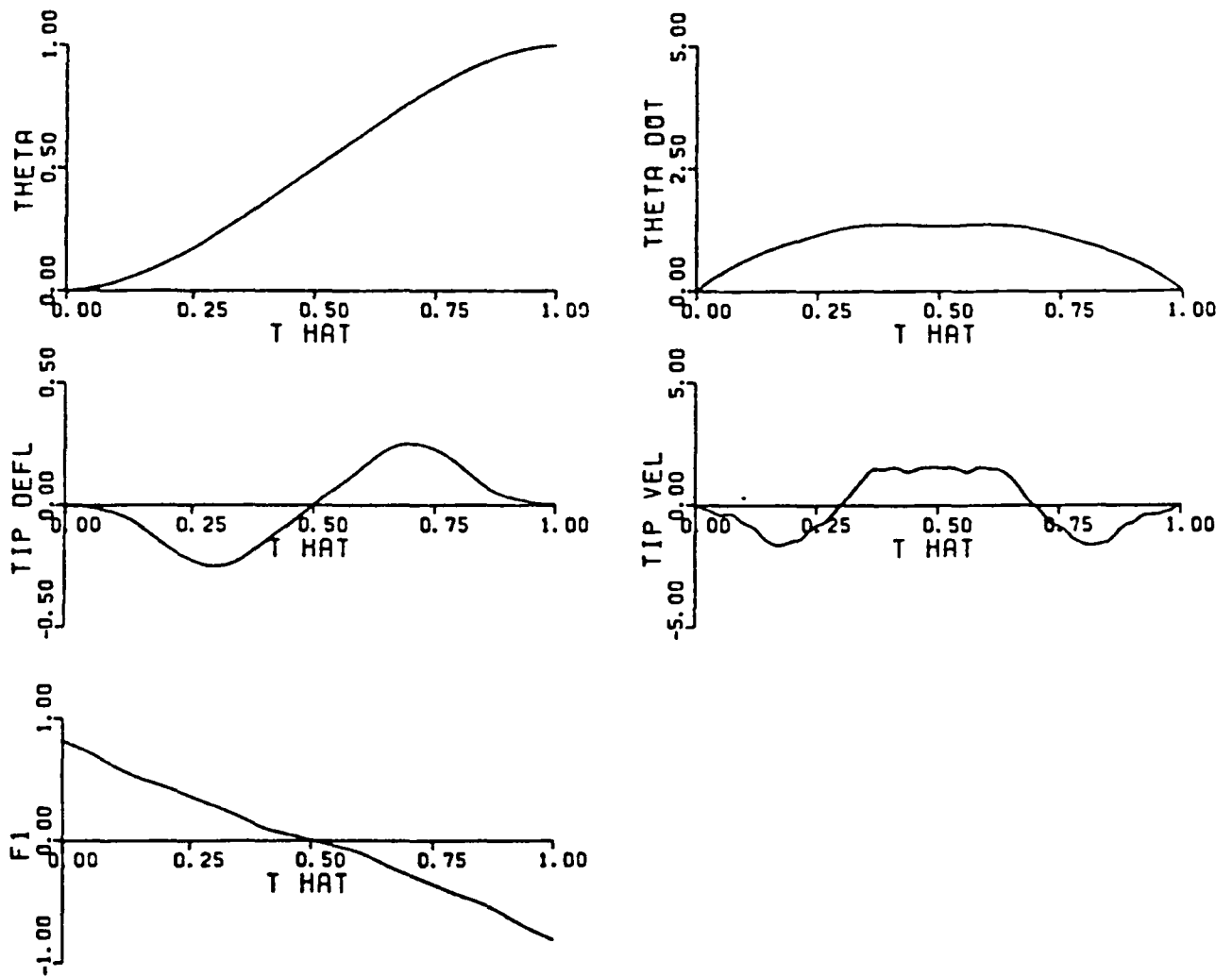
Figure 5
Time Histories for the Optimal Structure ($N_d=4$, $n=4$)
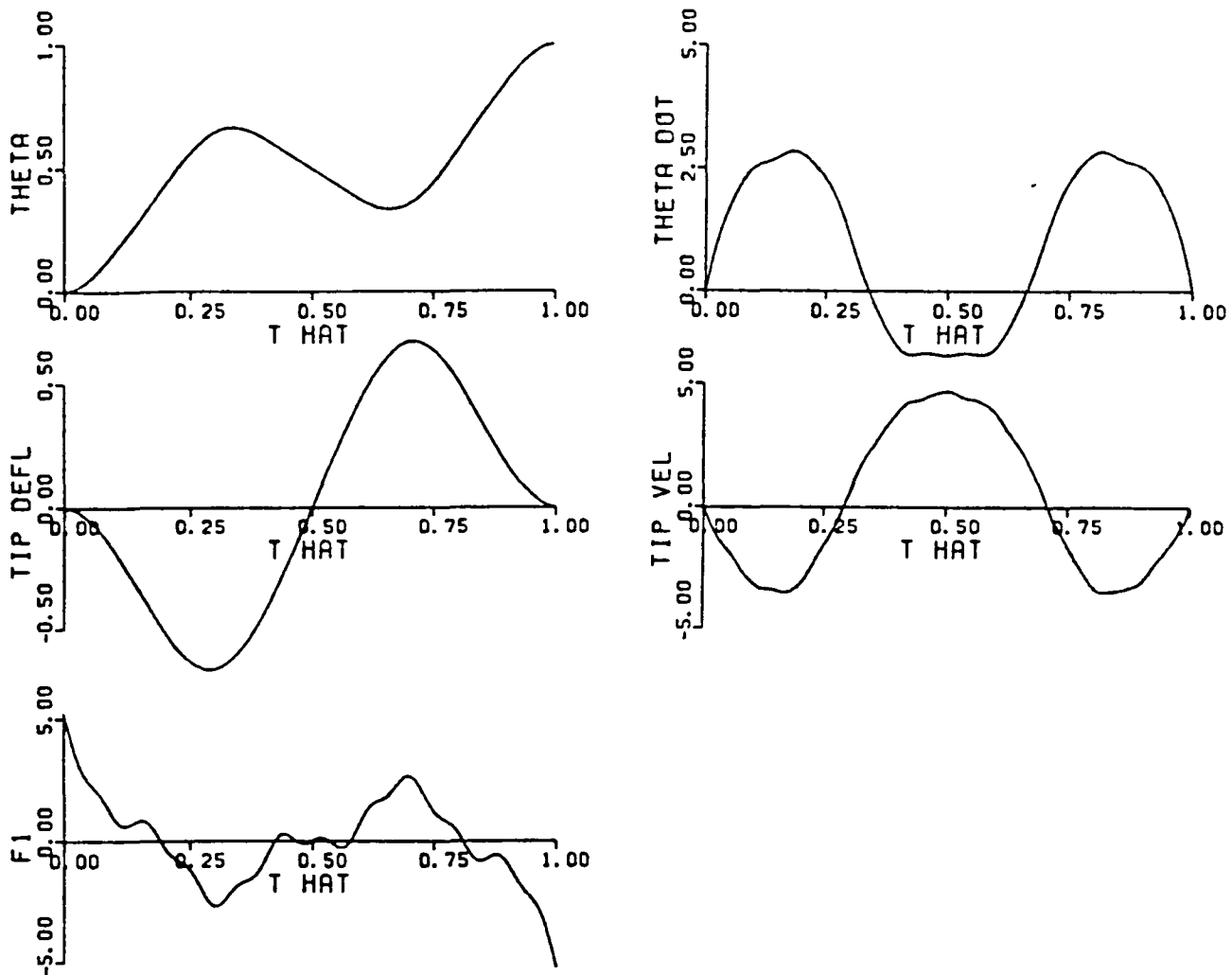
Figure 6
Time Histories for the Non-Optimal Structure ($N_d=4$, $n=4$)
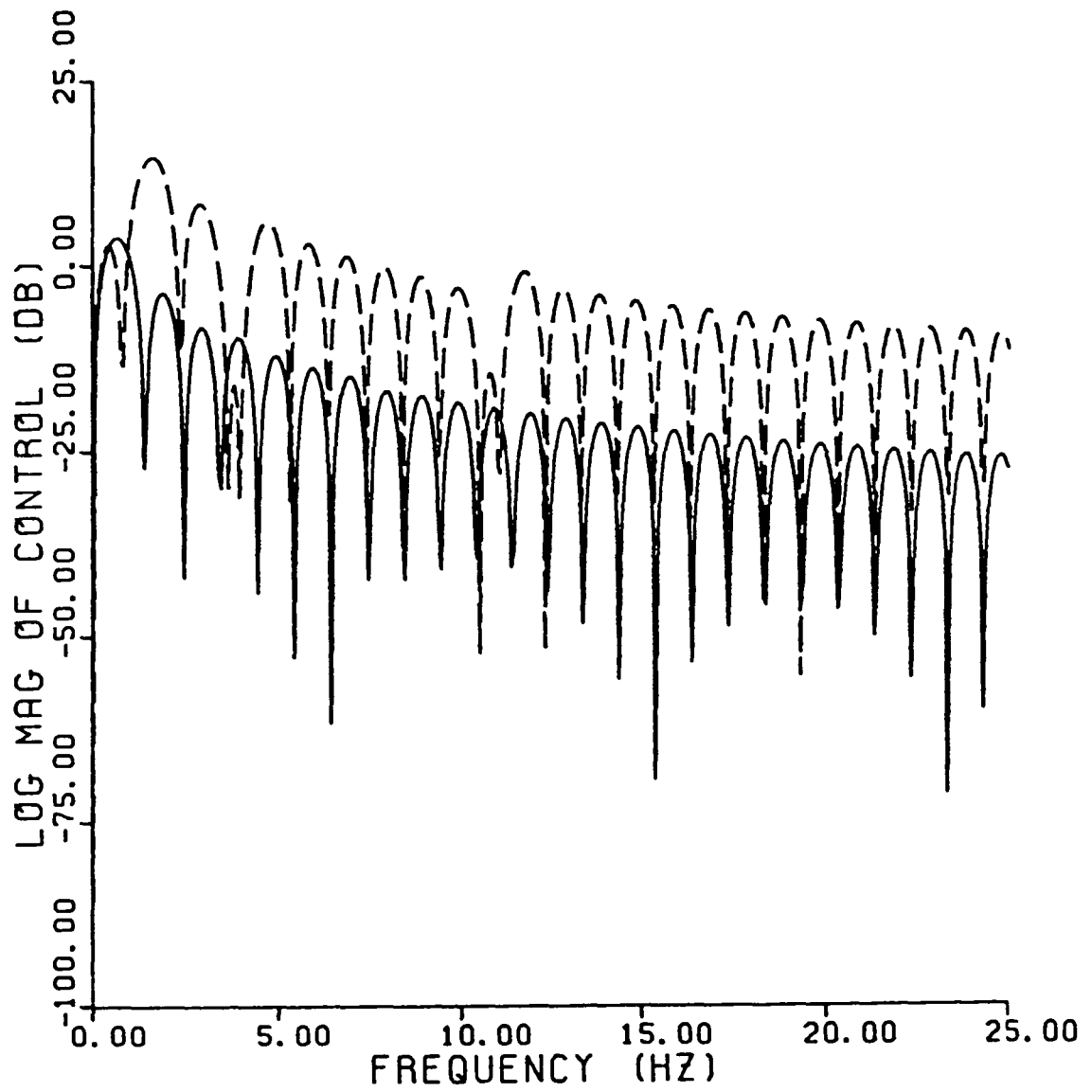
Figure 7
Magnitude Spectra of Optimal Control ($N_d=4$, $n=4$)
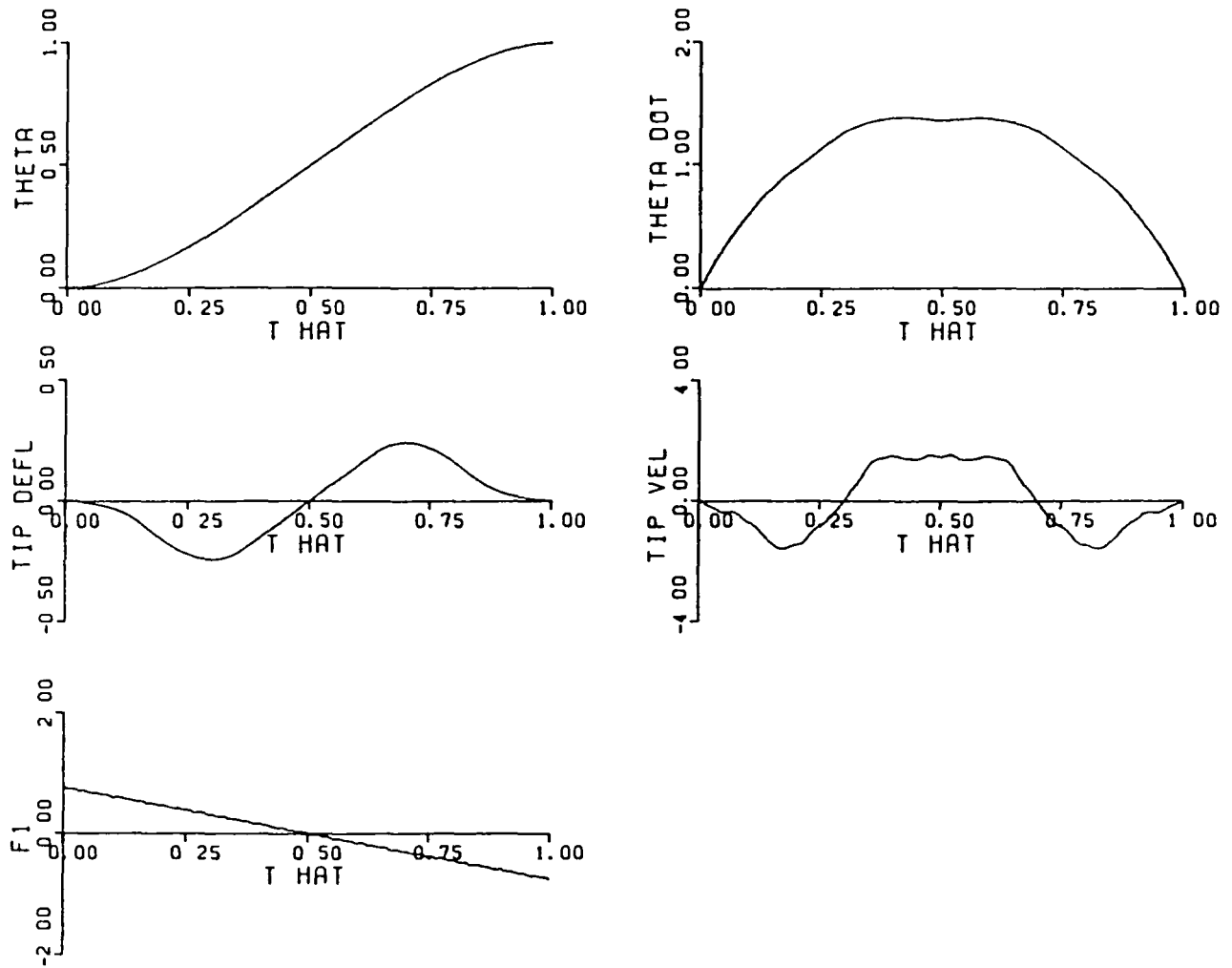
Figure 8
Optimal Control Time Histories for the Characteristic Structure
$(N_d=4,\ n=9)$
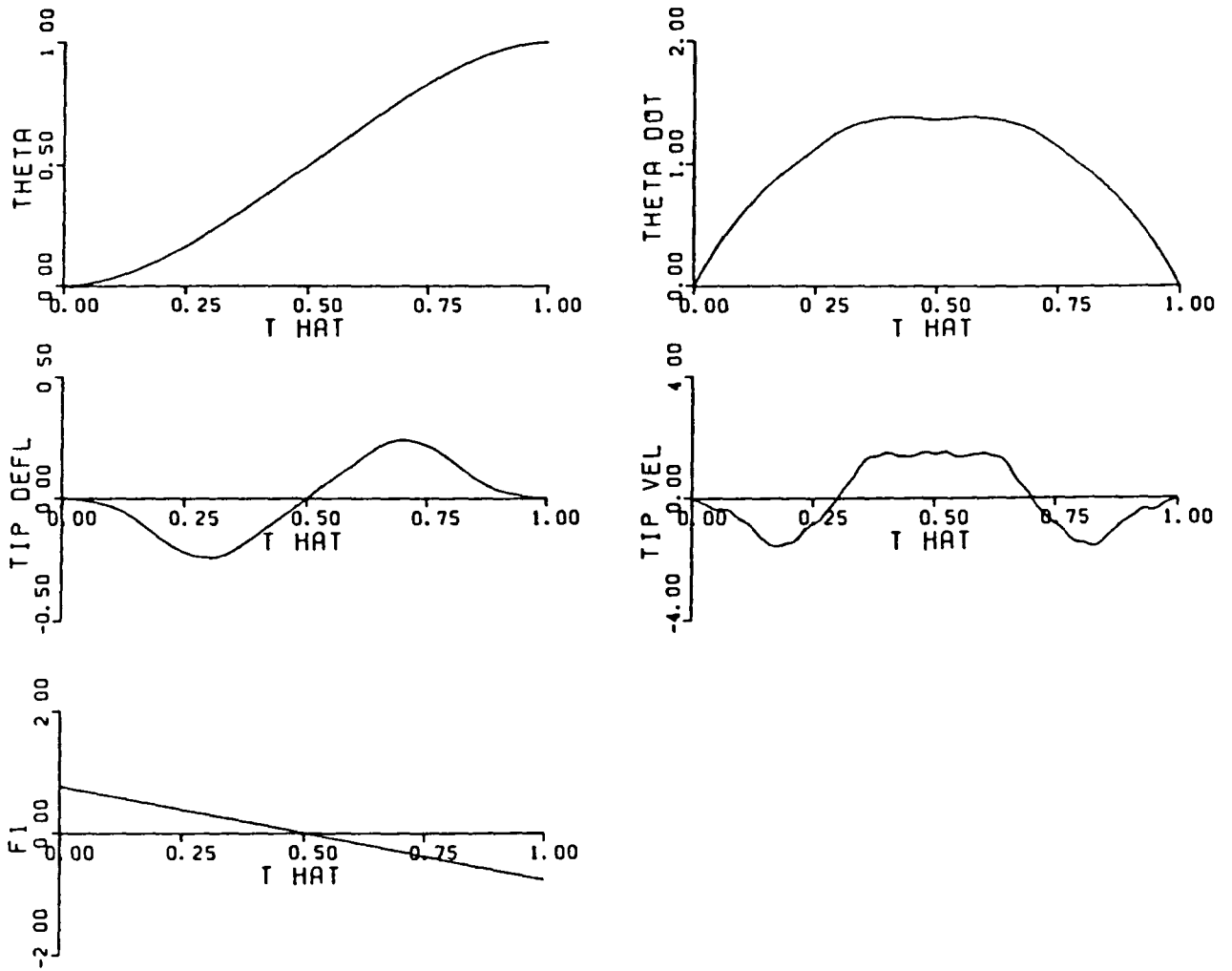
Figure 9
Time Histories for the Rigid Body Optimal Control
Applied to the Characteristic Structure
$(N_d=4)$
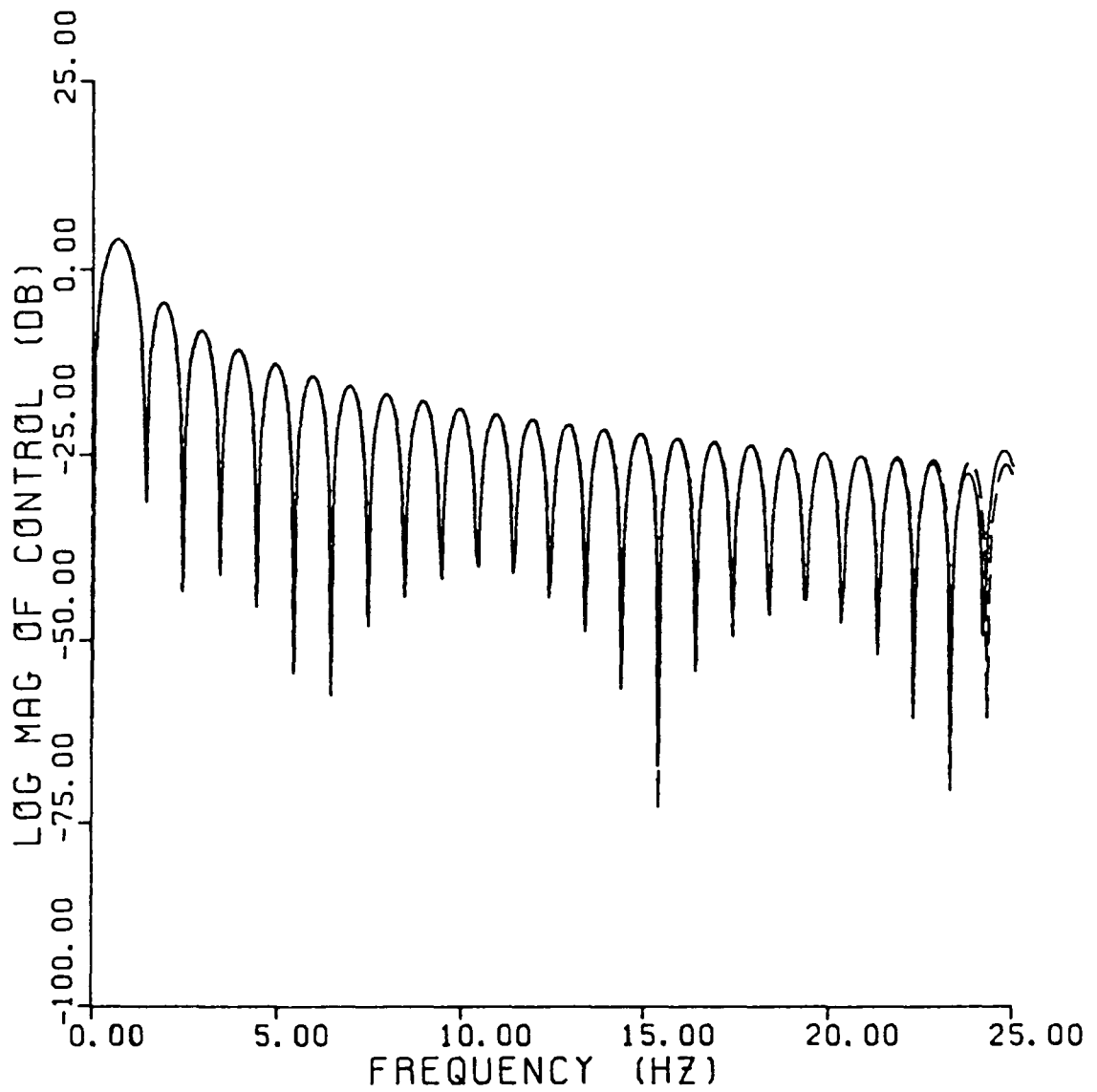
Figure 10
Magnitude Spectra of Optimal Controls For the Characteristic Structure
$(N_d=4)$

ISAAC (INTEGRATED STRUCTURAL ANALYSIS AND CONTROL) VIA CONTINUUM MODELING AND DISTRIBUTED FREQUENCY DOMAIN DESIGN TECHNIQUES

C. L. Gustafson, M. Aswani, A. L. Doran, and G. T. Tseng
The Aerospace Corporation
Los Angeles, CA 90009

ABSTRACT

This paper proposes a methodology for the integrated design of structures and their controls. The integration of design is accomplished through simultaneous selection, via optimization, of designer-specified parameters governing the structure and its controller. The cost function is chosen to address the primary structural and control goals. Inequality constraints are added to insure that additional design requirements are met.

The methodology is illustrated through development of an example involving a cantilever beam. A distributed transfer function is derived from the Bernoulli-Euler beam equation. A controller parametrization is then chosen, and performance requirements specified. A controller is then obtained via optimization, which is shown to give good performance.

287

I. Introduction

In this paper, we propose a methodology for the <u>integrated</u> design of structures and their controls. The integration of design is accomplished through <u>simultaneous</u> selection, via <u>optimization</u> [1, 2] (provide excellent references on optimization), of designer-specified parameters governing the structure and its controller ([3, 4, 5] present various optimization-based design approaches). The cost function of the optimization problem is chosen to address the primary <u>structural and control</u> design goals. Inequality constraints are added to insure that additional design requirements are met.

Historically, the design of a large, flexible space structure and its control policy has been an expensive and time consuming process. Because design goals have often necessitated the intertwining of control and structural frequencies, this process has become <u>sequential</u>, in which <u>separate</u> control and structural engineering groups <u>iterate</u> towards a final design. It is even possible that this process might not converge.

A hybrid model is developed for the structure using discrete modeling for rigid components, and equivalent continuum modeling [6, 7, 8, 9] for the flexible components. Partial differential equations (PDE's) are obtained from the equivalent continuum model, and solved in the <u>frequency</u> domain so that explicit dependence upon structural parameters is achieved. This solution is in <u>distributed</u> form, which thus retains all modal information available in the PDE.

This modeling approach necessitates the use of distributed frequency domain control design techniques; a parametrized design technique suggested by Zames [10] and later developed in [11, 12] is used. Using such a technique, the designer can specify control parameters best suited to a particular problem. This approach has been used in the past, with optimization, <u>solely</u> for control design [5, 13].

As the approaches to the modeling and control problems both allow <u>explicit</u> dependence on design parameters, the selection of the two sets of parameters

can be combined into a single optimization problem, thus avoiding an iterative design process.

To illustrate the methodology, a simple design example involving a cantilever beam is given in section III.

The paper is organized as follows:

Section I   -   Introduction and Notation
Section II   -   Design Methodology
Section III -   Design Example
Section IV   -   Conclusions

$a = b$ means "a denotes b." R denotes the real line and C denotes the complex plane. C_+ (C_-, resp.) denotes the closed right (left, resp.) plane $Re(s) \geq 0$ ($Re(s) \leq 0$).

$f \in A_-$ iff $f(t) = f_a(t) + \sum_{i=0}^{\infty} f_i \delta (t_i - t_1)$ where

f_a R$\rightarrow$R with $\bar{f}_a(t) = 0$ for $t<0$, and $t_o = 0$, $t_i>0$, $f_i \in R$, for $i \geq 1$

subject to:

(i) There exists $\epsilon > 0$, such that:

$$\int_o^{\infty} |f_a(t)| \, e^{\epsilon t} < \infty$$

(ii) There exists $\epsilon > 0$, such that

$$\sum_{i=0}^{\infty} |f_i| e^{\epsilon i} < \infty$$

$\hat{f}$ denotes the Laplace transform of f. $\hat{A}_- = \{\hat{f}: f \in A_-\}$. $\hat{A}_-^{\infty}$ ($\hat{A}_{-,o}$, resp.), denotes the subset of $\hat{A}_-$ consisting of those $\hat{f}$ that are bounded away from zero at infinity in C_+ ($\hat{f}$ that go to zero at infinity in C_+, resp.).

$\hat{B} := [\hat{A}_-] [\hat{A}_-^{\infty}]^{-1}$, the commutative algebra of fractions
$\hat{g} = \hat{n}/\hat{d}$ where $\hat{n} \in \hat{A}_-$ and $\hat{d} \in \hat{A}_-$ [14-16].

$\hat{B}_o := [\hat{A}_{-,o}] [\hat{A}_-^{\infty}]^{-1}$

Roughly speaking, $\hat{A}_-$ denotes the set of <u>proper stable, distributed</u> transfer functions, $\hat{A}_{-,o}$ denotes the set of <u>strictly proper, stable, distributed</u> transfer functions, $\hat{B}$ denotes the set of <u>proper, possibly unstable, distributed</u> transfer functions, and $\hat{B}_o$ denotes the set of <u>strictly proper, possibly unstable distributed</u> transfer functions. See [14-16] for more.

If S is a set, then E(S) denotes the set of <u>all</u> matrices having elements in S, and $S^{n \times m}$ denotes the set of all nxm matrices having elements in S.

For $H \in \hat{B}^{n \times m}$, H' denotes the derivative of H, i.e., $H'(s) := \frac{d}{ds} H(s)$, for almost all $s \in C$.

II. Design Methodology

II.1 Continuum modeling

A methodology was developed to obtain equivalent continuum models for truss type structures with a pattern of repeating elements. The procedure, summarized in Figure 1, essentially consists of deriving elastic and dynamic properties for the equivalent continuum model in terms of the geometric and material properties of the original truss structure. The details of the procedure may be found in [6]. Such an approach was used in obtaining an equivalent continuum model for a truss type beam problem discussed in Section III.

The ECM approach provides useful insight into the basic characteristics of a structure. In particular, useful trade studies can be carried out to enhance the structural performance. These studies are made possible because the ECM approach describes the structure by a set of PDE's. A closed form solution may exist, simplifying the simultaneous design process. The example covered in section III will show how useful such a closed form solution is. Even if closed form solutions are not easily obtained, writing the ECM as a PDE facilitates application of a numerical technique useful to the control design, as presented in [13].

APPROACH

Truss Structure - Solve Using FEM
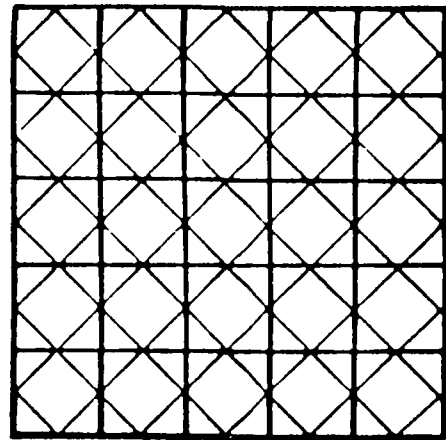
Isolate Repeating Element
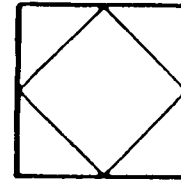
Geometric Properties
A, l
Material Properties
ρ, E

Repeating Element

Identical B. C.
and
Loading
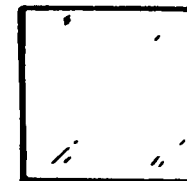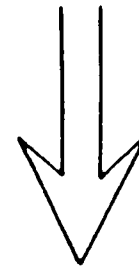
Determine Elastic
and
Dynamic Properties
in terms of E, ρ, l, A

Equivalent Continuum Element

Use Equivalent Continuum
Properties and Formulate
the Continuum Problem
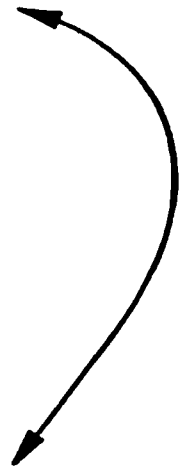
Equivalent Continuum Model
Closed Form/Numerical Solution

FIGURE 1

II.2 Control Theory

II.2.1 Preliminaries

We will consider the feedback system of Figure II throughout the paper.
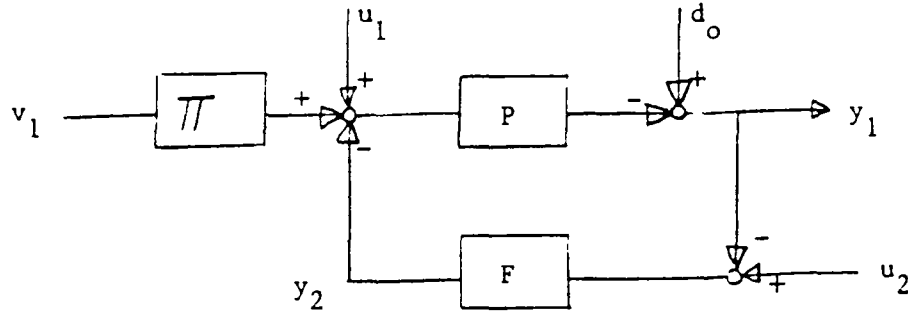
FIGURE II. S(P,F,Π)

In Figure II, P represents the plant, F the feedback compensator, and Π the pre-compensator. All are assumed to be linear distributed time-invariant MIMO transfer functions. We will need the following assumption.

(P1) $P \epsilon \hat{B}_o^{n_o \times n_1}$ (P is strictly proper)

(P2) $P \epsilon \hat{A}_{-,o}^{n_o \times n_1}$ (P is strictly proper and stable)

(F1) $F \epsilon \hat{B}^{n_1 \times n_o}$ (F is proper)

(Π1) $\Pi \epsilon \hat{A}^{n_1 \times n_i}$ (Π is proper and stable)

Under (P1) and (F1), $\det(I + PF)^{-1} \epsilon \hat{B}$ [14-16], and thus S(P,F,Π) is well-posed* and described by the following equations.

────────────────────

*well-posed means that $(I + PF)^{-1}$ and $(I + FP)^{-1} \epsilon E(\hat{B})$

292

$$
\begin{bmatrix} y_\iota \\ y_1 \\ y_2 \end{bmatrix} = \begin{bmatrix} \Pi & 0 & 0 & 0 \\ P(I+FP)^{-1}\Pi & P(I+FP)^{-1} & F(I+PF)^{-1} & (I+PF)^{-1} \\ FP(I+FP)^{-1}\Pi & FP(I+FP)^{-1} & -PF(I+PF)^{-1} & F(I+PF)^{-1} \end{bmatrix} \begin{bmatrix} v_1 \\ u_1 \\ u_2 \\ d_0 \end{bmatrix} \qquad (2.10)
$$

We define the individual transfer functions as follows:

$$
\begin{bmatrix} y_\iota \\ y_1 \\ y_2 \end{bmatrix} = \begin{bmatrix} H_{y_1 v_1} & H_{y_i u_1} & H_{y_1 u_2} & H_{y_i d_0} \\ H_{y_1 v_1} & H_{y_1 u_1} & H_{y_1 u_2} & H_{y_1 d_0} \\ H_{y_2 v_1} & H_{y_2 u_1} & H_{y_2 u_2} & H_{y_2 d_0} \end{bmatrix} \begin{bmatrix} v_1 \\ u_1 \\ u_2 \\ d_0 \end{bmatrix} \qquad (2.11)
$$

If we now define $u := [v_1^T \quad u_1^T \quad y_2^T \quad d_0^T]^T$ and $y := [y_i^T \quad y_1^T \quad y_2^T]^T$, then (2.11) defines $H_{yu} \in E(\hat{B})$ as follows:

$$
y = H_{yu} \cdot u \qquad (2.12)
$$

This leads to the following definition

Definition 2.1: The closed loop system $S(P,F,\Pi)$ is said to be $\hat{A}_-$- stable if and only if $H_{yu} \in E(\hat{A}_-)$.

The feedback system $S(P,F,\Pi)$ can be shown to have two degrees of freedom in the sense of Horowitz [17]. Roughly speaking, this is because $H_{y_1 d_0}$ and $H_{y_1 u_1}$ can be selected independently.

Stability analysis of $S(P,F,\Pi)$ is greatly simplified through use of the following matrix parameter [10].

$$
Q := H_{y_1 u_2} = H_{y_2 d_0} = F(I+PF)^{-1} \qquad (2.13)
$$

The equations (2.10) can be rewritten in terms of P, Q, and π.

$$
\begin{bmatrix} y_1 \\ y_1 \\ y_2 \end{bmatrix}
=
\begin{bmatrix}
\pi & 0 & 0 & 0 \\
P(I-QP)\pi & P(I-QP) & Q & I-PQ \\
QP\pi & QP & -PQ & Q
\end{bmatrix}
\begin{bmatrix} v_1 \\ u_1 \\ u_2 \\ d_0 \end{bmatrix}
\qquad (2.14)
$$

Note that F can be obtained from P and Q as follows.

$$
F = Q(I - PQ)^{-1} \qquad (2.15)
$$

II.2.2 Stability Theory and Design Parametrization

The following theory not only gives necessary and sufficient conditions for $\hat{A}_-$ - stability of $S(P,F,\Pi)$, but also gives a parametrization of all compensators which stabilize a given plant. This parametrization will be utilized in the design algorithm of section II.3.

Theorem 2.1: [11] Let P satisfy (P2). Then $S(P,F,\Pi)$ is $\hat{A}_-$ - stable with F satisfying (F1) if and only if

$$
(\mathrm{i}) \qquad Q \in \hat{A}_-^{\,n_i \times n_o} \qquad\qquad (2.16)
$$

$$
(\mathrm{ii}) \qquad \Pi \in \hat{A}_-^{\,n_i \times n_i} \qquad\qquad (2.17)
$$

Remark: The class of all compensators F stabilizing P is thus:

$$
F := \{ Q(I-PQ)^{-1} : Q \in \hat{A}_-^{\,n_i \times n_o} \} \qquad (2.18)
$$

This result can be extended to the case where P is unstable as follows.

Theorem 2.2: [12] Let P satisfy (P1). Additionally, let P be given by

$$P(s) = \frac{1}{(s-\lambda_1)^2} R_{12} + \frac{1}{s-\lambda_1} R_{11} + P_\alpha(s) \tag{2.19}$$

where $\lambda_1 \in C_+$, R_{12}, R_{11}, $\in C^{n_o \times n_i}$, and $P_\alpha \in \hat{A}_{-,o}^{n_o \times n_i}$. Then $S(P,F,\Pi)$ is $\hat{A}_-$-stable with F satisfying (F1)

(i) $Q \in \hat{A}_-^{n_1 \times n_o}$ \hfill (2.20)

(ii) $\Pi \in \hat{A}_-^{n_i \times n_1}$ \hfill (2.21)

(iii) $Q(\lambda_1)R_{12} = 0$ and $R_{12}Q(\lambda_1) = 0$ \hfill (2.22)

(iv) $Q(\lambda_1)R_{11} = -Q'(\lambda_1)R_{12}$ and $R_{11}Q(\lambda_1) = -R_{12}Q'(\lambda_1)$ \hfill (2.23)

(v) $R_{12} H_{y_1 u_1}(\lambda_1) = 0$ \hfill (2.24)

(vi) $R_{11} H_{y_1 u_1}(\lambda_1) + R_{12} H'_{y_1 u_1}(\lambda_1) = 0$ \hfill (2.25)

Remark: Conditions (iii) - (vi) simplify greatly when R_{12} has full rank, becoming:

(iii) $Q(\lambda_1) = 0$ \hfill (2.26)

(iv) $Q'(\lambda_1) = 0$ \hfill (2.27)

(v) $H_{y_1 u_1}(\lambda_1) = 0$ \hfill (2.28)

(vi) $H'_{y_1 u_1}(\lambda_1) = 0$ \hfill (2.29)

These results indicate that $(Q, Q', H_{y_1 u_1}$ and $H'_{y_1 u_1}$ must have <u>blocking zeros</u> at $s = \lambda_1$. In (2.22) - (2.25), only <u>transmission zeros</u> are required. Thus, (2.26) - (2.29) represent more conservative constraints.

II.3 Design Algorithm

In this section, we develop a general, somewhat conceptual algorithm for the integrated design of structures and controls. This algorithm incorporates the modeling techniques of section II.1 and the control theory of section II.2 to jointly parametrize the structural and control designs. A joint optimization problem is then formulated to simultaneously solve for the structural and control parameters.

Algorithm 2.1

Step 1: Using continuum modeling, develop partial differential equations (and ordinary differential equations) describing the motion of the structure, which depend explicitly on a designer-specified parameter vector $x \in R^{p1}$.

Step 2: Calculate a distributed transfer function $P \in \hat{B}_o^{n_o \times n_i}$ for the structure which maintains an explicit dependence on the structural parameters in x.

Step 3: Choose a representation for $Q \in \hat{A}_{-,o}^{n_i \times n_o}$ which is dependent upon a designer-specified control parameter vector $y \in R^{p2}$.

Step 4: Formulate a joint optimization problem which translates design goals into a cost function and inequality constraints as follows:

$$\min_{x,y} \quad f(x,y)$$

subject to:

$$\sup_{\omega_i \in \Omega_i} g_i(x,y,\omega_i) \le \ell_i(\omega_i) \qquad\qquad , i = 1,2,\ldots,n_g$$

$$h_k(x,y) \le b_k \qquad\qquad , k = 1,2,\ldots,n_k$$

The inequality constraints should be chosen so as to guarantee that the final values of x and y that result in structures and controllers that can actually be implemented.

Remark: This algorithm requires having $P \in \hat{B}_o^{n_o \times n_i}$, a distributed transfer function. Since the ECM of a structure is in PDE form, obtaining a distributed transfer requires taking a Laplace transform, and evaluating boundary conditions. In general these operations could be difficult. To avoid this problem, P can be calculated at discrete points (commonly along the $j\omega$-axis), directly from the PDE, using only complex arithmetic. Such an approach has been developed [13], and applications and extensions are being investigated.

III. Design Example

This section demonstrates the methodology of section II through application to the example of a cantilever beam. The beam considered (see Figure III) has a torque actuator and displacement sensor located at its tip. We assume that it has the truss structure of Figure IV, and has length $L = 1000$ ft. Finally, we assume that the displacement $v(x,t)$ is given by the Euler-Bernoulli beam equation:

$$EI \ v_{xxxx} = -\rho v_{tt} \tag{3.1}$$

subject to:
$$v(0,t) = 0 \tag{3.2}$$

$$v_x(0,t) = 0 \tag{3.3}$$

$$EI \ v_{xx}(L,t) = T(t) \tag{3.4}$$

$$EI \ v_{xxx}(L,t) = 0 \tag{3.5}$$

where E is the equivalent modulus of elasticity, I is the equivalent cross-sectional inertia, and ρ is the equivalent density. $T(t)$ is the applied torque.

BEAM MODEL
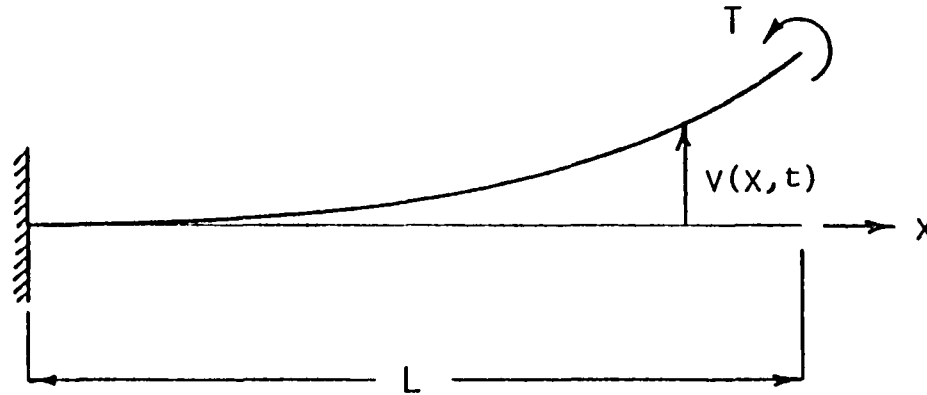
BEAM EQUATION: $EI\ v_{xxxx} = -\rho v_{tt}$

BOUNDARY CONDITIONS: $v(o,t) = 0$ $EI\ v_{xx}(L,t) = T(t)$

$v_x(o,t) = 0$ $EI\ v_{xxx}(L,t) = 0$

FIGURE   III

TRUSS STRUCTURE

E_{ROD} = 10×10^6 PSI

A_{ROD} = 0.2 IN^2

υ = 0.33

ρ_{ROD} = 0.1 LBS/IN^3

120"

120"

120"

L
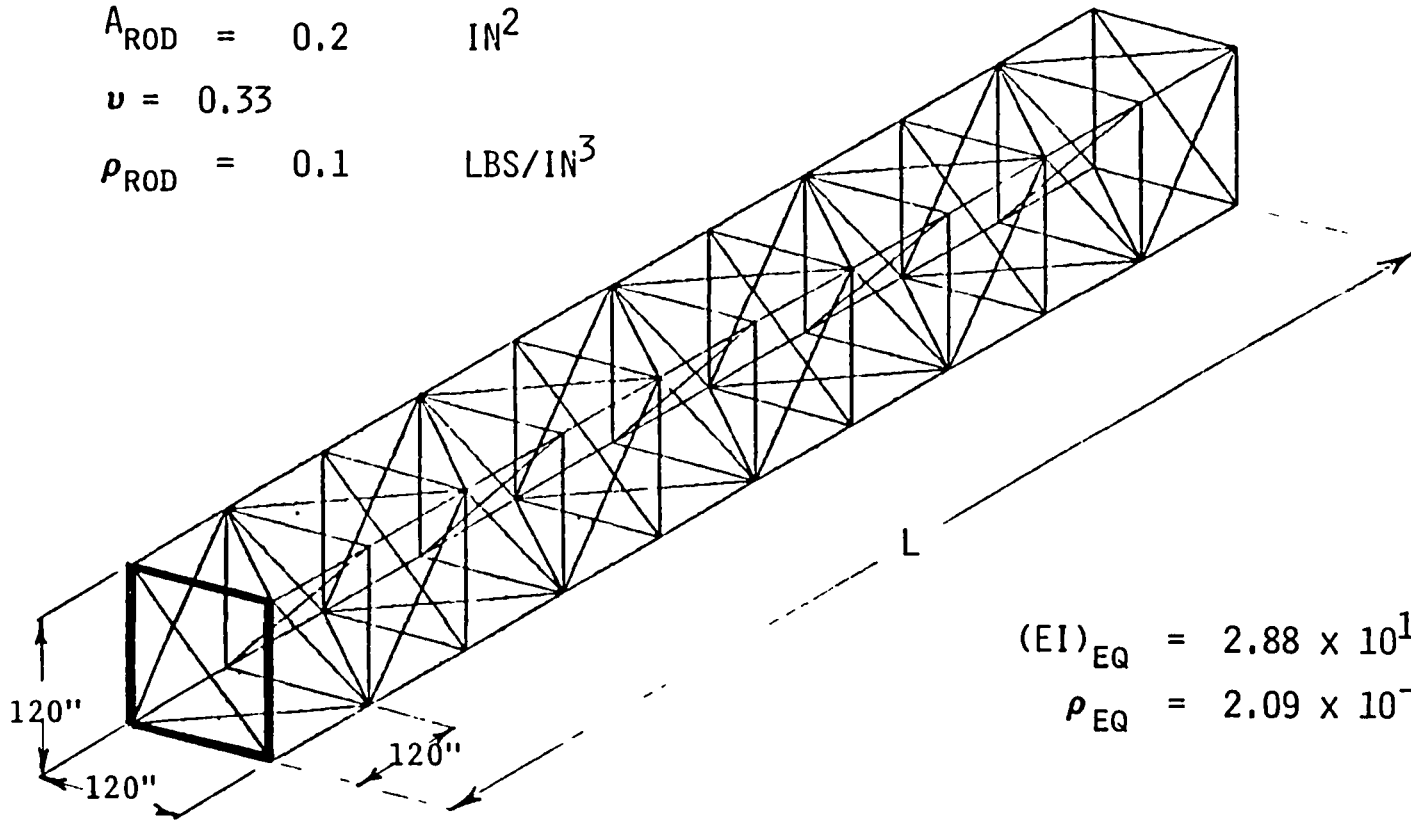
$(EI)_{EQ}$ = 2.88×10^{10} PSI

ρ_{EQ} = 2.09×10^{-5} LBS/IN^3

FIGURE IV

III.1 Equivalent Continuum Model

We parametrize the beam equations (3.1) - (3.5) by two structural parameters: EI and ρ. If the truss structure in Figure IV is made of aluminum, and the rods are assumed to have cross-sectional area $A = 0.2$ in^2, then the equivalent EI and ρ, as calculated by the method of [6] are:

$$EI = 4.15 \cdot 10^{12} \text{ lbf} - \text{ft}^2$$
$$\rho = .108 \text{ sl/ft}$$

If composite materials are substituted for the aluminum, stiffness increases and mass decreases. A reasonable range is:

$$4.15 \cdot 10^{12} \text{ lbf} - \text{ft}^2 \le EI \le 2.08 \cdot 10^{13} \text{ lbf} - \text{ft}^2 \qquad (3.6)$$

$$.054 \text{ sl/ft} \le \rho \le .108 \text{ sl/ft} \qquad (3.7)$$

These values were used in the optimization procedure.

III.2 Transfer Function Derivation

We define the transfer function p as mapping the torque T to the displacement v at $x = L$. Equivalently,

$$p(s) = \frac{V(L,s)}{T(s)} \qquad (3.8)$$

where $V(L,s) := \mathcal{L}[v(L,s)] \quad *$ $\qquad (3.9)$

$T(s) \quad := \mathcal{L}[T(t)]$ $\qquad (3.10)$

---

*$\mathcal{L}[f]$ denotes the Laplace transform of f.

To find p, we first take the Laplace transform of (3.1):

$$EI_{xxxx}(x,s) = -\rho s^2 \, V(x,s) \tag{3.11}$$

This is an ordinary differential equation in x, with solution:

$$V(x,s) = c_1 e^{-\gamma Lx\sqrt{s}} \cos\gamma Lx\sqrt{s} + c_2 e^{-\gamma Lx\sqrt{s}} \sin\gamma Lx\sqrt{s} \tag{3.12}$$

$$+ c_3 e^{\gamma Lx\sqrt{s}} \cos\gamma Lx\sqrt{s} + c_4 e^{\gamma Lx\sqrt{s}} \sin\gamma Lx\sqrt{s}$$

where

$$\gamma := \sqrt{2/(EI/\rho)} \tag{3.13}$$

By taking the Laplace transform of (3.2) – (3.5), c_1, c_2, c_3, and c_4 can be found. Evaluating $V(x,s)$ at $x = L$ (thus placing the sensor at $x = L$) yields

$$p(s) := \frac{V(L,s)}{T(s)} = \frac{\cosh L\gamma\sqrt{s} - \cos L\gamma\sqrt{s}}{\sqrt{\rho \, EI} \; s(2 + \cosh L\gamma\sqrt{s} + \cos L\gamma\sqrt{s})} \tag{3.14}$$

This can be rewritten in infinite product form:

$$p(s) = \frac{L^2}{2\,EI} \cdot \frac{\displaystyle\prod_{n=1}^{\infty}\left(1 + \frac{L^4 s^2}{k^2 \pi^4 n^4}\right)}{\displaystyle\prod_{n=1}^{\infty}\left(1 + \frac{L^4 s^2}{k^2 \pi^4 (n-1/2)^4}\right)} \tag{3.15}$$

where $k := \sqrt{\dfrac{EI}{\rho}}$

The poles of this form are approximate, with the exact poles given by:

$$P_n = \pm j \frac{k}{L^2} a \tag{3.16}$$

where $a \in R$ solves:

$$\cosh a \cos a = 1 \tag{3.17}$$

(3.14) and (3.15) clearly retain an explicit dependence on EI and, ρ (and L – though we have chosen a fixed L = 1000 ft.).

301

III.3 Control Problem and Parameterization

To illustrate the design methodology we will consider the following control problem: stabilize the closed-loop system, and suppress a 25 Hz disturbance torque applied at the end of the beam.

To provide a means for accomplishing this, we parameterize $q \in \hat{A}_-$ as follows (and choose $\pi = 1$):

$$q(s) = \frac{(a_n s^2 + b_n s + c_n)(s^2 + 2\zeta_n \omega_n s + \omega_n^2)(2 + \cosh L\gamma\sqrt{s} + \cos L\gamma\sqrt{s})}{\displaystyle\prod_{i=1}^{2}(s^2 + 2\zeta_{di}\omega_{di} s + \omega_{di}^2)\,\cosh\alpha\sqrt{s}} \qquad (3.18)$$

The third numerator term is included so that no plant poles occur in all transfer functions except $H_{y_1 v_1}$ and $H_{y_1 u_1}$. The third denominator term is included to insure the properness of q (only if $\alpha > L\gamma$). To keep q stable we must choose $\alpha > 0$ (guaranteeing that $\cosh \alpha \sqrt{s}$ is analyic in C_+).We define the vector $y \in R^{10}$, the vector of control parameters, by:

$$y := [\, a_n \;\vdots\; b_n \;\vdots\; c_n \;\vdots\; s_n \;\vdots\; \omega \;\vdots\; \xi_{d1} \;\vdots\; \xi_{d2} \;\vdots\; \omega_{d2} \;\vdots\; \alpha \,]^T$$

To formulate the optimization problem, we apply equality and inequality constraints on the control parameters as follows.

First, to guarantee closed-loop stability, in accordance with Thm. 2.1, we constrain q to be $\hat{A}_-$ stable:

$$.05 \leq \omega_{di} \leq 10^4 \qquad (3.20)$$

$$\text{for } i = 1,2$$

$$.05 \leq \xi_{di} \leq 1 \qquad (3.21)$$

$$L\gamma \leq \alpha \qquad (3.22)$$

The upper bounds in (3.20) and (3.21) represent "performance" bounds; they are not stability constraints. The lower bounds give stability "constraints". The lower bound in (3.22) not only guarantees that $\cosh \alpha \sqrt{s}$ has roots with only negative real part, but that q is proper (which is necessary for q to be in $\hat{A}_-$).*

Secondly, to guarantee that a physically reasonable q is selected, we constrain:

$$.05 \leq \omega_n \leq 10^4 \qquad (3.23)$$

$$.05 \leq \xi_n \leq 100 \qquad (3.24)$$

We are not greatly concerned with the damping of the numerator zeros, so (3.24) gives a loose upper bound on ζ_n.

The parameters a_n, b_n, and c_n are selected through imposition of equality constraints on q:

$$h_{y_1 d_0} (0) = 0 \qquad (3.25)$$

$$\left. \begin{array}{l} h_{y_1 u_1} (\lambda_1) = 1 \\ \\ h_{y_1 u_1} (\bar{\lambda}_1) = 1 \end{array} \right\} \ \lambda_1 \text{ is the first plant mode} \qquad \begin{array}{l} (3.26 \\ \\ (3.27) \end{array}$$

(3.25) guarantees that the closed-loop system will have low sensitivity to output noise at low frequencies. (3.26) - (3.27) will yield a closed-loop system in which the first bending mode of the plant, λ_1, will not be an eigenvalue of he closed-loop system. This follows from Theorem 2.2.

---

*Note that the $p \in \hat{A}_{-,o}$ - thus Thm. 2.1 technically does not apply. However, the introduction of damping in p would yield $p \in \hat{A}_{-,o}$, and realistically, p does have some damping. Thus, use of a controller designed by Thm. 2.1 would yield a stable closed-loop system.

The following cost function was chosen for the optimization problem:

$$\min \left[\beta_1 p(j\omega_d) + \beta_2 h_{y_1 d_0}(j\omega_d) + \beta_3 \rho^2 \right] \qquad (3.28)$$

where β_1, β_2, β_3 are scalar weighting factors and $\omega_d = 50\Pi r/s$. By minimizing the first two terms of (3.28), the steady-state response of to the 25 hz disturbance torque is minimized. And, by minimizing the third term, the weight of the beam is minimized.

Thus, the optimization problem solved is (3.28) subject to (3.6) - (3.7), and (3.20) - (3.27).

III.4 <u>Optimization and Results</u>

Upon solution of the above optimization problem, the following parameter values were obtained:

$$
\begin{array}{llll}
a_n & = & -4.9159 \times 10^6 & \qquad \zeta_{d1} & = & .050584 \\[2mm]
b_n & = & 9.4234 \times 10^8 & \qquad \omega_{d1} & = & 158.2 \\[2mm]
c_n & = & 6.8844 \times 10^7 & \qquad \zeta_{d2} & = & .051721 & (3.29) \\[2mm]
\zeta_n & = & .18394 & \qquad \omega_{d2} & = & 161.22 \\[2mm]
\omega_n & = 8038.9 & & \qquad \alpha & = & 1.4159 \\[2mm]
EI & = & 1.3678 \times 10^{13} \text{ ft-lb} & \qquad \rho & = & .054 \text{ sl/ft}
\end{array}
$$

The optimization problem was solved using the IMSL subroutine ZXSSQ.

The resulting compensator is infinite dimensional; the finite dimensional version shown below was obtained by truncation of the compensator above the disturbance frequency:

$$C(s) = \frac{17.521(s^2+1.25 \cdot 10^5)(s^2+2957s+6.462 \cdot 10^7)(s^2-191.69s-14.004)}{s^2(s^2+18.98s+23991)(s^2+11.61s+26261)}$$

As the Bode plot of $h_{y_1 d_0}(j\omega_d)$ in Figure V indicates, there is a notch at $\omega = 50$ r/s. This notch is present because the value of EI chosen places the first zero of the beam at $\omega = 50$ r/s (for minimum ρ). Additionally, there are two compensator poles near 50 r/s. Note that the first pole of p (56 r/s) does not appear.

IV. Conclusions

This paper has presented a methodology which <u>integrates</u> the design of a structure and its controller. The methodology achieves this integration of designs via <u>joint optimization</u> of structural and control parameters. The structural parameters are obtained through differential equations resulting from hybrid modeling, and the control parameters are obtained through <u>distributed</u> frequency domain design techniques.

The use of this methodology has been demonstrated in a simple example involving a cantilever beam. Currently, the methodology is being applied to a more complex model, and we anticipate its application to a wide vartiety of problems.

We feel that this methodology should be most useful in the conceptual and preliminary stages of the design process - in estblishing some of the tradeoffs between the structural and control problems. It should also be useful as a bridge to participation in system level designs involving other disciplines.
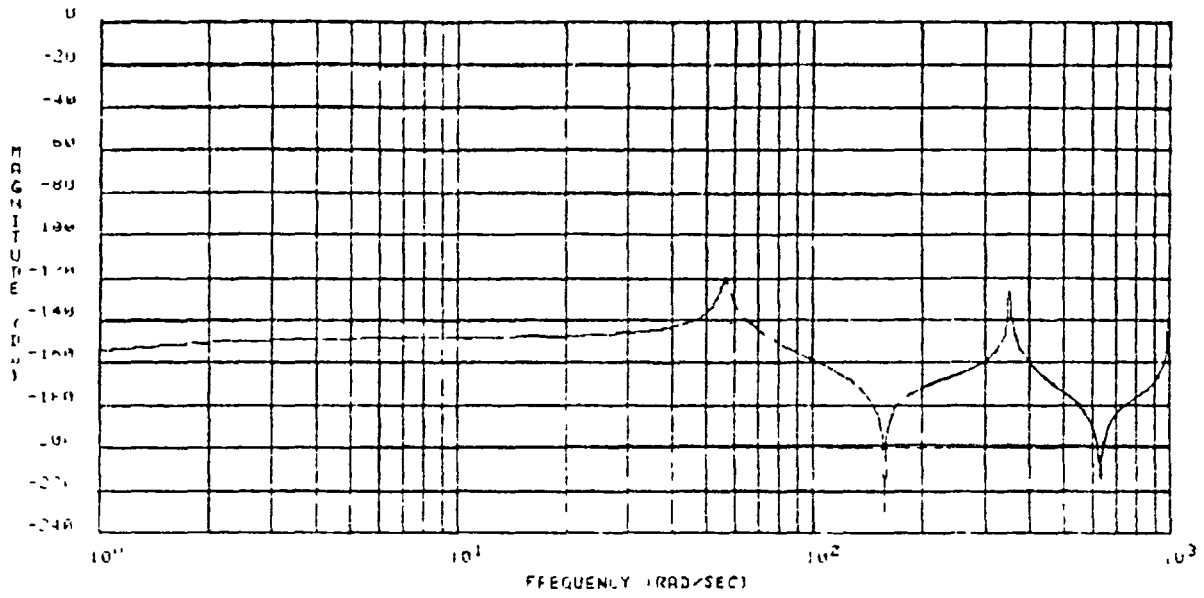
FIGURE V

References

[1]   W. T. Nye, E. Polak, A. Sangiovanni-Vincentelli, and A. L. Tits, "DELIGHT: An Optimization-Based Computer-Aided Design System," Proceedings of IEEE, ISCAS, Chicago, April 1981.

[2]   D. Q. Mayne, E. L. Polak, and A. L. M. Sangiovanni-Vincentelli, "Computer-Aided Design via Optimization: A Review," *Automatica*, Vol. 18, No. 2, pp. 147-155, March 1982.

[3]   A. Messac, J. D. Turner and K. Sossar, "An Integrated Control and Minimum Mass Structural Optimization Algorithm for Large Space Structures," NASA/ACC Workshop on Identification and Control of Flexible Space Structures, San Diego, June 1984.

[4]   J. S. Gibson, D. L. Mingori, A. Adamian and F. Jabbari, "Approximation of Optimal Infinite Dimensional Compensators for Flexible Structures," NASA/ACC Workshop on Identification and Control of Flexible Space Structures, San Diego, June 1984.

[5]   C. L. Gustafson and C. A. Desoer, "Controller Design for Linear Multivariable Feedback Systems with Stable Plant, Using Optimization with Inequality Constraints," *International Journal of Control*, vol. 37, no.5, pp. 881-907, May 1983.

[6]   M. Aswani, "Development of an Analytical Model for Large Space Structures," TR-0082(9975-1), The Aerospace Corporation, March 1982.

[7]   A. H. Nayfeh and M. S. Hefzy, "Continuum Modeling of the Mechanical and Thermal Behavior of Discrete Large Structures," AIAA 80-0679, 21st AIAA Structures, Structural Dynamics and Materials Conference, Seattle, May 1980.

References (cont'd)

[8]   C. T. Sun and T. Y. Yang, "A Continuum Approach Toward Dynamics of
      Gridworks," J. Appl. Mechanics, 40, 186, 1973.

[9]   W. R. Flower and L. C. Schmidt, "Analysis of Space Truss as
      Equivalent Plate," J. Struct. Div., 97, 2777, 1971.

[10] G. Zames, "Feedback and Optimal Sensitivity: Model Reference
      Transformations, Multiplicative Seminorms, and Approximate Inverse,"
      IEEE Trans. on Automat. Control, Vol. AC-26, pp.
      301-320, April 1981.

[11] C. A. Desoer and M. J. Chen, "Design of Multivariable Feedback
      Systems with Stable Plant," IEEE Trans on Automat. Control, vol.
      AC-26, pp. 408-415, April 1981.

[12] C. A. Desoer and C. L. Gustafson, "Design of Multivariable Feedback
      Systems with Simple Unstable Plant," University of California,
      Berkeley, Memo No. UCB/ERL M82/60, March 1982, to appear IEEE Trans.
      on Automat Control.

[13] C. L. Gustafson and C. A. Desoer, "A CAD Methodology for Linear
      Multivariable Feedback Systems based on Algebraic Theory," Memo No.
      M83/53, University of California, Berkeley, August 1983. to appear in
      International Journal of Control.

[14] F. M. Callier and C. A. Desoer, "An Algebra of Transfer Functions for
      Distributed Time-Invariant Systems," IEEE Trans. on Circuits and
      Systems, vol. CAS-25, pp. 651-662, Sept., 1978; corrections in vol.
      CAS-26, p. 360, May 1979.

References (cont'd)

[15]   F. M. Callier and C. A. Desoer, "Simplifications and Clarifications on the Paper, 'An Algebra of Transfer Functions for Distributed Time-Invariaent Systems,'" IEEE Trans. on Circuits and Systems, vol. CAS-27, pp. 320-323, April 1980.

[16]   F. M. Callier and C. A. Desoer, "Stabilization, Tracking and Distrubance Rejection in Multivariate Convolution Systems," Annales de la Societe Scientifique de Bruxelles, T. 94, I, pp. 7-51, 1980.

[17]   I. M. Horowitz, "Synthesis of Feedback Systems," Academic Press: New York and London, 1963.

OPTIMIZATION OF CONTROLLED STRUCTURES*

M. Salama, M. Hamidi, and **L. Demsetz**
Jet Propulsion Laboratory
California Institute of Technology
Pasadena, CA 91109

ABSTRACT

A formulation is presented for the coupled optimal design of a structural

system and its control by defining a composite objective function as a linear

combination of two components: a structural objective and a control objective.

For the case when the structural objective is a function of the structural

design variables only, and when the control objective is represented by the

quadratic functional of the response and control energy, one can analytically

express the optimal control in terms of any set of admissible structural design

variables. The expression for the optimal control is used recursively in an

iterative Newton-Raphson search scheme, the goal of which is to determine a

corresponding optimal set of structural design variables that minimize the

composite objective function. A numerical example is given to illustrate the

computational procedure.

I. INTRODUCTION

The optimal design of structural systems whose response to disturbances must be controlled to meet certain design objectives has traditionally proceeded along two separate paths. First, the structure is optimized by selecting an optimal set of structural design variables $\underset{\sim}{a}_1$, which minimize a structural objective function J_1-often taken as the mass of the structure - subjected to a set of pre-determined behavioral constraints $h_j(\underset{\sim}{a}) \geq 0$ on deformation, stresses, frequencies, etc.:

$$J_1(\underset{\sim}{a}_1) = \min_{\underset{\sim}{a}} J_1(\underset{\sim}{a},\underset{\sim}{u}) \; ; \; h_j(\underset{\sim}{a}) \geq 0 \; ; \quad \underset{\sim}{a}_1 \in \underset{\sim}{a} \tag{1}$$

During the structural optimization, the external loads are taken to be design-invariant quantities, regardless of whether they are due to external disturbances or due to commands for controlling the response of interest.

Second, having completely specified the structural design $\underset{\sim}{a}_1$, optimal control theory is used to determine an optimal set of control variables $\underset{\sim}{u}_1$ that minimize a control objective function J_2 - frequently taken as a quadratic cost functional of the response and control energy:

$$J_2(\underset{\sim}{u}_1) = J_2(\underset{\sim}{a}_1,\underset{\sim}{u}_1) = \min_{\underset{\sim}{u}} J_2(\underset{\sim}{a}_1,\underset{\sim}{u}) \; ; \quad \underset{\sim}{u}_1 \in \underset{\sim}{u} \tag{2}$$

This "separate" optimization procedure artificially decouples the design space into a structure design space and a control design space, without making use of dependency relations between them. It is possible, therefore, that the resulting optimal design $(\underset{\sim}{a}_1,\underset{\sim}{u}_1)$ of the uncoupled system may be suboptimal relative to the true optimal $(\underset{\sim}{a}^*,\underset{\sim}{u}^*)$ of the coupled system, i.e.

$$J(\underset{\sim}{a}^*, \underset{\sim}{u}^*) = \min_{\underset{\sim}{a}, \underset{\sim}{u}} \left[J_1(\underset{\sim}{a}, \underset{\sim}{u}) + J_2(\underset{\sim}{a}, \underset{\sim}{u}) \right] \leq J_1(\underset{\sim}{a}_1) + J_2(\underset{\sim}{u}_1) \tag{3}$$

The realization of the inequality expressed by (3) has high potential in the design of large flexible space structures. These structures tend to be spatially distributed. Their frequencies tend to be very low (fraction of a Hertz) and densely packed over a narrow range that overlaps with the control system frequencies. The corresponding vibration modes are usually poorly known and lightly damped. As a result, there can be considerable coupling between the optimal structure and optimal control designs. In addition, uncertainties in characterizing the structural design parameters, behavior of joints, tensioning devices and damping properties can adversely impact the control system performance and seriously reduce its stability margin. Conversely however, their controlled behavior can be made beneficial to the overall control system performance and stability, while simultaneously improving satisfaction of the structural optimality requirements.

The basic motivating idea embodied by Eq. (3) has also been recently recognized in somewhat different perspectives by other investigators [1-5]. However, due to the relatively high degree of mathematical and numerical complexity of the coupled structure - control optimization problem, there still remain many basic questions that begin with the formulation of the problem itself and the goals of the optimization process.

In this paper, we present a unified formulation which admits structural objective functions that do not depend on the control variables (e.g. structural mass), and assumes a quadratic control objective function. Coupled structure-control systems belonging to this class are shown here to lead to a simple formulation that enjoys the same theoretical guarantees regarding stability and controllability of the system as for the traditional state regulator problem. A numerical example is used to illustrate the computational procedure.

313

II. FORMULATION

A. Optimization Objective

A structure whose response to initial conditions $\underset{\sim}{v}(t_0) = \underset{\sim}{v}_0$, $\dot{\underset{\sim}{v}}(t_0) = \dot{\underset{\sim}{v}}_0$ must be controlled by a force vector $\underset{\sim}{u}$ is considered here. The discrete equations of motion of the system are:

$$\underset{\sim}{M}(\underset{\sim}{a})\dot{\underset{\sim}{v}} + \underset{\sim}{D}(\underset{\sim}{a})\dot{\underset{\sim}{v}} + \underset{\sim}{K}(\underset{\sim}{a})\underset{\sim}{v} = \underset{\sim}{B}_0 \underset{\sim}{u} \tag{4}$$

where $\underset{\sim}{M}(\underset{\sim}{a})$ is ($n_s \times n_s$) symmetric positive definite mass matrix, n_s being the number of dynamic degrees-of-freedom of the structure; $\underset{\sim}{K}(\underset{\sim}{a})$ is ($n_s \times n_s$) symmetric definite or semidefinite stiffness matrix; $\underset{\sim}{v}$ is n_s-dimensional vector of physical coordinates; and $\underset{\sim}{u}$ is n_c-dimensional vector of control forces whose points of application are mapped onto the structure by the ($n_s \times n_c$) control influence matrix $\underset{\sim}{B}_0$. Additionally, the damping matrix $\underset{\sim}{D}(\underset{\sim}{a})$ is congruent to a diagonal matrix through the modal transformation:

$$\underset{\sim}{v} = \underset{\sim}{\Phi} \underset{\sim}{\eta}$$

$$\underset{\sim}{\Phi}^T \underset{\sim}{M} \underset{\sim}{\Phi} = \underset{\sim}{I}$$

$$\underset{\sim}{\Phi}^T \underset{\sim}{K} \underset{\sim}{\Phi} = \text{diag}\left(\omega^2_{n_s}\right)$$

$$\underset{\sim}{\Phi}^T \underset{\sim}{D} \underset{\sim}{\Phi} = \text{diag}\left(2\zeta_{n_s} \omega_{n_s}\right) \tag{5}$$

The state form of Eq. (4) may be expressed in physical coordinates $\underset{\sim}{x}^T = (\underset{\sim}{v}, \dot{\underset{\sim}{v}})$, and leads to:

$$\dot{\underset{\sim}{x}} = \underset{\sim}{A}(\underset{\sim}{a})\underset{\sim}{x} + \underset{\sim}{B}(\underset{\sim}{a})\underset{\sim}{u} \tag{6}$$

where

$$\underset{\sim}{A}(\underset{\sim}{a}) = \begin{pmatrix} 0 & I \\ -\underset{\sim}{M}^{-1}\underset{\sim}{K} & -\underset{\sim}{M}^{-1}\underset{\sim}{D} \end{pmatrix} \quad ; \quad \underset{\sim}{B}(\underset{\sim}{a}) = \begin{pmatrix} 0 \\ \underset{\sim}{M}^{-1}\underset{\sim}{B}_0 \end{pmatrix} \tag{7}$$

The structural system described by (4), (5), and (6) is assumed to consist of n_a-number of independent design variables, $\underset{\sim}{a}$, whose magnitudes may be adjusted to create designs having various degrees of efficiency. For example, $\underset{\sim}{a}$, may designate member sizes of bars or beams, or thicknesses of plates or membranes. As such, M, D, K, A, B, and ω_{n_s} are all function of the design variables $\underset{\sim}{a}$.

We assume an output measurement vector $\underset{\sim}{z}$ of dimension n_m,

$$\underset{\sim}{z} = \underset{\sim}{c} \underset{\sim}{x} \tag{8}$$

where $\underset{\sim}{c} = [\underset{\sim}{c}_1 \ \underset{\sim}{c}_2]$ is $(n_m \times 2n_s)$ observation matrix.

In accordance with (3), the coupled optimization problem may be stated as follows:

Find the optimal set of variables $[\underset{\sim}{a}^*, \underset{\sim}{u}^*] \in [\underset{\sim}{a}, \underset{\sim}{u}]$ that minimize the objective functional

$$J(\underset{\sim}{a}, \underset{\sim}{u}) = \left[\rho_1 J_1(\underset{\sim}{a}) + \frac{1}{2} \rho_2 \int_{t=0}^{\infty} (\underset{\sim}{x}^T \underset{\sim}{Q} \underset{\sim}{x} + \underset{\sim}{u}^T \underset{\sim}{R} \underset{\sim}{u}) dt \right] \tag{9}$$

subject to the state equations (6), along with any n_h number of behavior constraints $h_j(a)$ on frequencies, deformations, stresses ... etc.

$$h_j(\underset{\sim}{a}) = \overline{U} - U_j(\underset{\sim}{a}) \geq 0 \quad j = 1, 2, \ldots n_h \tag{10}$$

and upper bound $\overline{a}$ or lower bound $\underline{a}$ on the ith design variable a_i:

$$\overline{a} \geq a_i \geq \underline{a} \quad i = 1, 2, \ldots n_a \tag{11}$$

315

In the present coupled structure - control optimization, the composite objective function in (9) is selected as a linear combination of two parts: a structural objective, and a control objective. The assumption is made further that the first part $J_1(\underset{\sim}{a})$ representing the structural measure of optimality is dependent only upon the structural design variables $\underset{\sim}{a}$, while the second part $J_2(\underset{\sim}{a},\underset{\sim}{u})$ representing the control measure of optimality - here taken as the traditional quadratic performance index - is dependent upon both $\underset{\sim}{a}$ and $\underset{\sim}{u}$. Since the two parts of the objective function do not necessarily have the same units or magnitudes, one may choose the scalar coefficients ρ_1 and ρ_2 so as to control the relative importance of the two objectives during computations.

Aside from the restrictions that the weighting matrix $\underset{\sim}{Q}$ must be non-negative, and $\underset{\sim}{R}$ must be positive definite, these matrices may be selected to achieve any desirable relations. For example, as noted in Ref. [5], one may select

$$
\underset{\sim}{Q} = \begin{pmatrix} \theta^2_k \underset{\sim}{K} & 0 \\ 0 & \theta^2_m \underset{\sim}{M} \end{pmatrix}
$$

and

$$
\underset{\sim}{R} = \underset{\sim}{\theta}^T_R \underset{\sim}{B}^T \underset{\sim}{K}^{-1} \underset{\sim}{B} \underset{\sim}{\theta}_R
$$

$$
\left. \phantom{\begin{pmatrix} \theta^2_k \underset{\sim}{K} & 0 \\ 0 & \theta^2_m \underset{\sim}{M} \end{pmatrix}} \right\} \quad (12)
$$

where θ_k, θ_m and θ_R are scaling parameters. If (12) is assumed, the integrand in (9) will have units of energy: strain, kinetic and potential.

B. Optimality Conditions

It should be noted that whether or not the relationship in (12) is assumed, the control objective in (9) is dependent upon both $\underset{\sim}{a}$ and $\underset{\sim}{u}$, while the structural objective is dependent only on $\underset{\sim}{a}$. As such, (9) may be restated as:

316

$$J(\underset{\sim}{a}^*, \underset{\sim}{u}^*) = \min_{\underset{\sim}{a}} \left[\rho_1 J_1(\underset{\sim}{a}) + \min_{\underset{\sim}{u}} \left[\frac{1}{2} \rho_2 \int_{t=0}^{\infty} (\underset{\sim}{x}^T \underset{\sim}{Q} \underset{\sim}{x} + \underset{\sim}{u}^T \underset{\sim}{R} \underset{\sim}{u}) dt \right] \right] \qquad (13)$$

For a specified initial condition $\underset{\sim}{x}(0) = \underset{\sim}{x}_0$, it is well known that [6]:

$$\min_{\underset{\sim}{u}} \left[\frac{1}{2} \int_{t=0}^{\infty} (\underset{\sim}{x}^T \underset{\sim}{Q} \underset{\sim}{x} + \underset{\sim}{u}^T \underset{\sim}{R} \underset{\sim}{u}) dt \right] = \frac{1}{2} \underset{\sim}{x}_0 \underset{\sim}{P}(\underset{\sim}{a}) \underset{\sim}{x}_0 \qquad (14)$$

and that the corresponding optimal control $\underset{\sim}{u}^*$ is obtained from:

$$\underset{\sim}{u}^* = - \underset{\sim}{R}^{-1}(\underset{\sim}{a}) \ B^T(\underset{\sim}{a}) \ \underset{\sim}{P}(\underset{\sim}{a}) \underset{\sim}{x} \qquad (15)$$

where $\underset{\sim}{P}(\underset{\sim}{a})$ is the positive definite solution of the algebraic Riccati equation:

$$\underset{\sim}{A}^T(\underset{\sim}{a}) \ \underset{\sim}{P}(\underset{\sim}{a}) + \underset{\sim}{P}(\underset{\sim}{a}) \ \underset{\sim}{A}(\underset{\sim}{a}) + \underset{\sim}{Q}(\underset{\sim}{a}) - \underset{\sim}{P}(\underset{\sim}{a}) \ \underset{\sim}{B}(\underset{\sim}{a}) \ \underset{\sim}{R}^{-1}(\underset{\sim}{a}) \ \underset{\sim}{B}^T(\underset{\sim}{a}) \ \underset{\sim}{P}(\underset{\sim}{a}) = 0 \qquad (16)$$

From the above, it is seen that the optimal control $\underset{\sim}{u}^*$ and the expression for the minimum in (14) are implicit functions of the design variables $\underset{\sim}{a}$. The stability of the closed loop system is assured by the positive definiteness of $\underset{\sim}{P}(\underset{\sim}{a})$ for all admissible values of $\underset{\sim}{a}$. It is assumed here that conditions for the existence of a positive definite solution to the Riccati equation are satisfied.

In deriving conditions (14), (15) and (16), use was made of the state equation (6), but the behavior and side constraints (10) and (11) were not enforced. The minimization of (9) is thus reduced to selecting an optimal set of structural design variables $\underset{\sim}{a}^*$ that minimize $F(\underset{\sim}{a})$:

$$F(\underset{\sim}{a}) = \left[\rho_1 \ J_1(a) + \frac{1}{2} \rho_2 \ \underset{\sim}{x}_0^T \ \underset{\sim}{P}(\underset{\sim}{a}) \ \underset{\sim}{x}_0 \right] \qquad (17)$$

317

subject to constraints (10) and (11). The relationship between the optimal con-

trol variables $\underset{\sim}{u}^*$ and optimal structural variables $\underset{\sim}{a}^*$ is implicitly preserved by

satisfying (10), (11), (15), (16), and (17). The constrained problem (17), (10)

and (11) may be converted to an unconstrained one of the form:

$$L = F + \sum_{j=1}^{n_h} \lambda_j h_j + \sum_{i=1}^{n_a} \left[\mu_i (a_i - \underline{a}) + \nu_i (\overline{a} - a_i) \right] \tag{18}$$

where λ_j, μ_i and ν_i respectively are unknown multipliers, one for each constraint.
A local optimum of (13) must necessarily satisfy the following first order Kuhn-
Tucker optimality conditions [7]:

$$F_{,a_i} + \sum_{j=1}^{} \lambda_j h_{j,a_i} + \mu_i + \nu_i$$

$$\lambda_j h_j = 0$$

$$\mu_i (a_i - \underline{a}) = 0$$

$$\nu_i (\overline{a} - a_i) = 0 \tag{19}$$

where the multipliers λ_j, μ_i, ν_i must be non-negative for all $j = 1, 2, \ldots n_h$, and

$i = 1, 2, \ldots n_a$.

III. COMPUTATIONAL ASPECTS

A. Recursive Relations

An iterative solution method based on a modified Newton-Raphson scheme is employed to insure satisfaction of the optimality condition (19). The method is relatively general so as to allow various forms of dependence of $Q(\underset{\sim}{a})$, $R(\underset{\sim}{a})$, $B(\underset{\sim}{a})$, and various types of constraints h_j. The set of design variables $\underset{\sim}{a}^*$ and multipliers $\underset{\sim}{\lambda}$ that satisfy (19) are obtained iteratively from the recursive relations:

$$
\left\{ \begin{array}{c} \underset{\sim}{a} \\ - \\ \underset{\sim}{\lambda} \end{array} \right\}_{r+1} = \left\{ \begin{array}{c} \underset{\sim}{a} \\ - \\ \underset{\sim}{\lambda} \end{array} \right\}_{r} - \alpha \left[\begin{array}{c|c} F_{,\underset{\sim}{a}\underset{\sim}{a}} + \sum_j \lambda_j \underset{\sim}{h}_{j,\underset{\sim}{a}\underset{\sim}{a}} & \underset{\sim}{h}_{j,\underset{\sim}{a}} \\ \hline \underset{\sim}{h}_{j,\underset{\sim}{a}} & 0 \end{array} \right]_r^{-1} \left\{ \begin{array}{c} F_{,\underset{\sim}{a}} + \sum_j \lambda_j \underset{\sim}{h}_{j,\underset{\sim}{a}} \\ \underset{\sim}{h}_j \end{array} \right\}_r
$$

(20)

Rather than including the multipliers μ_i and ν_i for the side constraints in (20), these are dealt with indirectly through the parameter α which limits the step size during an iteration so that none of the design variables go outside their range $\underline{a}$ and $\overline{a}$.

B. Expressions for Derivatives

The implementation of Eq. (20) requires the availability of the first and second derivatives of the Riccati solution P, structural cost function, and constraints, all with respect to the design variables $\underset{\sim}{a}$. The first derivatives $P_{,a_i}$, $i=1,2,\ldots n_a$ are obtained by differentiating (16), and are governed by the Lyapunov equation:

319

$$\underset{\sim}{c_1} + \underset{\sim}{c_2} \underset{\sim}{P}_{,a_i} + \underset{\sim}{P}_{,a_i} \underset{\sim}{c_2}^T = 0 \tag{21}$$

where

$$\left.\begin{aligned}
\underset{\sim}{c_1} &= \underset{\sim}{A}^T_{,a_i} \underset{\sim}{P} + \underset{\sim}{P} \underset{\sim}{A}_{,a_i} - \underset{\sim}{P} \underset{\sim}{E}_{,a_i} \underset{\sim}{P} + \underset{\sim}{Q}_{,a_i} \\
\underset{\sim}{c_2} &= \underset{\sim}{A}^T - \underset{\sim}{P} \underset{\sim}{E} \\
\underset{\sim}{E} &= \underset{\sim}{B} \underset{\sim}{R}^{-1} \underset{\sim}{B}^T
\end{aligned}\right\} \tag{22}$$

Similarly, the second derivatives $\underset{\sim}{P}_{,a_i a_k}$ ($i=1,2,\ldots n_a$, $k=1,2,\ldots n_a$) obey the Lyapunov equation:

$$\underset{\sim}{c_3} + \underset{\sim}{c_2} \underset{\sim}{P}_{,a_i a_k} + \underset{\sim}{P}_{,a_i a_k} \underset{\sim}{c_2}^T = 0 \tag{23}$$

where

$$\left.\begin{aligned}
\underset{\sim}{c_3} &= \underset{\sim}{c_4} + \underset{\sim}{c_4}^T + \underset{\sim}{c_5} + \underset{\sim}{c_5}^T \\
\underset{\sim}{c_4} &= \left(\underset{\sim}{A}^T_{,a_i} - \underset{\sim}{P}_{,a_i} \underset{\sim}{E} - \underset{\sim}{P} \underset{\sim}{E}_{,a_i}\right) \underset{\sim}{P}_{,a_k} \\
\underset{\sim}{c_5} &= \underset{\sim}{A}^T_{,a_i a_k} \underset{\sim}{P} + \underset{\sim}{A}^T_{,a_k} \underset{\sim}{P}_{,a_i} - \underset{\sim}{P}_{,a_i} \underset{\sim}{E}_{,a_k} \underset{\sim}{P} \\
&\quad - \frac{1}{2} \underset{\sim}{P} \underset{\sim}{E}_{,a_i a_k} \underset{\sim}{P} + \frac{1}{2} \underset{\sim}{Q}_{,a_i a_k}
\end{aligned}\right\} \tag{24}$$

Other derivative information for the structural objective function and constraints has been dealt with in the literature [8,9,10,11]. For example, if a lower bound is placed on the lowest open-loop frequency $\omega_1^2 \geq \omega^{*2}$, then

$$h_1 = \omega_1^2 - \omega^{*2} \geq 0 \tag{25}$$

320

According to (19), both ω^2_{1,a_1} and ω^2_{1,a_1a_k} are needed, and may be computed in a number of ways as discussed in Ref. [9 and 10].

C.   Numerical Example

To illustrate the computational procedure outlined above, the following numerical example is used.   Given a cantilever beam modeled by three finite bending elements of equal fixed lengths under the action of a lateral control force applied at the free tip, find the optimal distribution of cross-sectional areas that minimizes the cost function of equation (9), subject to a constraint on the structure's first open loop frequency.   The structure and relevant parameters are shown in Fig. 1.

Additional assumptions are made regarding the nature of the structural matrices M, K, and D.   The element mass matrices are assumed diagonal, with the mass linearly dependent upon the cross-sectional area.   The element bending stiffness is represented by a quadratic function of the cross-sectional area a_1. That is: $EI_1 = b_1a_1 + b_2a_1^2$.   For the circular tube under consideration with a fixed inner diameter d_1, it can be shown that $b_1 = (Ed_i^2/8)$ and $b_2 = (1/4\pi)$. Damping is assumed to be independent of the design variables, with values selected equal to 0.5% damping in each mode of the uniform beam satisfying the frequency constraint.

In the objective function (9), the structural objective J_1 is chosen to be the total mass, and the weighting matrices $\underset{\sim}{Q}$ and $\underset{\sim}{R}$ are arbitrarily taken as identity matrices. Values of (ρ_2/ρ_1) ranging from 0 to 5 were considered. The uniform beam satisfying a fundamental frequency constraint $\omega_1 = .35$ rad/sec has a cross-sectional area of $.01\,m^2$ corresponding to outer diameter = .11 m and inner diameter = .01 m.   For $\rho_2/\rho_1 = 0$, the optimization reduces to that for the structure alone, as in equation (1).   The resulting optimal structure gives 74% reduction in structural mass as

compared with the uniform beam. The area distribution and costs are shown in Table 1. These correspond to varying outer diameter, but fixed inner diameter = .01 m.

For $(\rho_2/\rho_1) > 0$, the cost depends on the initial conditions $\underset{\sim}{y}_0$ and $\dot{\underset{\sim}{y}}_0$. Two sets of initial conditions are considered. For the first case, the initial displacement $(\underset{\sim}{y}_0 = \underset{\sim}{x}_1)$ is taken as the fundamental mode of the uniform beam. For the second case, the second mode of the same structure was used: $(\underset{\sim}{y}_0 = \underset{\sim}{x}_2)$. In both cases, the assumed initial displacement shapes were made orthonormal to the mass matrix, and the initial velocities assumed zero.

Figures 2 and 3 show the iteration histories of the structural and control objectives of the composite function (9) with $(\rho_2/\rho_1) = 5$. Both figures are normalized to unit initial objectives. The initial control objective was roughly 1.7% of the initial structural objective. For this reason, a plot of the total objective is quite similar to Figure 2. Reduction in structural mass – as compared with a uniform beam – is therefore again nearly 74%. Also, Fig. 3 shows that depending on the initial conditions, the optimal beam requires approximately 93% to 95% less control cost than required by the initial uniform beam.

For the range of (ρ_2/ρ_1) considered, inclusion of the controller did not measurably alter the shape (relative sizes of a_i; i = 1,2,3) of the structure, because the frequency constraint appears to numerically dominate the optimization process. It is necessary therefore, to fully investigate the effect of other (ρ_2/ρ_1) values as well as other types of constraints.

IV. CONCLUSIONS

Being at the intersection of two relatively complex and computationally demanding problems, a successful simultaneous optimization of the coupled structure-control system crucially depends upon simplicity of the formulation and the strength of its theoretical foundation. The composite objective function introduced here as a linear combination of a structural objective (which is a function of the structural design variable $\underset{\sim}{a}$) and a control objective (which is a function of both $\underset{\sim}{a}$ and the control design variables $\underset{\sim}{u}$) allowed a simple and computationally tractable solution. By assuming the usual quadratic performance for the control objective it is possible to solve analytically for the optimal control variables $\underset{\sim}{u}^*(\underset{\sim}{a})$. As such, one is able to carry over without modification all mathematical bases for solution existence, stability, and robustness, readily available in the optimal control literature. Being valid for all feasible structural design variables $\underset{\sim}{a}$, the analytical expression for the optimal control $\underset{\sim}{u}^*$ is easily encapsulated within an iterative numerical search scheme to determine a corresponding optimal set of structural variables $\underset{\sim}{a}^*$, without increasing the dimensionality of the design space being searched. This is an important consideration for computational efficiency, especially as one seeks to solve practical problems having larger number of variables $\underset{\sim}{a}$ and $\underset{\sim}{u}$, and constraints h_j.

The example discussed in this paper illustrates the numerical results for one set of structural and control parameters. The constraint on the first open loop frequency used in the example seemed to dominate the optimal solution for the specific parameters presented. A more extensive study of the optimal design of this and other configurations and constraints over a broad range of parameter values will be the subject of a subsequent paper.

REFERENCES

1. Hanks, B., and Skelton, R., "Designing Structures for Reduced Response by Modern Control Theory", Paper No. 83-0815, presented at the 24th AIAA/ASME/ ASCE/AHS Structures, Structural Dynamics, and Materials Conference, Lake Tahoe, Nevada, May 1983.

2. Komkov, V., "Simultaneous Control and Optimization For Elastic Systems", Proceedings of the Workshop on Applications of Distributed System Theory to the Control of Large Space Structures, G. Rodriguez, Editor, JPL Publication 83-46, Jet Propulsion Laboratory, Pasadena, California, July 1983.

3. Hale, A., Lisowski, R., and Dahl, W., "Optimizing Both the Structure and the Control of Maneuvering Flexible Spacecrafts," Proceedings of the AAS/AIAA Astrodynamics Conference, Lake Placid, New York, August 1983.

4. Messac, A., and Turner, J., "Dual Structural-Control Optimization of Large Space Structures", presented at the 25th AIAA/ASME/ASCE/AHS Structures, Structural Dynamics and Materials Conference – Dynamics Specialists Conference, Palm Springs, California, May 1984.

5. Venkayya, V., and Tischler, V., "Frequency Control and the Effect on the Dynamic Response of Flexible Structures", Paper No. 84-1044-CP, presented at the 25th AIAA/ASME/ASCE/AHS Structures, Structural Dynamics and Materials Conference – Dynamics Specialists Conference, Palm Springs, California, May 1984.

6. Athans, M. and Falb, P., "Optimal Control", McGraw-Hill Book Co., 1966.

7. Hadley, G., "Nonlinear and Dynamic Programming", Addison-Wesley Publishing Co., 1964.

8. Fleury, C., "A Unified Approach to Structural Weight Minimization", Computer Methods in Applied Mechanics and Engineering, Vol. 20, 1979, pp. 17-38.

9. Fox, R., and Kapoor, M., "Rate of Change of Eigenvalues and Eigenvectors", AIAA Journal, Vol. 6, No. 12, 1968, pp. 2426-2429.

10. Nelson, R., "Simplified Calculation of Eigenvector Derivative", AIAA Journal, Vol. 14, No. 9, 1976, pp. 120-125.

11. Plaut, R., and Huseyin, K., "Derivatives of Eigenvalues and Eigenvectors in Non-Self-Adjoint Systems", AIAA Journal, Vol. 11, No. 2, 1973, pp. 250-251.
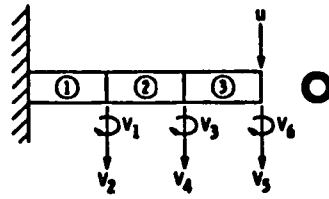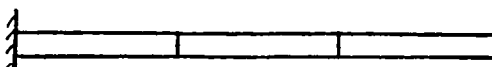
Element Length = 15 m
Inner Diameter = .01 m
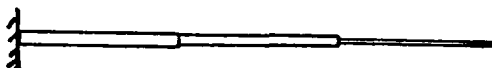
Graphite Epoxy:
ρ = 1660 kg/m^3
E = 9.56 $(10)^{10}$ N/m^2

Frequency Constraint:
ω_1 = .35 rad/sec

Figure 1. Structure and Parameters for Example

ρ_2/ρ_1	$\underset{\sim}{v}_0$	Optimal Shape (element areas, m)			Cost Ratio: Optimal Beam /Uniform Beam	
		a_1	a_2	a_3	Structure	Controller
0	-	.00354	.00176	.00024	.18	-
5	x_1	.00354	.00176	.00024	.18	.07
5	$\underset{\sim}{x}_2$	.00354	.00176	.00024	.18	.04

Uniform Beam :
(a = .01 m)

Optimal Shape:

lengths not to scale

Table 1. Cost Ratios

Figure 2. Iteration History, Structure

Figure 3. Iteration History, Controller

PARAMETRIC STIFFNESS CONTROL OF FLEXIBLE STRUCTURES*

F. C. Moon[+] and **R. H. Rand**[++]
Cornell University
Ithaca, NY 14853

ABSTRACT

We examine an unconventional method for control of flexible space structures using feedback control of certain elements of the stiffness matrix. The advantage of using this method of configuration control is that it can be accomplished in practical structures by changing the initial str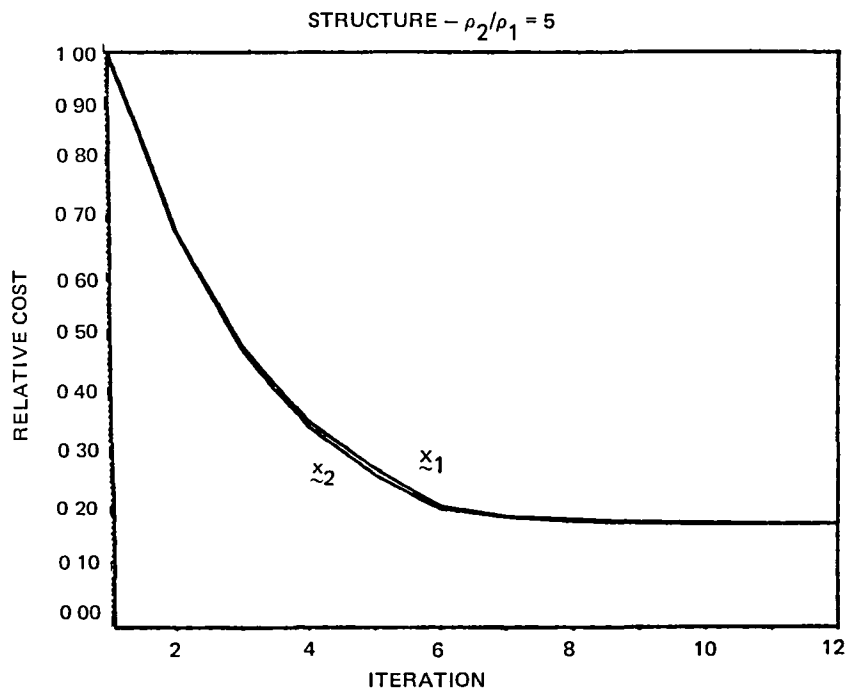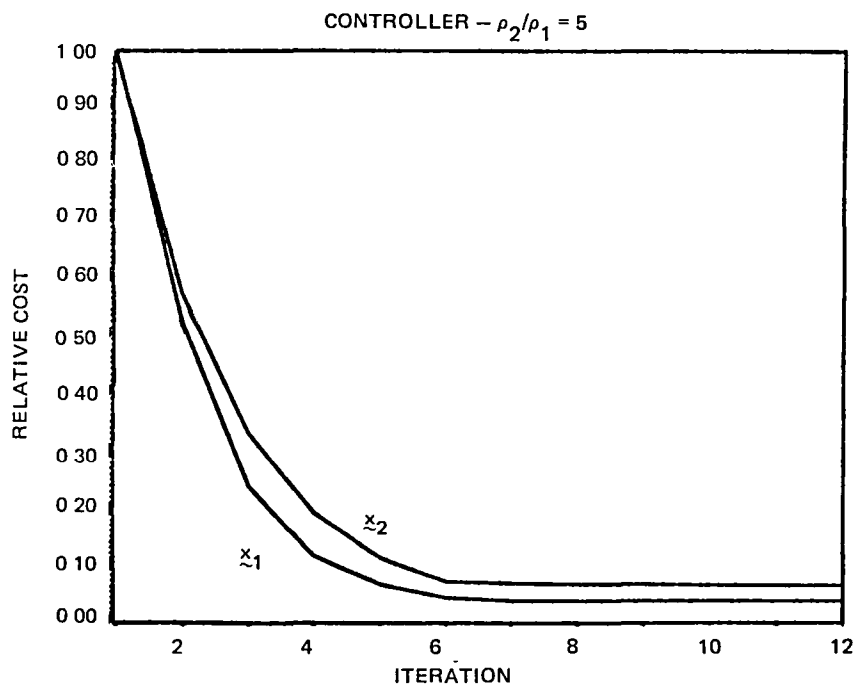ess state in the structure. The initial stress state can be controlled hydraulically or by cables. The method leads, however, to nonlinear control equations. In particular, we examine a long slender truss structure under cable induced initial compression. Both analytical and numerical analyses are presented. Nonlinear analysis using center manifold theory and normal form theory is used to determine criteria on the nonlinear control gains for stable or unstable operation. The analysis is made possible by the use of the exact computer algebra system MACSYMA.

INTRODUCTION

The use of linear feedback forces to control linear flexible structures has been studied for over a decade, [1]-[4]. The efficacy of these methods has been demonstrated experimentally in the laboratory for a few cases (see e.g. Ref. 2, 3). However, the problem of applying linear feedback forces to an actual structure in space is formidable. For structures with significant bending deformations, forces transverse to the major axis of the structure are required such as small distributed rocket motors. An alternative is to use a scheme used in nature to control animal structural configuration, namely active control of their internal stress or muscles. In a man-made structure this analogy can be exploited by applying a self-equilibrated internal stress state through the use of cables or hydraulic actuators (Figure 1). The tension in cables can be controlled by DC servomotors and gear reducers. Such a method for control of internal stresses is suited to low frequency applications where control of the lowest modes of the structure is desired. From elementary structural theory it is known that the initial stress state can change the elastic stiffness matrix. The simplest example is the beam-column. In this case, the initial axial stress can even make the stiffness go to zero at buckling. Stiffness control of a

---

vibrating string has been studied by Chen [5], and a two mode analysis of stiffness control has been presented by Fason et al. [6].

We propose the use of feedback to control elements of the stiffness matrix by controlling the internal stress. In one problem, we assume the structure is initially in a desired configuration and is impulsively disturbed. We examine the ability of several control laws to return the structure to its initial configuration. Both linear and nonlinear control laws are examined. Conditions for stable and unstable behavior of the system are derived.

STIFFNESS CONTROL – A SIMPLE EXAMPLE

The simplest structure for which an initial stress T can change the stiffness is the beam-column whose equation for the transverse displacement u is given below (Figure 2):

$$\frac{\partial^2}{\partial x^2} D \frac{\partial^2 u}{\partial x^2} + \gamma \frac{\partial^2 u}{\partial t^2} + \frac{\partial}{\partial x} T \frac{\partial u}{\partial x} = f + \frac{\partial g}{\partial x} \tag{1}$$

where f represents either distributed disturbances or linear control forces and g represents distributed torques such as those due to thermal or solar induced stresses. D is the bending stiffness and T is the axial compression induced by placing cables in tension along the beam. The mass density is γ.

Conventional control theory of flexible structures uses $f(x,t)$ to control the shape. In this paper we propose to use the initial stress or cable tension T to control the lowest mode. This eliminates the need for transverse control forces such as rockets or jets. When D and T are uniform along the beam, we have (neglecting distributed torques):

$$D \frac{\partial^4 u}{\partial x^4} + \gamma \frac{\partial^2 u}{\partial t^2} + T \frac{\partial^2 u}{\partial x^2} = f(x) \tag{2}$$

A single mode model may be derived using Galerkin's method where we assume the shape function is known

$$u(x,t) = A(t)U(x) \tag{3}$$

The equation for $A(t)$ takes the form,

$$\ddot{A} + (\omega^2 - \beta T)A = F(t) \tag{4}$$

Thus we can see that the stiffness term is linear in the initial stress T.

We propose a general control law for T, which includes both linear and nonlinear terms.

In general, the control law for the cable tension will have a lag due to servomotor or hydraulic system inertia or control circuit delay or stress waves propagating along the tension cables. (In a large structure the latter might not be negligible.) The tension will have a static and a dynamic part:

$$T = T_o + T_1(t) \tag{5}$$

where

$$\frac{1}{\alpha}\frac{dT_1}{dt} + T_1 = G(A,\dot{A}) \tag{6}$$

Three different control laws are examined

$$G = \Gamma_1 A + \Gamma_2 \dot{A} \tag{7}$$

$$G = \Gamma_3 A^2 + \Gamma_4 A\dot{A} + \Gamma_5 \dot{A}^2 \tag{8}$$

$$G = \frac{\Gamma_6 A\dot{A}}{(1 + \Gamma_7 A^2)} \tag{9}$$

Equations (4)-(6) constitute a nonlinear system of equations where the stiffness is controlled by a feedback parameter T , hence the term parametric stiffness control. This system is analogous to the Mathieu equation in which, however, the stiffness term is a known periodic function of time.

STIFFNESS CONTROL — GENERAL THEORY

For more general structures with a stiffness matrix (k) , mass matrix (m) and a set of cable tensions $\{T\}$ one has a set of linear coupled equations for the generalized displacements or modal amplitudes $\{x\}$.

$$(m)\{\ddot{x}\} + (k)\{x\} = \{f(t)\} \tag{10}$$

where $\{f\}$ represents disturbances. In classic control theory of flexible structures one would use $\{f\}$ to provide control. In the present theory however we recognize that the elements of (k) are linear functions of the tensions, i.e.,

$$k_{ij} = k_{ij}^o + \beta_{ijk}T_k \tag{11}$$

Thus one can try to vary the T_k to effect a change in any or all of the $\{x(t)\}$. To supplement these equations one requires a control law for the cable tensions. To account for lags in the cable control system, these control laws might take the form

$$\frac{1}{\alpha_k}\dot{T}_k + T_k = G_k(x_i, \dot{x}_j; S(t)) \tag{12}$$

where the $S(t)$ might be desired displacements. The system of equations (10)-(12) is clearly nonlinear. One can raise questions of observability, controllability, stability, etc. To effect all the modes one might require a combination of control force $\{f\}$ and stiffness control $\{T\}$. In the section below we examine a single mode problem and examine the question of stability for stiffness control alone.

ONE-MODE MODEL – STABILITY ANALYSIS

A) Nonlinear Quadratic Feedback Control

In this section we examine the stability of the equilibrium point at the origin under the quadratic feedback law (8). If one nondimensionalizes the modal amplitude so that the physical amplitude A is replaced by a dimensionless amplitude x, the equations (4), (6), and (8) can be put into the form of the rate of change of the state space vector $\underset{\sim}{r} = (x,y,z)^T$ where

$$\dot{x} = y \tag{13}$$

$$\dot{y} = -(1 + z)x \tag{14}$$

$$\dot{z} = -\alpha z + \alpha(G_{20}x^2 + G_{11}xy + G_{02}y^2) \tag{15}$$

where a general quadratic nonlinear control law has been assumed with control gains (G_{20}, G_{11}, G_{02}). We shall investigate the stability of this system of equations in the neighborhood of the equilibrium point at the origin $\underset{\sim}{r}=(0,0,0)$.

We note that the linearized system has eigenvalues 1, -1, and $-\alpha$. The last eigenvalue corresponds to the decay of the servomotor transient $z \rightarrow 0$. This suggests that any motion starting close to the origin will eventually move down onto the x,y plane. To obtain a more precise description one must account for the nonlinear terms. This situation is clarified by the Center Manifold Theorem [7], which states that there exists a surface

$$z = f(x,y) \tag{16}$$

which is tangent to the x,y plane at the origin to which all solutions starting sufficiently close to the origin tend asymptotically. The surface is moreover invariant under the motion or flow given by (13)-(15).

In order to formally approximate (16) we expand $f(x,y)$ in a power series:

$$z = \sum_{i=2}^{\infty} \sum_{j=2}^{\infty} m_{ij}x^i y^j \tag{17}$$

The constant and linear terms in (17) are dropped in order that the surface be tangent to the x,y plane at the origin. The coefficients m_{ij} may be found by differentiating (17) with respect to t and using (13)-(15) and (17) to eliminate $\dot{x}, \dot{y}, \dot{z}$ and z. Collecting terms of like powers of $x^i y^j$ one can obtain the constants m_{ij}. Needless to say this procedure involves much algebra which is easily handled by the computer using the exact symbolic computer algebra system MACSYMA (see e.g. Rand [8]). Proceeding in this fashion

we find that z consists of only even order terms. We expand (17) to powers up to fourth order and obtain expressions for the coefficients m_{20}, m_{11}, m_{02}, m_{04}, m_{31}, m_{22}, m_{13}, m_{04}. To illustrate the complexity of these coefficients we display four of them;

$$m_{20} = \frac{(\alpha^2 + 2)G_{20} + \alpha G_{11} + 2G_{02}}{\alpha^2 + 4}$$

$$m_{11} = \frac{-2\alpha G_{20} + \alpha^2 G_{11} + 2\alpha G_{02}}{\alpha^2 + 4}$$

(18)

$$m_{02} = \frac{2G_{20} - \alpha G_{11} + (\alpha^2 + 2)G_{02}}{\alpha^2 + 4}$$

$$m_{04} = -(2\alpha^6 G_{02}^2 - 10\alpha^5 G_{02} G_{11} + \alpha^4 (32 G_{02} G_{20} + 14 G_{11}^2 + 16 G_{02}^2) + \alpha^3 (-92 G_{11} G_{20} - 36 G_{02} G_{11})$$

$$+\alpha^2 (128 G_{20}^2 + 96 G_{02} G_{20} + 8 G_{11}^2 + 64 G_{02}^2) + \alpha(-176 G_{11} G_{20} - 176 G_{02} G_{11}) + 320 G_{20}^2$$

$$+256 G_{02} G_{20} - 64 G_{02}^2)/(\alpha^8 + 28\alpha^6 + 240\alpha^4 + 832\alpha^2 + 1024)$$

The full set will be given in a forthcoming paper with more details.

The Center Manifold Theorem [7] states that the stability of the origin in the full three dimensional flow (13)-(15) is the same as the stability of the equilibrium point $x = y = 0$ in the flow on the center manifold. Thus, we are led to study the stability of the system of equations

$$\dot{x} = y$$

(19)

$$\dot{y} = -(1 + \sum_{i=0}^{4} \sum_{j=0}^{4} m_{ij} x^i y^j)x + 0(7) \qquad i+j \leq 4$$

which may be considered as an oscillator with linear, cubic, and quintic forces. In the linearized case the eigenvalues $\pm i$ correspond to the "critical case" of Liapunov (see e.g., Minorsky, p. 150 [9]) and the stability cannot be determined on the basis of linear terms alone.

To study the stability of (19) we use the method of _normal forms_ (see e.g., Guckenheimer and Holmes [10]). We posit a "near identity" transformation from x,y to u,v coordinates of the form

$$x = u + g(u,v)$$

$$y = v + h(u,v)$$

(20)

where g,h are polynomials with terms cubic and quintic in u,v having undetermined coefficients. Takens [11], has shown that it is always possible to transform systems like (19) (which have linear parts equivalent to simple harmonic oscillators) into a form which may be expressed simply in polar coordinates in the u,v plane:

$$\dot{r} = a_1 r^3 + a_2 r^5 + 0(7)$$

(21)

$$\dot{\theta} = -1 + b_1 r^2 + b_2 r^4 + 0(6)$$

(22)

where $u = r\cos\theta$, $v = r\sin\theta$. Although this procedure is straightforward, the choice of functions g,h involves solving sixteen algebraic equations. Again this task was made tractable by using MACSYMA.

The result of this computation is that the quantities a_1 , a_2 , b_1 , b_2 in (21)-(22) are obtained in terms of the m_{ij} . We find

$$a_1 = -m_{11}/8$$

$$a_2 = -(2m_{31} - m_{11}m_{20} + 2m_{13} - m_{02}m_{11})/32$$

$$b_1 = -(96m_{20} + 32m_{02})/256$$

(23)

$$b_2 = -(80m_{40} + 16m_{22} - 21m_{20}^2 + 18m_{02}m_{20}$$

$$- 5m_{11}^2 + 16m_{04} + 3m_{02}^2)/256$$

In terms of the original control gains in (15) we find

$$a_1 = \frac{2\alpha G_{20} - \alpha^2 G_{11} - 2\alpha G_{02}}{8\alpha^2 + 32}$$

(24)

$$a_2 = -((2\alpha^5 + 48\alpha^3 + 96\alpha)G_{20}^2 + ((-\alpha^6 - 28\alpha^4 - 32\alpha^2)G_{11} + (4\alpha^5 + 64\alpha)G_{02})G_{20}$$

$$+ (2\alpha^5 - 8\alpha^3)G_{11}^2 + (-\alpha^6 - 4\alpha^4 - 64\alpha^2)G_{02}G_{11} + (2\alpha^5 + 16\alpha^3 - 32\alpha)G_{02}^2)$$

$$/(32\alpha^6 + 384\alpha^4 + 1536\alpha^2 + 2048)$$

The equation for $\dot{r}$, (21), governs the stability of the origin and the existence of limit cycles, while the equation for $\dot{\theta}$, (22), specifies the frequency of the periodic motion corresponding to a limit cycle.

In particular the origin will be asymptotically stable if $a_1 < 0$ and unstable of $a_1 > 0$. If $a_1 = 0$ then the sign of a_2 determines the

stability of the origin. Limit cycles correspond to equilibria of (21) and have a radius R given by

$$R^2 = -a_1/a_2 \tag{25}$$

Since the power series expansions (17) and (19) are only valid in a neighborhood of the origin, the expression (25) can only be expected to be valid in a neighborhood of $a_1 = 0$. In terms of the control gains we have

$$R^2 = 4(\alpha^2+4)^2(2G_{20}-\alpha G_{11}-2G_{02})/(2\alpha^4 G_{20}^2+48\alpha^2 G_{20}^2+96G_{20}^2-\alpha^5 G_{11}G_{20}$$

$$-28\alpha^3 G_{11}G_{20}-32\alpha G_{11}G_{20}+4\alpha^4 G_{02}G_{20}+64G_{02}G_{20}+2\alpha^4 G_{11}^2-8\alpha^2 G_{11}^2-\alpha^5 G_{02}G_{11}$$

$$-4\alpha^3 G_{02}G_{11}-64\alpha G_{02}G_{11}+2\alpha^4 G_{02}^2+16\alpha^2 G_{02}^2-32G_{02}^2) \tag{26}$$

From (24) the condition for the stability of the equilibrium point at the origin is given by

$$-\frac{\alpha^2 G_{11} + 2\alpha(G_{02}-G_{20})}{\alpha^2 + 4} < 0 \tag{27}$$

In the limit of zero servomotor lag $\alpha \to \infty$, (27) requires that $G_{11} > 0$. This corresponds to a quadratic damping feedback law where in (7) $G = \Gamma_5 A^2$. The stability condition (27) is a plane in control space (G_{11}, G_{02}, G_{20}) with a normal given by

$$\underset{\sim}{N} = (\alpha, 2, -2)$$

The maximum damping is obtained by choosing G_{11}, G_{02}, G_{20} so as to maximize the distance from this plane subject to the inequality (27).

Numerical integration of three specific quadratic feedback laws is shown in Figures 3, 4, and 5. A fourth order Runge-Kutta algorithm was used. In the stable case, we have $G_{02} = 1$, $G_{20} = 0$, $G_{11} = -1$, and $\alpha = 1$ which satisfies the stability criterion (27). We note the slow oscillatory decay which is characteristic of nonlinear quadratic damping (Figure 3).

In the second case (Figure 4) $\alpha = 3$, and the control system admits a limit cycle oscillation. In this case eq. (26) predicts a limit cycle radius of $R \simeq 0.86$ which agrees favorably with the numerical result. In the third example (Figure 5) we choose $G_{02} = G_{20} = 0$, $G_{11} = 1$. This case shows a stable damped spiral as in Figure 3.

B) Linear Feedback Control

The curious reader may wonder why we did not treat the case of the linear feedback (7) first. A linear feedback law, however, introduces quadratic terms in the dynamic equation (4) (or (13), (14)) in the limit of small lag $\alpha \to \infty$.

This introduces a saddle point in the phase plane and the system may not be globally bounded. However, using an analysis similar to that in the previous section we can show that the origin can be made stable in the limit of $\alpha \to \infty$. In this limit a linear feedback law

$$z = k_1 x + k_2 y \tag{28}$$

leads to the dynamic equation

$$\ddot{x} + x + k_1 x^2 + k_2 xy = 0 \tag{29}$$

Using normal form theory, an expression for the phase plane motion in polar coordinates can be found similar to (21)

$$\dot{r} = \frac{k_1 k_2 r^3}{8} + 0(5) \tag{30}$$

$$\dot{\theta} = \frac{1}{24} (k_2^2 + 10k_1^2) r^2 - 1 + 0(4) \tag{31}$$

By choosing $k_1 k_2 < 0$ a damped spiral motion can be obtained in the vicinity of the origin.

Numerical integration of the equation (29) confirms the result implied in (30), namely a stable spiral will result for $k_1 k_2 < 0$. This is illustrated in Figure 6. One can also observe in the Figure that for large initial conditions, the motion is not bounded because of the aforementioned saddle point at $y = 0$, $x = -1/k_1$.

C) Nonlinear Feedback -Rational Functions

As a final example we examine the case of stiffness control with a rational traction feedback law where the equations take the form

$$\dot{x} = y$$

$$\dot{y} = -(1 + z)x \tag{32}$$

$$\dot{z} = -\alpha z + \alpha P(x,y)/Q(x,y)$$

where P, Q are polynomials in the amplitude and velocity variables x,y. As a special case, we choose a form of P,Q such that for large amplitude $x \to \infty$ and small feedback lag $\alpha \to \infty$, the system (32) looks like a damped linear oscillator. One choice is the following

$$\dot{x} = y$$

$$\dot{y} = -(1+z)x \tag{33}$$

$$\dot{z} = -\alpha z + \alpha \Gamma xy/(1 + \eta x^2)$$

336

When $|x| \to \infty$ and $\alpha \to \infty$ this looks like

$$\ddot{x} + \frac{\Gamma}{\eta} \dot{x} + x = 0 \tag{34}$$

For small $|x|$, (33) reduces to the previous example A with $G_{02} = G_{20} = 0$, $\Gamma = G_{11}$. From the previous analysis we require $\Gamma > 0$ for stability. By choosing optimum values for Γ, η one can hope to get the state vector to approach the origin with little oscillation.

A numerical simulation of the equations (33) was carried out using a fourth order Runge-Kutta algorithm for the case $\Gamma = 10$, $\eta = 1$. The results are shown in Figure 7. This control law has clear advantages over the quadratic case.

CONCLUSION

This pilot study on the possibility of stiffness control of structural dynamics illustrates some of the complexities of this concept. First the nature of stiffness control leads to a nonlinear dynamical problem even when the feedback law is linear. Second the study shows that nonlinear feedback laws may be more desirable than linear control when stiffness control is used. Finally we note the power of exact computer algebra (MACSYMA) in allowing one to use powerful nonlinear perturbation techniques such as normal form theory to analyze the stability of these nonlinear systems.

REFERENCES

1. Knyazev, A.S. and Tartakowskii, "Application of Electromechanical Feedback for the Damping of Flexural Vibration in Rods." Soviet Physics Acoustics Vol. II, pp. 150-154, October-December 1965.

2. Moon, F.C. and Dowell, E.H., "Control of Flutter Instability in a Continuous Elastic System Using Feedback." Proc. AIAA/ASME 11th Structures, Structural Dynamics, an Materials Conference, 1970.

3. Horikawa, H., Dowell, E.H., and Moon, F.C., "Active Feedback Control of a Beam Subjected to a Nonconservative Force." Int. J. Solids and Structures 14, pp. 821-839, 1978.

4. Meirovich, L. and Baruh, H., "Control of Self-Adjoint Distributed-Parameter System." J. Guidance, Control and Dynamics, Vol. 5, No. 1, 1982.

5. Chen, J. C., "Response of Large Space Structures with Stiffness Control," AAS/AIAA Paper No. 83-344, Astrodynamics Specialist Conference, Lake Placid, New York, August 1983.

6. Fanson, J.L., Chen, J.C. and Caughey, T.K., "Stiffness Control of Large Space Structures," This Conference.

7. Carr, J., "Applications of Centre Manifold Theory." Springer Verlag, 1981.

8. Rand, R.H., "Computer Algebra in Applied Mathematics: An Introduction to MACSYMA." Pitman Publishing, 1984.

9. Minorsky, N., "Nonlinear Oscillations." D. Van Nostrand Co., 1962.

10. Guckenheimer, J. and Holmes, P.J., "Nonlinear Oscillations, Dynamical Systems, and Bifurcations of Vector Fields." Springer-Verlag, 1983.

11. Takens, F., "Singularities of Vector Fields." Publ. Math. Inst. Hautes Etudes Sci. 43, 47-100, 1974.
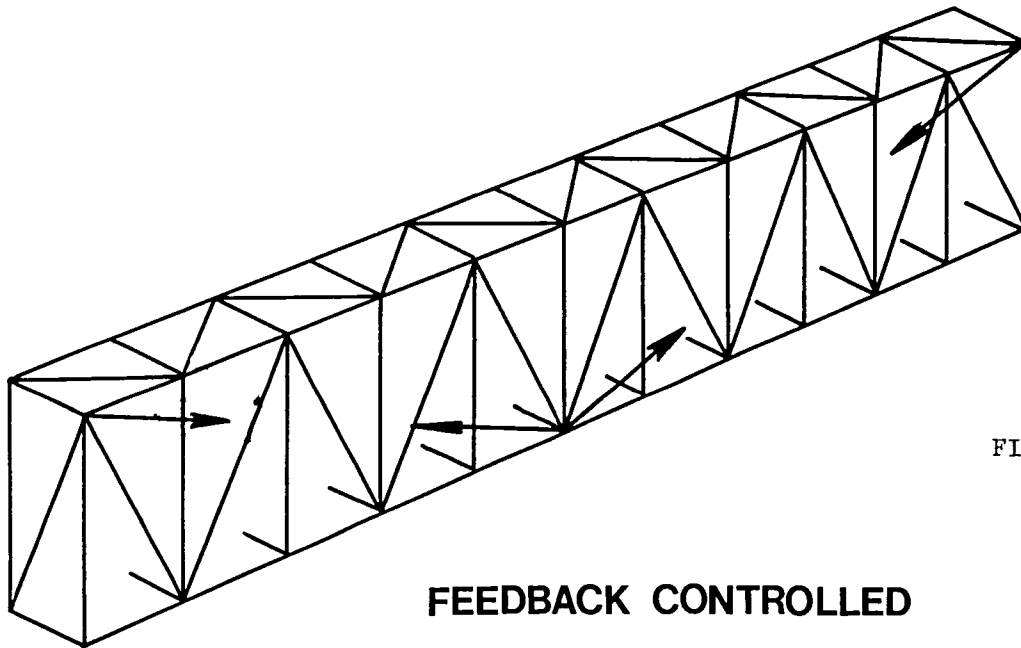
FEEDBACK CONTROLLED TENSION CABLES

FIGURE 1

BENDING DISTURBANCE

$u(x,t)$

X
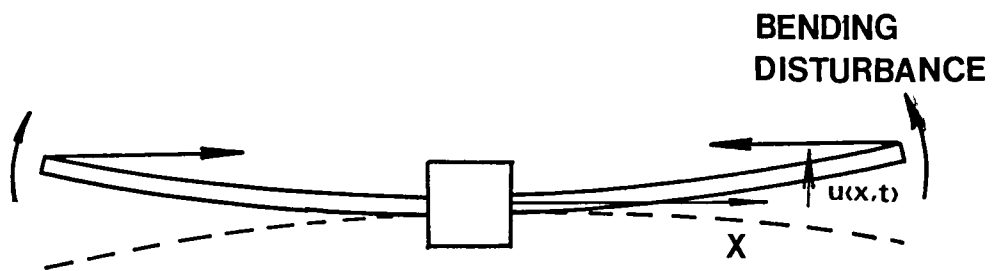
IDEALIZED MODEL

FIGURE 2
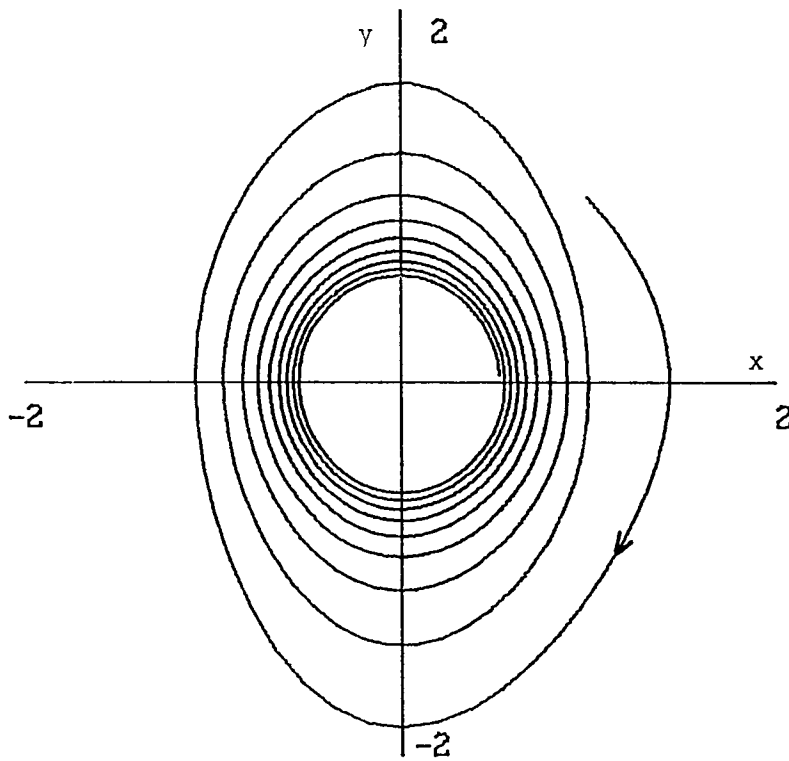
FIGURE 3. Numerical integration of eqs.(13)-(15) for parameter values $\alpha=1$, G02=1, G11=-1, G20=0. Note absence of limit cycle.
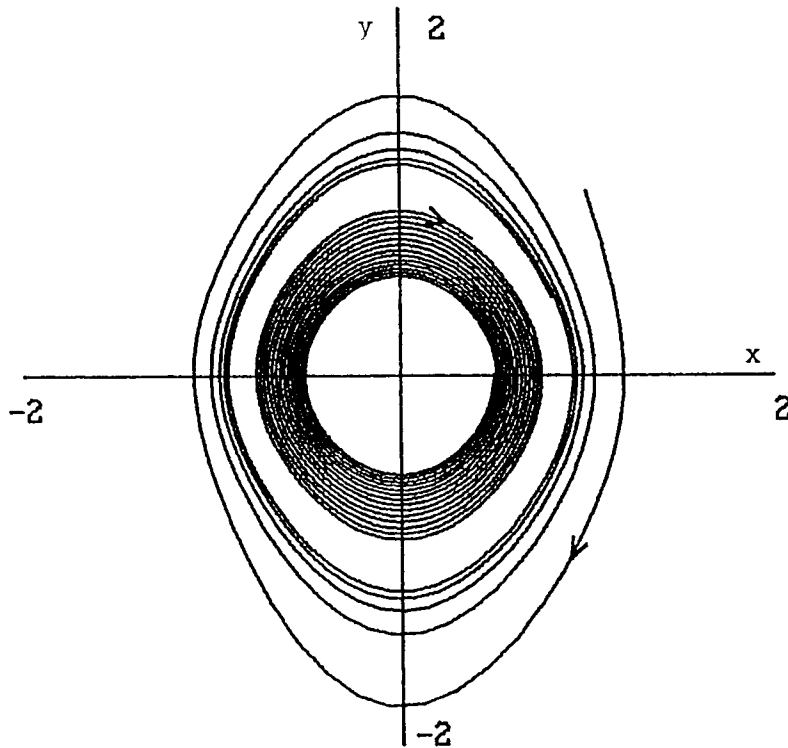
FIGURE 4. Numerical integration of eqs.(13)-(15) for parameter values $\alpha=3$, G02=1, G11=-1, G20=0. Presence of limit cycle indicated by growing inner trajectory and decaying outer trajectory.
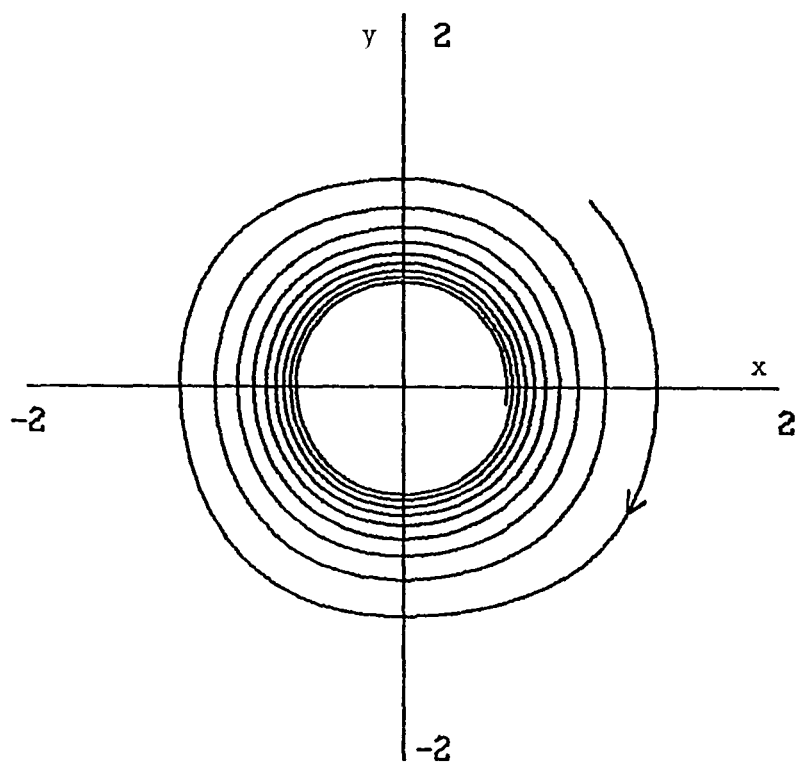
FIGURE 5. Numerical integration of eqs.(13)-(15) for parameter values $\alpha=1$, G02=0, G11=1, G20=0. The origin is aymptotically stable, in agreement with eq.(27).
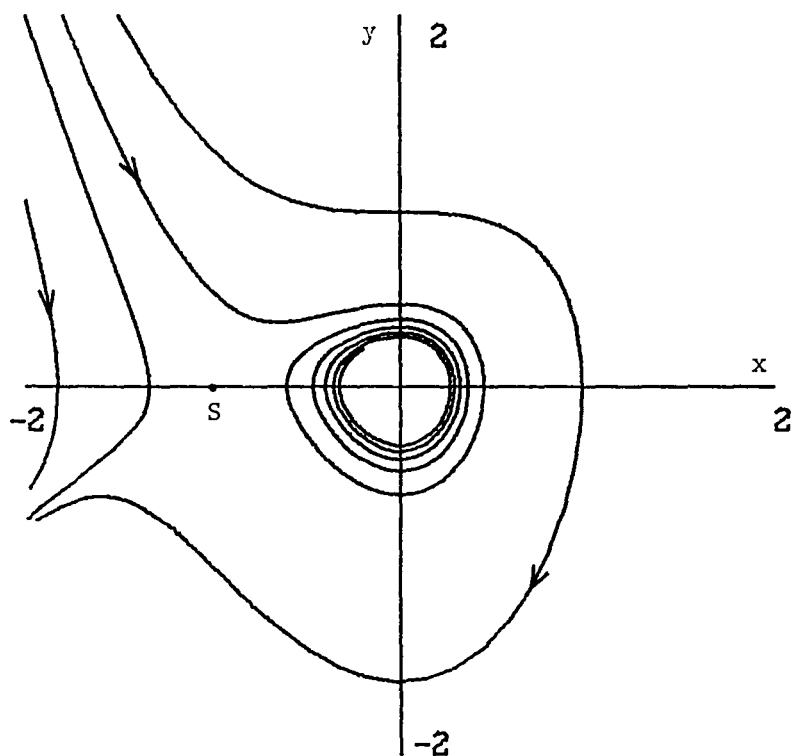
FIGURE 6. Numerical integration of eq.(29) with y=dx/dt for parameter values k1=1, k2=-1. Although the origin is aymptotically stable for sufficiently small initial conditions, the presence of a saddle S at x=-1, y=0 prevents the origin from exhibiting global asymptotic stability.
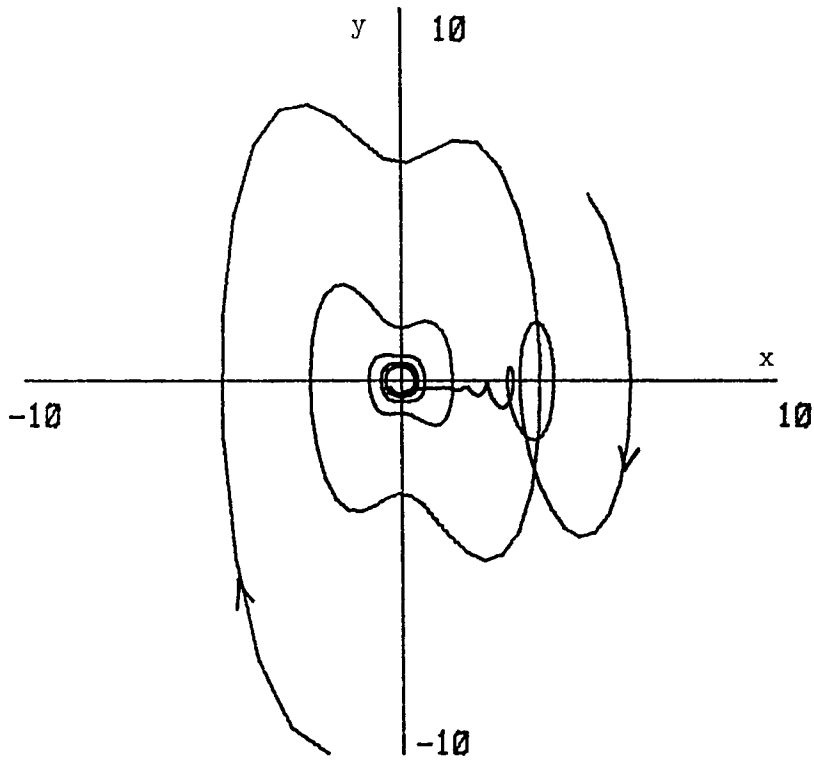
FIGURE 7. Numerical
integration of
eqs.(33) for
parameter values
α =1, Γ =10, η =1.

VIBRATIONAL STABILIZATION OF FLEXIBLE STRUCTURES

M. Zak

Jet Propulsion Laboratory
California Institute of Technology
Pasadena, CA 91109

ABSTRACT

The influence of high frequency excitations on flexible structure member characteristics is investigated. The response to these excitations is decomposed in two parts: "slow" motion, which practically remains unchanged during the vanishingly small period, and "fast" motion, whose value during this period is negligible in terms of displacements, but is essential in terms of velocities and the kinetic energy. After such a decomposition the "slow" (or the mean) motion becomes nonlinearly coupled with the "fast" motion (or the fluctuations) by the corresponding governing equations.

This coupling leads to an additional "effective" potential energy which changes the fundamental characteristic properties of the elastic continuum. The most important contribution of the high frequency excitation is the increase of the acoustic speed of longitudinal and shear wave propagation, i.e., the increase of the effective elastic moduli in the direction of the wave vector. This effect allows the stabilization and control of stiffness in any selected direction by the corresponding change in the intensity of the high frequency excitations.

This approach for dynamical stiffening can be applied to flexible structural elements (films, shells, etc.) for a temporary increase of their stiffness in the course of occasional loads to prevent buckling or wrinkling.

In practical terms, the high frequency excitations can be imparted by electromechanical transducers. It is implied that the exciting frequency is much smaller than frequencies characterizing molecular motions, as well as the wavelength of the exciting oscillations being much larger than the distances between the atoms in crystal lattices. At the same time, this frequency must be much higher than all the eigen-frequencies, whose energy contributions are essential.

Thus, this work addresses a new approach for dynamical stiffening and stiffness control which can be effective in large flexible structures. Such an approach may prove to be very practical in the sense that large structures need to be made as flimsy as possible for low cost under ordinary situations. However, for certain operations such as deployment, orbital transfer, docking, and other circumstances, it would be vital to have a means of temporarily stiffening certain structural members. If the structure was designed to meet these occasional loads without temporary stiffening, it would be considerably more massive and more expensive.

I. INTRODUCTION

The influence of high frequency excitations (HFE) on mechanical systems with relatively low eigen-frequencies is well known [1]. Some applications of this effect to vibrational control and stabilization are considered in [2]. The present paper is devoted to the HFE effect on special types of mechanical systems which have not been treated before. These systems are characterized by nonlinearities with respect to velocities and include all the continuous systems as well as some of the finite-degree-of-freedom systems (particularly the systems with non-euclidean metric of the configuration space). In contrast to the systems with euclidean metric of the configuration space (which were treated in [1], [2]) here HFE cannot be preassigned in advance: they are coupled with the basic ("slow") motions forming a nonlinear system of a higher order. This system possesses new fundamental properties such as different acoustic speeds, different stiffness characteristics, etc., so that HFE can be used as an actuator for its stabilization and control.

Herein, the feasibility of this new approach is analyzed.

II. CONTINUOUS SYSTEMS

a. <u>Governing Equations</u>. Assume that the motion of a continuous system is characterized by a time scale τ and a distance scale ℓ upon which the changes of the system parameters are negligible. Suppose now that the continuum is subjected to additional external excitations characterized by frequencies of the order of $\hat{\omega}$, where

$$\omega \gg \frac{1}{\ell} \tag{1}$$

Then the response can be sought in the form:

$$\overset{*}{v} = v \, (v,t) + \tilde{v}(r,t) \, e^{i(k \cdot r - \omega t)} \quad , \quad k = \frac{\omega}{c} \tag{2}$$

where $\overset{*}{v}$ is the total displacement, v and $\tilde{v}$ are smooth functions characterized by the scales τ and ℓ , and k is the wave vector:

$$k \gg \frac{1}{\ell} \tag{3}$$

and c is the acoustic speed in the k-direction.

Obviously,

$$\int_0^{2\pi/\omega} \tilde{v} \, e^{i \, (k \cdot r - \omega t)} \, dt = 0 \qquad \frac{\omega}{2\pi} \int_0^{2\pi/\omega} v \, dt = v \qquad \frac{\omega}{2\pi} \int_0^{2\pi/\omega} \tilde{v} \, dt = \tilde{v} \tag{4}$$

344

Thus, Eq. (2) decomposes the original motion into two parts: slow motion $\mathbf{v}$, and fast motion $\tilde{\mathbf{v}} \exp[i(\mathbf{k} \cdot \mathbf{r} - \omega t)]$. Due to the difference in scales they can be treated as geometrically independent, and therefore, formally the velocity speed becomes doublevalued.

Separating different scale motions in the momentum and continuity equations:

$$\rho(\frac{\partial \overset{*}{\mathbf{v}}}{\partial t}) + \overset{*}{\mathbf{v}} \nabla \overset{*}{\mathbf{v}}) = \nabla \cdot T \quad , \quad \frac{\partial \rho}{\partial t} + \nabla \cdot (\rho \overset{*}{\mathbf{v}}) = 0 \qquad (5)$$

where ρ is the density, and T is the elastic stress tensor, one arrives at the following equations:

$$\rho(\frac{\partial \mathbf{v}}{\partial t} + \mathbf{v} \nabla \mathbf{v} + \tilde{\mathbf{v}} \nabla \tilde{\mathbf{v}}) = \nabla \cdot T \qquad (6)$$

$$\rho(\frac{\partial \tilde{\mathbf{v}}}{\partial t} + \mathbf{v} \nabla \tilde{\mathbf{v}} + \tilde{\mathbf{v}} \nabla \mathbf{v}) = \nabla \cdot \tilde{T} \qquad (7)$$

$$\frac{\partial \rho}{\partial t} + \nabla \cdot (\rho \mathbf{v}) = 0 \qquad (8)$$

which nonlinearly couple the slow and fast motions through the convective terms of the acceleration.

For better physical interpretation Eqs. (6) and (7) are presented in the form:

$$\rho\left[\frac{\partial \mathbf{v}}{\partial t} + \mathbf{v} \nabla \mathbf{v} - \tilde{\mathbf{v}} \times \left(\nabla \times \tilde{\mathbf{v}}\right)\right] = \nabla \cdot T + \nabla\Pi \qquad (9)$$

$$\rho\left[\frac{\partial \mathbf{v}}{\partial t} - \mathbf{v} \times (\nabla \times \mathbf{v}) - \mathbf{v} \times \nabla \times \mathbf{v})\right] = \nabla \cdot T + \nabla \qquad (10)$$

where

$$\Pi = \frac{\tilde{\mathbf{v}}^2}{2} \quad , \quad \tilde{\Pi} = \mathbf{v} \cdot \tilde{\mathbf{v}} \qquad (11)$$

are the additional potential energies contributed by HFE.

b. Stabilization Effects.   For conservative continua if

$$\nabla \times \mathbf{v} = 0 \; , \quad \nabla \times \tilde{\mathbf{v}} = 0 \; , \quad \mathbf{v} \perp \tilde{\mathbf{v}} \; , \qquad (12)$$

Eqs. (9) and (10) are decoupled. Comparing now Eq. (9) with the corresponding equation without HFE:

$$\rho(\frac{\partial \mathbf{v}}{\partial t} + \mathbf{v} \nabla \mathbf{v}) = \nabla \cdot T \qquad (9a)$$

and applying the Rayleigh-Courant-Fisher theorem one concludes that

$$\lambda_1^* > \lambda_i^* \quad (i = 1,2,\ldots\ldots \text{ etc.})\tag{13}$$

where λ_i^*, λ_1 are the characteristic frequencies of the linearized Eqs. (9) and (9a), respectively.

In other words, HFE make a conservative continuous system more rigid if the conditions (12) are satisfied.

c. <u>Stiffening Effects</u>. An additional evidence of the stabilization effect of HFE on continua follows from a comparison of acoustic speeds before and after HFE.

For an elastic continuum

$$C_n = \pm\frac{\tilde{v}_n}{2} \pm \sqrt{\frac{E(1-\mu)}{\rho(1+\mu)(1-2\mu)} + \frac{\tilde{v}_n^2}{4}}\tag{14}$$

$$C_\tau = \pm\frac{\tilde{v}_n}{2} \pm \sqrt{\frac{G}{\rho} + \frac{\tilde{v}_n^2}{4}}\tag{15}$$

in which C_n, C_τ are the longitudinal and transverse acoustic speeds after HFE; E, G are the Young's and shear moduli, respectively; μ is the Poisson's ratio; $\tilde{v}_n$ is the excitation velocity in the direction of the wave propagation.

As follows from these expressions, the effective Young's and shear moduli can be introduced:

$$E' = E + \frac{(1+\mu)(1-2\mu)}{4(1-\mu)}\rho\tilde{v}_n^2 \quad E, \quad G' = G + \frac{\rho}{4}\tilde{v}_n^2 > G\tag{16}$$

which illustrates the stiffening effect.

For an inviscid fluid:

$$C_n = v_n \pm \sqrt{a^2 + \frac{1}{2}\tilde{v}_n^2}\tag{17}$$

$$C_\tau = v_n \pm \frac{\tilde{v}_n}{\sqrt{2}}\tag{18}$$

where a is the speed of sound.

Thus, HFE increase the effective speed of sound. Moreover, as follows from Eq. (18), they create a new elastic (transverse) wave transmitting vorticity.

All the results (14) - (18) hold true irrespective to the conditions (12).

346

d. <u>Damping Effects.</u> As follows from the above, the potential part of the HFE velocity field $\nabla(\tilde{v}^2/2)$ contributes into the potential energy of the system, and therefore, stabilizes it. At the same time, the rotational (vortex) part of the HFE velocity field $(\nabla \times \tilde{v})$ leads to dissipation of the mechanical energy through the material viscosity ν and contributes to the damping effect. The corresponding viscous stress T' contribution can be written as:

$$\nabla \cdot T' = -\rho\nu(\tilde{v}k) \cdot k \tag{19}$$

Thus, now the force $\nabla \cdot T$ in Eq. (10) includes the viscous component $\nabla \cdot T'$ expressed by Eq. (19). The effect of this force, i.e., the decrease of HFE amplitudes as well as the decrease of the depth of their penetration, is proportional to $\omega^2 = k^2c^2$.

Obviously, the energy dissipation is accompanied by the heat flow which, in general, will be coupled with the equations of motion (9), (10) through additional thermal forces.

e. <u>Remarks</u>

1. It is implied that the exciting frequency ω is much smaller than frequencies characterizing molecular motions, as well as the wavelength of the exciting oscillations, $1/k$, is much larger than the distances between the atoms in crystal lattices.

2. In elastic continua an additional limitation on the exciting frequency ω is imposed by the ultimate stress [T]:

$$\omega \leq \frac{[T]}{\rho\tilde{u}c_n} \tag{20}$$

where u is the displacement corresponding to the velocity u. As follows from (20):

$$\frac{E'}{E} \sim 1 + \frac{[T]}{E} , \quad \frac{G'}{G} \sim 1 + \frac{[T]}{G} \tag{21}$$

Hence, the longitudinal stiffening effect is practically negligible since usually $[T]/E \ll 1$. However, the transverse stiffening effect can be essential because the ratio $[T]/G$ can be large for flexible structural elements with low shear moduli such as strings, membranes, soft shells, and special types of laminated materials.

3. Theoretically, a continuous system possesses an infinite number of eigen-frequencies, the sequence of which is unbounded. However, practically, the energy contribution of very high eigen-frequency is negligible, and therefore, this sequence can be truncated, and the condition (1) is rewritten in the form:

$$\omega \gg \lambda_* \tag{22}$$

where λ_* is the greatest eigen-frequency whose energy contribution is essential.

III. EXAMPLE

In this item the theory will be illustrated by an example,

Stabilization of a String in the Gravity Field

The governing equation of equilibrium of a string subjected to longitudinal HFE in a gravity field is:

$$\frac{\partial}{\partial s} \left(T \frac{\partial r}{\partial s}\right) + \rho g = 0 \quad , \quad (T = T_0 + \rho \tilde{v}^2) \tag{23}$$

where r is the position vector, T_0 is the tension, ρg is the specific weight, and $\rho v^2/2$ is the kinetic energy of the stationary field of the longitudinal excitations. Obviously, an increase of the effective tension due to HFE stabilizes the string shape. In particular, longitudinal HFE can stabilize a vertical string which is attached below and has a free end at the top if

$$\tilde{v}^2 > 2g\,h \tag{24}$$

where h is the string length. Indeed, in this case the effective tension is positive (T>0) although the physical tension is negative (T_0<0).

CONCLUSION

It has been demonstrated that a HFE field significantly changes the fundamental properties of mechanical systems. The most important contribution of HFE is the stiffening effect of an elastic continuum in the direction of the wave vector. This effect allows control of stiffness in any selected direction by the corresponding changes in the intensity of HFE.

This new approach can be effective for large flexible space structures. Such an approach may prove to be very practical in the sense that large structures need to be made as flimsy as possible for low cost under ordinary situations. However, for certain operations such as deployment, orbital transfer, docking, and other circumstances, it would be vital to have a means of temporarily stiffening certain structural members. If the structure was designed to meet these occasional loads without temporary stiffening, it would be considerably more massive and more expensive.

REFERENCES

[1] Landou, L. D., and Lifshitz, E. M., "Course of Theoretical Physics", Vol. 1, Pergamon Press.

[2] Meerkov, S. M., "Conditions of Vibrational Stabilizability for Class of Nonlinear Systems", IEEE Transactions of Automatic Control, Vol. AC-27, No. 2, April 1982, pp. 485-487.

STIFFNESS CONTROL OF LARGE SPACE STRUCTURES

J. L. Fanson*, J. C. Chen**, and T. K. Caughey***
California Institute of Technology
Pasadena, CA 91109

ABSTRACT

A technique for using internal force producing dual element/actuators for vibration suppression of large space structures is proposed. The method is applied to a low order system. Selective modal damping is achieved. The actuators used in this method may be electrically powered. The method is suitable for structures which are too slender or flimsy to permit the use of reaction jet-type actuators.

I. INTRODUCTION

Large Space Structures (LSS) or Flexible Space Structures, as they are sometimes called, are a natural outgrowth of our rather recently acquired ability to transport and construct large objects in space. The capability of astronauts to do construction-like activities was demonstrated on the last Space Shuttle mission (STS-11). Already proposed LSS concepts include large antennas, solar sails, space stations, solar power satellites, and large orbiting platforms.

The performance of many of these systems depends critically on precise pointing or precise structural configuration. Since LSS are necessarily very flexible, numerous control problems become evident. LSS control objectives can be organized into three main categories. In increasing order of complexity they are: (1) Pointing accuracy, (2) Vibration suppression, and (3) Shape control. The problem of pointing accuracy is not new in spacecraft control, and has been largely solved over the last 25 years. The problems of vibration suppression and shape control are new. An important observation is that the objective of pointing can always be decoupled from the other two objectives. This is more clearly seen if one considers that pointing (in the rigid body sense) is affected by purely external forces, while vibration and shape are purely internal to the structure; they are "flexible body" concerns.

---

*Graduate Student, Applied Mechanics Department.
**Member Technical Staff, Jet Propulsion Laboratory
***Professor of Applied Mechanics.

The major differences then, between LSS control objectives and control objectives of the past, are seen to be due to structural complexity. When we approach the problems of vibration suppression and shape control we should bear in mind the structural nature of the problem.

It is also important to recognize that conventional-type actuators of the past may not be applicable to either the new class of control objectives or the new class of space structures. The primary actuators which have been used in space before are external force producing devices, namely, rockets and momentum wheels. These are consistent with the historical objective of pointing accuracy which requires external forces.

Since the new objectives do not require external forces, conventional actuators may not be the best way to meet them. Furthermore, rockets require fuel. Refueling a structure in high earth orbit may be prohibitively expensive; for a structure on an interplanetary trajectory, it may simply be impossible. Structures, such as solar sails or large antennas, may also be too thin and flimsy to allow the attachment of a massive actuator such as a rocket or a momentum wheel[1].

One source of power for a new class of actuator is the sun. If we can develop a technology which is electrically powered and provides control forces internal to the structure, we are well on the way to meeting the new objectives of vibration suppression and shape control.

II. APPROACH

We will approach the LSS control problem from a somewhat more structural viewpoint. We call the approach "stiffness control." There are different possible interpretations of the concept of stiffness control, so it need not be narrowly defined. This paper is concerned with one particular realization of stiffness control; there are others.

Before delving into the specifics of the approach it is useful to review some of the structural peculiarities of large space structures. LSS are continuous structures and therefore have essentially an infinite spectrum. We say "essentially" in view of Hughes' "absurd subspace"[2]. Related to this fact is the difficulty of system identification of LSS. Much work is being done on the problem of identification, but it seems safe to assume that, no matter how good identification becomes, we will be somewhat limited in our ability to estimate modal coordinates in real time. This implies possible difficulty for any control scheme which requires knowledge of modal coordinates, particularly of higher modes.

This does not mean, however, that such control schemes should be abandoned. Ideally, modal control, or the ability to damp out selected modes, is the most efficient means to damp out vibrations, since it makes the most intelligent use of knowledge of the structure. Secondly, vibrational energy will reside mainly in the lower modes, and these are the modes which are estimated best. Thirdly, the lower modes are the most troublesome from a

vibrational standpoint since they are associated with lower frequencies. At lower frequencies it takes longer for energy to dissipate by natural means. And lastly, for a given energy, lower modes vibrate at higher amplitude which results in a more degraded configuraton. So, while our knowledge of modal coordinates may be imperfect, this knowledge may still be useful and should not be abandoned a priori.

LSS may also have the property of very low inherent structural damping. This is a benefit from the control standpoint for two reasons: Low inherent damping makes the classical normal modes assumption closer to reality. Even more importantly, low inherent damping means that our control system does not have to introduce large damping into the structure to be useful. If only order ε damping is introduced by active control, it may double the overall damping in the structure. LSS are likely to exhibit many other peculiarities such as geometric nonlinearity, nonlinear modal coupling, etc., but these concerns are beyond the scope of this paper.

Chen investigated the stiffness control approach applied to a vibrating string[1]. For purposes of illustration the method will be reconstructed here. Consider the transverse vibration of a string described by the following differential equation:

$$\rho \frac{\partial^2 y}{\partial t^2} = \frac{\partial}{\partial x} \left(T \frac{\partial y}{\partial x} \right) \tag{1}$$

with the initial condition: $y = 0$, $\partial y/\partial t = \sin(\pi x/L)$ at $t = 0$, and the boundary condition: $y = 0$ at $x = 0,L$,

where
- y = transverse displacement
- x = axial coordinate
- t = time coordinate
- ρ = mass density per unit length of the string
- T = tension in the string
- L = string length

The tension T can be seen from Eq. (1) to represent the system "stiffness". By modulating the tension T by an amount $\Delta T(t)$ it is possible to introduce damping. Chen investigated various control laws for $\Delta T(t)$ and was able to produce various damping rates. Thus, by modulating the stiffness of the system, the string is rendered stable.

The string is a simple one-dimensional example. For a large space structure, even for a finite element model of one, the system typically has thousands of degrees of freedom. The stiffness of such a system is not a scalar quantity. The next step in investigating the application of stiffness control to LSS is to apply it to a multi-degree-of-freedom system. There are two approaches to choose from: one approach is to attempt some meaningful form of modal stiffness control, and the other approach is direct output feedback. Since modal control is attractive, the remainder of this paper is devoted to this first approach.

353

III. PROBLEM FORMULATION

In order to gain an insight into the basic physical relationships of stiffness control for multi-degree-of-freedom systems, we first confine ourselves to the simplest configuration, and postpone the consideration of structural complexities. Consider the following three mass-two spring system:
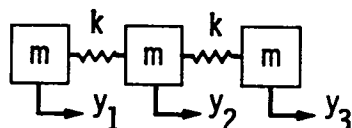
The differential equation of motion for this system is:

$$M\ddot{y} + Ky = 0 \qquad (2)$$

where

$$M = \begin{bmatrix} m & 0 & 0 \\ 0 & m & 0 \\ 0 & 0 & m \end{bmatrix} \quad , \quad K = \begin{bmatrix} k & -k & 0 \\ -k & 2k & -k \\ 0 & -k & k \end{bmatrix} \quad , \quad y = \begin{Bmatrix} y_1 \\ y_2 \\ y_3 \end{Bmatrix} \quad .$$

This is a three-degree-of-freedom system, but has only two vibratory modes. Label the first and second vibratory modal coordinates $\xi_1(t)$, and $\xi_2(t)$ respectively. As control actuators, consider the springs as having controllable effective stiffness. In other words, the spring elements themselves function dually as structural components and control actuators. We need not make every element an actuator, but for simplicity let us take them both to be.

The first two requirements for LSS control actuators are satisfied, namely, they can be electrically powered, and they apply only internal forces to the structure. The details of the design of the actuator/elements are unimportant so long as they exhibit the general property of controllable stiffness. We will assume that the actuators have an infinite bandwidth in order to avoid complications.

The equation of motion with stiffness modulation is given by:

$$M\ddot{y} + Ky = -C(t) Ky \qquad (3)$$

where $C(t)$ is a scalar gain which is yet to be constructed. Because the system stiffness matrix is modulated by a scalar, the modal matrix for the closed loop system is the same as for the system described by Eq. (2). Let ϕ

represent the mass normalized modal matrix. Premultiply Eq. (3) by ϕ^T and post-multiply by ϕ in the usual way to obtain:

$$\phi^T M \phi \dot{\underset{\sim}{y}} + \phi^T K \phi \underset{\sim}{y} = -C(t) \phi^T K \phi \underset{\sim}{y} \ . \tag{4}$$

Let
$$\underset{\sim}{\xi} = \left\{ \begin{matrix} \xi_0 \\ \xi_1 \\ \xi_2 \end{matrix} \right\} = \phi \underset{\sim}{y} \ .$$

Equation (4), now written in modal space, becomes:

$$I \ddot{\underset{\sim}{\xi}} + [\omega_0^2] \underset{\sim}{\xi} + C(t)[\omega_0^2] \underset{\sim}{\xi} = 0 \ , \tag{5}$$

where:
$$I = \text{identity matrix}$$

$$[\omega_0^2] = \begin{bmatrix} 0 & 0 & 0 \\ 0 & k/m & 0 \\ 0 & 0 & 3k/m \end{bmatrix} \ .$$

The equations governing the two vibratory modes are:

$$\ddot{\xi}_1 + k/m \ \xi_1 + C(t) \ k/m \ \xi_1 = 0$$

$$\ddot{\xi}_2 + 3k/m \ \xi_2 + C(t) \ 3k/m \ \xi_2 = 0 \tag{6}$$

The objective is to choose $C(t)$ in such a way as to render Eqs. (6) Liapunov asymptotically stable (LAS).

Let
$$C(t) = \frac{m}{k}(C_1 \xi_1 \dot{\xi}_1 + C_2 \xi_2 \dot{\xi}_2) \ , \tag{7}$$

This control law is motivated by the Reid's spring[3]. The true Reid's spring would use sgn $(\xi \dot{\xi})$. This would be expected to give better performance for small values of $\xi \dot{\xi}$, but for simplicity the sgn has been dropped.

This control law couples the two modes; however, since $C(t)$ is likely in practice to be a function of order ϵ, the coupling will also be order ϵ. Substituting Eq. (7) into Eq. (6) results in:

355

$$\ddot{\xi}_1 + (k/m + C_2\,\xi_2\dot{\xi}_2)\,\xi_1 + C_1\,\xi_1^2\dot{\xi}_1 = 0 \quad,$$

$$\ddot{\xi}_2 + (3k/m + 3\,C_1\xi_1\dot{\xi}_1)\,\xi_2 + 3\,C_2\,\xi_2^2\dot{\xi}_2 = 0 \quad. \tag{8}$$

If $C_2/C_1 = 3$, then system (8) is LAS.

To establish the asymptotic stability of (8) we will employ the Liapunov direct method.

Let E be a Liapunov function defined by:

$$E = \frac{1}{2}\dot{\xi}_1^2 + \frac{k}{2m}\xi_1^2 + \frac{1}{2}\dot{\xi}_2^2 + \frac{3k}{2m}\xi_2^2 \quad,$$

$$E = 0 \quad \text{at the origin:} \quad \xi_1 = \dot{\xi}_1 = \xi_2 = \dot{\xi}_2 = 0 \quad,$$

$$E > 0 \quad \text{away from the origin}$$

E is just the total system energy.

Differentiating E with respect to time gives:

$$\dot{E} = \underset{\sim}{x}^T\, P\, \underset{\sim}{x} \quad, \tag{9}$$

where

$$\underset{\sim}{x} = \left\{ \begin{array}{c} \xi_1\dot{\xi}_1 \\[4pt] \xi_2\dot{\xi}_2 \end{array} \right\} \quad, \qquad P = \begin{bmatrix} -C_1 & -\frac{1}{2}(C_2+3C_1) \\[4pt] -\frac{1}{2}(C_2+3C_1) & -3C_2 \end{bmatrix}$$

In Eq. (9), $\dot{E}$ can be made negative semidefinite by choosing $C_2/C_1 = 3$.

Hence $\qquad \dot{E} = 0 \quad$ at the origin,

$\qquad\qquad\quad \dot{E} \leq 0 \quad$ away from the origin.

This establishes the origin as Liapunov stable.

To show asymptotic stability notice that away from the origin the condition for $\dot{E} = 0$ is:

$$\left(\frac{\xi_2\dot{\xi}_2}{\xi_1\dot{\xi}_1}\right) = -\frac{1}{3} \quad. \tag{10}$$

which is a line in the $\xi_1\dot{\xi}_1 - \xi_2\dot{\xi}_2$ plane. This plane we call modal-product space.

A typical trajectory of system (8) in modal-product space is shown in Figure 1. Suppose the system is on the line:

$$\left(\frac{\xi_2\dot{\xi}_2}{\xi_1\dot{\xi}_1}\right) = -\frac{1}{3} \quad ,$$

and suppose that

$$\frac{d}{dt}\left(\frac{\xi_2\dot{\xi}_2}{\xi_1\dot{\xi}_1}\right) = 0 \quad .$$

It can be shown (see Appendix) that if these two conditions are met, then

$$\frac{d^2}{dt^2}\left(\frac{\xi_2\dot{\xi}_2}{\xi_1\dot{\xi}_1}\right) = \frac{8}{3}\frac{k}{m} \neq 0 \quad .$$

Therefore, away from the origin, $\dot{E}$ can be zero at most on a set of measure zero. Hence, system (8) is actually LAS.

Figure 2 shows a time history of the individual modal energies and the total system energy corresponding to the trajectory in Figure 1. It can be seen that if $C_2/C_1 = 3$, the second mode is damped out faster than the first mode. Plateaus in the total system energy can be readily correlated with trajectories approaching the line $(\xi_2\dot{\xi}_2/\xi_1\dot{\xi}_1) = -1/3$. Figures 3 and 4 show the time histories of the displacements and velocities. The initial conditions for all the examples are given by:

$$\xi_1 = 1.732 \quad , \quad \dot{\xi}_1 = 1 \quad ,$$

$$\xi_2 = 0 \quad \quad , \quad \dot{\xi}_2 = 2 \quad ,$$

$$k/m = 1 \quad \quad .$$

By altering the ratio C_2/C_1 the two modes can be damped out at different relative rates. Figure 5 shows the energy time history for $C_2/C_1 = 1$. This ratio violates the condition for $\dot{E} \leq 0$. A region now exists in modal-product space where $\dot{E} > 0$. On the boundary of this region $\dot{E} = 0$. The boundaries for the region in modal-product space are given by:

$$\left(\frac{\xi_2\dot{\xi}_2}{\xi_1\dot{\xi}_1}\right) = -\frac{1}{3} \text{ , and } \quad \left(\frac{\xi_2\dot{\xi}_2}{\xi_1\dot{\xi}_1}\right) = -\frac{C_1}{C_2} \quad .$$

Figure 6 shows the trajectory corresponding to the time history of Figure 5. The Liapunov stability result is seen to be quite conservative. The case for $C_2/C_1 = 1/3$ is shown in Figures 7 and 8. Performance still remains good even though the ratio C_2/C_1 is changed by a factor of 9 from that giving $\dot{E} \leq 0$.

DISCUSSION AND CONCLUSIONS

The method of stiffness control has been used successfully on a low order system. The technique allows the vibratory modes to be damped out selectively, even though these modes are not strictly uncoupled. The actuator/elements impart only internal forces to the structure. The actuators can conceivably be powered electrically. There is another possible benefit from using dual purpose actuator/structural elements. It may be possible to use these elements to affect shape control simultaneously with vibration suppression. This application requires further investigation.

Several other questions remain to be answered. Among these is the question of robustness: Can the control system tolerate perturbations in system parameters? What is the effect of observation spillover? How many structural elements must also be control actuators? What is the optimal location of actuators?

Work is underway at Caltech and JPL to answer these questions. Most importantly, the technique must be applied to a large order system; the results obtained so far are promising.

ACKNOWLEDGEMENTS

REFERENCES

[1] Chen, J. C., "Response of Large Space Structures with Stiffness Control," AAS/AIAA Paper No. 83-344, presented at AAS/AIAA Astrodynamics Specialist Conference, Lake Placid, New York, August 22-25, 1983.

[2] Hughes, P. C., "Space Structure Vibration Modes: How Many Exist? Which Ones are Important?," Proceedings of the Workshop on Applications of Distributed System Theory to the Control of Large Space Structures, NASA JPL-Publication 83-46, p. 34. July, 1983.

[3] Caughey, T. K., and Goh, C. J., "Analysis and Control of Quasi-Distributed Parameter Systems," Dynamics Laboratory Report DYNL-82-3, California Institute of Technology, November 1982.
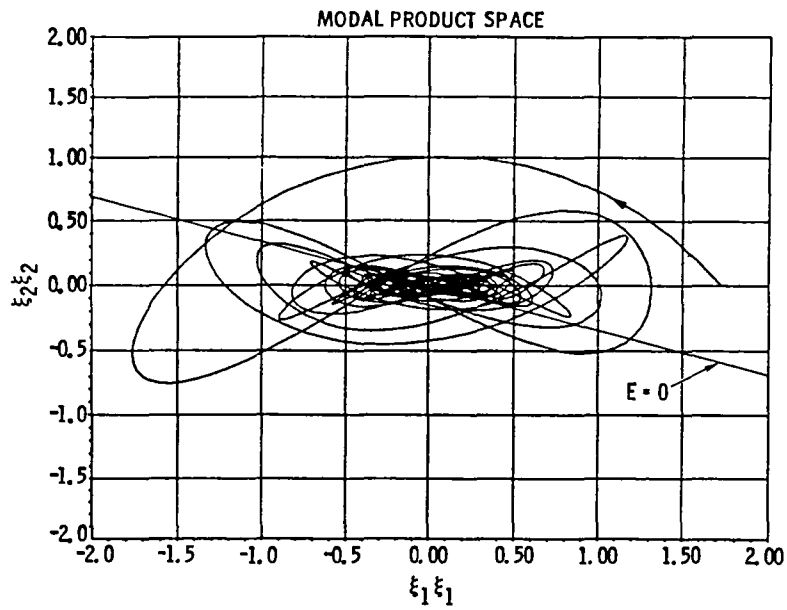
Figure 1. Trajectory for $C_2/C_1 = 3$.
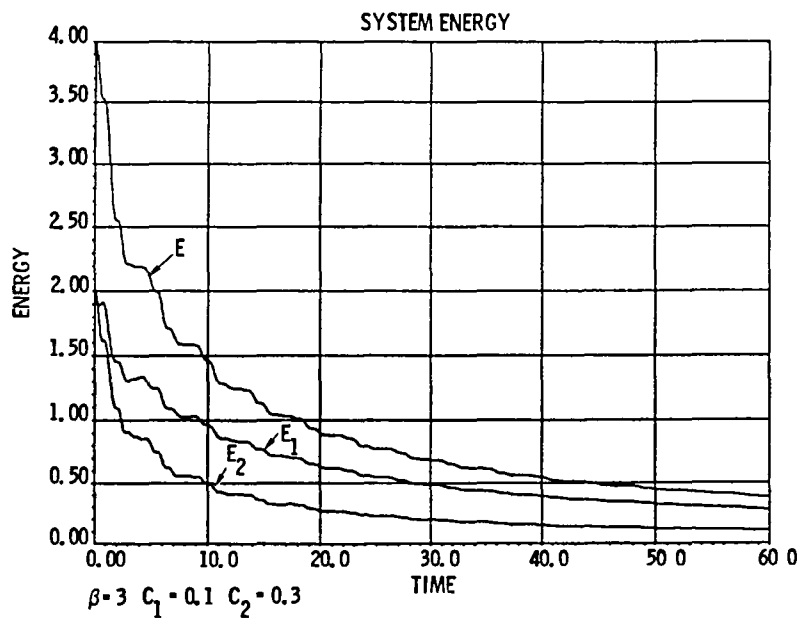
Figure 2. Energy for $C_2/C_1 = 3$.

SYSTEM POSITIONS
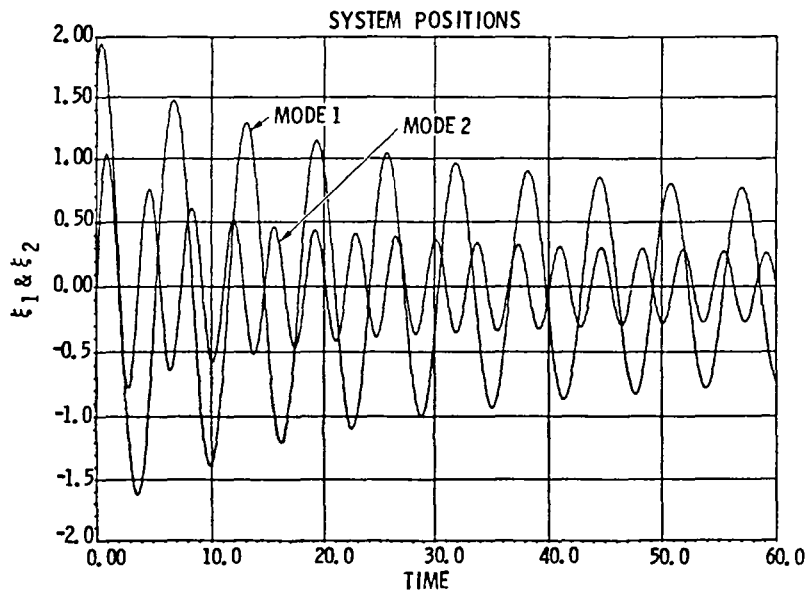
Figure 3. Displacements for $C_2/C_1 = 3$.
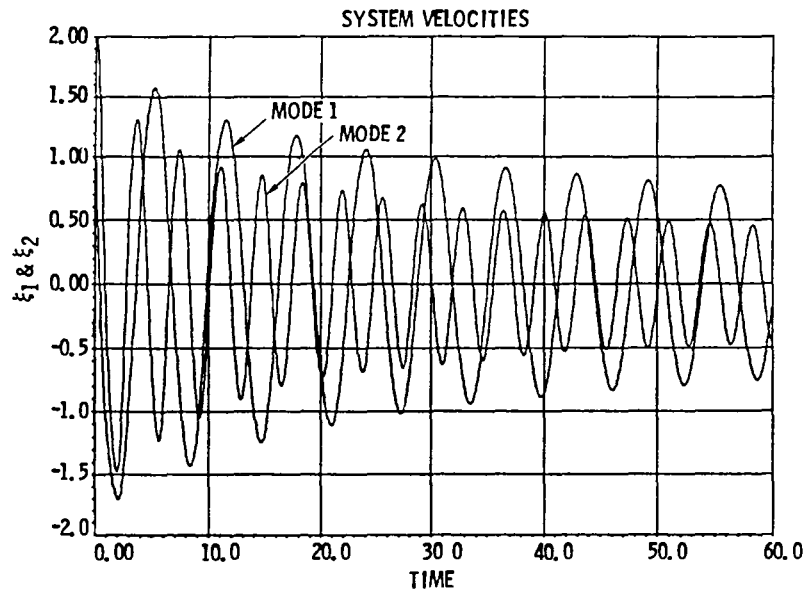
SYSTEM VELOCITIES

Figure 4. Velocities for $C_2/C_1 = 3$.

SYSTEM ENERGY

$\beta = 1.0 \quad C_1 = 0.5 \quad C_2 = 0.5$
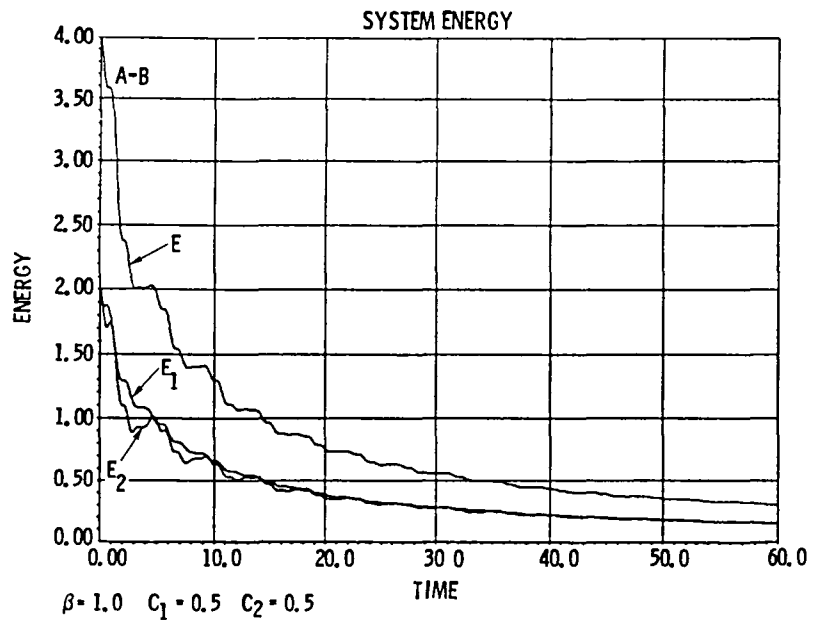
Figure 5.   Energy for $C_2/C_1 = 1$.

MODAL PRODUCT SPACE
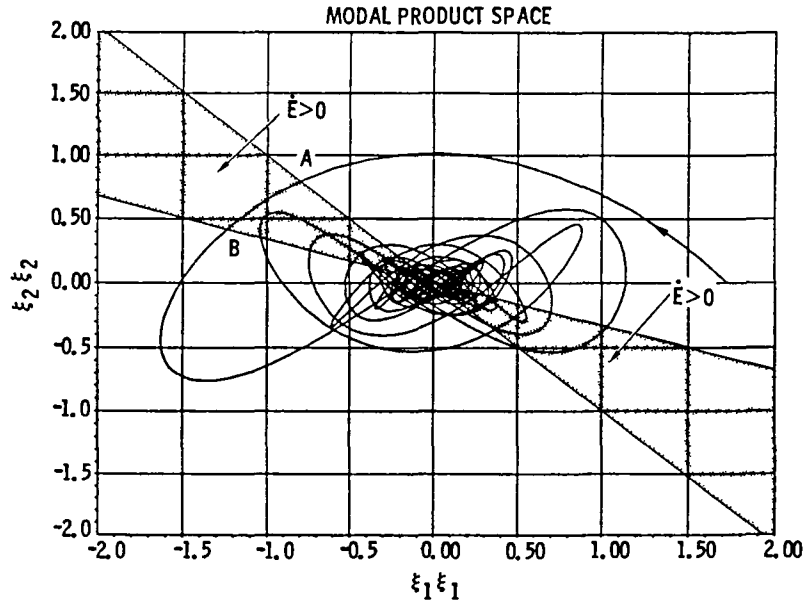
Figure 6.   Trajectory for $C_2/C_1 = 1$.

361
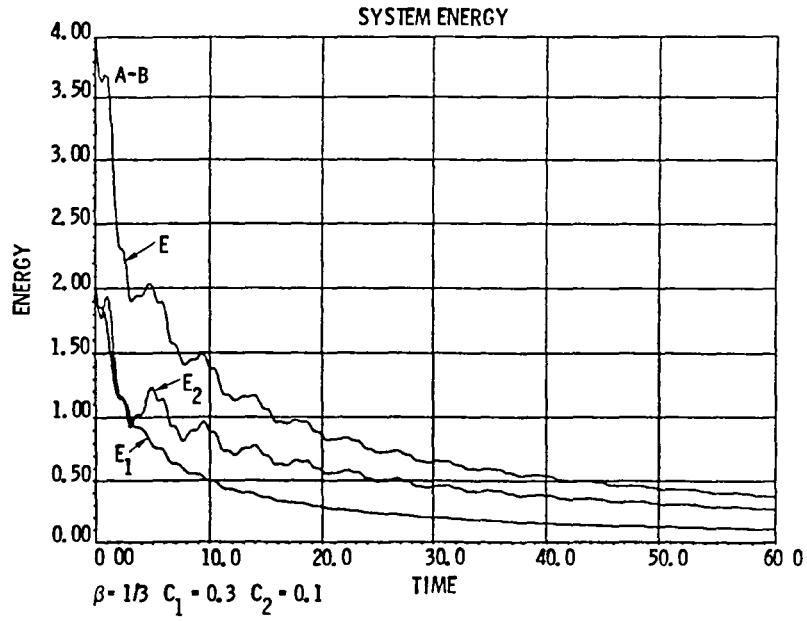
Figure 7. Energy for $C_2/C_1 = 1/3$.
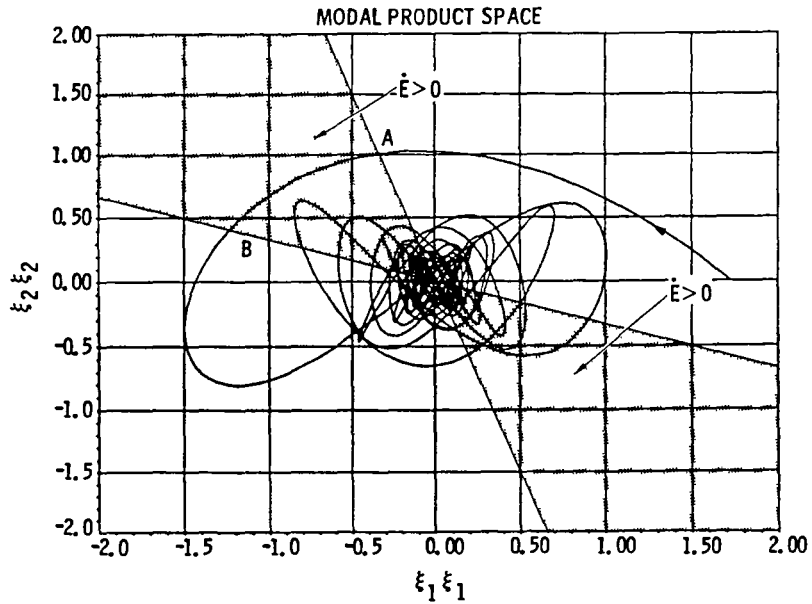
Figure 8. Trajectory for $C_2/C_1 = 1/3$.

362

APPENDIX:

In order for system (8) to remain on the line $\dot{E}=0$ away from the origin, the following relations must hold for all time:

1) $\quad \dfrac{\xi_2 \dot{\xi}_2}{\xi_1 \dot{\xi}_1} = -\dfrac{1}{3}$ $\hfill$ (A1)

2) $\quad \dfrac{d}{dt}\left(\dfrac{\xi_2 \dot{\xi}_2}{\xi_1 \dot{\xi}_1}\right) = 0$ $\hfill$ (A2)

3) $\quad \dfrac{d^2}{dt^2}\left(\dfrac{\xi_2 \dot{\xi}_2}{\xi_1 \dot{\xi}_1}\right) = 0$ $\hfill$ (A3)

Assume that relation (A1) holds. Expanding relation (A2) gives:

$$\frac{d}{dt}\left(\xi_2 \dot{\xi}_2\right) = -\frac{1}{3}\frac{d}{dt}\left(\xi_1 \dot{\xi}_1\right) \tag{A4}$$

Let $\xi_2 \dot{\xi}_2 = A$, then $\xi_1 \dot{\xi}_1 = -3A$ at a given instant of time. Expanding equation A4, and using equations (8) gives:

$$-9\frac{k}{m}\xi_2{}^2 + 3\dot{\xi}_2{}^2 - \frac{k}{m}\xi_1{}^2 + \dot{\xi}_1{}^2 = 0 \tag{A5}$$

In view of relation (A1) the variables in equation (A5) are not all independent. Let $\xi_1 = \alpha$, $\xi_2 = \beta$, then $\dot{\xi}_1 = -\dfrac{3A}{\alpha}$, $\dot{\xi}_2 = \dfrac{A}{\beta}$

Substituting into equation (A5) gives:

$$-9\frac{k}{m}\beta^2 + \frac{3A^2}{\beta^2} - \frac{k}{m}\alpha^2 + \frac{9A^2}{\alpha^2} = 0 \tag{A6}$$

Real solutions for α and β exist for equation (A6). For example: $\xi_1 = 1$, $\xi_2 = 1.083$, $\dot{\xi}_1 = -3$, $\dot{\xi}_2 = 0.923$, $\frac{k}{m} = 1$. Hence, relations (A1), and (A2) can be satisfied simultaneously for a given instant of time.

Now, to expand the third relation, let $\xi_1 \dot{\xi}_1 = f(t)$, $\xi_2 \dot{\xi}_2 = g(t)$

$$\frac{d^2}{dt^2}\left(\frac{g(t)}{f(t)}\right) = \frac{\ddot{g}(t)}{f(t)} - \frac{\dot{g}(t)\dot{f}(t)}{f^2(t)} - \frac{g(t)\ddot{f}(t) + \dot{g}(t)\dot{f}(t)}{f^2(t)} + \frac{2g(t)\dot{f}^2(t)}{f^3(t)}$$

Relations (A1), and (A2) give:

$$\frac{g(t)}{f(t)} = -\frac{1}{3} ,$$

and

$$\frac{\dot{g}(t)}{\dot{f}(t)} = -\frac{1}{3} ,$$

Substituting these relations and using equations (8) gives, after much algebra:

$$\frac{d^2}{dt^2}\left(\frac{g(t)}{f(t)}\right) = \frac{8}{3}\frac{k}{m}$$

This is, by assumption, nonzero. Thus conditions (A1), (A2), and (A3) cannot be satisfied simultaneously for any instant of time. Therefore system (8) cannot remain on the line $\dot{E} = 0$.   QED.

SUB-OPTIMAL CONTROL OF NONLINEAR FLEXIBLE SPACE STRUCTURES

T. J. Dehghanyar, S. F. Masri, R. K. Miller, and G. A. Bekey
University of Southern California
Los Angeles, CA 90089-0242

T. K. Caughey
California Institute of Technology
Pasadena, CA 91106

ABSTRACT

A simple yet efficient method is presented for the on-line vibration control of nonlinear distributed parameter systems, with constant or time-varying properties, responding to a wide class of dynamic environments. The control procedure uses pulse generators located at selected positions throughout a given system. The degree of system oscillation near each controller determines the controller's activation time and pulse amplitude. The direct method of Liapunov is used to establish that the response of the controlled nonlinear system is Lagrange stable. Analytical and experimental studies of a wing-like plate demonstrate the feasibility, reliability, and robustness of the proposed vibration-suppression method.

1. INTRODUCTION

One of the significant complications in the application of optimal control theory to flexible space structures is the need for precise information regarding the system order and parameters. In addition, the resulting control law may require the application of continuously generated control forces at one or more points in the structure. These issues are further exasperated in the case of large-scale distributed parameter systems (DPS) where the physical assembly is complex and incorporates components that are quite often nonlinear, with uncertain parameters.

This paper presents a sub-optimal control method suitable for on-line use to suppress vibrations in nonlinear flexible systems subjected to arbitrary dynamic environments. The method uses a form of open-loop velocity feedback to control pulse generators located at selected positions throughout the structure. The degree of system oscillation near each controller determines the controller's activation time and pulse amplitude.

The proposed control method is described in Section 2 and its stability analysis is given in Section 3. Digital computer simulation studies of a linear as well as a nonlinear hysteretic lumped parameter plate model under a variety of excitations are presented in Section 4. Experimental studies with a mechanical model resembling an aircraft wing are described in Section 5.

2. CONTROL PROCEDURE

Consider a nonlinear distributed parameter system whose governing partial differential equation (PDE) is known. Using suitable discretization techniques such as the finite element method (FEM), a large but finite-order mathematical

365

model can be obtained. An excellent discussion of and justification for using finite-dimensional models for structural control of continuous systems is given in the recent papers by Hughes [1] and Gran [2].

Assume that the finite-order mathematical model of the nonlinear system under discussion has n degrees of freedom and is governed by the differential equation

$$M\ddot{x} + D\dot{x} + Kx + f(x,\dot{x}) + \nabla F(x) = q(t) \tag{1}$$

with the following properties:

(1) $x(t)$ is the system displacement vector of order n,

(2) M is a diagonal positive definite matrix,

(3) D is a symmetric, positive semi-definite, small matrix such that

$$x^T K x > c x^T D x \tag{2}$$

where c is a positive constant, $0 < c < 1$,

(4) K is a symmetric, positive definite matrix,

(5) $f(x,\dot{x})$ represents nonconservative nonlinear forces

$$\text{and } |f_i(x,\dot{x})| \leq B_i \text{ with } i \in (1,n) \tag{3}$$

and B_i are bounded positive constants.

(6) $\nabla F(x)$ represents the conservative nonlinear forces which are equal to the gradiant of function F, and

$$F(x) > 0, \quad x^T \nabla F(x) \geq \alpha F(x) \tag{4}$$

with constant $\alpha > 1$.

(7) $q(t)$ is a bounded excitation vector that satisfies the condition

$$|q_i(t)| \leq Q_i \text{ with } i \in (1,n) \tag{5}$$

and Q_i are bounded constants.

Note from Eq. (3) that nonlinear damping forces of the type encountered in distributed systems incorporating mechanical components with joints and interface motion (such as damping forces inherent in hysteretic elements, limited-slip systems and Coulomb-type friction forces) can be handled within the restrictions imposed on f.

Since the damping matrix D is small and required to only be positive semi-definite, and since the presence of nonconservative nonlinear forces does not guarantee a bounded response in the presence of persistent disturbances (e.g.

Coulomb-damped or bilinear hysteretic systems under harmonic excitation), the response of the system governed by Eq. (1) may be large or even unbounded.

The active control procedure of this paper consists of using, at selected points in the structure, force actuators whose operation is triggered every time a zero crossing of the displacement of each of the points of interest is detected. The magnitude of each control pulse p_i will be given by

$$
p_i(t) = \begin{cases} -c_i \, \text{sgn}(v_i) \, |v_i|^{n_i} ; t_{o_i} < t < (t_{o_i} + T_{d_i}) \\ \\ 0 \qquad ; (t_{o_i} + T_{d_i}) < t < t_{o_{i+1}} \end{cases} \tag{6}
$$

where

c_i is a coefficient for scaling the needed control force at location i

$\text{sgn}(.)$ indicates the algebraic sign of its argument

v_i is the absolute or relative velocity of the structure at location i, depending on the nature of the problem

n_i is some appropriate power of the velocity at location i

t_{o_i} is the zero crossing time at location i

T_{d_i} is the pulse duration of the controlling force at location i.

Depending on the choice of control parameters in Eq. (6), the actuator will, at one extreme, behave as an open-loop control thruster, and at the other extreme perform as a negative feedback device whose action introduces nonlinear velocity-proportional damping.

In order to incorporate into the control algorithm constraints imposed by hardware limitations as well as to conserve the control energy, the control law of Eq. (6) can be augmented by the following constraints:

$$
p_i(t) = \begin{cases} \pm P_{max_i} \, , & |p_i| > P_{max_i} \\ \\ 0 \, , & |p_i| < P_{min_i} \end{cases} \tag{7}
$$

A more general form of Eq. (6) is to relate the magnitude of the control force at location i to both the displacement x_i and velocity v_i at that location:

$$p_i(t) = m_i(a_i x_i + b_i v_i) + g_i(x_i, v_i) \tag{8}$$

where m_i is the mass associated with i, and g_i is some suitable nonlinear function. The advantage of the formulation in Eq. (8) is that only <u>local</u> measurements of displacement and velocity are needed to determine the control force to be applied at a specific location. Since no global information regarding the stiffness and damping characteristics of the system is needed, the control law of Eq. (8) offers a distinct advantage in dealing with realistic distributed structural systems whose stiffness and damping parameters are difficult to identify accurately in practical cases.

3. STABILITY ANALYSIS

Referring back to Eq. (8), suppose that a control force $\underset{\sim}{h}$ is created and applied to the nonlinear system governed by Eq. (1), with

$$\underset{\sim}{h}(\dot{\underset{\sim}{x}} + c\underset{\sim}{x}) = -2cM(\dot{\underset{\sim}{x}} + c\underset{\sim}{x}) - \underset{\sim}{g}(\dot{\underset{\sim}{x}} + c\underset{\sim}{x}) \tag{9}$$

where c is a positive constant and

$$(\dot{\underset{\sim}{x}} + c\underset{\sim}{x})^T \underset{\sim}{g}(\dot{\underset{\sim}{x}} + c\underset{\sim}{x}) \geq 0 \quad . \tag{10}$$

The controlled dynamic system of Eq. (1) is now governed by

$$M\ddot{\underset{\sim}{x}} + (D+2cM)\dot{\underset{\sim}{x}} + (K+2c^2 M)\underset{\sim}{x} + \underset{\sim}{f}(\underset{\sim}{x},\dot{\underset{\sim}{x}}) + \nabla F(\underset{\sim}{x}) + \underset{\sim}{g}(\dot{\underset{\sim}{x}} + c\underset{\sim}{x}) = \underset{\sim}{q}(t) \quad . \tag{11}$$

Using Liapunov's direct method, the authors have shown in [3] that the solutions of Eq. (11) are Lagrange stable (bounded).

4. SIMULATION OF CONTROL STRATEGY

4.1 Linear Plate Model

Consider a thin triangular plate, that is clamped at one end, initially flat, subjected to forces acting perpendicular to it, and having the properties shown in Fig. 1(a). A discrete one-dimensional model of this distributed parameter system is shown in Fig. 1(b) and its corresponding lumped parameters (mass, stiffness and damping) are listed in Fig. 1(c).

The first six classical normal modes corresponding to the stick model with nonuniform properties shown in Fig. 1(b) are given in Fig. 2. These mode shapes are in close agreement with the corresponding beam modes obtained by using plate elements in a conventional finite element model of the plate shown in Fig. 1(a). The position of the various nodes of the mode shapes in Fig. 2 have a significant influence on the optimum number and location of the needed controllers.

4.2 Impulsive Excitation

If the linear model of Fig. 1(b) is subjected to an impulsive excitation consisting of a velocity-step input applied to the base, the resulting system response will consist of an exponentially decaying harmonic oscillation whose envelope varies with time as shown in Fig. 3. If the dynamic system is now provided with a single controller attached to the tip of the plate at station m_{10}, the resulting controlled motion will have a much more rapidly decaying envelope as shown in Fig. 3. The rate of vibration suppression is heavily influenced by the choice of control parameters.

In Fig. 4, the same situation as that of Fig. 3 is investigated except that parameter n is held fixed and the effects of varying the control gain parameter c are investigated. Clearly, considerable flexibility is available in the choice of control parameters to match a particular design situation and hardware limitations.

4.3 Nonstationary Random Excitation

If the broad-band nonstationary random excitation $\ddot{s}(t)$ shown in Fig. 5(a) is now applied to the base of the linear system in Fig. 1(b), the relative displacement and velocity response of the free end of the model will be as shown in Figs. 5(b,c). The time history segment shown in Fig. 5 corresponds to about 25 fundamental periods T_1 of the system.

The results in Fig. 6 show that the relative motion time history at three locations along the uncontrolled 10 DOF linear plate model under nonstationary random excitation is dominated by the contribution of the first mode illustrated in Fig. 2(a).

Applying the control strategy discussed above to this structure, the controlled response shown in Fig. 7 is obtained when four identical controllers, each with parameters n=0, c=1.0, and T_d=0.05 are used at stations m_3, m_5, m_7 and m_{10}. In order to simplify comparisons, the response amplitude scales are identical to the corresponding scales in Figs. 5 and 6 where no control action is appled.

The results in Figs. 8 and 9 correspond to identical situations as the one in Fig. 7, except that control parameters n and c are changed in each case as indicated. To facilitate comparison, the same amplitude scale is used to represent the needed control forces for all cases.

The effects of the number and location of controllers on the temporal rms response at stations m_3, m_5 and m_7 of the 10 DOF linear plate model under nonstationary random excitation, with control parameter n=0, is shown in Fig. 10. Similar results are shown in Fig. 11 for the temporal rms response of the tip of the plate when different control strategies are used: n=0 in Fig. 11(a), n=1 in Fig. 11(b), and n=2 in Fig. 11(c).

The results of Figs. 10 and 11 confirm the expected outcome that, with everything else being the same, the extent of vibration suppression throughout the structures is proportional to the number of controllers used.

4.4 Swept-Sine Excitation

To illustrate the applicability of the control algorithm under arbitrary dynamic environments, a swept-sine excitation is used in Fig. 12 where the control parameters are identical to those of Fig. 8 in which n=1.

4.5 Nonlinear Plate Model

The results shown in Fig. 13 correspond to a 10 DOF nonlinear lumped parameter plate model in which each of the ten discrete elements possesses bilinear hysteretic characteristics. If this nonlinear model is subjected to the non-stationary excitation of Fig. 5(a), its resulting motion without control will be as shown in Fig. 13(a-d). Providing this system with four identical controllers each with n=1, c=0.50, and T_d=0.05 results in the controlled motion in Fig. 13(e-h) and the corresponding control pulses shown in Fig. 13(i-ℓ). Comparable amounts of vibration attenuation is obtained at the other locations whose response is not plotted.

5. EXPERIMENTAL STUDIES

A mechanical model resembling an aircraft wing was designed and fabricated to investigate the control algorithm under realistic laboratory conditions. The photographs in Fig. 14 indicate the details of the test structure, vibration exciter, instrumentation, pneumatic power supply, and control thrusters.

Figure 15 shows sample results for the structure under harmonic excitation with a frequency close to the plate fundamental frequency. Because the control used in this experiment is to simply turn the controller on or off, this corresponds to using n=0 in Eq. (16) (i.e., active Coulomb damping). Thus, it is not surprising that the envelope of the decaying oscillations at the initiation of the control process exhibits the same characteristics associated with Coulomb friction: a straight-line decay envelope. On the other hand, it is seen from Fig. 15 that when the excitation is turned off, the envelope of the free vibrations can be well approximated by an exponential decay curve, which is a well known characteristic of viscously damped systems.

6. SUMMARY AND CONCLUSIONS

A simple, yet efficient method is presented for the on-line pulse control of linear as well as nonlinear distributed parameter systems, having constant or time-varying properties, and responding to arbitrary dynamic environments. A significant feature of the method is that detailed knowledge of the system structure is not needed; only local measurements of displacement and velocity are needed to determine the control force to be applied at a specific location in the nonlinear flexible structure.

Analytical and experimental studies with several models of different size and configuration have demonstrated the feasibility, reliability, and robustness of the proposed active control method.

370

ACKNOWLEDGMENT

REFERENCES

[1] Hughes, P. C., "Space Structure Vibration Modes: How Many Exist? Which Ones Are Important?" Proc. of the Workshop on Applications of Distributed Systems Theory to the Control of Large Space Structures, JPL Publication 83-46, 1 July 1983, pp. 31-47.

[2] Gran, R., "Control of Flexible Structures: A Systematic Overview of the Problem," Proc. of the Workshop on Applications of Distributed System Theory to the Control of Large Space Structures, JPL Publication 83-46, 1 July 1983, pp. 49-62.

[3] Masri, S. F., Bekey, G. A. and Caughey, T. K., "On-Line Control of Nonlinear Flexible Structures," ASME, Journal of Applied Mechanics, Vol. 49, December 1982, pp. 877-884.

(a) plate properties   (b) discrete model   (c) linear system characteristics
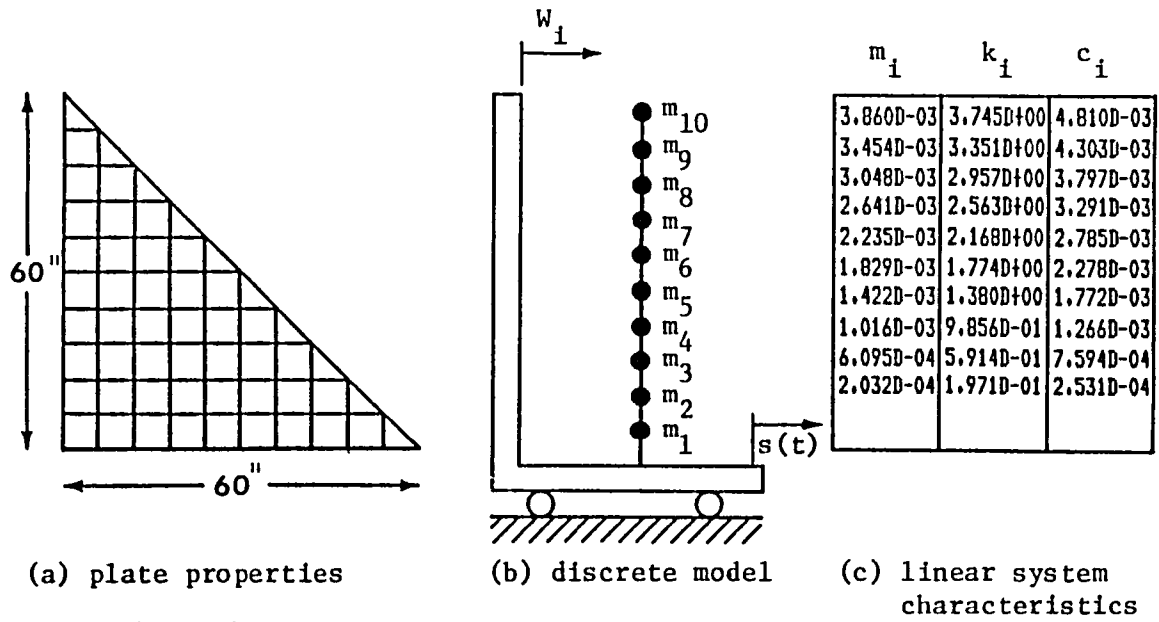
Figure 1. Ten-degree-of-freedom model of cantilever plate.

m_i	k_i	c_i
3.860D-03	3.745D+00	4.810D-03
3.454D-03	3.351D+00	4.303D-03
3.048D-03	2.957D+00	3.797D-03
2.641D-03	2.563D+00	3.291D-03
2.235D-03	2.168D+00	2.785D-03
1.829D-03	1.774D+00	2.278D-03
1.422D-03	1.380D+00	1.772D-03
1.016D-03	9.856D-01	1.266D-03
6.095D-04	5.914D-01	7.594D-04
2.032D-04	1.971D-01	2.531D-04

(a) $f_1 = 1.07$ Hz

(b) $f_2 = 4.54$ Hz

(c) $f_3 = 10.78$ Hz

(d) $f_4 = 19.45$ Hz

(e) $f_5 = 30.23$ Hz

(f) $f_6 = 43.45$ Hz
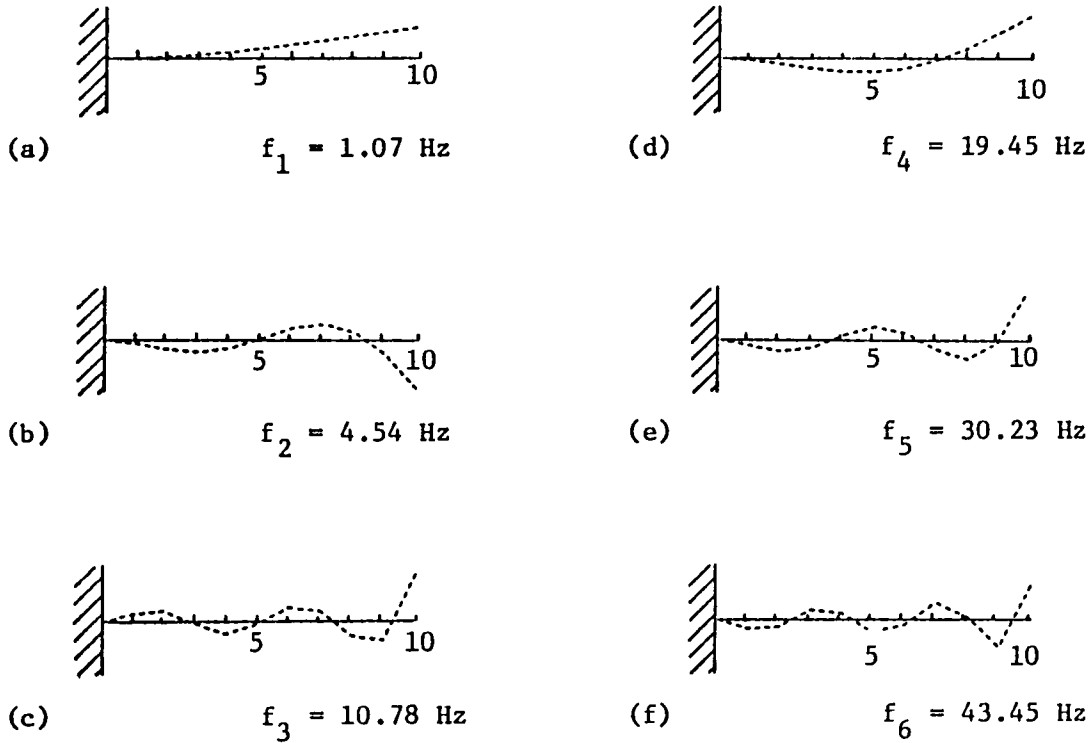
Figure 2. Dominant modal shapes of 10 DOF plate model.
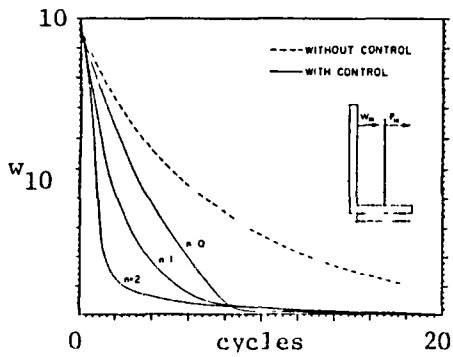
Fig. 3. Effects of control parameter n on the tip displacement of the linear plate model under velocity-step input at the base; one controller at m_{10}.
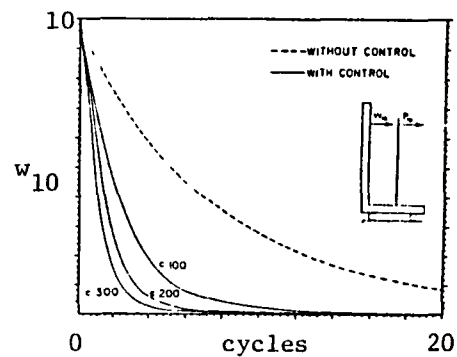
Fig. 4. Effects of control parameter c on the tip displacement of the linear plate model under velocity-step input at the base; one controller at m_{10}.
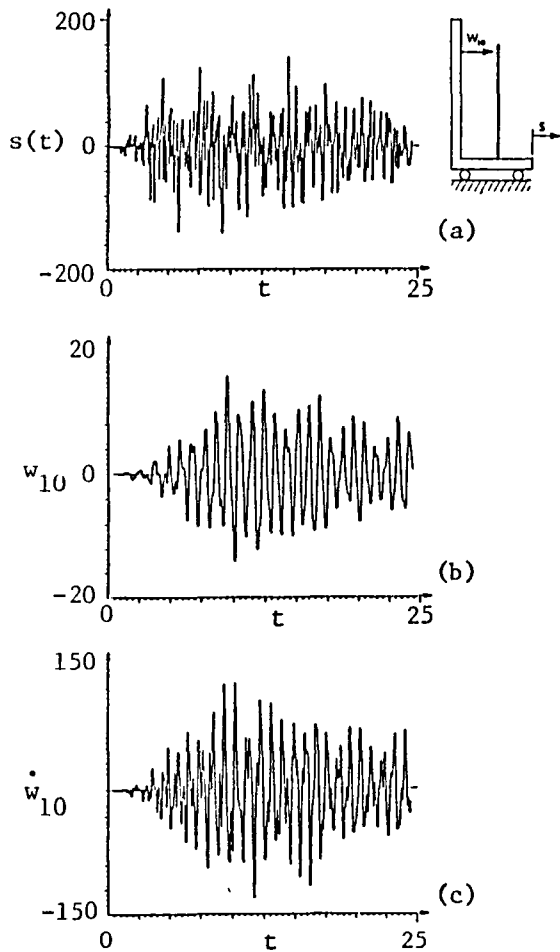
Fig. 5. Uncontrolled motion of 10 DOF linear plate model under nonstationary base excitation.
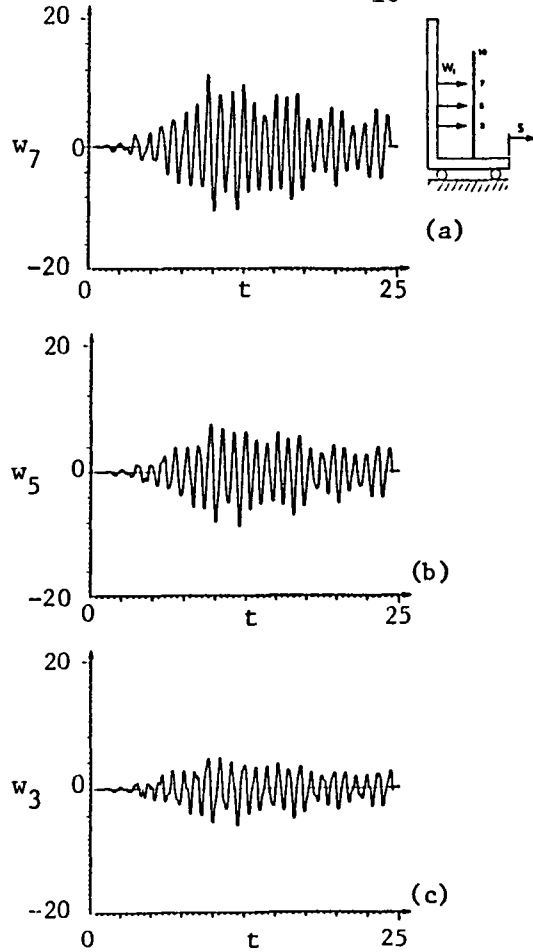
Fig. 6. Response time history at 3 locations along the uncontrolled 10 DOF linear plate model under nonstationary base excitation.

373
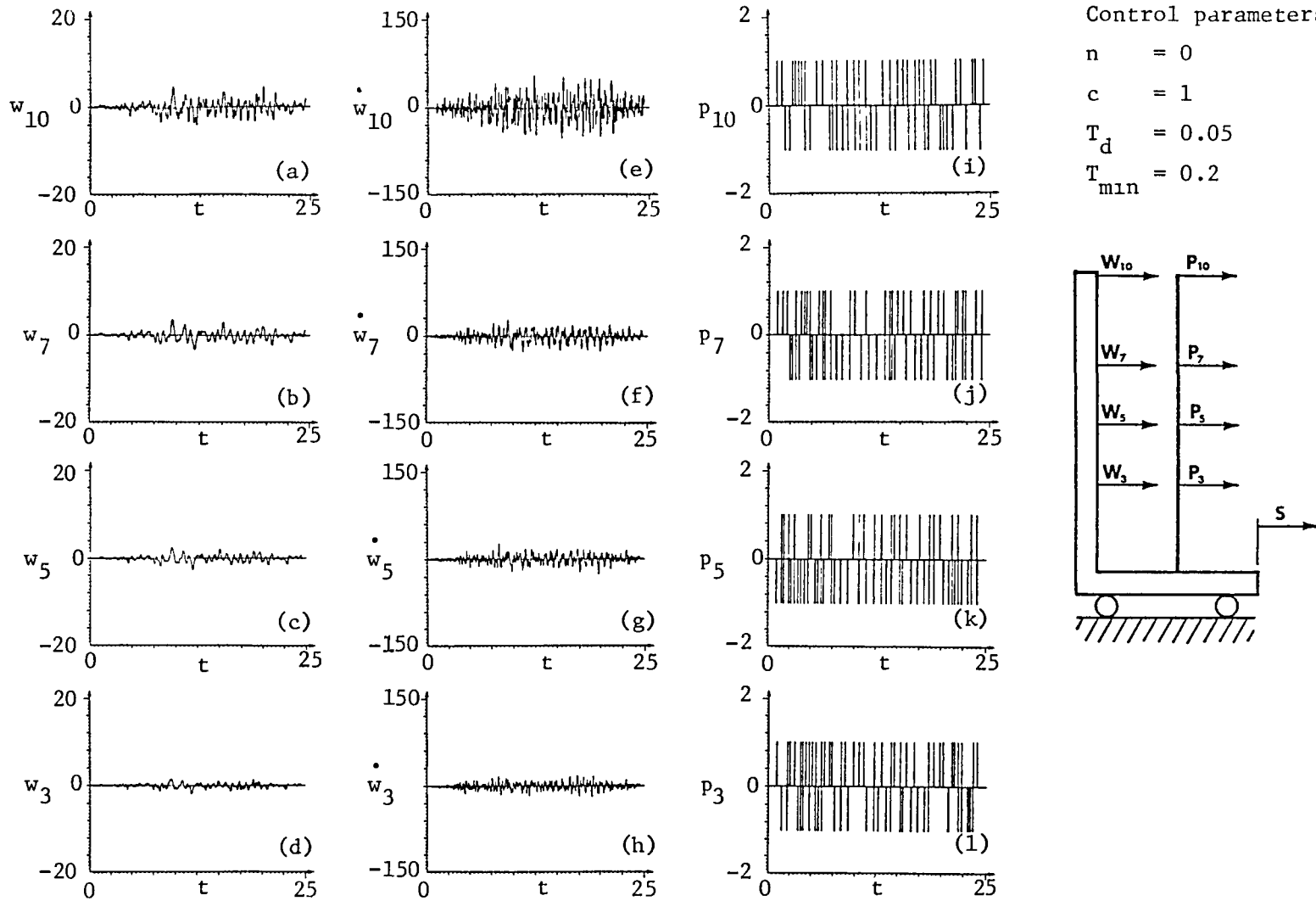
Figure 7.   Controlled motion of the 10 DOF linear plate model under nonstationary base excitation; 4 identical controllers used at locations m_3, m_5, m_7, m_{10}. Control parameter $n=0$; amplitude scales are identical to corresponding scales in Figs. 5 and 6.
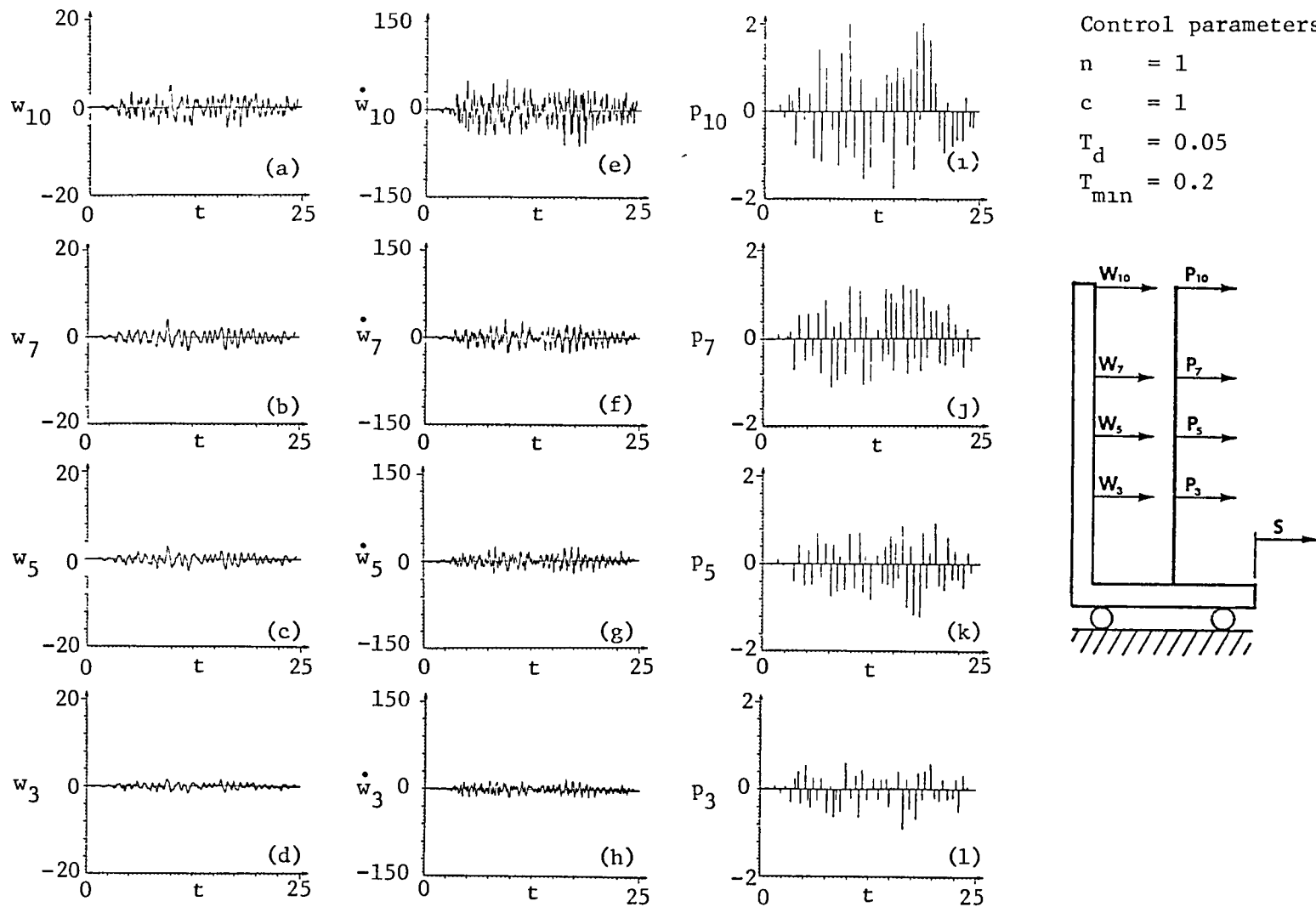
Figure 8.   Controlled motion of the 10 DOF linear plate model under nonstationary base excitation; 4 identical controllers used at locations m_3, m_5, m_7, m_{10}. Control parameter n=1; amplitude scales are identical to corresponding scales in Figs. 5 and 6.
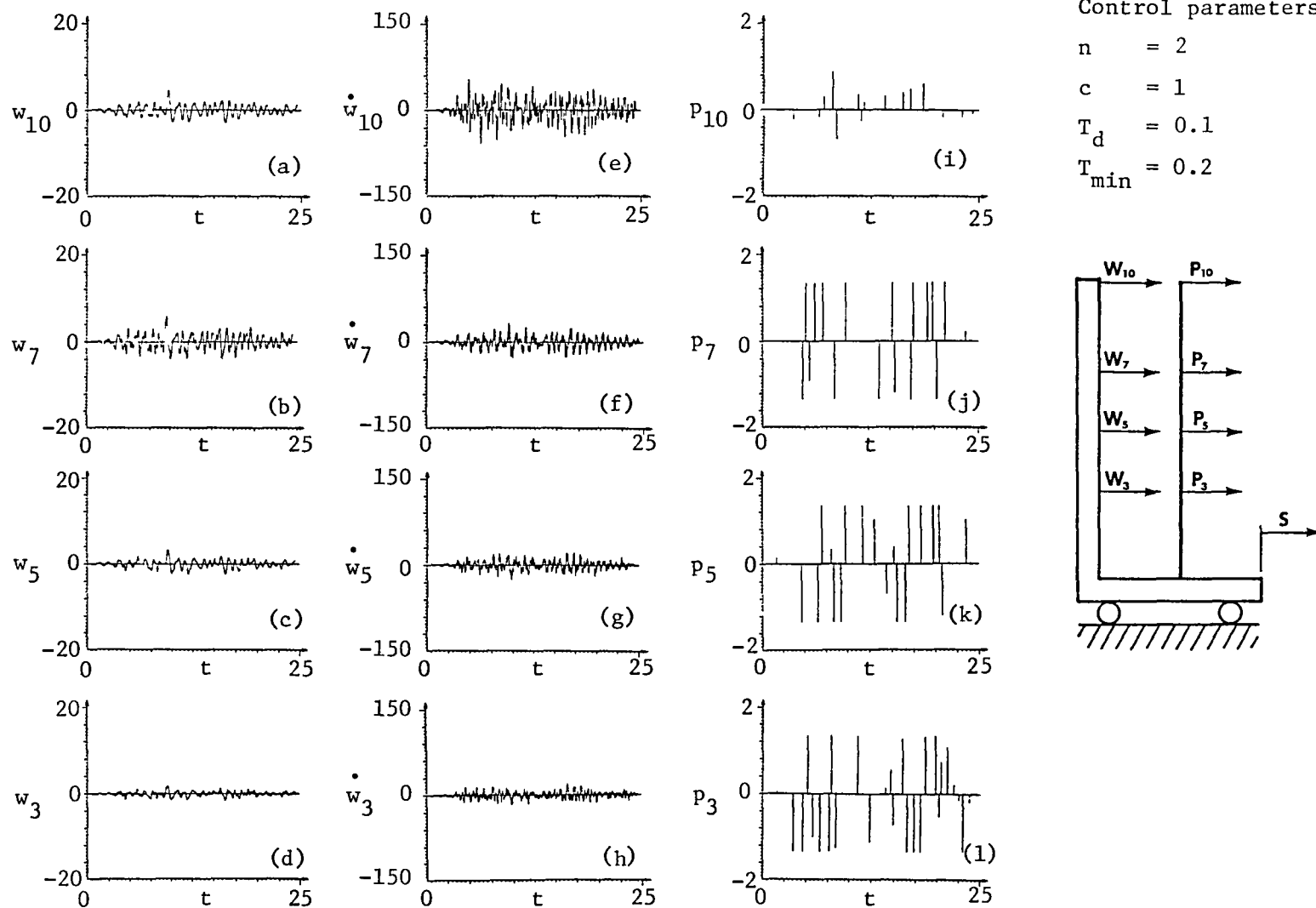
Figure 9. Controlled motion of the 10 DOF linear plate model under nonstationary base exictation; 4 identical controllers used at locations m_3, m_5, m_7, m_{10}. Control parameter n=2; amplitude scales are identical to corresponding scales in Figs. 5 and 6.

376

$n=0$, $c=1$, $T_d=0.5$, $T_{min}=0.2$

Case Number	Total Number of Controllers	Controller Location		Case Number	Total Number of Controllers	Controller Location
1	10	1,2,...,10		1	10	1,2,...,10
2	4	3,5,7,10		2	4	3,5,7,10
3	2	5,10		3	2	5,10
4	1	10		4	1	10
5	0	--		5	0	--
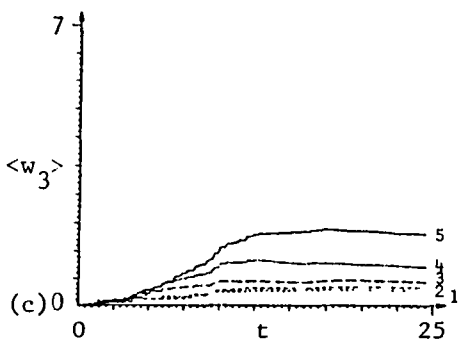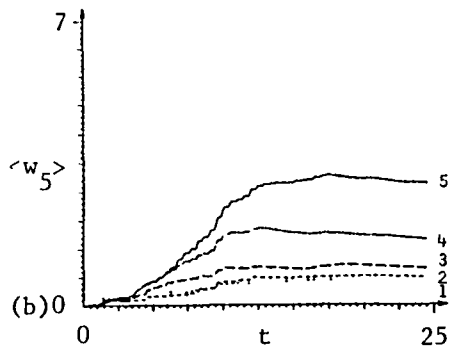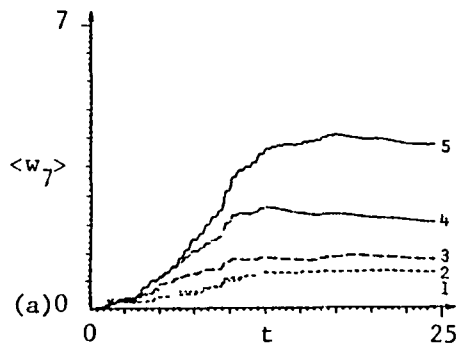
Fig. 10. Effects of the number and location of controllers on the temporal rms response at stations 3, 5, and 7 of the 10 DOF linear plate model under nonstationary random excitation; $n=0$.
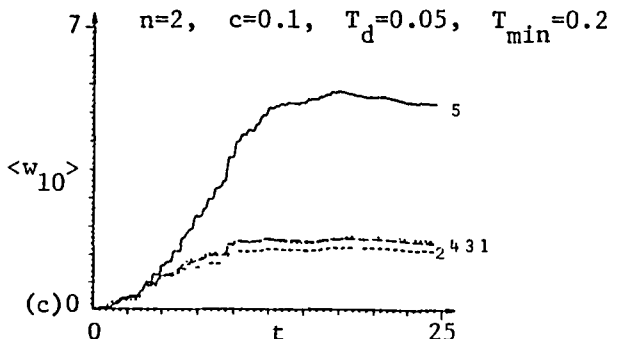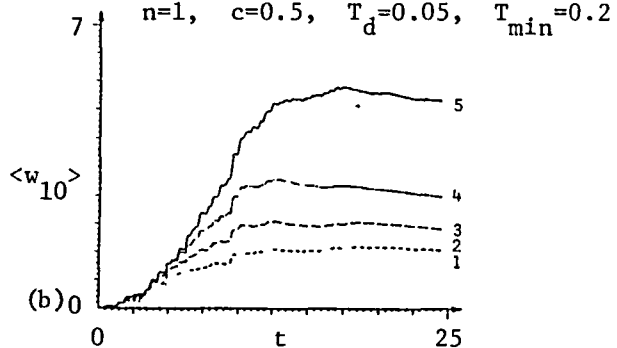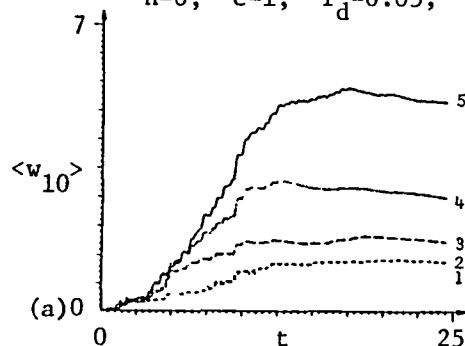
Fig. 11. Effects of controllers parameters, numbers, and locations on the temporal rms response of the tip of the 10 DOF linear plate model under nonstationary random excitation.

377
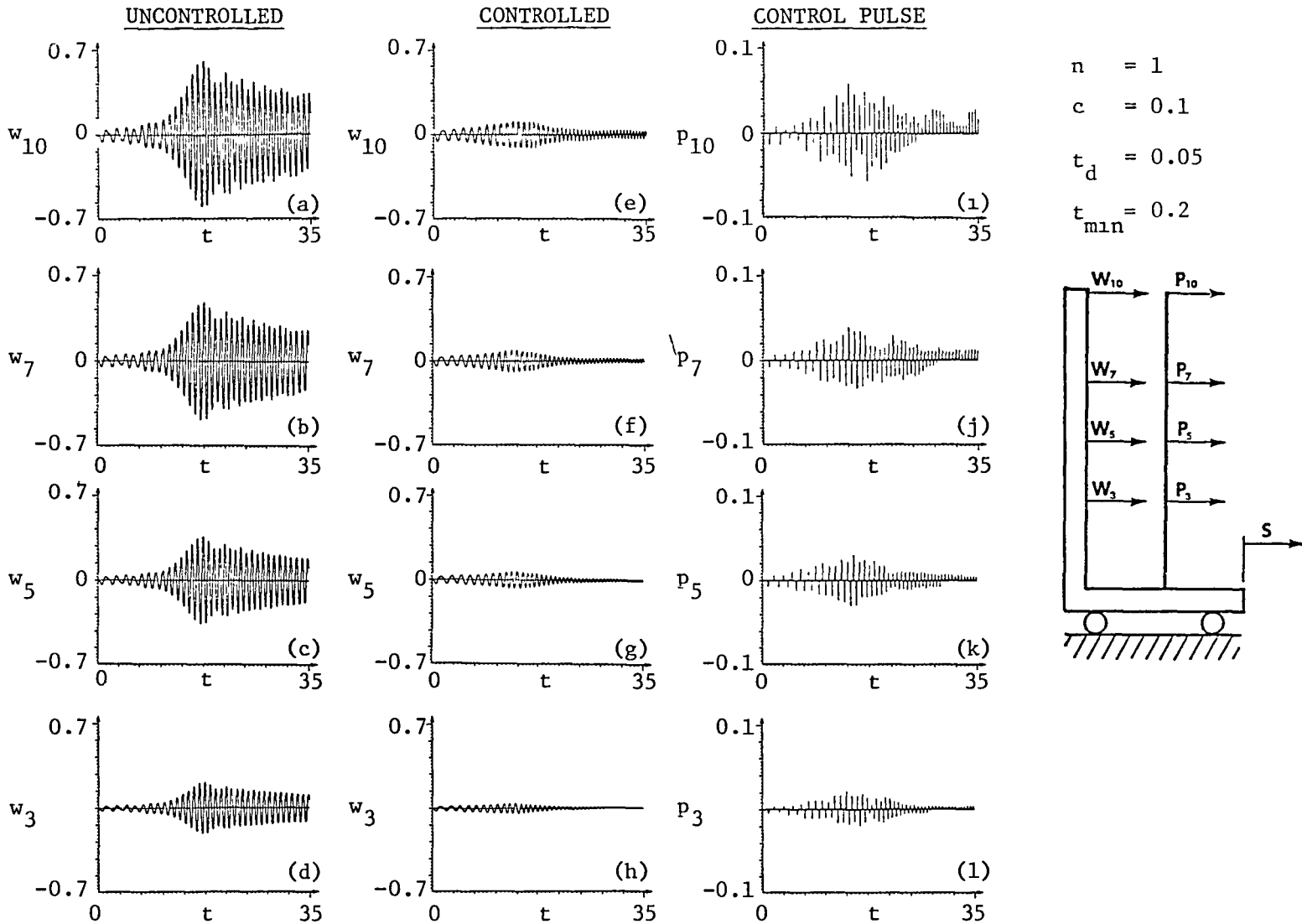
Figure 12. Controlled motion of the 10 DOF linear plate model under swept-sine base excitation; 4 identical controllers used at locations m_3, m_5, m_7, m_{10}. Control parameter $n = 1$.
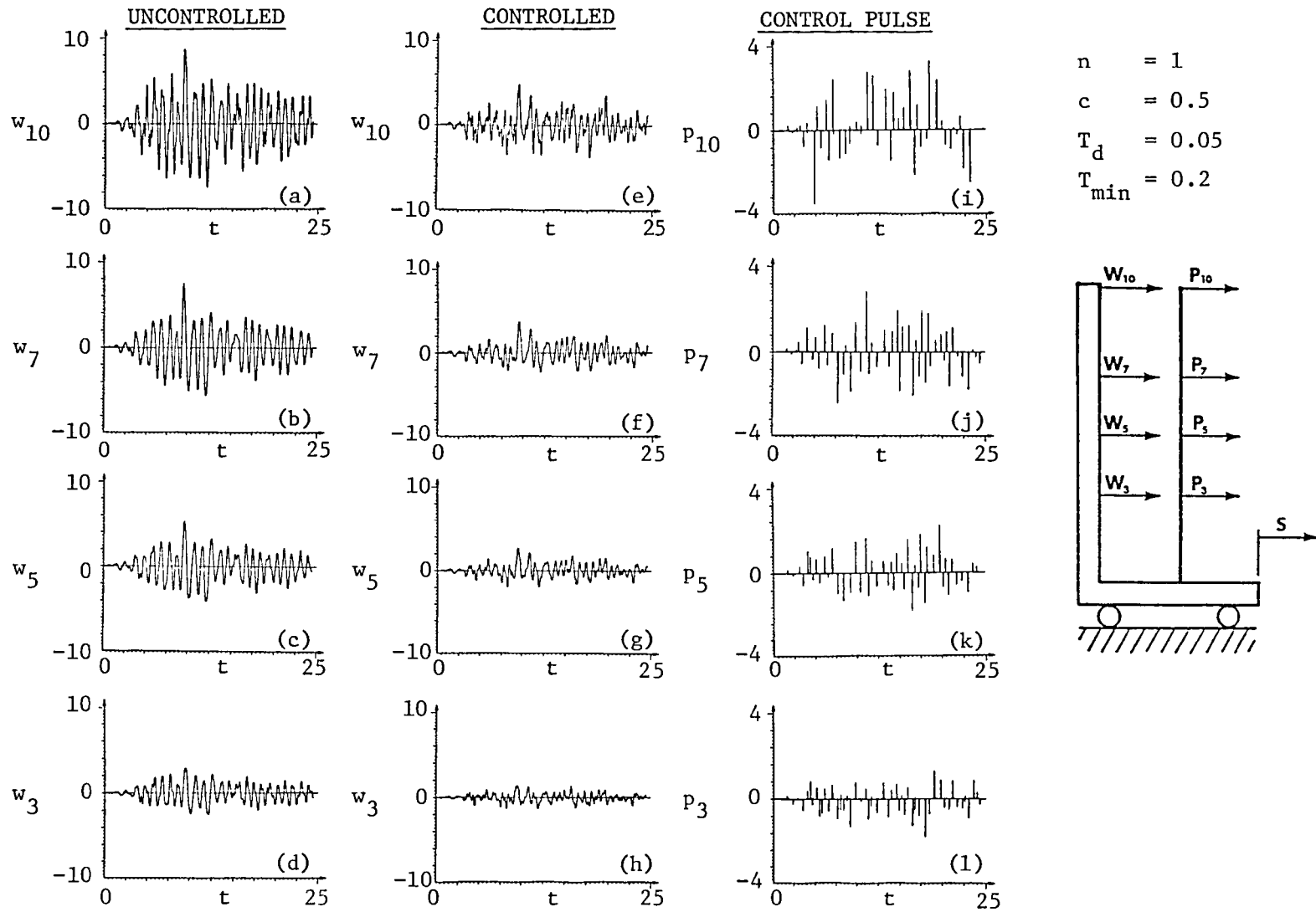
Figure 13. Motion of a hysteretic 10 DOF nonlinear plate model under nonstationary base
excitation; n = 1.

(a) Base-excited plate
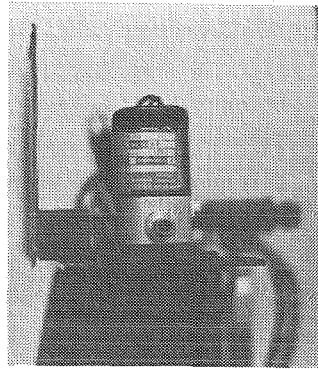
(b) Solenoid
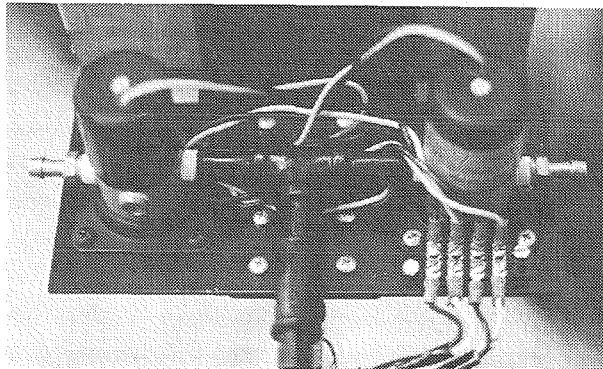
(c) Reaction-jet controllers

Figure. 14. Experimental setup.

$n=0$ $T_d=0.05$ $T_{min}=0.2$

NO CONTROL | CONTROLLER ON | CONTROLLER OFF | FREE VIBRATION

(a) Tip displacement vs TIME, 0 to 100

(b) Control signal vs TIME, 0 to 100

(c) Base displacement vs TIME, 0 to 100
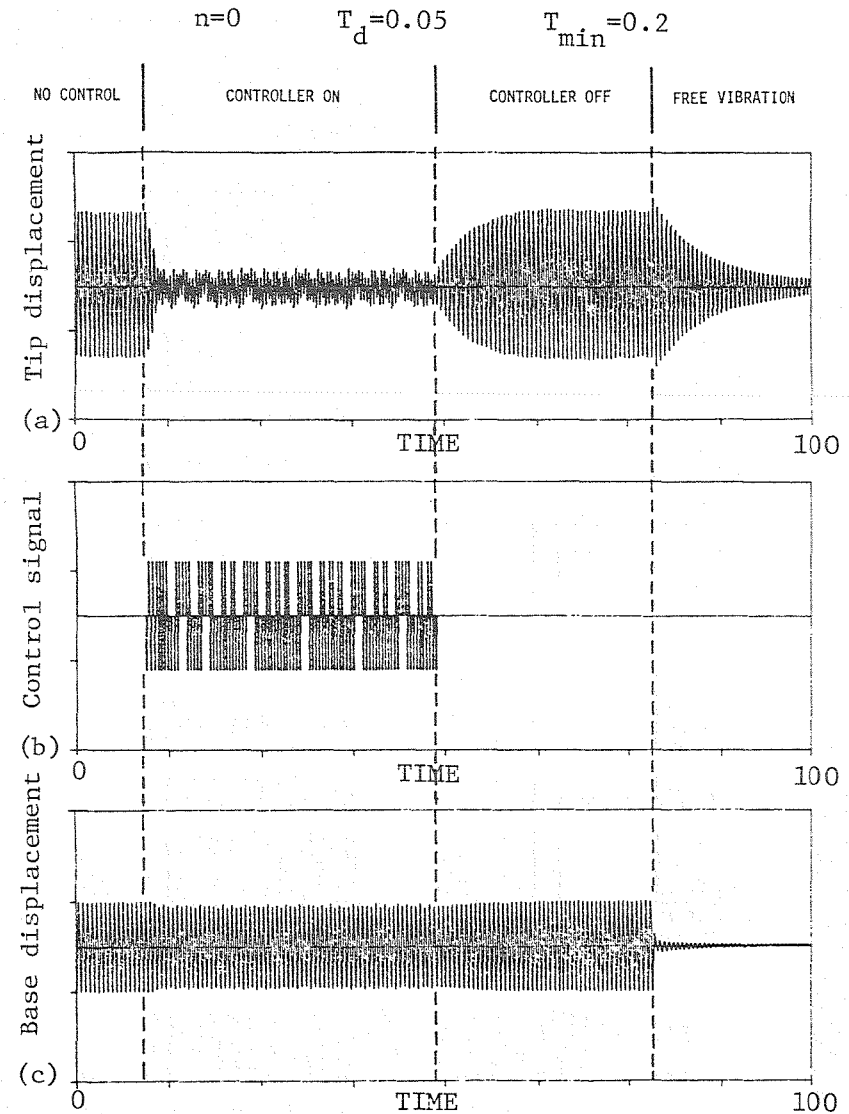
Figure 15. Measured response of plate with and without harmonic base excitation; one controller used at top of plate.

AN OVERVIEW OF LATEST MODEL REDUCTION AND CONTROL METHODS OF LARGE FLEXIBLE SPACE STRUCTURES

J. M. Santiago*, W. J. Lange, Jr.**, and M. Jamshidi
University of New Mexico
Albuquerque, NM 87131

Abstract.

This paper describes the latest trends and theoretical developments involved with the modeling and control of Large Flexible Space Structures (LFSS). The paper addresses first the basic problems, characteristics, and difficulties inherent in modeling and control of LFSS. Major source of difficulties and errors are the stiffness and damping operators of the dynamic model. Extensions of Linear Quadratic Gaussian (LQG) theory as applied to LFSS are presented, including frequency-shaped cost functionals and perturbation methods. The minimum data/maximum entropy approach which uses a stochastic design model to overcome difficulties found in LQG-based methods is described. Latest trends in system theory including balanced realization and singular-value analysis are used to determine reduced-order controllers and models. Ad hoc methods such as component cost analysis and modal cost analysis are discussed in context with the closed-loop reduction problem of controller order versus performance. The minimum data/maximum entropy approach also addresses controller order versus performance. The paper also attempts to identify those areas of control science and large scale systems that appear to have an important role in understanding and solving LFSS modeling and control.

* Graduate student and sponsored by the Air Force Institute of Technology, - Civilian Institute (AFIT-CI) education program.

** Graduate student and affiliated with the Air Force Weapons Laboratory (AFWL) Kirtland AFB, NM.

1. INTRODUCTION.

Large Flexible Space Structures (LFSS) are described as distributed parameter systems (DPS) whose dynamics may be modeled by a partial differential equation (PDE). LFSS refers to large flexible antennas with applications in global communications, astronomy (optical telescopes), surveillance, solar power (electric power) generation, and other space missions. Since LFSS are modeled by a partial differential equation, they are mathematical models having "infinite" dimension. A popular method to generate a finite-dimensional physical model for approximating a DPS uses finite element techniques in a model of very large order. The finite element model is impractical to design using current control schemes. Consequently, the LFSS problem has essentially two interrelated issues. The first involves model reduction and the second concerns controller design philosophy. The model reduction occurs in two phases. The first reduction is due to the impossibility of modeling the "infinite" number of vibrational modes of a pde. The second reduction is required because all of the modes that can be identified through off-line computation (e.g. Nastran, Stardyne) cannot be practically implemented and controlled because of computational and memory constraints.

Model reduction techniques include singular value decomposition, modal cost analysis, and modal truncation (or singular perturbation). The resulting reduced order model will be called the finite design model. With this design model, the goal of the design effort is to develop a controller of much lower dimension than the design model. Several approaches to accomplish these tasks is given below.

1) Open-Loop Model Reduction. Retain the primary (or critical) modes and ignore residual modes of th design model. Next, design a controller for the primary modes.

2) Closed-Loop Model Reduction. Design a full order controller. Then, reduce controller dimension for feasibility and performance.

3) Design a controller of specified form and dimension and determine its gains. As noted by Kosut [1], this may involve highly nonlinear equations and provides no guarantee of global solution.

All of the above reduced-order approaches do not take into account the effects of both spillover and parameter uncertainty. Spillover arises from model-reduction where unmodeled modes are measured and excited by the controller. This spillover effect occurs when the actuators and sensors are poorly placed driving the LFSS toward instability and has been demonstrated experimentally by Balas [2] for a simple beam. Much of the current control literature have dealt with the spillover effects and this fundamental problem has not been totally resolved. For example, expending control energy to suppress the spillover effects of unmodeled modes may lead to insufficient energy to control the lower vibrational modes for acceptable performance. For various methods to eliminate the spillover effect, see Longman [3], Sesak [4], Lin [5], and Gupta [6].

The second issue concerns control design philosophy. That is, state feedback versus output feedback, quadratic performance measures versus pole placement, centralized control versus decentralized control, stability robustness versus performance robustness. These different strategies or philosophies have not dealt with merging the control problem with the modeling problem and conversely.

The objective of this paper is to briefly describe the latest trends of theoretical developments involved with modeling and controlling LFSS from a finite dimensional viewpoint. Characteristics and difficulties of LFSS are reviewed. Latest trends in system theory for model-reduction involves the controllability and observability subspaces to

determine optimal projections and transformations of reduced-order models and controllers. Such ideas include balanced realizations and singular-value analysis. Ad hoc methods using component cost analysis attempts to combine relationships of cost sensitivity, eigenvalues, controllability, and observability norms of each vibrational mode. Extensions of Linear Quadratic Gaussian (LQG) theory as applied to LFSS are presented including frequency-shaped cost functionals and perturbation methods. This paper also attempts to identify those areas of control science and large-scale systems theory that appear to have an important role in understanding and solving LFSS modeling and control; this area includes chained aggregation and decentralized control. Hopefully, this paper will stimulate ideas to integrate and bridge the gap between the modeling and control problem.

2. LFSS CHARACTERISTICS.

LFSS is similar to other large scale system (LSS) problems in that the designer must meet stringent performance requirements while working with a system of large dimension with uncertain parameters that affect the performance in an unknown and possibly hostile environment. Specifically, the problem areas include

1) design of a practical finite dimensional controller for the infinite-dimensional LFSS model. This is the continuous-discrete nature of the problem; that is, the plant is a continuum while the controller consists of a discrete number of sensors and actuators.

2) incorporation of modeling errors and unmodeled modes in the control problem. Modes shapes and frequencies are in 10% error based on past spacecraft design experience (Herzberg, [7]).

3) satisfaction of ultra-high performance requirements

4) determination of actuator and sensor number, placement, and characteristics. This area involves seeking the optimal distribution of sensors and actuators to meet various control objectives and strategies.

For closed-loop evaluation, all these areas must be addressed. Additional characteristics of LFSS (Herzberg [7]) are model uncertainty in structural damping at low frequencies, instability effects or residual interaction between the controller bandwidth and unmodeled modes at high frequencies, densely packed low frequencies (some only .001 hz apart), and limited hardware testing for space behavior prediction. Any testing using numerical models will most likely involve insufficient and inaccurate data (Kosut, [1]). Finally, LFSS will be subject to many disturbances. These include thermal and gravity gradients, aerodynamic forces, solar pressure, and on-board disturbances.

From the above discussion, it is apparent that resolving all of the above issues represents a difficult and significant engineering challenge. Control laws must be developed suitable for systems of order of hundreds or thousands characterizing LFSS models and cope with the inherent uncertainties of the parameter plant models.

3. MODEL REDUCTION

3.1 INTRODUCTION

Model reduction scheme is a compromise between a complex, accurate models and a simple, less accurate model. It is a tradeoff between modeling order and accuracy of

plant characteristics. This compromise requires engineering judgement for the problem at hand. For LFSS applications, model-reduction is one method to reduce the gap between the high-order LFSS structural models and the relatively low-order control algorithms (Meirovich [8],[9]). The methods for developing reduced order models are needed to simplify controller structure and reduce any required computational simulations, analysis, and design. Any model reduction scheme should include appropriate criteria for selection of key model parameters or properties to meet high performance requirements.

LFSS structural models is usually represented by a finite-element model consisting of a large number of coupled ordinary differential equations (i.e. >1000). These equations contain varying degrees of importance and accuracy. The large order of LFSS models limits the controller performance due to computer limitations and thus model reduction is necessary. Techniques to accomplish this task include modal truncation, singular value decomposition (Moore [10] Jonckheere and Silverman [11], and modal cost analysis (MCA) (Skelton [12],[13]). Current control algorithms based on LQG methods are limited to plant models of orders approximately 100 states or 50 vibrational modes (Meirovich [8]). Controller order is even lower for practical implementation of processing capabilities of onboard computers and is not unique. The following subsections will present brief descriptions of the various model reduction schemes.

3.2 MODEL ERROR COMPENSATION

This scheme was developed to cope with the fundamental drawback of LQG theory which requires absolute modeling accuracy of the mathematical model [12]. This research effort attempts to provide a systematic guide toward the construction of a mathematical model which is appropriate for the control problem at hand. The method attempts to compensate for errors in the mathematical model of LFSS structures and solves the LQG problem subject to an augmented error system to the state equations. Here, a model error vector augments the system state vector to compensate for various modeling errors (parameter errors, truncated modes, neglected disturbances, and non-linearities of LFSS). Various model error systems can be viewed from this framework [12,14]. To cope with more than one type of modeling error, orthogonal functions (e.g. Chebyshev polynomials) are generated on-line to approximate the unknown model error vector. This latter concept yields a concept called orthogonal filtering for model error compensation. However, model error compensation requires additional states to model the nonwhite error characteristic of LFSS which raises an issue of applicability toward high order systems. The authors, Gupta, et al, [15] in LFSS have discovered connections between frequency-shaped costs functionals in LQG problems (to be discussed later) and orthogonal filtering. However, further research is required to explore these two points of view.

3.3 SINGULAR VALUE ANALYSIS AND BALANCED REALIZATIONS

This work was primarily initiated by Moore. Based on this approach, References [16]-[30] demonstrate the interest of approximating a high order model with a reduced order model and some applications toward LFSS has been done. Much of this work is based on open-loop model reduction and Jonckheere [16] has applied this approach to closed-loop model reduction.

The method of analysis is based on the input-output characteristics of the state-space model. A criteria is defined to measure the contribution of the modes to the input-output characteristics of a state-space model (e.g. finite element model). Based on

this criteria, those modes having the lowest contribution or weighting are then deleted. The singular values provide a measure of controllability and observability for each state of the system. An alternative view is that singular values provide a measure of the contribution of each subsystem to the overall interconnected system.

Balanced realization is built around singular value decomposition or principal component analysis [10,25]. Although balanced realizations has not been specifically developed for LFSS due to ill-conditioning problems, this method does provide useful analytical tools and guidelines for coping with structural instabilities and model reduction. The method of solution consists of solving two Lyapunov equations and a symmetric eigenvalue/eigenvector problem (or singular value analysis problem). For asymptotically stable systems, these Lyapunov equations determine the observability and controllability subspaces. The method uses principal component analysis to measure the observability and controllability of the system by evaluating the singular values of the controllability and observability Grammians. Singular values provide a crude measure of the impulse response error between the full-order and the reduced-order impulse response matrix. The model reduction scheme eliminates any weak subsystem which provides little contribution to the overall system response. Laub [26] provides an alternative computational schemes to the calculation of balanced transformations. Balanced realization has been applied to suboptimal LQG-design (Verriest, [27]). Other studies have shown that for discrete time variable systems, both balanced realization and Hankel-norm yields identical reduced models and guaranteed stable reduced order models.

3.4 EXTENSIONS OF BALANCED REALIZATIONS.

Jonckheere [16] extended Moore's open-loop balanced realization or approximation to closed-loop systems. The approach is based on designing a full order controller using standard LQG techniques. Next, the contribution of each state component to the closed-loop LQG is evaluated based on a new set of variables (i.e. similarity invariants) which are similar to singular values, described earlier. As before, unimportant states are deleted to yield a reduce-order controller. The reduced-order controller is selected to be optimal (in the LQG sense) for the reduced-order model. Most important, if the similarity invariants which are suppressed are small, closing the loop with the above LQG reduced-order controller on the full order system is guaranteed.

Instead of solving a pair of Lyapunov equations developed in balanced realization, the method is based on solving a pair of algebraic Riccati equations. A unique transformation, based on the AREs, will result to decouple the state components. Those state components which contribute very little to closed loop behavior, are deleted during the design of the reduced order controller.

Jonckheere developed sufficient conditions for stability of the full system closed by the reduced-order controller. The most interesting part concerning these conditions involves both the gains   and its associated phase. Note that phase information has been generated as well as gains using this approach.

The above approach has been applied for a simple LFSS model (24-dimensional tetrahedral finite-element model). For LFSS, the open-loop singular values are widely spread (where the smallest singular value corresponds to the high vibrational modes). Unfortunately, it is well-known that even unmodeled high-frequency modes can lead to instability called spillover. Thus, these open-loop singular values do not provide a useful measure of closed-loop contribution along with the numerical difficulties of singular value analysis. This is due to the widely spread singular values inherent in LFSS. How-

385

ever, Jonckheere's similarity invariants are not widely spread. In summary, closed-loop analysis revealed (where closed-loop characteristic values are moderately spread) important contributions of those modes which were discarded found in the open-loop analysis.

Other efforts by Santiago and Jamshidi [31] have extended Moore's open-loop balancing concepts to linear time-invariant unstable systems with weighted inputs and outputs. This extension includes using modified Lyapunov equations. Preliminary results by Santiago [32] also indicate systematic choices for Q and R matrices of the quadratic cost function for optimal control is possible. Additionally, if the system is unobservable and uncontrollable, another model reduction technique called chained aggregation, can be used. Balanced realization can then be applied on the reduced order model generated by chained aggregation. This combined approach has been successfully done by Santiago [32]. References [33]-[50] provide further insight into the balanced approach and demonstrate a collective interest of applying the balanced approach as a model-reduction tool by various researchers.

3.5 MODAL COST ANALYSIS

Another reduction method is called Modal Cost Analysis and is similar to Moore's balanced approach, with respect to model reduction criteria. This scheme attempts to combine the modeling and control problem by closed-loop modal truncation [13,51]. The method is based on a cost analysis for a linear system. This is done by connecting a white noise source at the input and measuring the amount of noise at the output. Then, those states having the least cost are deleted. Various criteria (i.e. disturbability norm, observability norm, modal frequency) are chosen to eliminate those closed loop modes that do not contribute significantly to the quadratic performance cost. The approach yields an iterative scheme for developing a series of state feedback controllers of successably lower dimension obtained from closed loop equations for a controller of higher dimension. Skelton relates the modeling and control problem using a "model quality index" which measures the performance of the higher order system when control is applied upon the lower-order model. Those modal coordinates that have smaller sensitivity to the model quality index is truncated. The model quality index measures controllability and observability. In summary closed-loop model reduction is performed in the presence of state dependent feedback using a performance criteria to study the cost contribution of each mode with the overall quadratic cost function.

4. EXTENSIONS OF LQG THEORY

4.1 LAC/HAC CONTROLLER

One extension of LQG theory consists of a two-level approach. The formulation is made up of a broadband, low damping controller called low-authority control (LAC) [52-54] and a narrowband, high damping controller called high-authority control (HAC) [55-57]. Low-authority control provides limited damping and uses root perturbation techniques for controller synthesis. The purpose of LAC is to provide low-damping (low authority) in a wide range of vibrational frequencies for robustness. Spillover reduction in the residual modes is accomplished by LAC. LAC takes care of the instabilities characteristics found in HAC. HAC redistributes the vibrational energy and provides high-damping or mode shaping in a narrow range of frequencies to achieve high performance. HAC synthesis uses LQG frequency-shaped cost functionals where increased penalties in a frequency-dependent cost function are placed on those frequencies where less response is desired. HAC applications in LFSS control includes spillover manage-

ment, disturbance rejection, and state estimation. Both HAC and LAC are then integrated properly such that their bandwidths overlapped and designed iteratively to yield a high-performance, stable, and robust controller.

4.2 MESS ALGORITHM

MESS stands for Model Error Sensitivity Suppression and is described briefly below (developed by Sesak [58]). This method uses LQG extensions to cope with the unknown high frequency residual modes. The formulation consists of a quadratic cost functional containing information concerning the unmodelled but known vibrational states (i.e. suppressed states). These states are known, reliably computed, and appreciably affect controller performance but are not included in the plant model due to on board computer limitations. MESS constrains both control and observation spillover for the known modes. With proper placement of actuators and sensors, the undesirable spillover terms are removed. The MESS algorithm penalizes the spillover effects directly through the quadratic cost function. The design technique developed in MESS uses the alpha-shift approach with known stability margin by Anderson and Moore. The alpha value measures control effort and sets an exponentially weighted quadratic cost function. Other researchers [59] describes this specialized LQG formulation as attempts to make the controller more positive (energy dissipative). The formulation also requires frequent parameter changes or "tuning" to yield acceptable performance.

4.3 MINIMUM DATA/MAXIMUM ENTROPY

Developed by Hyland, et al [60]-[62] and unlike the previous LQG formulations which require frequent design iterations, this approach attempts to provide a one-step design procedure for robust controllers. The design procedure addresses the effects of modelling uncertainty in large order systems and offers a new perspective in LQG theory. The approach accounts for parameter uncertainties directly into the design using minimum data/maximum entropy models. The approach handles the spillover effects and other modeling uncertainties by limiting information in the control law. The control design formulation includes measures of uncertainty to eliminate the dimensionality and modeling errors in vibrational control of LFSS. One of the major contributions of the work is a stochastic design model to compensate for the dimensionality and parameter sensitivity problems inherent in LFSS. The approach recognizes that an accurate and precise system model does not exist and develops the model from a severely limited set of parameter data. this restricted data set generates a probability model consistent with the data set and accounts for the large modeling errors in high order modal parameters. With this stochastic design model, a control law, based on the ensemble average of the quadratic criterion, is computed. This method assumes complete knowledge of the parameter probability distributions and is induced by the data set consisting of modal decorrelation times. This data set was chosen since they provide significant modelling fidelity. The modal decorrelation times reflect the frequency uncertainties in the mean response, the covariance and the expected cost. This data set adequately models the open-loop system second moment response.

Following this modeling philosophy, the objective is to minimize the average of a quadratic cost function. With the above data set, a full probability model for frequency uncertainties is constructed which is maximally unconstrained based on the entropy principle. The design method posed by Hyland reduces the number of measures of parameter uncertainties to a reasonable level. The system model generated by this approach accounts for the large uncertainties in high order modal parameters with rela-

387

tively little input data. The resulting design model permits formulation of closed equations for the expected cost matrix and explicit solution of the linear regulator problem. The formulation yields a modified Riccati equation having important implications to the dimensionality problem. The stochastic Riccati equation based on the minimum data/maximum entropy approach has a unique positive semi-definite solution. Its special structure permits quantitative distinction between coherent and incoherent modes. As a result, very high order models are applicable in regulator design computations. In addition, this method assures complete stability for high order stochastic (Minimum information) design model. The formulation has asympotic properties securing stochastic stability over the actual parameter set and models various levels of modeling uncertainties for design conservatism.

The method has demonstrated that the stochastic Riccati equation provides a robust rate-feedback control for those modes having large priori frequency uncertainties, and a deterministic LQ design for modes having small frequency uncertainties yielding a stable, mean-square optimal design. In other words, to account for the uncertainties in the plant as part of the control design model, a robust and high performance controller is assured. The effective dimension of the system model is not dictated the number of modes retained but by the quantity of parameter information rests in the model.

4.4 FIXED ORDER COMPENSATION

This strategy uses the minimum data/maximum entropy approach discussed earlier. However, this control strategy seeks a quadratically dynamic optimal controller of prespecified dimension and is based on a relatively high order plant mode. Major results from this effort include optimality under incomplete system information, robustness comparable with modelled uncertainty, and the resolution of the dimensionality problem. When the order of the compensator is equal to the dimension of the plant, standard LQG results are obtained. Necessary conditions for controllers of prespecified and lesser order consists of two modified Riccati equations and two modified Lyapunov equations. Along with these conditions, and optimal projection defines the geometric structure of the controller. The projection, an idempotent matrix, contains the observation and control subspaces of the controller. It is interesting to note that this research effort has found that the optimal subspaces for this formulation are not modal subspaces. In summary, these conditions and equations provide an optimal controller of fixed order. One can observe that this treatment is analogous to designing reduced-order observers (Luenberger [63]). The necessary conditions can serve as a reference for comparing other suboptimal design methods. Solving these equations yields a control law which guarantees closed-loop stochastic stability and optimal in the mean-square sense.

4.5 POSITIVITY CONCEPTS

Developed by Benhabib [59], this formulation does not rely on modal truncation. The concept uses positive (energy dissipative) and embedding operators and the design method has been successfully applied to the design of the attitude control and active structural damping systems for Draper model #2. A strictly positive operator has a physical interpretation as one that is always dissipative and does not create energy. The performance is not optimal and system "tuning" is required to yield acceptable performance. This method relies on on-orbit model parameter identification and subsequent controller tuning via ground communication to achieve acceptable performance. Balas [64], direct innovations feedthrough (LQG-type concept) results in a more positive controller. The work also sheds light in the placement of collocated sensors and actua-

tors combined with the above LQG formulation. Here, a positive controller results. Noncollocated sensors and actuators destroy the positivity conditions by losing the spatial and time phase relationships that exist between sensors and actuators. Others have described this effect as unstably interacting, Gran [65].

The positivity design approach is one of the few methods that tackled the discrete-time control for LSS. With the rapid technological change and flexibility of microprocessors, LSS digital control is inevitable.

5. LARGE-SCALE SYSTEMS THEORY

Due to the vast complexities of LFSS, as it has been argued throughout our discussions, there are very few modeling or control strategies available for these effectively infinite-dimensional systems. One of the few possibilities may be large-scale systems theory. However, within the framework of large-scale system modeling very few schemes are appropriate for LFSS. Most of such schemes either require knowledge of the eigenstructure of the system or are limited to single-input single-output systems. One of the more promising schemes for modeling and model reduction of LFSS is perhaps "Chained aggregation", introduced first by Perkins and associates [66], discussed by Jamshidi [67] and extended by Kwong [68]. References [69]-[78] provide further information and insight into this modeling scheme. Chained aggregation has been successfully applied with the balanced approach, Santiago [31]-[32], using Kwong's example [68].

In the area of control, large-scale systems theory provides us with hierarchical and decentralized control strategies [79] both of which can be interpreted as local control schemes. Hierarchical control is based on two key issues - "Decomposition" and "Coordination" both of which would be very unfeasible and impractical for a LFSS. Decentralized control, on the other hand, does not require any tearing of the system structure and can utilize local measurements for local control and yet provide an overall stabilizing effect for the system. Among decentralized control schemes, decentralized robust servomechanism introduced by Davison [79], described in text book context by Jamshidi [67] and applied for LFSS by West-Vukovich et al. [80] seems to be a promising control law for LFSS. In this section one modeling and one control strategy of large-scale systems i.e. *chained aggregation* and *decentralized robust servomechanism control* are briefly discussed.

5.1 CHAINED AGGREGATION

One of the more recent approaches in aggregating large-scale linear time-invariant systems is "chained aggregation", developed by Perkins and associates [66]. The usual linear time-invariant system model is transformed through a transformation matrix consisting of the output matrix columns depicting the strongly and weakly observable modes. This would partition the system into an "aggregated" and a "residual" subsystems. At this point if the aggregated subsystem is completely aggregatable [66] then the residual subsystem is discarded and process is complete. Otherwise, a new transformation matrix would be constructed to add on to strongly observable components of the system. In other words, the aggregation process continues by choosing an output for the residual subsystem and obtain an aggregation with respect to this output and by expanding the size of the aggregated subsystem. This process continues until the off-diagonal 1-2 submatrix of the resulting GHF is null. A few points need to be mentioned regarding chained aggregation. One is that its GHR formulation is not unique. The weak couplings of modes is not identified easily. In spite of these, chained aggregation stands a good chance for use in the model reduction of LFSS.

389

5.2 DECENTRALIZED ROBUST CONTROL

One of the more promising control strategies for LFSS can be decentralized robust control. West-Vukovich et al [80] have applied decentralized robust controlled, to be briefly introduced here, to a 100-mode of Purdue's LFSS [81].

Consider a large-scale linear time-invariant system

$$\dot{x} = Ax + \sum_{i=1}^{N} B_i u_i + Ez$$

$$y_i = c_i x + D_i u + F_i z, i=1,...,N$$

$$y_i^m = c_i^m + D_i^m + F_i^m z, \ i=1,...,N$$

where $x \epsilon R^n$ is the state, $u_i \epsilon R^{m_i}$ are the control inputs, $y_i \epsilon R^{r_i}$ are the outputs to be regulated and $y_i^m \epsilon R^{r_i^m}$ are the outputs to be measured. The vector $z \epsilon R^3$ is a constant disturbance. The existence of a decentralized control

$$u_i = K_i y_i + v_i$$

is guaranteed by having none of the fixed modes [67] of the system in the right-half plane. A system has a fixed mode if one or more of its modes (eigenvalues) are not excited regardless of what decentralized controller is chosen. West-Vukovich et al. [80] have obtained conditions for a LFSS and have applied the decentralized control notion to a 200th order Purdue [81] model.

6. CONCLUSIONS

Although the structural control of LFSS has been approached by many researchers for several years, much theoretical and practical work still remains. There exists a gap to combine various model reduction schemes with control strategies and vice versa and how and when these two disciplines should be combined during the entire design process. Various criteria and approaches have been presented to provide an initial step toward combining these two disciplines. Santiago's dissertation [32] is a first attempt to combine the various modeling and control issues with applications to large-space flexible structures. The main thrusts of his dissertation include: (1) Systematic model reduction (2) Systematic placement of actuators and sensors (3) Systematic selection of Q and R matrices of the linear quadratic optimal control problem (4) Integrate (1)-(3) and apply to a large space structural model. In this paper an effort has been made to introduce ideas by other researchers to take on this infinitely challenging problem.

REFERENCES

[1]. R. L. Kosut, "Robust Control of Flexible Spacecraft", *Journal of Guidance, Control, and Dynamics*, Vol. 6, No. 2, March 1983.

[2]. M. Balas, "Modal Control of Certain Flexible Dynamic Systems", *SIAM Journal of Control and Optimization*, Vol. 16, No. 3, May 1978.

[3]. R. W. Longman, "Annihilation of Suppression of Control and Observation Spillover in the Optimal Shape Control of Flexible Aircraft", *Journal of Asthronautical Sciences*, Vol. XXVII, No. 4, Oct-Nov 1979.

[4]. J. R. Sesak, P. W. Likens, "Model Error Sensitivity Suppression: Quasi-static Optimal Control for Flexible Structures", *18th IEEE CDC*, December 1979.

[5]. J. G. Lin, "Three Steps to Alleviate Control and Observation Problems of Large Space Structures, *19th IEEE CDC*, December 1980.

[6]. N. K. Gupta, M. G. Lyons, J. N. Aubrun, G. Margulies, "Modeling, Control, and System Identification Methods for Large Space Structures", Paper obtained from Advance Beam Control Branch of Air Force Weapons Laboratory, Kirtland AFB, NM (Private correspondence with LtCol Donald Washburn), 1982.

[7]. R. J. Herzberg, "Dynamics and Control of Large Satellites", *Astronautics and Aeronautics*, October 1978.

[8]. L. Meirovitch, H. Oz, "Computational Aspects of the Control of Large Flexible Structures", *18th IEEE CDC*, December 1979.

[9]. L. Meirovitch, H. Oz, "An Assessment of Methods for the Control of Large Space Structures", *Proceedings of the 1979 Joint Automatic Control Conference*, 1979.

[10]. B. C. Moore, "Singular value analysis of linear systems, Part I," Dep.Elec.Eng., Univ. Toronto, Toronto, Ont., Canada Syst. Contr. Rep 7801, July 1973; and "Singular value analysis of linear systems, Part II," Dep. Elec.Engr., Univ. Toronto, Toronto, Ont., Canada Syst. Contr. Rep 7802, July 1978.

[11]. E. A. Jonckheere, L. M. Silverman, "A new Set of Invariants for Linear Systems-Application to Reduced Order Compensator Design, *IEEE Transactions on Automatic Control*, Vol. AC-28, 1983.

[12]. R. Skelton, Likens P., "Techniques of Modeling and Model Error Compensation in Linear Regulator Problems", *Advances in Control and Dynamic Systems*, Vol. 14. C. T. Leondes, Ed., 1978.

[13]. R. Skelton and C. Z. Gregory, "Measurement Feedback and Model Reduction by Modal Cost Analysis", *Proceedings of the JACC*, Denver, Colorado, 1979.

[14]. C. D. Johnson, "Theory of Disturbance-Accommodating Controllers", *Advances in Control and Dynamic Systems*, Vol. 14, C. T. Leondes, Ed., 1976.

[15]. N. K. Gupta, et al., ACOSS THREE (Active Control of Space Structures) Phase 1, DTICADA089142, Rome Air Development Center Final Report (RADC-TR-80-131), May 1980.

[16]. E. A. Jonckheere and L. M. Silverman, "A new set of invariants for linear systems - Application to approximation," presented the 1981 Int. Symo. Math. Theory Networks and Syst., Santa Monica, CA 1981.

[17]. S. Kung, "Optimal Hankel-Norm Nodel Reductions-Scalar Systems", Proceedings, 1980, JACC, San Francisco, CA.

[18]. S. Y. Kung and D. W. Lin, "Optimal Hankel-Norm Model Reductions-Multivariable Systems," *IEEE Transactions on Automatic Control*, Vol. ACk-26, No. 4, August 1981.

[19]. Adamjan, V. M., D. Z. Arov, M. G. Krein, "Analytic Properties of Schmidt pairs for a Hankel Operator and the Generalized Schur-Takagi problem", Math. USSR Sbirbik, Vol. 15, 1971.

[20]. -, "Infinite Hankel block matrices and related extension problems", *Amer. Math. Soc. Trans.*, Vol. 1, pp. 133-156, 1978.

[21]. L. M. Silverman and M. Bettayeb, "Optimal Approximation of Linear Systems", JACC, San Francisco, CA 1980.

[22]. A. Bultheel, and P. Dewilde, "One the Adamjan-Arov-Krein approximation, identification, and balanced realization", IEEE Trans. Automatic Control, submitted for publication.

[23]. L. Pernebo and L. M. Silverman, "Model reduction via balanced state space representation," IEEE Trans. Automatic Control, vol. AC-27, April 1982.

[24]. R. E. Skelton, "A control design algorithm for flexible structures," Proc. of 19th IEEE CDC, Albuquerque, NM., Dec. 10-12, 1980, pp. 1232-1234.

[25]. B. C. Moore, "Principal Component Analysis in Linear Systems, Controllability, Observability, and Model-Reduction, *IEEE Transactions on Automatic Control*, Vol. AC-26, 1981.

[26]. A. Laub, "Computation of Balancing Transformations", JACC, 1980.

[27]. E. I. Verriest, "Suboptimal LQG-design via Balanced Realization", *20th IEEE CDC*, December 1981.

[28]. M. Bettayeb, L. M. Silverman, M. G. Safonov, "Optimal Approximation of Continuous-Time Systems", *19th IEEE CDC*, December 1980.

[29]. J. L. Tietze, "Singular Value Analysis of the Model Error Sensitivity Suppression Technique", *20th IEEE CDC*, December 1981.29.

[30]. E. A. Jonckheere, L. M. Silverman, "Singular Value Analysis of Deformable Systems", *20th IEEE CDC*, December 1981.

[31]. J. Santiago and M. Jamshidi, "Extensions of the Balanced Approach", to be published,1985.

[32]. J. Santiago, "Systematic Optimal Model Reduction based on Signal Injections with Application to Large Flexible Space Structures", Ph.D. dissertation, Dept. of Elect.Engr. and Compt. Engr., University of New Mexico, Albuquerque, N.M. (to be published in 1985).

[33]. K. V. Fernando and H. Nicholson, "Singular Perturbation Model Reduction" of Balanced Systems", *IEEE Trans. Auto. Contr.*, Vol. AC-27, April 1982.

[34]. A. Yousuff and R. E. Skelton, "A Note on Balanced Controller Reduction," *IEEE Trans. Auto.Contr.*, Vol. AC-29, March 1984.

[35]. D. A. Wilson and A. Kumar, "Symmetry Properties of Balanced Systems", *IEEE Trans. Auto. Contr.*, Vol. AC-28, September 1983.

[36]. L. Pernebo, L. M. Silverman, "Model Reduction via Balanced State Space Representations", *IEEE Trans. Auto. Contr.*, Vol. AC-27, April 1982.

[37]. K. V. Fernando and H. Nicholson, "On the Structure of Balanced and other Principal Representations of SISO Systems", *IEEE Trans. Auto. Contr.*, Vol. AC-28, February 1983.

[38]. K. V. Fernando and H. Nicholson, "Singular Perturbational Model Reduction in the Frequency Domain", *IEEE Trans. Auto. Contr.*, Vol. AC-27, August 1982.

[39]. K. V. Fernando and H. Nicholson, "On the Cauchy Index of Linear Systems", *IEEE Trans. Auto. Contr.*, Vol. AC-28, February 1983.

[40]. K. V. Fernando and H. Nicholson, "Reciprocal Transformations in Balanced Model-Order Reduction", *IEE Proceedings*, Vol. 130, Pt. D, No. 6, November 1983.

[41]. K. V. Fernando and H. Nicholson, "Singular Perturbational Approximations for Discrete-Time Balanced Systems", *IEEE Trans. Auto. Contr.*, Vol. AC-28, No. 2, February 1983.

392

[42]. K. V. Fernando and H. Nicholson, "Karhunen-Loeve Expansion with Reference to Singular-Value Decomposition and Separation of Variables", *IEE Proceedings*, Vol. 127. Pt. D, No. 5, September 1980.

[43]. K. V. Fernando and H. Nicholson, "Discrete Double-Sided Karhunen-Loeve Expansion", *IEE Proceedings*, Vol. 127. Pt. D, No. 4, July 1980.

[44]. S. Shokoohi, L. M. Silverman, and P. M. Van Dooren, "Linear Time-Variable Systems: Balancing and Model Reduction", *IEEE Trans. Auto. Contr.*, Vol. AC-28, August 1983.

[45]. E. I. Verriest and T. Kaliath, "On Generalized Balanced Realizations", *IEEE Trans. Auto. Contr.*, Vol. AC-28, August 1983.

[46]. K. Glover and D. J. N. Lemebeer, "Robust Multivariable Control System Design using Optimal Reduced Order Plant Models", *Automatic Control Conference*, San Francisco, CA., June 1983.

[47]. G. J. Lastman and N. K. Sinha, "A Comparison of the Balanced Matrix Method and the Aggregation Method of Model Reduction", *IEEE CDC*, December 1983.

[48]. P. Harshavardhana, E. A. Jonckheere, and L. M. Silverman, "Stochastic Balancing and Approximation- Stability and Minimality", *IEEE CDC*, December 1983.

[49]. W. L. Mills, C. T. Mullis, R. A. Roberts, "Low Roundoff Noise and Normal Realizations of Fixed Point IIR Digital Filters", *IEEE Trans. on Acoust., Speech, Signal Processing*, Vol. ASSP-24, pp. 538-549, December 1976.

[50]. C. T. Mullis, R. A. Roberts, "Roundoff Noise in Digital Filters: Frequency Transformations and Invariants", Vol. ASSP-24, December 1976.

[51]. R. Skelton, A. Yousuff, "Component Cost Analysis of Large-Scale Systems", *Advances in Control and Dynamics Systems*, Vol. 18, C. T. Leondes, Ed., 1982.

[52] J. N. Auburn, "Theory of the Control of Structures by Low-Authority Controllers", *Journal of Guidance and Control*, Vol. 3, No. 5, Article No. 7-168R.

[53] J. N. Aubrun, J. A. Breakwell, C. J. Chambers, "Experimental Results for Active Structural Control", *20th IEEE CDC*, December 1981.

[54] J. N. Aubrun, N. K. Gupta, M. G. Lyons, "Large Space Structures Control: An Integrated Approach", *AIAA Guidance and Control Conference*, Boulder, Colorado, August 1979.

[55] N. K. Gupta, M. G. Lyons, J. N. Aubrun, G. Margulies, "Modeling, Control, and System Identification Methods for Large Space Structures", Paper obtained from Advance Beam Control Branch of Air Force Weapons Laboratory, Kirtland AFB, NM (Private correspondence with LtCol Donald Washburn), 1982.

[56]. N. K. Gupta, "Frequency-Shaped Cost Functionals: Extensions of Linear-Quadratic-Gaussian Design Methods", *Journal of Guidance and Control*, Vol. 3, No. 6, Nov-Dec 1980.

[57]. N. K. Gupta, M. G. Lyons, J. N. Aubrun, G. Margulies, "Frequency-Shaping Methods in Large-Space Structures Control", AIAA paper.

[58]. J. R. Sesak, P. W. Likens, "Model Error Sensitivity Suppression: Quaso-static Optimal Control for Flexible Structures", *18th IEEE CDC*, December 1979.

[59]. R. J. Benhabib, "Discrete Large Space Structure Control System Design Using Positivity", *20th IEEE CDC*, Dec. 1981.

[60]. D. C. Hyland, "Optimal Regulation of Structural Systems with Uncertain Parameters", TR-80-246 Feb. 1981. Electronic Systems Command, Hanscom AFB, Bedford MA. 01731.

[61]. D. C. Hyland, "Mean-Square Optimal Fixed-Order Compensation - Beyond Spillover Suppression", AIAA Astrodynamics Conf., Paper No. 82-1403, August 1982.

[62]. D. C. Hyland, A. N. Madiwale, "A Stochastic Design Approach for Full-Order Compensation of Structural Systems with Uncertain Parameters", Paper 81-1830, AIAA Guidance and Control Conference, Albuquerque, NM August 1981.

[63]. D. G. Luenberger, "Observers for Multivariable Systems", *IEEE Trans. on Automatic Control*, Vol. AC-II, No. 2, April 1966.

[64]. M. J. Balas, "Active Control of Flexible Systems", *Journal of Optimization Theory and Applications*, Vol. 25, No. 3, July 1978.

[65]. R. Gran, "Qualitative Stability of Large Space Structures with Non-Collocated Actuators and Sensors", *20th IEEE CDC*, December 1981.

[66]. E.C.Y. Tse, J.V. Medanic, W.R. Perkins, "Chained Aggregation of Linear Time Invariant Systems," *Proc. JACC.* San Francisco, CA.

[67]. M. Jamshidi *Large-Scale Systems - Modeling and Control*, Elsevier Science (North-Holland), New York, 1983.

[68]. C. P. Kwong, "Optimal Chained Aggregation for Reduced-Order Modelling", *International Journal of Control*, 1982, Vol. 35, No. 6, 965-982.

[69]. M. Aoki, "Control of Large-Scale Dynamic Systems by Aggregation", *IEEE Trans. Auto, Contr.*, Vol. AC-13, June 1968.

[70]. M. Aoki, "Some Approximation Methods for Estimation and Control of Large Scale Systems", *IEEE Trans. Auto. Contr.*, Vol. AC-23, April 1978.

[71]. M. Aoki, "Aggregation", in *Optimization Methods for Large-Scale Systems...with Applications*, D. A. Wilson, ed., Mcgraw-Hill Book Co., New York, 1971.

[72]. C. P. Kwong, "Disaggregation, Approximate Disaggregation, and Design of Suboptimal Control", *International Journal of Control*, Vol. 37, no. 4, 1983.

[73]. C. P. Kwong and C. F. Chen, "A Quotient Space Analysis of Aggregated Models", *IEEE Trans. Auto. Contr.*, AC-27, February 1982.

[74]. D. Lindner, W. R. Perkins, J. Medanic, "Chained Aggregation and Three-control-component design: a geometric analysis", *International Journal of Control*, Vol. 35, No. 4, 1982.

[75]. D. Lindner, W. R. Perkins, "The Generalized Hessenberg Representation and Near Observability in Model Reduction", *Automatic Control Conference*, San Francisco, CA., June 1983.

[76]. E. C. Tse, J. Medanic, and W. R. Perkins, "Generalized Hessenberg Transformations for Reduced-Order Modeling of Large-Scale Systems, *International Journal of Control*, Vol. 27, 1978.

[77]. W. R. Perkins, "Reduced-Order Modeling of Large-Scale Systems by Chained Aggregation", *IEEE CDC*, December 1979.

[78]. V. C. Klema, A. J. Laub, "The Singular Value Decomposition: Its Computation and Some Applications", *IEEE Trans. Auto. Contr.*, Vol. AC-25, April 1980.

[79]. E. J. Davison, "The robust Decentralized Control of a General Servomechanism Problem", *IEEE Trans. Auto. Cont.* AC-21: 14-24.

[80]. G. West-Vukovich, E. J. Davison, P.C. Hughes, "The Decentralized Control of Large Flexible Space Structures," 1981 CDC, Albuquerque, NM, pp. 949-955.

[81]. H. B. Hablani, R.E. Skelton, "Generic Model of a Large Flexible Space Structure for Control Concept Evaluation," submitted J. Guidance and Control.

FREQUENCY DOMAIN CONTROL DESIGN OF LARGE SPACE STRUCTURES; A PRACTICAL APPROACH

R. Harding and A. Das
General Electric Space Division
Valley Forge, PA 19481

ABSTRACT

New requirements indicate the need for much larger, more accurate, and in some cases, very dynamic satellites. Large control system bandwidths are needed to meet accuracy and response requirements while maintaining tight control over appendage oscillations. Studies in recent years have shown that linear quadratic Gaussian (LQG) controllers can achieve the desired performance if the system is linearizable and if the system model is accurate. This paper presents results of an LQG controller applied to a single axis satellite with large solar arrays. A reduced order model (ROM) comprises rigid body motion with dominant structural modes. Optimal control and estimation gains are calculated based on an extremely conservative 0.0005 critical damping ratio. In order to examine stability characteristics, single-input single-output (SISO) frequency response concepts are generalized to develop a method of displaying open loop frequency response of a multi-input multi-output (MIMO) control system. The method is developed, verified, and used to predict unstable conditions.

INTRODUCTION

As space structures grow in dimension and requirements for attitude determination and control become more stringent, control systems engineers need an increasingly sophisticated approach to control design and analysis. Spacecraft flexibility is no longer a secondary concern. In fact, it becomes of paramount importance which drives the design of the control system so that distributed parameter system control, state obervability and controllability, control and estimation spillover, multivariable control analyses, and critical parameter error sensitivities are key concerns during preliminary design. Some of these concerns are relatively well understood even though few systems have implemented the underlying principles. Other concerns, such as multivariable control, have only recently been investigated in detail. This study is motivated by the desire to apply modern control theory to a linear time-invariant flexible space structure and perform frequency domain analyses as an investigation of the stated concerns.

A high accuracy pointing requirment brings to light a fundamental conflict for a Large Space Structure (LSS) control design. To

satisfy pointing accuracy requirements, the bandwidths of the attitude control system (ACS) have to be at least one or two orders of magnitude higher than what classical development techniques can provide. Higher bandwidths can be achieved for spacecraft with linearizable dynamic systems by optimizing quadratic cost functionals in the presence of gaussian noise. These optimal linearizable quadratic Gaussian (LQG) designs seem to be a good choice, although, they have several drawbacks. Good estimates of the modeshapes, the modal critical damping ratios and the natural frequencies of the spacecraft structure are required for the LQG controllers to be effective. Therefore, LSS design requires analysis techniques that aid the investigation of parameter error sensitivities and overall MIMO controller robustness.

OPTIMAL CONTROL SYNTHESIS

Most previous satellite controller designs have been able to meet the performance specification while avoiding active control of any structural modes. The standard design procedure rolls off the controller response at higher frequencies so that the system response is highly attenuated at the modal natural frequencies. A quadratic performance index optimization method that allows the designer to choose the states to be controlled has gained widespread appreciation as an alternative to the classical approach. In this manner, identifiable structural modes can be included in the controller instead of avoided as in the case of a classical control design. This type of control will actively damp controllable and observable modes and enhance attitude control performance. Development of an LQG controller is outlined in the following paragraphs.

A linear time-invariant system can be represented in the form

$$\dot{x} = Ax + Bu + w \tag{1}$$

$$y = Cx + v \tag{2}$$

where,

A = nxn system matrix

B = nxr control matrix

C = mxn measurement matrix

x = nx1 state vector

y = mx1 sensor output vector

u = rx1 control vector

w = nxl noise vector

v = mxl measurement noise vector

n = number of states

r = number of actuators

m = number of sensors

The controller is designed based on estimates of A,B,C, and x so the equations for the LQG design become

$$\dot{x} = \hat{A}x + \hat{B}u + w \tag{3}$$

$$y = \hat{C}x + v \tag{4}$$

where, , signifies an estimated entity and w and v are uncorrelated white noise vectors with zero mean. Detailed information for minimizing a scalar performance index as a function of the weighted norm of the state and control effort can be found in several optimization texts [1-3]. Minimizing the performance index leads to an optimal control law

$$u(t) = K1(t)\hat{x}(t) \tag{5}$$

where K1 is rxn optimal gain matrix which is found via the following relation.

$$K1(t) = -R1^{-1}(t)\hat{B}^T(t)P1(t) \tag{6}$$

and,

R1 = constant mxm control weighting matrix

The P1(t) matrix is obtained by solving the backward matrix Riccatti equation [3].

In a similar fashion, the optimal state estimate, $\hat{x}$, is found by solving the following equation.

$$\dot{\hat{x}} = \hat{A}\hat{x} + \hat{B}u + K2(y - \hat{C}\hat{x}) \tag{7}$$

The optimal estimation gains, K2, are found via

$$K2(t) = P2(t)\hat{C}^T(t)R2^{-1}(t) \tag{8}$$

where,

R2 = constant mxm measurement noise covariance matrix

and P2(t) is found by solving the forward matrix Riccatti equation [2,3].

FREQUENCY DOMAIN ANALYSES

A designer must aquire control system margin and sensitivity
information in order to show the robustness of the design in a
quantitative fashion. Many studies during the last several years
have shown that ROM controllers are sensitive to certain critical
parameters [4]. Modelling errors of parameters such as damping
ratios, modal natural frequencies, and modal admittances can
invalidate whatever stability margins the designer thought
existed in the approximated plant. Appropriate truncation of the
distributed parameter system is also crucial to controller
robustness for residual mode rejection. Further, inclusion of a
particular mode in the ROM state space does not assure adequate
modal control. Identifying problem modes early in the design
phase is extremely useful for structure and control design
iterations. All these concerns motivate development of analysis
tools to show strengths and weakness of a control system design.
Recent MIMO frequency response techniques draw parallels with
SISO stability criteria in a quest to assure global stability
over some range of plant perturbations. However, these MIMO
techniques seem to give a stability indication at the system
level with little insight into the stability or sensitivity of
the individual state elements.

This paper presents the results of a frequency analysis method
that answers many of the stated concerns as well as provide
insight into the state elements of a ROM controller. The
examples highlight these capabilities and include simulation
results to support frequency response predictions.

FREQUENCY DOMAIN APPROACH

All frequency response analyses rely on development of the system
transfer function. The concept of relating a systems output to
the input is fundamental to system dynamics and feedback control.
The open loop forward transfer function can be derived from the
equations for the plant, (1),(2),(5),and (8). Rewriting these
four equations with proper substitutions one finds the following
equations for the optimal controller and the Kalman state
estimator.

$$\dot{x} = Ax + BK1\hat{x} \tag{9}$$

$$\dot{\hat{x}} = \hat{A}\hat{x} + \hat{B}K1\hat{x} + K2(Cx - \hat{C}\hat{x}) \tag{10}$$

Taking the Laplace transform of both equations gives

$$x_O = [sI - A]^{-1}BK1\hat{x} \tag{11}$$

400

$$\hat{x} = [sI - \hat{A} - \hat{B}K1 + K2\hat{C}]^{-1}K2Cx_I \tag{12}$$

Combining (11) and (12) leads to the open loop system transfer function, G, so that

$$G = - (x_0 /x_I)$$

where,

$$G = G(A,\hat{A},B,\hat{B},C,\hat{C},K1,K2,s)$$

At this point in the frequency response analysis, a new transfer function is derived, g_{OL}. This is accomplished by appropriate partitioning of G to isolate the state element of interest and closing all other loops. The resulting transfer function is a scalar equation which can be used to generate familiar Bode, Nyquist, and Nichols plots or other frequency domain type graphs which have been widely used for SISO analyses.

Once the open loop response is obtained, the closed loop frequency response is easily calculated from the relation

$$g_{CL} = g_{OL}/(1+g_{OL}) \tag{13}$$

With this approach, the gain and phase margins for the particular state element as well as the effects of all other loops on that state element are accurately depicted. The authors have noted that each state should be examined when using this method in order to assure complete system stability. For example, a truth model of the plant may comprise ten state elements so that a thorough analysis would require ten open loop calculations using this approach. Effects of modes which are carried in the truth model and residual to the ROM can be predicted. The usefulness and validity of the method is shown in the following sections.

REDUCED ORDER MODEL

Truncation of the structural modes to only those modes that must be controlled is very important in order to minimize onboard processing. However, a robust controller must include the minimum set of dominant modes in its state space, otherwise instability will result. The phenomenon of exciting structural modes outside the controller state space is commonly referred to as control spillover. A similar phenomenon, estimator spillover, occurs when residual mode inputs to the estimation equations cause estimation errors which can also lead to instability. The capability of the controller to maintain attitude and modal control without knowledge of residual modes is one aspect of the robustness of the system in the presence of destabilizing factors. All structural modes respond in varying degrees to an actuating input, but, a robust controller does not excite

residual modes to the point of instability. Instead, it ignores these modes allowing the structure to damp their response passively.

Truncation of an infinite set of structural modes to a reduced order model (ROM) is based upon the determination of the dominant modes which will yield maximum deflections for a given input. Identifying dominant modes for a structure is a straight forward procedure that starts with the flexible motion differential equation.

$$\ddot{q}_j + 2\zeta_j \omega_{nj} \dot{q}_j + \omega_{nj}^2 q_j = \emptyset_{ij} f_i \tag{14}$$

or,

$$q_j = \frac{\emptyset_{ij} f_i}{s^2 + 2\zeta_j \omega_{nj} s + \omega_n^2} \tag{15}$$

where,

q_j = jth generalized coordinate

$\emptyset_{ij}$ = jth modal admittance at the ith node

ζ_j = jth modal critical damping ratio (0.0005)

ω_{nj} = jth modal frequency

f_i = torque at the ith node

s = Laplace operator

The generalized coordinate, q , is related to the spacecraft body axis, θ , by

$$\theta_i = \emptyset_{ij} q_j \tag{16}$$

so that (16) becomes

$$\theta_i = \frac{\emptyset_{ij}^2 f_i}{s^2 + 2\zeta_j \omega_{nj} s + \omega_{nj}^2} \tag{17}$$

Equation (17) is the open loop transfer function relating input torques to flexible displacement. This function takes on maximum values at structure natural frequencies, so that

$$\frac{\theta_{imax}}{f_{imax}} = \frac{\emptyset_{ij}^2}{2\zeta_j \omega_{nj}^2} \tag{18}$$

which relates maximum modal deflection for a maximum input torque. The greatest deflections are due to the modes with the largest admittances and lowest natural frequencies. For this study, a finite element method provides structural information for the first thirty modes, all of which are evaluated for maximum deflections using (18). From the thirty modes, six modes dominate all others by a minimum of two orders of magnitude. The six dominant modes and natural frequencies are

First Symmetric Bending	(.0407 Hz)
First Asymmetric Bending	(.0904 Hz)
Second Symmetric Bending	(.0957 Hz)
Second Asymmetric Bending	(.1500 Hz)
Third Symmetric Bending	(.1641 Hz)
Third Asymmetric Bending	(.2212 Hz)

The following four modes are the next largest. These modes are included in the true plant model and are residual to the controller.

First Symmetric Torsion	(.0649 Hz)
Solar Array Blanket Mode	(.1450 Hz)
Solar Array Blanket Mode	(.1453 Hz)
Third Symmetric Torsion	(.2074 Hz)

It seems prudent to carry all six dominant modes in the ROM. However, further ROM reduction is desirable provided that stability margins and performance is not seriously degraded by neglecting one or more of the six dominant modes. To follow through with this investigation, some actuator and sensor configurations need to be established so that the state equations of the previous section can be constructed.

Reference [5] outlines the procedure that was used to select actuator and sensor configurations for this study. That procedure made use of two approaches for the selection. A familiar eigenvalue analysis was compared with observer and controller Gramian matrices of various closed loop controllers and estimators [3]. For the sake of brevity, assume these configurations are finalized. In practice, actuator and sensor selections will probably be iterated with ROM definition selections to provide the best control system possible. Baseline actuator and sensor locations are shown in Fig. 1. The sensor and actuator complements that are used throughout the anlaysis portion of this study are listed in Table 1.
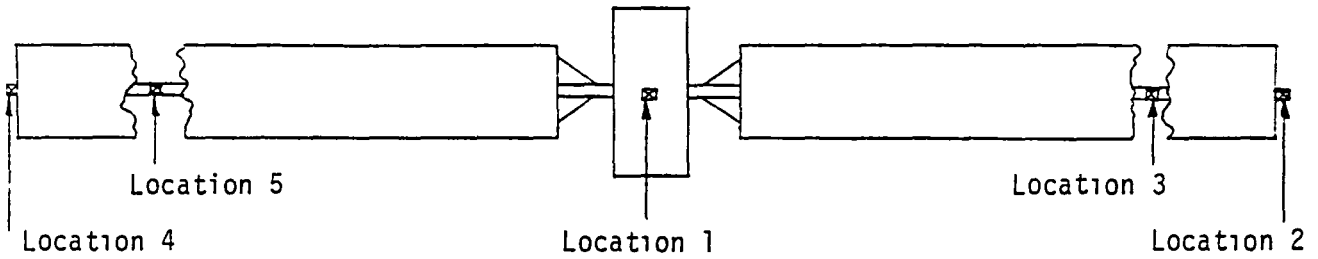
Figure 1. Actuator and Sensor Locations

ELEMENT	LOCATION	TYPE
Actuator	1	Torque producing
Actuator	2	Torque producing
Actuator	4	Torque producing
Sensor	1	Angular rate
Sensor	1	Angular position
Sensor	2	Relative angular position (1)
Sensor	3	Relative angular position
Sensor	4	Relative angular position
Sensor	5	Relative angular position

Table 1. ACTUATOR AND SENSOR COMPLEMENT

Note 1. A relative position sensor measures local angular deflections relative to the center body.

Fig. 2a and b are the yaw axis position Bode plots depicting gain and phase for the LQG controller (that includes the six dominant modes). The LQG controller has a bandwidth one order of magnitude greater than a classical controller that was developed for the same structure [5]. Yaw axis control is severly notched at the natural frequency of the first asymmetric bending mode due to poor controllability. Bode plots, Fig. 2c and d, and a Nyquist plot, 0% curve in Fig. 6, for the first asymmetric bending mode indicate a stable loop. All frequency response curves for all the state elements, as well as curves for the residual modes also indicate a stable system. This prediction compares very well with transient response simulation data shown in Fig. 3a-g. The first asymmetric bending mode is not successfully damped whereas the other controlled modes are damped quite well.


FURTHER ROM REDUCTION

The desire to minimize computational burdens for onboard processing leads to the desire to minimize the number of controlled modes. Application of the frequency response analysis to the six dominant modes can facillitate this procedure so that a smaller ROM which meets performance and stability specifications can be found. Carrying out the analysis on the six dominant modes, one finds that a minimum of two dominant modes must be kept in the controller state space. They are

First Symmetric Bending   (.0407 Hz)

Third Asymmetric Bending   (.2212 Hz)

All other modes are residual to the controller. It is interesting to note that the first symmetric bending is the largest modeshape and the third asymmetric mode is the third largest modeshape using (18). Also, any ROM selection neglecting either of these two modes is unstable. The yaw axis Bode plots for this ROM controller are shown in Fig. 4a and b. Two observations can be made: One, the effects of the first asymmetric bending and third symmetric bending modes are in evidence whereas before the ROM reduction, both were notched from the controller; and two, the bandwidth of the controller has been increased 20%. However, examination of the Bode plots for the first asymmetric bending mode, Fig. 4c and d, show a 20 DB increase of the peak gain and a 27 Deg loss in phase when this mode becomes residual to the controller.

Simulation of the reduced ROM controller, Fig. 5a-g, verifies the frequency response findings. The increased bandwidth results in a quicker transient response and a 28% faster settling time. This enhanced pointing capability is done at the expense of greater modal deflections. The first symmetric, first
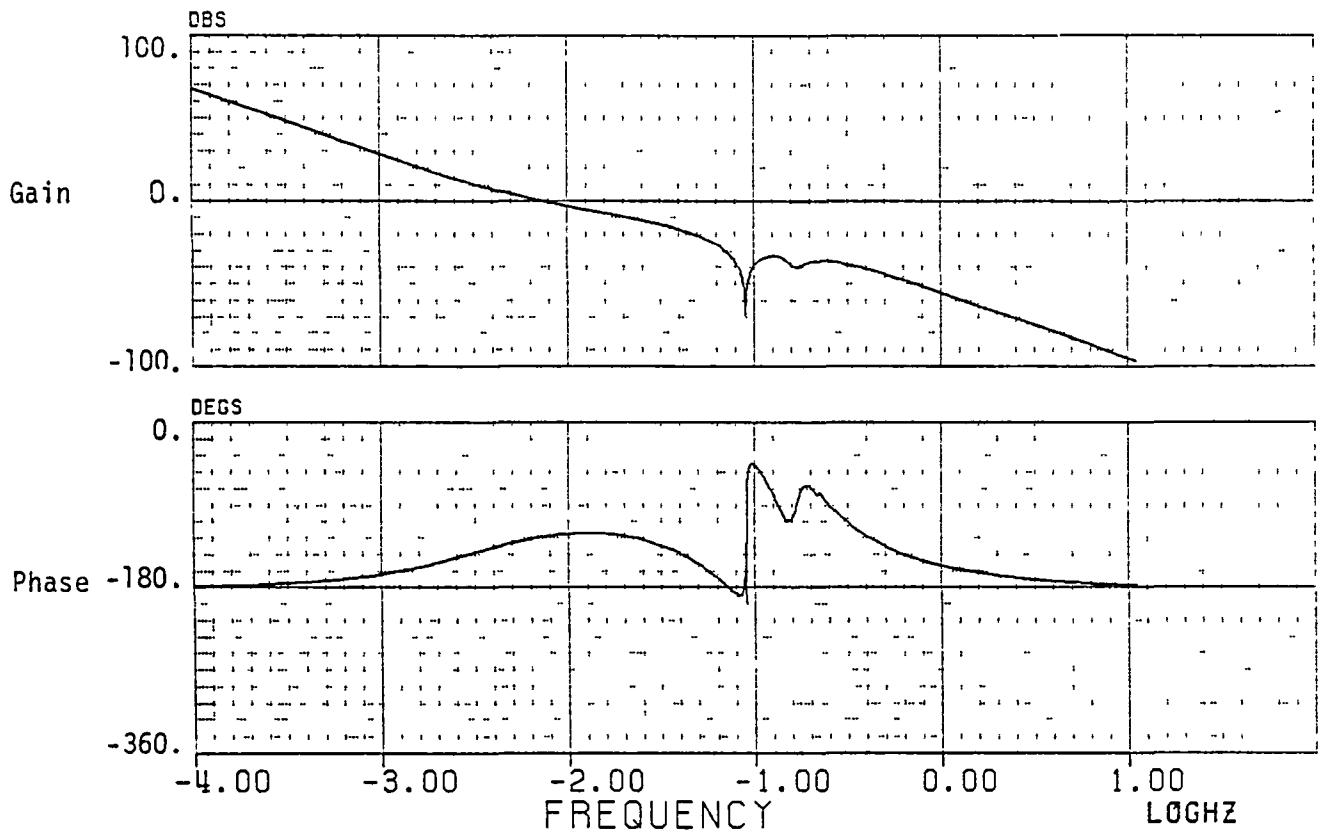
Figures 2a and b.   Yaw Axis Open Loop Gain and Phase
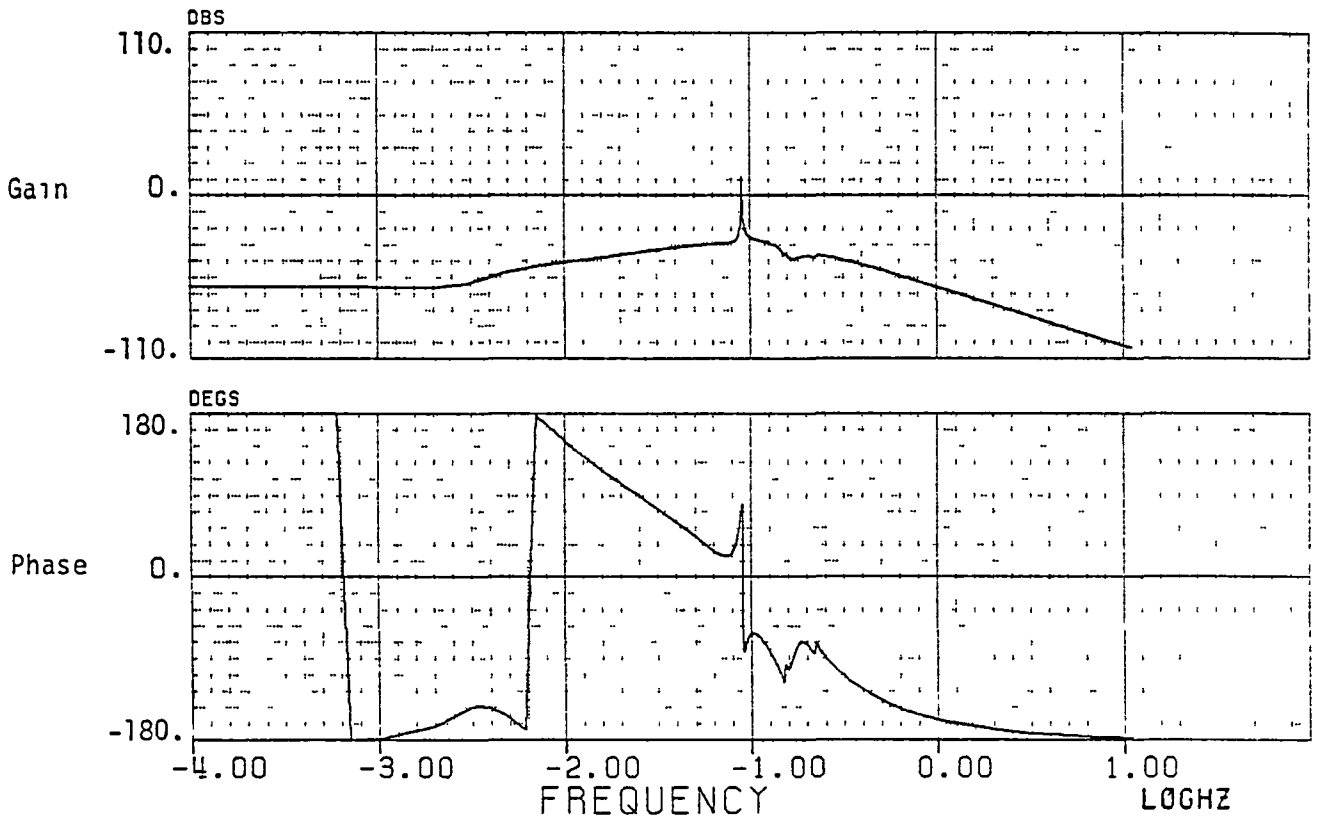
Figures 2c and d.   First Asymmetric Bending Open Loop Gain and Phase

406
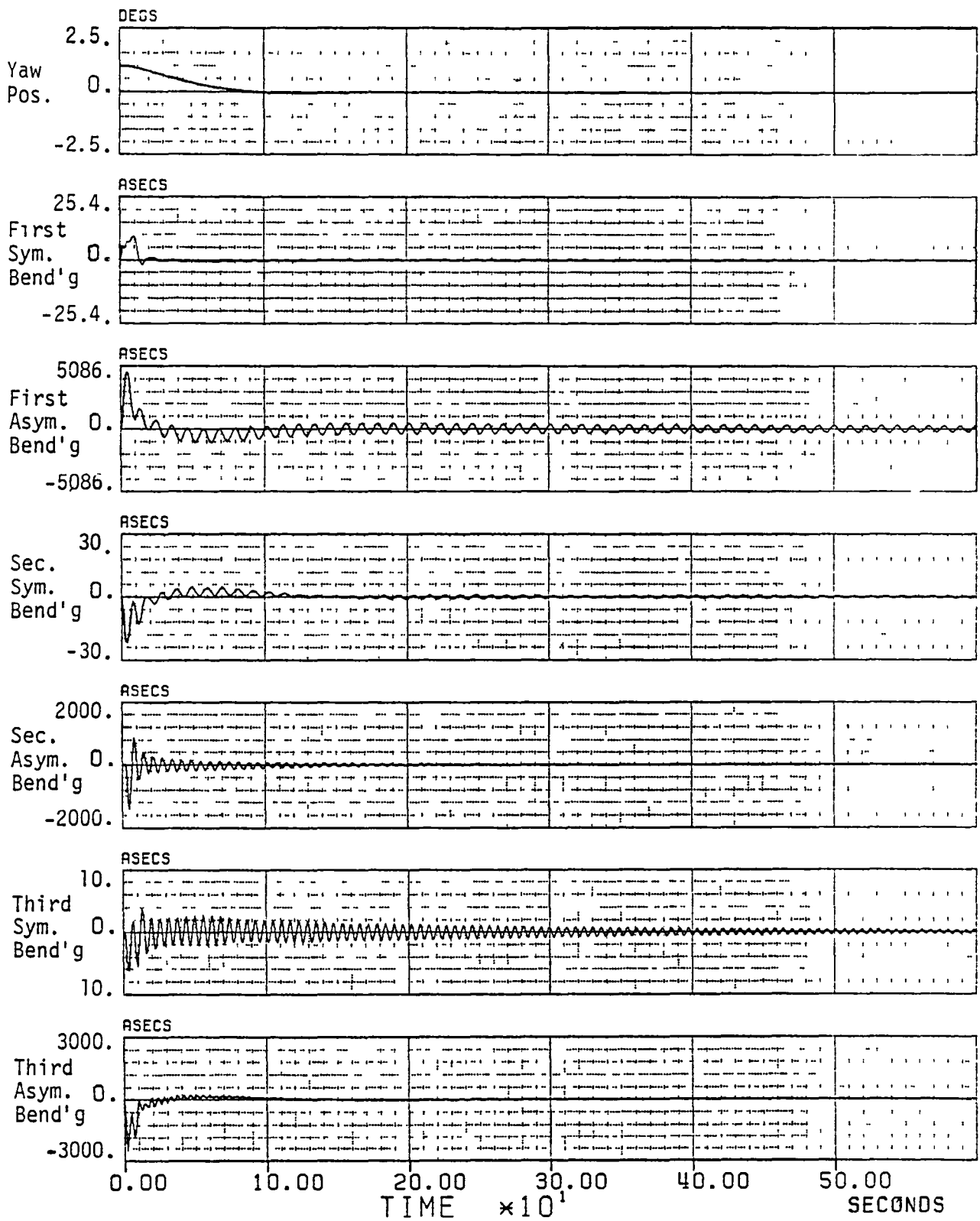
Figures 3a-g.   Transient Response with Six Controlled Dominant Modes

407
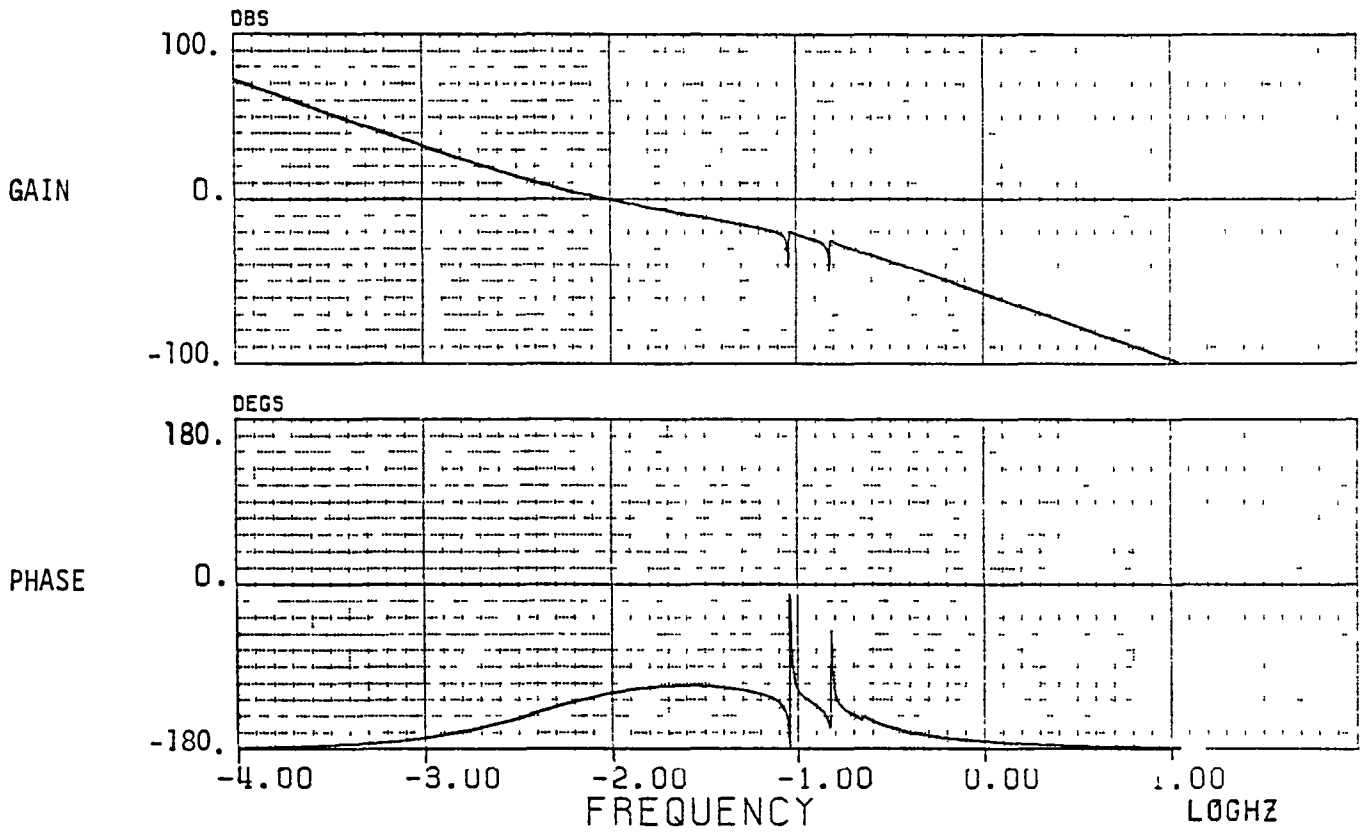
Figures 4a and b. Yaw Axis Open Loop Gain and Phase
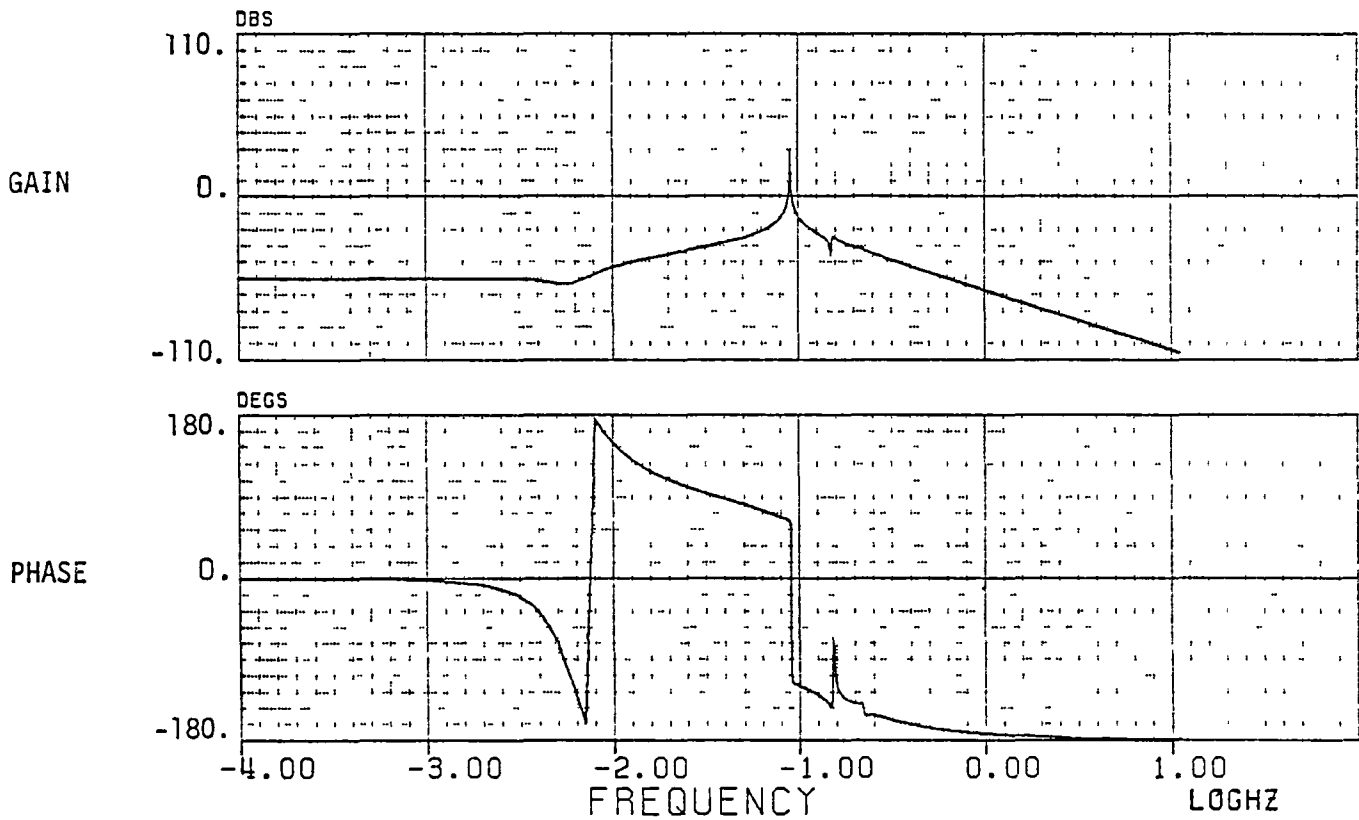
Figures 4c and d.   First Asymmetric Bending Open Loop Gain and Phase

408
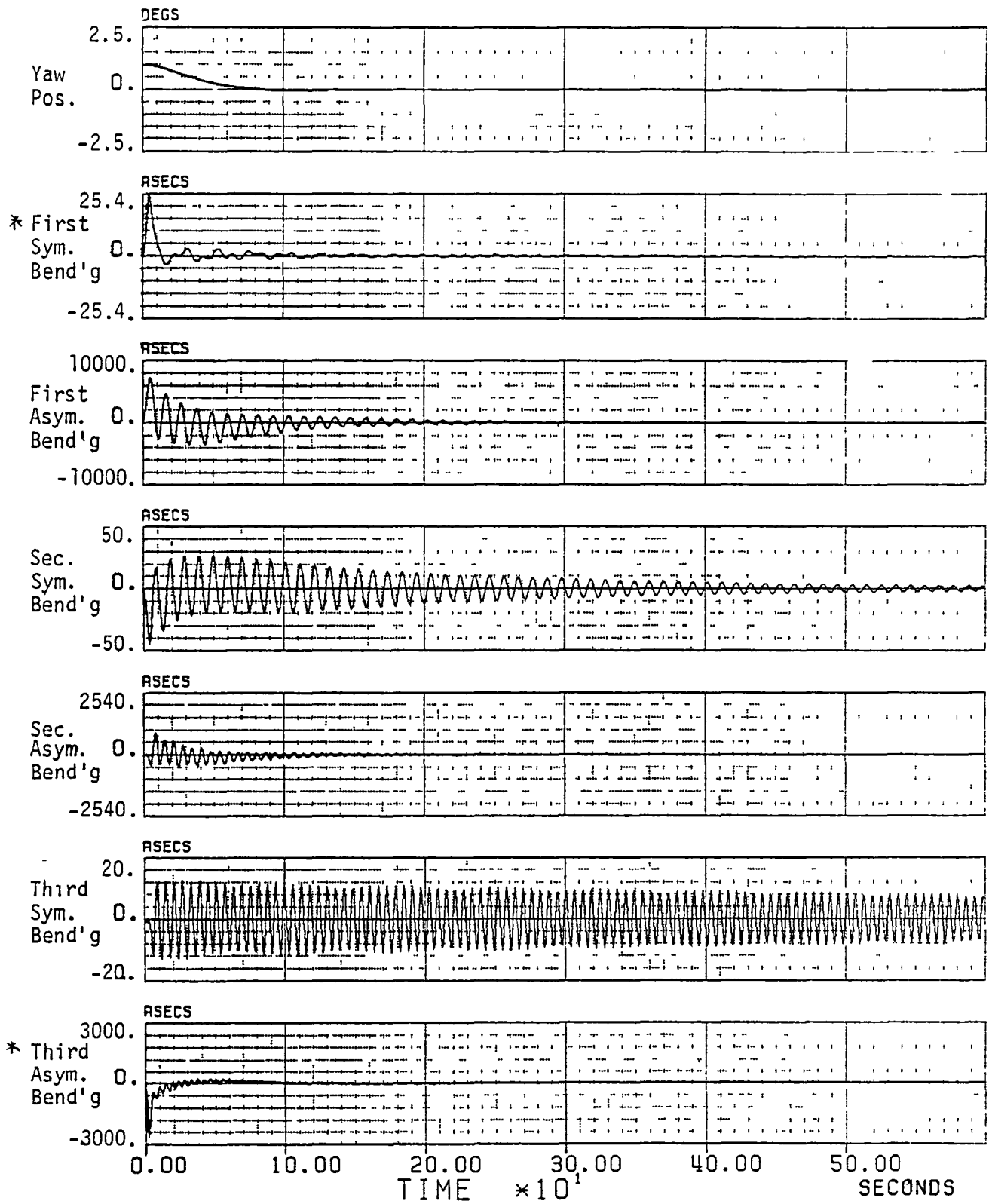
Figures 5a-g. Transient Response with Two Controlled Dominant Modes*

asymmetric, and third symmetric modes have significantly increased peak deflections. Interestingly, the first asymmetric mode is damped quicker as a residual mode than as a controlled mode. Investigation of the larger ROM controller shows that the state estimation errors for the first asymmetric mode are very large and slow to converge due to small observability of this mode. This accounts for the poor performance in controlling this mode. Combining this observation with the Bode plot information in Fig. 4c and d, one concludes that not including the first asymmetric mode in the ROM controller is a viable alternative if the designer is willing to trade reduced stability margin of the first asymmentric bending mode loop in order to achieve greater system pointing perfomance.

ERROR TOLERANCE CALCULATIONS

LQG derived control and estimation gains are based on critical, a priori structure parameters. Errors in the assumed dynamics will result in non-optimal gain calculations such that the system becomes unstable. Tolerances to this type of error is essential because the true plant parameters are unknown to the control systems designer.

EXAMPLE: NATURAL FREQUENCY ERROR TOLERANCE

This example investigates the first asymmetric mode natural frequency error tolerance as a controlled mode. It is apparent from Fig. 2d that the phase margin of the control loop may be negative if the true natural frequency for this mode occured at .014 Hz (i.e. an 84% error) in the frequency spectrum. Therefore, one expects the system to be unstable if the natural frequency of this mode is overestimated by some amount greater than 84%. Nyquist plots are very useful for modal analysis because of the characteristic circular contour of a mode when mapped onto the G plane. Nyquist stability criterion relates the number of encirclements of the (-1 + j0) point to system poles and zeroes in the right half plane. The Nyquist plot, Fig. 6 exhibits an encirclement of (-1 + j0) with an 84% natural frequency error as expected from the Bode plots. Transient response simulation data, Fig. 7, correlate very well with the Bode and Nyquist stability predictions that successful control is possible until the a priori second dominant modal frequency is overestimated by approximately 84%.

EXAMPLE: MODAL ADMITTANCE ERROR TOLERANCE

Any ROM controller is susceptable to controller spillover. Fig. 8a and b depict the Bode plots for the third symmetric bending mode as a residual mode. Closer inspection at'the modal
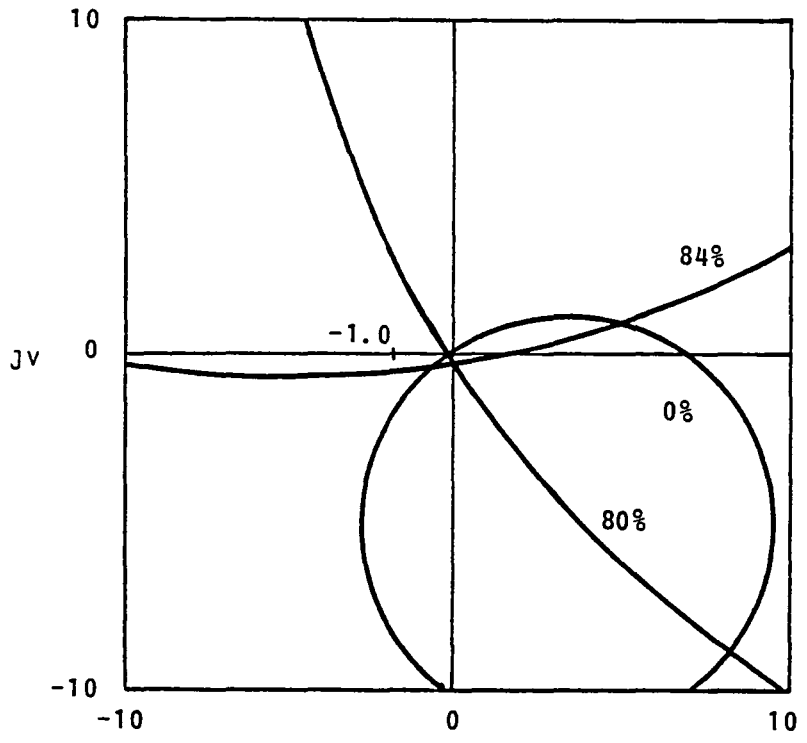
Figure 6. First Asymmetric Bending Nyquist for Various ω_n Errors
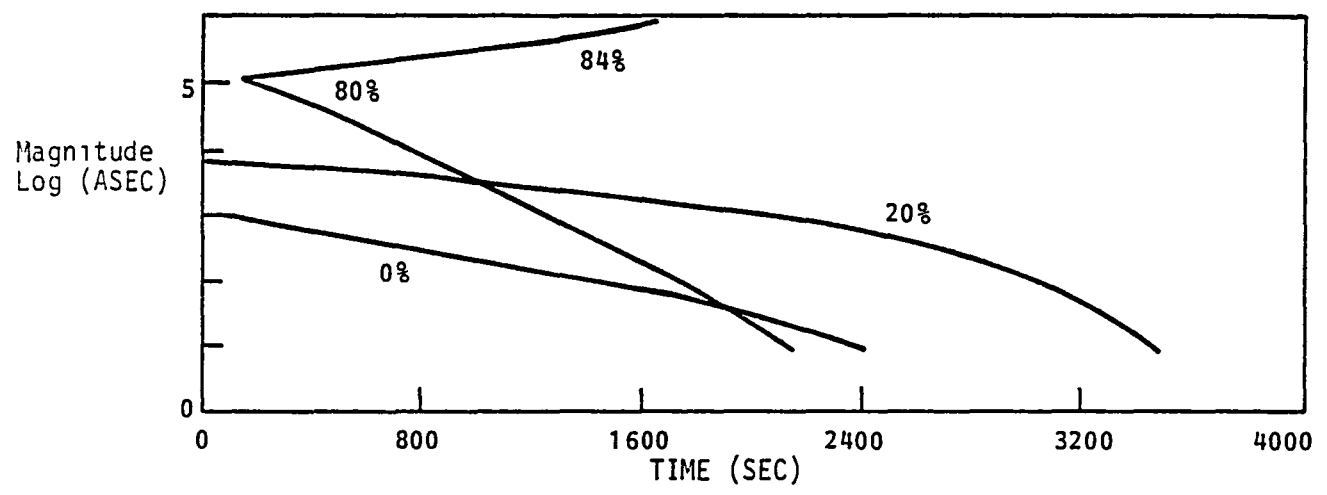

Figure 7. First Asymmetric Bending Transient Response Envelopes

411
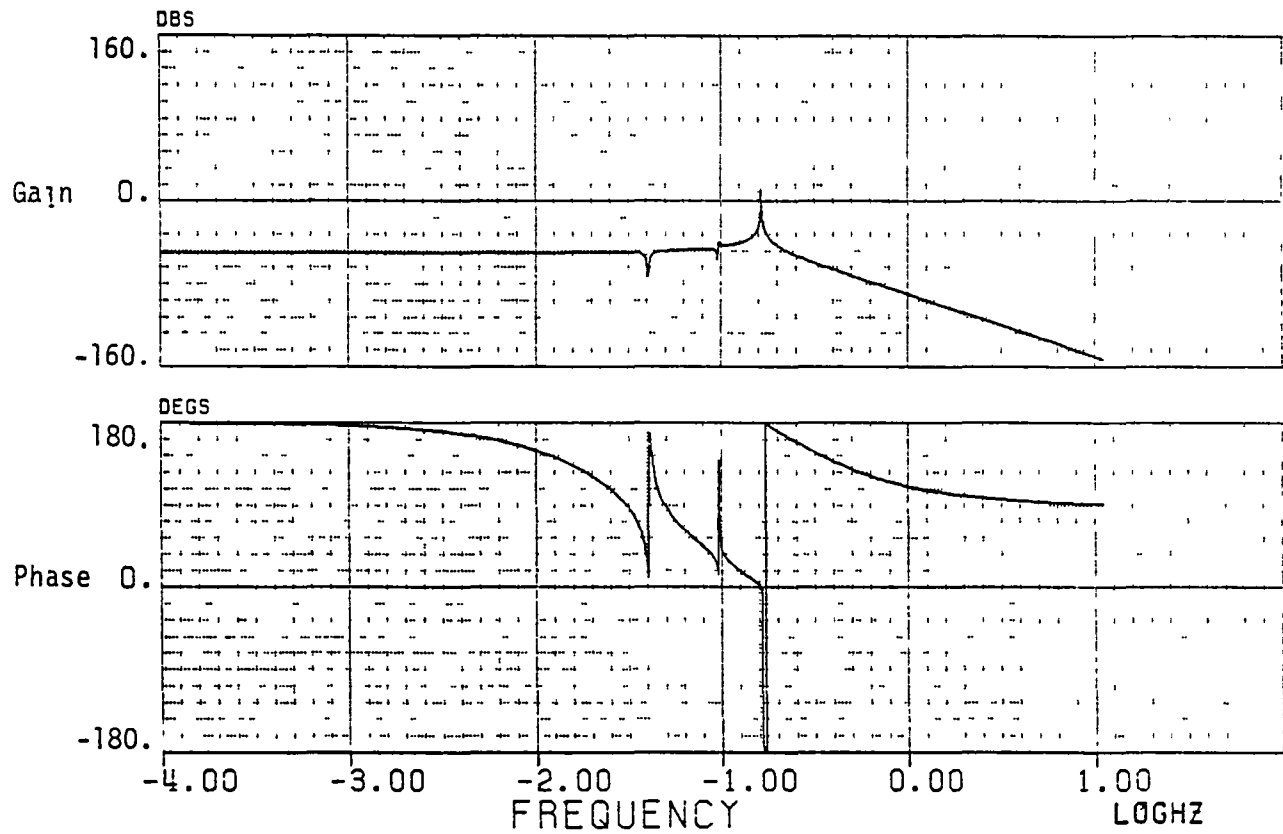
Figures 8a and b. Third Symmetric Bending Open Loop Gain and Phase
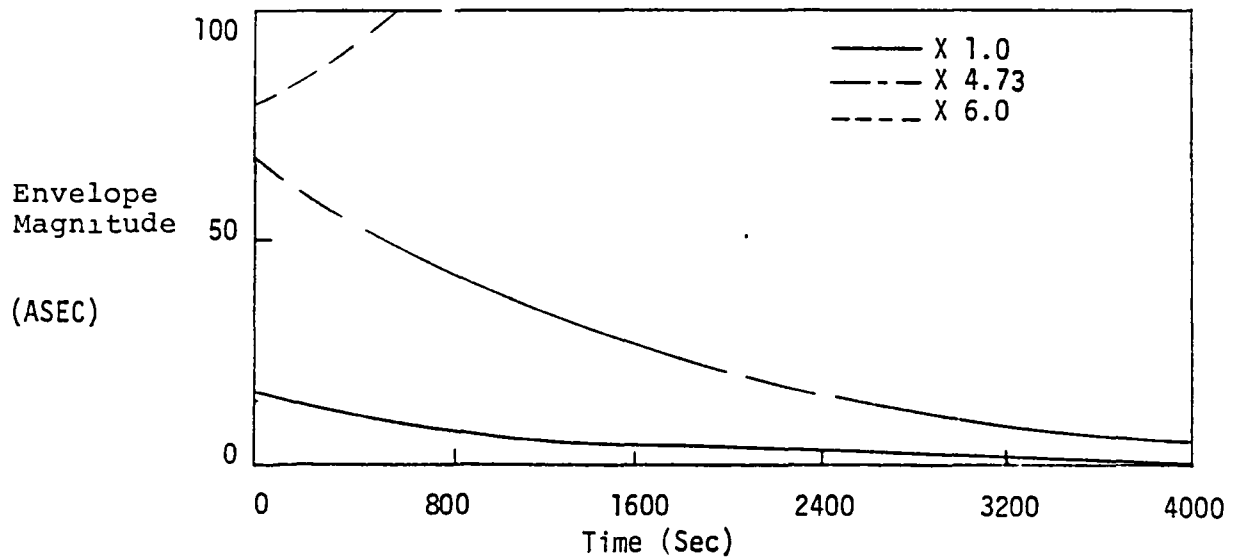
Figure 9. Third Symmetric Bending Mode Transient Response Envelopes

natural frequency shows 27 DB of gain margin which at first glance appeared to be marginally stable. This is actually an indication of modal admittance error margin because the mode shape magnitude defines the height of this curve. In short,

$$\text{gain margin (DB)} = 20 \ \log(f(\phi^2 \ ))$$

where   is the modal admittance. Working backward, one finds that 27 DB of gain margin equates to a factor of 4.73 error margin in the modal admittance values. Multiplying the admittances by 4.73 raises the gain curve so that the system is marginally stable due to zero gain and phase margins. Multiplying by a factor greater than 4.73 results in negative gain margin thus predicting system instability. Transient response simulation data, Fig. 9, support the frequency response predictions.

CONCLUSIONS

The performance advantages of LQG controllers for LSS are readily apparent. Precision pointing and quick transient response are very desirable attributes that an LQG controller can provide even with negligible structural damping. LQG control methods can be well suited to the distributed parameter problem of flexible structure control if the dominant characteristics of the system are known. The LQG controller developed for this investigation is robust such that four of six dominant modes can be residual to the controller with little adverse impact to active flexible control performance.

The frequency response method outlined herein is accurate for MIMO controller performance and stability analysis and critical parameter error margin predictions. This method is also useful in ROM definition by identifying modes which lead to system instability if they are not included in the controller state space. One concludes that this frequency response anlaysis technique is useful and the wealth of information derived for SISO systems is applicable to MIMO systems as well.

REFERENCES

1. Bryson and Ho, "Applied Optimal Control", Blaisdell Publishing Co., 1969.

2. Gelb, A. (Editor), "Applied Optimal Estimation", M.I.T. Press, 1974.

3. Sage, A. P. and White, C. C., "Optimum Systems Control", 2nd Edition, Prentice-Hall Inc., 1977.

4. Balas, M.J.,"Trends in Large Space Structure Control Theory: Fondest Hopes, Wildest Dreams", IEEE Transactions on Automatic Control, Vol. AC-27, No. 3, June 1982.

5. Harding, R. and Das, A.,"Flexible Structure Control in the Frequency Domain", Vibration Damping Workshop Procedings, 1984.

6. Benhabib, R., et al, "Stability of Large Space Structure Control Systems Using Positivity Concepts", J. Guidance and Control, Vol. 4, No. 5, Sep.-Oct., 1981.

7. Chan, S. and Athans, M., "Applications of Robustness Theory to Power System Models", IEEE Transactions on Automatic Control, Vol. 29, No. 1, Jan. 1984.

8. Dazzo and Houpis, "Linear Control Systems Analysis and Design", McGraw Hill Inc., 1975.

9. DeCarlo, R., et al, "Multivariable Nyquist Theory", Int. Journal of Control, Vol. 25, No. 5, 1977.

10. Frame, J. and Garrett, S., "Robust Control: An Overview", IEEE Conference, CH1749-1/82.

11. Postlewaite, I., et al, "Principal Gains and Principal Phases in the Analysis of Linear Multivariable Feedback Systems", IEEE Transactions Automatic Control, Vol. 26, No. 1, Feb. 1981.

A CONTROL CONCEPT FOR LARGE FLEXIBLE SPACECRAFT USING ORDER REDUCTION TECHNIQUES

G. Thieme and **H. Roth**
DORNIER SYSTEM GmbH
Postfach 1360
7990 Friedrichshafen 1, Germany

ABSTRACT

This paper presents some results found during the investigation of control problems of large flexible spacecraft. A triple plate configuration of such a spacecraft is defined and studied. The model is defined by modal data derived from finite element modelling. The order reduction method applied is briefly described. An attitude control concept with low and high authority control has been developed to design an attitude controller for the reduced model. The stability and response of the original system together with the reduced controller is analysed.

I. INTRODUCTION

This paper concentrates on theoretical aspects of the attitude control problem of large flexible spacecraft. It reports on baseline investigations for the test and comparison of design approaches and techniques.

The objectives of the study carried out are the investigation of control problems of large flexible spacecraft and the identification of basic problems that will be studied experimentally. The first steps have been the analysis and definition of requirements for the attitude control design and the dynamics model set up. Then order reduction methods have been applied to test the reduction methods and to achieve reduced order models. The next step is the controller design itself, but it is clear that order reduction and controller design have to be seen as elements of an iteration loop, in order to come to a final reduced order controller. The design is finished by a performance evaluation and critical assessment of the designed systems and the design methods applied. The identification of basic problems leads to the definition of an appropriate test set up and test program to study those problems experimentally. Fig. 1-1 shows the study task flow in phase 1.
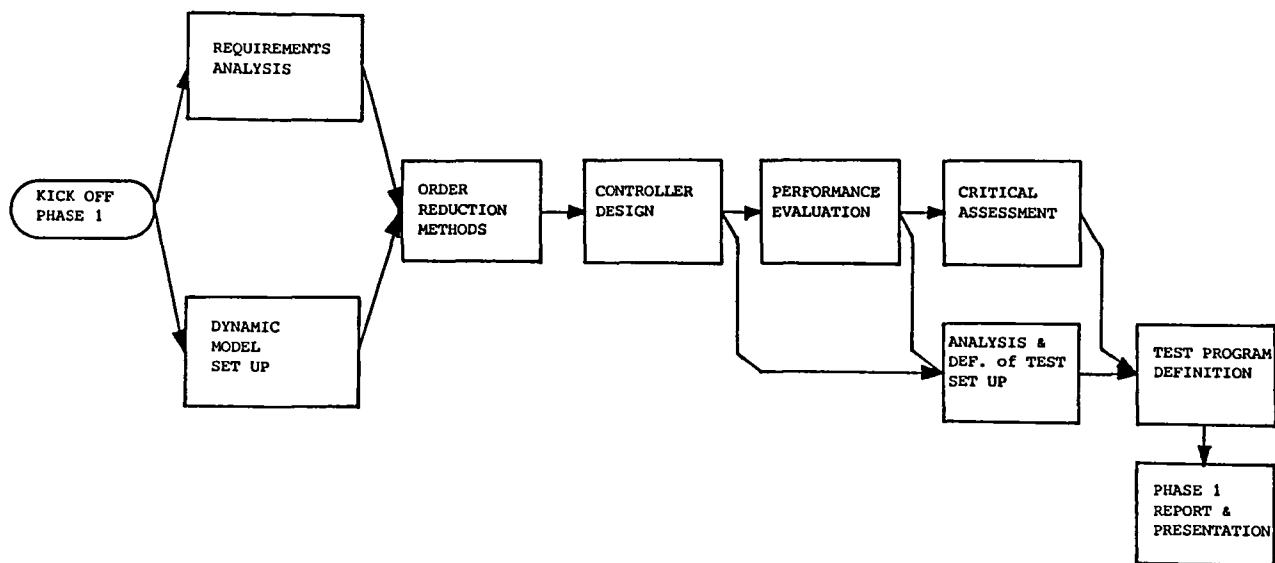
Fig. 1.1:   STUDY TASK FLOW PHASE 1

II.   DISTRIBUTED FLEXIBILITY MODEL

Three models were used as reference spacecraft in the studies. The models do no represent real or planned spacecraft, but they are representative for the characteristics which play a role in the design of attitude control systems for future large spacecraft. The simplest model is a free beam. The second model has been proposed in the literature as a generic model. It is a flat plate with a rigid centre body and has been developed at Purdue University. The third model is constructed of three coupled plates with the goal to have a spacecraft with nonhomogeneous flexibility. This three plate model proved to be the most interesting model, giving the most design problems. We will therefore concentrate on this model. The model consists of a central plate, having higher stiffness and mass density, which is coupled to two identical plates with lower eigenfrequencies. The modal data of this triple plate configuration has been derived from a finite element model. The physical size is 100 m by 150 m. Each of the three plates has a width of 50 m.

The thickness of the inner plate is set to 2 m, whereas the outer plates are 1 m thick. The elasticity modules is 2. E5 N/m^2 for the outer plates and 7.E5 N/m^2 for the centre plate. The mass density is 2 kg/m^3. These values are quite arbitrary. They have been selected in order to get densly packed frequencies starting at about O.02 Hz. From the 40 element model with 171 degrees of freedom the following 20 lowest eigenfrequencies were found:

416
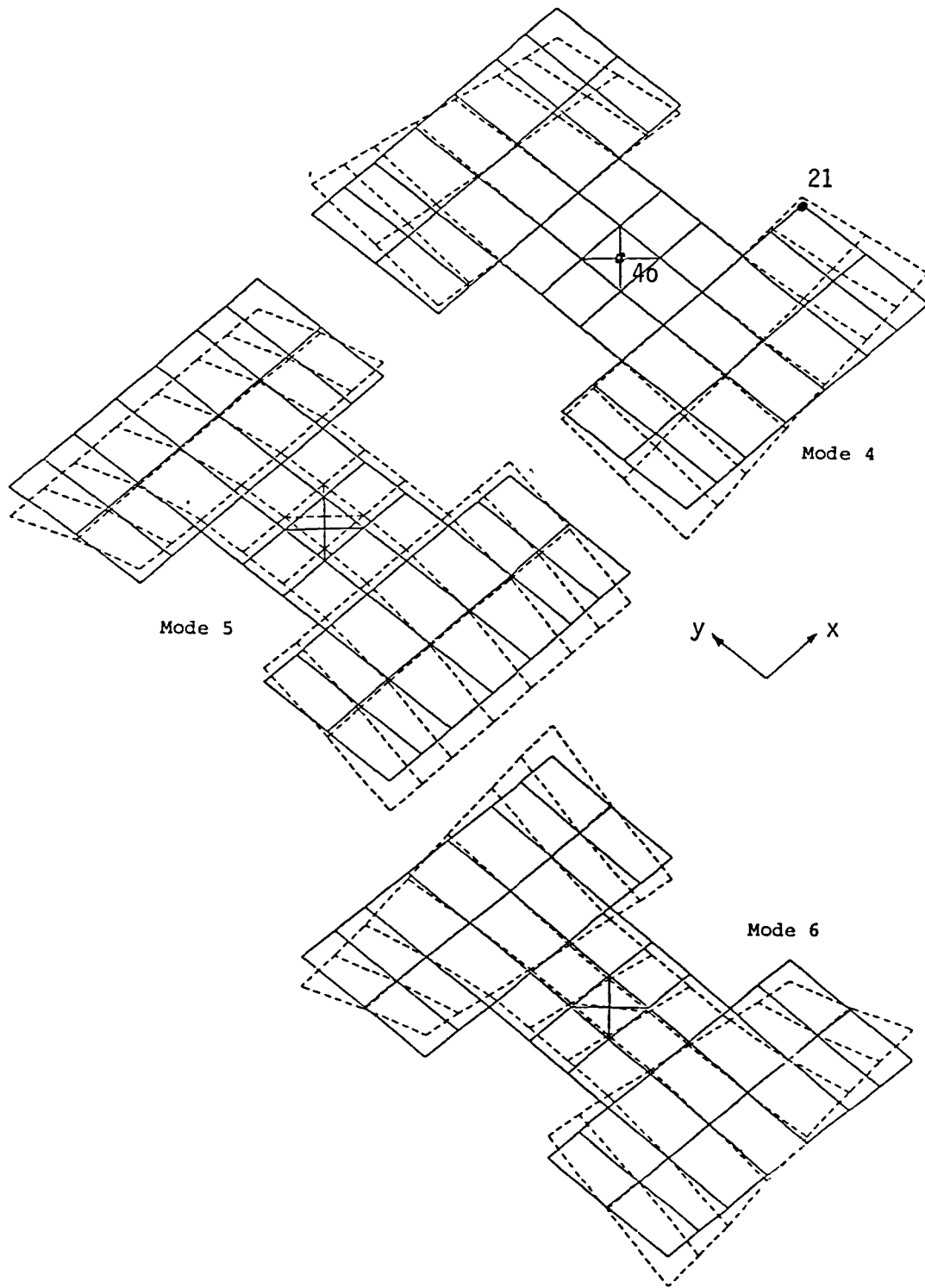
Fig. 2.1:   FLEXIBLE MODES

Mode	Omega [rad/s]	Frequency [Hz]
1	0	0
2	0	0
3	0	0
4	0.139	0.022
5	0.146	0.023
6	0.269	0.043
7	0.281	0.045
8	0.292	0.047
9	0.311	0.050
10	0.483	0.077
11	0.628	0.100
12	0.668	0.106
13	0.763	0.121
14	0.793	0.126
15	0.972	0.155
16	1.001	0.159
17	1.173	0.187
18	1.243	0.198
19	1.259	0.200
20	1.459	0.232

Table 2.1:   EIGENFREQUENCIES OF THE DISTRIBUTED FLEXIBILITY MODEL

Plots of the first three flexible Modes are given in Fig. 2.1. Input/Output transfer functions of the model are evaluated directly from the eigenvector solutions of the free-free structure.

The transfer function consists of parallel second order terms with resonant frequencies according to the eigenfrequencies and weight factors according to the modal gains. It can be expressed in state space form by decoupled second order state space forms for each mode. Hence the system matrix consists of a band of 2 by 2 matrices along their diagonal.

So far each node of the structural model can be defined as input or output station. For the use of the model in the studies different sensor/actuator stations have been defined. The following configuration proved to be most reasonable:

- Rotation sensor x, y at the centre node
- Translation sensors z and force actuators z at the edges of the outer plates.

The centre node is considered as a reference for attitude control.

III.   ORDER REDUCTION BY THE MODAL APPROACH OF LITZ

The idea of order reduction is to try to approximate a system of high order by a lower order system in order to ease the simulation, analysis and controller design. The design based on a reduced order system may also be less costly and reduces the controller order, which may be important for the implementation in the control computer aboard a spacecraft.

The finite element model itself is already a reduced model and the original system order is determined by the number of eigensolutions computed from the FEM. In our case the original order is 40. The mathematical methods of order reduction are then applied to this 40th order system called evaluation model. Since our model is based on modal data it appears reasonable to use modal methods for order reduction.

Modal approaches to order reduction require a transformation of the original system to the Jordan canonical form and take only the dominant eigenvalues of the original model into a reduced model. Methods have been developed since the mid sixties. The techniques of E.J. Davison, S.A. Marshall and M.R. Chidambara in their original versions have some shortcomings, which have been avoided by a newer technique of L. Litz [1]. In [2] a unified derivation and critical review of modal approaches has been given. Litz' technique is shown to be both highly accurate and powerful. Therefore this technique has been selected for application to the flexible spacecraft model. Litz' method links modal techniques to least square reduction techniques. It gives an explicit formulation for the reduced model and is optimal in the sense that it minimizes the weighted integral of the square of the deviations between the original and the reduced model.

The original states are sorted such as to have the relevant states in a subvector $\underline{x}_1$:

$$\begin{bmatrix} \dot{\underline{x}}_1 \\ \dot{\underline{x}}_2 \end{bmatrix} = A \quad \underline{x}_1 \quad + B \underline{u}. \tag{3.1}$$

The relevant states may be identified by their physical meaning or it may be the states which contribute to the output vector:

$$\underline{y} = [C_1 \ 0] \ \underline{x}_1. \tag{3.2}$$

The reduced model yields an approximation for the substates $\underline{x}_1$:

$$\dot{\tilde{\underline{x}}}_1 = A_R \tilde{\underline{x}}_1 + B_R \underline{u} \tag{3.3a}$$

and for the output $\underline{y}$:

$$\tilde{\underline{y}} = C_R \tilde{\underline{x}}_1. \tag{3.3b}$$

As for all modal methods the original system (3.1) is transformed by:

$$\underline{x} = V \underline{z} = \begin{bmatrix} V_{11} & V_{12} \\ V_{21} & V_{22} \end{bmatrix} \underline{z} \tag{3.4}$$

to Jordan canonical form:

$$
\begin{bmatrix} \dot{\underline{z}}_1 \\ \dot{\underline{z}}_2 \end{bmatrix} = \begin{bmatrix} \Lambda_1 & o \\ o & \Lambda_2 \end{bmatrix} \begin{bmatrix} \underline{z}_1 \\ \underline{z}_2 \end{bmatrix} + \begin{bmatrix} B_1^* \\ B_2^* \end{bmatrix} \underline{u} \qquad (3.5)
$$

where

$$
\begin{bmatrix} B_1^* \\ B_2^* \end{bmatrix} = B^* = V^{-1} B.
$$

Now again the transformed state vector is reordered such that $\underline{z}_1$ represents the dominant part, found by certain dominance measures. The structure of the original model is shown in Fig. 3.1.
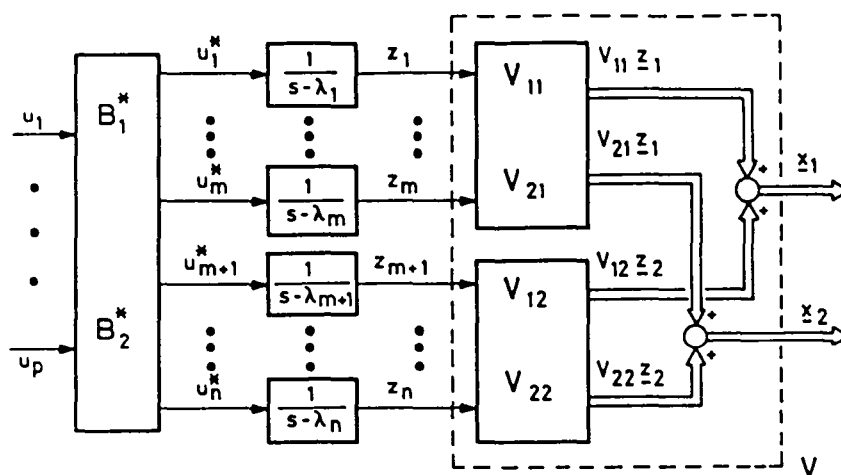
Fig. 3.1:   STRUCTURE OF ORIGINAL MODEL

The reduced model is not derived by neglecting the nondominant eigenmotions $\underline{z}_2$, but by reconstructing the $\underline{z}_2$ out of the retained states $\underline{z}_1$ (see Fig. 3.2):

$$
\tilde{\underline{z}}_2 = E \, \underline{z}_1 \qquad (3.6)
$$

giving

$$
\tilde{\underline{x}}_1 = (V_{11} + V_{12} E) \, \underline{z}_1 = M \, \underline{z}_1 \qquad (3.7)
$$

$$
\tilde{\underline{x}}_2 = (V_{21} + V_{22} E) \, \underline{z}_1 = L \, \underline{z}_1 \qquad (3.8)
$$

and the reduced model (3.3) as:

$$
\dot{\tilde{\underline{x}}}_1 = M \, \Lambda_1 \, M^{-1} \, \tilde{\underline{x}}_1 + M \, B_1^* \, \underline{u}. \qquad (3.9)
$$

420

Fig. 3.2:   REDUCED MODEL OF LITZ

The matrix E is determined such that the following performance index is minimized:

$$I = \sum_{i=1}^{r} q_i^2 \int_0^\infty /\underline{\varepsilon}_i (t)/^2 \, dt \tag{3.10}$$

with $\underline{\varepsilon}_i (t) = \underline{z}_{2i} (t) - \overset{\sim}{\underline{z}}_{2i} (t)$ (r number of inputs).

The index i indicates that only the i-th input is excited by a unity step. The weight factors q_i allow different weighting of the system inputs.

The optimization problem can be solved explicitly for:

$$E = E (B^*, \Lambda, q_1, \ldots, q_r).$$

The solution also guarantees stationary accuracy by:

$$\underline{\varepsilon}_i (t \to \infty) = \underline{O} \text{ for } i = 1, r.$$

In order to determine the low-order system completely, the output matrix C_R of eqn. (3.3b) has to be defined. If the high-order system output equation has the form of eqn. (3.2) this problem is easy to solve:

$$C_R = C_1. \tag{3.11}$$

But if variables of $\underline{x}_2$ are also necessary to evaluate the output $\underline{y}$ of the high-order system, that means:

$$\underline{y} = C_1 \underline{x}_1 + C_2 \underline{x}_2, \tag{3.12}$$

421

there are two possibilities, on principle, to get C_R.

The first one is to approximate the state variables of $\underline{x}_2$ by means of the eqns. (3.7) and (3.8):

$$\underset{\sim}{\underline{x}}_2 = LM^{-1} \underset{\sim}{\underline{x}}_1 .$$

Substituting the state vector $\underline{x}$ in eqn. (3.12) by its approximation $\underset{\sim}{\underline{x}}_1$, $\underset{\sim}{\underline{x}}_2$ yields the low-order output equation:

$$\underset{\sim}{\underline{y}} = C_1 \underset{\sim}{\underline{x}}_1 + C_2 \underset{\sim}{\underline{x}}_2 = (C_1 + C_2 \, LM^{-1}) \, \underset{\sim}{\underline{x}}_1 .$$

Thus the low-order output matrix is given by:

$$C_R = C_1 + C_2 \, LM^{-1} . \tag{3.13}$$

The second possibility is a so-called "transformation to sensor-coordinates". A transformation T is applied to the state vector $\underline{x}$ of the high-order system:

$$\underline{x} = T \, \underline{x}_N \tag{3.14}$$

yielding a new state vector $\underline{x}_N$, which contains the measurable variables $\underline{y}$ (sensor-coordinates) as an element:

$$\underline{x}_N = \begin{bmatrix} \underline{y} \\ \underline{x}_A \end{bmatrix}$$

The other subvector $\underline{x}_A$ consists of a linear combination of the original vector $\underline{x}$. The transformation matrix T has to be defined by the demand:

$$C \cdot T = [I_q, \; 0] . \tag{3.15}$$

The so transformed high-order model:

$$\dot{\underline{x}}_N = T^{-1} \, AT \, \underline{x}_N + T^{-1} \, B \, \underline{u}, \tag{3.16}$$

$$\underline{y} = [I, \; 0] \, \underline{x}_N \tag{3.17}$$

is of the same form as the system of eqns. (3.1) and (3.2).

Thus, the low-order system is obtained by reducing this transformed high-order model. Then the output matrix C_R is given by eqn. (3.11).

Remark 1: The main numerical difficulty when evaluating the low-order system matrices with LITZ's method lies in the fact that three matrices have to be inverted. Therefore they must be regular. Two of the inversions are necessary to get the matrix E and another one is the inversion of $\underline{M}$ in eqns. (3.9) and (3.13). One of the first mentioned matrices can always be inverted by an appropriate choice of the weighting parameters q_1 in eqn. (3.10). The other

two matrices depend on parameters of the mathematical model and cannot be influenced. Therefore these matrices can get singular. If such a case occurs the desired matrix E can be set to zero yielding the low-order system matrices without optimization of the criterion in eqn. (3.10). This result is identical with the low-order model derived by the approach of Davison [3].

LITZ has also proposed a method of generating a dominance measure. This measure does not only take into account the stability of the eigenvalue, i.e. its distance to the imaginary axis, but in addition its controllability and observability characteristics. To keep the presentation clear a single input single output system with single eigenvalues λ_1, ..., λ_n is considered. The state space description in Jordan canonical form is:

$$\dot{\underline{z}} = \Lambda \underline{z} + \underline{b}^* u$$

$$y = \underline{c}^{*T} \underline{z}.$$

The vector elements b_1^* and c_1^* determine the controllability and observability of the system. For $b_1^* = 0$ the eigenmotion z_1 is not controllable with u, and for $c_1^* = 0$ it is not observable from y.

The unity step response can be expressed as:

$$y = \sum_{k=1}^{n} \frac{b_k^* c_k^*}{\lambda_k} (e^{\lambda_k \cdot t} - 1), \quad t > 0.$$

From this:

$$q_k = \frac{b_k^* c_k^*}{\lambda_k}$$

can be taken as a measure of the influence of eigenvalue λ_k on the dynamic behaviour of the output. The definition of the equivalent measure for multiple input multiple output systems is easy, considering each signal path from input u_j to output y_i:

$$q_{ijk} = \frac{b_{kj}^* c_{ik}^*}{\lambda_k}.$$

If this q_{ijk} is related to the stationary value $y_{ij\infty}$, the dimensionless value

$$r_{ijk} = \frac{/q_{ijk}/}{/y_{ij\infty}/}$$

gives a measure how the response $y_{ij}(t)$ is influenced by the eigenvalue λ_k. As a criterion it can be stated that eigenvalues with small r_{ijk} are not dominant within the path (i, j).

A dominance measure, which also reflects that the output is influenced differently from the inputs, which may also have different amplitudes, can be defined by:

$$d_{ijk} = r_{ijk} \cdot N_{ij}$$

with

$$N_{ij} = \frac{/y_{ij\infty} \, u_{jmax}/}{\max_{j=1,r} (/y_{ij\infty} \, u_{jmax}/)}$$

The evaluation of the dominance with respect to the overall system can be done by either the maximum or the sum of all measures d_{ijk} which belong to the eigenvalue λ_k:

$$M_k = \max_{(i,j)} d_{ijk}$$

$$S_k = \sum_{i,j} d_{ijk}.$$

In reference [2] LITZ formulates the dominance criterion:

The eigenvalues λ_k with the highest measures M_k, S_k are dominant.

Remark 2: Because the dominance measure implies a division by λ_k it would not be suitable for zero-eigenvalues. But on the other side a zero-eigenvalue represents an integrator. Therefore it is always dominant and has to remain in a low-order reduced model.

IV. CONTROLLER DESIGN

Beside the high order of mathematical models of flexible spacecraft the generally low natural damping is of relevance. The control problems can be largely reduced with increased damping of the structural vibrations. One idea is to increase modal damping by velocity feedback. The feedback with distributed sensors and actuators which only moderately modifies the natural modes and frequencies of the structure has been named by Aubrun [4] as Low-Authority Control.

The controller design has been separated into two tasks:

- Low-Authority Control (LAC) for damping augmentation
- High-Authority Control (HAC) for attitude control.

As a design goal the modal damping should be increased to 5% due to LAC. The LAC design in the frame of this study has been done by G. Schulz at DFVLR using numerical optimization [5]. Eight sensors and actuators have been placed at the edges of the outer plates.

The low authority controller has been designed as feedback of the velocity sensor output $\underline{y}$:

$$\underline{u} = -K \, \underline{y} + \underline{w} \tag{4.1}$$

for the system

$$\dot{\underline{x}} = A\,\underline{x} + B\,\underline{u}, \qquad (4.2)$$

$$\underline{y} = C\,\underline{x}. \qquad (4.3)$$

The vector $\underline{w}$ represents the control variable of the high authority controller. The LAC gains K have been derived such as to yield 5% damping.

During the study two approaches to controller design have been compared:

Step	Approach 1	Approach 2
1	Order reduction of original high order model	LAC design for high order model
2	LAC design for (reduced model or) high order model	Order reduction for LAC loop closed
3	HAC design for reduced model, LAC closed	HAC design for reduced model from step 2

These two approaches will be discussed in the following and the most promissing approach will be identified.

The LAC design algorithm showed no problems when applied to high order models and the more modes are included in the design model the more the problem of spillover is reduced. On the other hand the order of the design model has no impact on the controller implementaton effort, because not full state feedback but output feedback is used. Therefore the use of high order models for LAC design is preferable. To make the model manageable some order reduction prior to LAC may be reasonable, but the model needs not to be reduced to such a low order as used for HAC design.

IV.1 HAC DESIGN WITH REDUCED-ORDER MODEL OF THE UNCONTROLLED SYSTEM

Approach 1 starts with the order reduction of the uncontrolled high order system (4.2). This yields the low-order model:

$$\dot{\tilde{\underline{x}}}_1 = A_R\,\tilde{\underline{x}}_1 + B_R\,\underline{u}, \qquad (4.4)$$

$$\tilde{\underline{y}} = C_R\,\tilde{\underline{x}}_1. \qquad (4.5)$$

Connecting the output feedback (4.1) with the low-order model one gets:

$$\dot{\tilde{\underline{x}}}_1 = (A_R - B_R K\,C_R)\,\tilde{\underline{x}}_1 + B_R\,\underline{w}, \qquad (4.6)$$

$$\tilde{\underline{y}} = C_R\,\tilde{\underline{x}}_1.$$

425

For this LAC controlled low-order model a linear state controller

$$\underline{w} = -R_1 \, \underset{\sim}{\hat{\underline{x}}}_1 \qquad\qquad (4.7)$$

is designed, minimizing a quadratic performance index.

The state variables are generalized coordinates and cannot be measured directly. Therefore an observer is necessary to estimate $\underset{\sim}{\hat{\underline{x}}}_1$.
The observer design is also based on the low-order model (4.6):

$$\dot{\underset{\sim}{\hat{\underline{x}}}}_1 = (A_R - B_R K \, C_R) \, \underset{\sim}{\hat{\underline{x}}}_1 + B_R \, \underline{w} + G_1 \, (\underset{\sim}{\underline{y}} - \hat{\underline{y}}), \qquad (4.8)$$

$$\hat{\underline{y}} = C_R \, \underset{\sim}{\hat{\underline{x}}}_1.$$

The observer matrix G_1 can be evaluated as a stationary Kalman filter gain or by designing a controller for the transposed system.

The estimated state vector $\underset{\sim}{\hat{\underline{x}}}_1$ is used in the HAC control law:

$$\underline{w} = -R_1 \, \underset{\sim}{\hat{\underline{x}}}_1 \qquad\qquad (4.9)$$

Although the observer has been designed for the system in Eqn. (4.8), it is assumed for the controller realization, that the observer still gives estimates of the state variables $\underline{x}_1$ when the output $\underline{y}$ of the physical system is replacing $\underset{\sim}{\underline{y}}$.

Applying the low authority controller K, high authority controller R_1 and observer G_1 to the high-order system yields the overall system:

$$\begin{bmatrix} \dot{\underline{x}} \\ \dot{\hat{\underline{x}}}_1 \end{bmatrix} = \begin{bmatrix} A - BKC & -BR_1 \\ G_1 \, C & A_R - B_R K \, C_R - B_R \, R_1 - G_1 \, C_R \end{bmatrix} \begin{bmatrix} \underline{x} \\ \hat{\underline{x}}_1 \end{bmatrix}. \qquad (4.10)$$

Since controller and observer have been designed for a low-order model the eigenvalues assigned in the design steps may change in general, the overall system may even become unstable.

IV.2 HAC DESIGN WITH REDUCED-ORDER MODEL OF THE LAC-CONTROLLED SYSTEM

The second approach first couples the LAC to the high-order system before order reduction is applied. The system of equation (4.2) is controlled by the LAC of equation (4.1) yielding:

$$\dot{\underline{x}} = A_L \, \underline{x} + B \, \underline{w}, \qquad\qquad (4.11)$$

$$\underline{y} = C \, \underline{x} \qquad\qquad (4.12)$$

with $\qquad A_L = A - BKC \qquad\qquad (4.13)$

426

This system has been reduced using the approach of Litz. The reduced order system is:

$$\dot{\tilde{\underline{x}}}_1 = \tilde{A}_L \, \tilde{\underline{x}}_1 + \tilde{B}_L \, \underline{w}, \tag{4.14}$$

$$\tilde{\underline{y}} = \tilde{C}_L \, \tilde{\underline{x}}_1. \tag{4.15}$$

As before for the system of equation (4.14) a complete state feedback R_2 is designed:

$$\underline{w} = -R_2 \, \tilde{\underline{x}}_1 \tag{4.16}$$

minimizing a quadratic performance index.

The observer for the state vector $\tilde{\underline{x}}_1$ is designed for the low-order system (4.14), giving a gain matrix G_2.

The overall system with observer G_2, low-authority control K and high-authority control R_2 becomes:

$$\begin{bmatrix} \dot{\underline{x}} \\[1ex] \dot{\hat{\underline{x}}}_1 \end{bmatrix} = \begin{bmatrix} A - BKC & -B \, R_2 \\[1ex] G_2 \, C & \tilde{A}_L - G_2 \, \tilde{C}_L - \tilde{B}_L \, R_2 \end{bmatrix} \begin{bmatrix} \underline{x} \\[1ex] \hat{\underline{x}}_1 \end{bmatrix} \tag{4.17}$$

The structure is described in Figure 4.1. Both design approaches result in formally the same structure. This can be seen from the equations (4.10) and (4.17). The differences between both systems are in the parameter values of the observer and the high-authority controller. Also the observer order is different.
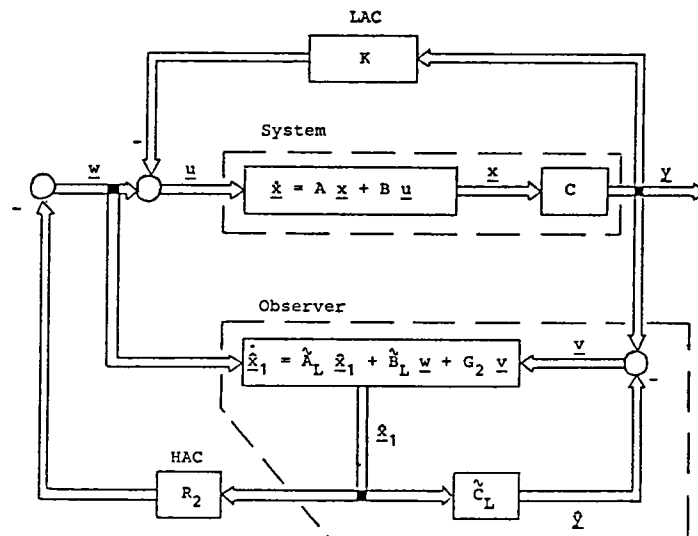

Fig. 4.1: STRUCTURE OF THE OVERALL SYSTEM

427

In order to design an overall controller for the distributed flexibility model derived in chapter 2 the LAC controller is designed first. To do so a so-called local feedback has been designed by parameter optimization meaning that the velocity of a sensor at one certain point has been used to excite only the actuator positioned at the same position (collocated positioning). The LAC gains of the output feedback K of eqn. (4.1) are given in Table 4.1:

$$
\begin{bmatrix}
0 & 0 & -43.8785 & 0 & 0 & 0 & 0 & 0 & 0 & 0 \\
0 & 0 & 0 & -43.8785 & 0 & 0 & 0 & 0 & 0 & 0 \\
0 & 0 & 0 & 0 & -43.8785 & 0 & 0 & 0 & 0 & 0 \\
0 & 0 & 0 & 0 & 0 & -43.8785 & 0 & 0 & 0 & 0 \\
0 & 0 & 0 & 0 & 0 & 0 & -96.2619 & 0 & 0 & 0 \\
0 & 0 & 0 & 0 & 0 & 0 & 0 & -96.2619 & 0 & 0 \\
0 & 0 & 0 & 0 & 0 & 0 & 0 & 0 & -96.2733 & 0 \\
0 & 0 & 0 & 0 & 0 & 0 & 0 & 0 & 0 & -96.2733
\end{bmatrix}
$$

Table 4.1:   OUTPUT FEEDBACK GAINS FOR LAC

It has been designed on the base of the high-order system yielding 5% damping for all eigenvalues at a minimum. Without LAC the lowest damping has been 0.5%.

According to the first approach a low-order model of the original high-order system has to be evaluated. The dominance analysis of Litz presented in chapter 3 marks 9 flexible modes as dominant. They are underlined in Table 4.2 where the dominance values are depicted. In addition with the 3 rigid body modes the low system order has to be 24. But with this eigenvalue configuration it was impossible to get a low-order system applying the method of Litz because always one of the matrices mentioned in the Remark 1 of chapter 3 becomes singular. Thus the low-order system matrices have been evaluated with Davion's approach (see Remark 1).

Now, the LAC and this low-order model have been switched together and for this closed loop the high authority controller as well as an observer have been designed. Finally, the LAC, the HAC and the observer are connected with the 40th-order original model. This overall system is stable but it is only weakly damped and needs very high control variables u_j. These facts are demonstrated in Figs. 4.2 and 4.3. For the second approach the low authority controller of Table 4.1 is switched to the high-order system. For this closed loop a dominance analysis has been performed. In addition to the three zero-eigenvalues which are always dominant (see Remark 2) there are 11 eigenvalues with high dominance values (see Table 4.3). Thus, the system order 14 seems to be suitable for a good approximation. This system order is essentially lower than in the first approach where the system order 24 has been necessary.

428

Table 4.2:

NO	EIGENVALUES REAL	IMAGINARY	OBS/CONT MAXIMUM	-DOMINANCY SUM
1	-0 0007	0 1386	0 0137	0 3189
2	-0 0007	-0 1386	0 0137	0 3189
3	-0 0007	0 1462	0 0185	0 5447
4	-0 0007	-0 1462	0 0185	0 5447
5	-0 0013	0 2688	0 0362	0 5619
6	-0 0013	-0 2688	0 0362	0 5619
7	-0 0014	0 2811	0 0071	0 0813
8	-0 0014	-0 2811	0 0071	0 0813
9	-0 0015	0 2922	0 0023	0 0513
10	-0 0015	-0 2922	0 0023	0 0513
11	-0 0016	0 3110	0 0446	0 4735
12	-0 0016	-0 3110	0 0446	0 4735
13	-0 0024	0 4830	0 0007	0 0213
14	-0 0024	-0 4830	0 0007	0 0213
15	-0 0031	0 6279	0 0023	0 0401
16	-0 0031	-0 6279	0 0023	0 0401
17	-0 0033	0 6685	0 0009	0 0249
18	-0 0033	-0 6685	0 0009	0 0249
19	-0 0038	0 7630	0 0061	0 0552
20	-0 0038	-0 7630	0 0061	0 0552
21	-0 0040	0 7934	0 0012	0 0391
22	-0 0040	-0 7934	0 0012	0 0391
23	-0 0049	0 9716	0 0000	0 0006
24	-0 0049	-0 9716	0 0000	0 0006
25	-0 0050	1 0006	0 0048	0 0596
26	-0 0050	-1 0006	0 0048	0 0596
27	-0 0059	1 1733	0 0016	0 0203
28	-0 0059	-1 1733	0 0016	0 0203
29	-0 0062	1 2432	0 0000	0 0008
30	-0 0062	-1 2432	0 0000	0 0008
31	-0 0063	1 2589	0 0002	0 0013
32	-0 0063	-1 2589	0 0002	0 0013
33	-0 0073	1 4587	0 0001	0 0034
34	-0 0073	-1 4587	0 0001	0 0034

Table 4.2: DOMINANCE MEASURES OF LITZ (only flexible modes; the dominant eigenvalues are underlined)

Table 4.3:

| NO	EIGENVALUES REAL	IMAGINARY	OBS/CONT MAXIMUM	-DOMINANCY SUM
1	0 0	0 0	0 0	0 0
2	0 0	0 0	0 0	0 0
3	0 0	0 0	0 0	0 0
4	-0 0199	0 0	0 8660	51 7091
5	-0 0245	0 2824	0 0302	0 3582
6	-0 0245	-0 2824	0 0302	0 3582
7	-0 0376	0 6277	0 0130	0 1787
8	-0 0376	-0 6277	0 0130	0 1787
9	-0 0449	0 0	1 1656	21 1308
10	-0 0456	0 1509	0 0341	1 1107
11	-0 0456	-0 1509	0 0341	1 1107
12	-0 0509	0 9616	0 0022	0 0468
13	-0 0509	-0 9616	0 0022	0 0468
14	-0 0667	0 2689	0 0212	0 7984
15	-0 0667	-0 2689	0 0212	0 7984
16	-0 0708	1 1631	0 0038	0 0749
17	-0 0708	-1 1631	0 0038	0 0749
18	-0 0715	1 4315	0 0004	0 0189
19	-0 0715	-1 4315	0 0004	0 0189
20	-0 0789	0 1216	0 0737	1 9312
21	-0 0789	-0 1216	0 0737	1 9312
22	-0 0821	0 0	1 0377	20 0716
23	-0 0896	0 4914	0 0121	0 4094
24	-0 0896	-0 4914	0 0121	0 4094
25	-0 1026	0 2541	0 1112	1 7788
26	-0 1026	-0 2541	0 1112	1 7788
27	-0 1091	0 2872	0 0477	0 7328
28	-0 1091	-0 2872	0 0477	0 7328
29	-0 1252	1 2224	0 0039	0 0672
30	-0 1252	-1 2224	0 0039	0 0672
31	-0 1252	1 2396	0 0034	0 0922
32	-0 1252	-1 2396	0 0034	0 0922
33	-0 1408	0 7188	0 0104	0 3677
34	-0 1408	-0 7188	0 0104	0 3677
35	-0 1461	0 7278	0 0058	0 1490
36	-0 1461	-0 7278	0 0058	0 1490
37	-0 1672	0 6288	0 0074	0 4409
38	-0 1672	-0 6288	0 0074	0 4409
39	-0 2150	0 9202	0 0165	0 2979
40	-0 2150	-0 9202	0 0165	0 2979

Table 4.3: DOMINANCE ANALYSIS OF THE LAC CONTROLLED HIGH-ORDER SYSTEM (the dominant eigenvalues are underlined)

With the reduction technique of Litz the low-order system matrices have been evaluated. Because the high-order system output matrix C has only 20 zero-columns the output equation isn't of the form of eqn. (3.2). Therefore the low-order system output matrix C_R has to be evaluated by eqn. (3.13).

A transformation to sensor-coordinates according to eqn. (3.14) has not been successful because then always singular matrices prevent the computation of the low-order system matrices with Litz' reduction technique.

On the base of the reduced-order system of order 14 the HAC design as well as the observer design have been performed. Now, the overall system consisting of the 40th-order system the 14th-order observer, the HAC and LAC has not only been stable but although the dynamic behaviour is considerably smoother but nevertheless fast. In spite of this the actuating variables are one or two orders of magnitude lower than with the first approach. This statement is demonstrated by the Figs. 4.2 and 4.3.

These favourable characteristics of the second approach have been possible although the order of the observer and of the HAC have been considerably lower than in the first one. This affects not only the off-line effort during the design steps of the HAC and of the observer but also the online computation of the control law.
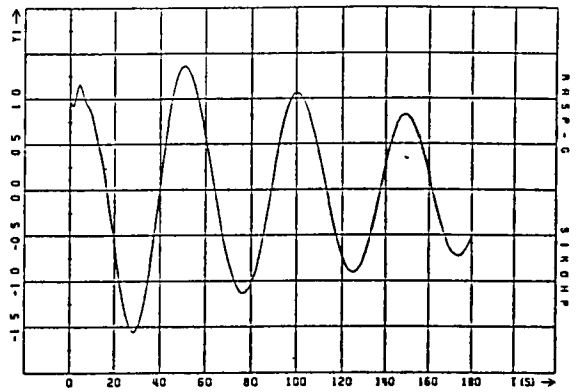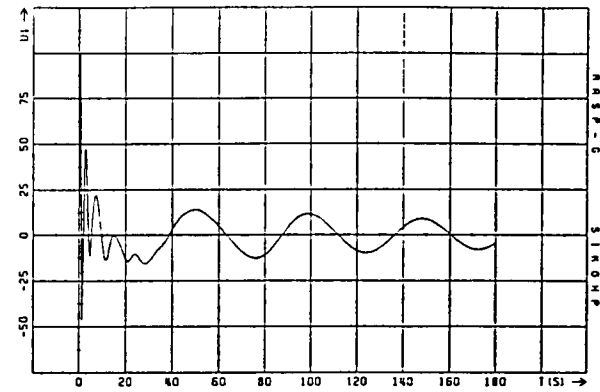
a) First proposal Overall system consisting of 40th-order system, 24th-order observer, LAC, and HAC
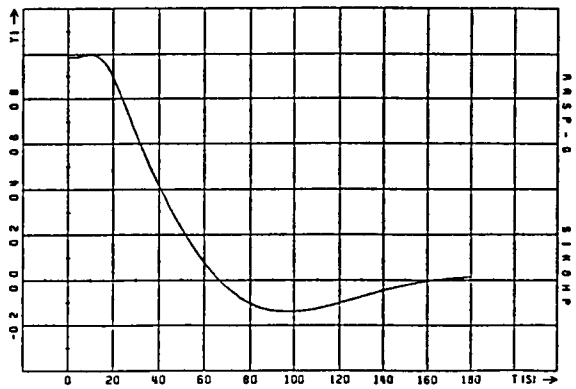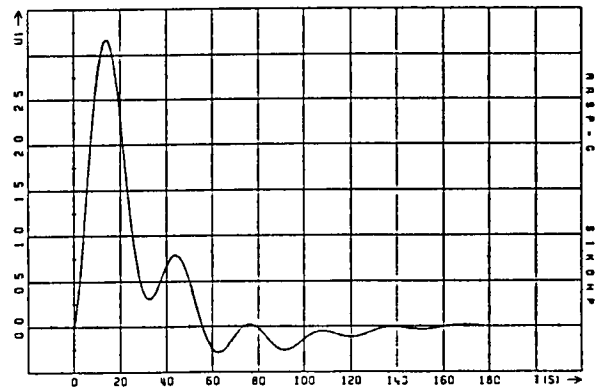
b) Second proposal Overall system consisting of 40th-order system, 14th-order observer, LAC, and HAC

Fig. 4.2   OUTPUT VARIABLE y_1; ROTATION ABOUT x-COORDINATE IN NODE 40

a) First proposal Overall system with the 24th-order observer

b) Second proposal Overall system with the 14th-order observer

Fig. 4.3   ACTUATOR QUANTITY u_1; FORCE ACTUATOR IN NODE 21

V. CONCLUSIONS

From the experiences made the following design concept has been identified as most promissing:

- Definition of sensors and actuators for low authority control (type, number, location)

- Design of LAC feedback gains for a high-order model (output feedback)

- Order reduction of the high-order system with LAC loop closed

- Design of a high authority controller for this low-order system. The HAC may use sensors and actuators different from those used for LAC.

- Design of a state estimator/observer for the low-order system. An observer is needed since the HAC is conceived as state feedback including non-measurable variables. The low-order system should be used in order to decrease the computational effort of the high authority controller.

- Combine LAC and HAC with a high-order evaluation model in order to analyze stability and dynamic behaviour. Since HAC feedback gains and state observer have been designed for low-order systems, the influence of those modes which have not been included in the design model has to be investigated. If there are problems with some modes the HAC design steps, or even LAC, have to be repeated including those critical modes into the design model.
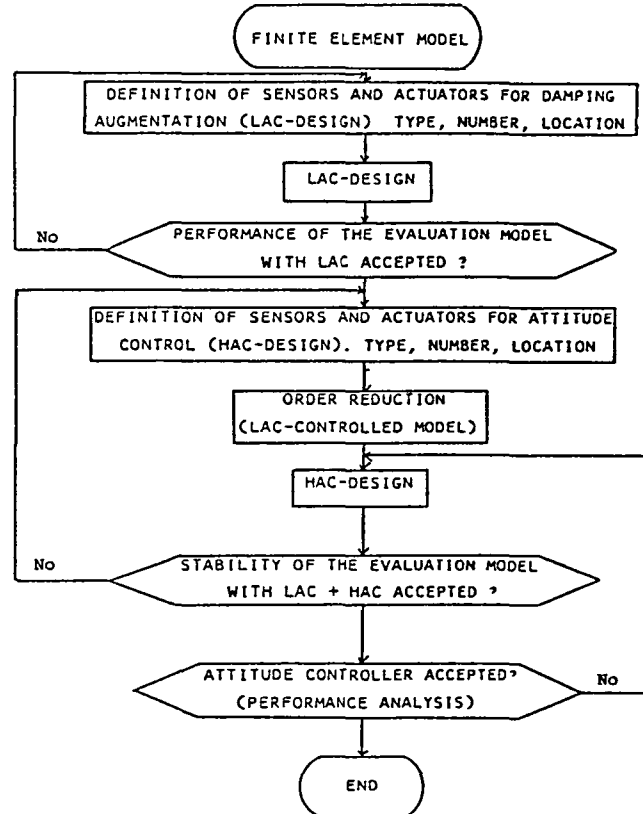The design concept is summarized in the flow chart Fig. 5.

Fig. 5: CONTROLLER DESIGN CONCEPT FOR DISTRIBUTED FLEXIBILITY MODELS

431

REFERENCES

[1] Litz, L., "Reduktion der Ordnung linearer Zustandsraummodelle mittels modaler Verfahren", Hochschulverlag Stuttgart, 1979

[2] Bonvin, D. and Mellichamp D.A., "A Unified Derivation and Critical Review of Modal Approaches to Model Reduction", Int. J. Control, 1982, Vol. 35, No. 5, pp. 828-848

[3] Davison, E.J., "A Method for Simplifying Linear Dynamic Systems", IEEE Trans. AC, 1966, pp. 93 - 101

[4] Aubrun, J.N., "Theory of the Control of Structures by Low-Authority Controllers". Journal of Guidance and Control, Vol. 3, No. 5, Sept./Oct. 1980, pp. 444-451.

[5] Schulz, G., "Low Authority Control of Flexible Spacecraft via Numerical Optimization", AGARD-CP-350

WIDEBAND DISTURBANCE ACCOMMODATION IN PRECISION FLEXIBLE SPACE STRUCTURES

D. R. Hegg
Charles Stark Draper Laboratory
Cambridge, MA 02139

G. J. Kissel
Massachusetts Institute of Technology*
Cambridge, MA 02139

ABSTRACT

Numerous spacecraft missions currently being formulated exhibit several basic and sharply conflicting features: selected components (e.g., an optical train) of inherently flexible structures are to maintain precision pointing performance in a wideband disturbance environment. Within the overall process of synthesizing an active controller to deal with this difficult problem, the aspects of reduced-order modeling and of actuator and sensor selection are crucial to the successful implementation of any controller feedback strategy. The principal focus in this paper is on the influence of actuator and sensor selection upon the effectiveness of a specified controller strategy for wideband disturbance accommodation. A generic optical support structure is used for a number of design examples. Active transducer selections are made systematically based upon their direct contribution to optical pointing error. Controller designs incorporating the various transducer selections exhibit stability in the presence of unmodeled modes over a frequency range substantially beyond the bandwidth of the disturbance.

1. INTRODUCTION

The anticipated need for active control to quench vibrations in flexible space structures arises principally because of stringent performance requirements involving certain structural components. High-precision pointing requirements for optical systems provide an important example. Synthesis of an active controller for flexible supporting structures is strongly influenced by inherent structural dynamic characteristics, such as low and clustered characteristic frequencies, and small inherent damping. Accommodation of anticipated disturbances without an unacceptable deterioration in system performance is fundamental. From the control synthesis viewpoint, a (small) number of periodic disturbances at known frequencies poses only mild difficulty. However, aperiodic disturbances with non-negligible power spectral density over a wide band of frequencies pose unusually severe difficulties, especially for the class of structures to be controlled. The purpose of this paper is to give a preliminary account of progress with a systematic approach to wideband disturbance accommodation in precision flexible space structures.

---

* Draper Laboratory Fellow

2. AN EXPERIMENTAL APPROACH

The process of synthesis for active control of flexible space structures requires the consideration of at least four principal factors, as illustrated in Figure 1: (1) the basic design of the structure to be controlled; (2) the selection of reduced-order models for design and for evaluation; (3) the selection of active transducers (actuators and sensors) both by functional type and by location; and (4) the determination of the controller feedback strategy. Much has been written regarding each of these factors standing alone, but very little is known about the detailed interactions of one factor with another. Especially important for flexible structure control is a mutual compatibility between the second and third factors listed. In order to gain a deeper understanding of the influence of each factor upon an overall design, and of their interactions, a scientific experiment for examination of the synthesis process has been defined. This approach is in the spirit of the recent comments of Ho [1] in which he proposed a wider adoption of experimental investigation--not necessarily in hardware--in preference to attempts at manipulating new problems so as to fit into a known solution framework. The principal idea behind the proposed experiment is to execute a planned sequence of designs from beginning to end, at each stage of which some aspect of one of the principal factors in the synthesis process is changed. The objective at each stage of this sequence is not necessarily to obtain the best possible design, but rather to isolate the influence of one of the principal factors, or of one of the mutual interactions, upon the overall synthesis process.

In the work reported here, the basic structural design (first factor) and the controller feedback strategy (fourth factor) are fixed, attention being focused on the influence that reduced-order model selections and active transducer selections have upon closed-loop stability and performance. The object of control is the ACOSS Model No. 2 generated by Henderson [2,3], which represents a generic optical support structure as illustrated in Figure 2. Revision 1 is chosen as the specific structural design, representing a compromise which retains certain improvements on the original structural design while avoiding the extremes of relatively high inherent flexibility or relatively high inherent stiffness, respectively, reflected in the other revisions. The controller feedback strategy is determined using a standard disturbance-rejection control design as described by Kwakernaak and Sivan [4]; i.e., a linear-quadratic-Gaussian (LQG) design in which the model of the plant to be controlled is augmented with a dynamic model of the disturbances, based on their statistical description.

3. ACTIVE TRANSDUCER SELECTION

The approach to active transducer selection incorporates two notable features. First, each transducer selected has relatively strong influence upon the design-problem variables to be regulated (for the demonstration examples--optical pointing error). Second, the aggregate of transducers selected is relatively sparse, containing fewer selections than the number of controlled modes. The approach was originally outlined by Fogel [5], and has been amplified recently in Reference 6. A brief summary is presented here.

434

Mathematical Formulation of a Selection Problem

The relevant structural dynamic equations in modal coordinates are:

$$\ddot{\eta} + 2Z\Omega\dot{\eta} + \Omega^2\eta = (\Phi^T B_A)u_A + (\Phi^T B_D)u_D \tag{1}$$

$$y = (C_P\Phi)\eta + (C_V\Phi)\dot{\eta} \tag{2}$$

$$z = (D\Phi)\eta \tag{3}$$

where $\eta \equiv (\eta_1, \cdots, \eta_n)^T$ is the vector of modal coordinates retained in the reduced-order model; $\Omega \equiv \text{diag}(\omega_i)$: $n \times n$ is the matrix of characteristic structural frequencies; Φ: $\nu \times n$ is the truncation of the principal-axis transformation to modal coordinates (mode shapes of the reduced-order model), ν being the number of physical generalized coordinates; $Z \equiv \text{diag}(\zeta_i)$: $n \times n$ is the matrix of modal damping ratios assumed to represent inherent structural damping; $u_A \equiv (u_1, \cdots, u_m)^T$ is the vector of inputs to the actuators; $u_D \equiv (w_1, \cdots, w_\gamma)^T$ is the vector of disturbance inputs; $y \equiv (y_1, \cdots, y_\ell)^T$ is the vector of outputs from the sensors; $z \equiv (z_1, \cdots, z_s)^T$ is the vector of variables to be regulated; and B_A: $\nu \times m$, B_D: $\nu \times \gamma$, C_P: $\ell \times \nu$, C_V: $\ell \times \nu$, and D: $s \times \nu$ are the influence matrices associated with the actuators, disturbances, displacement sensors, rate sensors, and regulated variables, respectively. The superscript (T) denotes matrix transpose. In the treatment presented here, it is assumed that the actuators and sensors are equal in number and colocated, and that each has infinite bandwidth. To clarify the exposition, the regulated variable z in Eq. (3) is identified in what follows with the optical line-of-sight (LOS) rotation error and defocus

$$z \equiv z_{LOS} \overset{\Delta}{=} (z_{LOSX}, z_{LOSY}, z_{DEFOCUS})^T \tag{4}$$

relative to local body axes (cf. Fig. 2) that is used in the design examples.

Any candidate class of actuators may be identified with the columns of a matrix

$$A \overset{\Delta}{=} [a^1 \vdots \cdots \vdots a^\mu] : n \times \mu \tag{5}$$

where the j-th column vector is the modal influence vector $\Phi^T b_A^j$ (j-th column of matrix $\Phi^T B_A$) associated with the actuator input u_j in Eq. (1). The vectors

$$b^{LOSX} \overset{\Delta}{=} \Phi^T d_{LOSX}, \qquad b^{LOSY} \overset{\Delta}{=} \Phi^T d_{LOSY} \tag{6}$$

where d^T_{LOSX} and d^T_{LOSY} are the first two row vectors of the line-of-sight influence matrix D in Eq. (3), are taken as objective vectors for the selection problem. With a sufficiently large class of actuator candidates, the equations

$$b^{LOSX} = Ax \equiv \sum_{j=1}^{\mu} a^j x_j \tag{7}$$

$$b^{LOSY} = Ay \equiv \sum_{j=1}^{\mu} a^j y_j \tag{8}$$

have solutions $x \equiv (x_1, \cdots, x_\mu)^T$ and $y \equiv (y_1, \cdots, y_\mu)^T$, respectively. An <u>ideal selection problem</u> is to realize the representation of Eqs. (7) and (8) with fewer actuators:

$$b^{LOSX} = A'x' \equiv \sum_j a^j x'_j \tag{9}$$

$$b^{LOSY} = A'y' \equiv \sum_j a^j y'_j \tag{10}$$

where the sums in Eqs. (9) and (10) extend over the column indices of some submatrix A' of A formed by a selection of columns from A.

In the absence of a linear algebraic solution to the ideal selection problem, an <u>approximate selection problem</u> using a least-squares formulation is a feasible alternative. This problem consists of seeking submatrices A' (formed by a selection of columns from A) and vectors x' and y' (having reduced dimension compatible with A') that minimize

$$J(x'; A', b^{LOSX}) \triangleq \| b^{LOSX} - A'x' \|^2_W \tag{11}$$

and

$$J(y'; A', b^{LOSY}) \triangleq \| b^{LOSY} - A'y' \|^2_W \tag{12}$$

respectively, and such that the columns of A' constitute a minimal set with respect to acceptable increases in the least-squares-minimum values realized in Eqs. (11) and (12). The notation $\|\alpha\|^2_W$ denotes the weighted inner product $\alpha^T W \alpha$, for a real symmetric positive-definite weighting matrix W: n× n.

Theoretical Foundations

Well-known theoretical tools are available for solving the approximate selection problem. The first of these is the representation theory for solutions to least-squares problems. An excellent summary may be found in Peters and Wilkinson [7], with a more complete treatment available in Lawson and Hanson [8]. In brief, minima of Eq. (11) (similarly for Eq. (12)) are characterized by solutions of the normal equations

$$A^T(b - Ax) = 0 \tag{13}$$

where the superscripts on A, b, and x appearing in Eq. (11) have been suppressed in an obvious way, and the weighting matrix has been taken to be the identity matrix (an equivalent problem under a simple scaling). The result in Eq. (13) represents an orthogonality relation satisfied by the residual vector b − Ax at a least-squares solution. An explicit representation of solutions for Eq. (13) is given by:

$$x = A^\dagger b + (I - A^\dagger A)\omega, \quad \omega : n \times 1 \text{ arbitrary} \tag{14}$$

where (†) represents the Moore-Penrose [9,10] inverse, and I represents the identity matrix of appropriate dimension. The minimum value realized in Eq. (11) by any of the minima in Eq. (14) is

$$J_{min} = \|(I - AA^\dagger)b\|^2 \tag{15}$$

and is zero when b is in the column space of A.

The representations of Eqs. (14) and (15) can be sharpened considerably if a full-rank factorization such as the QR-decomposition of Francis [11] is used to represent the A matrix. This decomposition for a matrix A: n × m having full rank k = min {n, m} has the form

$$AP = QR \tag{16}$$

where P: m × m is a column permutation matrix, Q: n × n is an orthogonal matrix, and R: n × m has the form

$$\begin{bmatrix} R_1 & \vdots & S \end{bmatrix} \tag{17}$$

$$\begin{bmatrix} R_1 \end{bmatrix} \tag{18}$$

or

$$\begin{bmatrix} R_1 \\ \cdots \\ 0 \end{bmatrix} \tag{19}$$

according as the matrix A is underdetermined (k = n < m), determinate (k = n = m), or overdetermined (k = m < n), respectively. The matrix R_1: k × k is upper triangular, its elements having the important diagonal dominance property

$$r_{\ell\ell}^2 \geq \sum_{i=\ell}^{j} r_{ij}^2, \quad j = \ell, \cdots, k; \quad \ell = 1, \cdots, k \tag{20}$$

with diagonal elements positive. The relations in Eq. (20) are not obvious from the usual interpretation of Eq. (16) as the matrix representation of a

Gram-Schmidt orthogonalization. However, they result from the construction process involving the Householder [12] triangularization lemma that is employed in the LINPACK [13] algorithms for generating the decomposition. In particular, Eq. (20) implies that the diagonal elements of the matrix R_1 form a non-increasing sequence. The expressions for Eqs. (14) and (15) in the over-determined case are especially significant; they are

$$x = R_1^{-1} Q_1^T b \qquad (21)$$

and

$$J_{min} = \| Q_2^T b \|^2 \qquad (22)$$

where $Q \equiv [Q_1 \vdots Q_2]$ is partitioned compatibly with the block matrix in Eq. (19).

A Selection Algorithm

Once an actuator candidate class is selected, with corresponding matrix A (cf. Eq. (5)), the selection algorithm is executed as follows.

Step 1--Compute a QR-decomposition for A (cf. Eqs. (16), (17)).

Step 2--Truncate the rearranged matrix AP (cf. Eq. (16)) by retaining only the first n columns. The truncated matrix $A^{(1)}$ has linearly independent columns and inherits a QR-decomposition from Step 1. Further eliminations from $A^{(1)}$ produce an overdetermined system with generally nonzero least-squares-minimum values representable by Eq. (22).

Step 3--Compute least-squares solutions corresponding to $A^{(1)}$ (cf. Eqs. (11), (12)). The result corresponding to Eq. (15) is zero.

Step 4--Select an actuator for elimination from $A^{(1)}$ using one of the following considerations:

Fact I: A small value for the ratio $r_{nn}/r_{n-1,n-1}$ is a measure of near-linear-dependence of column a^n upon the other columns a^j, $j < n$, in the truncated matrix $A^{(1)}$.

Fact II: Small values of products $r_{\sigma\sigma}x_\sigma$ (resp. $r_{\tau\tau}y_\tau$) appearing in the matrix product $A^{(1)}x$ (resp. $A^{(1)}y$) in Eq. (11) (resp. Eq. (12)), where $x \equiv (x_i)$ (resp. $y \equiv (y_i)$) is a least-squares solution to Eq. (11) (resp. Eq. (12)) from Step 3, is an indication that a^σ (resp. a^τ) contributes less to the approximation measured by Eq. (11) (resp. Eq. (12)) than the other a^j, $j > \sigma$ (resp. $j > \tau$). This follows from Eq. (20). [6]

Denote the reduced $A^{(1)}$ matrix (using either Fact I or Fact II) by $A^{(2)}$.

Step 5--Compute a QR-decomposition of $A^{(2)}$ (cf. Eqs. (16), (19)).

Step 6--Compute least-squares solutions corresponding to Eqs. (11) and (12) for $A^{(2)}$.

438

Step 7—Repeat Steps 4 through 6, iteratively, generating a sequence of matrices $\{A^{(i)}\}$ with successively fewer columns.

Step 8—Termination occurs when a reduced A matrix, say A', is obtained such that further eliminations result in exceeding a prespecified tolerance on the minimum values corresponding to Eq. (22) for either Eq. (11) or Eq. (12). The actuator selections corresponding to A' then constitute a minimal selection.

Remarks—Since each execution of Step 4 may suggest up to three distinct candidates for elimination, the aggregate of alternatives for elimination generated by the algorithm is generally an expanding lattice. The number p of actuators in a minimal selection is of special interest. Results may be described in terms of the non-negative parameter $\Delta \overset{\Delta}{=} n - p$ called the level of reduction (from the number of controlled modes). The qualitative richness of the elimination lattice is also of interest.

4. DESIGN EXAMPLES

An artist's conception of a generic optical support structure represented by ACOSS Model No. 2 and used as the object of control for the design examples of the experiment is depicted in Figure 2. Also indicated are the locations (node 37 on the upper support truss and node 46 on the equipment section) and lines of application of a wideband disturbance. A profile of the power spectral density assumed for each disturbance is shown in Figure 3. In order to reduce computation costs, each disturbance has been assumed fixed in direction (at an equal angle with each body axis).

To assist in selecting reduced-order models for design, the structural modes are ranked in accordance with their open-loop response to the two disturbances. The optical pointing error equation for the full-order system has the form of Eqs. (3), (4), and can be written (only the first two components contribute to the pointing error) as

$$z_{LOS} = (D\Phi)\eta = \sum_{\alpha=1}^{N} z_{LOS}^{\alpha} \eta_{\alpha} \tag{23}$$

where z_{LOS}^{α}: 2×1 is the line-of-sight pointing error due to a unit displacement in mode α, and $N = 150$ is the number of flexible modes in the full-order system. The root-mean-square (RMS) values of the Euclidean norm of the modal error coefficients z_{LOS}^{α} of Eq. (23) in response to the total disturbance are listed in Table 1. By comparison, the specification for the optical pointing error arising from all the modal influences is that each of the two components of the variable z_{LOS} be less that 0.05 μ-radians in magnitude. An inevitable feature of such a ranking is that, in general, a selected group G of consecutively-ranked modes is not contiguous in frequency; i.e., there exist modes not in G which are interlaced in frequency with modes in G. This is seen by comparing Tables 1 and 2 for the first eleven modes in the ranking of Table 1.

A reduced-order model having this property is called _interlaced_; otherwise it is called _contiguous_.

Principal observations with respect to the performance of the selection algorithm that have emerged from the work to date are the following:

(1) Column ordering with respect to initial elimination that is generated by the initial factorization (cf. Step 1) of the matrix of actuator candidates may be represented approximately by the following partition (cf. Eq. (16)):

$$AP = \begin{bmatrix} A_{Translation} & \vdots & A_{Rotation} & \vdots & A_{Axial} \end{bmatrix} \qquad (24)$$

where the subscripts of each block submatrix represent groupings of actuators of the same functional type (the rank within the ordering decreasing toward the right in Eq. (24));

(2) The level of reduction increases when:

(a) Interlaced reduced-order design models on which active transducer selection is based are made contiguous, or

(b) The class of actuator candidates is enlarged from the axial type to include either translational or rotational types;

(3) Minimal selections which realize the same level of reduction are not necessarily unique.

The four design examples which follow demonstrate the first two observations. The following are assumed in each design example: the modal damping in Eq. (1) is taken as $\zeta_i = 0.001$ for all modes; the weighting matrix W in Eqs. (11) and (12) is the diagonal matrix whose nonzero entries are the disturbance-induced error values listed in Table 1 for the modes selected; the tolerance parameter for Step 8 of the selection algorithm is taken as $\tau_0 = 10^{-6}$.

Specifications for the four examples are summarized in Table 3. The reduced-order model for Example A consists of the first eleven modes in the ranking of Table 1. For the remaining examples, this model is augmented so as to become contiguous as indicated in Table 2. An exception is that mode 19 is not included in the numerical implementation of the active transducer selection because the very small associated weighting from Table 1 results in ill-conditioning. Its influence upon the optical pointing error is also negligibly small. The actuator candidate class for Examples A and B consists of all node-connecting elements of the finite-element model as axial actuators. For Examples C and D, this class is enlarged to include translational and rotational actuators, respectively, at nodes.

A summary of the selection results for each example is also shown in Table 3, and pictorial representations of the minimal selections are shown in Figures 4 through 7, respectively. The principal observations noted above may be deduced from Table 3, except for the existence of nonunique minimal selections.

Disturbance-rejection control designs employing the active transducer selections in Examples A through D were made. The specific form of the functional being minimized in the LQ designs is:

$$J \overset{\Delta}{=} \int_0^\infty \left(z^T Q z + \rho_R u_A^T u_A \right) dt$$

where u_A and z are the variables in Eqs. (1) and (4), respectively, $Q \equiv \text{diag}(q_i)$: 3×3 is the regulated-variable weighting matrix, and ρ_R is the actuator-input weighting parameter. Although the measurement equation Eq. (2) does not model sensor noise, a matrix $\rho_0 I_\ell$, where $\rho_0 > 0$ is small and I_ℓ is the $\ell \times \ell$ identity matrix, is introduced into the calculations playing the role of a fictitious sensor noise covariance matrix to permit a nonsingular approach to the Kalman filter design. Each LQ design is stable and meets performance specifications relative to the optical pointing error. In addition, each LQG design is examined for stability in the presence of residual modes using an expanding family of contiguous evaluation models. Table 4 summarizes the results. For clarification, it should be noted that the design in Example A is stable when connected across the interlaced reduced-order model depicted in Table 2, but is unstable when connected across the contiguous closure (i.e., modes 7 through 24) of that interlaced model. Such unacceptable behavior is one of the reasons for restricting attention subsequently to contiguous reduced-order models for design. The results in the remaining examples indicate a range of stability in the presence of unmodeled modes substantially beyond the 5 Hz extent of the reduced-order design models. It can also be demonstrated (not shown here) that an appropriate augmentation of a minimal selection by a larger number of actuators (yet fewer than the number of controlled modes) can enhance the stability robustness indicated.

5. CONCLUSIONS AND FUTURE DIRECTIONS

Preliminary results from a systematic approach to the accommodation of wideband disturbances for precision pointing in flexible space structures have been encouraging. Substantial insight into an appropriate procedure for selecting active transducers has been obtained. A capability for making selections which have direct influence upon the variables to be regulated and which are substantially fewer in number than the controlled modes has been demonstrated. The selection process itself, as well as the selections it produces, exhibits potentially beneficial design flexibility.

Linear-quadratic-Gaussian disturbance-rejection controllers employing transducer selections generated as described herein demonstrate stability in

the presence of residual modes over a frequency range substantially beyond the bandwidth of the disturbance. These demonstrations are significant in that stability-enhancing adjustments of the controller feedback strategy have been deliberately postponed so as to focus on the influence that the selection of reduced-order models and of active transducers have upon closed-loop stability and performance. With appropriate modification of the estimator portion of the LQG designs, compensators may readily be found that employ the transducer selections in Examples C and D and which are capable of stabilizing the full 150-mode structural model. This will be discussed in a future paper.

Finally, the active transducer selection procedure outlined here is by no means restricted to the consideration of colocated actuator-sensor pairs. In fact, it can be readily modified to provide for an independent selection of sensors (e.g., so as to provide improved information on disturbance effects). The efficacy of such a modification is currently being investigated.

ACKNOWLEDGEMENT

REFERENCES

1. Ho, Y.C., "Is It Application or Is It Experimental Science?" (Editorial), IEEE Trans. Automatic Control, Vol. AC-27, No. 6, December 1982, p. 1142.

2. Henderson, T., "Active Control of Space Structures (ACOSS) Model 2," Charles Stark Draper Laboratory Report C-5437, September 1981.

3. Henderson, T., "Modifications to ACOSS Model #2 Design; Technical Report, Data Base (Final)," Charles Stark Draper Laboratory Report CSDL-R-1585, October 1982 (also Rome Air Development Center Report RADC-TR-83-56, March 1983).

4. Kwakernaak, H., and Sivan, R., Linear Optimal Control Systems, Wiley, New York, NY, 1972.

5. Fogel, E., "Sensor/Actuator Selection," ACOSS Eleven Second Semiannual Technical Report, Vol. 2: Active Controller Designs, Charles Stark Draper Laboratory Report CSDL-R-1583, August 1982 (also Rome Air Development Center Report RADC-TR-82-295, Vol. II, November 1982), Section 3.

6. Hegg, D.R., "Progress on Synthesis of Active Control for Broadband Disturbance Accommodation — Part 1: Active Transducer Selection," ACOSS Eleven Fourth Semiannual Technical Report, Vol. 2, Charles Stark Draper Laboratory Report CSDL-R-1648, August 1983 (also Rome Air Development Center Report RADC-TR-83-261, Vol. II, December 1983), Section 2.

7. Peters, G., and Wilkinson, J.H., "The Least-Squares Problem and Pseudo-Inverses," Computer J. (United Kingdom), Vol. 13, No. 3, August 1970, pp. 309-316.

8. Lawson, C.L. and Hanson, R.J., Solving Least Squares Problems, Prentice-Hall, Englewood Cliffs, NJ, 1974.

9. Moore, E.H., "On the Reciprocal of the General Algebraic Matrix," Bull. American Mathematical Society, Vol. 26, June 1920, pp. 394-395.

10. Penrose, R., "A Generalized Inverse for Matrices," Proc. Cambridge Philosophical Society, Vol. 51, July 1955, pp. 406-413.

11. Francis, J.G.F., "The QR Transformation: A Unitary Analogue to the LR Transformation -- Part 1," Computer J. (United Kingdom), Vol. 4, October 1961, pp. 265-271.

12. Householder, A.S., "Unitary Triangularization of a Nonsymmetric Matrix," J. Association for Computing Machinery, Vol. 5, No. 4, 1958, pp. 339-342.

13. Dongarra, J.J., Moler, C.B., Bunch, J.R., and Stewart, G.W., LINPACK Users Guide, SIAM, Philadelphia, PA, 1979.
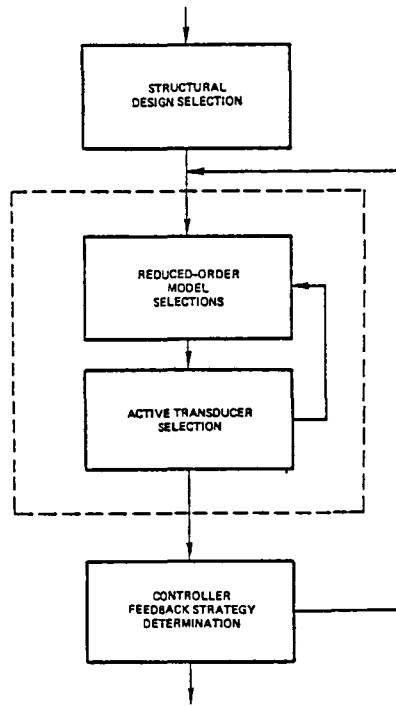
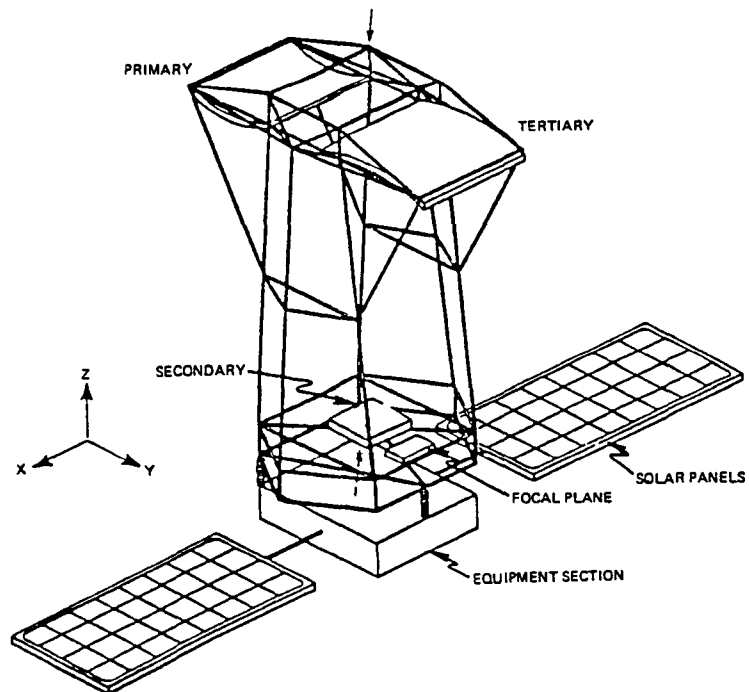Figure 1. Process for active control synthesis.

Figure 2. Generic optical support structure (ACOSS Model No. 2) -
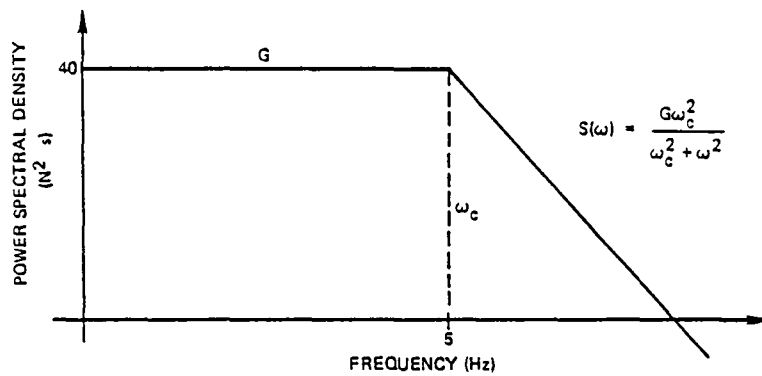artist's conception.

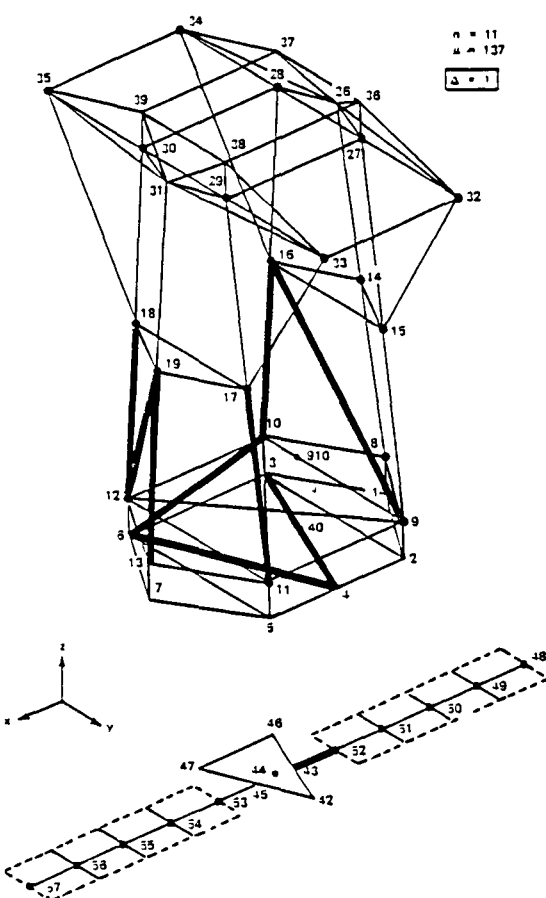Figure 3. Power spectral density of wideband disturbance.

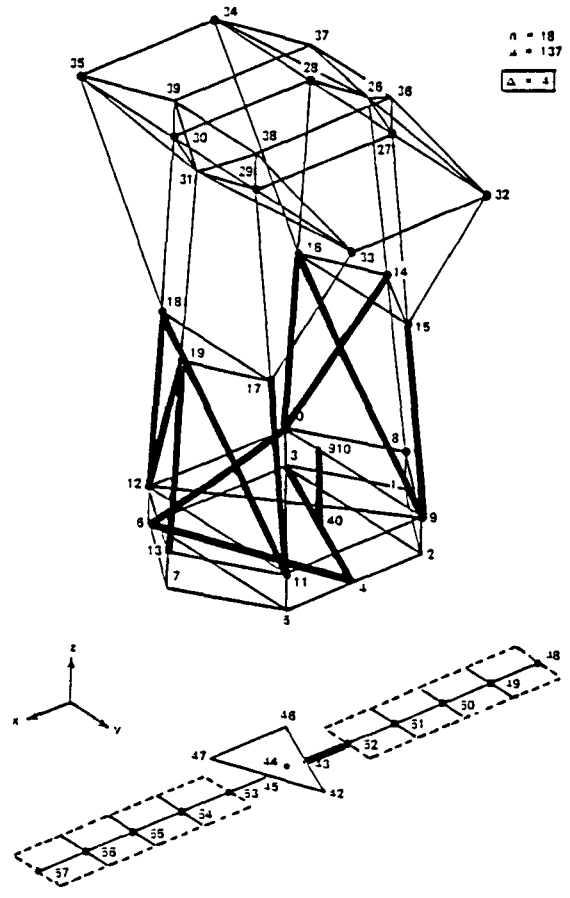Figure 4. Minimal selection, Example A.
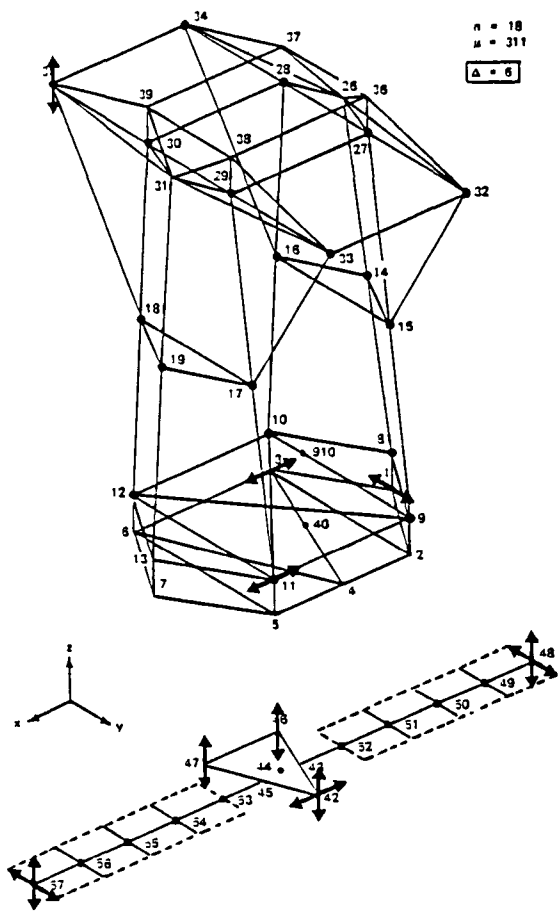
Figure 5. Minimal selection, Example B.

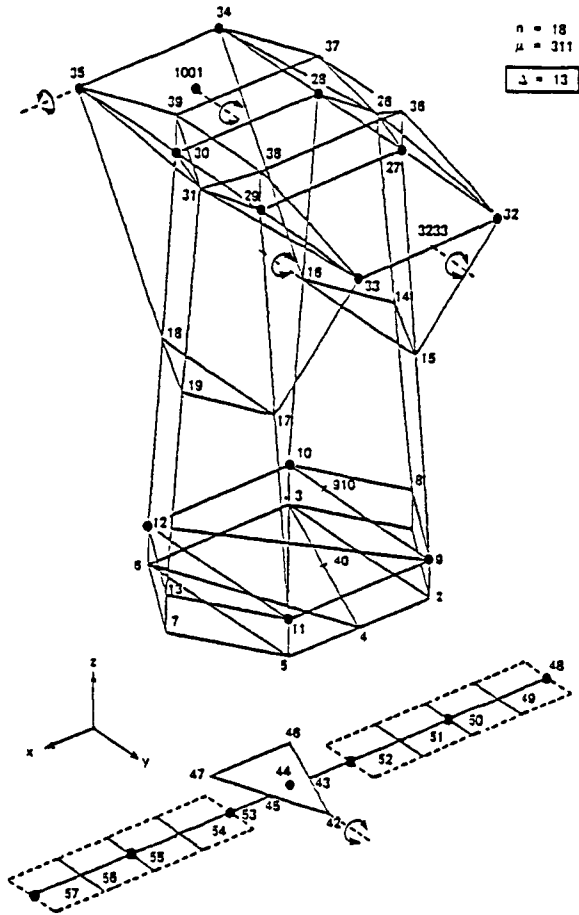Figure 6. Minimal selection, Example C.

Figure 7. Minimal selection, Example D.

Table 1. Ranking of open-loop modal responses to wideband disturbance.

Rank	Mode		RMS LOS-Error (μ-rad)	Rank	Mode	RMS LOS-Error (μ-rad)
1	7	o	600.97	26	11	1.19
2	24	o	455.77	.	.	.
3	23	o	105.89	.	.	.
4	13	o	92.65	35	21	0.72
5	22	o	77.04	.	.	.
6	12	o	72.43	.	.	.
7	16	o	32.47	42	20	0.25
8	14	o	15.91	.	.	.
9	10	o	12.94	.	.	.
10	8	o	12.22	47	17	0.09
11	9	o	5.06	.	.	.
12	39		5.01	.	.	.
.	.		.	78	18	0.005
.	.		.	.	.	.
22	15		1.45	.	.	.
.	.		.	145	19	1E-22

Table 2. Characteristic frequencies for ACOSS Model No. 2 and reduced-order models; o Design (interlaced) ● Design (contiguous) ■ Evaluation (contiguous).

Mode				Frequency (Hz)	Mode		Frequency (Hz)
7	o	●	■	0.148	25	■	5.162
8	o	●	■	0.282	26	■	5.170
9	o	●	■	0.319	27	■	7.877
10	o	●	■	0.335	28	■	7.918
11		●	■	0.468	29	■	8.772
12	o	●	■	0.583	30	■	8.776
13	o	●	■	0.601	31	■	8.838
14	o	●	■	0.673	32	■	8.980
15		●	■	0.960	33	■	9.620
16	o	●	■	1.092	34	■	10.40
17		●	■	1.839	35	■	11.67
18		●	■	1.844	36	■	12.27
19		●	■	1.889	37	■	13.39
20		●	■	1.990	38	■	13.62
21		●	■	2.060	39	■	14.77
22	o	●	■	2.452	40	■	16.43
23	o	●	■	2.472	41		20.83
24	o	●	■	3.242	42		21.79
					43		21.84

Table 3. Active transducer selection: design example specifications and results.

Example	Design Model	Actuator Candidate Class	Richness	Minimal Selection Size (p) & Type	Level of Reduction (Δ)
A	Rank 1-11 Interlaced (n = 11)	Axial only (μ = 137)	Sparse	10 (axial)	1
B	Rank 1-11 Contiguous* (n = 18)	Axial only (μ = 137)	Moderate (-)	14 (axial)	4
C	Rank 1-11 Contiguous* (n = 18)	Axial and Nodal Translation (μ = 311) ———————— Axial and Nodal Transl. & Rotation (μ = 485)	Moderate (+)	12 (translation)	6
D	Rank 1-11 Contiguous* (n = 18)	Axial and Nodal Rotation (μ = 311)	Very rich	5 (rotation)	13

* Mode 19 excluded numerically

Table 4. Controller design and evaluation.

Actuator/ Sensor Selection	Weights				LQ (modes 7-24)			LQG (modes 7-24)			LQG (modes 7-36)			Modes in Stable Evaluation
	q_1	q_2	q_3	ρ_R and ρ_0	LOSX (μr)	LOSY (μr)	DEFOCUS (10^{-3}m)	LOSX (μr)	LOSY (μr)	DEFOCUS (10^{-3}m)	LOSX (μr)	LOSY (μr)	DEFOCUS (10^{-3}m)	
Design Objective	–	–	–	–	0.05	0.05	0.025	0.05	0.05	0.025	0.05	0.05	0.025	7-156
A (10 axial)	10^3	10^1	10^{-4}	10^{-17}	0.0364	0.02093	0.00180							*Un-stable
B (14 axial)	10^3	10^1	10^{-4}	10^{-17}	0.01958	0.01146	0.00408							7-29
C (12 transl.)	10^0	10^{-1}	10^{-5}	10^{-17}	0.00532	0.00851	0.00136	0.00644	0.05073	0.00136'	31.44	19.16	0.03848	7-39
D (5 rot.)	10^1	10^{-1}	10^{-5}	10^{-17}	0.05587	0.04776	0.00496	0.06019	0.16216	0.00496				7-33

* Unstable over modes 7-24 inclusive

End of Document